Development and Mechanistic Studies of Chiral Silanol-Containing Ligands for Enantioselective Catalysis

By

YUN-PU CHANG
DISSERTATION

Submitted in partial satisfaction of the requirements for the degree of

DOCTOR OF PHILOSOPHY

in

Chemistry

in the

OFFICE OF GRADUATE STUDIES

of the

UNIVERSITY OF CALIFORNIA

DAVIS

Approved:

Annaliese K. Franz, Chair

Mark Mascal

David E. Olson

Committee in Charge

2024

© 2024 by Yun-Pu Chang
All rights reserved.

# Table of Contents

*Table of Contents* ..... *ii*

*Acknowledgements* ..... *v*

*Abstract* ..... *viii*

*List of Symbols and Abbreviations* ..... *x*

*Introduction* ..... *1*

**I. Organic Synthesis and Catalysis in Drug Discovery** ..... **1**
Ia. Transition Metal Catalysis ..... 2
Ib. Asymmetric Catalysis ..... 3
Ic. Metal Choice and Importance of Ligand Design ..... 4
Id. Organic Photoredox Catalysis ..... 6

**II. General Overview of the Dissertation** ..... **8**

**III. References** ..... **9**

*Chapter One: Chiral Silanol Ligands for Copper-catalyzed Enantioselective N−H Insertion Reactions* ..... *12*

**I. Introduction and Background** ..... **12**
Ia. Silanols and Siloxides ..... 12
Ib. Metal-siloxides in Catalysis ..... 14

**II. Synthesis of Chiral Silanol Ligands** ..... **17**
IIa. Synthesis of Imidazoline Silanols and the Discovery of the Aminoamide Silanol Ligand ..... 17
IIb. Pd-catalyzed Hydrolysis at Elevated Temperature ..... 18
IIc. Efforts toward the Synthesis of Imidazoline Silanols ..... 19
IId. Exploring Alternative Routes for the Synthesis of Aminoamide Silanols ..... 23

**III. Investigation of Catalytic Properties of Chiral Aminoamide-silanol Ligands** ..... **24**
IIIa. Enantioselective N−H Insertions ..... 24
IIIb. Preliminary Ligand Screening for the Enantioselective N−H Insertion ..... 25
IIIc. Addition of Molecular Sieves Affects Enantioselectivity ..... 26
IIId. Optimization of the Cu-catalyzed Enantioselective N−H Insertion ..... 27
IIIe. Screening of Chiral Silanol Ligand for the Enantioselective N−H Insertion ..... 30
IIIf. Silanol Ligand Validation and Control Experiments ..... 33

**IV. Scope of the Enantioselective N−H Insertion of Diazoesters with Anilines** ..... **34**
IVa. Unsuccessful Amide/Amine Substrates ..... 37
IVb. Screening of Metal Catalysts for the Enantioselective N−H Insertion ..... 38

**V. Conclusions** ..... **39**

**VI. Experimental Procedure and Characterization** ..... **39**
VIa. General Information ..... 39
VIb. General Procedure ..... 41
Vlc. Characterization Data ..... 47
VId. X-ray Crystallography Data ..... 99

**VII. References** ..... **109**

*Chapter Two: Mechanistic Insights into the Aminoamide Silanol Ligand in the Copper-catalyzed Enantioselective N−H Insertion Reaction* ..... *115*

**I. Introduction** ..... **115**

**II. Modularity of Aminoamide-silanol Ligands** ..... **116**

**III. Discussion of Pd-free Hydrolysis During Ligand Synthesis** ..... **119**

**IV. Mechanistic Studies of the Metal-ligand Binding Mode ..... 122**
IVa. Silanol Ligand Analog Study ..... 122
IVb. Evaluation of Non-linear Behavior and M/L Ratio Experiments ..... 125
IVc. Investigation of the Silanol Ligand in Reactions with a Concerted Mechanism ..... 127
IVd. Silanols with Bulky [Cu] Catalyst ..... 128
IVe. Metal-ligand Binding Experiments using NMR and IR Spectroscopy ..... 129
IVf. Results of NMR Binding Experiments with Different Metal Salts ..... 131
IVg. Crystallization Experiments for the Understanding of Metal-ligand Binding Interactions 134
IVh. DFT Calculations on the Metal-ligand Binding Modes ..... 135
IVi. Proposed chiral induction model for the N−H insertions ..... 137
IVj. Proposed Mechanism of the Formation of Active Metal Complex ..... 139

**V. Conclusions ..... 140**

**VI. Experimental Procedure and Characterization ..... 140**
VIa. General Information ..... 140
VIb. General Procedure ..... 141
VIc. Characterization Data ..... 143
VId. X-ray Crystallography Data ..... 157

**VII. References ..... 160**

***Chapter Three: NMR Quantification of Halogen-Bonding Donor Ability to Evaluate Catalyst Activity ..... 162***

**I. Introduction ..... 162**
Ia. Halogen-bonding ..... 163
Ib. X-bonding in Organocatalysis ..... 164
Ic. Quantification Methods of X-bonding ..... 165
Id. Quantification of Lewis Acidity Using $^{31}$P NMR Spectroscopy ..... 166

**II. Method Validation ..... 167**
IIa. Titration Experiments ..... 167
IIb. Job Plots ..... 168
IIc. Changing the Halogen-donating Atom on Substrates ..... 169
IId. Hammett Plot ..... 170
IIe. Effect on Impurities on $\Delta\delta(^{31}P)$ Values ..... 170

**III. Results and discussion ..... 173**
IIIa. Low $\Delta\delta(^{31}P)$ Values of Neutral XBDs ..... 174
IIIb. Structure Effect: Benzimidazolium- *vs* Imidazolium-based XBD ..... 175
IIIc. Counteranion Effect ..... 176
IIId. Denticity Effect: Bis(imidazolium)-based XBDs ..... 177
IIIe. Correlation of $\Delta\delta(^{31}P)$ and $\Delta G^{\ddagger}$ values ..... 178
IIIf. Kinetic Analysis of Catalytic Activity in Friedel−Crafts Indole Additions ..... 179
IIIg. Correlation of $\Delta\delta(^{31}P)$ and Catalytic Activity ..... 183

**IV. Conclusions ..... 185**

**V. Experimental procedure and characterization ..... 185**
Va. General Information ..... 185
Vb. Experimental Procedures ..... 186
Vc. $^{31}$P NMR Spectroscopy Titration Data and Determination of Association Constants ..... 201
Vd. Job Plot Analysis of XBD Binding with TEPO ..... 205
Ve. Kinetic Analysis of Indole Addition to *trans*-Crotonophenone ..... 207
Vf. Kinetic Data for Indole Addition to *trans*-Crotonophenone Reaction Catalyzed by XBDs .208

**VI. References ..... 233**

*Chapter Four: Evaluation of NMR Quantification for H-bonding Ability of Photoacids* ..... *237*

**I. Introduction** ..... **237**
Ia. Photoacids ..... 237
Ib. Photoacids in Catalysis ..... 238

**II. Results and Discussion** ..... **240**
IIa. Concentration Tests ..... 240
IIb. Synthesis of Merocyanine-type Photoacids (MEH) ..... 241
IIc. Solvent Screen ..... 242
IId. Assessment of the HBD−TEPO Binding Equilibrium in $d^6$-Acetone ..... 243
IIe. Benchtop Irradiation of MEH ..... 244
IIf. Preliminary $^{31}P$ NMR Quantification Experiments of MEH ..... 246
IIg. Evaluation of n-Butyl MEH for $^{31}P$ NMR Quantification ..... 247

**III. Conclusions and Future Work** ..... **249**

**IV. Experimental Procedure** ..... **250**

**V. References** ..... **251**

*Appendix A: Photoredox Catalysis for the Synthesis of Functionalized Polyhedral Oligomeric Silsesquioxanes* ..... *253*

**I. Introduction** ..... **253**

**II. Method Development** ..... **256**
IIa. Solvent Screen ..... 257
IIc. Additive Screen ..... 258
IId. Base Screen ..... 259
IIe. Catalyst Loading Screen ..... 263

**III. Substrate Scope** ..... **263**

**IV. Conclusions** ..... **268**

**V. Experimental Procedure and Characterization** ..... **268**
Va. General Information ..... 268
Vb. General Procedure ..... 268
Vc. Characterization Data ..... 269

**VI. References** ..... **277**

*Appendix B: Copies of Spectra* ..... *278*

# Acknowledgements

My deepest gratitude goes to my parents. Though I have often walked a path different from what you might have expected, you never pushed me toward your expectations. Instead, you allowed me to explore my passions and find my way. Your unwavering support, regardless of my choices, gave me the courage to chase my dreams without fear, knowing I could always come back home. Dad, your reminder of Grandma's saying, "Slow is fast," has become a guiding principle in my scientific journey. Mom, thank you for filling my summers with science camps—even butterfly camps—which sparked my love for science.

To my sister, thank you for those childhood fights—they shaped who I am today. Thank you for always bringing me the foods I miss most when I return home. To my brother-in-law and nieces, thank you for the joy you bring into my life. I appreciate all of you for overcoming the challenges of bringing two toddlers to the US for my graduation. Sharing that special moment with you all meant the world to me. A heartfelt thanks to my Aunt and Uncle: Your home is always my first and last stop when I return to Taiwan, and your meals always make me feel right at home.

To my best friend, Wan-Fang: Thank you for always illuminating my path. You have been the one to push me toward my dreams and encourage me to pursue them fearlessly. I couldn't have completed all the journey without your love and support. Thank you to Papa Chou and Mama Chou for treating me like one of your own and for all your kindness and support.

To my high school friends, the So-Called Circle Island Group: Thank you for all the laughter, tears, and craziness we have shared over the years. Distance has never affected our friendship—after all, the US feels closer to Kaohsiung than Hualien! Thank you for keeping your five-year promise to come to the US for my graduation ceremony.

Amanda, thank you for being an amazing housemate for five years. I will always treasure our time together and the memories we made in APT248. Your dedication and passion for cardiology have been a constant inspiration, reminding me to stay committed to what I love.

Alice and Chris, thank you for always accommodating us in SoCal. Those trips were the perfect way to recharge both mentally and physically. Your perspectives on handling life's challenges always inspire me.

To my Master: Thank you for always being there for me and helping me keep my faith through difficult times. Your words, "Everything happens for the best," have been a guiding reminder to embrace both the highs and lows.

To Jack: I am grateful for the fate of always having our labs next to each other, both in Taiwan and the US. We helped each other to stay on top of things and handle them at the right time. You are one of the most brilliant chemists I have known, and I feel fortunate to have had your support throughout grad school.To Bao, Herra, and Hervin: I could not imagine going through grad school without your friendship and support. I have cherished our meals together and conversations—they were a much-needed break from the grind.

I want to thank both past and present members of the Franz group. Thank you for tackling challenging topics, embracing the negative results, and celebrating successes together.

Ady: I cannot imagine finishing grad school without you. Thank you for the constructive venting sessions in the office and all your support. I have learned many valuable skills from you, especially soft skills. You have always been there to offer the right words when I needed them. You are a true fighter and a great mentor, and I am excited to see all the success that lies ahead for you. Ravi: I have missed sharing an office with you and the excitement (and nerves) of fighting for concert tickets. Thank you for those Accountability Fridays motivating me to dive into dissertation writing. Hannah: I enjoyed the short period we worked next to each other in the lab and office, but that life was too short. Your attentiveness and intelligence will take you far, and I believe in you. 'Cause you are a real tough kid! Kevin: I will forever be grateful for the NH insertion suggestion you made—it was a game-changer. The passion and enthusiasm you bring to chemistry have always been inspiring. Jacob: It was an honor to share the fume hood with you and witness your impressive skills in stereogenic silicon chemistry. Linnea, the sunshine: thank you for your motivation and support during grad school. I am grateful for

you always standing by for me. Leah: Your dedication to teaching and to your project as well as the kindness and respect you show to others, has inspired me. Your future students will be incredibly lucky to have you. David: Thank you for always working your magic to bring our HPLC back to life. Your expertise has saved the day more times than I can count. Andrew: I had a great time working on the POSS project with you. Your insights and collaborative spirit made the process enjoyable and productive. Wendy: Please don't leak that embarrassing photo of me! It was wonderful getting to know you better during my last summer here. Don't forget to take time off when you need it! Catherine: Thank you for allowing me to learn and reflect on my role as a mentor. Your meticulous nature and respectfulness will serve you well in your future endeavors. Thank you, Jake and Teresa, for being incredible X-team members and for working together to push the project forward. I also want to thank the Shaw lab members—Jack, Garrett, Linda, Rose, Andy, and Dylan—for the fun conversations in the break room and the Thursday happy hours.

I am grateful for the feedback and guidance from my dissertation committee, Professor David Olson and Professor Mark Mascal. I want to thank Professor Peng Liu and Turki Alturaifi for their collaboration on the DFT studies of silanol ligands. My thanks go to Dr. Derrick Kaseman and Dr. Ping Yu for their collaboration on LED NMR and for providing training in advanced NMR techniques. I appreciate Dr. Jim Fettinger for his assistance with X-ray analysis and for the valuable discussions.

To my advisor and mentor, Annaliese Franz: Thank you for your support, both in research and life. Your optimism has been a source of inspiration, and I have learned to approach challenges with a more positive outlook, turning setbacks into great learning opportunities—not just in research, but in all aspects of life. Thank you for trusting me and giving me the freedom to explore my ideas in lab. I appreciate for all the training and guidance you have provided throughout the years.

Lastly, I want to thank myself—and my lab shoes with holes—for being resilient through the challenges, embracing the ups and downs, and staying committed to this journey. This accomplishment reflects my determination and passion; I am proud of how far I have come.

# Abstract

Catalysis plays a crucial role in modern organic synthesis and has significant applications in drug discovery. This dissertation explores advanced catalytic strategies in organic chemical synthesis, with a focus on novel ligand discovery featuring a silanol coordinating group for transition-metal-catalyzed asymmetric reactions. The introduction chapter provides an overview of transition-metal catalysis, asymmetric catalysis, and organophotoredox catalysis, along with a discussion of selected examples demonstrating their applications in drug discovery.

Chapter One details the discovery and synthesis of novel chiral silanol ligands for asymmetric catalysis. In the process of designing a new chelating silanol ligand, a new aminoamide silanol ligand was discovered that enables a Cu-catalyzed enantioselective N−H insertion, yielding enantioenriched amino acid derivatives with up to 98:2 enantiomeric ratio and 88% yield. Control experiments validate the crucial role of silanol in both catalytic activity and selectivity. This research represents the first example of a transition metal-catalyzed enantioselective reaction facilitated by chiral silanol-containing ligands. Additionally, the chapter explores alternative synthetic routes and discusses efforts to address challenges related to the synthesis of certain ligand analogs.

Chapter Two extends the investigation of the novel chiral silanol ligand into mechanistic studies, proposing a metal-ligand binding mode based on experimental and computational studies. The exploration involves the design and synthesis of silanol ligand analogs to gain insights into the roles of amide, amino, and silanol components on the ligand in catalysis. The chapter presented further investigations into the silanol coordination mode, including DFT calculations, ligand analog studies, NMR, and X-ray structure analyses, to support the formation of an H-bond stabilized silanol-chelating copper carbenoid complex. Additionally, DFT calculations revealed a π-π stacking interaction proposed to enable selectivity for aryl diazoacetate substrates, overcoming traditional limitations associated with these substrates.

Chapter Three introduces a quantification method for evaluating the catalytic ability of halogen-bonding catalysts, utilizing $^{31}$P NMR spectroscopy and a commercially available molecular probe, TEPO. The method has proved to be a sensitive indicator for analyzing residual acidic impurities,

and fellow researchers in the field have applied it to verify the X-bonding ability and purity of their newly designed catalysts.

Chapter Four presents efforts to quantify the H-bonding capabilities of photoacids, aiming to broaden the applications of the $^{31}P$ NMR quantification method detailed in Chapter Three. The assessment includes the exploration of in-situ LED-NMR spectroscopy, the identification of the optimal solvent for the quantification method, and the synthesis of photoacids with prolonged relaxation times.

Appendix A presents parallel collaborative work to develop the first photocatalysis methodology for functionalizing polyhedral oligomeric silsesquioxanes (POSS), forming a new C−C bond with up to 88% yield. The chapter discusses the evolution from initial exploration in transition-metal catalysis to a new direction with organophotoredox catalysis using POSS, highlighting the versatility and potential of this emerging catalytic strategy.

# List of Symbols and Abbreviations

| | |
|---|---|
| Å | Angstrom |
| CSP | Chiral stationary phase |
| d | Days |
| DCE | Dichloroethane |
| DCM | Dichloromethane |
| DMF | *N,N*-Dimethylformamide |
| DMSO | Dimethylsulfoxide |
| dr | Diastereomeric ratio |
| ee | Enantiomeric excess |
| eq | Equation |
| equiv | Equivalents |
| er | Enantiomeric ratio |
| ESI-MS | Electrospray ionization-mass spectrometry |
| EtOAc | Ethyl acetate |
| EWG | Electron-withdrawing group |
| g | Grams |
| h | Hours |
| HPLC | High Pressure Liquid Chromatography |
| HRMS | High Resolution Mass Spectrometry |
| IR | Infrared radiation |
| $K_a$ | Association constant |
| $k_{obs}$ | Observed rate constant |
| L | Ligands |
| LED | Light-emitting diode |
| Ln | Natural logarithm |

| | |
|---|---|
| M | Molar |
| m/z | Mass to charge ratio |
| mg | Milligrams |
| MHz | Megahertz |
| min | Minutes |
| mL | Milliliter |
| mm | Millimeter |
| mM | Millimolar |
| mmol | Millimole |
| mol | Mole |
| MS | Molecular sieves |
| MW | Molecular weight |
| NMR | Nuclear magnetic resonance |
| PA | Photoacids |
| PC | Photocatalysts |
| POSS | Polyhedral oligomeric silsesquioxane |
| ppm | Parts per million |
| rt | Room temperature |
| Temp | Temperature |
| TLC | Thin layer chromatography |
| Δ | Changes in the indicated quantity |
| δ | Chemical shift |

# Introduction

This introduction chapter presents the significance of catalysis in organic chemical synthesis, which is particularly relevant to the research in this dissertation. This discussion encompasses transition metal catalysis, asymmetric catalysis, and organophotoredox catalysis. With a specific focus on the application of catalysis in drug discovery, this chapter also provides examples showcasing their relevance in the pharmaceutical industry.

## I. Organic Synthesis and Catalysis in Drug Discovery

Organic synthesis presents opportunities for advancing drug discovery, playing a pivotal role throughout the drug development process—from the discovery and optimization of lead molecules to their transformation into pharmaceuticlas.[1–3] However, organic synthesis also emerges as a substantial bottleneck in drug discovery, with one common challenge being the presence of unprotected polar groups, such as amines and N-heterocycles (Figure 0.1).[1] This poses a substantial hurdle in the synthesis and purification processes. To address this challenge, researchers design and develop innovative synthetic strategies capable of accommodating these functionalities. Consequently, the focus of organic chemists revolves around developing practical methods for synthesizing organic molecules. This includes enhancing reaction efficiency by reducing the number of steps and optimizing yields, or adopting more sustainable approaches such as catalysis, green solvents and reagents, and reduced energy usage, thereby making synthetic routes more appealing.[3–5]

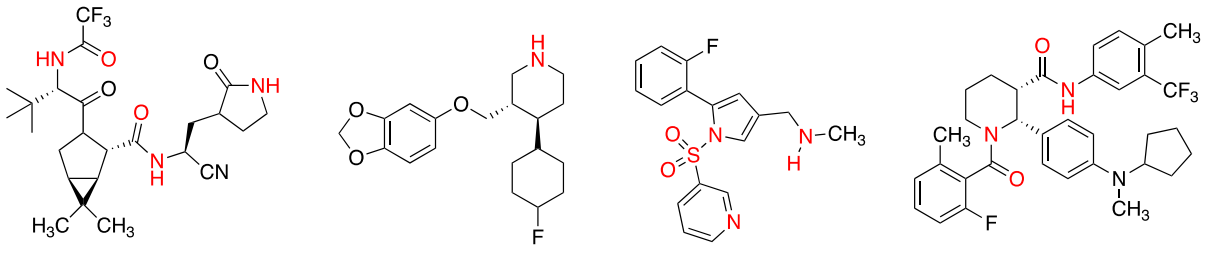
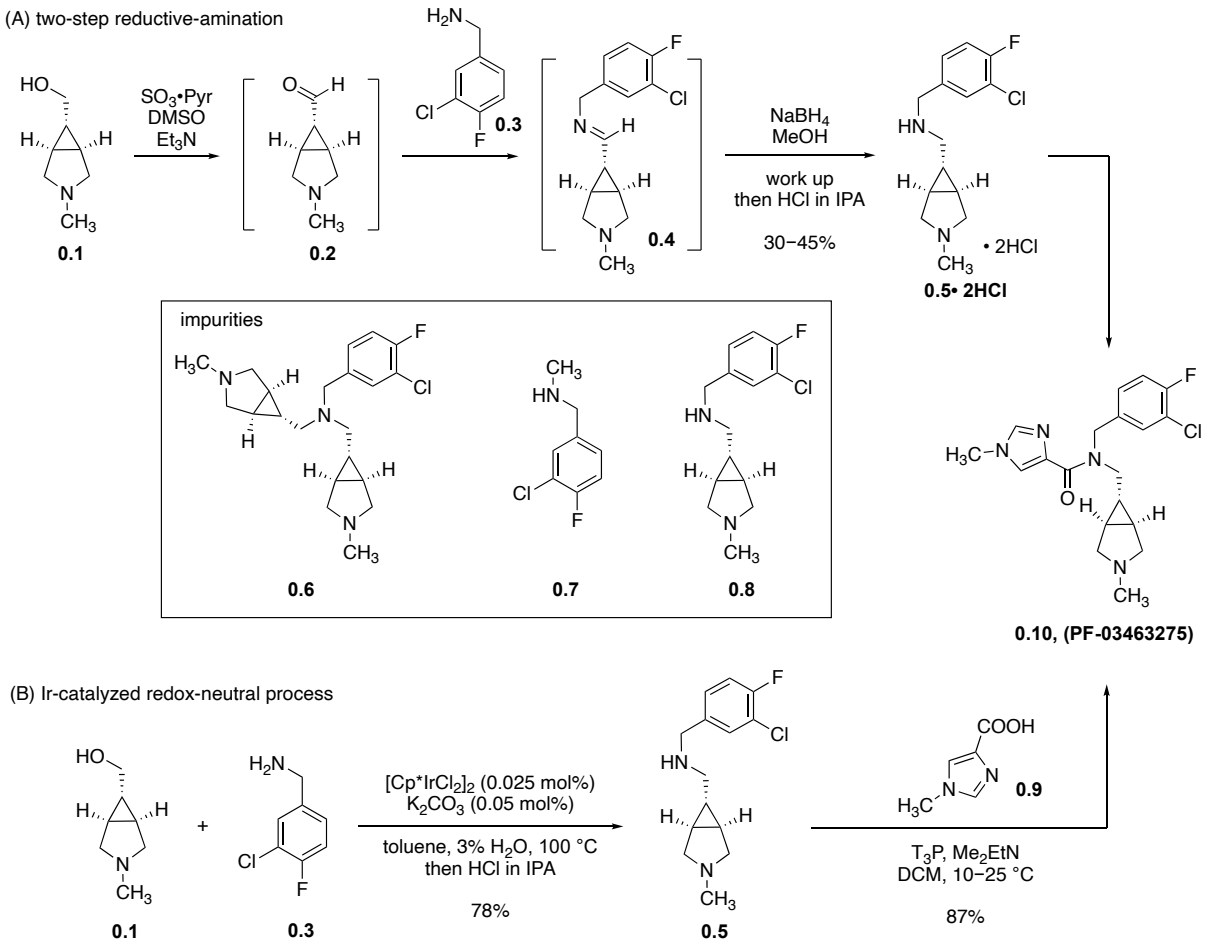



**Figure 0.1.** Examples of drug molecules incorporating amines, N-heterocycles, and other exposed polar groups.

## Ia. Transition Metal Catalysis

Transition metals catalysis plays a crucial role in modern chemistry,[5–9] enabling key bond formations for the construction of C−C and C−X bonds through powerful cross-coupling methodologies. This catalytic approach has widespread applications in the chemical community, particularly in the pharmaceutical industry.[6,7,9] The utilization of transition metal catalysis facilitates synthetic disconnections that would otherwise be challenging or even impossible. The use of transition metal catalysis often leads to shorter, more efficient, and ideally more sustainable syntheses of drug candidates and pharmaceutical products.

For example, Pfizer employed an Ir-catalyzed hydrogen-borrowing coupling in the kilo-scale synthesis of the GlyT1 inhibitor, PF-03463275 (**0.10**), in place of the tradition reductive amination route, which had issues with the lengthy workup process and low yields (Scheme 0.2).[10] The initial route for the synthesis of the key intermediate **0.5** was a two-step oxidation/reductive amination reaction, starting with Swern oxidation to form aldehyde **0.2**, followed by reductive amination (Scheme 0.2A). However, this approach led to the formation of impurities and side-products, including the bis-alkylation product **0.6**, *N*-methylated amine **0.7** and reduction product **0.8**. The latter two impurities were generated from the reduction of the methyleneiminium species **0.4** derived from the Swern oxidation. The overall yield of **0.5•2HCl** in the two-step synthesis was 30−45%. Consequently, an alternative process was developed: an Ir-catalyzed redox-neutral process adapted from Fujita and Yamaguchi's method (Scheme 0.2B).[11] The Pfizer team successfully increased the step-economy and avoided the generation of stoichiometric byproducts by employing the Ir-catalyzed process. Lastly, PF-03463275 was synthesized through the amide coupling of amine **0.5** and imidazole carboxylic acid **0.9** using a propanephosphonic acid anhydride ($T_3P$)-mediated process. This example showcases the ability of transition metal catalysis in simplifying synthetic processes, reducing the number of synthetic steps, and improving overall sustainability.

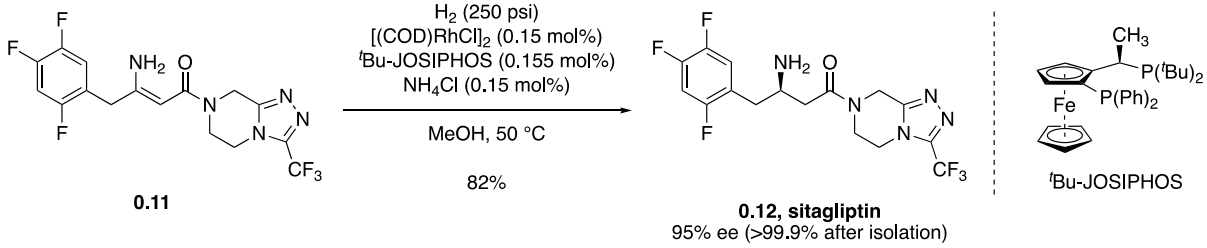



**Scheme 0.1.** The synthesis of PF-03463275 precursor **0.5** through (A) a two-step reductive-amination and (B) an Ir-catalyzed process.[10]

## Ib. Asymmetric Catalysis

Asymmetric catalysis is widely considered the most efficient method to prepare enantioenriched compounds.[4,12–14] The quest for increased environmental sustainability has driven the advancement of asymmetric synthesis. In asymmetric synthesis, catalysis stands out as a particularly advantageous strategy, as only a fractional amount of chiral material is needed to induce enantioenrichment in a significantly larger quantity of material in the final product. In transition metal-catalyzed asymmetric reactions, chiral ligands are utilized to enhance reactivity and promote stereoselectivity. The distinctive feature of transition metals lies in their ability to control both reactivity and selectivity through the metal-ligand partnership. A common strategy involves using a multidentate chiral ligand complexed with a transition metal, leading to many successful reactions. As a result, considerable efforts have been dedicated to design and synthesize classes of ligands for various chemical transformations.[15,16]

Asymmetric synthesis enhances material efficiency and step economy by eliminating the need for an enantiomer separation step or the transformation of raw materials from chiral pools. Numerous active pharmaceutical ingredients (APIs) are chiral molecules, and industry commonly employs transition metal-catalyzed asymmetric reactions for their synthesis. For example, the Merck team utilized a Rh-catalyzed asymmetric hydrogenation of an unfunctionalized enamide **0.11** as a key step in the synthesis of sitagliptin (**0.12**, Scheme 0.2).[17] The strategy of using a well-designed ligand in asymmetric catalysis facilitated the formation of enantiopure product without requiring the installation and subsequent removal of a chiral activating group. Avoidance of additional steps streamlined the synthetic route and contributed to enhancing overall efficiency in the synthesis of sitagliptin (**0.12**).



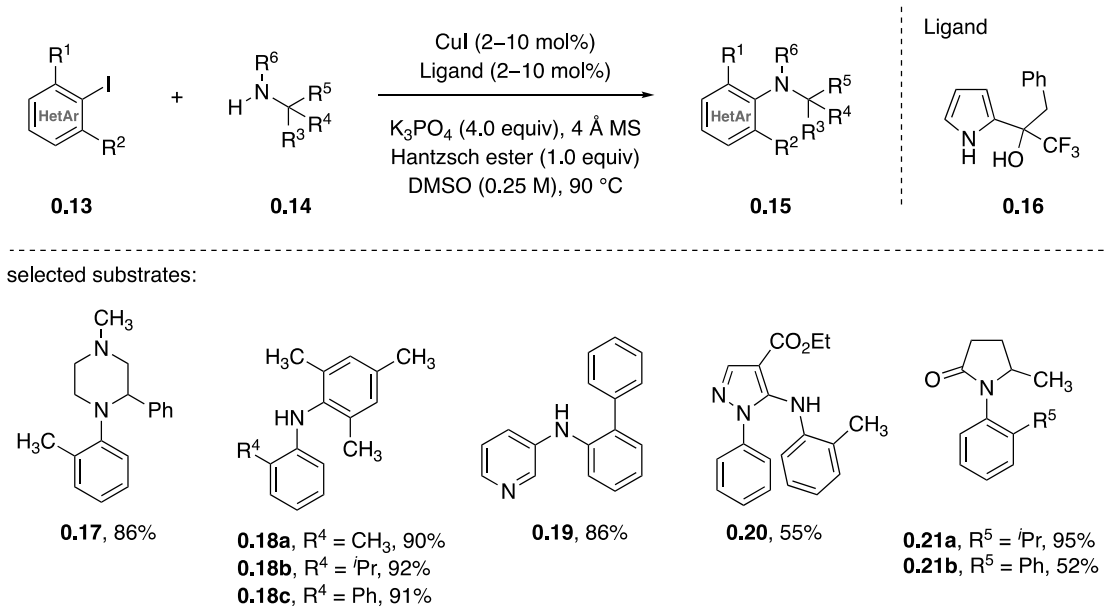

**Scheme 0.2.** A rhodium-catalyzed asymmetric hydrogenation of an unfunctionalized enamide.[17]

## Ic. Metal Choice and Importance of Ligand Design

The majority of transition metal-catalyzed transformations are used in routine organic synthesis involving second- and sometime third-row transition metals, particularly Pd catalysts for C−C[18] and C−N cross-coupling.[19] In addition, Rh and Ru are utilized in asymmetric hydrogenations.[20,21] The significant advantages of using precious metals as catalyst stem from their broad functional group tolerance, substrate scope, and well-studied mechanisms. These mechanisms typically involve predictable oxidation states and two-electrons redox processes. Moreover, the extensive development of chiral phosphine ligands contributes to these advantages. Many of the reaction systems exhibit high turnover numbers, allowing for very low catalyst loadings. However, a notable drawback of using precious metal catalysts is their inherent low earth-abundance, leading to higher environmental impact and cost.

There is particular interest in forming new C−N bonds through Cu-catalyzed reactions within the field of earth-abundant transition metal catalysis. This interest is driven by the frequent occurrence of these structural motifs in pharmaceuticals and agrochemicals. Ullmann-type cross-couplings are commonly employed for C−N bond formation. Nevertheless, Cu-catalyzed C−N coupling reactions with hindered partners remain a challenging problem, and thus, Buchwald−Hartwig amination using a Pd catalyst remains the most frequently used strategy.[22–25] The relatively limited development of ligands in Cu catalysis is one of the factors constraining the application of Cu-catalyzed C−N coupling. To overcome this limitation, an AbbVie team has recently introduced a novel ligand **0.16**, enabling the facilitation of challenging and previously unreported direct amination with sterically hindered coupling partners using Cu catalysis (Scheme 0.3).[22,26] The ligand facilitated the coupling of ortho- and ortho, ortho'-disubstituted aryl iodides **0.13** with sterically hindered amines, anilines, heterocycles, and amides.

Ligand design has proven essential for tuning the properties and performance of transition metal catalysts, allowing control over reaction feasibilities, selectivities, and efficiencies in various chemical processes. The discovery of the pyrrole-ol ligand **0.16** resulted from screening the AbbVie internal compound library, demonstrating the importance of compound library screening for ligand discovery in challenging transition metal-catalyzed reactions.




**Scheme 0.3.** Cu-catalyzed C−N coupling reactions with sterically hindered coupling partners.[22]

With the emergence of transition metal catalysis as a crucial method in organic synthesis, the need for effective impurity control becomes apparent. Transition metal-catalyzed reactions are frequently employed at the final stages of a synthetic route, introducing distinct challenges related to impurity control.[5,7] These challenges include the management of byproducts and elemental impurities to comply with regulatory and quality standards. Toxicology evaluation of metal impurities is complex, given its correlation with metabolism factors such as oxidation state, particle sizes, and coordination sphere, which influence the solubility and bioavailability of trace metals.[27,28] Despite this complexity, the overarching goal remains the removal of metal impurities as completely as possible. In response to the prevalence of Pd-catalyzed transformations, various methods have been developed to eliminate Pd from reactions, aiming to meet stringent limits for residual metal content in APIs. However, these methods often require the use of expensive scavengers or resins, thereby elevating process complexity and costs.

**Id. Organic Photoredox Catalysis**

Photochemistry has found extensive applications in organic synthesis.[29–34] The field has expanded rapidly in terms of photochemical transformations and reaction conditions, especially in the field of photoredox chemistry. The significant potential of photoredox catalysis in organic synthesis was initially explored through the development of Ru and Ir complexes, pioneered by the Yoon[35] group and the MacMillan[36] group (Figure 0.2A). However, the use of rare metals contributes to the high cost of the catalysts, restricting their use in large-scale organic synthesis. In response to this limitation, there has been a notable surge in the development and utilization of organic photoredox catalysts in recent years (Figure 0.2B).[33,34,37,38] This trend holds the promise of significantly enhancing the overall sustainability of synthetic approaches. The advancement of organic photoredox catalysis is not only attributed to the advantages of metal-free processes but also to its capability of achieving unique chemical reactivity under mild conditions.

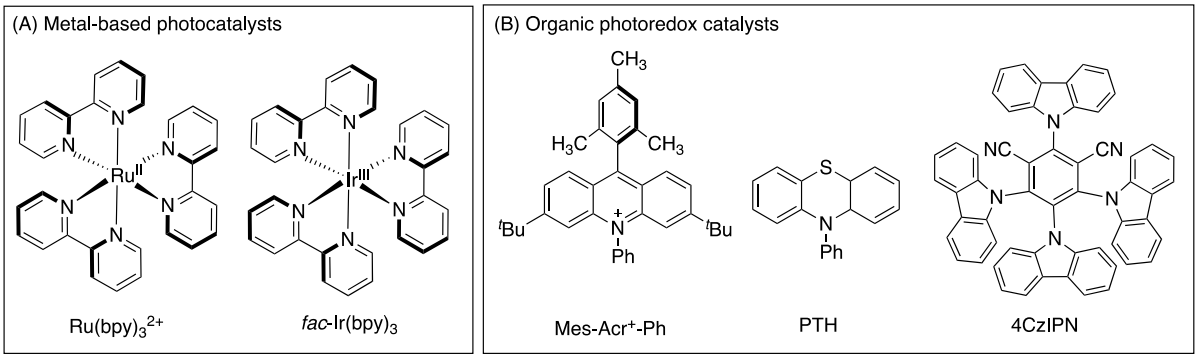
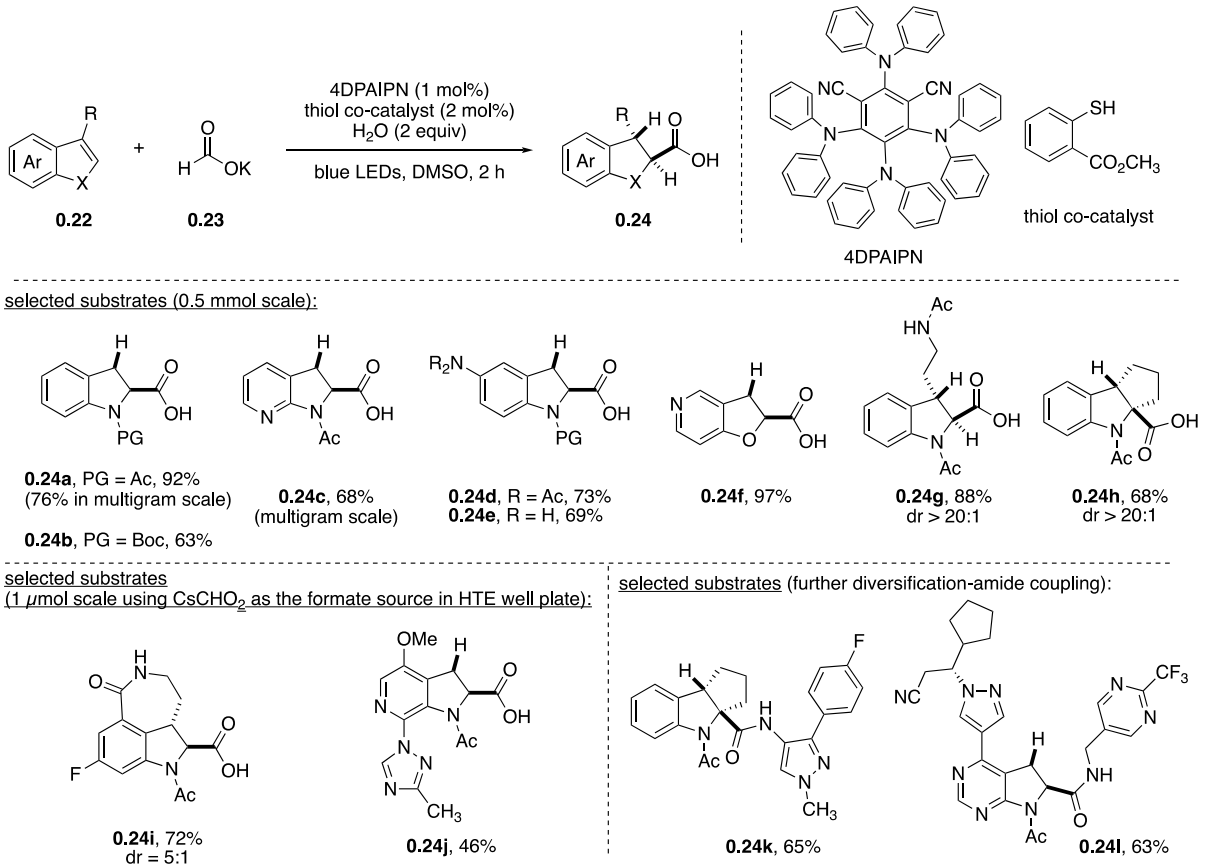



**Figure 0.2.** Selected examples of (A) Metal-based photocatalysts; (B) Organic photoredox catalysts.

A recent demonstration by Merck and the Wickens group showcased the utilization of employing organic photoredox catalysis in drug discovery.[39] They illustrated the application of organic photoredox catalysis in a dearomative hydrocarboxylation reaction, involving the coupling of heteroarenes (**0.22**) with formate (**0.23**) through a $CO_2^{\bullet-}$ intermediate (Scheme 0.4). This transformation exhibited high chemoselectivity and broad functional group tolerance (**0.24a**−**i**). Moreover, the methodology has the capability to yield hydrocarboxylation products **0.24a** and **0.24d** on a multigram scale, as well as more than 80 substrates in high-throughput experimentation (HTE). This methodology is applicable in late-stage functionalization without concern regarding metal residues.




**Scheme 0.4.** An example of dearomative hydrocarboxylation through organophotoredox catalysis and the selected substrates.

## II. General Overview of the Dissertation

My research is focused on the theme of catalysis, and it will be presented in three chapters and two appendixes in this dissertation. Chapter One will discuss the discovery and development of novel silanol ligands for asymmetric catalysis. The catalytic activity of these silanol ligands is showcased through a Cu-catalyzed N−H insertion, yielding enantioenriched unnatural amino acid derivatives. Chapter Two delves into mechanistic studies and the investigation of the contributions of the silanol ligands in catalysis, including proposing a metal-ligand binding mode. Chapter Three will discuss the development of a $^{31}$P NMR quantification method for the catalytic ability of halogen-bonding catalysts, an emerging class of organocatalysts. Appendix A explores the potential expansion of the $^{31}$P NMR quantification method to evaluate the H-bonding ability of photoacids. Lastly, Appendix B presents the pioneering functionalization of Polyhedral Oligomeric Silsesquioxanes (POSS) through organophotoredox catalysis.

## III. References


(1) Blakemore, D. C.; Castro, L.; Churcher, I.; Rees, D. C.; Thomas, A. W.; Wilson, D. M.; Wood, A. Organic Synthesis Provides Opportunities to Transform Drug Discovery. *Nat. Chem.* **2018**, *10* (4), 383–394. https://doi.org/10.1038/s41557-018-0021-z.

(2) *Organic synthesis toward small-molecule probes and drugs*. https://doi.org/10.1073/pnas.1103205108.

(3) Ilaria, M. Organic Synthesis Empowering Drug Discovery: Innovations and Applications in the Pharmaceutical Industry.

(4) Busacca, C. A.; Fandrick, D. R.; Song, J. J.; Senanayake, C. H. The Growing Impact of Catalysis in the Pharmaceutical Industry. *Adv. Synth. Catal.* **2011**, *353* (11–12), 1825–1864. https://doi.org/10.1002/adsc.201100488.

(5) Hayler, J. D.; Leahy, D. K.; Simmons, E. M. A Pharmaceutical Industry Perspective on Sustainable Metal Catalysis. *Organometallics* **2019**, *38* (1), 36–46. https://doi.org/10.1021/acs.organomet.8b00566.

(6) Johansson Seechurn, C. C. C.; Kitching, M. O.; Colacot, T. J.; Snieckus, V. Palladium-Catalyzed Cross-Coupling: A Historical Contextual Perspective to the 2010 Nobel Prize. *Angew. Chem. Int. Ed.* **2012**, *51* (21), 5062–5085. https://doi.org/10.1002/anie.201107017.

(7) Wu, H.; Qu, B.; Nguyen, T.; Lorenz, J. C.; Buono, F.; Haddad, N. Recent Advances in Non-Precious Metal Catalysis. *Org. Process Res. Dev.* **2022**, *26* (8), 2281–2310. https://doi.org/10.1021/acs.oprd.2c00124.

(8) Hartwig, J. F.; Shaughnessy, K. H.; Shekhar, S.; Green, R. A. Palladium-Catalyzed Amination of Aryl Halides. In *Organic Reactions*; Denmark, S. E., Ed.; Wiley, 2019; pp 853–958. https://doi.org/10.1002/0471264180.or100.14.

(9) Chirik, P. J.; Engle, K. M.; Simmons, E. M.; Wisniewski, S. R. Collaboration as a Key to Advance Capabilities for Earth-Abundant Metal Catalysis. *Org. Process Res. Dev.* **2023**, *27* (7), 1160–1184. https://doi.org/10.1021/acs.oprd.3c00025.

(10) Berliner, M. A.; Dubant, S. P. A.; Makowski, T.; Ng, K.; Sitter, B.; Wager, C.; Zhang, Y. Use of an Iridium-Catalyzed Redox-Neutral Alcohol-Amine Coupling on Kilogram Scale for the Synthesis of a GlyT1 Inhibitor. *Org. Process Res. Dev.* **2011**, *15* (5), 1052–1062. https://doi.org/10.1021/op200174k.

(11) Fujita, K.; Li, Z.; Ozeki, N.; Yamaguchi, R. N-Alkylation of Amines with Alcohols Catalyzed by a Cp*Ir Complex. *Tetrahedron Lett.* **2003**, *44* (13), 2687–2690. https://doi.org/10.1016/S0040-4039(03)00371-X.

(12) Noyori, R. Asymmetric Catalysis: Science and Opportunities (Nobel Lecture). *Angew. Chem. Int. Ed.* **2002**, *41* (12), 2008–2022. https://doi.org/10.1002/1521-3773(20020617)41:12<2008::AID-ANIE2008>3.0.CO;2-4.

(13) Fanourakis, A.; Docherty, P. J.; Chuentragool, P.; Phipps, R. J. Recent Developments in Enantioselective Transition Metal Catalysis Featuring Attractive Noncovalent Interactions between Ligand and Substrate. *ACS Catal.* **2020**, *10* (18), 10672–10714. https://doi.org/10.1021/acscatal.0c02957.

(14) MacMillan, D. W. C. The Advent and Development of Organocatalysis. *Nature* **2008**, *455* (7211), 304–308. https://doi.org/10.1038/nature07367.

(15) Connon, R.; Roche, B.; Rokade, B. V.; Guiry, P. J. Further Developments and Applications of Oxazoline-Containing Ligands in Asymmetric Catalysis. *Chem. Rev.* **2021**, *121* (11), 6373–6521. https://doi.org/10.1021/acs.chemrev.0c00844.

(16) Yoon, T. P.; Jacobsen, E. N. Privileged Chiral Catalysts. *Science* **2003**, *299* (5613), 1691–1693. https://doi.org/10.1126/science.1083622.

(17) Hansen, K. B.; Hsiao, Y.; Xu, F.; Rivera, N.; Clausen, A.; Kubryk, M.; Krska, S.; Rosner, T.; Simmons, B.; Balsells, J.; Ikemoto, N.; Sun, Y.; Spindler, F.; Malan, C.; Grabowski, E. J. J.; Armstrong, J. D. III. Highly Efficient Asymmetric Synthesis of Sitagliptin. *J. Am. Chem. Soc.* **2009**, *131* (25), 8798–8804. https://doi.org/10.1021/ja902462q.

(18) Pagett, A. B.; Lloyd-Jones, G. C. Suzuki–Miyaura Cross-Coupling. In *Organic Reactions*; John Wiley & Sons, Ltd, 2019; pp 547–620. https://doi.org/10.1002/0471264180.or100.09.

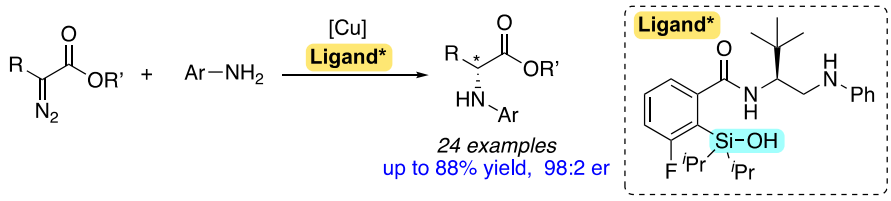
(19) Hartwig, J. F.; Shaughnessy, K. H.; Shekhar, S.; Green, R. A. Palladium-Catalyzed Amination of Aryl Halides. In *Organic Reactions*; John Wiley & Sons, Ltd, 2019; pp 853–958. https://doi.org/10.1002/0471264180.or100.14.
(20) Etayo, P.; Vidal-Ferran, A. Rhodium-Catalysed Asymmetric Hydrogenation as a Valuable Synthetic Tool for the Preparation of Chiral Drugs. *Chem. Soc. Rev.* **2013**, *42* (2), 728–754. https://doi.org/10.1039/C2CS35410A.
(21) Genet, J.-P. Asymmetric Catalytic Hydrogenation. Design of New Ru Catalysts and Chiral Ligands: From Laboratory to Industrial Applications. *Acc. Chem. Res.* **2003**, *36* (12), 908–918. https://doi.org/10.1021/ar020152u.
(22) Modak, A.; Nett, A. J.; Swift, E. C.; Haibach, M. C.; Chan, V. S.; Franczyk, T. S.; Shekhar, S.; Cook, S. P. Cu-Catalyzed C–N Coupling with Sterically Hindered Partners. *ACS Catal.* **2020**, *10* (18), 10495–10499. https://doi.org/10.1021/acscatal.0c02965.
(23) Kwong, F. Y.; Buchwald, S. L. Mild and Efficient Copper-Catalyzed Amination of Aryl Bromides with Primary Alkylamines. *Org. Lett.* **2003**, *5* (6), 793–796. https://doi.org/10.1021/ol0273396.
(24) Kim, S.-T.; Strauss, M. J.; Cabré, A.; Buchwald, S. L. Room-Temperature Cu-Catalyzed Amination of Aryl Bromides Enabled by DFT-Guided Ligand Design. *J. Am. Chem. Soc.* **2023**, jacs.3c00500. https://doi.org/10.1021/jacs.3c00500.
(25) Yang, Q.; Zhao, Y.; Ma, D. Cu-Mediated Ullmann-Type Cross-Coupling and Industrial Applications in Route Design, Process Development, and Scale-up of Pharmaceutical and Agrochemical Processes. *Org. Process Res. Dev.* **2022**, *26* (6), 1690–1750. https://doi.org/10.1021/acs.oprd.2c00050.
(26) de Gombert, A.; Darù, A.; Ahmed, T. S.; Haibach, M. C.; Li-Matsuura, R.; Yang, C.; Henry, R. F.; Cook, S. P.; Shekhar, S.; Blackmond, D. G. Mechanistic Insight into Cu-Catalyzed C–N Coupling of Hindered Aryl Iodides and Anilines Using a Pyrrol-Ol Ligand Enables Development of Mild and Homogeneous Reaction Conditions. *ACS Catal.* **2023**, 2904–2915. https://doi.org/10.1021/acscatal.2c06201.
(27) Egorova, K. S.; Ananikov, V. P. Toxicity of Metal Compounds: Knowledge and Myths. *Organometallics* **2017**, *36* (21), 4071–4090. https://doi.org/10.1021/acs.organomet.7b00605.
(28) Egorova, K. S.; Ananikov, V. P. Which Metals Are Green for Catalysis? Comparison of the Toxicities of Ni, Cu, Fe, Pd, Pt, Rh, and Au Salts. *Angew. Chem. Int. Ed.* **2016**, *55* (40), 12150–12162. https://doi.org/10.1002/anie.201603777.
(29) Romero, N. A.; Nicewicz, D. A. Organic Photoredox Catalysis. *Chem. Rev.* **2016**, *116* (17), 10075–10166. https://doi.org/10.1021/acs.chemrev.6b00057.
(30) Ravelli, D.; Fagnoni, M.; Albini, A. Photoorganocatalysis. What For? *Chem Soc Rev* **2013**, *42* (1), 97–113. https://doi.org/10.1039/C2CS35250H.
(31) Marzo, L.; Pagire, S. K.; Reiser, O.; König, B. Visible-Light Photocatalysis: Does It Make a Difference in Organic Synthesis? *Angew. Chem. Int. Ed.* **2018**, *57* (32), 10034–10072. https://doi.org/10.1002/anie.201709766.
(32) Speckmeier, E.; Fischer, T. G.; Zeitler, K. A Toolbox Approach To Construct Broadly Applicable Metal-Free Catalysts for Photoredox Chemistry: Deliberate Tuning of Redox Potentials and Importance of Halogens in Donor–Acceptor Cyanoarenes. *J. Am. Chem. Soc.* **2018**, *140* (45), 15353–15365. https://doi.org/10.1021/jacs.8b08933.
(33) Bortolato, T.; Cuadros, S.; Simionato, G.; Dell'Amico, L. The Advent and Development of Organophotoredox Catalysis. *Chem. Commun.* **2022**, *58* (9), 1263–1283. https://doi.org/10.1039/D1CC05850A.
(34) Joshi-Pangu, A.; Lévesque, F.; Roth, H. G.; Oliver, S. F.; Campeau, L.-C.; Nicewicz, D.; DiRocco, D. A. Acridinium-Based Photocatalysts: A Sustainable Option in Photoredox Catalysis. *J. Org. Chem.* **2016**, *81* (16), 7244–7249. https://doi.org/10.1021/acs.joc.6b01240.
(35) Ischay, M. A.; Anzovino, M. E.; Du, J.; Yoon, T. P. Efficient Visible Light Photocatalysis of [2+2] Enone Cycloadditions. *J. Am. Chem. Soc.* **2008**, *130* (39), 12886–12887. https://doi.org/10.1021/ja805387f.
(36) *Merging Photoredox Catalysis with Organocatalysis: The Direct Asymmetric Alkylation of Aldehydes*. https://doi.org/10.1126/science.1161976.
(37) Romero, N. A.; Nicewicz, D. A. Organic Photoredox Catalysis. *Chem. Rev.* **2016**, *116* (17), 10075–10166. https://doi.org/10.1021/acs.chemrev.6b00057.

(38) Bogdos, M. K.; Pinard, E.; Murphy, J. A. Applications of Organocatalysed Visible-Light Photoredox Reactions for Medicinal Chemistry. *Beilstein J. Org. Chem.* **2018**, *14*, 2035–2064. https://doi.org/10.3762/bjoc.14.179.
(39) Mikhael, M.; Alektiar, S. N.; Yeung, C. S.; Wickens, Z. K. Translating Planar Heterocycles into Three-Dimensional Analogs by Photoinduced Hydrocarboxylation. *Angew. Chem. Int. Ed.* **2023**, *62* (30), e202303264. https://doi.org/10.1002/anie.202303264.

# Chapter One: Chiral Silanol Ligands for Copper-catalyzed Enantioselective N−H Insertion Reactions*

## I. Introduction and Background

This chapter presents the synthesis and evaluation of novel chiral metal-chelating ligands featuring a silanol coordinating group and a chiral aminoamide scaffold. The chapter showcases the ligand development and catalytic properties of these silanol ligands by a Cu-catalyzed enantioselective N−H insertion, affording enantioenriched unnatural amino acid derivatives in high selectivity (Scheme 1.1). Notably, this work represents the first example of enantioselective transition metal catalysis using chiral silanol-containing ligands. The ligand highlights the effectiveness of silanols as coordinating groups in transition metal catalysis.

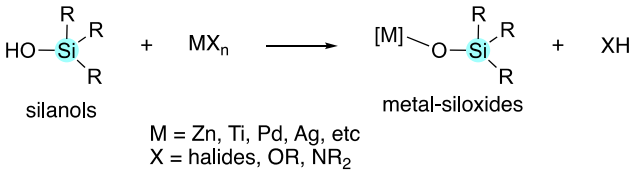



**Scheme 1.1.** Project overview.

### Ia. Silanols and Siloxides

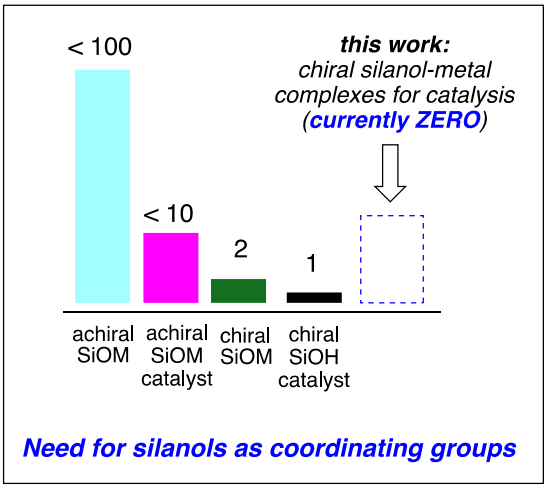
Silanol compounds contain a unique Si−OH group, providing an opportunity to design ligands with new coordination sites. These silanol ligands exhibit both σ- and π-donating capabilities.[1,2] In comparison to their carbon counterparts, silanol ligands bind with greater ionic character, owing to the electropositive nature of silicon versus carbon.[3,4] Silanols, silanediols, and other silanol-containing species are recognized for their capability to generate metal siloxides when exposed to various main groups and transition metals (Equation 1.1).[2,5,6]

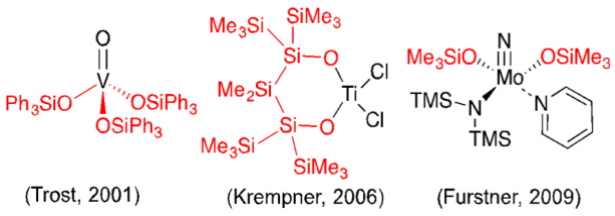
*Reproduced in part with permission from Chang, Y.-P.; Blanco-Herrero, K.; Alturaifi, T. M.; Fettinger, J. C.; Liu, P.; Franz, A. K. "Multifunctional Chiral Silanol Ligands for Enantioselective Catalysis." *Angew. Chem. Int. Ed. (manuscript under revision)*



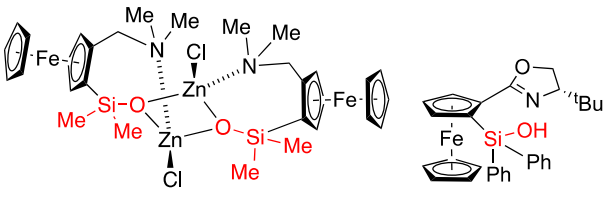

**Equation 1.1.** Formation of metal-siloxides.

Metal complexes with achiral siloxy ligands have been synthesized and examined with 23 transition metals (Figure 1.1). However, the examples are limited to simple achiral siloxy groups, such as $OSiAr_3$ or $OSiMe_3$.[7,8] While there are no examples of chiral silanol ligands used in enantioselective catalysis, there is precedent for the catalytic activity of achiral metal-siloxide complexes in organic transformations.[1,2] Despite the incorporation of silyl groups into the backbone of ligand scaffolds,[9–14] enantioenriched metal-siloxide complexes remain significantly underexplored. Strohmann and coworkers reported the only class of enantiomerically pure metal-siloxides with chiral amine-containing, ferrocene-based chiral zinc(II)-silanoates,[15,16] although no catalytic activity was documented. The only reported example using a chiral silanol ligand for asymmetric induction is a ferrocene-based organosilanol in a zinc-mediated asymmetric phenyl transfer.[17]




Examples of ***achiral*** metal-siloxide complexes used in catalysis
(demonstrated for 23 transition metals)




Two examples of ***chiral*** metal-siloxide reported (no catalytic activity reported)

One example of a ***chiral*** silanol used for $Ph_2Zn$ transfer reaction

**Figure 1.1.** Examples of previously reported metal-siloxide complexes for structural and catalytic studies.

The silanol (Si−OH) group provides an opportunity to design ligands with new coordination modes for enhanced activity and stereoselectivity in asymmetric catalysis. Studies have shown that metal siloxides exhibit more Lewis acidic character than metal alkoxides due to backbonding interactions ($O_{lp}\rightarrow\sigma^*_{Si-C}$).[18,19] Furthermore, the elongated Si−O bonds could improve steric modulation and selectivity (Figure 1.2A). Fürstner proposed that the donating capacity of metal siloxides, which is dependent on the Si−O−M angle, plays a crucial role in balancing reactivity within catalytic cycles.[20,21] At an Si−O−M angle closer to 180˚, oxygen exhibits maximum electron donation into the vacant metal d-orbitals. This occurs because both orthogonal electron pairs on the oxygen can engage in bonding to the metal, resulting in a shorter M−O bond and a reduction in the Lewis acidity of the metal center. However, when the Si−O−M angle deviates further from 180°, only one of the oxygen lone pairs effectively overlaps, leading to longer M−O bonds and an increased Lewis acidic character at the metal center (Figure 1.2B).

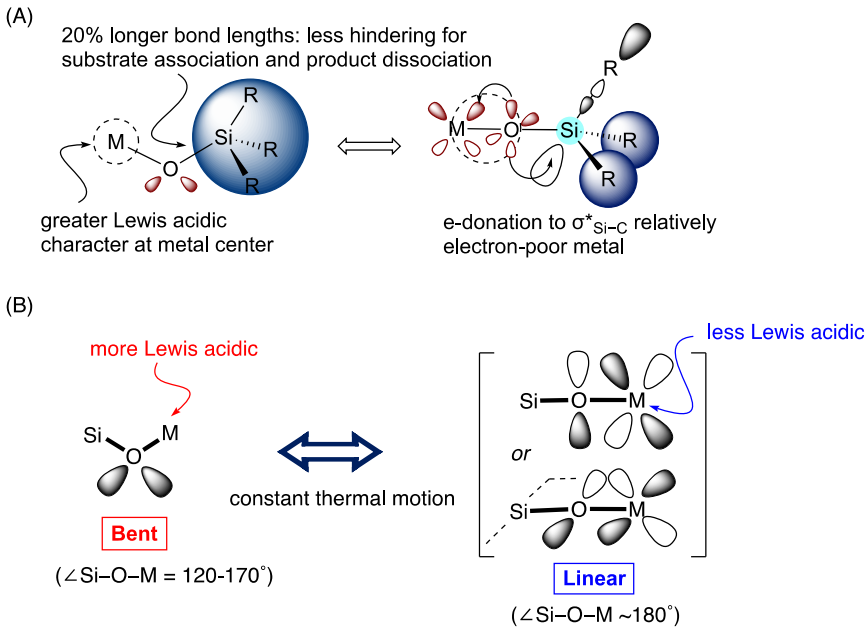
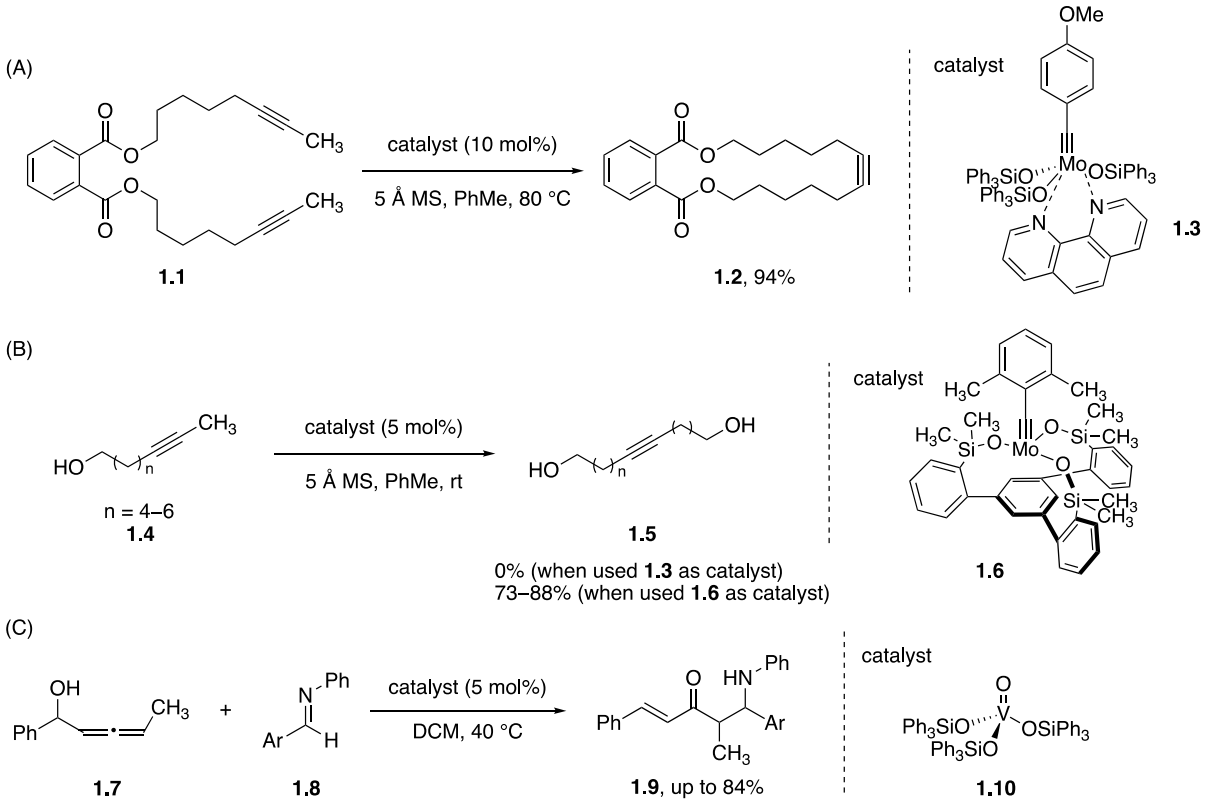



**Figure 1.2.** Structures, bonding, and properties of metal-siloxides.

## Ib. Metal-siloxides in Catalysis

Silanols have been previously utilized as ancillary ligands or reagents for a variety of metal-catalyzed transformations such as alkyne metatheses,[21–23] Pd-catalyzed cross-couplings[24–27] and ortho-metalations.[28–32] Among these examples, Fürstner reported using siloxides as ancillary ligands in

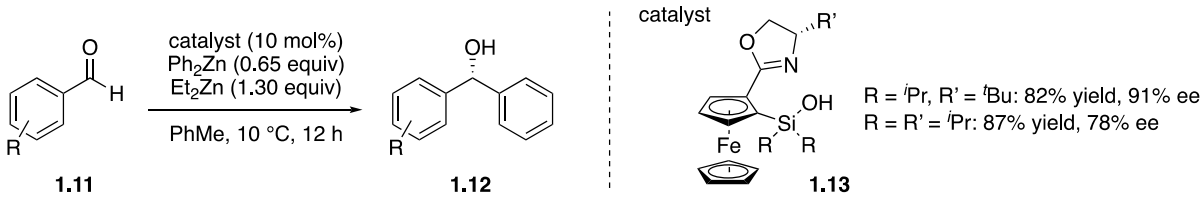
molybdenum-silanolate complexes, demonstrating their superior reactivity and exceptional tolerance towards various functional groups when employed as catalysts for alkyne metathesis (Scheme 1.2A). This molybdenum-silanolate complex **1.3** exhibited heightened activity and stability compared to their carbon-based analogs in facilitating alkyne metatheses. Subsequently, the development of catalyst **1.6** marked a significant improvement by maintaining comparable reactivity to its best predecessor **1.3** while displaying improved functional group tolerance. These newly developed catalysts have demonstrated excellent performance in the presence of unprotected alcohols and diverse protic groups (Scheme 1.2B). Furthermore, Trost reported an $O{=}V(OSiR_3)_3$ catalyst for addition of allenic alcohols to aldehydes/imines where the $O{=}V(OSiPh_3)_3$ catalyst is uniquely active relative to $O{=}V(OSiMe_3)_3$ and $O{=}V(O\textit{i}\text{-}Pr_3)_3$ complexes (Scheme 1.2C).[33–35]




**Scheme 1.2.** (A−B) Molybdenum-catalyzed alkyne metathesis reactions reported by Fürstner and coworkers. (C) A vanadium-catalyzed reaction of an allenic alcohol and imines reported by Trost and coworkers.

Bolm and coworkers introduced ferrocene-based chiral organosilanol ligand **1.13** in an asymmetric phenyl-transfer reaction involving substituted benzaldehydes (**1.11**), using a stoichiometric amount of

both diethylzinc and diphenylzinc (Scheme 1.3).[17] Although a catalytic amount of silanol ligand is utilized, their application was limited to stoichiometric Zn reagents rather than transition metal-catalyzed processes. Despite previous work on using silanols in organic transformations, using silanols as chelating ligands in transition-metal catalyzed enantioselective catalysis has yet to be reported.




**Scheme 1.3.** Ferrocene-based chiral silanol ligands in asymmetric phenyl-transfer reactions.

We hypothesized that metal siloxides could lead to enhanced activity and stereoselectivity in asymmetric catalysis with the appropriate silanol ligand structure and metal combination. Enantioselective catalysis is widely considered the most efficient method to prepare enantioenriched compounds.[36–38] In metal-catalyzed reactions, chiral ligands are utilized to enhance reactivity and promote stereoselectivity. Considerable efforts have been made to design and synthesize classes of ligands for various chemical transformations.[39,40] The heteroatoms serving as coordinating sites are key to chiral ligand design principles,[41,42] where stereocontrol and reactivity can be tuned by incorporating different coordinating groups. Common coordinating groups applied in ligands include phosphines,[43–47] phosphites,[48–50] amines,[43,51] imines,[52,53] and alcohols[51–56] (Figure 1.3A).[42] Silicon has previously been incorporated as part of a chiral ligand scaffold backbone (Figure 1.3B),[9–14] and the hydridosilane introduced as a coordinating group for achiral[57–61] and recently enantioselective[62] catalysis. The use of silanols as coordinating groups in enantioselective catalysis has been underexplored due to challenges in synthesis and limited investigations.[63]

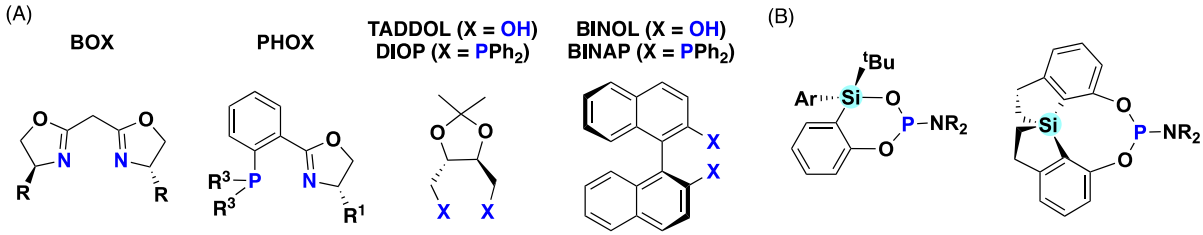



**Figure 1.3.** (A) Examples of common ligand scaffolds and coordinating groups in asymmetric catalysis. (B) Examples of ligands with silicon as part of a chiral ligand scaffold backbone.

## II. Synthesis of Chiral Silanol Ligands

At the beginning of our investigation, we aimed to integrate silanols into chiral scaffolds commonly utilized in various enantioselective transformations for their modular construction, providing convenient variability.[39,64–66] The project was initiated by Dr. Taewoo Min, a former member of the Franz group, who introduced the silanol group onto a chiral oxazoline scaffold to synthesize **L1** (Figure 1.4A).[67] Subsequently, Dr. Kayla Diemoz, another former member of the Franz group, assessed its catalytic capacity in asymmetric catalysis and metal-ligand binding properties.[68] However, initial assessments of **L1** showed moderate reactivity and low selectivity across several test reactions. We later proposed incorporating the silanol group onto chiral imidazoline scaffolds **L2** (Figure 1.4B). Pfaltz and coworkers introduced the imidazoline scaffold to chiral ligand design.[46] We hypothesized that the compact torsion angle of the imidazoline might bring the chiral steric group closer to the reaction center (Figure 1.4C), as previously noted by Pfaltz and coworkers.[46]

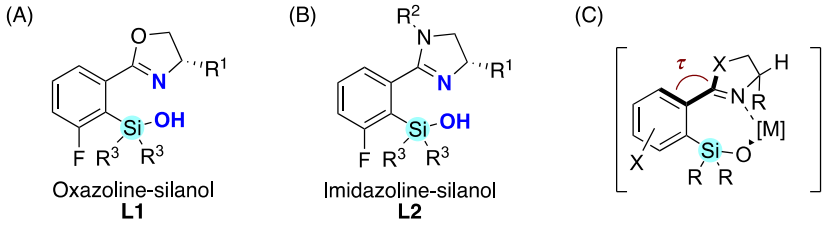
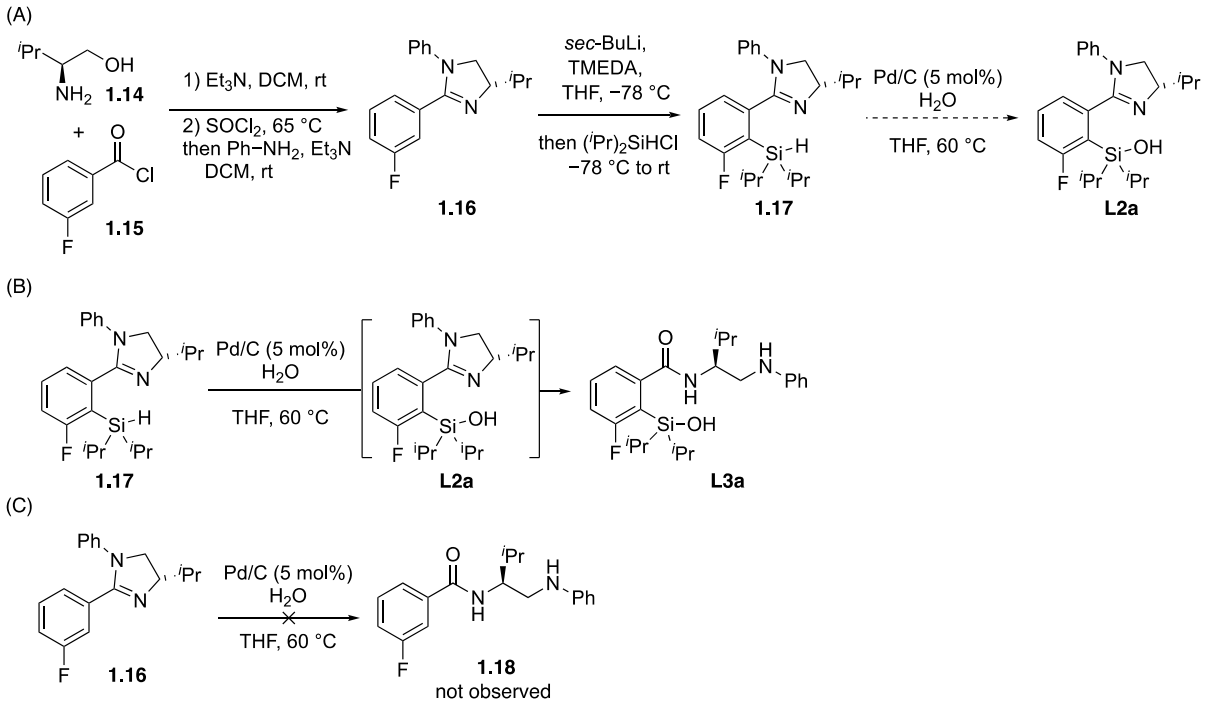



**Figure 1.4.** (A) Oxazoline-silanol synthesized by Dr. Taewoo Min and assessed by Dr. Kayla Diemoz. (B) My proposal on incorporating silanol onto chiral imidazoline. (C) Proposed metal-siloxide complex.

### IIa. Synthesis of Imidazoline Silanols and the Discovery of the Aminoamide Silanol Ligand

The proposed synthetic route for imidazoline silanol **L2** is outlined in Scheme 1.4A. This synthetic route involves an initial amide coupling followed by cyclization to generate the imidazoline group **1.16**. Further steps include a direct *ortho*-lithiation[69] using *sec*-BuLi and subsequent addition of a chlorosilane to afford silane **1.17**. The anticipated final step was a Pd-catalyzed hydrolysis to achieve the desired imidazoline silanol **L2**. However, an unexpected product formed during the Pd-catalyzed hydrolysis process at 60 °C: the imidazoline underwent a ring-opening, forming an aminoamide silanol **L3** (Scheme 1.4B). It was unexpected for the imidazoline to undergo a ring-opening reaction, especially

considering the lack of reaction observed in the control experiment where the imidazoline was subjected to the same Pd-catalyzed hydrolysis conditions at 60 °C for 16 h (Scheme 1.4C).



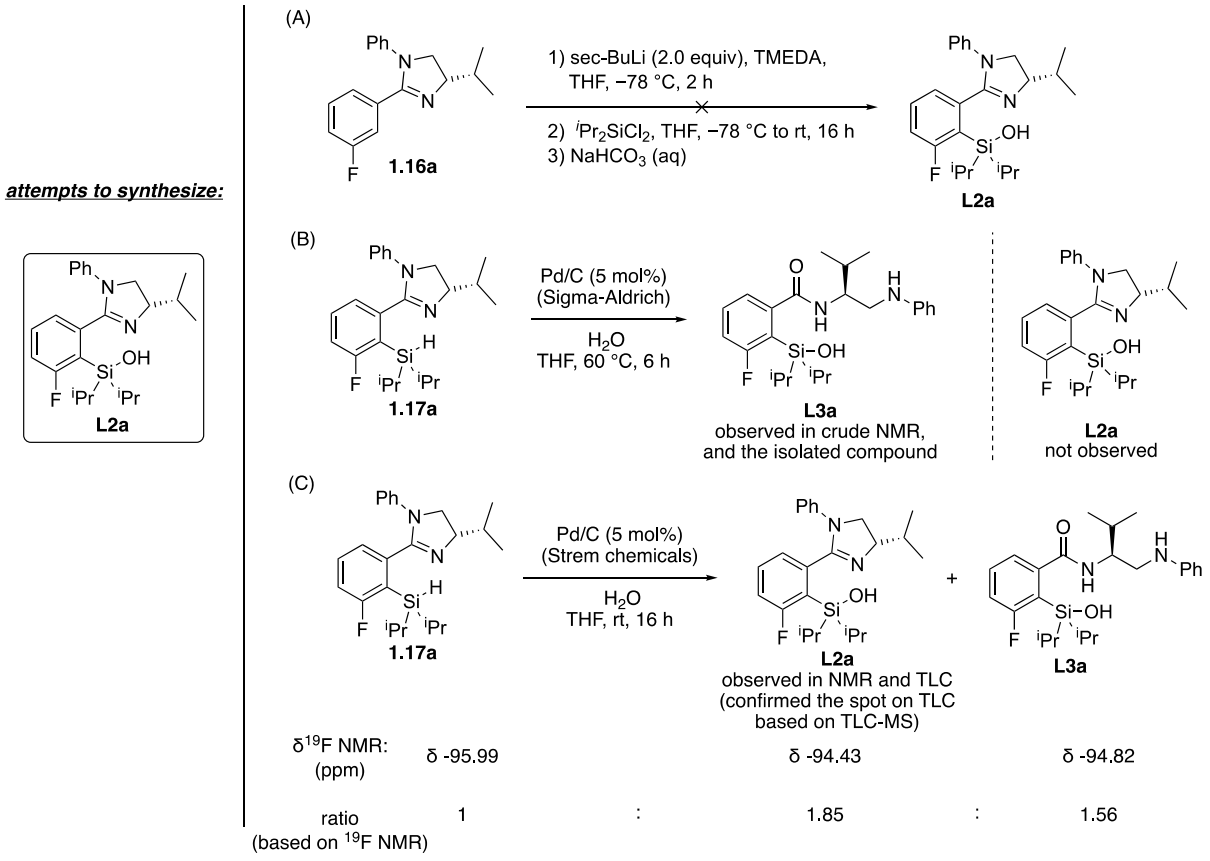

**Scheme 1.4.** (A) Proposed synthetic route to access imidazoline silanol **L2**. (B) Unexpected formation of aminoamide silanol **L3**. (C) Control experiment of imidazoline under the hydrolysis conditions.

## IIb. Pd-catalyzed Hydrolysis at Elevated Temperature

Typically, silane hydrolysis to produce a silanol occurs smoothly at room temperature, completing the reaction within less than 16 h.[70–73] This also applies to oxazoline silane hydrolysis, where oxazoline silanol **L1** was obtained in a 92% yield under Pd-catalyzed hydrolysis at room temperature in 4 h. However, with imidazoline silane **1.17**, no silane consumption was observed under Pd-catalyzed hydrolysis at room temperature over a 3-day period. Subsequently, raising the reaction temperature to 60 °C led to successful hydrolysis (Scheme 1.4B). The lack of reactivity for imidazoline silane **1.17** hydrolysis at room temperature could be attributed to several factors: 1) the hindered torsion angle that impedes the oxidative addition of Pd to the Si−H bond, 2) the declining activity of the oxidized Pd/C catalyst over time due to the presence of PdO or potential aggregation of catalyst particles, and 3) variations in the particle size of Pd/C sourced from different manufacturers.[74]

## IIc. Efforts toward the Synthesis of Imidazoline Silanols

Several attempts were made to synthesize the proposed imidazoline silanol **L2a** depicted in Scheme 1.5. An alternative route illustrated in Scheme 1.5A was explored, aiming to generate the silanol by hydrolyzing an *in-situ* generated imidazoline silylchloride. While it is our preference to use the Pd/C-catalyzed hydrolysis of silanes to obtain pure silanols that do not contain HCl,[75] we still attempted to synthesize **L2a** by quenching an *in-situ* generated imidazoline silylchloride with $NaHCO_3$. This method did not yield the desired **L2a** based on $^{1}H$, $^{19}F$ NMR analysis and TLC of the unpurified mixture.




**Scheme 1.5.** Efforts toward the synthesis of imidazoline silanol **L2a**.

Scheme 1.5B and 1.8C compare various sources of Pd/C catalyst for the silane hydrolysis. Different sources of Pd/C catalysts can significantly influence reaction time, yield, and selectivity. An article published in *Organic Process Research & Development* in 2021 identified the following key catalyst properties for efficiency: (1) small Pd/PdO particle size, (2) homogeneous distribution of Pd/PdO on the carbon support, and (3) palladium oxidation state.[74] This study highlighted that 5% Pd/C from Strem Chemicals is the most effective; conversely, Pd/C from Sigma-Aldrich, characterized by larger particle

sizes and a higher quantity of PdO, exhibited lower catalyst activity. Given that our group was generally using Pd/C from Sigma-Aldrich for the silane hydrolysis reaction, this might explain why aminoamide silanol **L3a** was the sole product formed after the hydrolysis at elevated temperature (Scheme 1.5B), and no hydrolysis was observed at room temperature over a 3-day period. We revisited the Pd/C hydrolysis at room temperature using the newly purchased Pd/C catalyst from Strem chemicals, which was evaluated to be the more active catalyst (Scheme 1.5C).[74] Initially, the formation of imidazoline silanol was observed after 2 h of reaction time, and the reaction was continuously monitored for an additional 4 h. The presence of imidazoline silanol on the TLC plate was confirmed based on TLC-MS (Figure 1.5A). Although some silane remained and protodesilylation occurred, the reaction was allowed to proceed overnight. After 16 h, $^{19}F$ NMR analysis of an aliquot from the reaction solution was performed, which showed the formation of both imidazoline silanol and aminoamide silanol, with their respective ratios depicted in Scheme 1.5C. To prevent further conversion of imidazoline silanol to aminoamide silanol, standard procedures were followed to work up the reaction. This involved the dilution of the reaction mixture, addition of $MgSO_4$, filtration through Celite to remove the Pd/C catalyst, and rotavapping. However, during the rotavapping process at 34 °C in a water bath for approximately 7 minutes, the unpurified mixture changed from yellow to black. Subsequent TLC and $^{19}F$ NMR analyses confirmed the conversion of both imidazoline silane and imidazoline silanol to aminoamide silanol. The TLC analysis and $^{19}F$ NMR spectra obtained before and after workup are shown in Figure 1.5B.

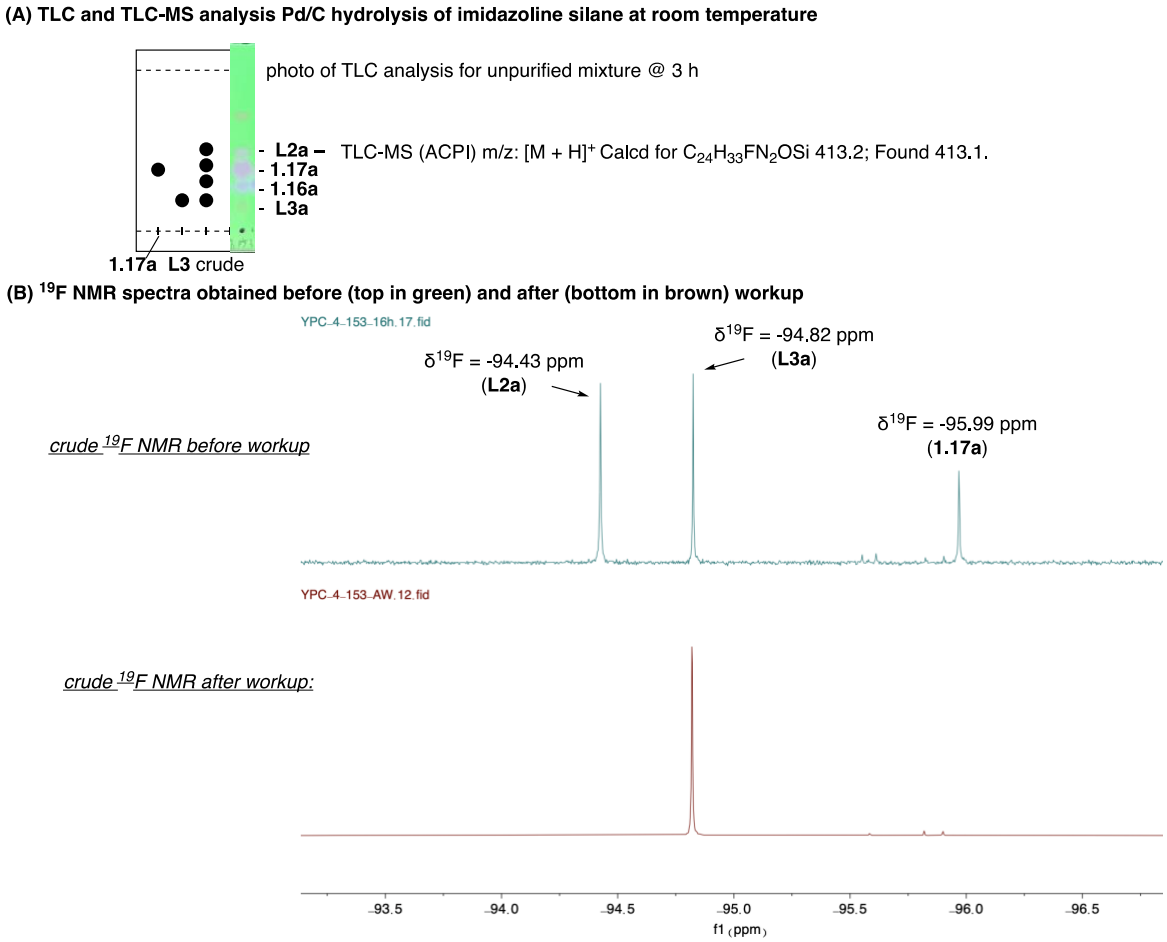
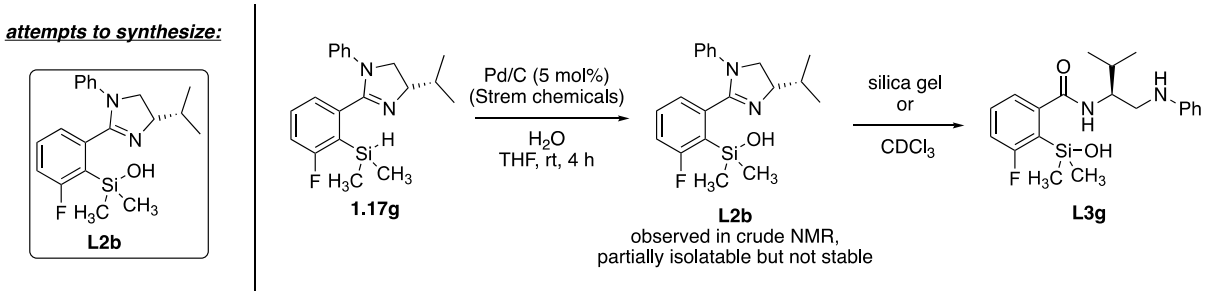



**Figure 1.5.** TLC analysis and $^{19}F$ NMR spectra of the hydrolysis reaction in Scheme 1.5C.

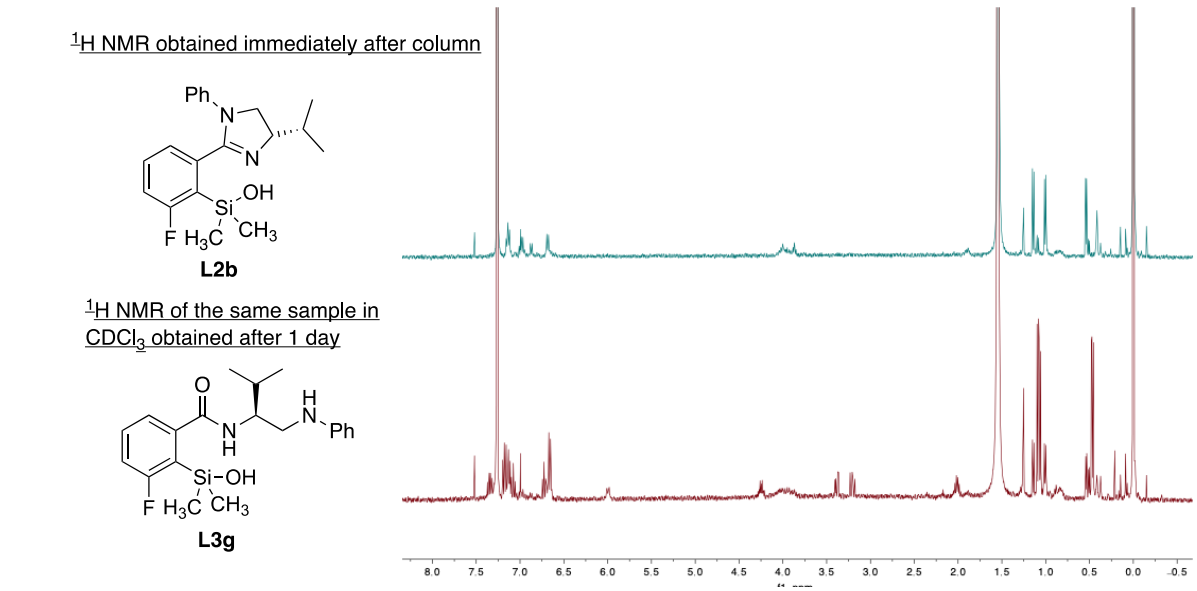
A Pd/C hydrolysis was conducted on dimethyl-substituted imidazoline silane **1.17g** at room temperature. This process resulted in the observation and isolation of imidazoline silane **L2b** (Scheme 1.6). In the NMR analysis of the unpurified mixture, the reaction showed 60% desilylation of the silane and 40% imidazoline silanol formation. However, during purification on a silica gel column, the aminoamide silanol **L3g** was formed. Despite isolating a small quantity of imidazoline silanol **L2b** and collecting $^{1}H$ and $^{19}F$ NMR data (Figure 1.6, top), its instability was observed as it converted to aminoamide silanol **L3g** in $CDCl_3$ within a day (Figure 1.6, bottom). The spectral data obtained after a day align with the spectra of the aminoamide silanol synthesized using an alternative route (see the characterization data of **L3g**). These findings suggests that the unstable imidazoline silanol tends to undergo conversion into the aminoamide silanol under the given conditions. Given the observations

made during the synthesis of the imidazoline silanol, it can be inferred that its instable nature renders it unsuitable for use as a ligand.




**Scheme 1.6.** Efforts toward the synthesis of imidazoline silanol **L2b**.

**(A) $^{1}$H NMR spectra in $CDCl_3$ obtained immediately after column purification (top) and in $CDCl_3$ after 1day (bottom)**




**(B) $^{19}$F NMR spectra in $CDCl_3$ obtained immediately after column purification (top) and in $CDCl_3$ after 1day (bottom)**

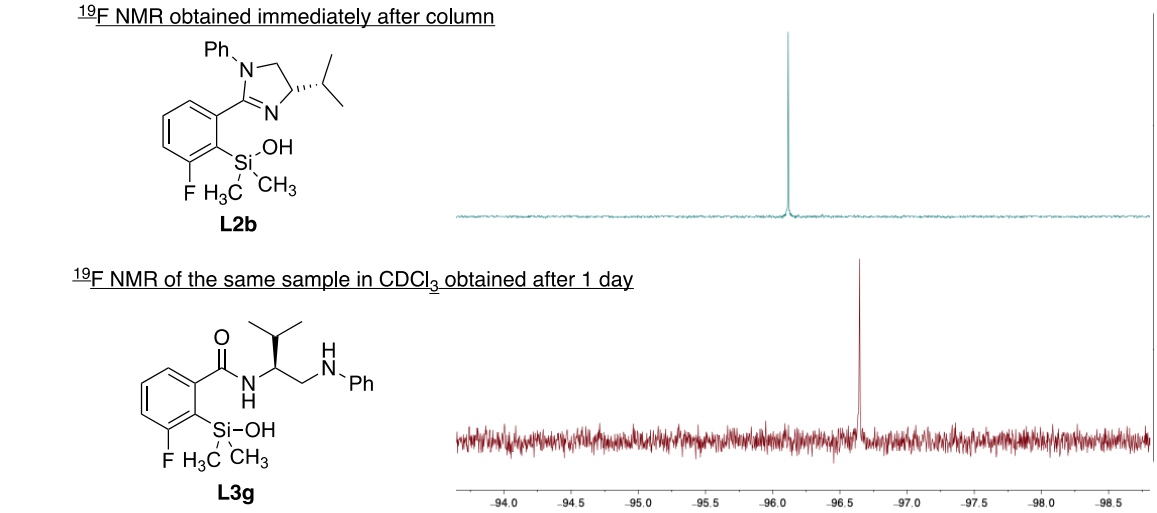
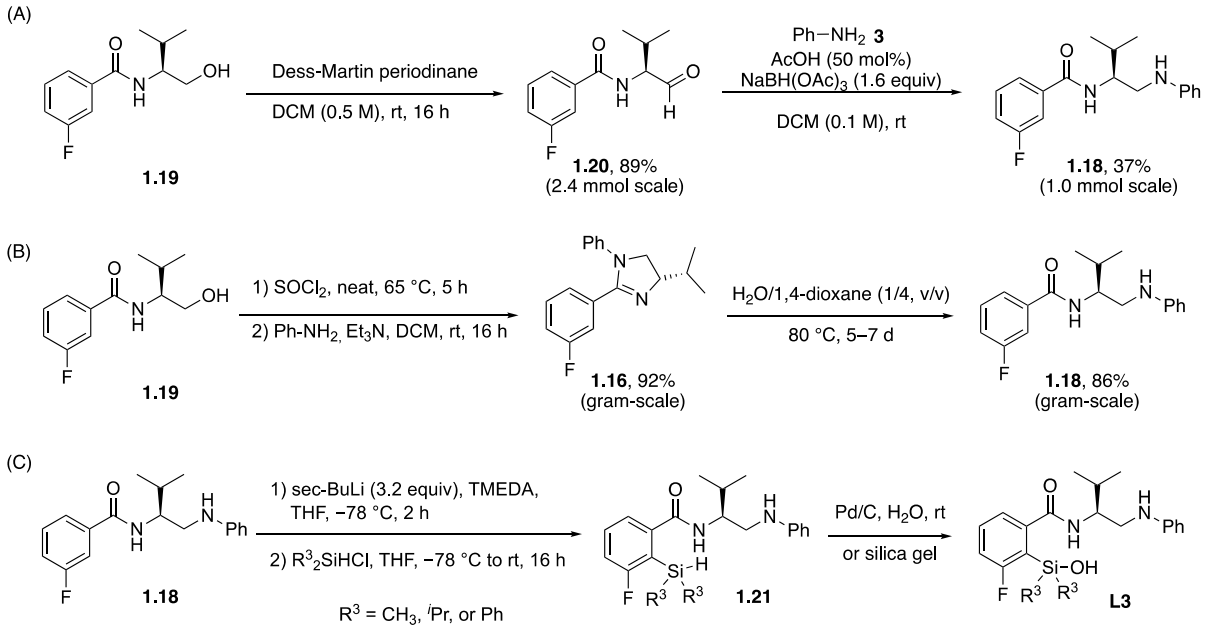


**Figure 1.6.** Comparison of (A)$^{1}$H NMR spectra and (B) $^{19}$F NMR spectra obtained immediately after column purification and after 1 day.

## IId. Exploring Alternative Routes for the Synthesis of Aminoamide Silanols

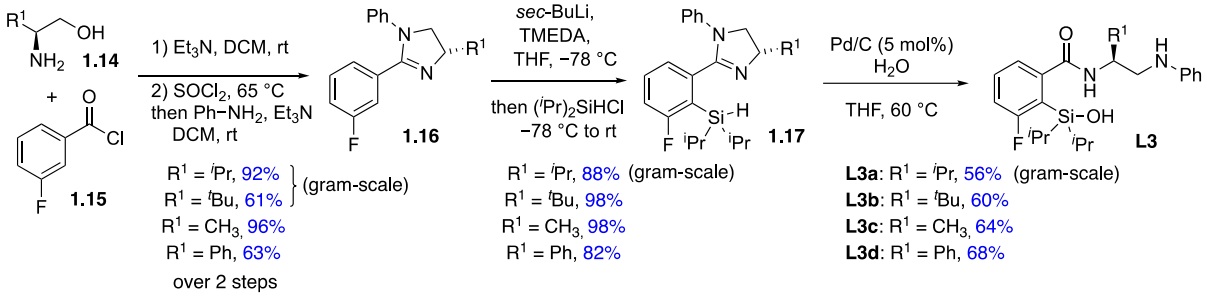
After concluding that the proposed imidazoline silanol (**L2**) lacks the stability essential for its role as a ligand in reactions, we explored alternative pathways to synthesize the newly discovered ligand, aminoamide silanol **L3** (Scheme 1.7).

In Scheme 1.7A, aldehyde **1.20** was synthesized from the oxidation of β-hydroxy amide (**1.19**) using the Dess-Martin periodinane, followed by a reductive-amination to form the aminoamide. However, there was a risk of potential racemization of **1.20**. We had to use the aldehyde for the next step immediately to prevent racemization. Despite this concern, we utilized route A to validate the spectroscopic data of **1.18** for comparison with route B. Scheme 1.7B involved synthesizing imidazoline **1.16** via the cyclization of β-hydroxy amide **1.19**. Following this, acid-catalyzed hydrolysis induced ring-opening to form aminoamide **1.18**. Both steps gave high yields of the desired product. However, this entire process required more than 10 days to complete, making it time-consuming. In addition, the lithiation of the aminoamide requires more than 3 equivalents of both *sec*-BuLi and chlorosilane, making it cost-ineffective (Scheme 1.7C).




**Scheme 1.7.** Exploration of alternative pathways for the synthesis of **L3**.

Considering the above, the most efficient approach to synthesizing the desired aminoamide silanol **L3** involves the imidazoline silane, as illustrated in Scheme 1.8. The imidazoline silane **1.17** undergoes the ring-opening reaction to convert the silane into a silanol during Pd/C hydrolysis in a single step. This approach overcomes the challenges associated with the direct synthesis of the aminoamide scaffold, which typically requires a three- to four-step process. The entire process can be completed in 6 days with up to 60% yield over four steps. A collection of aminoamide silanol ligands (**L3**) were prepared through this synthetic sequence that provides straightforward access to ligands with varied steric properties. All of the aminoamide silanol products are air-stable crystalline white solids. **L3a** and **L3b** were found to be stable to air and atmospheric moisture for >30 months with minimal decomposition and no loss of catalytic activity. The next section will discuss the catalytic properties of aminoamide-silanol ligands (**L3**) through enantioselective reactions.



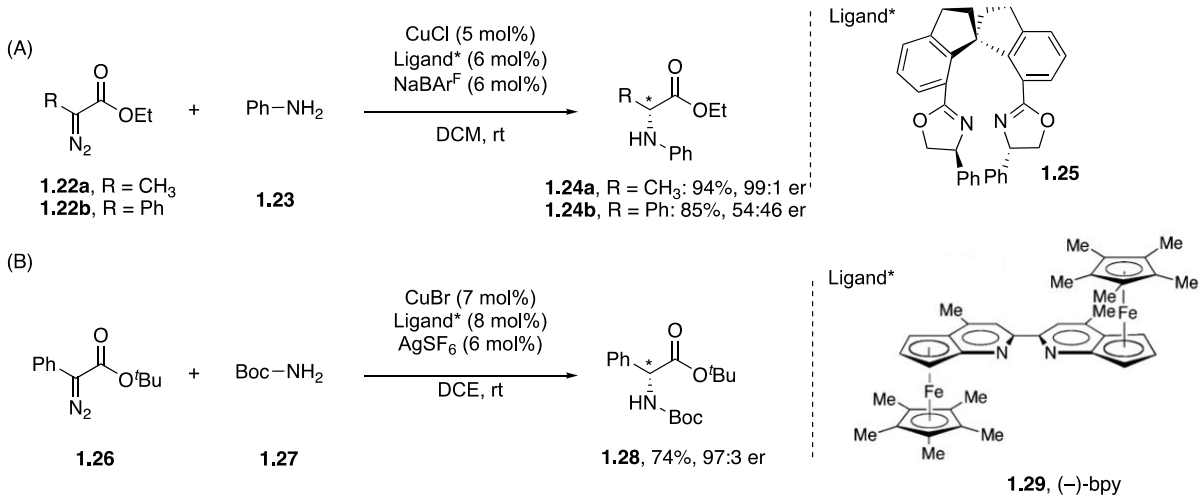

**Scheme 1.8.** Synthesis of chiral aminoamide-silanol ligands (**L3**).

## III. Investigation of Catalytic Properties of Chiral Aminoamide-silanol Ligands

### IIIa. Enantioselective N−H Insertions

An investigation was conducted to comprehend the effectiveness of aminoamide-silanol ligands (**L3**), focusing on their catalytic potential. This investigation primarily focuses on evaluating the catalytic properties of these silanol ligands through enantioselective N−H insertions. This test reaction was suggested by a Franz group member, Kevin Blanco-Herrero, who was designing and evaluating other novel silicon-containing ligands. Enantioselective N−H insertions have proven to be a highly efficient way to form C−N bonds and can be used for the enantioselective synthesis of unnatural chiral amino acids.[76–86] Previous chiral ligands employed for enantioselective N−H insertions include rigid spirobox,[76,77,85] bipyridines,[84] or *N,N*-dioxides.[83] Zhu and coworkers introduced the chiral SpiroBox

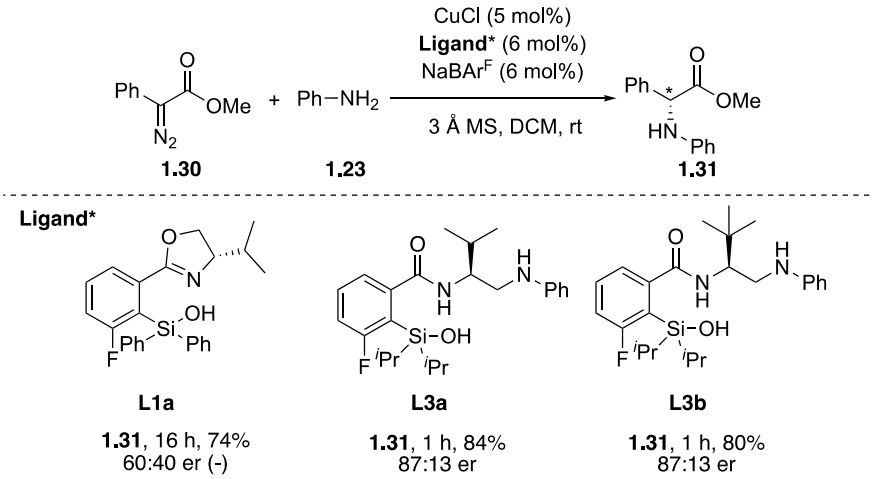
ligand **1.25** for the insertion of alkyl diazoesters **1.22** into the N−H bond of aniline, obtaining up to 94% yield of product with 99:1 er (Scheme 1.9A).[76] Fu and coworkers developed a copper-catalyzed enantioselective N−H insertion of aryldiazo ester **1.26** into the N−H bond of carbamates using a chiral bipyridine ligand **1.29** (Scheme 1.9B).[84] The resulting products **1.28** can be readily deprotected and form unnatural arylglycines.




**Scheme 1.9.** Examples of enantioselective N−H insertions.

## IIIb. Preliminary Ligand Screening for the Enantioselective N−H Insertion

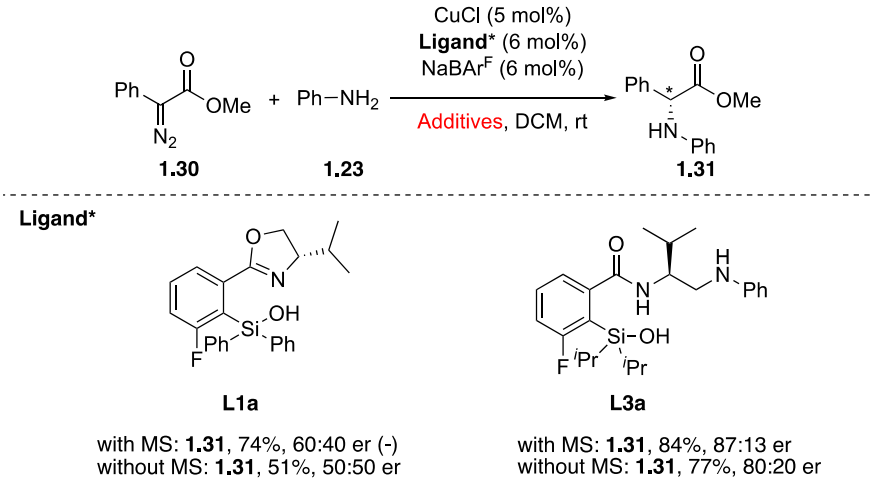
We investigated the catalytic activity of the silanol ligands via an enantioselective N−H insertion of α-phenyl-α-diazoesters with anilines, as depicted in Scheme 1.10. In the previous example by the Zhu group, excellent enantioselectivity was achieved using alkyl diazoesters; however, no selectivity was observed when phenyl diazoester **1.22b** was utilized (Scheme 1.9A).[76] To comprehensively evaluate ligand performance, we specifically utilized phenyl diazoester **1.30** for our evaluation. Initially, we conducted a preliminary ligand screening to identify the most suitable ligand for further reaction optimization. The results indicated that aminoamide ligands **L3** exhibited superior reactivity and enantioselectivity compared to **L1a**. Both **L3a** and **L3b**, with *i*-Pr or *t*-Bu as the steric group, demonstrated identical enantioselectivity (87:13 er) with good yields of the N−H insertion product. Considering the quantity of available ligands in hand and the cost of the chiral amino alcohol starting material **1.14**. we selected isopropyl as the chiral substituent for the subsequent reaction optimization.




**Scheme 1.10.** Preliminary ligand screening for enantioselective N–H insertion of α-phenyl-α-diazoesters with aniline.

## IIIc. Addition of Molecular Sieves Affects Enantioselectivity

Moisture was identified as a significant factor affecting enantioselectivity, as reported by the Zhu group.[76] Consequently, they conducted reactions within a glove box, and all reagents were required to undergo fresh distillation before use. In our experimental setup, we conducted the reaction under an Ar-balloon atmosphere and introduced 3 Å spherical molecular sieves to adsorb moisture. It is worth noting that we did not perform distillation of diazoester or aniline before use. Importantly, we observed decreases in selectivity when molecular sieves were omitted from the reaction setup (Scheme 1.11).

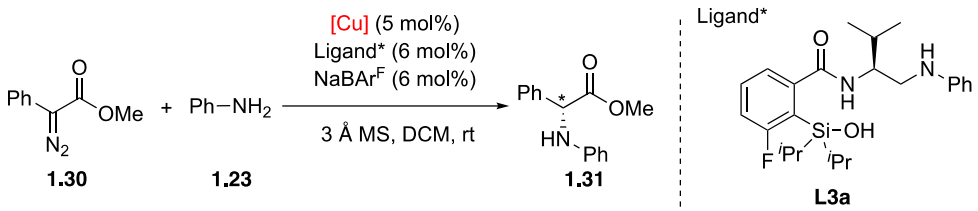



**Scheme 1.11.** Comparison in with or without the addition of molecular sieves.

## IIId. Optimization of the Cu-catalyzed Enantioselective N−H Insertion

The enantioselectivity of the N−H insertion of α-phenyl-α-diazoesters with aniline was evaluated with various copper salts (Table 1.1). CuCl demonstrated the highest enantioselectivity (87:13 er). The enantioselectivity levels remained consistent, except when $Cu(OTf)_2$ and $Cu(OAc)_2$ were used (55:45 and 64:35 er, respectively). This deviation in selectivity could be attributed to potential coordination between triflate or acetate anions and the catalyst or ligand, which may disrupt the formation of an active metal-ligand complex essential for high enantioselectivity in product formation.

**Table 1.1.** Copper salt screen for the enantioselective N−H insertions

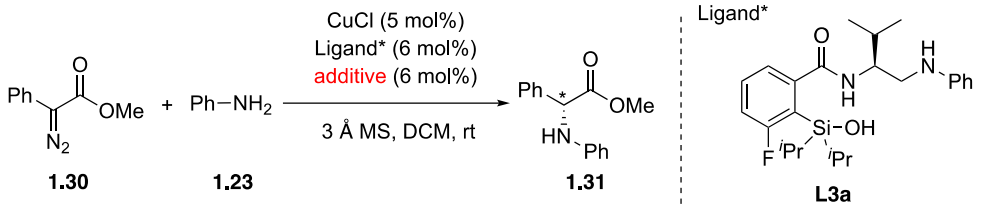



| Entry[a] | [Cu] | Counteranion | Time (h) | Yield (%)[b] | er[c] |
|---|---|---|---|---|---|
| 1 | CuCl | $NaBAr^F$ | 1 | 84 | 87:13 |
| 2 | [Cu(OTf)•½$C_6H_6$] | $NaBAr^F$ | 1 | 77 | 84:16 |
| 3 | CuBr | $NaBAr^F$ | 1 | 71 | 83:17 |
| 4 | $Cu(OTf)_2$ | $NaBAr^F$ | 16 | 89 | 55:45 |
| 5 | $Cu(OAc)_2$ | $NaBAr^F$ | 1 | 84 | 64:36 |
| 6 | $CuCl_2$ | $NaBAr^F$ | 1 | 80 | 83:17 |
| 7 | $CuBr_2$ | $NaBAr^F$ | 1 | 72 | 84:16 |

[a]Reactions performed under standard reaction conditions (General procedure-Procedure G): Diazo compound **1.30** (0.2 mmol), aniline **1.23** (0.2 mmol), CuCl (5 mol%), $NaBAr^F$ (6 mol%), ligand (6 mol%), and activated spherical 3 Å mol sieves (50 mg) at room temperature. [b]NMR yield using Ph−TMS as internal standard. [c]Determined using CSP-HPLC with a Chiralpak OD-H column.

The counteranion screening revealed the critical role of $NaBAr^F$ in enhancing enantioselectivity (Table 1.2). Sodium tetrakis(3,5-bis(trifluoromethyl)phenyl)borate, commonly known as $NaBAr^F$, functions as a non-coordinating or weakly coordinating counteranion in organometallic chemistry. Its utilization elevates the Lewis acidity of the metal center, thereby increasing reactivity. Substituting $NaBAr^F$ with $AgSbF_6$ maintained the reactivity but failed to achieve selectivity (Table 1.2, entry 3). Additionally, the reaction did not proceed in the absence of CuCl.

**Table 1.2.** Additive screen for the enantioselective N−H insertions.

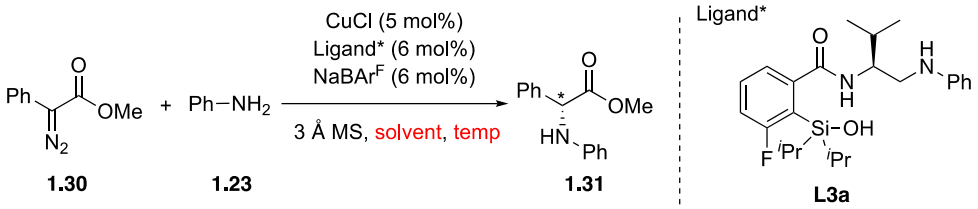



| Entry[a] | Catalyst | Additive | Time (h) | Yield (%)[b] | er[c] |
|---|---|---|---|---|---|
| 1 | CuCl | $NaBAr^F$ | 1 | 84 | 87:13 |
| 2 | CuCl | -- | 1 | 72 | 51:49 |
| 3 | CuCl | $AgSbF_6$ | 1 | 85 | 56:44 |
| 4 | -- | $NaBAr^F$ | 16 | <5 | nd[d] |

[a]Reactions performed under standard reaction conditions (General procedure-Procedure G) [b]NMR yield using Ph−TMS as internal standard. [c]Determined using CSP-HPLC with a Chiralpak OD-H column. [d]Not determined.

The optimization process extended to solvent and reaction temperature adjustments (Table 1.3). Aromatic solvents such as toluene, benzene, and chlorobenzene exhibited similar enantioselectivity (Table 1.3, entries 2−4). Lewis basic solvents like THF notably diminished both reactivity and enantioselectivity. Among chlorinated solvents, chloroform exhibited decreased enantioselectivity, while dichloroethane (DCE) maintained enantioselectivity (85:15 er) but showed reduced reactivity (49%). Dichloromethane emerged as the optimal solvent due to its best performance in both enantioselectivity and reactivity. Lowering the temperature resulted in a decreased in the reaction rate and did not aid in improving enantioselectivity (Table 1.3, entries 8−11).

**Table 1.3.** Solvent and temperature screen for the enantioselective N−H insertions

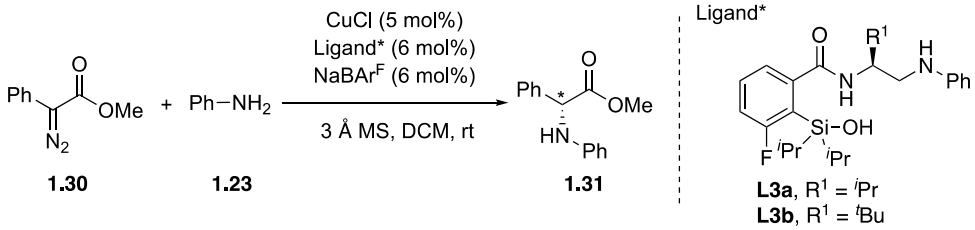



| Entry[a] | Solvent | Temp | Time (h) | Yield (%)[b] | er[c] |
|---|---|---|---|---|---|
| 1 | DCM | rt | 1 | 84 | 87:13 |
| 2 | PhMe | rt | 1 | 66 | 78:22 |
| 3 | $C_6H_6$ | rt | 16 | 44 | 78:22 |
| 4 | PhCl | rt | 1 | 74 | 79:21 |
| 5 | THF | rt | 16 | 37 | 50:50 |
| 6 | $CHCl_3$ | rt | 1 | 66 | 66:34 |
| 7 | DCE | rt | 1 | 49 | 85:15 |
| 8 | DCM | 0 °C | 6 | 37 | 78:22 |
| 9 | DCM | −78 °C | 24 | <5 | 64:36 |
| 10 | DCM | 0 °C to rt | 3 | 69 | 81:19 |
| 11 | DCM | −78 °C to rt | 3 | 69 | 80:20 |

[a]Reactions performed under standard reaction conditions (General procedure-Procedure G) [b]NMR yield using Ph−TMS as internal standard. [c]Determined using CSP-HPLC with a Chiralpak OD-H column.

The reaction concentration and pre-complexation time were tested (Table 1.4). Lowering the concentration aimed to disrupt ligand aggregation, resulting in higher enantioselectivity. When the concentration was reduced to 0.013 M, an enantioselectivity of 92:8 er was achieved (Table 1.4, entry 3); however, such a low concentration was deemed impractical for use. Furthermore, pre-complexation time was explored. The standard pre-complexation time was set at 2 hours to premix CuCl, NaBArF, and the ligand before the addition of reagents. While maintaining the reaction performance with a reduced time of 1 hour from the standard 2 hours (Table 1.4, entry 4), variations in enantioselectivity and reactivity were observed during substrate scope investigations. Consequently, the 2-hour pre-complexation time was retained to ensure consistent reaction performance. Finally, we revisited the examination of ligand **L3b**, with *t*-Bu as the steric group, under the optimal conditions. The results indicated an enhanced enantioselectivity compared to **L3a** at a concentration of 0.05 M. From these results, optimized conditions for the enantioselective N−H insertions using silanol ligand were 5 mol% CuCl, 6 mol% of $NaBAr^F$ , and 6 mol% of ligand **L3b** in DCM (0.05 M) with the addition of 3Å MS.

**Table 1.4.** Concentration screen for the enantioselective N−H insertions



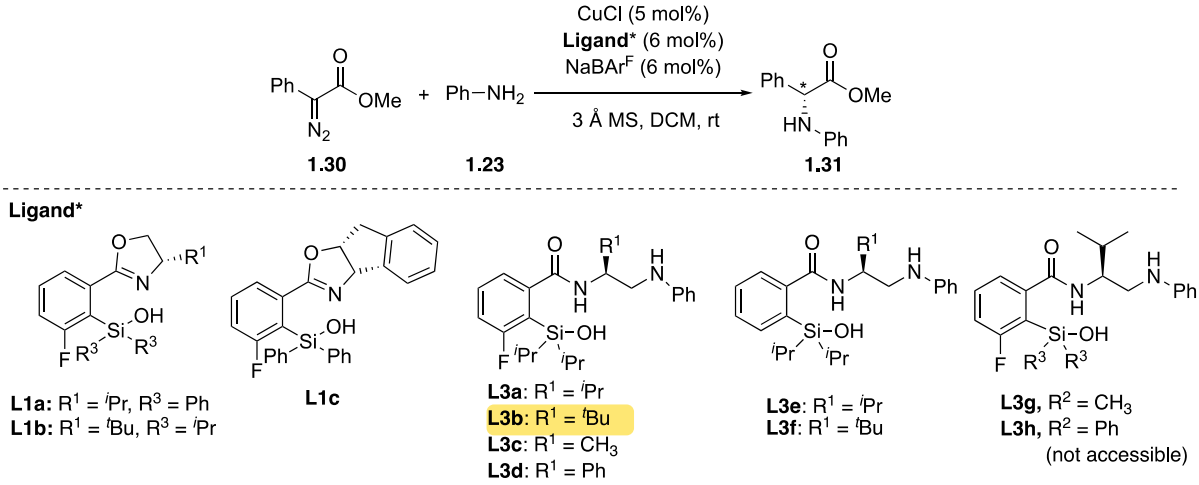

| Entry[a] | Ligand | Conc. (M) | Time(h) | Yield (%)[b] | er[c] |
|---|---|---|---|---|---|
| 1 | **L3a** | 0.1 | 1 | 84 | 87:13 |
| 2 | **L3a** | 0.05 | 1 | 83 | 89:11 |
| 3 | **L3a** | 0.013 | 1 | 60 | 92:8 |
| 4[d] | **L3a** | 0.05 | 1 | 79 | 88:12 |
| 5 | **L3b** | 0.1 | 1 | 80 | 87:13 |
| 6 | **L3b** | 0.05 | 1 | 80 | 91:9 |
| 7 | **L3b** | 0.025 | 1 | 75 | 91:9 |

[a]Reactions performed under standard reaction conditions (General procedure-Procedure G) [b]NMR yield using Ph−TMS as internal standard. [c]Determined using CSP-HPLC with a Chiralpak OD-H column. [d]CuCl and NaBAr$^F$ were precomplexed for 1 h, followed by the addition of ligand. The pre-complexation was stirred for an additional hour, and then the starting materials were added.

## IIIe. Screening of Chiral Silanol Ligand for the Enantioselective N−H Insertion

To identify the most effective ligand, a series of silanol ligands, including oxazoline silanol (**L1**) and aminoamide silanol (**L3**) were evaluated (Table 1.5) under the optimal conditions. The poor enantioselectivity observed using oxazoline silanols (**L1**) shows the advantage of using aminoamide silanol ligands in the system (Table 1.5, entries 1−3). The enantioselectivity of the N−H insertion (**L3a**−**L3d**) is influenced by the steric groups ($R^1$) at the chiral center (Table 1.5, entries 4−7). We then turned our attention to the effect of the aryl fluoride, which was originally incorporated into the backbone for synthetic purposes. Two ligands without the fluorine substituent (**L3e** and **L3f**) were synthesized; in both cases, a slight reduction in enantioselectivity was observed (86:14 and 80:20 er, respectively), suggesting the electron density of the aryl ring influences the enantioselectivity (Table 1.5, entries 8−9).

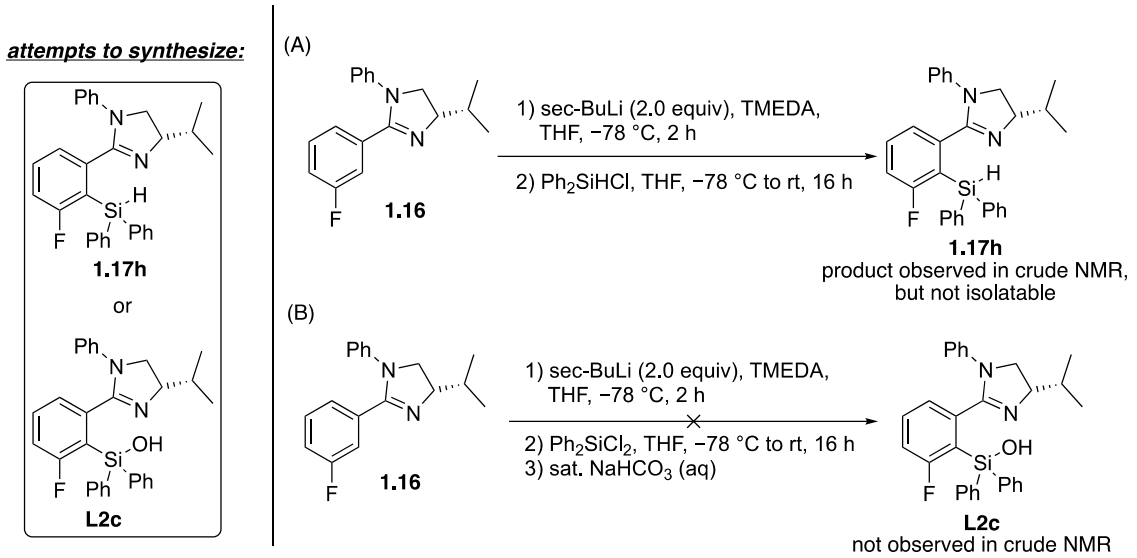
**Table 1.5.** Ligand screening for enantioselective N−H insertion of α-phenyl-α-diazoesters with aniline




| Entry[a] | Ligand | Time | Yield (%)[b] | er[c] |
|---|---|---|---|---|
| 1 | **L1a** | 16 h | 74 | 60:40 (-) |
| 2 | **L1b** | 16 h | 63 | 61:39 (-) |
| 3 | **L1c** | 22 h | 42 | 55:45 (-) |
| 4 | **L3a** | 1 h | 84 | 89:11 |
| 5 | **L3b** | **1 h** | **80** | **91:9** |
| 6 | **L3c** | 2 h | 71 | 77:23 |
| 7 | **L3d** | 1 h | 69 | 79:21 |
| 8 | **L3e** | 1 h | 70 | 86:14 |
| 9 | **L3f** | 1 h | 70 | 80:20 |
| 10 | **L3g** | 1 h | 59 | 56:44 |

[a]Reactions performed under standard reaction conditions (General procedure-Procedure G): Diazo compound **1.30** (0.2 mmol), aniline **1.23** (0.2 mmol), CuCl (5 mol%), NaBAr$^F$ (6 mol%), ligand (6 mol%), and activated spherical 3 Å mol sieves (50 mg) at room temperature. [b]NMR yield using Ph−TMS as internal standard [c]Determined using CSP-HPLC with a Chiralpak OD-H column. [d]**L1a**, [d]**L1b**, and **L1c** produced the opposite enantiomer.

Next, we examined the effect of the silicon substituents ($R^3$) on enantioselectivity (Table 1.5, entry 10). Introducing the less sterically demanding methyl groups on the silicon using **L3g** resulted in a significant decrease in enantioselectivity (89:11 vs 56:44 er). Unfortunately, the diphenyl aminoamide-silanol analog **L3h** was not isolatable due to its apparent instability. We were unable to access diphenyl substituents on the silicon **L3h** via either silane **1.17h** or *in-situ* chlorosilane (Scheme 1.12). Although **1.17h** was observed in >95% conversion in the NMR analysis of the unpurified mixture after work-up, purification on silica gel led to complete protodesilylation (Scheme 1.12A). Furthermore, attempts to generate the desired product via *in-situ* chlorosilane quenching did not prove successful (Scheme 1.12B).

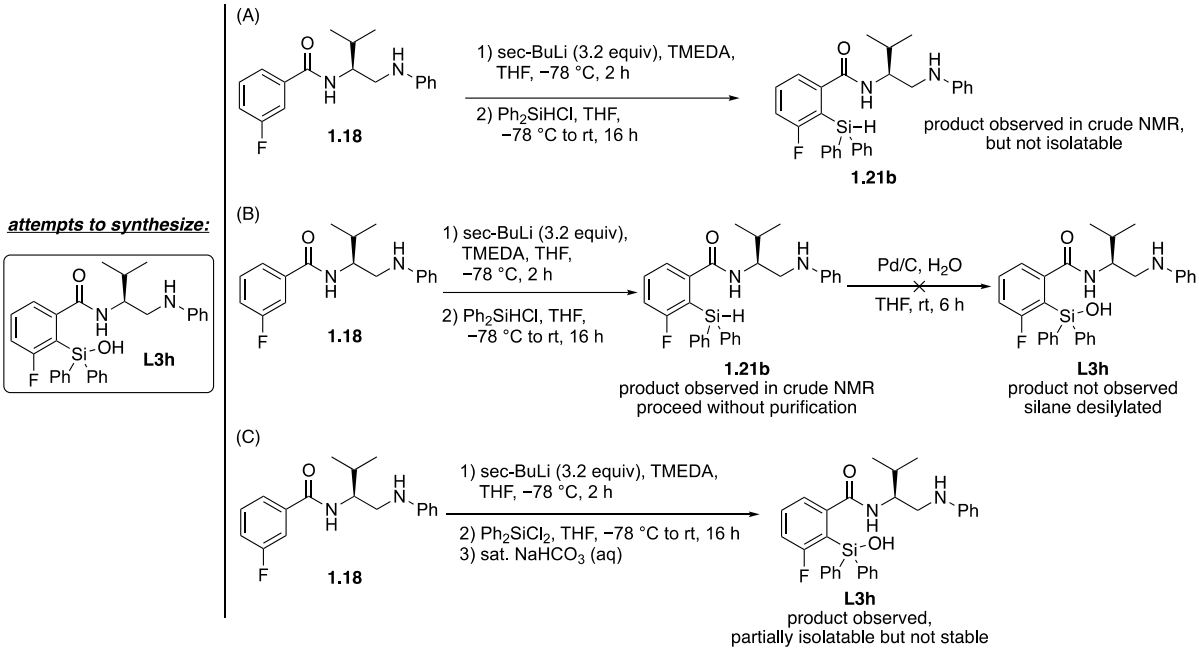



**Scheme 1.12.** Efforts toward the synthesis of (A) imidazoline silane **1.17h** and (B) imidazoline silanol **L2c**.

As we could not access the imidazoline silanol with diphenyl substituents on the silicon (Scheme 1.13), we decided to use the aminoamide as starting material to install the silicon. Our hypothesis was that the flexible amimoamide scaffold could prevent the protodesilylation during purification on silica gel. Upon the silylation of aminoamide using sec-BuLi, the aminoamide silane **1.21b** was the major product observed in the NMR analysis of the unpurified mixture (Scheme 1.13A); however, during purification on the silica column, it underwent protodesilylation, resulting in the loss of the silane moiety. Vigorous bubbling was observed when loading the unpurified material onto the silica gel, leading to the isolation of a quantitative amount of aminoamide **1.18**.

We also made attempts to use the unpurified aminoamide silane **1.21b** for hydrolysis (Scheme 1.13B). The reaction mixture, containing the aminoamide silane, only underwent filtration through Celite prior to hydrolysis. However, during the hydrolysis, the aminoamide silane underwent protodesilylation, and no silanol product was observed. Furthermore, we explored an alternative approach by quenching the *in-situ* generated aminoamide silylchloride with $NaHCO_3$ to synthesize the silanol **L3h** (Scheme 1.13C). Although we observed the desired silanol in the NMR analysis of the unpurified mixture, its isolation on silica gel led to protodesilylation. While we were able to isolate trace amounts of the desired silanol and confirm its structure using ASAP-ACPI-MS, the product underwent protodesilylation before

confirming the structure using NMR spectroscopy. Based on the challenges encountered in isolating the silanol **L3h**, it can be concluded that the compound is too unstable for use as a ligand.



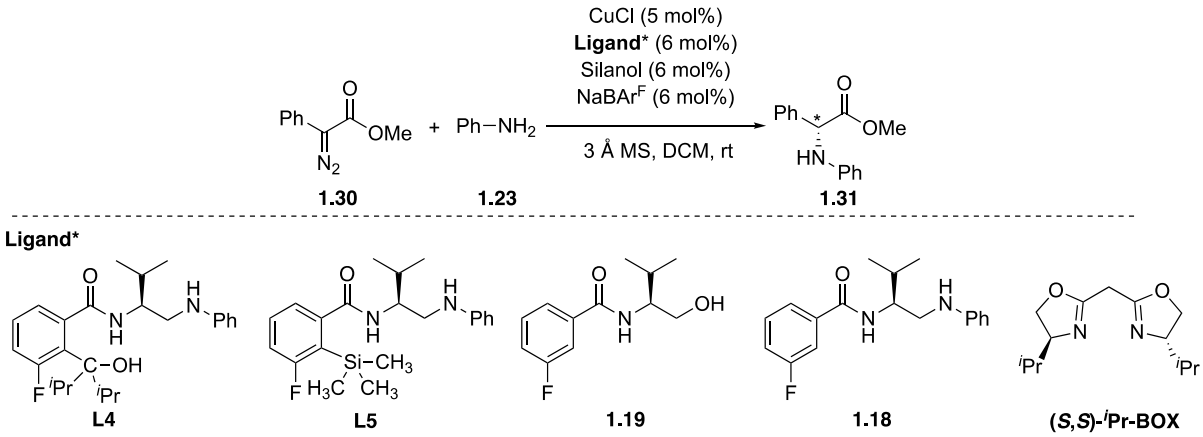

**Scheme 1.13.** Efforts toward the synthesis of aminoamide silanol **L3h**.

## IIIf. Silanol Ligand Validation and Control Experiments

Several control ligands were synthesized to verify the essential role of silanol and aminoamide functionalities in metal-ligand binding and their impact on the reactivity and selectivity of N−H insertion (Table 1.6). A carbon ligand analog (**L4**) with the silanol replaced by a trimethylsilyl group (**L5**) resulted in a complete loss of enantioselectivity for the insertion reaction. This highlights the essential role of the silanol group to coordinate with the metal center, imparting enantioselectivity. It is worth noting that the direct comparison ligand to the standard ligand **L3a** is to replace the diisopropylsilanol with diisopropylmethylsilyl; however, the ligand is inaccessible. The trimethyl silyl group serves as the next best alternative for comparing silanol (**L3g**) and trialkylsilyl (**L4**), showing a decrease in selectivity from 56:44 er to 50:50 er. Using β-hydroxy amide (**1.19**) and aminoamide (**1.18**) as ligands resulted in the formation of the N−H insertion product with good yield but exhibited almost no enantioselectivity (Table 1.6, entries 2−3). The widely employed BOX ligand displayed low enantioselectivity (Table 1.6, entry 4). In a competition experiment between the silanol ligand **L3b** and

aminoamide **1.18**, low reactivity was observed, suggesting that both ligands bind with the Cu, causing the deactivation of the catalyst (Table 1.6, entry 5). Moreover, using aminoamide **1.18** with an external silanol as a co-ligand increased the reactivity of N−H insertion. However, both reactions resulted in the formation of racemic insertion products (Table 1.6, entries 6−7). This observation highlights the significance of the silanol and the resultant metal siloxide in the ligand **L3a** in contributing significantly to the observed enantioselectivity.

**Table 1.6.** Silanol ligand validation of enantioselective N−H insertion of α-phenyl-α-diazoester with aniline




| Entry[a] | Ligand | Silanol | Time (h) | Yield (%)[b] | er[c] |
|---|---|---|---|---|---|
| 1 | **L4** | - | 1 | 48 | 50:50 |
| 2 | **L5** | - | 1 | 82 | 50:50 |
| 3 | **1.19** | - | 1 | 65 | 51:49 |
| 4 | **1.18** | - | 1 | 63 | 52:48 |
| 5 | **(*S*,*S*)-$^i$Pr-BOX**[d] | - | 2 | 38 | 52:48 |
| 6 | **1.18** | **L3a** | 16 | 35 | 59:41 |
| 7 | **1.18** | $^i$Pr$_2$PhSiOH | 0.5 | 80 | 50:50 |
| 8 | **1.18** | Ph$_3$SiOH | 0.5 | 78 | 50:50 |

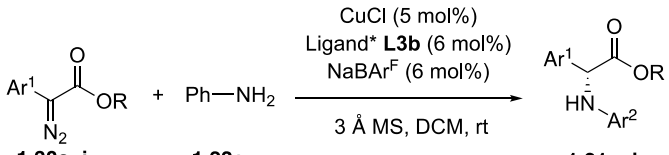
[a]Standard reaction conditions: **1.30** and **1.23** (0.2 mmol), CuCl (5 mol%), NaBAr$^F$ (6 mol%), ligand (6 mol%), silanol (6 mol%, if applicable), and spherical 3Å mol sieves (50 mg) in DCM (0.05 M) at room temperature. [b]Yield determined using NMR spectroscopy with Ph−TMS as internal standard. [c]Determined using CSP-HPLC analysis with a Chiralpak OD-H column. [d](*S*,*S*)-$^i$Pr-BOX, 2,2'-methylenebis[(4*S*)-4-isopropyl-2-oxazoline].

### IV. Scope of the Enantioselective N−H Insertion of Diazoesters with Anilines

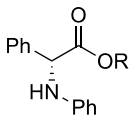
The N−H insertion reactions of α-aryl-α-diazoesters with various substituted anilines were performed (Scheme 1.14). The enantioselectivity (91:9 er) was not affected by steric bulk on the ester (**1.31a**−**7c**). Electronic effects at the insertion center were investigated by Kevin Blanco-Herrero (**1.31d**−**j**) across

substituted aryl diazo compounds. The general mechanism of N−H insertions involve an ylide intermediate (Figure 1.7B).[79,85] When the substituents stabilize the ylide, then the free ylide tends to form preferentially and the N−H insertion product is obtained with poor enantioselectivity. However, when the catalyst-associated ylide is favored, high enantioselectivity is usually observed. Based on these generally accepted hypotheses, a good correlation of the log (er) values of the products with the Hammett substituent constants[87] should be observed.[85,86] Higher enantioselectivity in the N−H insertion was observed with electron-donating substituents on the aryl diazo **1.30d**−**j**, which generally aligned with this trend.

**Scheme 1.14.** Scope of the enantioselective N−H insertion of α-aryl-α-diazoesters with aniline

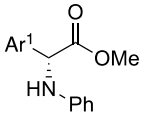



**1.30a–j** **1.23a** **1.31a–j**



**1.31a–c**

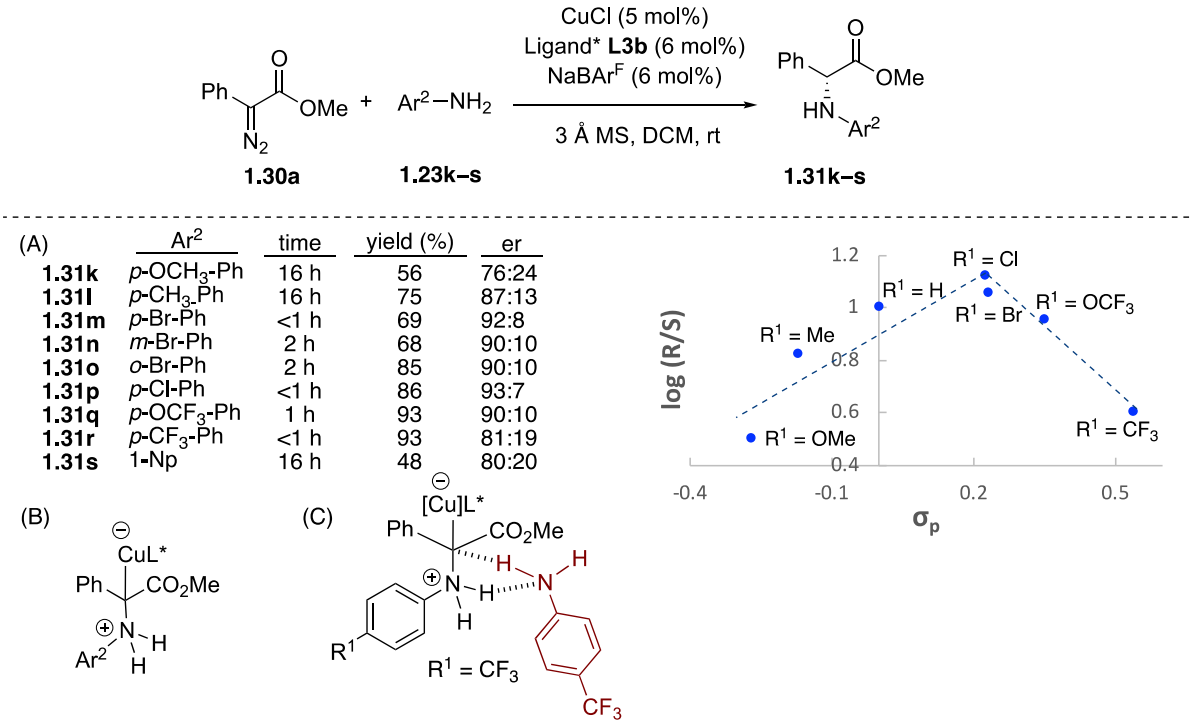
| | R | time | yield (%) | er |
|---|---|---|---|---|
| **1.31a** | $CH_3$ | 1 h | 80 | 91:9 |
| **1.31b** | Et | 1 h | 86 | 92:8 |
| **1.31c** | $^t$Bu | <1 h | 89 | 91:9 |



**1.31d–j**

| | $Ar^1$ | time | yield (%) | er |
|---|---|---|---|---|
| **1.31d** | *p*-$OCH_3$-Ph | 1 h | 53 | 90:10 |
| **1.31e** | *p*-$CH_3$-Ph | 1 h | 84 | 89:11 |
| **1.31f** | *m*-$CH_3$-Ph | 1 h | 76 | 90:10 |
| **1.31g** | *o*-$CH_3$-Ph | 1 h | 67 | 71:29 |
| **1.31h** | *p*-Br-Ph | 2 h | 72 | 86:14 |
| **1.31i** | *p*-F-Ph | 1 h | 92 | 82:18 |
| **1.31j** | 1-Np | 2 h | 87 | 82:18 |

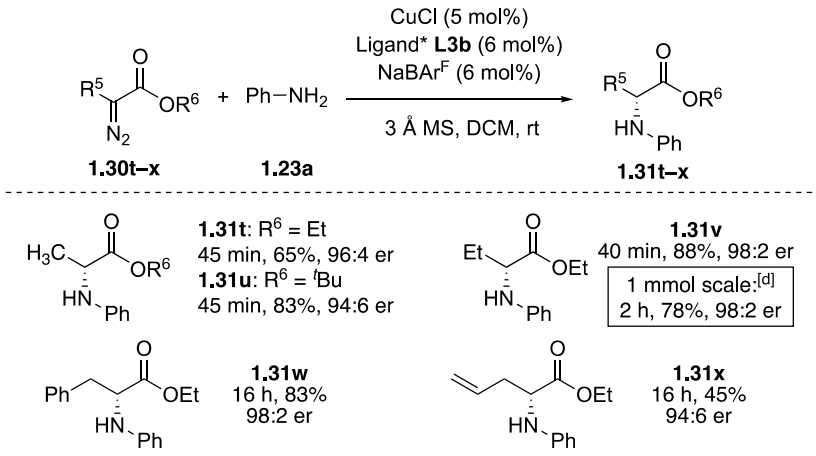
The electronic profile of the aniline reactant was also explored via a Hammett analysis (Figure 1.7, **1.31k**−**r**). Interestingly, a crossover point in the Hammett plot was observed (Figure 1.7A), suggesting a change in mechanism where the highly electron-withdrawing anilines (**1.23q** and **1.23r**) start functioning as achiral proton-shuttle catalysts (Figure 1.7C). This change led to a decrease in enantioselectivity.




| | $Ar^2$ | time | yield (%) | er |
|---|---|---|---|---|
| **1.31k** | *p*-$OCH_3$-Ph | 16 h | 56 | 76:24 |
| **1.31l** | *p*-$CH_3$-Ph | 16 h | 75 | 87:13 |
| **1.31m** | *p*-Br-Ph | <1 h | 69 | 92:8 |
| **1.31n** | *m*-Br-Ph | 2 h | 68 | 90:10 |
| **1.31o** | *o*-Br-Ph | 2 h | 85 | 90:10 |
| **1.31p** | *p*-Cl-Ph | <1 h | 86 | 93:7 |
| **1.31q** | *p*-$OCF_3$-Ph | 1 h | 93 | 90:10 |
| **1.31r** | *p*-$CF_3$-Ph | <1 h | 93 | 81:19 |
| **1.31s** | 1-Np | 16 h | 48 | 80:20 |

**Figure 1.7.** Scope of the enantioselective N−H insertion of α-phenyl-α-diazoesters with anilines. (A) Substituent effects of **1.31k**−**r** on enantiomeric ratio. (B) Ylide intermediate of the N−H insertion (C) Proposed *p*-$CF_3$-aniline-assisted proton-transfer mechanism.

Alkyl diazoesters also proceed in the N−H insertion reaction (Scheme 1.15) with good to excellent enantioselectivity (94:6 to 98:2 er). Steric bulk on the α-diazopropanoate slightly erodes the selectivity (96:4 vs 94:6 er) albeit with a higher yield of product (**1.31t** and **1.31u**). With ethyl 2-diazobutanoate, excellent yield and enantioselectivity (88%, 98:2 er) were observed (**1.31v**), and the reactivity and selectivity were unaffected by scaling up to a 1.0 mmol scale. With a phenyl at the β-position of the diazoester (**1.30w**), it is commonly observed that the β-H elimination competes with insertion to form conjugated products; however, using the silanol ligand in the catalysis leads to a high yield of the desired N−H insertion product (**1.31w**). An olefin functional group (**1.31x**) is tolerated under the reaction conditions with high selectivity observed, albeit only moderate yield, which is attributed to the competitive β-H elimination.




**Scheme 1.15.** Scope of the enantioselective N−H insertion of α-alkyl-α-diazoesters with aniline.

## IVa. Unsuccessful Amide/Amine Substrates

Unfortunately, when employing Boc-amide **1.32**, secondary amine **1.33**, or alkyl amines **1.34**, we observed either low enantioselectivity or no reaction at all (Figure 1.8A). These substrates are recognized as challenging due to specific reasons.[79,84,85,88] In the case of amides and secondary amines, they tend to stabilize the ylide intermediate, leading to the formation of racemic products (Figure 1.8B).[85,86] The stabilization of the ylide by these substituents allows the free ylide to form independently of CuL*, resulting in the reaction proceeding without CuL*, ultimately leading to racemic product formation. On the other hand, alkyl amines, due to their strong Lewis basicity, have the capability to interfere with the metal catalyst by binding with the metal. This interaction can hinder the formation of the metal carbenoid or replace CuL* on the ylide, disrupting the desired reaction pathway.[80,81]

The approach to tackle the challenges posed by Boc-amides **1.32** and secondary amines **1.33** involves destabilizing the ylide by experimenting with less polar solvents and exploring the use of donor/donor diaryl carbenes. Kevin Blanco-Herrero is currently investigating this approach. In the case of addressing the challenges related to using alkyl amines, our strategy revolves around enhancing the Lewis acidity of the silanol ligand. This can be achieved by incorporating more electron-deficient aryl groups or increasing the steric hindrance on the silicon substituent to prevent the binding of the amine substrate with [Cu]. A Franz group member, James Vesto, is currently synthesizing derivatives of these silanol ligands to pursue this strategy.

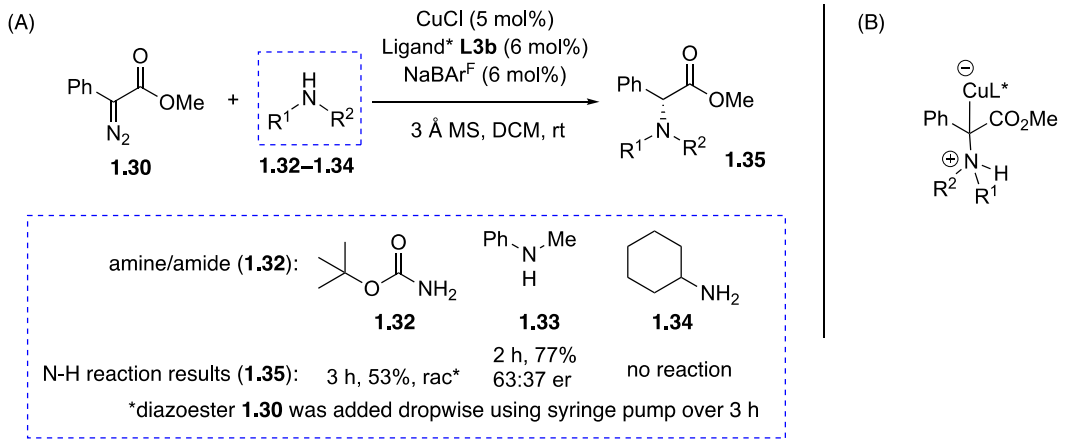
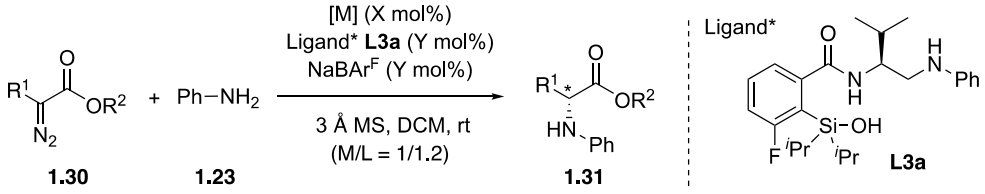



**Figure 1.8.** (A) Challenges of amide and amine substrates under the current conditions. (B) The ylide intermediate.

## IVb. Screening of Metal Catalysts for the Enantioselective N−H Insertion

Several metal catalysts were screened for the N−H insertion reaction (Table 1.7). The findings illustrate the compatibility and efficiency of aminoamide silanol **L3a** in inducing asymmetry using alternative transition metals in the enantioselective N−H insertion, with Pd and Ag showing the most encouraging initial outcomes. This suggests the potential versatility of the silanol ligand for various other organic transformations.

**Table 1.7.** Evaluation of different metal salts with silanol ligands for the enantioselective N−H insertion of α-phenyl-α-diazoesters with aniline




***conditions not yet optimized for different [M]***

| Entry[a] | $R^1$ | $R^2$ | [M] | X (mol%) | Y (mol%) | Time | Yield (%)[b] | er[c] |
|---|---|---|---|---|---|---|---|---|
| 1 | Ph | Me | $Pd(dba)_2$/$NaBAr^F$ | 2 | 2.4 | 45 min | 93 | 82:18 |
| 2 | Ph | Me | Ag(OAc)/$NaBAr^F$ | 10 | 12 | 16 h | 51 | 81:19 |
| 3 | Ph | Me | $Rh_2(OAc)_4$ | 2 | 2.4 | 30 min | 78 | 60:40 |
| 4 | Et | Et | $Pd(dba)_2$/$NaBAr^F$ | 2 | 2.4 | 30 min | 31 | 90:10 |

[a]Reactions performed under standard reaction conditions (General procedure-Procedure G): Diazo compound **1.30** and aniline **1.23** (0.2 mmol), M (X mol%), $NaBAr^F$ (Y mol%), ligand (Y mol%), and activated spherical 3 Å mol sieves (50 mg) at room temperature. [b]NMR yield using Ph−TMS as internal standard [c]Determined using CSP-HPLC with a Chiralpak OD-H column.

## V. Conclusions

In conclusion, this chapter discussed the synthesis and evaluation of novel aminoamide silanol ligands. The catalytic properties of the silanol ligands have been demonstrated through an enantioselective N−H insertion, which has received constant attention as an important method for the synthesis of chiral amine building blocks. Using a copper salt with a chiral aminoamide silanol ligand, we have obtained enantioenriched unnatural amino acid derivatives with up to 98:2 enantiomeric ratio and up to 88% yield. The control experiments validate the crucial role of silanol in the model N−H insertion reaction. This work represents the first case of a transition-metal catalyzed enantioselective reaction induced by chiral silanol-containing ligands. This pioneering use of silanol ligands in transition-metal catalysis provides valuable insights for the design and development of future ligands. Chapter 2 will extend the investigations, including additional mechanistic studies, examination of additional silanol ligands, and the distinct contributions of silanol ligands in catalysis.

## VI. Experimental Procedure and Characterization

### VIa. General Information

**Synthesis, Purification, and Analysis.** Dry DCM, THF, $Et_2O$ and PhMe were dispensed from a solvent purification system that passes solvent through two columns of dry neutral alumina prior to use. All other reagents, unless otherwise noted, were purchased from commercial sources.

Chlorosilanes were purchased from Gelest; CuCl, aniline, 3-fluorobenzoyl chloride, 3Å spherical molecular sieves, *sec*-BuLi (1.4 M in cyclohexane), chloroform were purchased from Sigma-Aldrich; $NaBAr^F$ was purchased from AA Blocks LLC; Pd/C (10 wt%, dry support) used for general ligand synthesis was purchased from Sigma-Aldrich (unless otherwise indicated in Scheme 1.5. ); L-tert-leucinol was purchased from Ambeed; L-valinol was purchased from Chem-Impex International, Inc.; Diazo **1.30** known compounds were synthesized based on previously published literature. $^1H$ NMR data was consistent with literature results.

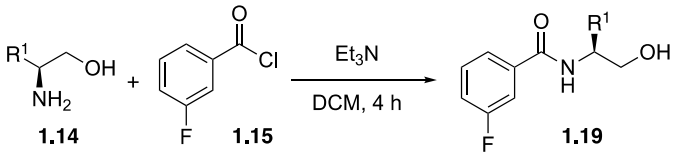
All reactions were performed in flame-dried and argon-purged glassware (including 8 mL KIMAX borosilicate glass vials fitted with rubber septa). Spherical 3Å molecular sieves were activated by flame-drying, then cooled under vacuum (<1 torr). Reactions were analyzed by thin layer chromatography (TLC) on EMD glass plates that were pre-coated with silica gel 60 F254. The reactions were purified by column chromatography using Acros silica gel 60 Å (0.035−0.070 mm).

Nuclear magnetic resonance (NMR) spectra obtained on Bruker Avance III equipped with Bruker CPTCI Cryoprobe (800 MHz for $^{1}H$; 200 MHz for $^{13}C$), 600 MHz Bruker Avance III equipped with Bruker CPTCI Cryoprobe (600 MHz for $^{1}H$; 151 MHz for $^{13}C$), Bruker Avance IIIHD Nanobay Spectrometer (400 MHz for $^{1}H$; 101 MHz for $^{13}C$; 376 MHz for $^{19}F$; 79 MHz for $^{29}Si$), 300 MHz Bruker Avance-NEO Spectrometer (300 MHz for $^{1}H$; 76 MHz for $^{13}C$; 283 MHz for $^{19}F$), and/or Varian VNMRS (600 MHz for $^{1}H$; 151 MHz for $^{13}C$). The $^{1}H$ spectral data are reported as follows: chemicals shifts were reported in parts per million downfield from tetramethylsilane internal standard on the δ scale, multiplicity (s, singlet; d, doublet; t, triplet; q, quartet; m, multiplet; dd, doublet of doublets, ddd, doublet of doublet of doublet, dddd, doublet of doublet of doublet of doublets and br, broadened), coupling constant (Hz), and integration. Apparent signals are indicated with app. and are used when signals with multiple couplings appear to form a certain peak type. Carbon NMR chemical shifts are reported in ppm from tetramethylsilane (TMS at 0.0 ppm) with the solvent reference employed as the internal standard (deuterochloroform ($CDCl_3$) at 77.16 ppm or deuterobenzene ($C_6D_6$) at 128.06 ppm). $^{19}F$ NMR chemical shifts were reported relative to external reference of trifluorotoluene in $CDCl_3$ at −62.86 ppm. Infrared data were collected using a Thermo Fisher Scientific Nicolet™ iS10 FT-IR spectrometer with a Smart iTX™ accessory (diamond ATR). Data was normalized to base peak in all cases. Crystal structures were measured on a Bruker APEX-II CCD. High-resolution mass spectra (HRMS) were acquired on a Thermo Fisher Scientific Electron LTQ-Orbitrap XL Hybrid mass spectrometer on positive ESI mode. Low-resolution mass spectra (LRMS) ASAP-ACPI-MS data were acquired on a Advion Interchim Scientific expression® Compact Mass Spectrometer (CMS) with Atmospheric Solids Analysis Probe (ASAP®). TLC-MS data were acquired on a Advion Plate Express™ combined with Advion CMS. Melting points were taken on an EZ-melting apparatus and were

uncorrected. High performance liquid chromatography (HPLC) data were obtained on Shimadzu LC-20AB system with CHIRALPAK® AD-H column (4.6 x 250 mm, 5 μm), CHIRALPAK® OD-H column (4.6 x 250 mm, 5 μm) or CHIRALPAK® AS column (4.6 x 250 mm, 5 μm) and Shimadzu SPD-M20A photodiode array detector. Each HPLC sample was eluted at a constant flow rate with isocratic hexanes/isopropanol system and 40 or 30 °C column oven temperature.

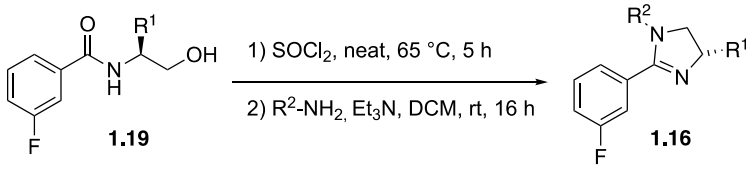
## VIb. General Procedure

**Procedure A: Synthesis of β-hydroxy amides (1.19)**




Amino alcohol (1.05 equiv) was added directly into a flame-dried round-bottom flask, dissolved in DCM (0.3 M) and purged with argon. Dry triethylamine was added (1.50 equiv) followed by the dropwise addition of 3-fluorobenzoyl chloride (1.00 equiv). The reaction was exothermic and the evolution of HCl gas could be observed. After 4 h of stirring the reaction was quenched with saturated 1M NaOH (30 mL). The aqueous phase was extracted with DCM (3 × 20 mL), and the combined organic phase was dried over $MgSO_4$, filtered, and concentrated *in vacuo*. The product was dried under high vacuum for over 6 h to fully remove triethylamine. The product was carried on without further purification.

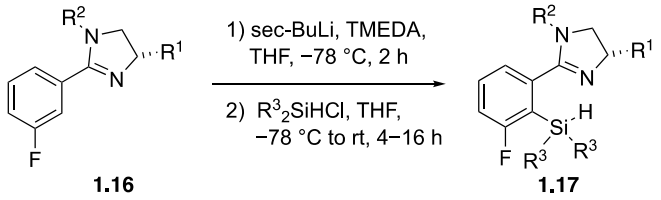
**Procedure B: Synthesis of imidazolines (1.16)**




The experimental procedure was adapted from a previous literature report.[46] Amide (1.0 equiv) was added by difference (directly from reagent bottle or flask to reaction vial) into a flame-dried microwave vial, followed by the addition of thionyl chloride (4.0 equiv). (Caution: HCl and $SO_2$ gas evolves as the reaction proceeds). The vial was capped with a septum and a balloon to collect the evolved gas. The

solution was stirred for 4−5 h at 65 °C. The resulting yellow unpurified oil mixture was transferred to a separate flame-dried 24/40 single-neck round bottom flask. (*Note*: A 24/40 neck round-bottom flask is used to increase the efficiency of $SOCl_2$ removal via rotary evaporation). Excess thionyl chloride was removed by rotary evaporation with the water-bath temperature set to 40 °C. (*Note*: Residual $SOCl_2$ must be removed to avoid reacting with $Et_3N$ in the next step, which causes the reaction mixture to turn a dark brown color; leading to lower yields). The resulting unpurified dichloride was dissolved in 30 mL of dry DCM (30 mL). To this solution, dry triethylamine (3.0 equiv) was added, followed by the addition of $R^2$–$NH_2$ (1.2 equiv). The resulting orange reaction mixture was stirred at room temperature for 16 h. Afterward, the solution was stirred with 20 mL of 2.5 M NaOH solution for 10 min to remove excess aniline. The aqueous phase was then extracted with DCM (2 × 20 mL). The combined organic phase was dried over $MgSO_4$, filtered, and concentrated *in vacuo*. The resulting reaction mixture was purified using flash column chromatography ($SiO_2$, hexanes/EtOAc/$Et_3N$, 140:20:3 *v*/*v*/*v*).

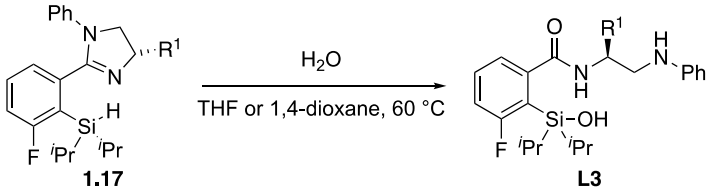
**Procedure C: Synthesis of imidazoline silanes (1.17)**




The imidazoline (1.0 equiv) was added directly into a flame-dried round-bottom flask, dissolved in THF (0.15 M), and purged under argon for 5 min. The reaction was cooled to –78 °C and tetramethylethylenediamine (TMEDA) (2.0 equiv, unless otherwise indicated) was added followed by the dropwise addition of *sec*-butyl lithium (1.4 M in cyclohexane, 2.0 equiv, unless otherwise indicated). The reaction was stirred at –78 °C for 2 h and then chlorosilane (2.1 equiv, unless otherwise indicated) was added. The reaction was stirred for an additional 6−16 h while gradually reaching room temperature. The solution was quenched with saturated aq. $NaHCO_3$ (10 mL) and the aqueous phase was extracted with diethyl ether (3 × 5 mL). The combined organic phase was dried over $MgSO_4$, filtered, and concentrated *in vacuo*. The reaction mixture was purified using flash column chromatography ($SiO_2$, hexanes/EtOAc/$Et_3N$, 140:20:3 *v*/*v*/*v*) to yield the corresponding silane (**1.17**).

**Procedure D: Synthesis of aminoamide-silanols (L3)**

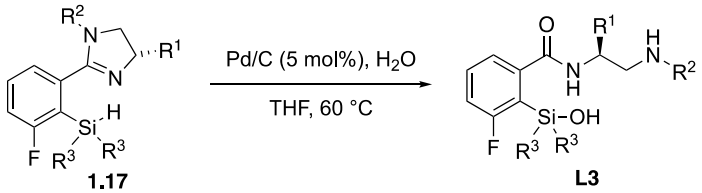
Method A: Metal-free hydrolysis




In a flask, the silane (1.0 equiv) was dissolved in THF or 1,4-dioxane (0.15 M, unless otherwise indicated). Then, deionized water (10 equiv) was added. The reaction was capped and stirred at 60 °C (unless otherwise indicated). The reaction was monitored using TLC and/or $^{19}$F NMR spectroscopy for the consumption of starting material silane. TLC conditions: hexanes/EtOAc/$Et_3N$, 7:1:0.15 v/v/v. Once the silane was fully consumed, the reaction was diluted with $Et_2O$, dried over $MgSO_4$, filtered, and concentrated in vacuo. The reaction mixture was purified using flash chromatography ($SiO_2$, hexanes/EtOAc/$Et_3N$, 140:20:1.5 v/v/v) to yield silanol.

(*Note*: We obtained consistent results with both THF and 1,4-dioxane. However, for longer reaction times, 1,4-dioxane is preferred to prevent solvent evaporation).

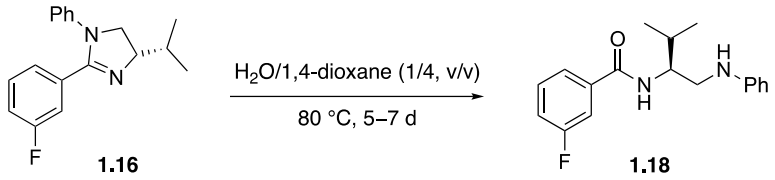
Method B: Pd-catalyzed hydrolysis




In a flask, the silane and imidazoline mixture (1.0 equiv) was dissolved in THF (0.15 M, unless otherwise indicated). Pd/C (10 wt% Pd on C, 0.05 equiv) was added followed by the addition of deionized water (10 equiv). (Caution: $H_2$ gas evolves as the reaction proceeds.) The reaction was capped with a septum equipped with a needle and was stirred at 60 °C (unless otherwise indicated). The reaction was monitored using TLC and/or $^{19}$F NMR spectroscopy for the consumption of starting material silane. TLC conditions: hexanes/EtOAc/$Et_3N$, 7:1:0.15 *v/v/v*. Once silane was fully consumed, the reaction was diluted with $Et_2O$ and filtered through a pad of Celite to remove Pd/C. The filtrate was dried over

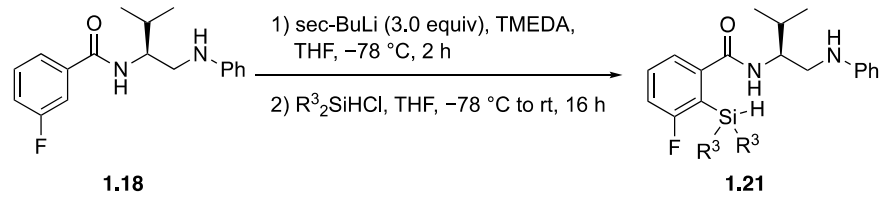
$MgSO_4$, filtered, and concentrated *in vacuo*. The reaction mixture was purified using flash chromatography ($SiO_2$, hexanes/EtOAc/$Et_3N$, 140:20:1.5 *v*/*v*/*v*) to yield silanol.

**Procedure E: Synthesis of aminoamide from imidazoline**




To a flask, the imidazoline starting material was dissolved in 1,4-dioxane/$H_2O$ (0.4 M, 4:1 *v*/*v*) and the reaction mixture was heated to 80 ˚C. Typically, the reaction required approximately 5−7 days for complete consumption of the starting material when performed in the absence of Pd/C and without a silane/silanol. The progress of the reaction was monitored by TLC to track the consumption of the imidazoline starting material. TLC conditions: hexanes/EtOAc/$Et_3N$, 7:1:0.15 *v*/*v*/*v*. Once the imidazoline was fully consumed, the reaction mixture was diluted with $Et_2O$ and extracted with brine. The combine organic layer was dried over $MgSO_4$, filtered, and concentrated *in vacuo*. The reaction mixture was purified using flash column chromatography ($SiO_2$, hexanes/EtOAc/$Et_3N$, 140:40:3 *v*/*v*/*v*) to yield the corresponding aminoamide.

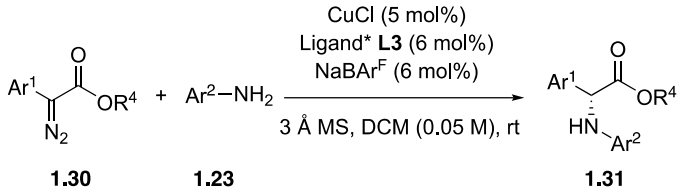
**Procedure F: Synthesis of aminoamide silane from aminoamide**




The aminoamide (1.0 equiv) was dissolved in THF (0.15 M) and purged under argon for 5 min. The reaction was cooled to –78 °C and tetramethylethylenediamine (TMEDA) (3.0 equiv, unless otherwise indicated) was added followed by the dropwise addition of *sec*-butyl lithium (1.4 M in cyclohexane, 3.0 equiv, unless otherwise indicated). The reaction was stirred at –78 °C for 2 h and then chlorosilane (3.1 equiv, unless otherwise indicated) was added. The reaction was stirred for an additional 6−16 h while gradually reaching room temperature. The solution was quenched with saturated aq. $NaHCO_3$ (10

mL) and the aqueous phase was extracted with diethyl ether (3 × 5 mL). The combine organic layer was dried over $MgSO_4$, filtered, and concentrated *in vacuo*. The reaction mixture was purified using flash column chromatography ($SiO_2$, hexanes/EtOAc/$Et_3N$, 140:20:3 *v*/*v*/*v*) to yield the corresponding silane.

**Procedure G: Procedure for the enantioselective N−H insertions**



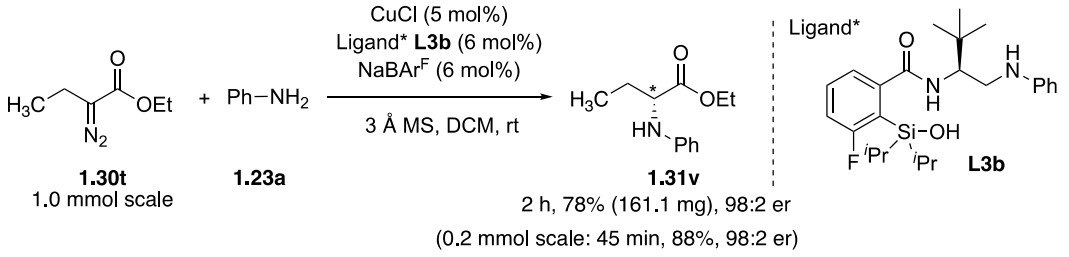

A 7 mL vial containing 50 mg of 3Å molecular sieves (MS) and a stir bar was flame-dried under high vacuum (<1 torr). After the vial cooled to room temperature, it was purged with argon. CuCl (1.0 mg, 0.010 mmol, 0.050 equiv), $NaBAr^F$ (10.6 mg, 0.012 mmol, 0.060 equiv) and the corresponding ligand (0.06 equiv, 0.012 mmol) were added by difference measurement (directly from reagent bottle or flask to the reaction vial). The vial was re-purged with argon three times and capped with a septum and an Ar-balloon. Anhydrous DCM (2.0 mL) was then added, and the resulting mixture was stirred (~270 rpm to avoid molecular sieves being pulverized) for 2 h at room temperature. In a separate 7 mL vial, 50 mg of 3Å molecular sieves was added and flame-dried under high vacuum (<1 torr). After the vial cooled to room temperature, it was purged with argon and capped with a septum and an Ar-balloon. The corresponding diazo ester (1.0 equiv, 0.2 mmol), amine (1.0 equiv, 0.2 mmol) and anhydrous DCM (2.0 mL) were added into the vial. This solution was drawn into a 3-mL syringe with long needle and added dropwise into the stirring solution over 2 min. The appearance of $N_2$ gas bubbles during the reaction is sometimes observed, and this can be taken as an indication of good reactivity. The reaction mixture was stirred at room temperature and the reaction progress was monitored using TLC. TLC conditions: hexanes/EtOAc, 9.5:0.5 *v*/*v*. After the diazo ester was fully consumed or the reaction time reached 16 h, the mixture was filtered through a silica plug (~0.5 cm of silica gel in a Pasteur pipette), washed with ~1 mL DCM, and evaporated *in vacuo*. The products were purified using flash column chromatography ($SiO_2$, hexanes/EtOAc, 95:5 *v*/*v*) to furnish pure chiral amino acid derivatives.

**Procedure H: Procedure for HPLC Analysis**

The silica-filtered reaction mixture was spotted onto a TLC plate (4 × 4 cm). The plate was placed in a TLC chamber to develop, and the product band was etched off the plate with a razor blade. The loose silica was washed with hexanes/isopropanol (IPA) (0.6 mL, 70:30 *v/v*) and filtered through glass fiber to furnish HPLC samples.

**Note:** *The enantiomeric ratios were not affected by using different HPLC sample preparation methods. The three different HPLC sampling methods are listed: a) etched-off from TLC plate described above; b) filtered unpurified reaction mixtures diluted with hexanes/IPA (70:30 v/v); c) purified product after flash column chromatography diluted with hexanes/IPA (70:30 v/v).*

**Procedure I: Procedure for 1 mmol-scale enantioselective N−H insertions of diazo 1.30t and aniline 1.23a**

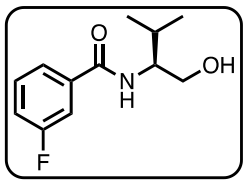



A 50 mL round bottom flask containing 250 mg of 3Å spherical molecular sieves (MS) and a stir bar was flame-dried under high vacuum (<1 torr). After the vial cooled to room temperature, it was purged with argon. CuCl (5.0 mg, 0.050 mmol, 0.05 equiv), $NaBAr^F$ (53 mg, 0.060 mmol, 0.06 equiv) and silanol-containing ligand **L3b** (26 mg, 0.060 mmol, 0.06 equiv) were added. The vial was re-purged with argon three times and capped with a septum and an Ar-balloon. Anhydrous DCM (10 mL) was then added, and the resulting mixture was stirred (~360 rpm to avoid molecular sieves being pulverized) for 2 h at room temperature. In a separate 20 mL vial, 250 mg of 3Å molecular sieves was added and flame-dried under high vacuum (<1 torr). After the vial cooled to room temperature, it was purged with argon and capped with a septum and an Ar-balloon. The corresponding diazo ester **1.30t** (142 mg, 1.00

mmol, 1.00 equiv), amine (93 mg, 1.00 mmol, 1.00 equiv) and anhydrous DCM (10 mL) were added into the vial. This solution was drawn into a 12-mL syringe with long needle and added dropwise into the stirring solution over 5 min. The reaction mixture was stirred at room temperature and the reaction progress was monitored using TLC. After diazo ester was fully consumed, the mixture was filtered through a silica plug (~1 cm of silica gel in a Pasteur pipette), washed with ~3 mL DCM, and evaporated *in vacuo*. The products were purified using flash chromatography to furnish pure chiral amine (88%, 161 mg).

## VIc. Characterization Data

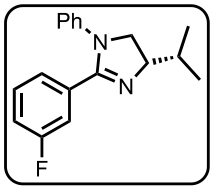
**(*S*)-3-fluoro-*N*-(1-hydroxy-3-methylbutan-2-yl)benzamide (1.19a)**




Synthesized according to the General Procedure A using L-valinol (1.50 g, 13.0 mmol), 3-fluorobenzoyl chloride (1.50 mL, 12.3 mmol) and $Et_3N$ (2.60 mL, 18.5 mmol). The product was purified using extraction and dried under high vacuum to give the β-hydroxy amide (**1.14a**) as a white powder (2.77 g, >99%).

$^1$H NMR (400 MHz, $CDCl_3$) δ 7.57 – 7.45 (m, 2H), 7.39 (td, $J$ = 8.0, 5.5 Hz, 1H), 7.19 (td, $J$ = 8.0, 2.7 Hz, 1H), 6.42 (s, 1H), 3.99 – 3.89 (m, 1H), 3.80 (d, $J$ = 4.3 Hz, 2H), 2.67 (s, 1H), 2.10 – 1.93 (m, $J$ = 6.9 Hz, 1H), 1.03 (d, $J$ = 6.8 Hz, 3H), 1.01 (d, $J$ = 6.8 Hz, 3H); $^{13}$C{$^1$H} NMR (101 MHz, $CDCl_3$) δ 167.1 (d, $^4J_{C,F}$ = 2.2 Hz), 162.9 (d, $^1J_{C,F}$ = 248.0 Hz), 137.0 (d, $^3J_{C,F}$ = 6.6 Hz), 130.4 (d, $^3J_{C,F}$ = 8.1 Hz), 122.5 (d, $^4J_{C,F}$ = 2.9 Hz), 118.7 (d, $^2J_{C,F}$ = 21.3 Hz), 114.5 (d, $^2J_{C,F}$ = 22.7 Hz), 63.8, 57.6, 29.4, 19.7, 19.2; $^{19}$F{$^1$H} NMR (376 MHz, $CDCl_3$): δ −111.71; HRMS (ESI/Orbitrap) m/z: $[M + H]^+$ Calcd for $C_{12}H_{17}FNO_2$ 226.1243; Found 226.1244.

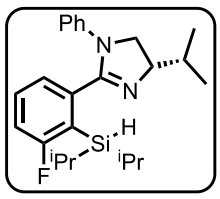
**(*S*)-2-(3-fluorophenyl)-4-isopropyl-1-phenyl-4,5-dihydro-1*H*-imidazole (1.16a)**




Synthesized according to the General Procedure B for imidazoline formation using β-hydroxy amide (**1.16a**) (1.50 g, 6.66 mmol), thionyl chloride (1.90 mL, 26.6 mmol), $Et_3N$ (2.80 mL, 20.0 mmol) and aniline (0.73 mL, 7.8 mmol). The reaction mixture was purified using flash column chromatography ($SiO_2$, hexanes/EtOAc/$Et_3N$, 7:1:0.15 *v*/*v*/*v*) to give the imidazoline as a yellow oil (1.73 g, 92%).

$^1$H NMR (400 MHz, $CDCl_3$): δ 7.27 − 7.14 (m, 5H), 7.07−6.96 (m, 2H), 6.78 − 6.75 (m, 2H), 4.14 − 4.02 (m, 2H), 3.73 − 3.61 (m, 1H), 1.98 − 1.85 (m, 1H), 1.05 (d, $J$ = 6.7 Hz, 3H), 0.96 (d, $J$ = 6.7 Hz, 3H). $^{13}$C{$^1$H} NMR (101 MHz, $CDCl_3$): δ 162.5 (d, $^1J_{C,F}$ = 246.5 Hz), 160.4 (d, $^4J_{C,F}$ = 2.6 Hz), 143.0, 133.8 (d, $^3J_{C,F}$ = 8.1 Hz), 129.9 (d, $^3J_{C,F}$ = 8.1 Hz), 128.9, 124.6 (d, $^4J_{C,F}$ = 2.9 Hz), 123.6, 122.6, 116.9 (d, $^2J_{C,F}$ = 21.3 Hz), 115.9 (d, $^2J_{C,F}$ = 23.1 Hz), 70.4, 56.6, 33.2, 19.00, 18.0; $^{19}$F{$^1$H} NMR (376 MHz, $CDCl_3$): δ −112.71; IR (neat) 2958, 2871, 1594, 1576, 1495, 1444, 1306, 1207, 847, 754, 694 cm$^{-1}$; HRMS (ESI/Orbitrap) m/z: $[M + H]^+$ Calcd for $C_{18}H_{20}FN_2$ 283.1610; Found 283.1595.

**(*S*)-2-(2-(diisopropylsilyl)-3-fluorophenyl)-4-isopropyl-1-phenyl-4,5-dihydro-1*H*-imidazole (1.17a)**

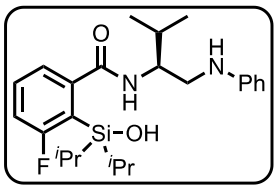



Synthesized according to the General Procedure C for silane formation using imidazoline (**1.16a**) (980 mg, 3.54 mmol), *sec*-BuLi (1.4 M in cyclohexane, 3.0 mL, 4.3 mmol), TMEDA (0.63 mL, 4.3 mmol) and diisopropylchlorosilane (0.79 mL, 4.6 mmol). The reaction mixture was purified via flash column chromatography (hexanes/EtOAc/$Et_3N$, 7:1:0.15 *v*/*v*/*v*) to yield the silane as a pale yellow oil (1.24 g, 88%).

$^{1}$H NMR (400 MHz, $CDCl_3$): δ 7.37 (ddd, *J* = 8.2, 7.5, 6.0 Hz, 1H), 7.24 (d, *J* = 6.6 Hz, 1H), 7.10 – 6.97 (m, 3H), 6.88 – 6.78 (m, 1H), 6.68 – 6.58 (m, 2H), 4.03 – 3.88 (m, 2H), 3.82 – 3.68 (m, 2H), 1.99 – 1.84 (m, 1H), 1.28 – 1.14 (m, 2H), 1.13 (d, *J* = 6.7 Hz, 3H), 1.05 – 0.93 (m, 9H), 0.80 (d, *J* = 7.4 Hz, 3H), 0.69 (d, *J* = 7.4 Hz, 3H); $^{13}$C{$^{1}$H} NMR (76 MHz, $CDCl_3$) δ 167.1 (d, $^{1}J_{C,F}$ = 240.3 Hz), 160.6 (d, $^{4}J_{C,F}$ = 2.5 Hz), 141.9 (d, $^{3}J_{C,F}$ = 12.0 Hz), 141.0, 131.7 (d, $^{3}J_{C,F}$ = 9.3 Hz), 128.7, 125.6 (d, $^{4}J_{C,F}$ = 2.7 Hz), 122.0, 121.8 (d, $^{2}J_{C,F}$ = 34.6 Hz), 119.4, 115.5 (d, $^{3}J_{C,F}$ = 26.7 Hz), 70.8, 54.5, 33.6, 19.8, 19.0, 19.0, 18.9, 11.6 (d, $^{4}J_{C,F}$ = 2.2 Hz), 11.3 (d, $^{4}J_{C,F}$ = 2.2 Hz); $^{19}$F{$^{1}$H} NMR (376 MHz, $CDCl_3$): δ −95.99; $^{29}$Si{$^{1}$H} NMR (79 MHz, $CDCl_3$) δ 2.05 (d, $^{3}J_{Si,F}$ = 3.3 Hz); IR (neat) 2941, 2862, 2127, 1595, 1498, 1379, 1223, 1003, 879, 796 cm$^{-1}$; HRMS (ESI/Orbitrap) m/z: $[M + H]^+$ Calcd for $C_{24}H_{34}FN_2Si$ 394.2475; Found 397.2459.

***Note:*** *The silane (**1.17a**) was found to be unstable and completely converted into aminoamide silanol (**L3a**) under air in 3 months. However, stored at -20 °C it remained stable for >3 months with minimal decomposition.*

**(*S*)-3-fluoro-2-(hydroxydiisopropylsilyl)-*N*-(3-methyl-1-(phenylamino)butan-2-yl)benzamide (L3a)**




**Method A:**

Synthesized according to the General Procedure D (Method A) for silanol formation using the silane (**1.17a**) from previous step (954 mg, 2.41 mmol) and $H_2O$ (434 µL, 24.1 mmol) in THF (16 mL, 0.15 M) at 60 °C for 53 h. The reaction mixture was purified using flash column chromatography ($SiO_2$, hexanes/EtOAc/$Et_3N$, 140:20:1.5 *v*/*v*/*v*) to give the silanol (**L3a**) as a crystalline white solid (544 mg, 54%).

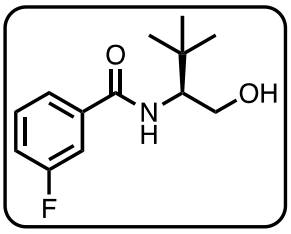
**Method B:**

Synthesized according to the General Procedure D (Method B) for silanol formation using the silane (**1.17a**) mixture from previous step (1.02 g, 2.58 mmol), Pd/C (10 wt%, 137.2 mg, 0.129 mmol) and $H_2O$ (0.46 mL, 25.8 mmol) in THF (0.15 M) at 60 °C for 6 h. The reaction mixture was purified using flash column chromatography ($SiO_2$, hexanes/EtOAc/$Et_3N$, 140:20:1.5 *v*/*v*/*v*) to give the silanol (**L3a**) as a crystalline white solid (622 mg, 56%).

$^1$H NMR (400 MHz, $CDCl_3$) δ 7.39 – 7.30 (m, 1H), 7.21 – 7.14 (m, 2H), 7.11 (d, *J* = 7.4 Hz, 1H), 7.10 – 7.03 (m, 1H), 6.77 – 6.60 (m, 3H), 5.92 (d, *J* = 9.6 Hz, 1H), 4.25 (dddd, *J* = 9.6, 9.6, 6.0, 3.8 Hz, 1H), 3.97 (br, 2H), 3.39 (dd, *J* = 12.3, 3.8 Hz, 1H), 3.17 (dd, *J* = 12.3, 9.6 Hz, 1H), 2.07 – 1.92 (m, 1H), 1.35 – 1.25 (m, 2H), 1.14 – 1.02 (m, 12H), 0.99 (dd, *J* = 7.4, 1.0 Hz, 3H), 0.97 – 0.90 (m, 3H); $^{13}$C{$^1$H} (101 MHz, $CDCl_3$) δ 172.9 (d, $^4J_{C,F}$ = 2.6 Hz), 166.8 (d, $^1J_{C,F}$ = 240.3 Hz), 148.4, 145.3 (d, $^3J_{C,F}$ = 11.4 Hz), 131.5 (d, $^3J_{C,F}$ = 9.2 Hz), 129.4, 122.9 (d, $^2J_{C,F}$ = 34.8 Hz), 122.8 (d, $^4J_{C,F}$ = 2.6 Hz), 117.8, 116.8 (d, $^2J_{C,F}$ = 27.9 Hz), 113.0, 55.4, 46.4, 31.1, 19.8, 18.5, 17.84 (d, $^5J_{C,F}$ = 2.6 Hz), 17.81 (d, $^5J_{C,F}$ = 2.2 Hz), 17.42, 17.38, 14.2 (d, $^4J_{C,F}$ = 2.0 Hz), 13.8 (d, $^4J_{C,F}$ = 2.9 Hz); $^{19}$F{$^1$H} NMR (376 MHz, $CDCl_3$): δ −94.81; $^{29}$Si{$^1$H} NMR (79 MHz, $CDCl_3$) δ 9.06 (d, $^3J_{Si,F}$ = 4.8 Hz). IR (neat) 3356, 3265, 2943, 2866, 1635, 1603, 1508, 1221, 849, 748 cm$^{-1}$; HRMS (ESI/Orbitrap) m/z: [M – $H_2O$ + H]$^+$ Calcd for $C_{24}H_{34}FN_2OSi$ 413.2424; Found 413.2413; mp: 94 −96 °C; $R_f$ = 0.20 (hexanes/EtOAc/$Et_3N$, 7:1:0.15 *v*/*v*/*v*); HPLC analysis: Chiralpak AD-H column, n-hexane/2-propanol = 97/3, 1.0 mL/min, λ = 254 nm, 40 °C, $t_R$ (*S*, major) = 6.1 min; $t_R$ (*S*, minor) = 8.4 min, >99:1 er.

***Note:*** *The silanol was found to be stable to air for >30 months with minimal decomposition and no loss of catalytic activity.*

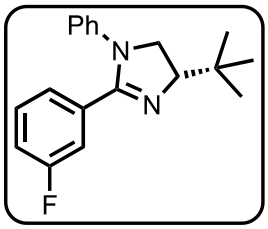
**(*S*)-3-fluoro-*N*-(1-hydroxy-3,3-dimethylbutan-2-yl)benzamide (1.19b)**




Synthesized according to the General Procedure A using L-tert-leucinol (1.51 g, 13.0 mmol), 3-fluorobenzoyl chloride (1.50 mL, 12.3 mmol) and $Et_3N$ (2.60 mL, 18.5 mmol). The product was purified using extraction and dried under high vacuum to give the β-hydroxy amide as a white powder (2.95 g, >99%).

$^1$H NMR (400 MHz, $CDCl_3$) δ 7.58 – 7.48 (m, 2H), 7.43 (ddd, *J* = 8.0, 7.8, 5.6 Hz, 1H), 7.22 (dddd, *J* = 8.3, 8.3, 2.6, 1.0 Hz, 1H), 6.27 (d, *J* = 7.9 Hz, 1H), 4.05 (ddd, *J* = 7.9, 7.2, 3.5 Hz, 1H), 3.95 (dd, *J* = 11.2, 3.5 Hz, 1H), 3.71 (dd, *J* = 11.2, 7.2 Hz, 1H), 2.23 (s, 1H), 1.04 (s, 9H); $^{13}$C{$^1$H} NMR (101 MHz, $CDCl_3$) δ 167.5 (d, $^4J_{C,F}$ = 2.6 Hz), 162.9 (d, $^1J_{C,F}$ = 248.0 Hz), 137.1 (d, $^3J_{C,F}$ = 7.0 Hz), 130.5 (d, $^3J_{C,F}$ = 8.1 Hz), 122.5 (d, $^4J_{C,F}$ = 2.9 Hz), 118.7 (d, $^2J_{C,F}$ = 21.3 Hz), 114.6 (d, $^2J_{C,F}$ = 23.1 Hz), 63.2, 60.0, 34.1, 27.2; $^{19}$F{$^1$H} NMR (376 MHz, $CDCl_3$) δ –111.74; IR (neat): 3296, 3076, 2962, 2871, 1637, 1585, 1541, 1221, 802, 679 cm$^{-1}$; HRMS (ESI/Orbitrap) m/z: $[M + H]^+$ Calcd for $C_{13}H_{19}FNO_2$ 240.1400; Found 240.1403; mp: 100 −102 °C.

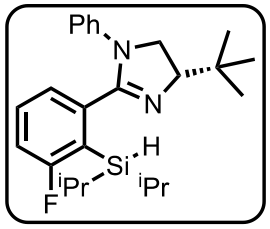
**(*S*)-4-(*tert*-butyl)-2-(3-fluorophenyl)-1-phenyl-4,5-dihydro-1*H*-imidazole (1.16b)**




Synthesized according to the General Procedure B for imidazoline formation using β-hydroxy amide (**1.19b**) (900 mg, 3.76 mmol), thionyl chloride (1.10 mL, 13.4 mmol), $Et_3N$ (1.58 mL, 10.1 mmol), and aniline (0.41 mL, 4.0 mmol). The reaction mixture was purified using flash column chromatography ($SiO_2$, hexanes/EtOAc/$Et_3N$, 140:20:3.0 *v*/*v*/*v*) to give the imidazoline as a yellow oil (699 mg, 63%).

$^{1}$H NMR (400 MHz, $CDCl_3$) δ 7.30 – 7.21 (m, 3H), 7.20 – 7.12 (m, 2H), 7.08 – 6.95 (m, 2H), 6.80 – 6.72 (m, 2H), 4.13 (dd, *J* = 11.0, 9.5 Hz, 1H), 3.99 (dd, *J* = 11.0, 7.6 Hz, 1H), 3.67 (dd, *J* = 9.5, 7.5 Hz, 1H), 0.98 (s, 9H); $^{13}$C{$^{1}$H} NMR (101 MHz, $CDCl_3$) δ 162.5 (d, *J* = 246.1 Hz), 160.5 (d, *J* = 2.6 Hz), 143.1, 133.8 (d, *J* = 7.7 Hz), 129.9 (d, *J* = 8.1 Hz), 128.9, 124.6 (d, *J* = 2.9 Hz), 123.7, 122.8, 116.9 (d, *J* = 21.3 Hz), 115.9 (d, *J* = 22.7 Hz), 74.0, 55.5, 34.4, 26.0; $^{19}$F{$^{1}$H} NMR (376 MHz, $CDCl_3$) δ –112.73; HRMS (ESI/Orbitrap) m/z: $[M + H]^+$ Calcd for $C_{19}H_{22}FN_2$ 297.1767; Found 297.1760; mp: 84−86 °C.

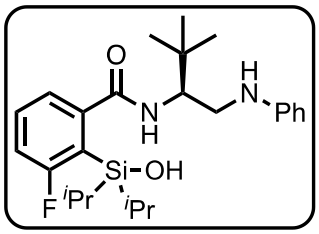
**(*S*)-4-(*tert*-butyl)-2-(2-(diisopropylsilyl)-3-fluorophenyl)-1-phenyl-4,5-dihydro-1*H*-imidazole (1.17b)**




Synthesized according to the General Procedure C for silane formation using imidazoline (**1.16b**) (600 mg, 2.03 mmol), *sec*-BuLi (1.4 M in cyclohexane, 1.74 mL, 2.43 mmol), TMEDA (0.45 mL, 2.6 mmol) and diisopropylchlorosilane (0.36 mL, 2.43 mmol). The reaction mixture was purified via flash column chromatography (140:20:3.0 *v*/*v*/*v*) to yield the silane as a pale yellow oil (0.731 g, 88%).

$^{1}$H NMR (400 MHz, $CDCl_3$) δ 7.43 – 7.33 (m, 1H), 7.31 – 7.26 (m, 1H), 7.10 – 6.98 (m, 3H), 6.84 (dd, *J* = 7.4, 7.4 Hz, 1H), 6.67 – 6.60 (m, 2H), 4.03 – 3.81 (m, 3H), 3.78 (ddd, *J* = 3.4, 3.4, 3.3 Hz, 1H), 1.26 – 1.16 (m, 1H), 1.18 – 1.07 (m, 1H), 1.04 (s, 9H), 1.04 – 0.94 (m, 6H), 0.78 (d, *J* = 7.4 Hz, 3H), 0.72 (d, *J* = 7.5 Hz, 3H); $^{13}$C{$^{1}$H} NMR (101 MHz, $CDCl_3$) δ 167.2 (d, *J* = 240.3 Hz), 160.8, 141.2, 131.7 (d, *J* = 9.2 Hz), 128.7, 125.7 (d, *J* = 2.9 Hz), 122.0, 122.0 (d, *J* = 34.8 Hz), 119.6, 115.5 (d, *J* = 26.8 Hz), 74.2, 52.7, 34.0, 26.6, 19.29, 19.21, 19.18, 19.17, 11.5 (d, *J* = 2.2 Hz), 11.4 (d, *J* = 2.2 Hz); $^{19}$F{$^{1}$H} NMR (376 MHz, $CDCl_3$) δ –95.81; $^{29}$Si{$^{1}$H} NMR (79 MHz, $CDCl_3$) δ 1.81 (d, $^{3}J_{Si,F}$ = 3.4 Hz); IR (neat) 2946, 2861, 2131, 1595, 1498, 1379, 1221, 1005, 879, 798 $cm^{-1}$; HRMS (ESI/Orbitrap) m/z: $[M + H]^+$ Calcd for $C_{25}H_{36}FN_2Si$ Si 411.2632; Found 411.2638.

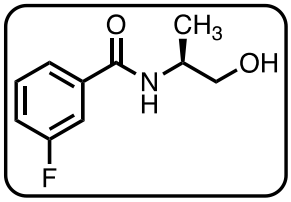
**(*S*)-*N*-(3,3-dimethyl-1-(phenylamino)butan-2-yl)-3-fluoro-2-(hydroxydiisopropylsilyl)benzamide (L3b)**




Synthesized according to the General Procedure D for silanol formation using silane (**1.17b**) from previous step (650 mg, 1.70 mmol), Pd/C (10 wt%, 90 mg, 0.085 mmol) and $H_2O$ (0.30 mL, 17 mmol) in THF (0.1 M) at 60 °C for 16 h. The reaction mixture was purified using flash column chromatography ($SiO_2$, gradient from hexanes/EtOAc/$Et_3N$, 140:20:3.0 *v*/*v*/*v* to 140:40:3.0 *v*/*v*/*v*) to give the silanol as a crystalline white solid (522 mg, 60%). $R_f$ = 0.23 (hexanes/EtOAc/$Et_3N$, 7:1:0.15 *v*/*v*/*v*).

$^1$H NMR (400 MHz, $CDCl_3$) δ 7.36 (ddd, *J* = 8.2, 7.9, 5.8 Hz, 1H), 7.21 – 7.10 (m, 3H), 7.07 (dd, *J* = 8.5, 8.5 Hz, 1H), 6.74 – 6.65 (m, 3H), 5.89 (d, *J* = 10.8 Hz, 1H), 4.27 (ddd, *J* = 10.8, 10.8, 3.1 Hz, 1H), 3.98 (br, 1H), 3.47 (dd, *J* = 10.8, 3.1 Hz, 1H), 3.02 (dd, *J* = 10.8, 10.8 Hz, 1H), 1.40 – 1.22 (m, 2H), 1.16 – 1.05 (m, 15H), 1.02 (dd, *J* = 7.5, 1.4 Hz, 3H), 0.91 (d, *J* = 7.5 Hz, 3H); $^{13}$C{$^1$H} NMR (101 MHz, $CDCl_3$) δ 173.0 (d, $^4J_{C,F}$ = 2.6 Hz), 166.8 (d, $^1J_{C,F}$ = 240.6 Hz), 148.5, 145.5 (d, $^3J_{C,F}$ = 11.7 Hz), 131.6 (d, $^3J_{C,F}$ = 9.2 Hz), 129.3, 122.9 (d, $^2J_{C,F}$ = 34.8 Hz), 122.6 (d, $^4J_{C,F}$ = 2.6 Hz), 117.6, 116.8 (d, $^2J_{C,F}$ = 27.5 Hz), 113.0, 58.2, 44.6, 34.6, 26.9, 17.85 (d, $^5J_{C,F}$ = 1.6 Hz), 17.82 (d, $^5J_{C,F}$ = 2.1 Hz), 17.42, 17.37, 14.3 (d, $^4J_{C,F}$ = 2.2 Hz), 13.6 (d, $^4J_{C,F}$ = 2.9 Hz); $^{19}$F{$^1$H} NMR (376 MHz, $CDCl_3$): δ −94.80; $^{29}$Si{$^1$H} NMR (79 MHz, $CDCl_3$) δ 9.36 (d, $^3J_{Si,F}$ = 4.9 Hz); IR (neat) 3373, 2945, 2866, 1645, 1603, 1506, 1221, 1107, 748 cm$^{-1}$; HRMS (ESI/Orbitrap) m/z: [M – $H_2O$ + H]$^+$ Calcd for $C_{25}H_{36}FN_2OSi$ 427.2581; Found 427.2588; mp: 92−96 °C.

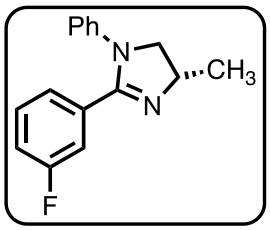
**(*S*)-3-fluoro-*N*-(1-hydroxypropan-2-yl)benzamide (1.19c)**




Synthesized according to the General Procedure A using L-alaninol (649 mg, 8.64 mmol), 3-fluorobenzoyl chloride (1.00 mL, 8.22 mmol) and $Et_3N$ (1.72 mL, 12.3 mmol). The product was purified using extraction and dried under high vacuum to give the β-hydroxy amide as a white powder (>99%).

$^1H$ NMR (400 MHz, $CDCl_3$) δ 7.49 (d, *J* = 7.7 Hz, 1H), 7.44 (ddd, *J* = 8.3, 2.6, 2.6 Hz, 1H), 7.29 (ddd, *J* = 8.3, 7.7, 5.5 Hz, 1H), 7.12 (ddd, *J* = 8.3, 8.3, 2.6 Hz, 1H), 7.03 (d, *J* = 7.8 Hz, 1H), 4.27 – 4.13 (m, 1H), 4.08 (s, 1H), 3.70 (dd, *J* = 11.2, 4.0 Hz, 1H), 3.60 (dd, *J* = 11.2, 5.6 Hz, 1H), 1.24 (d, *J* = 6.8 Hz, 3H); $^{13}C\{^1H\}$ NMR (101 MHz, $CDCl_3$) δ 166.9 (d, *J* = 2.2 Hz), 162.6 (d, *J* = 247.6 Hz), 136.6 (d, *J* = 7.0 Hz), 130.2 (d, *J* = 7.7 Hz), 122.6 (d, *J* = 2.9 Hz), 118.5 (d, *J* = 21.3 Hz), 114.4 (d, *J* = 22.7 Hz), 66.0, 48.2, 17.0; $^{19}F\{^1H\}$ NMR (376 MHz, $CDCl_3$) δ –111.74; HRMS (ESI/Orbitrap) m/z: $[M + H]^+$ Calcd for $C_{10}H_{13}FNO_2$ 198.0929; Found 198.0923.

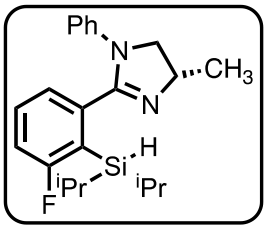
**(*S*)-2-(3-fluorophenyl)-4-methyl-1-phenyl-4,5-dihydro-1*H*-imidazole (1.16c)**




Synthesized according to the General Procedure B for imidazoline formation using β-hydroxy amide (**1.19c**) (604 mg, 2.22 mmol), thionyl chloride (0.65 mL, 8.9 mmol), $Et_3N$ (930 μL, 6.67 mmol) and aniline (240 μL, 2.67 mmol). The reaction mixture was purified using flash column chromatography ($SiO_2$, hexanes/EtOAc/$Et_3N$, 7:1:0.15 *v*/*v*/*v*) to give the imidazoline as a clear oil (542 mg, 96%).

$^{1}$H NMR (400 MHz, $CDCl_3$) δ 7.27 – 7.20 (m, 3H), 7.17 (dddd, *J* = 7.4, 7.4, 2.9, 1.9 Hz, 2H), 7.07 – 7.01 (m, 1H), 6.99 (dd, *J* = 7.4, 1.2 Hz, 1H), 6.77 (ddd, *J* = 8.7, 2.9, 1.9 Hz, 2H), 4.32 (ddq, *J* = 9.9, 8.0, 6.6 Hz, 1H), 4.13 (dd, *J* = 9.9, 9.1 Hz, 1H), 3.62 (dd, *J* = 9.1, 8.0 Hz, 1H), 1.41 (d, *J* = 6.6 Hz, 3H); $^{13}$C{$^{1}$H} NMR (101 MHz, $CDCl_3$) δ 162.4 (d, *J* = 246.5 Hz), 160.2 (d, *J* = 2.6 Hz), 143.0, 133.6 (d, *J* = 8.1 Hz), 129.8 (d, *J* = 8.1 Hz), 128.9, 124.6 (d, *J* = 3.3 Hz), 123.6, 122.5, 117.0 (d, *J* = 20.9 Hz), 115.9 (d, *J* = 23.1 Hz), 61.1, 60.0, 22.3; $^{19}$F{$^{1}$H} NMR (376 MHz, $CDCl_3$) δ –112.68; HRMS (ESI/Orbitrap) m/z: $[M + H]^+$ Calcd for $C_{16}H_{16}FN_2$ 255.1297; Found 255.1287. $R_f$ = 0.29 (hexanes/EtOAc/$Et_3N$, 7:2:0.15 *v*/*v*/*v*).

**(*S*)-2-(2-(diisopropylsilyl)-3-fluorophenyl)-4-methyl-1-phenyl-4,5-dihydro-1*H*-imidazole (1.17c)**

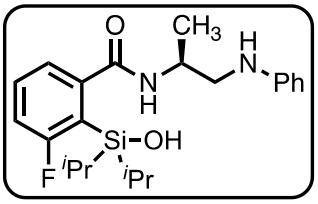



Synthesized according to the General Procedure C for silane formation using imidazoline (**3c**) (254 mg, 1.00 mmol), *sec*-BuLi (1.4 M in cyclohexane, 1.50 mL, 2.10 mmol), TMEDA (315 µL, 2.10 mmol) and diisopropylchlorosilane (320 µL, 2.20 mmol). The reaction mixture was purified via flash column chromatography (140:20:3.0 *v*/*v*/*v*) to yield the silane as a pale yellow oil (332 mg, 98%).

$^{1}$H NMR (400 MHz, $CDCl_3$) δ 7.39 (ddd, *J* = 8.3, 7.5, 6.0 Hz, 1H), 7.26 (dt, *J* = 7.6, 1.1 Hz, 1H), 7.14 – 6.97 (m, 3H), 6.85 (tt, *J* = 6.9, 1.1 Hz, 1H), 6.68 – 6.60 (m, 2H), 4.31 (ddq, *J* = 9.7, 8.5, 6.6 Hz, 1H), 4.11 (dd, *J* = 9.7, 8.7 Hz, 1H), 3.78 (dd, *J* = 6.6, 3.5 Hz, 1H), 3.65 (dd, *J* = 8.7, 8.7 Hz, 1H), 1.45 (d, *J* = 6.6 Hz, 3H), 1.32 – 1.10 (m, 2H), 1.04 (d, *J* = 7.6 Hz, 3H), 0.99 (d, *J* = 7.6 Hz, 3H), 0.84 (dd, *J* = 7.6, 1.0 Hz, 3H), 0.69 (dd, *J* = 7.6, 1.0 Hz, 3H); $^{13}$C{$^{1}$H} NMR (101 MHz, $CDCl_3$) δ 166.99 (d, *J* = 240.3 Hz), 160.32 (d, *J* = 2.2 Hz), 141.76 (d, *J* = 12.1 Hz), 140.88, 131.56 (d, *J* = 8.8 Hz), 128.69, 125.41 (d, *J* = 2.9 Hz), 121.94, 121.70 (d, *J* = 34.5 Hz), 119.27, 115.44 (d, *J* = 26.8 Hz), 59.58, 58.07, 21.96, 19.22, 19.15, 19.08 (d, *J* = 1.5 Hz), 18.87 (d, *J* = 1.5 Hz), 11.53 (d, *J* = 1.8 Hz), 11.19 (d, *J* = 2.6 Hz); $^{29}$Si{$^{1}$H} NMR (79 MHz, $CDCl_3$) δ 2.09 (d, *J* = 3.3 Hz); $^{19}$F{$^{1}$H} NMR (376 MHz, $CDCl_3$) δ –96.03; HRMS

(ESI/Orbitrap) m/z: $[M + H]^+$ Calcd for $C_{22}H_{30}FN_2Si$ 369.2162; Found 369.2149. $R_f$ = 0.34 (hexanes/EtOAc/$Et_3N$, 7:2:0.15 *v*/*v*/*v*).

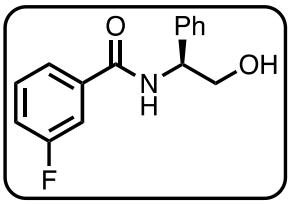
**(*S*)-3-fluoro-2-(hydroxydiisopropylsilyl)-*N*-(1-(phenylamino)propan-2-yl)benzamide (L3c)**




Synthesized according to the General Procedure D for silanol formation using silane (**1.17c**) from previous step (262 mg, 0.711 mmol), Pd/C (10 wt%, 38 mg, 0.036 mmol) and $H_2O$ (130 µL, 7.11 mmol) in THF (5 mL, 0.15 M) at 60 °C for 6 h. The reaction mixture was purified using flash column chromatography ($SiO_2$, gradient from hexanes/EtOAc/$Et_3N$, 140:20:3 *v*/*v*/*v* to 140:40:3 *v*/*v*/*v*) to give the silanol as a white solid (183 mg, 64%).

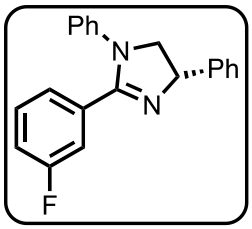
$^1H$ NMR (400 MHz, $CDCl_3$) δ 7.32 (ddd, *J* = 8.2, 8.1, 5.8 Hz, 1H), 7.16 (ddd, *J* = 8.1, 2.3, 1.2 Hz, 2H), 7.13 – 6.99 (m, 2H), 6.75 – 6.61 (m, 3H), 6.05 (d, *J* = 8.5 Hz, 1H), 4.41 (dqdd, *J* = 8.5, 7.9, 6.6, 4.6 Hz, 1H), 3.31 (dd, *J* = 12.8, 4.6 Hz, 1H), 3.19 (dd, *J* = 12.8, 7.9 Hz, 1H), 1.38 – 1.18 (m, 5H), 1.09 (dd, *J* = 7.3, 2.1 Hz, 6H), 0.96 (ddd, *J* = 7.3, 7.0, 1.1 Hz, 6H); $^{13}C\{^1H\}$ NMR (101 MHz, $CDCl_3$) δ 172.20 (d, *J* = 2.2 Hz), 166.73 (d, *J* = 240.6 Hz), 148.20, 145.03 (d, *J* = 11.7 Hz), 131.37 (d, *J* = 9.2 Hz), 129.42, 122.97 (d, *J* = 2.6 Hz), 122.75 (d, *J* = 34.5 Hz), 117.88, 116.78 (d, *J* = 27.9 Hz), 113.11, 49.49, 46.38, 18.97, 17.81 (d, *J* = 2.2 Hz), 17.74 (d, *J* = 2.2 Hz), 17.38, 17.36, 14.12 (d, *J* = 2.2 Hz), 13.99 (d, *J* = 2.9 Hz); $^{19}F\{^1H\}$ NMR (376 MHz, $CDCl_3$) δ –94.86; $^{29}Si\{^1H\}$ NMR (79 MHz, $CDCl_3$) δ 9.02 (d, *J* = 4.8 Hz); HRMS (ESI/Orbitrap) m/z: $[M + H]^+$ Calcd for $C_{22}H_{32}FN_2O_2Si$ 403.2217; Found 403.2227. $R_f$ = 0.22 (hexanes/EtOAc/$Et_3N$, 7:2:0.15 *v*/*v*/*v*).

**(*S*)-3-fluoro-*N*-(2-hydroxy-1-phenylethyl)benzamide (1.19d)**




Synthesized according to the General Procedure A using (*S*)-(+)-2-phenylglycinol (1.77 g, 13.0 mmol), 3-fluorobenzoyl chloride (1.50 mL, 12.3 mmol) and $Et_3N$ (2.60 mL, 18.5 mmol). The product was dried under high vacuum to fully remove triethylamine and was carried on without further purification.

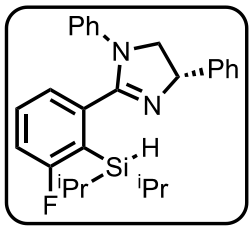
**(*S*)-2-(3-fluorophenyl)-1,4-diphenyl-4,5-dihydro-1*H*-imidazole (1.16d)**




Synthesized according to the General Procedure B for imidazoline formation using β-hydroxy amide (**1.19d**) (650 mg, 2.51 mmol), thionyl chloride (0.73 mL, 10 mmol), $Et_3N$ (1.05 mL, 7.53 mmol) and aniline (0.28 mL, 3.0 mmol). The reaction mixture was purified using flash column chromatography ($SiO_2$, hexanes/EtOAc/$Et_3N$, 140:20:3.0 *v*/*v*/*v*) to give the imidazoline as a yellow oil (500 mg, 63%).

$^1$H NMR (300 MHz, $CDCl_3$) δ 7.41 – 7.23 (m, 8H), 7.22 – 7.15 (m, 2H), 7.08 (ddd, *J* = 8.3, 2.6, 1.3 Hz, 1H), 7.05 – 6.98 (m, 1H), 6.88 – 6.74 (m, 2H), 5.35 (dd, *J* = 10.8, 8.3 Hz, 1H), 4.47 (dd, *J* = 10.8, 9.5 Hz, 1H), 3.93 (dd, *J* = 9.5, 8.3 Hz, 1H); $^{13}$C{$^1$H} NMR (101 MHz, $CDCl_3$) δ 162.5 (d, *J* = 246.5 Hz), 161.5 (d, *J* = 2.6 Hz), 143.8, 142.8, 133.3 (d, *J* = 8.1 Hz), 129.9 (d, *J* = 8.4 Hz), 129.1, 128.8, 127.5, 126.9, 124.8 (d, *J* = 2.9 Hz), 124.1, 123.0, 117.2 (d, *J* = 21.3 Hz), 116.2 (d, *J* = 23.1 Hz), 67.9, 62.0; $^{19}$F{$^1$H} NMR (283 MHz, $CDCl_3$) δ –112.51; HRMS (ESI/Orbitrap) m/z: $[M + H]^+$ Calcd for $C_{21}H_{18}FN_2$ 317.1454; Found 317.1448. $R_f$ = 0.24 (hexanes/EtOAc/$Et_3N$, 7:1:0.15 *v*/*v*/*v*).

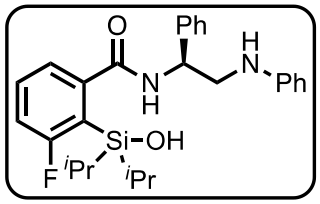
**(*S*)-2-(2-(diisopropylsilyl)-3-fluorophenyl)-1,4-diphenyl-4,5-dihydro-1*H*-imidazole (1.17d)**




Synthesized according to the General Procedure C for silane formation using imidazoline (**1.16d**) (222 mg, 0.706 mmol), *sec*-BuLi (1.4 M in cyclohexane, 1.1 mL, 1.5 mmol), TMEDA (220 µL, 1.48 mmol) and diisopropylchlorosilane (270 µL, 1.55 mmol). The reaction mixture was purified via flash column chromatography (hexanes/EtOAc/$Et_3N$, 140:20:3.0 *v*/*v*/*v*) to yield the silane as a pale orange oil (248 g, 82%).

$^1$H NMR (400 MHz, $CDCl_3$) δ 7.54 – 7.49 (m, 2H), 7.47 – 7.36 (m, 4H), 7.33 – 7.27 (m, 1H), 7.13 – 7.03 (m, 3H), 6.88 (t, *J* = 7.4 Hz, 1H), 6.68 (d, *J* = 8.0 Hz, 2H), 5.36 (dd, *J* = 9.8, 9.8 Hz, 1H), 4.39 (dd, *J* = 9.8, 9.8 Hz, 1H), 4.04 (ddd, *J* = 9.8, 9.8, 1.8 Hz, 1H), 3.89 – 3.80 (m, 1H), 1.29 – 1.11 (m, 2H), 1.06 – 0.92 (m, 6H), 0.81 (d, *J* = 7.4 Hz, 3H), 0.68 (d, *J* = 7.4 Hz, 3H); $^{13}$C{$^1$H} NMR (101 MHz, $CDCl_3$) δ 167.0 (d, *J* = 240.3 Hz), 161.7 (d, *J* = 2.2 Hz), 143.4, 141.4 (d, *J* = 12.1 Hz), 140.6, 131.7 (d, *J* = 9.2 Hz), 128.7 (d, *J* = 22.0 Hz), 127.3, 127.2, 125.7 (d, *J* = 2.9 Hz), 122.4, 121.8 (d, *J* = 34.8 Hz), 119.6, 115.7 (d, *J* = 26.4 Hz), 67.6, 58.9, 19.1, 18.9, 11.5, 11.2; $^{19}$F{$^1$H} NMR (376 MHz, $CDCl_3$) δ –95.77; $^{29}$Si{$^1$H} NMR (79 MHz, $CDCl_3$) δ 2.06 (d, *J* = 3.3 Hz); HRMS (ESI/Orbitrap) m/z: $[M + H]^+$ Calcd for $C_{27}H_{32}FN_2Si$ 431.2319; Found 431.2314. $R_f$ = 0.27 (hexanes/EtOAc/$Et_3N$, 7:1:0.15 *v*/*v*/*v*).

**(*S*)-3-fluoro-2-(hydroxydiisopropylsilyl)-*N*-(1-phenyl-2-(phenylamino)ethyl)benzamide (L3d)**

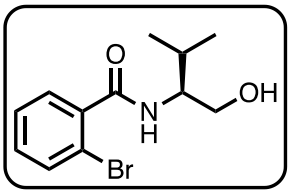



Synthesized according to the General Procedure D for silanol formation using silane (**1.17d**) from previous step (215 mg, 0.500 mmol), Pd/C (10 wt%, 27 mg, 0.025 mmol) and $H_2O$ (90 µL, 5.0 mmol)

in THF (3 mL, 0.15 M) at 60 °C for 16 h. The reaction mixture was purified using flash column chromatography ($SiO_2$, hexanes/EtOAc/$Et_3N$, 140:20:3.0 *v*/*v*/*v* to 140:40:3.0 *v*/*v*/*v*) to give the silanol as a crystalline white solid (157 mg, 68%).

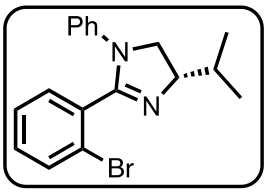
$^1$H NMR (400 MHz, $CDCl_3$) δ 7.46 – 7.29 (m, 6H), 7.22 – 7.13 (m, 3H), 7.12 – 7.03 (m, 1H), 6.74 (dddd, *J* = 7.3, 7.3, 1.1, 1.1 Hz, 1H), 6.68 (dd, *J* = 8.7, 1.2 Hz, 2H), 6.53 (d, *J* = 8.3 Hz, 1H), 5.47 (ddd, *J* = 7.7, 7.7, 5.4 Hz, 1H), 4.00 (br, 1H), 3.70 – 3.55 (m, 2H), 1.37 – 1.22 (m, 2H), 1.09 (dd, *J* = 11.3, 7.4 Hz, 6H), 0.96 (ddd, *J* = 7.4, 3.0, 1.2 Hz, 6H); $^{13}$C{$^1$H} NMR (101 MHz, $CDCl_3$) δ 172.0 (d, $^4J_{C,F}$ = 2.6 Hz), 166.8 (d, $^1J_{C,F}$ = 240.6 Hz), 147.9, 144.7 (d, $^3J_{C,F}$ = 11.7 Hz), 139.2, 131.5 (d, $^3J_{C,F}$ = 9.2 Hz), 129.5, 129.3, 128.3, 126.6, 123.1 (d, $^2J_{C,F}$ = 34.5 Hz), 123.1 (d, $^4J_{C,F}$ = 2.9 Hz), 118.4, 117.0 (d, $^2J_{C,F}$ = 28.2 Hz), 113.5, 53.8, 49.1, 17.9 (d, $^5J_{C,F}$ = 2.2 Hz), 17.8 (d, $^5J_{C,F}$ = 2.2 Hz), 17.43, 17.39, 14.2 (d, $^4J_{C,F}$ = 2.6 Hz), 14.0 (d, $^4J_{C,F}$ = 2.9 Hz); $^{19}$F{$^1$H} NMR (376 MHz, $CDCl_3$) δ –94.72; $^{29}$Si{$^1$H} NMR (79 MHz, $CDCl_3$) δ 8.95 (d, *J* = 4.8 Hz); IR (neat) 3294, 2945, 2835, 1641, 1585, 1495, 1448, 750, 694 cm$^{-1}$; HRMS (ESI/Orbitrap) m/z: [M – $H_2O$ + H]$^+$ Calcd for $C_{27}H_{32}FN_2OSi$ 447.2268; Found 447.2264; mp: 85−87 °C. $R_f$ = 0.17 (hexanes/EtOAc/$Et_3N$, 7:1:0.15 *v*/*v*/*v*).

**(*S*)-2-bromo-*N*-(1-hydroxy-3-methylbutan-2-yl)benzamide (1.36)**




Synthesized according to the General Procedure A using L-valinol **1.14a** (994 mg, 9.64 mmol), 3-fluorobenzoyl chloride **1.15b** (1.20 mL, 9.18 mmol) and $Et_3N$ (2.00 mL, 13.8 mmol). The product was dried under high vacuum to fully remove triethylamine and was carried on without further purification.

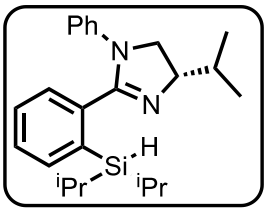
**(*S*)-2-(2-bromophenyl)-4-isopropyl-1-phenyl-4,5-dihydro-1*H*-imidazole (1.37)**




Synthesized according to the General Procedure B for imidazoline formation using β-hydroxy amide (**1.36**) (900 mg, 2.50 mmol), thionyl chloride (0.73 mL, 10 mmol), $Et_3N$ (1.05 mL, 7.53 mmol) and aniline (0.28 mL, 3.0 mmol). The reaction mixture was purified using flash column chromatography ($SiO_2$, hexanes/EtOAc/$Et_3N$, 140:20:3.0 *v*/*v*/*v*) to give the imidazoline as a yellow oil (638 mg, 75%).

$^1$H NMR (400 MHz, $CDCl_3$) δ 7.48 (dd, *J* = 7.6, 1.8 Hz, 2H), 7.32 (ddd, *J* = 7.7, 7.6, 1.3 Hz, 1H), 7.22 (ddd, *J* = 7.7, 7.7, 1.9 Hz, 1H), 7.13 – 7.04 (m, 2H), 6.89 (tt, *J* = 6.9, 1.2 Hz, 1H), 6.66 (dd, *J* = 8.6, 1.2 Hz, 2H), 4.15 – 3.97 (m, 2H), 3.77 (dd, *J* = 8.6, 8.6 Hz, 1H), 1.99 (dh, *J* = 13.5, 6.8 Hz, 1H), 1.10 (d, *J* = 6.8 Hz, 3H), 1.04 (d, *J* = 6.8 Hz, 3H); $^{13}$C{$^1$H} NMR (101 MHz, $CDCl_3$) δ 159.7, 141.0, 134.3, 133.1, 131.0, 130.8, 128.7, 127.6, 122.5, 122.2, 119.4, 70.2, 53.7, 33.0, 19.1, 18.4; HRMS (ESI/Orbitrap) m/z: $[M + H]^+$ Calcd for $C_{18}H_{20}BrN_2$ 343.0810; Found 343.0803.

**(*S*)-2-(2-(diisopropylsilyl)phenyl)-4-isopropyl-1-phenyl-4,5-dihydro-1*H*-imidazole (1.38)**

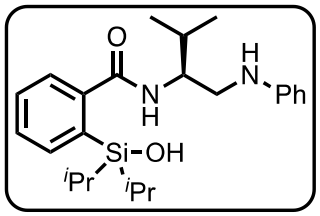



Synthesized according to the General Procedure C for silane formation using imidazoline (**1.37**) (684 mg, 2.00 mmol), *sec*-BuLi (1.4 M in cyclohexane, 2.10 mL, 3.00 mmol), TMEDA (450 µL, 3.00 mmol) and diisopropylchlorosilane (470 µL, 3.20 mmol). The reaction mixture was purified via flash column chromatography (hexanes/EtOAc/$Et_3N$, 140:20:3 *v*/*v*/*v*) to remove the protonated imidazoline. However, the silane was found to be unstable and started turning into silanol in the silica column, and hence, pure

characterization data was not collected. A mixture (3:1, 171 mg) of imidazoline silane (**S6**) and aminoamide silanol (**L3e**) was isolated.

***Note**: The silane was found to be unstable and started turning into aminoamide silanol **L3e** under air and atmospheric moisture after the flash silica column. Confirmation of the product was achieved through* $^{29}Si\{^{1}H\}$ *NMR (79 MHz, $CDCl_3$) with δ 2.60 ppm and ASAP-MS (ACPI) m/z: [M + H]+ Calcd for $C_{24}H_{35}N_2Si$ 379.3; Found 379.4.*

**(*S*)-2-(hydroxydiisopropylsilyl)-*N*-(3-methyl-1-(phenylamino)butan-2-yl)benzamide (L3e)**




**Method A:**

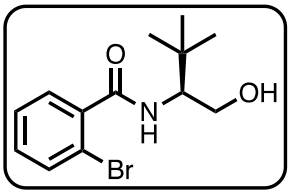
Synthesized according to the General Procedure D (Method A) for silanol formation using a mixture of imidazoline silane (**1.37**) and aminoamide silanol (**L3e**) from previous step (3:1, 84 mg, 0.22 mmol) and $H_2O$ (40 μL, 2.2 mmol) in THF (1.5 mL, 0.15 M) at 60 °C for 16 h. The reaction mixture was purified using flash column chromatography ($SiO_2$, hexanes/EtOAc/$Et_3N$, 140:20:3 *v*/*v*/*v* to 140:40:3 *v*/*v*/*v*) to give the silanol as a crystalline white solid (75 mg, 83%).

**Method B:**

Synthesized according to the General Procedure D (Method B) for silanol formation using a mixture of imidazoline silane (**1.37**) and aminoamide silanol (**L3e**) from previous step (3:1, 80 mg, 0.21 mmol), Pd/C (10 wt%, 11 mg, 0.011 mmol) and $H_2O$ (38 μL, 2.1 mmol) in THF (1.5 mL, 0.15 M) at 60 °C for 6 h. The reaction mixture was purified using flash column chromatography ($SiO_2$, hexanes/EtOAc/$Et_3N$, 140:20:3 *v*/*v*/*v* to 140:40:3 *v*/*v*/*v*) to give the silanol as a crystalline white solid (43 mg, 50%).

$^{1}$H NMR (400 MHz, $CDCl_3$) δ 7.62 (d, *J* = 7.2 Hz, 1H), 7.44 (td, *J* = 6.9, 2.2 Hz, 1H), 7.39 – 7.33 (m, 2H), 7.17 (tt, *J* = 7.3, 2.2 Hz, 2H), 6.71 (tt, *J* = 7.4, 1.2 Hz, 1H), 6.65 (dd, *J* = 8.7, 1.2 Hz, 2H), 6.04 (d, *J* = 9.5 Hz, 1H), 4.31 – 4.18 (m, 1H), 3.98 (br, 1H), 3.38 (dd, *J* = 12.4, 4.1 Hz, 1H), 3.22 (dd, *J* = 12.4, 8.9 Hz, 1H), 2.08 – 1.94 (m, 1H), 1.37 – 1.23 (m, 2H), 1.07 (t, *J* = 7.5 Hz, 12H), 0.97 (dd, *J* = 7.5, 6.3 Hz, 6H); $^{13}$C{$^{1}$H} NMR (101 MHz, $CDCl_3$) δ 172.9, 148.4, 142.1, 137.2, 135.6, 129.8, 129.4, 129.0, 126.5, 117.8, 113.0, 55.3, 46.5, 30.8, 19.8, 18.5, 17.9, 17.9, 17.6, 17.6, 13.6, 13.5; $^{29}$Si{$^{1}$H} NMR (79 MHz, $CDCl_3$) δ 6.42; HRMS (ESI/Orbitrap) m/z: $[M + H]^+$ Calcd for $C_{24}H_{37}N_2O_2Si$ 413.2624; Found 413.2615. $R_f$ = 0.21 (hexanes/EtOAc/$Et_3N$, 7:1:0.15 *v*/*v*/*v*).

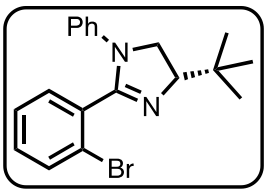
**(*S*)-2-bromo-*N*-(1-hydroxy-3,3-dimethylbutan-2-yl)benzamide (1.38)**




Synthesized according to the General Procedure A using L-tert-leucinol **1.14b** (0.56 g, 4.8 mmol), 2-bromobenzoyl chloride **1.15b** (0.60 mL, 4.6 mmol) and $Et_3N$ (0.96 mL, 6.9 mmol). The product was purified using extraction and dried under high vacuum to give the β-hydroxy amide as a white powder (1.38 g, >99%).

$^{1}$H NMR (400 MHz, $CDCl_3$) δ 7.64 – 7.54 (m, 2H), 7.37 (ddd, *J* = 7.5, 7.5, 1.2 Hz, 1H), 7.32 – 7.24 (m, 1H), 4.07 (ddd, *J* = 9.4, 7.4, 3.5 Hz, 1H), 3.96 (dd, *J* = 11.4, 3.5 Hz, 1H), 3.69 (dd, *J* = 11.4, 7.4 Hz, 1H), 1.05 (s, 9H); $^{13}$C{$^{1}$H} NMR (101 MHz, $CDCl_3$) δ 168.8, 138.1, 133.5, 131.5, 129.9, 127.8, 119.2, 63.3, 60.5, 33.9, 27.2; HRMS (ESI/Orbitrap) m/z: $[M + H]^+$ Calcd for $C_{13}H_{19}BrNO_2$ 300.0599; Found 300.0605.

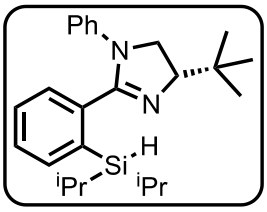
**(*S*)-2-(2-bromophenyl)-4-(*tert*-butyl)-1-phenyl-4,5-dihydro-1*H*-imidazole (1.39)**




Synthesized according to the General Procedure B for imidazoline formation using β-hydroxy amide (**1.19**) (500 mg, 1.67 mmol), thionyl chloride (0.49 mL, 6.7 mmol), $Et_3N$ (0.70 mL, 5.0 mmol) and aniline (0.18 mL, 2.0 mmol). The reaction mixture was purified using flash column chromatography ($SiO_2$, gradient from 100% DCM to 20:1 DCM/MeOH) to give the imidazoline as a yellow oil (466 mg, 79%).

$^1$H NMR (400 MHz, $CDCl_3$) δ 7.48 (ddd, *J* = 8.0, 1.5, 1.5 Hz, 2H), 7.33 (ddd, *J* = 7.5, 7.5, 1.3 Hz, 1H), 7.22 (ddd, *J* = 7.6, 7.5, 1.8 Hz, 1H), 7.14 – 7.04 (m, 2H), 6.94 – 6.86 (m, 1H), 6.71 – 6.63 (m, 2H), 4.08 – 3.96 (m, 2H), 3.88 – 3.76 (m, 1H), 1.05 (s, 9H); $^{13}$C{$^1$H} NMR (101 MHz, $CDCl_3$) δ 159.8, 141.1, 134.3, 133.2, 131.2, 130.9, 128.8, 127.6, 122.6, 122.3, 119.7, 74.0, 52.6, 34.4, 26.3. HRMS (ESI/Orbitrap) m/z: $[M + H]^+$ Calcd for $C_{19}H_{22}BrN_2$ 357.0966; Found 357.0961.

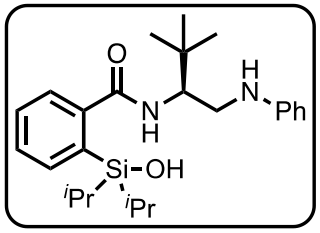
**(*S*)-4-(*tert*-butyl)-2-(2-(diisopropylsilyl)phenyl)-1-phenyl-4,5-dihydro-1*H*-imidazole (1.40)**




Synthesized according to the General Procedure C for silane formation using imidazoline (**1.39**) (380 mg, 1.07 mmol), *sec*-BuLi (1.4 M in cyclohexane, 1.52 mL, 2.13 mmol), TMEDA (320 µL, 2.13 mmol) and diisopropylchlorosilane (330 µL, 2.25 mmol). The reaction mixture was purified via flash column chromatography (hexanes/EtOAc/$Et_3N$, 140:20:3 *v*/*v*/*v*) to yield the silane as a pale yellow oil (252 mg, 60%).

$^{1}$H NMR (400 MHz, $CDCl_3$) δ 7.51 (dd, *J* = 5.7, 3.1 Hz, 1H), 7.42 – 7.37 (m, 1H), 7.37 – 7.30 (m, 2H), 7.09 – 7.00 (m, 2H), 6.82 (t, *J* = 7.4 Hz, 1H), 6.62 (d, *J* = 8.2 Hz, 2H), 3.96 (dd, *J* = 10.2, 10.2 Hz, 1H), 3.91 – 3.81 (m, 3H), 1.24 – 1.16 (m, 1H), 1.16 – 1.08 (m, 1H), 1.07 – 1.01 (m, 15H), 0.83 (t, *J* = 7.1 Hz, 6H); $^{13}$C{$^{1}$H} NMR (101 MHz, $CDCl_3$) δ 161.7, 141.8, 139.4, 135.9, 135.4, 129.3, 129.1, 128.5, 128.2, 121.8, 119.9, 77.5, 77.2, 76.8, 74.1, 53.1, 34.0, 26.5, 19.3, 19.2, 19.0, 11.6, 11.3; $^{29}$Si{$^{1}$H} NMR (79 MHz, $CDCl_3$) δ 2.54; HRMS (ESI/Orbitrap) m/z: $[M + H]^+$ Calcd for $C_{25}H_{36}N_2Si$ 393.2726; Found 393.2719; $R_f$ = 0.76 (hexanes/EtOAc/$Et_3N$, 7:1:0.15 *v*/*v*/*v*).

**(*S*)-*N*-(3,3-dimethyl-1-(phenylamino)butan-2-yl)-2-(hydroxydiisopropylsilyl)benzamide (L3f)**

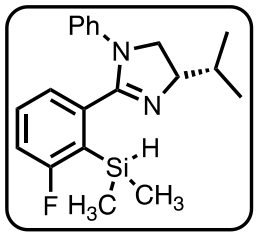



Synthesized according to the General Procedure D for silanol formation using silane (**1.40**) from the previous step (200 mg, 0.51 mmol), Pd/C (10 wt%, 27 mg, 0.025 mmol) and $H_2O$ (92 μL, 5.1 mmol) in THF (0.15 M) at 60 °C for 16 h. The reaction mixture was purified using flash column chromatography ($SiO_2$, hexanes/EtOAc/$Et_3N$, 140:20:3 *v*/*v*/*v* to 140:40:3 *v*/*v*/*v*) to give the silanol as a crystalline white solid (132 mg, 61%).

$^{1}$H NMR (400 MHz, $CDCl_3$) δ 7.61 (d, *J* = 7.3 Hz, 1H), 7.48 – 7.41 (m, 1H), 7.41 – 7.33 (m, 2H), 7.22 – 7.10 (m, 2H), 6.74 – 6.58 (m, 3H), 5.98 (d, *J* = 10.1 Hz, 1H), 4.27 (ddd, *J* = 10.6, 10.6, 3.1 Hz, 1H), 4.00 (br, 2H), 3.48 (dd, *J* = 10.6, 3.1 Hz, 1H), 3.11 – 3.02 (m, 1H), 1.34 – 1.26 (m, 2H), 1.11 – 1.04 (m, 15H), 0.99 (d, *J* = 7.5 Hz, 3H), 0.95 (d, *J* = 7.5 Hz, 3H); $^{13}$C{$^{1}$H} NMR (101 MHz, $CDCl_3$) δ 173.19, 148.54, 142.28, 137.19, 135.57, 129.73, 129.35, 129.02, 126.34, 117.64, 112.96, 77.48, 77.16, 76.84, 58.18, 45.10, 34.49, 26.97, 17.90, 17.89, 17.58, 17.56, 13.76, 13.45; $^{29}$Si{$^{1}$H} NMR (79 MHz, $CDCl_3$) δ 6.47; IR (neat) 3334, 2947, 2864, 1639, 1603, 1508, 1462, 1014, 881, 744 $cm^{-1}$; HRMS (ESI/Orbitrap)

m/z: $[M - H_2O + H]^+$ Calcd for $C_{25}H_{37}N_2OSi$ 409.2675; Found 409.2674; mp: 82 −84 °C; $R_f$ = 0.25 (hexanes/EtOAc/$Et_3N$, 7:1:0.15 *v*/*v*/*v*).

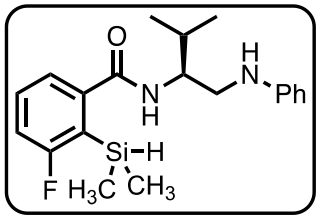
**(*S*)-2-(2-(dimethylsilyl)-3-fluorophenyl)-4-isopropyl-1-phenyl-4,5-dihydro-1*H*-imidazole (1.17j)**




Synthesized according to the General Procedure C for silane formation using imidazoline (**1.16a**) (282 mg, 1.0 mmol), *sec*-BuLi (1.4 M in cyclohexane, 1.5 mL, 2.1 mmol), TMEDA (0.31 mL, 2.1 mmol) and diisopropylchlorosilane (0.24 mL, 2.2 mmol). The reaction mixture was purified via flash column chromatography ($SiO_2$, hexanes/EtOAc/$Et_3N$, 7:1:0.15 *v*/*v*/*v*) to yield the silane as a pale yellow oil (0.260 g, 76%).

$^1$H NMR (400 MHz, $CDCl_3$) δ 7.36 (ddd, *J* = 8.2, 7.9, 6.0 Hz, 1H), 7.25 (d, *J* = 7.5 Hz, 1H), 7.12 – 7.03 (m, 2H), 7.00 (t, *J* = 8.5 Hz, 1H), 6.86 (tt, *J* = 7.1, 1.1 Hz, 1H), 6.61 – 6.53 (m, 2H), 4.29 – 4.18 (m, *J* = 3.7 Hz, 1H), 4.04 – 3.92 (m, 2H), 3.80 – 3.68 (m, 1H), 2.01 – 1.88 (m, 1H), 1.11 (d, *J* = 6.7 Hz, 3H), 1.01 (d, *J* = 6.8 Hz, 3H), 0.11 (dd, J = 3.8, 1.5 Hz, 3H), 0.02 (dd, J = 3.8, 1.5 Hz, 3H); $^{13}$C NMR (101 MHz, $CDCl_3$) δ 167.72 (d, J = 241.0 Hz), 160.64 (d, J = 2.2 Hz), 140.78, 140.39 (d, J = 11.0 Hz), 131.67 (d, J = 9.2 Hz), 128.64, 125.20 (d, J = 2.9 Hz), 123.58 (d, J = 31.2 Hz), 122.11, 119.53, 115.79 (d, J = 26.0 Hz), 70.33, 54.00, 33.14, 19.37, 18.71, –3.65 (d, J = 2.9 Hz), –3.90 (d, J = 3.3 Hz); $^{19}$F{$^1$H} NMR (376 MHz, $CDCl_3$) δ –98.84; $^{29}$Si{$^1$H} NMR (79 MHz, $CDCl_3$) δ –20.99 (d, J = 9.2 Hz); HRMS (ESI/Orbitrap) m/z: $[M + H]^+$ Calcd for $C_{20}H_{26}FN_2Si$ 341.1849; Found 341.1835.

**(*S*)-2-(dimethylsilyl)-3-fluoro-*N*-(3-methyl-1-(phenylamino)butan-2-yl)benzamide (1.21b)**

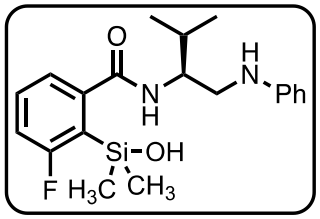


Synthesized according to the General Procedure F for silane formation using aminoamide (**1.18**) (85 mg, 0.28 mmol), *sec*-BuLi (1.4 M in cyclohexane, 0.61 mL, 0.85 mmol), TMEDA (0.13 mL, 0.85 mmol) and dimethylchlorosilane (100 µL, 0.88 mmol). The reaction mixture was purified via flash column chromatography ($SiO_2$, hexanes/EtOAc/$Et_3N$, 7:2:0.15 *v*/*v*/*v*) to yield the silane as a clear oil (31 mg, 31%).

**Note**: *Aminoamide silanol (**L3g**) formed during purification on silica gel chromatography. The silanol was isolated as a clear oil (52 mg, 49%).*

$^1$H NMR (400 MHz, $CDCl_3$) δ 7.47 (dd, *J* = 7.6, 5.3 Hz, 1H), 7.41 (dd, *J* = 7.3, 1.8 Hz, 1H), 7.33 (dd, *J* = 8.8, 1.5 Hz, 1H), 7.20 – 7.11 (m, 2H), 6.70 (tt, *J* = 7.3, 1.1 Hz, 1H), 6.66 – 6.58 (m, 2H), 6.09 (d, *J* = 9.1 Hz, 1H), 4.47 (pd, *J* = 3.8, 2.2 Hz, 1H), 4.24 (tdd, *J* = 8.5, 6.1, 4.1 Hz, 1H), 4.00 (s, 1H), 3.38 (dd, *J* = 12.5, 4.1 Hz, 1H), 3.25 (dd, *J* = 12.5, 8.4 Hz, 1H), 2.10 – 1.93 (m, *J* = 6.8 Hz, 1H), 1.05 (dd, *J* = 7.6, 6.9 Hz, 6H), 0.38 (dd, *J* = 3.8, 0.9 Hz, 6H); $^{13}$C{$^1$H} NMR (101 MHz, $CDCl_3$) δ 167.31 (d, *J* = 242.8 Hz), 167.16 (d, *J* = 2.6 Hz), 148.43, 138.27 (d, *J* = 7.3 Hz), 136.29 (d, *J* = 11.0 Hz), 129.42, 128.05 (d, *J* = 30.8 Hz), 122.12 (d, *J* = 2.9 Hz), 117.67, 113.46 (d, *J* = 27.5 Hz), 112.86, 55.22, 46.54, 30.57, 19.67, 18.57, –3.96, –3.98; $^{19}$F{$^1$H} NMR (376 MHz, $CDCl_3$) δ –100.00; $^{29}$Si{$^1$H} NMR (79 MHz, $CDCl_3$) δ –18.84 (d, *J* = 7.3 Hz); IR (neat) 3296, 2960, 2139, 1633, 1602, 1541, 1508, 1392, 879, 748 cm$^{-1}$; HRMS (ESI/Orbitrap) m/z: $[M + H]^+$ Calcd for $C_{20}H_{28}FN_2Si$ 359.1948; Found 359.1955. $R_f$ = 0.48 (hexanes/EtOAc/$Et_3N$, 7:2:0.15 *v*/*v*/*v*).

**(S)-3-fluoro-2-(hydroxydimethylsilyl)-N-(3-methyl-1-(phenylamino)butan-2-yl)benzamide (L3g)**




**Method A:**

Synthesized according to the General Procedure F for silane formation using aminoamide (**1.18**) (85 mg, 0.28 mmol), *sec*-BuLi (1.4 M in cyclohexane, 0.61 mL, 0.85 mmol), TMEDA (0.13 mL, 0.85 mmol) and dimethylchlorosilane (100 µL, 0.88 mmol). The reaction mixture was purified via flash column chromatography ($SiO_2$, hexanes/EtOAc/$Et_3N$, 7:2:0.15 *v*/*v*/*v*) to yield the silane as a clear oil (31 mg, 31%). Aminoamide silanol (**L3g**) formed during purification in silica gel chromatography. The silanol was isolated as a clear oil (52 mg, 49%).

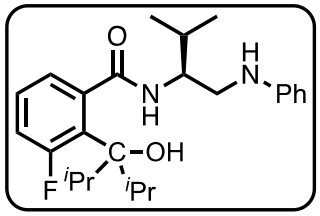
**Method B:**

Synthesized according to the General Procedure D for silanol formation using imidazoline silane (**1.21b**) (89 mg, 0.26 mmol), Pd/C (10 wt%, 18 mg, 0.013 mmol) and $H_2O$ (47 µL, 2.6 mmol) in THF (2 mL, 0.15 M) at room temperature for 2 h. The reaction mixture was purified using flash column chromatography ($SiO_2$, hexanes/EtOAc/$Et_3N$, 140:40:1.5 *v*/*v*/*v*) to give the silanol as a white solid (54 mg, 55%).

$^1$H NMR (600 MHz, $CDCl_3$) δ 7.41 – 7.28 (m, 1H), 7.24 – 7.02 (m, 4H), 6.72 (tt, *J* = 7.3, 1.2 Hz, 1H), 6.66 (dd, *J* = 8.7, 1.1 Hz, 2H), 6.00 (d, *J* = 9.8 Hz, 1H), 4.25 (dddd, *J* = 9.8, 9.3, 6.9, 3.9 Hz, 1H), 4.03 (s, 1H), 3.38 (dd, *J* = 12.3, 4.0 Hz, 1H), 3.20 (dd, *J* = 12.3, 9.3 Hz, 1H), 2.01 (dq, *J* = 13.6, 6.9 Hz, 1H), 1.08 (t, *J* = 6.9 Hz, 6H), 0.47 (d, *J* = 2.5 Hz, 3H), 0.46 (d, *J* = 2.9 Hz, 3H); $^{13}$C{$^1$H} NMR (151 MHz, $CDCl_3$) δ 172.31 (d, *J* = 2.3 Hz), 167.13 (d, *J* = 242.1 Hz), 148.32, 143.98 (d, *J* = 10.5 Hz), 131.52 (d, *J* = 9.4 Hz), 129.48, 125.71 (d, *J* = 31.4 Hz), 122.49 (d, *J* = 2.8 Hz), 118.03, 117.53 (d, *J* = 27.5 Hz), 113.14, 55.42, 46.68, 30.96, 29.85, 19.81, 18.53, 1.82 (d, *J* = 3.3 Hz), 1.48 (d, *J* = 4.4 Hz); $^{19}$F{$^1$H} NMR (283 MHz, $CDCl_3$) δ –96.64; $^{29}$Si{$^1$H} NMR (79 MHz, $CDCl_3$) δ 5.25 (d, *J* = 8.4 Hz); IR (neat)

3364, 3280, 3055, 2960, 1633, 1602, 1508, 1256, 1223, 829, 748, 692 $cm^{-1}$; HRMS (ESI/Orbitrap) m/z: $[M - H_2O + H]^+$ Calcd for $C_{20}H_{28}FN_2O_2Si$ 357.1798; Found 357.1791; $R_f$ = 0.22 (hexanes/EtOAc/$Et_3N$, 7:2:0.15 *v*/*v*/*v*).

**(*S*)-3-fluoro-2-(3-hydroxy-2,4-dimethylpentan-3-yl)-*N*-(3-methyl-1-(phenylamino)butan-2-yl)benzamide (L4)**

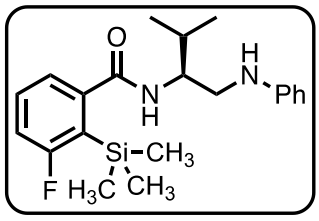



Aminoamide (**1.18**, 170 mg, 0.57 mmol, 1.0 equiv) was added directly into a flame-dried round bottom flask, dissolved in THF (2 mL), and purged under argon for 5 min. The reaction was cooled to –78 °C and TMEDA (270 μL, 3.2 equiv) was added followed by the dropwise addition of *sec*-butyl lithium (1.4 M in cyclohexane, 3.2 equiv, 1.3 mL). The mixture was stirred at –78 °C for 2 h to form the lithiated aminoamide. In a separate flask, $CeCl_3$ (461 mg, 1.88 mmol, 3.3 equiv) was added and flame-dried under high vacuum (<1 torr). After the vial cooled to room temperature, it was purged with argon and capped with a septum with an Ar-balloon. 2,4-Dimethylpentan-3-one (265 mg, 1.88 mmol, 3.3 equiv) and anhydrous THF (2 mL) were added into the flask. The mixture was stirred at room temperature for 1 h to activate the ketone. Subsequently, the lithiated aminoamide solution was drawn into a 5-mL syringe with long needle and added dropwise into the stirring solution at –78 °C. The reaction was allowed to stir at room temperature and stirred for 40 h. The solution was quenched with saturated aq. $NH_4Cl$ (7 mL) and the aqueous phase was extracted with EtOAc (3 × 5 mL). The combined organic phase was dried over $MgSO_4$, filtered, and concentrated *in vacuo*. The reaction mixture was purified using flash column chromatography ($SiO_2$, hexanes/EtOAc/$Et_3N$, 140:40:3 *v*/*v*/*v*) to yield the corresponding carbon analog **L4** (9 mg, 4%).

$^1H$ NMR (800 MHz, $CDCl_3$) δ 7.67 (t, *J* = 6.9 Hz, 1H), 7.40 (dd, *J* = 8.1, 1.9 Hz, 1H), 7.37 (dd, *J* = 12.8, 1.9 Hz, 1H), 7.15 (dd, *J* = 8.6, 7.3 Hz, 2H), 6.69 (tt, *J* = 7.3, 1.1 Hz, 1H), 6.63 (dd, *J* = 8.7, 1.1

Hz, 2H), 6.03 (d, *J* = 8.9 Hz, 1H), 4.26 (dddd, *J* = 8.8, 8.8, 6.1, 4.0 Hz, 1H), 4.02 (s, 1H), 3.39 (dd, *J* = 12.4, 4.1 Hz, 1H), 3.25 (dd, *J* = 12.4, 8.8 Hz, 1H), 2.55 – 2.51 (m, 2H), 2.06 – 1.98 (m, *J* = 6.8 Hz, 1H), 1.06 (dd, *J* = 12.0, 6.8 Hz, 6H), 0.87 (dd, *J* = 6.7, 2.0 Hz, 6H), 0.80 (dd, *J* = 6.9, 2.1 Hz, 6H); $^{13}C\{^{1}H\}$ NMR (151 MHz, $CDCl_3$) δ 167.02 (d, *J* = 2.0 Hz), 159.65 (d, *J* = 244.0 Hz), 148.46, 135.23 (d, *J* = 7.7 Hz), 133.68 (d, *J* = 13.2 Hz), 131.38 (d, *J* = 5.5 Hz), 129.47, 121.50 (d, *J* = 2.8 Hz), 117.76, 115.28 (d, *J* = 28.1 Hz), 112.92, 82.16 (d, *J* = 5.5 Hz), 55.15, 46.87, 33.91 (d, *J* = 2.8 Hz), 33.88 (d, *J* = 2.8 Hz), 30.67, 29.85, 19.77, 18.55, 17.98, 17.97, 16.72; $^{19}F\{^{1}H\}$ NMR (376 MHz, $CDCl_3$) δ –106.60; HRMS (ESI/Orbitrap) m/z: [M + H]+ Calcd for $C_{25}H_{36}FN_2O_2$ 415.2761; Found 415.2761. $R_f$ = 0.35 (hexanes/EtOAc/$Et_3N$, 7:2:0.15 v/v/v).

**(S)-3-fluoro-N-(3-methyl-1-(phenylamino)butan-2-yl)-2-(trimethylsilyl)benzamide (L5)**

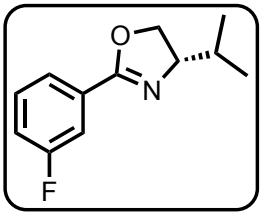



Synthesized according to the General Procedure F for silane formation using aminoamide (**1.18**) (150 mg, 0.50 mmol), *sec*-BuLi (1.4 M in cyclohexane, 1.14 mL, 1.60 mmol, 3.2 equiv), TMEDA (240 µL, 1.60 mmol, 3.2 equiv) and trimethylchlorosilane (210 µL, 1.65 mmol). The reaction mixture was purified via flash column chromatography ($SiO_2$, hexanes/EtOAc/$Et_3N$, 7:1:0.15 *v*/*v*/*v*) to yield the silane as a clear oil (67 mg, 36%).

$^{1}H$ NMR (400 MHz, $CDCl_3$) δ 7.31 (ddd, *J* = 8.2, 7.5, 5.6 Hz, 1H), 7.25 – 7.15 (m, 2H), 7.15 – 7.01 (m, 2H), 6.74 (tt, *J* = 7.3, 1.1 Hz, 1H), 6.65 (dd, *J* = 8.6, 1.1 Hz, 2H), 5.90 (d, *J* = 9.1 Hz, 1H), 4.27 – 4.18 (m, 1H), 3.45 (d, *J* = 7.2 Hz, 1H), 3.39 (dd, *J* = 12.4, 4.3 Hz, 1H), 3.27 (dd, *J* = 12.4, 8.3 Hz, 1H), 2.13 – 2.04 (m, 1H), 1.10 (d, *J* = 3.0 Hz, 3H), 1.09 (d, *J* = 3.0 Hz, 3H), 0.40 (d, *J* = 2.1 Hz, 9H); $^{13}C$ NMR (101 MHz, $CDCl_3$) δ 171.05 (d, *J* = 2.6 Hz), 168.01 (d, *J* = 243.2 Hz), 148.33, 145.14 (d, *J* = 10.3 Hz), 131.07 (d, *J* = 9.5 Hz), 129.47, 125.38 (d, *J* = 30.4 Hz), 122.61 (d, *J* = 2.6 Hz), 117.75, 117.17 (d, *J* = 28.2 Hz), 112.88, 55.06, 46.40, 30.57, 29.85, 19.63, 18.59, 1.00, 0.96; $^{19}F$ NMR (376 MHz, $CDCl_3$) δ -

94.72; $^{29}$Si NMR (79 MHz, $CDCl_3$) δ -3.78 (d, $J$ = 6.2 Hz); HRMS (ESI/Orbitrap) m/z: $[M + H]^+$ Calcd for $C_{21}H_{30}FNOSi$ 373.2111; Found 373.2097; $R_f$ = 0.20 (hexanes/EtOAc/$Et_3N$, 7:2:0.15 *v*/*v*/*v*).

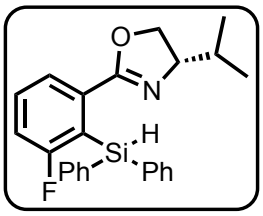
**(*S*)-2-(3-fluorophenyl)-4-isopropyl-4,5-dihydrooxazole (1.41a)**




β-Hydroxy amide (**1.19a**) (1.850 g, 8.22 mmol, 1.00 equiv), *p*-toluenesulfonyl chloride (2.06 g, 10.9 mmol, 1.32 equiv) and 4-dimethylaminopyridine (0.005g, 0.04 mmol, 0.005 equiv) were dissolved in DCM (27 mL) and the flask was purged under argon for 5 min. Triethylamine (3.43 mL, 24.7 mmol, 3.00 equiv) was added dropwise and the reaction was allowed to stir for 14 h. The reaction was diluted with diethyl ether (10 mL) and quenched with saturated aq. $NaHCO_3$ (10 mL). The aqueous phase was extracted with diethyl ether (3 × 20 mL), and the combined organic phase was washed with brine (2 × 10 mL). The combined organic phase was dried over $MgSO_4$, filtered, and concentrated *in vacuo.* The reaction mixture was purified by column chromatography (8:1 hexanes/EtOAc to 5:1 hexanes/EtOAc) to yield the titled product as a clear oil (1.410 g, 83 %).

$^1$H NMR (300 MHz, $CDCl_3$) δ 7.74 (ddd, $J$ = 7.7, 1.3, 1.3 Hz, 1H), 7.65 (ddd, $J$ = 9.6, 2.7, 1.3 Hz, 1H), 7.37 (ddd, $J$ = 8.0, 7.9, 5.7 Hz, 1H), 7.16 (dddd, $J$ = 8.3, 8.3, 2.7, 1.1 Hz, 1H), 4.42 (ddd, $J$ = 6.5, 6.5, 2.5 Hz, 1H), 4.20 – 4.03 (m, 2H), 1.96 – 1.75 (m, 1H), 1.03 (d, $J$ = 6.7 Hz, 3H), 0.93 (d, $J$ = 6.7 Hz, 3H); $^{13}$C{$^1$H} NMR (76 MHz, $CDCl_3$) δ 162.6 (d, $J$ = 246.0 Hz), 162.4 (d, $J$ = 3.0 Hz), 130.2 (d, $J$ = 8.2 Hz), 130.0 (d, $J$ = 8.2 Hz), 124.1 (d, $J$ = 3.0 Hz), 118.2 (d, $J$ = 21.3 Hz), 115.4 (d, $J$ = 23.4 Hz), 72.8, 70.5, 32.9, 19.0, 18.2; $^{19}$F{$^1$H} NMR (283 MHz, $CDCl_3$) δ –112.84. IR (neat) 2958, 2873, 1653, 1614, 1587, 1450, 1190, 1070, 968, 847, 793 cm$^{-1}$; HRMS (ESI/Orbitrap) m/z: $[M + H]^+$ Calcd for $C_{12}H_{15}FNO$ 208.1137; Found 208.1126.

**(*S*)-2-(2-(diphenylsilyl)-3-fluorophenyl)-4-isopropyl-4,5-dihydrooxazole (1.42)**

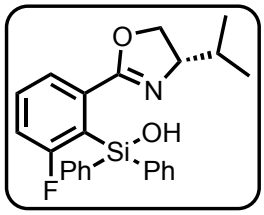



Synthesized according to the General Procedure C for silane formation using oxazoline (**1.41a**) (600 mg, 2.90 mmol, 1.00 equiv), *sec*-BuLi (1.4 M in cyclohexane, 2.69 mL, 3.77 mmol, 1.20 equiv), TMEDA (0.52 mL, 3.77 mmol, 1.20 equiv) and diphenylchlorosilane (0.73 mL, 3.8 mmol, 1.3 equiv). The reaction mixture was preliminary purified via flash column chromatography (hexanes/EtOAc, 8:1 *v*/*v*) to yield the silane as a clear oil (0.802 g, 71%).

$^{1}$H NMR (400 MHz, $CDCl_3$) δ 7.70 – 7.63 (m, 3H), 7.63 – 7.57 (m, 2H), 7.45 (ddd, *J* = 8.0, 7.7, 5.7 Hz, 1H), 7.41 – 7.30 (m, 6H), 7.11 (ddd, *J* = 8.5, 8.5, 1.2 Hz, 1H), 5.58 (d, *J* = 7.2 Hz, 1H), 3.95 (dd, *J* = 9.8, 8.5 Hz, 1H), 3.78 (t, *J* = 8.5 Hz, 1H), 3.63 (td, *J* = 9.8, 6.8 Hz, 1H), 1.65 – 1.55 (m, 1H), 0.90 (d, *J* = 6.7 Hz, 3H), 0.80 (d, *J* = 6.7 Hz, 3H); $^{13}$C{$^{1}$H} NMR (101 MHz, $CDCl_3$) δ 168.0 (d, *J* = 244.3 Hz), 163.7 (d, *J* = 2.9 Hz), 137.0 (d, *J* = 9.5 Hz), 135.6, 135.4, 133.7 (d, *J* = 2.2 Hz), 133.4 (d, *J* = 2.2 Hz), 132.3 (d, *J* = 9.2 Hz), 129.58, 129.47, 127.91, 127.90, 125.5 (d, *J* = 2.9 Hz), 120.9 (d, *J* = 27.5 Hz), 117.8 (d, *J* = 26.4 Hz), 73.0, 70.5, 32.8, 19.2, 18.7; $^{19}$F{$^{1}$H} NMR (376 MHz, $CDCl_3$) δ –94.15; $^{29}$Si{$^{1}$H} NMR (79 MHz, $CDCl_3$) δ –27.51 (d, *J* = 11.7 Hz). IR (neat) 3068, 2958, 2143, 1655, 1595, 1429, 1226, 1109, 804, 731, 696 cm$^{-1}$; HRMS (ESI/Orbitrap) m/z: $[M + H]^+$ Calcd for $C_{24}H_{25}FNOSi$ 390.1689; Found 390.1673.

***Note:*** *The silane was found to be stable at benchtop to air for >24 months with minimal decomposition.*

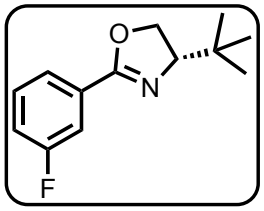
**(*S*)-(2-fluoro-6-(4-isopropyl-4,5-dihydrooxazol-2-yl)phenyl)diphenylsilanol (L1a)**




Synthesized according to the General Procedure D for silanol formation using oxazoline silane (**S12**) (0.500 g, 1.28 mmol, 1.00 equiv), Pd/C (10 wt%, 70 mg, 0.07 mmol) and $H_2O$ (0.23 mL, 13 mmol) in diethyl ether (15 mL) at room temperature for 3 h and monitored using TLC for the consumption of starting material. The reaction mixture was purified by flash chromatography (5:1 hexanes/EtOAc) to yield silanol as a white solid (0.478 g, 92%).

$^1$H NMR (400 MHz, $CDCl_3$) δ 8.53 (s, 1H), 7.79 (dd, *J* = 7.8, 1.1 Hz, 1H), 7.63 (ddt, *J* = 13.3, 6.5, 1.7 Hz, 4H), 7.44 (ddd, *J* = 8.0, 8.0, 5.8 Hz, 1H), 7.40 – 7.30 (m, 6H), 7.07 (ddd, *J* = 9.3, 8.2, 1.2 Hz, 1H), 4.25 (dd, *J* = 9.7, 8.3 Hz, 1H), 3.96 (dd, *J* = 8.5, 8.5 Hz, 1H), 3.86 (ddd, *J* = 9.9, 8.8, 6.9 Hz, 1H), 1.70 – 1.54 (m, *J* = 6.8 Hz, 1H), 0.94 (d, *J* = 6.7 Hz, 3H), 0.83 (d, *J* = 6.7 Hz, 3H); $^{13}$C{$^1$H} NMR (101 MHz, $CDCl_3$) δ 167.22 (d, *J* = 242.5 Hz), 165.32 (d, *J* = 3.3 Hz), 137.11 (d, *J* = 2.9 Hz), 136.76 (d, *J* = 2.6 Hz), 134.82, 134.79 (d, *J* = 2.2 Hz), 134.72, 134.54 (d, *J* = 2.2 Hz), 131.86 (d, *J* = 9.5 Hz), 129.66 (d, *J* = 11.7 Hz), 127.66, 126.87 (d, *J* = 2.6 Hz), 124.42 (d, *J* = 28.6 Hz), 118.95 (d, *J* = 27.9 Hz), 72.48, 70.57, 32.76, 18.91, 18.72; $^{19}$F{$^1$H} NMR (376 MHz, $CDCl_3$) δ –89.29; $^{29}$Si{$^1$H}NMR (79 MHz, $CDCl_3$) δ –17.33 (d, *J* = 11.0 Hz); IR (neat) 3447, 3068, 2960, 1641, 1593, 1427, 1250, 1113, 974, 887, 804, 698 cm$^{-1}$; HRMS (ESI/Orbitrap) m/z: $[M + H]^+$ Calcd for $C_{24}H_{25}FNO_2Si$ 406.1638; Found 406.1625.

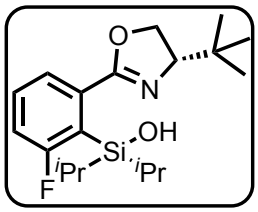
**(*S*)-4-(*tert*-butyl)-2-(3-fluorophenyl)-4,5-dihydrooxazole (1.41b)**



β-Hydroxy amide (**1.19b**) (650 mg, 2.72 mmol, 1.00 equiv), *p*-toluenesulfonyl chloride (673 mg, 3.53 mmol, 3.53 equiv) and 4-dimethylaminopyridine (2.6 mg, 0.013 mmol, 0.005 equiv) were dissolved in DCM (20 mL) and the flask was purged under argon for 5 min. Triethylamine (1.13 mL, 8.16 mmol, 3.00 equiv) was added dropwise and the reaction was allowed to stir for 16 h. The reaction was diluted with diethyl ether (10 mL) and quenched with saturated aq. $NaHCO_3$ (10 mL). The aqueous phase was extracted with diethyl ether (3 × 20 mL), and the combined organic phase was washed with brine (2 × 10 mL). The combined organic phase was dried over $MgSO_4$, filtered, and concentrated *in vacuo.* The reaction mixture was purified by column chromatography (10:1 hexanes/EtOAc to 8:1 hexanes/EtOAc) to yield the title product as a clear oil (230 mg, 38 %).

$^1$H NMR (300 MHz, $CDCl_3$) δ 7.74 (ddd, *J* = 7.8, 1.3, 1.3 Hz, 1H), 7.65 (ddd, *J* = 9.6, 2.7, 1.5 Hz, 1H), 7.37 (ddd, *J* = 8.1, 8.0, 5.7 Hz, 1H), 7.16 (dddd, *J* = 8.4, 8.4, 2.7, 1.1 Hz, 1H), 4.36 (dd, *J* = 10.1, 8.2 Hz, 1H), 4.24 (dd, *J* = 8.2, 8.2 Hz, 1H), 4.05 (dd, *J* = 10.1, 8.2 Hz, 1H), 0.95 (s, 9H); $^{13}$C{$^1$H} NMR (101 MHz, $CDCl_3$) δ 162.6 (d, *J* = 245.8 Hz), 162.4 (d, *J* = 3.3 Hz), 130.3 (d, *J* = 8.1 Hz), 130.0 (d, *J* = 8.1 Hz), 124.1 (d, *J* = 3.3 Hz), 118.2 (d, *J* = 21.3 Hz), 115.4 (d, *J* = 23.5 Hz), 76.4, 69.1, 34.2, 26.0; $^{19}$F{$^1$H} NMR (283 MHz, $CDCl_3$) δ –112.90; HRMS (ESI/Orbitrap) m/z: $[M + H]^+$ Calcd for $C_{13}H_{16}FNO$ 222.1294; Found 222.1284.

**(*S*)-(2-(4-(*tert*-butyl)-4,5-dihydrooxazol-2-yl)-6-fluorophenyl)diisopropylsilanol (L1b)**



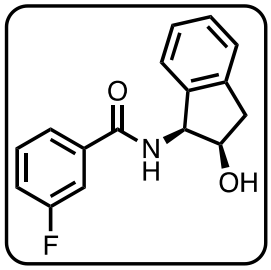

Synthesized according to the General Procedure C for silane formation using oxazoline (**1.41b**) (215 mg, 0.970 mmol), *sec*-BuLi (1.4 M in cyclohexane, 0.84 mL, 1.20 mmol), TMEDA (180 μL, 1.20 mmol) and diisopropylchlorosilane (220 μL, 1.30 mmol). The reaction mixture was filtered through a silica plug (hexanes/EtOAc, 6:1 *v*/*v*) to yield the mixture of unreacted oxazoline (**1.41b**) and the corresponding oxazoline-silane **1.42b**. The resulting mixture was carried on to the next step.

Confirmation of the product was obtained through diagnostic peaks in the $^{1}H$ NMR and $^{19}F$ NMR with a diagnostic peak at δ –95.70 ppm.

For silanol formation, a mixture of unreacted oxazoline and oxazoline-silane (**1.41b**:**1.42b**, 1:20, 263 mg, 0.785 mmol, calculated based off silane), Pd/C (10 wt%, 42 mg, 0.039 mmol) and $H_2O$ (140 μL, 7.8 mmol) was used in THF (0.15 M) at room temperature for 16 h. The reaction mixture was purified using flash column chromatography ($SiO_2$, hexanes/EtOAc, 10:1 *v*/*v*/*v*) to give the silanol as a crystalline white solid (223 mg, 65%) over two steps.

$^{1}H$ NMR (400 MHz, $CDCl_3$) δ 8.58 (s, 1H), 7.85 (dd, *J* = 7.9, 1.1 Hz, 1H), 7.40 (ddd, *J* = 8.0, 7.9, 6.1 Hz, 1H), 7.13 (ddd, *J* = 8.0, 7.9, 1.1 Hz, 1H), 4.36 (dd, *J* = 10.1, 8.5 Hz, 1H), 4.22 (dd, *J* = 8.5, 8.5 Hz, 1H), 4.14 (dd, *J* = 10.1, 8.5 Hz, 1H), 1.38 – 1.18 (m, 2H), 1.09 (dd, *J* = 7.0, 7.0 Hz, 6H), 1.04 – 0.98 (m, 3H), 0.97 (s, 9H), 0.91 (dd, *J* = 7.4, 1.2 Hz, 3H); $^{13}C\{^{1}H\}$ NMR (101 MHz, $CDCl_3$) δ 166.98 (d, *J* = 237.0 Hz), 165.47 (d, *J* = 3.3 Hz), 134.63 (d, *J* = 12.8 Hz), 130.76 (d, *J* = 9.9 Hz), 127.50 (d, *J* = 2.2 Hz), 125.85 (d, *J* = 34.5 Hz), 118.29 (d, *J* = 29.3 Hz), 76.00, 68.28, 34.06, 26.01, 18.03, 18.00, 17.95, 17.92, 17.64, 15.29 (d, *J* = 4.0 Hz), 14.46 (d, *J* = 5.9 Hz); $^{19}F\{^{1}H\}$ NMR (376 MHz, $CDCl_3$) δ –93.20; $^{29}Si\{^{1}H\}$NMR (79 MHz, $CDCl_3$) δ 7.09 (d, *J* = 7.3 Hz); HRMS (ESI/Orbitrap) m/z: $[M + H]^+$ Calcd for $C_{19}H_{31}FNO_2Si$ 352.2108; Found 352.2099.

**3-fluoro-*N*-((1*S*,2*R*)-2-hydroxy-2,3-dihydro-1*H*-inden-1-yl)benzamide (1.41c)**

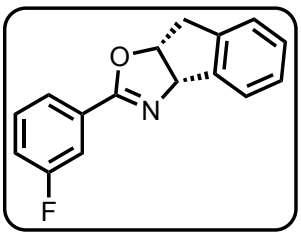



(1*S*,2*R*)-(-)-*cis*-1-Amino-2-indanol (1.29 g, 8.64 mmol, 1.05 equiv) was added to a round-bottom flask, dissolved in DCM (27 mL) and the flask was purged with argon for 5 min. Triethylamine was added (1.81 mL, 12.96 mmol, 1.50 equiv) followed by the dropwise addition of 3-fluorobenzoyl chloride (1.00

mL, 8.23 mmol, 1.00 equiv). The reaction was exothermic and the evolution of HCl gas could be observed. After 1 h of stirring the reaction was quenched with 1M NaOH (10 mL). The aqueous phase was extracted with DCM (3 × 5 mL), and the combined organic phase was washed with brine (2 × 5 mL). The combined organic phase was and dried over $MgSO_4$, filtered, and concentrated *in vacuo*. The reaction mixture was carried on without further purification.

$^1$H NMR (400 MHz, $CDCl_3$) δ 7.63 – 7.54 (m, 2H), 7.42 (ddd, *J* = 8.1, 7.9, 5.5 Hz, 1H), 7.35 (d, *J* = 6.8 Hz, 1H), 7.31 – 7.27 (m, 2H), 7.26 – 7.16 (m, 2H), 6.85 (d, *J* = 6.8 Hz, 1H), 5.60 (dd, *J* = 7.9, 5.2 Hz, 1H), 4.75 (br, 1H), 3.26 (dd, *J* = 16.6, 5.2 Hz, 1H), 3.01 (dd, *J* = 16.6, 2.2 Hz, 1H), 2.14 (br, 1H); $^{13}$C{$^1$H} NMR (101 MHz, $CDCl_3$) δ 166.8 (d, *J* = 2.6 Hz), 162.9 (d, *J* = 248.0 Hz), 140.6, 140.0, 136.6 (d, *J* = 7.0 Hz), 130.4 (d, *J* = 7.7 Hz), 128.6, 127.5, 125.6, 124.8, 122.7 (d, *J* = 3.3 Hz), 118.9 (d, *J* = 21.3 Hz), 114.7 (d, *J* = 23.1 Hz), 73.8, 58.1, 40.1; $^{19}$F{$^1$H} NMR (376 MHz, $CDCl_3$) δ –111.66; HRMS (ESI/Orbitrap) m/z: $[M + H]^+$ Calcd for $C_{16}H_{15}FNO_2$ 272.1087; Found 272.1086.

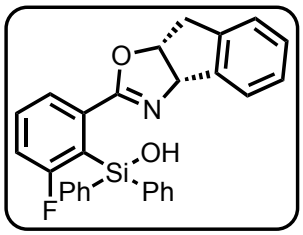
**(3a*S*,8a*R*)-2-(3-fluorophenyl)-3a,8a-dihydro-8*H*-indeno[1,2-*d*]oxazole (1.44)**




Titanium(IV) tetraisopropoxide (4.546 g, 16 mmol, 4.00 equiv) was added to a round-bottom flask containing amide (**1.41c**) (1.09 g, 4.00 mmol, 1.00 equiv). The mixture was stirred at 150 °C for 14 h with a Dean-Stark trap to remove isopropanol. After cooling to room temperature, 3-(dimethylamino)-1,2-propanediol (1.89 mL, 16 mmol, 4.00 equiv) was added and then the reaction was allowed to stir for 0.5 h. EtOAc (20 mL) and deionized water (20 mL) were added and a white solid formed which became soluble after 2 h of stirring. The aqueous layer was extracted with ethyl acetate (3 × 10 mL) and the combined organic phase was washed with brine (2 × 5 mL). The combined organic phase was dried over $MgSO_4$, filtered and concentrated *in vacuo.* The reaction mixture was purified via column chromatography (3:1 hexanes/EtOAc) to yield the indanol as a white solid (0.932 g, 92%).

$^{1}$H NMR (400 MHz, $CDCl_3$) δ 7.71 (d, *J* = 7.8 Hz, 1H), 7.62 (ddd, *J* = 9.6, 2.7, 1.6 Hz, 1H), 7.55 (dd, *J* = 6.9, 3.0 Hz, 1H), 7.37 – 7.22 (m, 4H), 7.17 – 7.07 (m, 1H), 5.73 (d, *J* = 8.2 Hz, 1H), 5.48 (ddd, *J* = 8.2, 6.8, 1.8 Hz, 1H), 3.50 (dd, *J* = 17.9, 6.8 Hz, 1H), 3.35 (dd, *J* = 17.9, 1.8 Hz, 1H); $^{13}$C{$^{1}$H} NMR (101 MHz, $CDCl_3$) δ 163.1 (d, *J* = 2.9 Hz), 162.5 (d, *J* = 246.1 Hz), 141.9, 139.8, 130.1 (d, *J* = 8.1 Hz), 130.0 (d, *J* = 8.1 Hz), 128.7, 127.6, 125.7, 125.4, 124.2 (d, *J* = 2.9 Hz), 118.3 (d, *J* = 21.3 Hz), 115.5 (d, *J* = 23.5 Hz), 83.5, 77.2, 39.9; $^{19}$F{$^{1}$H} NMR (376 MHz, $CDCl_3$) δ –112.78; HRMS (ESI/Orbitrap) m/z: $[M + H]^+$ Calcd for $C_{16}H_{13}FNO$ 254.0981; Found 254.0977.

**(2-((3a*S*,8a*R*)-3a,8a-dihydro-8*H*-indeno[1,2-*d*]oxazol-2-yl)-6-fluorophenyl)diphenylsilanol (L1c)**




Indanol (**1.41c**) (1.00 g, 3.95 mmol, 1.00 equiv) was dissolved in THF (13 mL) and purged under argon for 5 min. The reaction was cooled to –78 °C and TMEDA (0.71 mL, 4.7 mmol, 1.2 equiv) was added followed by the dropwise addition of *sec*-butyl lithium (1.4 M, 3.64 mL, 4.74 mmol, 1.20 equiv). The reaction was allowed to stir at –78 °C for 2 h and then diphenylchlorosilane (1.12 mL, 5.14 mmol, 1.30 equiv) was added. The reaction was allowed to warm to room temperature and then stirred for an additional 30 min at which time it was quenched with saturated aq. $NaHCO_3$ (10 mL). The aqueous phase was extracted with diethyl ether (3 × 5 mL), and the combined organic phase was washed with brine (2 × 5 mL). The combined organic phase was dried over $MgSO_4$, filtered, and concentrated *in vacuo*. The reaction mixture was filter through a silica plug (hexanes/EtOAc, 3:1 *v*/*v*) to yield the mixture of unreacted indanol and the corresponding silane. The resulting mixture was carried on to the next step. Confirmation of the product was obtained through diagnostic peaks in the $^{1}$H NMR and $^{19}$F NMR with a diagnostic peak at δ -94.09 ppm.

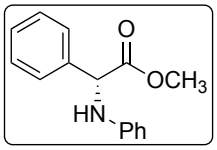
For silanol formation, a mixture of unreacted indanol and silane (4:1, 800 mg, 1.8 mmol, 1.0 equiv, calculated based off silane) was dissolved in diethyl ether (30 mL). Pd/C (0.20 g, 0.090 mmol, 0.050 equiv, 5 wt %) was added followed by the dropwise addition of deionized water (0.331 mL, 18.4 mmol,

10.0 equiv). The reaction was capped with a septum was stirred at room temperature for 3 h and monitored by TLC for the consumption of starting material (Caution: $H_2$ gas evolves as the reaction proceeds). The Pd/C was removed by filtration and the filtrate was dried over $MgSO_4$. The reaction mixture was purified by flash chromatography (5:1 hexanes/EtOAc) to yield silanol as a white solid (0.678 g, 82%).

$^1$H NMR (400 MHz, $CDCl_3$) δ 8.05 (s, 1H), 7.75 (dd, *J* = 7.8, 1.1 Hz, 1H), 7.69 – 7.60 (m, 2H), 7.49 – 7.29 (m, 7H), 7.28 (d, *J* = 7.4 Hz, 1H), 7.27 – 7.15 (m, 5H), 7.04 (ddd, *J* = 8.6, 8.2, 1.1 Hz, 1H), 5.57 (d, *J* = 8.2 Hz, 1H), 5.27 (ddd, *J* = 8.3, 7.0, 1.8 Hz, 1H), 3.41 (dd, *J* = 18.0, 7.0 Hz, 1H), 3.17 (dd, *J* = 18.0, 1.8 Hz, 1H); $^{13}$C{$^1$H} NMR (101 MHz, $CDCl_3$) δ 167.2 (d, *J* = 242.8 Hz), 165.7 (d, *J* = 3.3 Hz), 140.6, 139.4, 137.0 (d, *J* = 2.9 Hz), 136.6 (d, *J* = 2.6 Hz), 134.9 (d, *J* = 9.9 Hz), 134.62, 134.60, 134.58, 134.56, 131.8 (d, *J* = 9.5 Hz), 129.7, 129.5, 128.9, 127.9, 127.7, 127.6, 126.7 (d, *J* = 2.9 Hz), 125.6 (d, *J* = 11.0 Hz), 124.4 (d, *J* = 28.6 Hz), 118.9 (d, *J* = 27.5 Hz), 83.3, 76.2, 39.7; $^{19}$F{$^1$H} NMR (376 MHz, $CDCl_3$) δ –89.56; $^{29}$Si{$^1$H} NMR (79 MHz, $CDCl_3$) δ -17.55 (d, *J* = 10.6 Hz); IR (neat) 3321, 3068, 2918, 1633, 1593, 1427, 1113, 1022, 999, 883, 698 cm$^{-1}$; HRMS (ESI/Orbitrap) m/z: $[M + H]^+$ Calcd for $C_{28}H_{23}FNO_2Si$ 452.1482; Found 452.1500.

**Enantioselective N−H insertion products:**

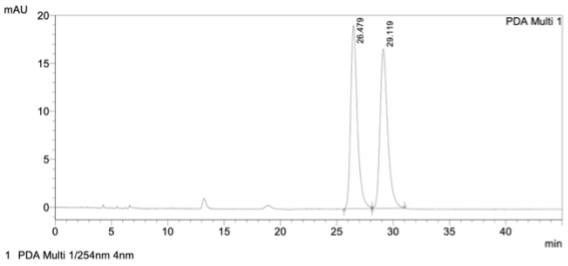
**methyl (*R*)-2-phenyl-2-(phenylamino)acetate (1.31a)**




According to the General Procedure G, diazoacetate **1.30a** (35.2 mg, 0.200 mmol) and aniline (18.6 mg, 0.200 mmol) were used and the reaction was stirred for 1 h. The product was purified using flash column chromatography ($SiO_2$, hexanes/EtOAc, 95:5 *v*/*v*) and isolated as a white solid (38.6 mg, 80%). $^1$H NMR spectral data matches that of a previous report.[89]

HPLC analysis: Chiralpak OD-H column, n-hexane/2-propanol = 99/1, 0.7 mL/min, λ = 254 nm, 40 °C, $t_R$ (*R*, major) = 26.3 min; $t_R$ (*S*, minor) = 36.8 min, 91:9 er.

*HPLC trace for: (A) racemic standard of **1.31a***



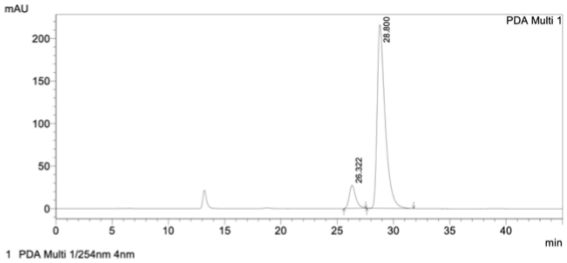

**< Peak Table >**

PeakTable C:\LabSolutions\Training1107\YPC\YPC-2-190-RAC.lcd

PDA Ch1 254nm 4nm

| Peak# | Ret. Time | Area | Height | Area % | Height % |
|---|---|---|---|---|---|
| 1 | 26.479 | 788858 | 19076 | 50.360 | 53.460 |
| 2 | 29.119 | 777588 | 16606 | 49.640 | 46.540 |
| Total | | 1566446 | 35682 | 100.000 | 100.000 |

*(B) enantiomerically enriched **(R)-1.31a***



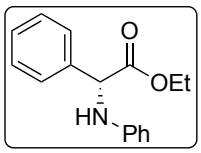

**< Peak Table >**

PeakTable C:\LabSolutions\Training1107\YPC\YPC-3-40-L.lcd

PDA Ch1 254nm 4nm

| Peak# | Ret. Time | Area | Height | Area % | Height % |
|---|---|---|---|---|---|
| 1 | 26.322 | 1069979 | 27039 | 9.217 | 11.132 |
| 2 | 28.800 | 10538294 | 215852 | 90.783 | 88.868 |
| Total | | 11608273 | 242892 | 100.000 | 100.000 |

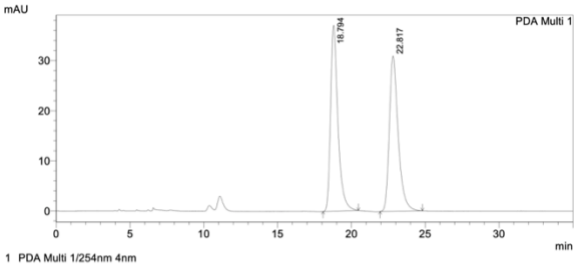
**ethyl (*R*)-2-phenyl-2-(phenylamino)acetate (1.31b)**




According to the General Procedure G, diazoacetate **1.30b** (38.0 mg, 0.200 mmol) and aniline (18.6 mg, 0.200 mmol) were used and the reaction was stirred for 1 h. The product was purified using flash column chromatography ($SiO_2$, hexanes/EtOAc, 95:5 *v*/*v*) and isolated as a white solid (43.9 mg, 86%). $^1$H NMR spectral data matches that of a previous report.[89]

HPLC analysis: Chiralpak OD-H column, n-hexane/2-propanol = 99/1, 0.7 mL/min, λ = 254 nm, 40 °C, $t_R$ (*R*, major) = 18.2 min; $t_R$ (*S*, minor) = 22.0 min, 92:8 er.

*HPLC trace for: (A) racemic standard of **1.31b***



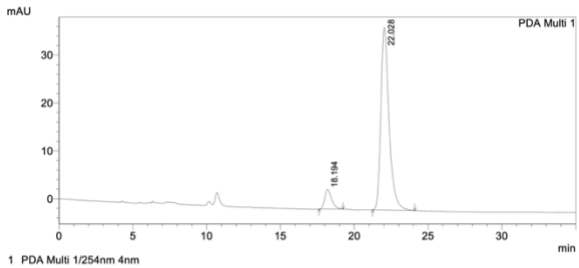

< Peak Table >

PeakTable C:\LabSolutions\Training1107\YPC\YPC-3-57-OEt-rac-OD-99-1-0.7ml-032922.lcd

PDA Ch1 254nm 4nm

| Peak# | Ret. Time | Area | Height | Area % | Height % |
|---|---|---|---|---|---|
| 1 | 18.794 | 1282963 | 37042 | 49.831 | 54.475 |
| 2 | 22.817 | 1291660 | 30956 | 50.169 | 45.525 |
| Total | | 2574623 | 67998 | 100.000 | 100.000 |

*(B) enantiomerically enriched **(R)-1.31b***



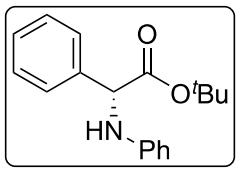

< Peak Table >

PeakTable C:\LabSolutions\Training1107\YPC\Optimization\YPC-3-57-OEt--2h-L-OD-99-1-0.7ml-2.lcd

PDA Ch1 254nm 4nm

| Peak# | Ret. Time | Area | Height | Area % | Height % |
|---|---|---|---|---|---|
| 1 | 18.194 | 133169 | 4108 | 8.344 | 9.728 |
| 2 | 22.028 | 1462768 | 38122 | 91.656 | 90.272 |
| Total | | 1595937 | 42230 | 100.000 | 100.000 |

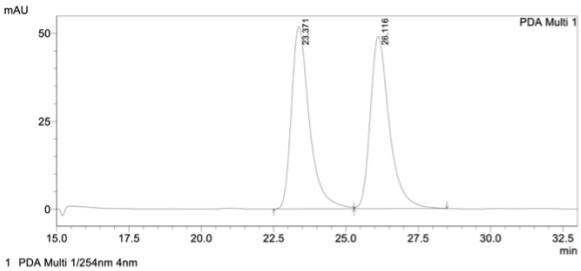
**_tert_-butyl (*R*)-2-phenyl-2-(phenylamino)acetate (1.31c)**




According to the General Procedure G, diazoacetate **1.30c** (43.6 mg, 0.200 mmol) and aniline (18.6 mg, 0.200 mmol) were used and the reaction was stirred for 1 h. The product was purified using flash column chromatography ($SiO_2$, hexanes/EtOAc, 95:5 *v*/*v*) and isolated as a white solid (50.0 mg, 89%). $^1$H NMR spectral data matches that of a previous report.[89]

HPLC analysis: Chiralpak OD-H column, n-hexane/2-propanol = 99.5/0.5, 0.2 mL/min, λ = 254 nm, 40 °C, $t_R$ (*R*, major) = 25.4 min; $t_R$ (*S*, minor) = 25.8 min, 91:9 er.

*HPLC trace for: (A) racemic standard of **1.31c*** *(B) enantiomerically enriched **(R)-1.31c***

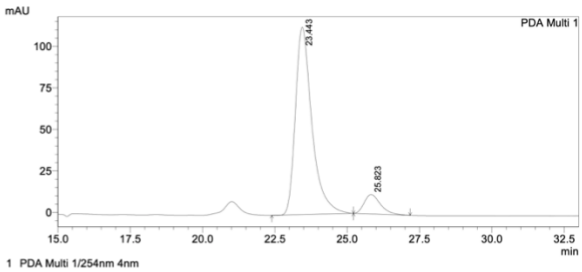



< Peak Table >

PeakTable C:\LabSolutions\Training1107\YPC\Optimization\YPC-3-16-OtBu-rac-OD-95-5-0.2-2.lcd

PDA Ch1 254nm 4nm

| Peak# | Ret. Time | Area | Height | Area % | Height % |
|---|---|---|---|---|---|
| 1 | 23.371 | 2241643 | 51826 | 50.093 | 51.435 |
| 2 | 26.116 | 2233363 | 48935 | 49.907 | 48.565 |
| Total | | 4475006 | 100760 | 100.000 | 100.000 |




< Peak Table >

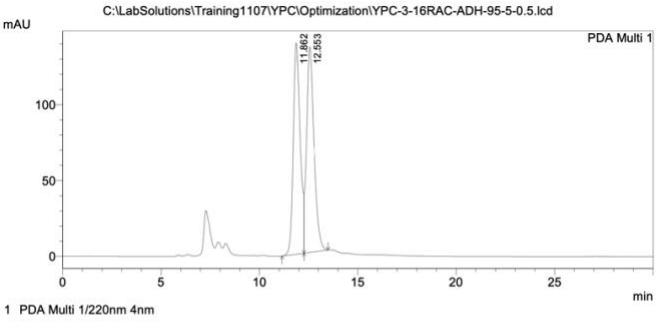
PeakTable C:\LabSolutions\Training1107\YPC\YPC-3-53-OtBu-L-OD-95-5-0.2.lcd

PDA Ch1 254nm 4nm

| Peak# | Ret. Time | Area | Height | Area % | Height % |
|---|---|---|---|---|---|
| 1 | 23.443 | 4479188 | 112853 | 90.697 | 90.587 |
| 2 | 25.823 | 459460 | 11727 | 9.303 | 9.413 |
| Total | | 4938648 | 124581 | 100.000 | 100.000 |

***Note***: The HPLC data obtained below using Chiralpak AD-H column was utilized to determine the absolute configuration of compound **1.31a−s**. The major and minor peaks are discernible and used for comparison with previous HPLC data.[89]

HPLC analysis: Chiralpak AD-H column, n-hexane/2-propanol = 95/5, 0.5 mL/min, λ = 220 nm, 40 °C, $t_R$ (*R*, major) = 11.7 min; $t_R$ (*S*, minor) = 12.3 min.

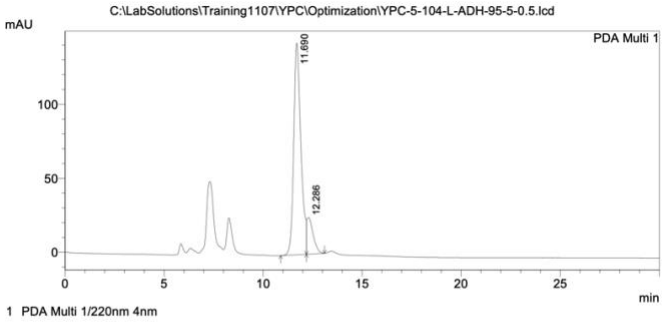



< Peak Table >

PeakTable C:\LabSolutions\Training1107\YPC\Optimization\YPC-3-16RAC-ADH-95-5-0.5.lcd

PDA Ch1 220nm 4nm

| Peak# | Ret. Time | Area | Height | Area % | Height % |
|---|---|---|---|---|---|
| 1 | 11.862 | 3399579 | 139314 | 48.512 | 50.699 |
| 2 | 12.553 | 3608123 | 135471 | 51.488 | 49.301 |
| Total | | 7007702 | 274784 | 100.000 | 100.000 |



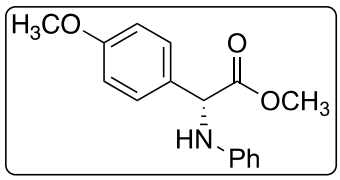

< Peak Table >

PeakTable C:\LabSolutions\Training1107\YPC\Optimization\YPC-5-104-L-ADH-95-5-0.5.lcd

PDA Ch1 220nm 4nm

| Peak# | Ret. Time | Area | Height | Area % | Height % |
|---|---|---|---|---|---|
| 1 | 11.690 | 3600855 | 142969 | 86.605 | 85.254 |
| 2 | 12.286 | 556916 | 24728 | 13.395 | 14.746 |
| Total | | 4157771 | 167697 | 100.000 | 100.000 |

**methyl (*R*)-2-(4-methoxyphenyl)-2-(phenylamino)acetate (1.31d)**

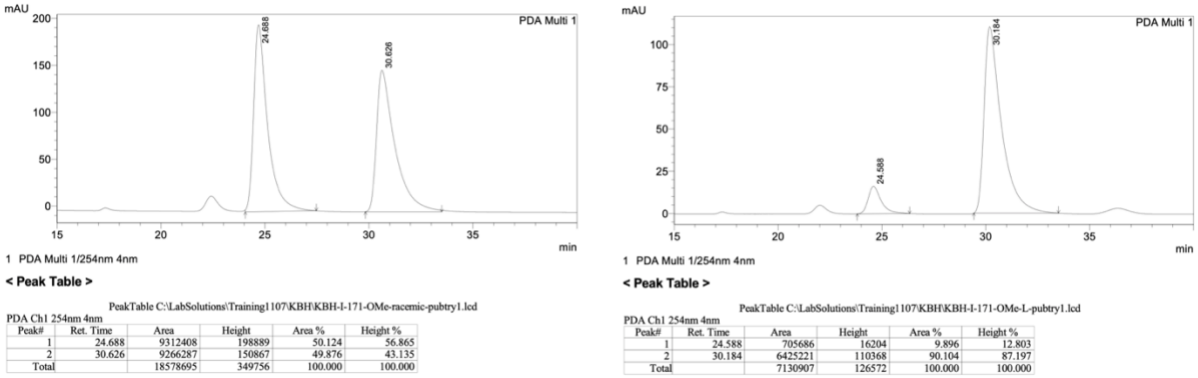



According to the General Procedure G, diazoacetate **1.30d** (41.2 mg, 0.200 mmol) and aniline (18.6 mg, 0.200 mmol) were used and the reaction was stirred for 1 h. The product was purified using flash column

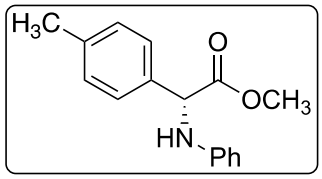
chromatography ($SiO_2$, hexanes/EtOAc, 96:4 *v*/*v*) and isolated as a white solid (28.7 mg, 53%). $^1$H NMR spectral data matches that of a previous report.[89]

HPLC analysis: Chiralpak OD-H column, n-hexane/2-propanol = 99/1, 1.0 mL/min, λ = 254 nm, 40 °C, $t_R$ (*S*, minor) = 24.6 min; $t_R$ (*R*, major) = 30.2 min, 90:10 er.

*HPLC trace for: (A) racemic standard of* ***1.31d*** *(B) enantiomerically enriched* ***(R)-1.31d***



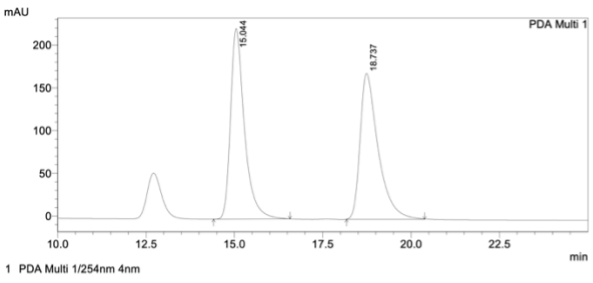

**methyl (*R*)-2-(phenylamino)-2-(*p*-tolyl)acetate (1.31e)**




According to the General Procedure G, diazoacetate **1.30e** (38.1 mg, 0.200 mmol) and aniline (18.6 mg, 0.200 mmol) were used and the reaction was stirred for 1 h. The product was purified using flash column chromatography ($SiO_2$, hexanes/EtOAc, 90:10 *v*/*v*) and isolated as a white solid (43 mg, 84%). $^1$H NMR spectral data matches that of a previous report.[78]

HPLC analysis: Chiralpak OD-H column, n-hexane/2-propanol = 99/1, 1.0 mL/min, λ = 254 nm, 40 °C, $t_R$ (*S*, minor) = 15.2 min; $t_R$ (*R*, major) = 18.9 min, 89:11 er.

*HPLC trace for: (A) racemic standard of* ***1.31e*** *(B) enantiomerically enriched* ***(R)-1.31e***

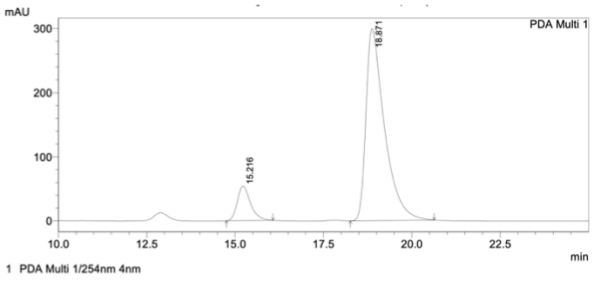



< Peak Table >

PeakTable C:\LabSolutions\Training1107\KBH\KBH-I-171-Me-racemic-pubtry1.lcd

PDA Ch1 254nm 4nm

| Peak# | Ret. Time | Area | Height | Area % | Height % |
|---|---|---|---|---|---|
| 1 | 15.044 | 6099927 | 222729 | 50.161 | 56.602 |
| 2 | 18.737 | 6060710 | 170773 | 49.839 | 43.398 |
| Total | | 12160637 | 393502 | 100.000 | 100.000 |



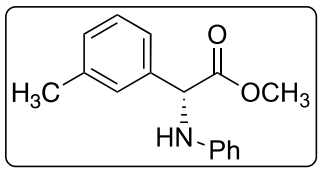

< Peak Table >

PeakTable C:\LabSolutions\Training1107\KBH\KBH-I-171-Me-L-pubtry1.lcd

PDA Ch1 254nm 4nm

| Peak# | Ret. Time | Area | Height | Area % | Height % |
|---|---|---|---|---|---|
| 1 | 15.216 | 1401259 | 53811 | 11.406 | 15.244 |
| 2 | 18.871 | 10884094 | 299180 | 88.594 | 84.756 |
| Total | | 12285353 | 352991 | 100.000 | 100.000 |

**methyl (*R*)-2-(phenylamino)-2-(*m*-tolyl)acetate (1.31f)**

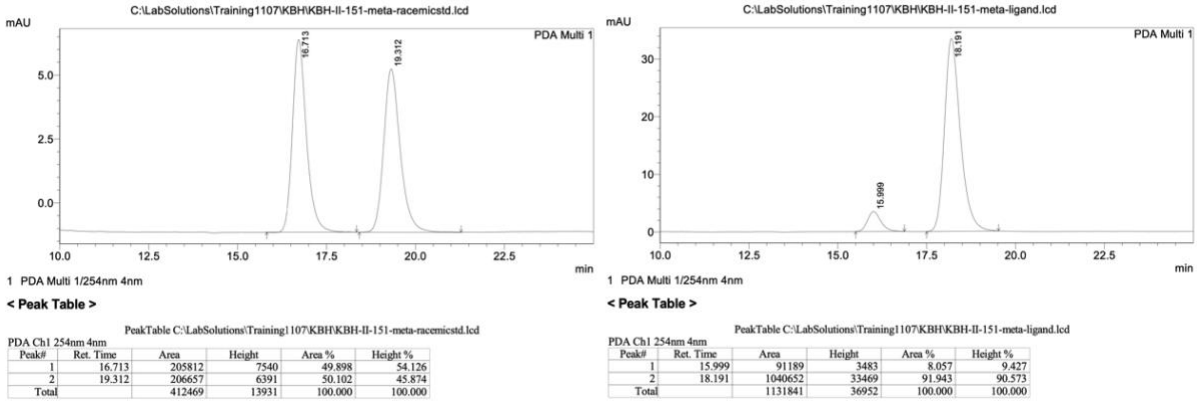



According to the General Procedure G, diazoacetate **1.30f** (38.1 mg, 0.200 mmol) and aniline (18.6 mg, 0.200 mmol) were used and the reaction was stirred for 1 h. The product was purified using flash column chromatography ($SiO_2$, hexanes/EtOAc, 90:10 *v*/*v*) and isolated as a white solid (39 mg, 76%).

$^1$H NMR (300 MHz, $CDCl_3$) δ 7.33 – 7.22 (m, 2H), 7.27 – 7.18 (m, 1H), 7.19 – 7.06 (m, 3H), 6.70 (tt, *J* = 7.3, 1.1 Hz, 1H), 6.56 (dd, *J* = 8.7, 1.1 Hz, 2H), 5.03 (d, *J* = 5.8 Hz, 1H), 4.90 (d, *J* = 5.8 Hz, 1H), 3.72 (s, 3H), 2.34 (s, 3H); $^{13}$C NMR (76 MHz, $CDCl_3$) δ 172.6, 146.2, 138.8, 137.7, 129.4, 129.3, 128.9, 128.0, 124.5, 118.2, 113.5, 60.9, 52.9, 21.6; HRMS (ESI/Orbitrap) m/z: $[M + H]^+$ Calcd for $C_{16}H_{18}NO_2$ 256.1337; Found 256.1333.

HPLC analysis: Chiralpak OD-H column, n-hexane/2-propanol = 99/1, 1.0 mL/min, λ = 254 nm, 40 °C, $t_R$ (*S*, minor) = 16.0 min; $t_R$ (*R*, major) = 18.2 min, 92:8 er.

*HPLC trace for: (A) racemic standard of **1.31f*** *(B) enantiomerically enriched **(R)-1.31f***



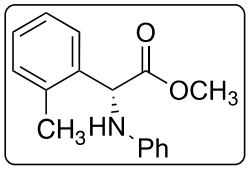

PeakTable C:\LabSolutions\Training1107\KBH\KBH-II-151-meta-racemicstd.lcd
PDA Ch1 254nm 4nm

| Peak# | Ret. Time | Area | Height | Area % | Height % |
|---|---|---|---|---|---|
| 1 | 16.713 | 205812 | 7540 | 49.898 | 54.126 |
| 2 | 19.312 | 206657 | 6391 | 50.102 | 45.874 |
| Total | | 412469 | 13931 | 100.000 | 100.000 |

PeakTable C:\LabSolutions\Training1107\KBH\KBH-II-151-meta-ligand.lcd
PDA Ch1 254nm 4nm

| Peak# | Ret. Time | Area | Height | Area % | Height % |
|---|---|---|---|---|---|
| 1 | 15.999 | 91189 | 3483 | 8.057 | 9.427 |
| 2 | 18.191 | 1040652 | 33469 | 91.943 | 90.573 |
| Total | | 1131841 | 36952 | 100.000 | 100.000 |

**methyl (*R*)-2-(phenylamino)-2-(*o*-tolyl)acetate (1.31g)**

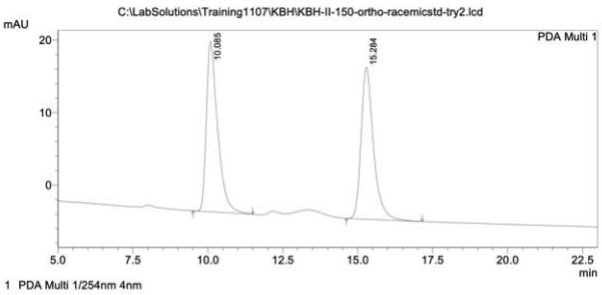



According to the General Procedure G, diazoacetate **1.30g** (38.1 mg, 0.200 mmol) and aniline (18.6 mg, 0.200 mmol) were used and the reaction was stirred for 1 h. The product was purified using flash column chromatography ($SiO_2$, hexanes/EtOAc, 90:10 *v*/*v*) and isolated as a white solid (34 mg, 67%).

HPLC analysis: Chiralpak OD-H column, n-hexane/2-propanol = 99/1, 1.0 mL/min, λ = 254 nm, 40 °C, $t_R$ (*R*, major) = 10.3 min; $t_R$ (*S*, minor) = 15.5 min, 71:29 er.

$^1$H NMR (400 MHz, $CDCl_3$) δ 7.39 (d, *J* = 6.8 Hz, 1H), 7.24 – 7.14 (m, 3H), 7.12 (tt, *J* = 7.3, 2.1 Hz, 2H), 6.70 (tt, *J* = 7.3, 1.2 Hz, 1H), 6.57 – 6.48 (m, 2H), 5.28 (d, *J* = 6.1 Hz, 1H), 4.80 (d, *J* = 6.1 Hz, 1H), 3.72 (s, 3H), 2.53 (s, 3H); $^{13}$C NMR (101 MHz, $CDCl_3$) δ 172.9, 146.3, 136.7, 136.0, 131.1, 129.4, 128.3, 126.8, 126.6, 118.3, 113.3, 57.5, 52.8, 19.6; HRMS (ESI/Orbitrap) m/z: $[M + H]^+$ Calcd for $C_{16}H_{18}NO_2$ 256.1337; Found 256.1333.

*HPLC trace for: (A) racemic standard of **1.31g*** *(B) enantiomerically enriched **(R)-1.31g***

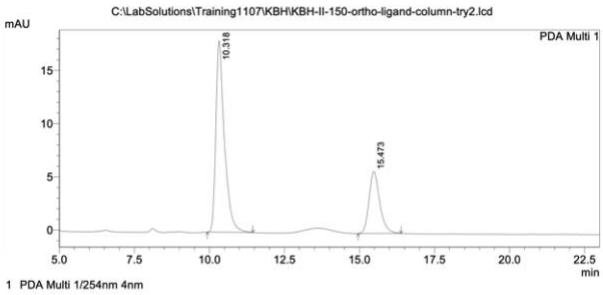



< Peak Table >

PeakTable C:\LabSolutions\Training1107\KBH\KBH-II-150-ortho-racemicstd-try2.lcd

PDA Ch1 254nm 4nm

| Peak# | Ret. Time | Area | Height | Area % | Height % |
|---|---|---|---|---|---|
| 1 | 10.085 | 610792 | 23525 | 50.286 | 52.891 |
| 2 | 15.284 | 603833 | 20953 | 49.714 | 47.109 |
| Total | | 1214624 | 44479 | 100.000 | 100.000 |



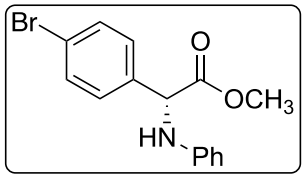

< Peak Table >

PeakTable C:\LabSolutions\Training1107\KBH\KBH-II-150-ortho-ligand-column-try2.lcd

PDA Ch1 254nm 4nm

| Peak# | Ret. Time | Area | Height | Area % | Height % |
|---|---|---|---|---|---|
| 1 | 10.318 | 356654 | 17990 | 71.224 | 75.567 |
| 2 | 15.473 | 144098 | 5817 | 28.776 | 24.433 |
| Total | | 500752 | 23807 | 100.000 | 100.000 |

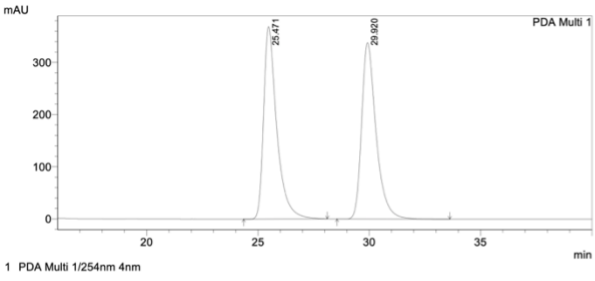
**methyl (*R*)-2-(4-bromophenyl)-2-(phenylamino)acetate (1.31h)**




According to the General Procedure G, diazoacetate **1.30h** (50.8 mg, 0.200 mmol) and aniline (18.6 mg, 0.200 mmol) were used and the reaction was stirred for 2 h. The product was purified using flash column chromatography ($SiO_2$, hexanes/EtOAc, 95:5 *v*/*v*) and isolated as a white solid (46.0 mg, 72%). $^1$H NMR spectral data matches that of a previous report.[89]

HPLC analysis: Chiralpak OD-H column, n-hexane/2-propanol = 97/3, 0.5 mL/min, λ = 254 nm, 40 °C, $t_R$ (*R*, major) = 25.9 min; $t_R$ (*S*, minor) = 30.4 min, 86:14 er.

*HPLC trace for: (A) racemic standard of **1.31h*** *(B) enantiomerically enriched **(R)-1.31h***

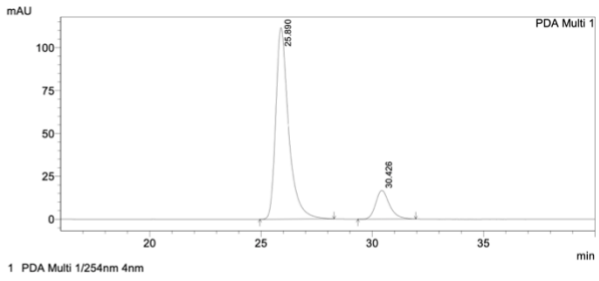



< Peak Table >

PeakTable C:\LabSolutions\Training1107\YPC\YPC-3-76-4-Br-DA-rac-OD-97-3-0.5ml.lcd

PDA Ch1 254nm 4nm

| Peak# | Ret. Time | Area | Height | Area % | Height % |
|---|---|---|---|---|---|
| 1 | 25.471 | 15155418 | 368890 | 49.885 | 52.173 |
| 2 | 29.920 | 15225217 | 338158 | 50.115 | 47.827 |
| Total | | 30380635 | 707049 | 100.000 | 100.000 |



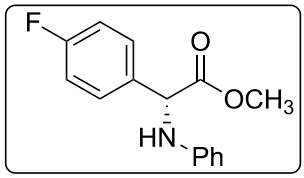

< Peak Table >

PeakTable C:\LabSolutions\Training1107\YPC\YPC-3-76-4-Br-DA-L-OD-97-3-0.5ml.lcd

PDA Ch1 254nm 4nm

| Peak# | Ret. Time | Area | Height | Area % | Height % |
|---|---|---|---|---|---|
| 1 | 25.890 | 4506985 | 111555 | 86.255 | 86.989 |
| 2 | 30.426 | 718177 | 16685 | 13.745 | 13.011 |
| Total | | 5225163 | 128240 | 100.000 | 100.000 |

**methyl (*R*)-2-(4-fluorophenyl)-2-(phenylamino)acetate (1.31i)**

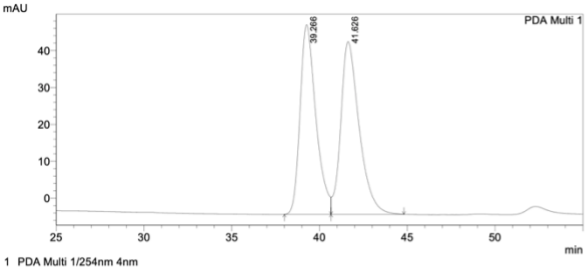



According to the General Procedure G, diazoacetate **1.30i** (38.8 mg, 0.200 mmol) and aniline (18.6 mg, 0.200 mmol) were used and the reaction was stirred for 1 h. The product was purified using flash column chromatography ($SiO_2$, hexanes/EtOAc, 95:5 *v*/*v*) and isolated as a white solid (47.7 mg, 92%).

$^1$H NMR (400 MHz, $CDCl_3$) δ 7.53 – 7.43 (m, 2H), 7.13 (dd, *J* = 8.6, 7.3 Hz, 2H), 7.05 (t, *J* = 8.6 Hz, 2H), 6.72 (tt, *J* = 7.3, 1.1 Hz, 1H), 6.55 (dd, *J* = 8.7, 1.1 Hz, 2H), 5.07 (d, *J* = 5.7 Hz, 1H), 4.97 (d, *J* = 5.7 Hz, 1H), 3.75 (s, 3H); $^{13}$C{$^1$H} NMR (101 MHz, $CDCl_3$) δ 172.1, 162.7 (d, *J* = 246.9 Hz), 145.7, 133.4 (d, *J* = 3.3 Hz), 129.3, 128.9 (d, *J* = 8.1 Hz), 118.3, 115.8 (d, *J* = 21.6 Hz), 113.4, 60.0, 52.9; $^{19}$F{$^1$H} NMR (376 MHz, $CDCl_3$) δ –113.84; HRMS (ESI/Orbitrap) m/z: $[M + H]^+$ Calcd for $C_{15}H_{15}FNO_2$ 260.1087; Found 260.1083.

HPLC analysis: Chiralpak OD-H column, n-hexane/2-propanol = 99.5/0.5, 0.8 mL/min, λ = 254 nm, 40 °C, $t_R$ (*S*, minor) = 39.7 min; $t_R$ (*R*, major) = 42.0 min, 82:18 er.

*HPLC trace for: (A) racemic standard of **1.31i***




1 PDA Multi 1/254nm 4nm

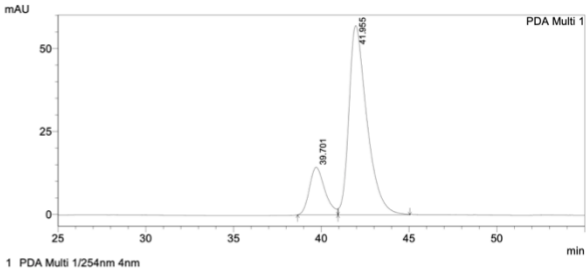
**< Peak Table >**

PeakTable C:\LabSolutions\Training1107\KBH\KBH-I-171-F-racemic-pubtry1.lcd

PDA Ch1 254nm 4nm

| Peak# | Ret. Time | Area | Height | Area % | Height % |
|---|---|---|---|---|---|
| 1 | 39.266 | 3218658 | 51347 | 48.583 | 52.337 |
| 2 | 41.626 | 3406352 | 46761 | 51.417 | 47.663 |
| Total | | 6625010 | 98108 | 100.000 | 100.000 |

*(B) enantiomerically enriched **(R)-1.31i***




1 PDA Multi 1/254nm 4nm

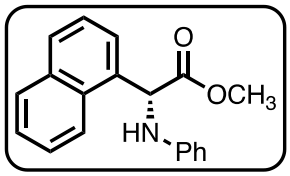
**< Peak Table >**

PeakTable C:\LabSolutions\Training1107\KBH\KBH-I-171-F-L-pubtry1.lcd

PDA Ch1 254nm 4nm

| Peak# | Ret. Time | Area | Height | Area % | Height % |
|---|---|---|---|---|---|
| 1 | 39.701 | 877792 | 14337 | 17.717 | 20.105 |
| 2 | 41.955 | 4076842 | 56976 | 82.283 | 79.895 |
| Total | | 4954633 | 71313 | 100.000 | 100.000 |

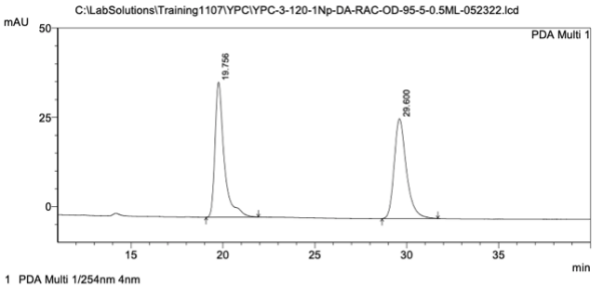
**methyl (*R*)-2-(naphthalen-1-yl)-2-(phenylamino)acetate (1.31j)**




According to the General Procedure G, diazoacetate **1.30j** (45.2 mg, 0.200 mmol) and aniline (18.6 mg, 0.200 mmol) were used and the reaction was stirred for 2 h. The product was purified using flash column chromatography ($SiO_2$, hexanes/EtOAc, 95:5 *v*/*v*) and isolated as a white solid (50.4 mg, 87%). $^1$H NMR spectral data matches that of a previous report.[89]

HPLC analysis: Chiralpak OD-H column, n-hexane/2-propanol = 95/5, 0.5 mL/min, λ = 254 nm, 40 °C, $t_R$ (*R*, major) = 19.0 min; $t_R$ (*S*, minor) = 27.8 min, 82:18 er.

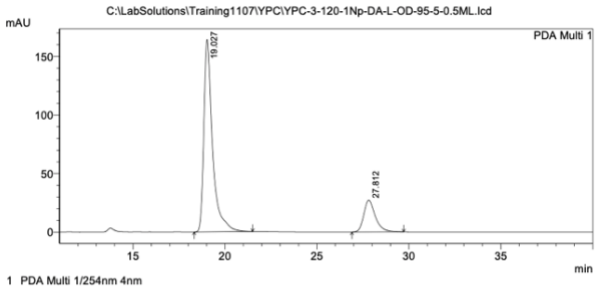
*HPLC trace for: (A) racemic standard of **1.31j***




PeakTable C:\LabSolutions\Training1107\YPC\YPC-3-120-1Np-DA-RAC-OD-95-5-0.5ML-052322.lcd
PDA Ch1 254nm 4nm

| Peak# | Ret. Time | Area | Height | Area % | Height % |
|---|---|---|---|---|---|
| 1 | 19.756 | 1318768 | 37825 | 50.507 | 57.493 |
| 2 | 29.600 | 1292294 | 27965 | 49.493 | 42.507 |
| Total | | 2611062 | 65790 | 100.000 | 100.000 |

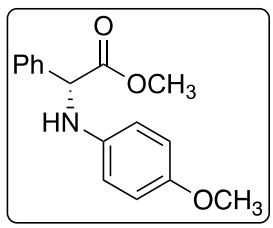
*(B) enantiomerically enriched **(R)-1.31j***




PeakTable C:\LabSolutions\Training1107\YPC\YPC-3-120-1Np-DA-L-OD-95-5-0.5ML.lcd
PDA Ch1 254nm 4nm

| Peak# | Ret. Time | Area | Height | Area % | Height % |
|---|---|---|---|---|---|
| 1 | 19.027 | 5398404 | 164151 | 81.961 | 85.791 |
| 2 | 27.812 | 1188163 | 27186 | 18.039 | 14.209 |
| Total | | 6586567 | 191337 | 100.000 | 100.000 |

**methyl (*R*)-2-((4-methoxyphenyl)amino)-2-phenylacetate (1.31k)**

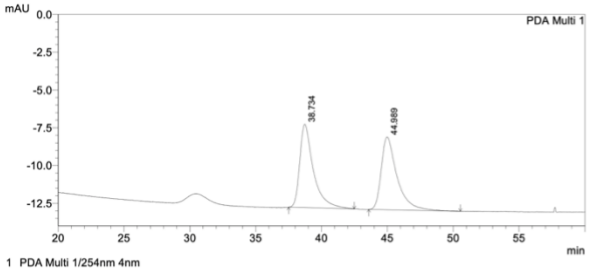



According to the General Procedure G, α-phenyl-α-diazoesters **1.30a** (35.2 mg, 0.200 mmol) and *p*-anisidine **1.23k** (24.6 mg, 0.200 mmol) were used and the reaction was stirred for 16 h. The product

was purified using flash column chromatography ($SiO_2$, hexanes/EtOAc, 95:5 *v*/*v*) and isolated as a white solid (30.2 mg, 56%). $^1$H NMR spectral data matches that of a previous report.[89]

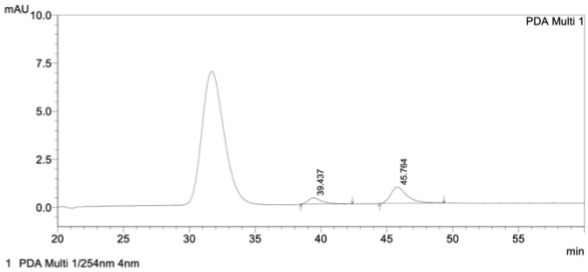
HPLC analysis: Chiralpak OD-H column, n-hexane/2-propanol = 99.5/0.5, 1.0 mL/min, λ = 254 nm, 40 °C, $t_R$ (*S*, minor) = 39.4 min; $t_R$ (*R*, major) = 45.8 min, 76:24 er.

*HPLC trace for: (A) racemic standard of **1.31k***



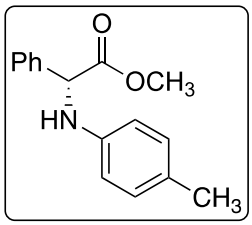

| Peak# | Ret. Time | Area | Height | Area % | Height % |
|---|---|---|---|---|---|
| 1 | 38.734 | 396475 | 5514 | 49.715 | 53.354 |
| 2 | 44.989 | 401024 | 4820 | 50.285 | 46.646 |
| Total | | 797499 | 10334 | 100.000 | 100.000 |

*(B) enantiomerically enriched **(R)-31k***




| Peak# | Ret. Time | Area | Height | Area % | Height % |
|---|---|---|---|---|---|
| 1 | 39.437 | 23183 | 324 | 24.156 | 27.787 |
| 2 | 45.764 | 72790 | 841 | 75.844 | 72.213 |
| Total | | 95973 | 1164 | 100.000 | 100.000 |

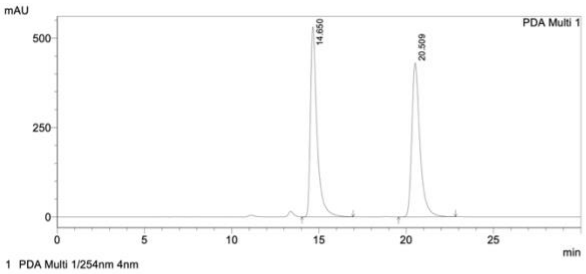
**methyl (*R*)-2-phenyl-2-(*p*-tolylamino)acetate (1.31l)**




According to the General Procedure G, α-phenyl-α-diazoesters **1.30a** (35.2 mg, 0.200 mmol) and *p*-toluidine **1.23l** (21.4 mg, 0.200 mmol) were used and the reaction was stirred for 16 h. The product was purified using flash column chromatography ($SiO_2$, hexanes/EtOAc, 95:5 *v*/*v*) and isolated as a white solid (38.3 mg, 75%). $^1$H NMR spectral data matches that of a previous report.[90]

HPLC analysis: Chiralpak OD-H column, n-hexane/2-propanol = 97/3, 0.5 mL/min, λ = 254 nm, 40 °C, $t_R$ (*R*, major) = 14.7 min; $t_R$ (*S*, minor) = 20.2 min, 87:13 er.

*HPLC trace for: (A) racemic standard of **1.31l*** *(B) enantiomerically enriched **(R)-1.31l***

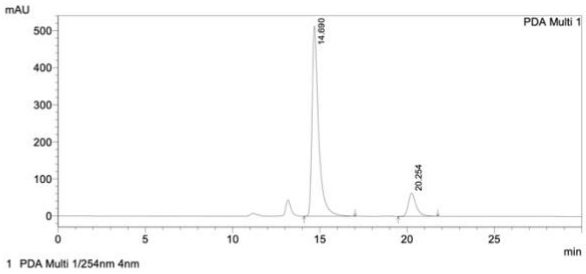



< Peak Table >

PeakTable C:\LabSolutions\Training1107\YPC\YPC-3-91-4-Me-NH2-rac-OD-97-3-0.5ml.lcd

PDA Ch1 254nm 4nm

| Peak# | Ret. Time | Area | Height | Area % | Height % |
|---|---|---|---|---|---|
| 1 | 14.650 | 13875020 | 530958 | 49.952 | 55.224 |
| 2 | 20.509 | 13901843 | 430505 | 50.048 | 44.776 |
| Total | | 27776863 | 961463 | 100.000 | 100.000 |



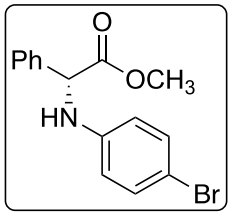

< Peak Table >

PeakTable C:\LabSolutions\Training1107\YPC\YPC-3-91-4-Me-NH2-L-OD-97-3-0.5ml.lcd

PDA Ch1 254nm 4nm

| Peak# | Ret. Time | Area | Height | Area % | Height % |
|---|---|---|---|---|---|
| 1 | 14.690 | 13402270 | 512636 | 87.198 | 89.111 |
| 2 | 20.254 | 1967649 | 62642 | 12.802 | 10.889 |
| Total | | 15369919 | 575277 | 100.000 | 100.000 |

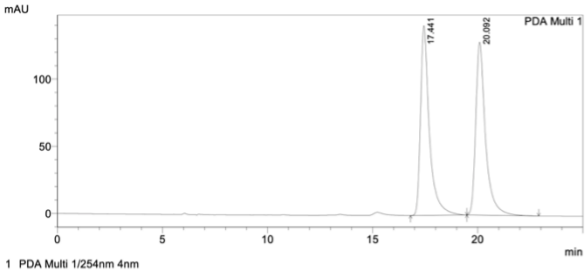
**methyl (*R*)-2-((4-bromophenyl)amino)-2-phenylacetate (1.31m)**




According to the General Procedure G, α-phenyl-α-diazoesters **1.30a** (35.2 mg, 0.200 mmol) and 4-bromoaniline (34.4 mg, 0.200 mmol) were used and the reaction was stirred for 45 min. The product was purified using flash column chromatography ($SiO_2$, hexanes/EtOAc, 95:5 *v*/*v*) and isolated as a white solid (43.8 mg, 69%). $^1$H NMR spectral data matches that of a previous report.[89]

HPLC analysis: Chiralpak OD-H column, n-hexane/2-propanol = 97/3, 0.5 mL/min, λ = 254 nm, 40 °C, $t_R$ (*R*, major) = 17.0 min; $t_R$ (*S*, minor) = 19.7 min, 92:8 er.

*HPLC trace for: (A) racemic standard of **1.31m*** *(B) enantiomerically enriched **(R)-1.31m***

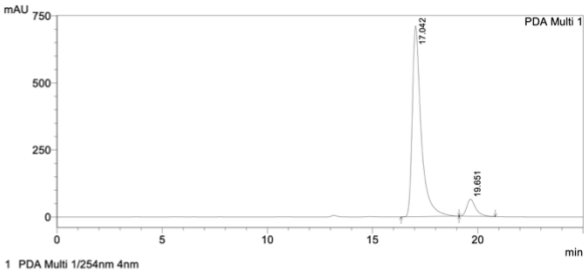



< Peak Table >

PeakTable C:\LabSolutions\Training1107\YPC\YPC-3-87-4-Br-NH2-rac-OD-97-3-0.5ml.lcd

PDA Ch1 254nm 4nm

| Peak# | Ret. Time | Area | Height | Area % | Height % |
|---|---|---|---|---|---|
| 1 | 17.441 | 4144528 | 141243 | 49.978 | 52.313 |
| 2 | 20.092 | 4148122 | 128756 | 50.022 | 47.687 |
| Total | | 8292650 | 269999 | 100.000 | 100.000 |



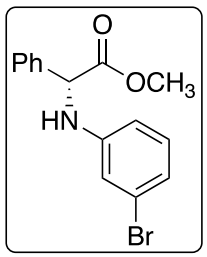

< Peak Table >

PeakTable C:\LabSolutions\Training1107\YPC\YPC-3-87-4-Br-NH2-L-OD-97-3-0.5ml.lcd

PDA Ch1 254nm 4nm

| Peak# | Ret. Time | Area | Height | Area % | Height % |
|---|---|---|---|---|---|
| 1 | 17.042 | 20949940 | 710931 | 91.659 | 91.792 |
| 2 | 19.651 | 1906447 | 63572 | 8.341 | 8.208 |
| Total | | 22856387 | 774503 | 100.000 | 100.000 |

**methyl (*R*)-2-((3-bromophenyl)amino)-2-phenylacetate (1.31n)**

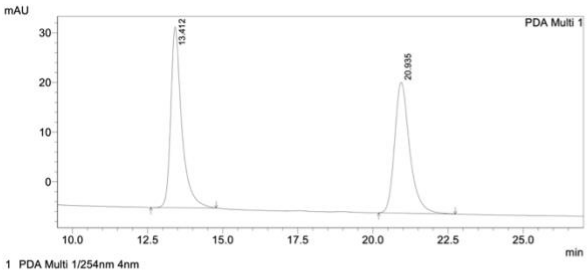



According to the General Procedure G, α-phenyl-α-diazoesters **1.30a** (35.2 mg, 0.200 mmol) and 3-bromoaniline (34.4 mg, 0.200 mmol) were used and the reaction was stirred for 2 h. The product was purified using flash column chromatography ($SiO_2$, hexanes/EtOAc, 98:2 *v*/*v*) and isolated as a white solid (43.3 mg, 68%). $R_f$ = 0.37 (hexanes/EtOAc, 97:3 *v*/*v*).

$^1$H NMR (400 MHz, $CDCl_3$) δ 7.52 – 7.42 (m, 2H), 7.40 – 7.27 (m, 3H), 6.95 (dd, *J* = 8.0, 8.0 Hz, 1H), 6.80 (ddd, *J* = 7.9, 1.8, 1.0 Hz, 1H), 6.70 (dd, *J* = 2.1, 2.1 Hz, 1H), 6.44 (ddd, *J* = 8.3, 2.4, 1.0 Hz, 1H), 5.09 – 5.00 (m, 2H), 3.73 (s, 3H); $^{13}$C NMR (101 MHz, $CDCl_3$) δ 172.0, 147.3, 137.1, 130.6, 129.1, 128.6, 127.3, 123.3, 121.1, 116.3, 112.1, 60.5, 53.1; HRMS (ESI/Orbitrap) m/z: $[M + H]^+$ Calcd for $C_{15}H_{15}BrNO_2$ 320.0286; Found 320.0287.

HPLC analysis: Chiralpak OD-H column, n-hexane/2-propanol = 99/1, 1.0 mL/min, λ = 254 nm, 40 °C, $t_R$ (*R*, major) = 12.9 min; $t_R$ (*S*, minor) = 20.0 min, 90:10 er.

*HPLC trace for: (A) racemic standard of **1.31n***



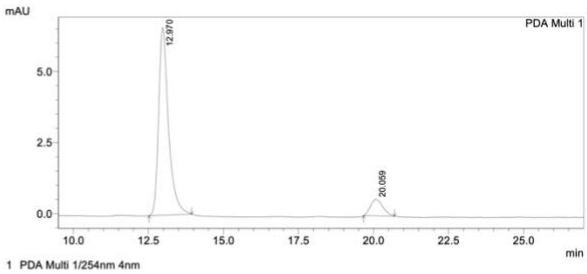

**< Peak Table >**

PeakTable C:\LabSolutions\Training1107\YPC\YPC-4-67-3-Br-NH2-L-OD-99-1-1.0ml.lcd

PDA Ch1 254nm 4nm

| Peak# | Ret. Time | Area | Height | Area % | Height % |
|---|---|---|---|---|---|
| 1 | 13.412 | 928921 | 36417 | 50.226 | 58.008 |
| 2 | 20.935 | 920566 | 26362 | 49.774 | 41.992 |
| Total | | 1849487 | 62780 | 100.000 | 100.000 |

*(B) enantiomerically enriched **(R)-1.31n***



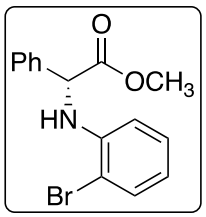

**< Peak Table >**

PeakTable C:\LabSolutions\Training1107\YPC\YPC-4-67-3-Br-NH2-L-OD-99-1-1.0ml-122222.lcd

PDA Ch1 254nm 4nm

| Peak# | Ret. Time | Area | Height | Area % | Height % |
|---|---|---|---|---|---|
| 1 | 12.970 | 150237 | 6595 | 90.100 | 91.919 |
| 2 | 20.059 | 16507 | 580 | 9.900 | 8.081 |
| Total | | 166745 | 7175 | 100.000 | 100.000 |

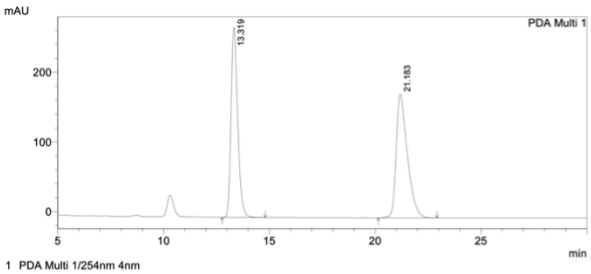
**methyl (*R*)-2-((2-bromophenyl)amino)-2-phenylacetate (1.31o)**




According to the General Procedure G, α-phenyl-α-diazoesters **1.30a** (35.2 mg, 0.200 mmol) and 2-bromoaniline (34.4 mg, 0.200 mmol) were used and the reaction was stirred for 2 h. The product was purified using flash column chromatography ($SiO_2$, hexanes/EtOAc, 98:2 *v*/*v*) and isolated as a white solid (54.4 mg, 85%). $R_f$ = 0.52 (hexanes/EtOAc, 98:2 *v*/*v*). $^1$H NMR (400 MHz, $CDCl_3$) δ 7.53 – 7.47 (m, 2H), 7.43 (dd, *J* = 7.9, 1.6 Hz, 1H), 7.39 – 7.29 (m, 3H), 7.06 – 6.97 (m, 1H), 6.56 (ddd, *J* = 7.7, 7.7, 1.5 Hz, 1H), 6.35 (dd, *J* = 8.2, 1.6 Hz, 1H), 5.73 (d, *J* = 5.5 Hz, 1H), 5.10 (d, *J* = 5.8 Hz, 1H), 3.75 (s, 3H); $^{13}$C NMR (101 MHz, $CDCl_3$) δ 171.8, 143.0, 137.1, 132.7, 129.1, 128.6, 128.5, 127.3, 118.7, 112.3, 110.3, 60.8, 53.1. HRMS (ESI/Orbitrap) m/z: $[M + H]^+$ Calcd for $C_{15}H_{15}BrNO_2$ 320.0286; Found 320.0290.

HPLC analysis: Chiralpak OD-H column, n-hexane/2-propanol = 99/1, 1.0 mL/min, λ = 254 nm, 40 °C, $t_R$ (*S*, minor) = 14.2 min; $t_R$ (*R*, major) = 21.4 min, 90:10 er.

*HPLC trace for: (A) racemic standard of **1.31o***




1 PDA Multi 1/254nm 4nm

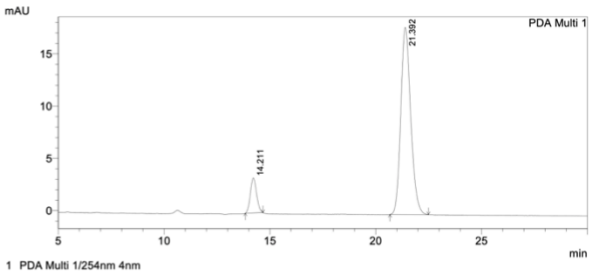
**< Peak Table >**

PeakTable C:\LabSolutions\Training1107\YPC\YPC-4-66-2-Br-NH2-RAC-OD-99-1-1.0ml.lcd

PDA Ch1 254nm 4nm

| Peak# | Ret. Time | Area | Height | Area % | Height % |
|---|---|---|---|---|---|
| 1 | 13.319 | 5955366 | 272677 | 47.912 | 60.540 |
| 2 | 21.183 | 6474306 | 177732 | 52.088 | 39.460 |
| Total | | 12429672 | 450409 | 100.000 | 100.000 |

*(B) enantiomerically enriched **(R)-1.31o***




1 PDA Multi 1/254nm 4nm

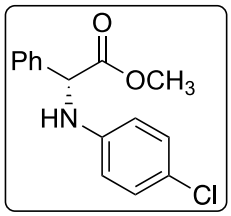
**< Peak Table >**

PeakTable C:\LabSolutions\Training1107\YPC\YPC-4-66-2-Br-NH2-L-OD-99-1-1.0ml--.lcd

PDA Ch1 254nm 4nm

| Peak# | Ret. Time | Area | Height | Area % | Height % |
|---|---|---|---|---|---|
| 1 | 14.211 | 68245 | 3348 | 10.478 | 15.754 |
| 2 | 21.392 | 583051 | 17904 | 89.522 | 84.246 |
| Total | | 651296 | 21252 | 100.000 | 100.000 |

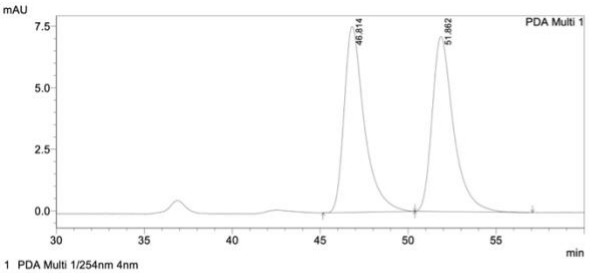
**methyl (*R*)-2-((4-chlorophenyl)amino)-2-phenylacetate (1.31p)**




According to the General Procedure G, α-phenyl-α-diazoesters **1.30a** (35.2 mg, 0.200 mmol) and 4-chloroaniline (25.5 mg, 0.200 mmol) were used and the reaction was stirred for 45 min. The product was purified using flash column chromatography ($SiO_2$, hexanes/EtOAc, 95:5 *v*/*v*) and isolated as a white solid (47.5 mg, 86%). $^1$H NMR spectral data matches that of a previous report.[89]

HPLC analysis: Chiralpak OD-H column, n-hexane/2-propanol = 98/2, 0.2 mL/min, λ = 254 nm, 40 °C, $t_R$ (*R*, major) = 48.4 min; $t_R$ (*S*, minor) = 51.5 min, 93:7 er.

*HPLC trace for: (A) racemic standard of **1.31p***



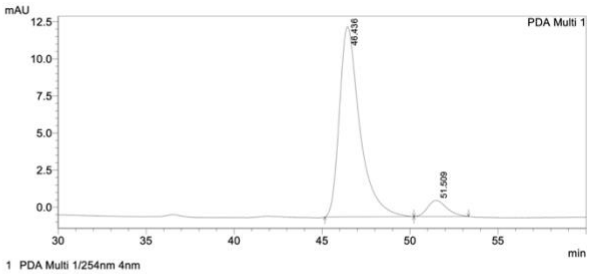

**< Peak Table >**

PeakTable C:\LabSolutions\Training1107\YPC\YPC-3-109-4-Cl-NH2-rac-OD-98-2-0.2ml.lcd

PDA Ch1 254nm 4nm

| Peak# | Ret. Time | Area | Height | Area % | Height % |
|---|---|---|---|---|---|
| 1 | 46.814 | 604322 | 7556 | 50.208 | 51.501 |
| 2 | 51.862 | 599320 | 7116 | 49.792 | 48.499 |
| Total | | 1203642 | 14672 | 100.000 | 100.000 |

*(B) enantiomerically enriched **(R)-1.31p***



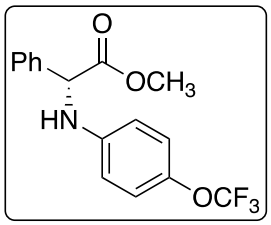

**< Peak Table >**

PeakTable C:\LabSolutions\Training1107\YPC\YPC-3-109-4-Cl-NH2-L-OD-98-2-0.2ml.lcd

PDA Ch1 254nm 4nm

| Peak# | Ret. Time | Area | Height | Area % | Height % |
|---|---|---|---|---|---|
| 1 | 46.436 | 1031832 | 12806 | 92.660 | 92.191 |
| 2 | 51.509 | 81734 | 1085 | 7.340 | 7.809 |
| Total | | 1113567 | 13891 | 100.000 | 100.000 |

**methyl (*R*)-2-phenyl-2-((4-(trifluoromethoxy)phenyl)amino)acetate (1.31q)**

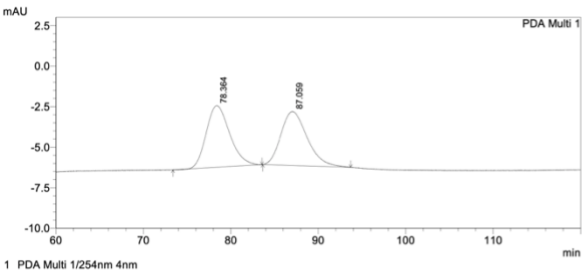



According to the General Procedure G, α-phenyl-α-diazoesters **1.30a** (35.2 mg, 0.200 mmol) and 4-trifluoromethoxy aniline (35.4 mg, 0.200 mmol) were used and the reaction was stirred for 1 h. The product was purified using flash column chromatography ($SiO_2$, hexanes/EtOAc, 95:5 *v*/*v*) and isolated as a white solid (60.4 mg, 93%). $R_f$ = 0.16 (hexanes/EtOAc, 95:5 *v*/*v*).

$^1$H NMR (400 MHz, $CDCl_3$) δ 7.51 – 7.43 (m, 2H), 7.41 – 7.26 (m, 3H), 7.01 – 6.92 (m, 2H), 6.54 – 6.45 (m, 2H), 5.06 (d, *J* = 5.7 Hz, 1H), 5.02 (d, *J* = 5.7 Hz, 1H), 3.73 (s, 3H); $^{13}$C{$^1$H} NMR (101 MHz, $CDCl_3$) δ 172.2, 144.8, 141.1 (q, *J* = 1.8 Hz), 137.3, 129.1, 128.6, 127.3, 122.5, 120.8 (q, *J* = 255.5 Hz), 113.8, 60.9, 53.1; $^{19}$F{$^1$H} NMR (376 MHz, $CDCl_3$) δ -58.45; HRMS (ESI/Orbitrap) m/z: $[M + H]^+$ Calcd for $C_{16}H_{15}F_3NO_3$ 326.1004; Found 326.1012.

HPLC analysis: Chiralpak OD-H column, n-hexane/2-propanol = 98/2, 0.2 mL/min, λ = 254 nm, 40 °C, $t_R$ (*S*, minor) = 78.9 min; $t_R$ (*R*, major) = 87.5 min, 90:10 er.

*HPLC trace for: (A) racemic standard of **1.31q***



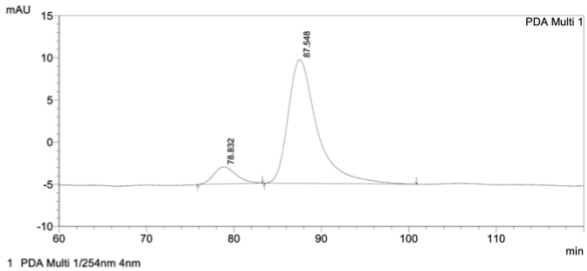

< Peak Table >

PeakTable C:\LabSolutions\Training1107\YPC\YPC-4-71-4-OCF3-NH2-rac-AD-94-6-0.1ml-120min.lcd

PDA Ch1 254nm 4nm

| Peak# | Ret. Time | Area | Height | Area % | Height % |
|---|---|---|---|---|---|
| 1 | 78.364 | 706909 | 3801 | 50.389 | 53.313 |
| 2 | 87.059 | 695984 | 3328 | 49.611 | 46.687 |
| Total | | 1402893 | 7129 | 100.000 | 100.000 |

*(B) enantiomerically enriched **(R)-1.31q***



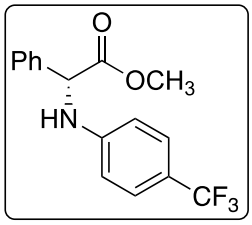

< Peak Table >

PeakTable C:\LabSolutions\Training1107\YPC\YPC-4-71-4-OCF3-NH2-L-AD-94-6-0.1ml-122122-.lcd

PDA Ch1 254nm 4nm

| Peak# | Ret. Time | Area | Height | Area % | Height % |
|---|---|---|---|---|---|
| 1 | 78.832 | 360258 | 2034 | 9.597 | 12.183 |
| 2 | 87.548 | 3393449 | 14664 | 90.403 | 87.817 |
| Total | | 3753707 | 16698 | 100.000 | 100.000 |

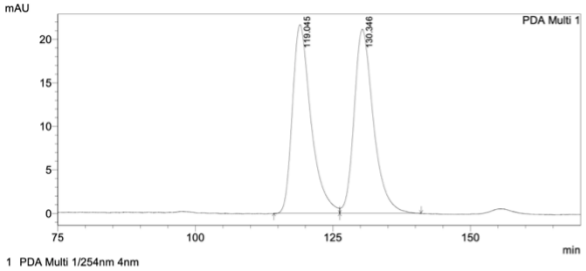
**methyl (*R*)-2-phenyl-2-((4-(trifluoromethyl)phenyl)amino)acetate (1.31r)**




According to the General Procedure G, α-phenyl-α-diazoesters **1.30a** (35.2 mg, 0.200 mmol) and 4-(trifluoromethyl)aniline (32.2 mg, 0.200 mmol) were used and the reaction was stirred for 45 min. The product was purified using flash column chromatography ($SiO_2$, hexanes/EtOAc, 95:5 *v*/*v*) and isolated as a white solid (57.2 mg, 93%). $^1$H NMR spectral data matches that of a previous report.[91]

HPLC analysis: Chiralpak OD-H column, n-hexane/2-propanol = 99/1, 0.1 mL/min, λ = 254 nm, 30 °C, $t_R$ (*R*, major) = 118.2 min; $t_R$ (*S*, minor) = 129.6 min, 81:19 er.

*HPLC trace for: (A) racemic standard of **1.31r***

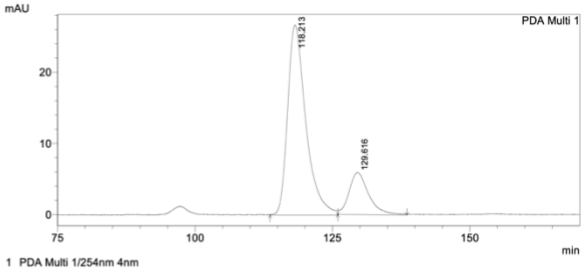



**< Peak Table >**

PeakTable C:\LabSolutions\Training1107\YPC\YPC-3-90-4-CF3-NH2-RAC-OD-99-1-0.1ml-30C-B-170min-..lcd
PDA Ch1 254nm 4nm

| Peak# | Ret. Time | Area | Height | Area % | Height % |
|---|---|---|---|---|---|
| 1 | 119.045 | 5097109 | 21672 | 49.722 | 50.597 |
| 2 | 130.346 | 5154024 | 21160 | 50.278 | 49.403 |
| Total | | 10251133 | 42832 | 100.000 | 100.000 |

*(B) enantiomerically enriched **(R)-1.31r***

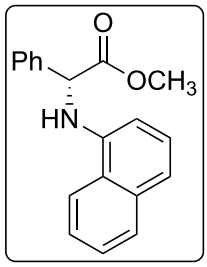



**< Peak Table >**

PeakTable C:\LabSolutions\Training1107\YPC\YPC-3-90-4-CF3-NH2-L-OD-99-1-0.1ml-30C-170min-..lcd
PDA Ch1 254nm 4nm

| Peak# | Ret. Time | Area | Height | Area % | Height % |
|---|---|---|---|---|---|
| 1 | 118.213 | 6174987 | 26717 | 80.682 | 81.860 |
| 2 | 129.616 | 1478504 | 5921 | 19.318 | 18.140 |
| Total | | 7653491 | 32638 | 100.000 | 100.000 |

**methyl (*R*)-2-(naphthalen-1-ylamino)-2-phenylacetate (1.31s)**

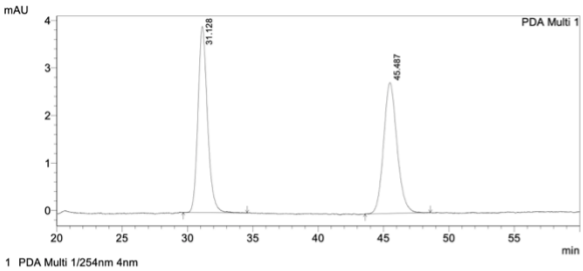



According to the General Procedure G, α-phenyl-α-diazoesters **1.30a** (35.2 mg, 0.200 mmol) and 1-naphthyl aniline (28.6 mg, 0.200 mmol) were used and the reaction was stirred for 16 h. The product

was purified using flash column chromatography ($SiO_2$, hexanes/EtOAc, 95:5 *v*/*v*) and isolated as a white solid (27.9 mg, 48%). $^1$H NMR spectral data matches that of a previous report.[89]

HPLC analysis: Chiralpak OD-H column, n-hexane/2-propanol = 99/1, 1.0 mL/min, λ = 254 nm, 40 °C, $t_R$ (*R*, major) = 31.3 min; $t_R$ (*S*, minor) = 45.9 min, 80:20 er.

*HPLC trace for: (A) racemic standard of* ***1.31s*** *(B) enantiomerically enriched* ***(R)-1.31s***

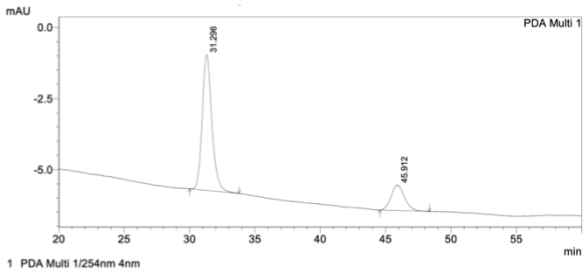



< Peak Table >

PeakTable C:\LabSolutions\Training1107\YPC\YPC-3-67-Np-rac-OD-99-1-1.0ml-2.lcd

PDA Ch1 254nm 4nm

| Peak# | Ret. Time | Area | Height | Area % | Height % |
|---|---|---|---|---|---|
| 1 | 31.128 | 197655 | 3915 | 50.135 | 58.735 |
| 2 | 45.487 | 196589 | 2751 | 49.865 | 41.265 |
| Total | | 394244 | 6666 | 100.000 | 100.000 |



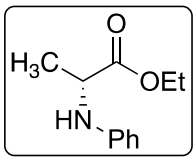

< Peak Table >

PeakTable C:\LabSolutions\Training1107\YPC\YPC-3-67-Np-L-OD-99-1-1.0ml.lcd

PDA Ch1 254nm 4nm

| Peak# | Ret. Time | Area | Height | Area % | Height % |
|---|---|---|---|---|---|
| 1 | 31.296 | 246231 | 4776 | 79.557 | 84.219 |
| 2 | 45.912 | 63272 | 895 | 20.443 | 15.781 |
| Total | | 309504 | 5671 | 100.000 | 100.000 |

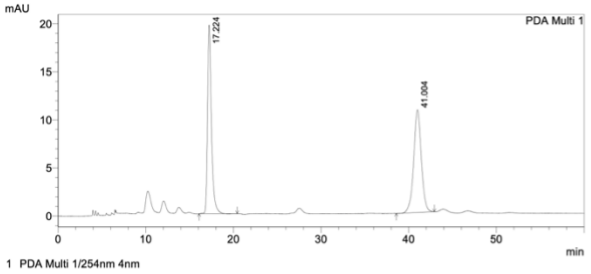
**ethyl phenyl-*D*-alaninate (1.31t)**




According to the General Procedure G, diazoester **1.30t** (25.6 mg, 0.200 mmol) and aniline (18.6 mg, 0.200 mmol) were used and the reaction was stirred for 45 min. The product was purified using flash column chromatography ($SiO_2$, hexanes/EtOAc, 98:2 *v*/*v*) and isolated as a clear oil (25.1 mg, 65%). $^1$H NMR spectral data matches that of a previous report.[92]

HPLC analysis: Chiralpak OD-H column, n-hexane/2-propanol = 99/1, 0.7 mL/min, λ = 254 nm, 40 °C, $t_R$ (*S*, minor) = 16.3 min; $t_R$ (*R*, major) = 40.8 min, 96:4 er.

*HPLC trace for: (A) racemic standard of **1.31t***  *(B) enantiomerically enriched **(R)-1.31t***

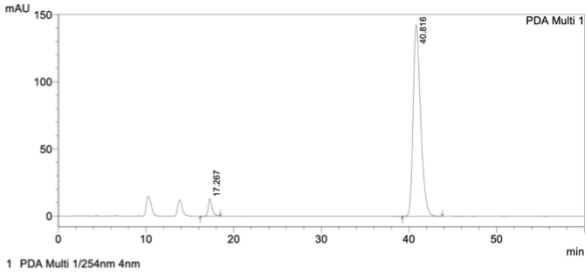



< Peak Table >

PeakTable C:\LabSolutions\Training1107\YPC\YPC-3-83-Me-DA-rac-OD-99-1-0.7ml-60min.lcd

PDA Ch1 254nm 4nm

| Peak# | Ret. Time | Area | Height | Area % | Height % |
|---|---|---|---|---|---|
| 1 | 17.224 | 606839 | 19608 | 48.493 | 64.763 |
| 2 | 41.004 | 644563 | 10669 | 51.507 | 35.237 |
| Total | | 1251402 | 30277 | 100.000 | 100.000 |



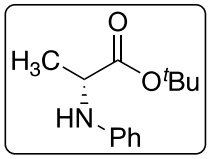

< Peak Table >

PeakTable C:\LabSolutions\Training1107\YPC\YPC-3-83-Me-DA-L-OD-99-1-0.7ml.lcd

PDA Ch1 254nm 4nm

| Peak# | Ret. Time | Area | Height | Area % | Height % |
|---|---|---|---|---|---|
| 1 | 17.267 | 394113 | 12869 | 4.463 | 8.285 |
| 2 | 40.816 | 8437517 | 142459 | 95.537 | 91.715 |
| Total | | 8831630 | 155329 | 100.000 | 100.000 |

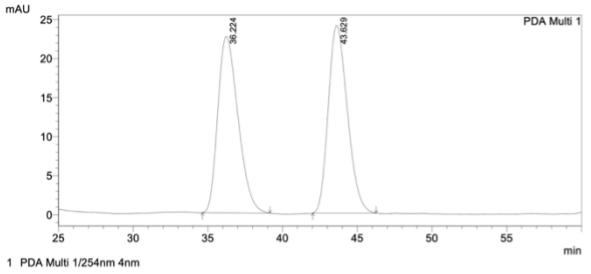
### *tert*-butyl phenyl-*D*-alaninate (1.31u)




According to the General Procedure G, diazoester **1.30u** (31.2 mg, 0.200 mmol) and aniline (18.6 mg, 0.200 mmol) were used and the reaction was stirred for 45 min. The product was purified using flash column chromatography ($SiO_2$, hexanes/EtOAc, 98:2 *v*/*v*) and isolated as a clear oil (36.7 mg, 83%). $^1$H NMR spectral data matches that of a previous report.[92]

HPLC analysis: Chiralpak OD-H column, n-hexane/2-propanol = 99/1, 0.2 mL/min, λ = 254 nm, 40 °C, $t_R$ (*R*, major) = 36.1 min; $t_R$ (*S*, minor) = 43.4 min, 94:6 er.

*HPLC trace for: (A) racemic standard of **1.31u***  *(B) enantiomerically enriched **(R)-1.31u***

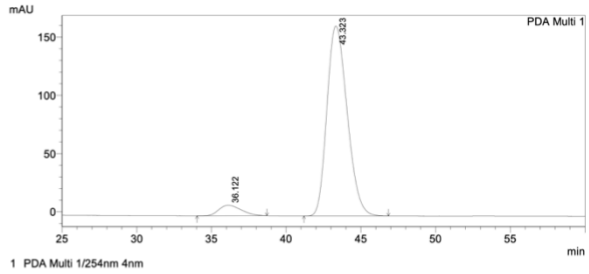



< Peak Table >

PeakTable C:\LabSolutions\Training1107\YPC\YPC-3-102-Me-OtBu-DA-rac-OD-99-1-0.2ml.lcd

PDA Ch1 254nm 4nm

| Peak# | Ret. Time | Area | Height | Area % | Height % |
|---|---|---|---|---|---|
| 1 | 36.224 | 2131888 | 22595 | 49.857 | 48.478 |
| 2 | 43.629 | 2144159 | 24014 | 50.143 | 51.522 |
| Total | | 4276047 | 46609 | 100.000 | 100.000 |



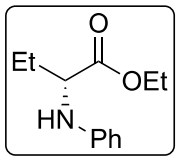

< Peak Table >

PeakTable C:\LabSolutions\Training1107\YPC\YPC-3-102-Me-OtBu-DA-L-OD-99-1-0.2ml.lcd

PDA Ch1 254nm 4nm

| Peak# | Ret. Time | Area | Height | Area % | Height % |
|---|---|---|---|---|---|
| 1 | 36.122 | 942076 | 9065 | 5.776 | 5.266 |
| 2 | 43.323 | 15366834 | 163078 | 94.224 | 94.734 |
| Total | | 16308910 | 172143 | 100.000 | 100.000 |

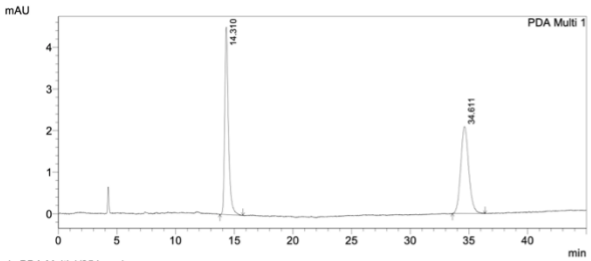
**ethyl (*R*)-2-(phenylamino)butanoate (1.31v)**




According to the General Procedure G, diazoester **1.30v** (28.4 mg, 0.200 mmol) and aniline (18.6 mg, 0.200 mmol) were used and the reaction was stirred for 40 min. The product was purified using flash column chromatography ($SiO_2$, hexanes/EtOAc, 98:2 *v*/*v*) and isolated as a clear oil (36.7 mg, 88%). $^1$H NMR spectral data matches that of a previous report.[93]

HPLC analysis: Chiralpak OD-H column, n-hexane/2-propanol = 99/1, 0.7 mL/min, λ = 254 nm, 40 °C, $t_R$ (*S*, minor) = 13.4 min; $t_R$ (*R*, major) = 33.4 min, 98:2 er.

*HPLC trace for: (A) racemic standard of **1.31v***  *(B) enantiomerically enriched **(R)-1.31v***

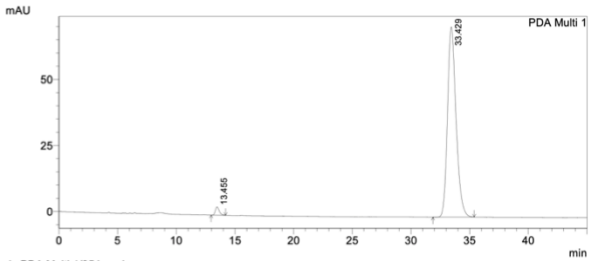



< Peak Table >

PeakTable C:\LabSolutions\Training1107\YPC\YPC-3-98-Et-DA-rac-OD-99-1-0.7ml-.lcd

PDA Ch1 254nm 4nm

| Peak# | Ret. Time | Area | Height | Area % | Height % |
|---|---|---|---|---|---|
| 1 | 14.310 | 98041 | 4508 | 49.836 | 68.315 |
| 2 | 34.611 | 98687 | 2091 | 50.164 | 31.685 |
| Total | | 196728 | 6599 | 100.000 | 100.000 |




< Peak Table >

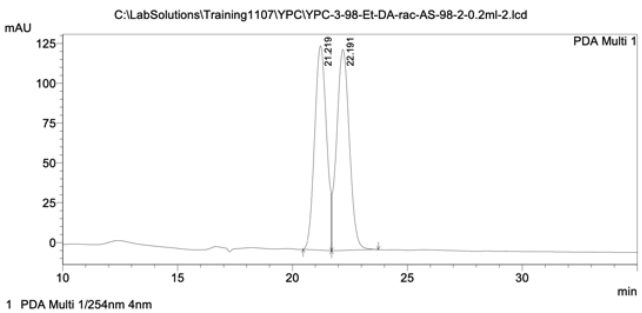
PeakTable C:\LabSolutions\Training1107\YPC\YPC-3-98-Et-DA-L-OD-99-1-0.7ml.lcd

PDA Ch1 254nm 4nm

| Peak# | Ret. Time | Area | Height | Area % | Height % |
|---|---|---|---|---|---|
| 1 | 13.455 | 72410 | 3156 | 1.948 | 4.202 |
| 2 | 33.429 | 3644669 | 71943 | 98.052 | 95.798 |
| Total | | 3717079 | 75098 | 100.000 | 100.000 |

***Note***: The HPLC data below using Chiralpak AS-H column was utilized to determine the absolute configuration of compound **1.31t−x**. The major and minor peaks are discernible and used for comparison with previous HPLC data.[76]

HPLC analysis: Chiralpak AS-H column, n-hexane/2-propanol = 98/2, 0.2 mL/min, λ = 254 nm, 40 °C, $t_R$ (*R*, major) = 21.5 min; $t_R$ (*S*, minor) = 22.5 min.

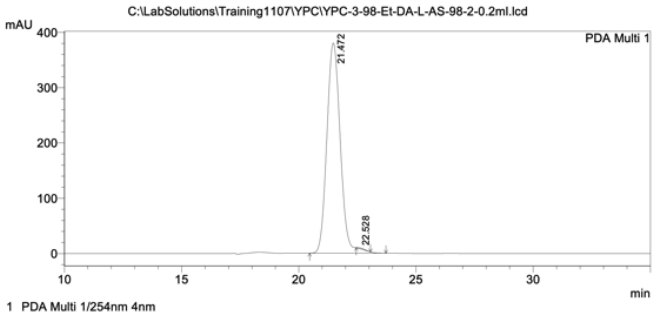



< Peak Table >

PeakTable C:\LabSolutions\Training1107\YPC\YPC-3-98-Et-DA-rac-AS-98-2-0.2ml-2.lcd

PDA Ch1 254nm 4nm

| Peak# | Ret. Time | Area | Height | Area % | Height % |
|---|---|---|---|---|---|
| 1 | 21.219 | 4632904 | 128331 | 48.800 | 50.400 |
| 2 | 22.191 | 4860834 | 126295 | 51.200 | 49.600 |
| Total | | 9493738 | 254626 | 100.000 | 100.000 |



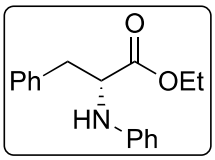

< Peak Table >

PeakTable C:\LabSolutions\Training1107\YPC\YPC-3-98-Et-DA-L-AS-98-2-0.2ml.lcd

PDA Ch1 254nm 4nm

| Peak# | Ret. Time | Area | Height | Area % | Height % |
|---|---|---|---|---|---|
| 1 | 21.472 | 15160243 | 379920 | 99.767 | 99.750 |
| 2 | 22.528 | 35452 | 953 | 0.233 | 0.250 |
| Total | | 15195695 | 380872 | 100.000 | 100.000 |

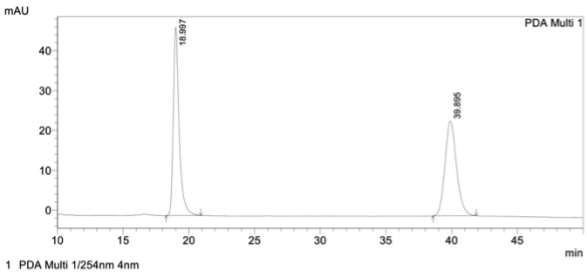
**ethyl phenyl-*D*-phenylalaninate (1.30w)**




According to the General Procedure G, diazoester **1.30w** (40.8 mg, 0.200 mmol) and aniline (18.6 mg, 0.200 mmol) were used and the reaction was stirred for 16 h. The product was purified using flash column chromatography ($SiO_2$, hexanes/EtOAc, 95:5 *v*/*v*) and isolated as a clear oil (44.5 mg, 83%). $^1$H NMR spectral data matches that of a previous report.[94]

HPLC analysis: Chiralpak OD-H column, n-hexane/2-propanol = 95/5, 0.5 mL/min, λ = 254 nm, 40 °C, $t_R$ (*S*, minor) = 19.4 min; $t_R$ (*R*, major) = 40.0 min, 98:2 er.

*HPLC trace for: (A) racemic standard of **1.31w***



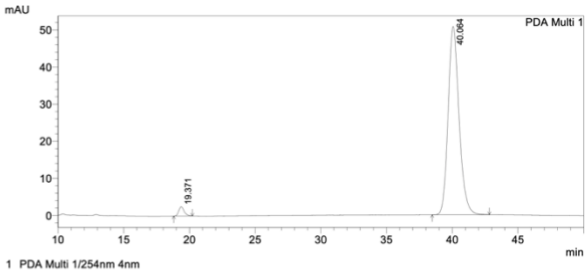

< Peak Table >

PeakTable C:\LabSolutions\Training1107\YPC\YPC-3-113-Bn-DA-rac-OD-95-5-0.5ML-60MIN-OD.lcd

PDA Ch1 254nm 4nm

| Peak# | Ret. Time | Area | Height | Area % | Height % |
|---|---|---|---|---|---|
| 1 | 18.997 | 1458124 | 47260 | 50.126 | 66.538 |
| 2 | 39.895 | 1450782 | 23767 | 49.874 | 33.462 |
| Total | | 2908906 | 71027 | 100.000 | 100.000 |

*(B) enantiomerically enriched **(R)-1.31w***



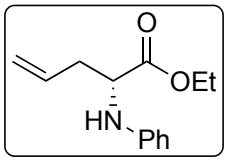

< Peak Table >

PeakTable C:\LabSolutions\Training1107\YPC\YPC-3-113-Bn-DA-L-OD-95-5-0.5ML-60MIN-OD.lcd

PDA Ch1 254nm 4nm

| Peak# | Ret. Time | Area | Height | Area % | Height % |
|---|---|---|---|---|---|
| 1 | 19.371 | 72729 | 2539 | 2.417 | 4.767 |
| 2 | 40.064 | 2935941 | 50737 | 97.583 | 95.233 |
| Total | | 3008670 | 53277 | 100.000 | 100.000 |

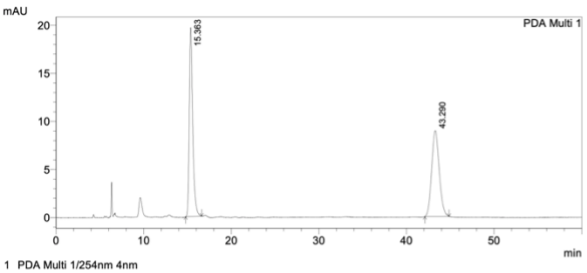
**ethyl (*R*)-2-(phenylamino)pent-4-enoate (1.31x)**




According to the General Procedure G, diazoester **1.30x** (30.8 mg, 0.200 mmol) and aniline (18.6 mg, 0.200 mmol) were used and the reaction was stirred for 16 h. The product was purified using flash column chromatography ($SiO_2$, hexanes/EtOAc, 98:2 *v*/*v*) and isolated as a clear oil (19.7 mg, 45%). $^1$H NMR spectral data matches that of a previous report.[95]

HPLC analysis: Chiralpak OD-H column, n-hexane/2-propanol = 99/1, 0.7 mL/min, λ = 254 nm, 40 °C, $t_R$ (*S*, minor) = 14.8 min; $t_R$ (*R*, major) = 42.6 min, 94:6 er.

*HPLC trace for: (A) racemic standard of **1.31x***



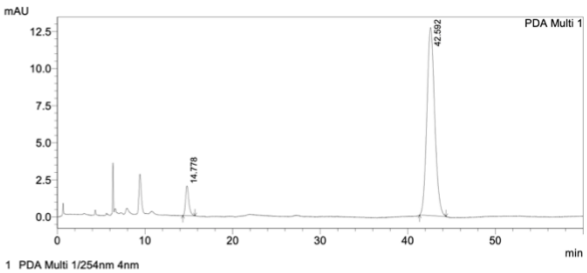

**< Peak Table >**

PeakTable C:\LabSolutions\Training1107\YPC\YPC-3-114-ALLYL-DA-rac-OD-99-1-0.7ML-.lcd

PDA Ch1 254nm 4nm

| Peak# | Ret. Time | Area | Height | Area % | Height % |
|---|---|---|---|---|---|
| 1 | 15.363 | 538548 | 19646 | 50.289 | 68.757 |
| 2 | 43.290 | 532354 | 8927 | 49.711 | 31.243 |
| Total | | 1070903 | 28573 | 100.000 | 100.000 |

*(B) enantiomerically enriched **(R)-1.31x***




**< Peak Table >**

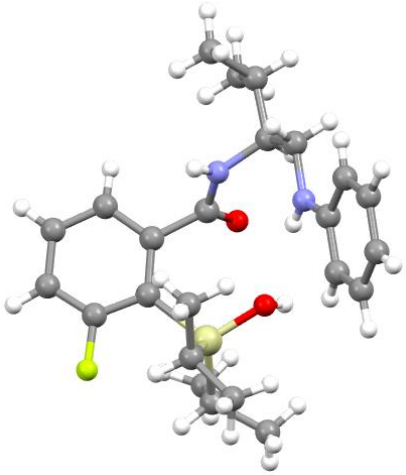
PeakTable C:\LabSolutions\Training1107\YPC\YPC-3-114-2-ALLYL-DA-L-OD-99-1-0.7ML-TLC-2.lcd

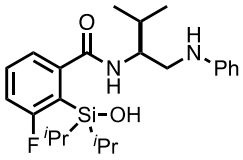
PDA Ch1 254nm 4nm

| Peak# | Ret. Time | Area | Height | Area % | Height % |
|---|---|---|---|---|---|
| 1 | 14.778 | 51949 | 2014 | 6.208 | 13.715 |
| 2 | 42.592 | 784802 | 12670 | 93.792 | 86.285 |
| Total | | 836750 | 14684 | 100.000 | 100.000 |

## VId. X-ray Crystallography Data

**Table 1.8.** Crystal data and structure refinement for **L3a** (CCDC 2289933).

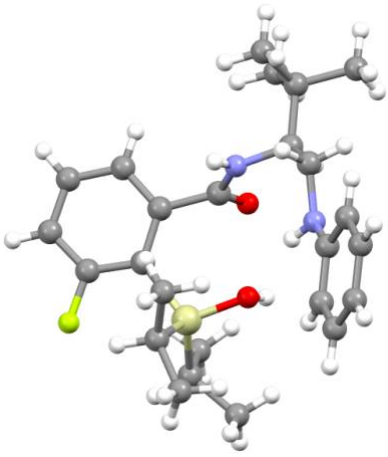


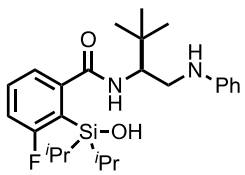



| | | |
|---|---|---|
| Identification code | JF3111F3_60MI | (YPC-2-49) |
| Empirical formula | C24 H35 F N2 O2 Si | |
| Formula weight | 430.63 | |
| Temperature | 100(2) K | |
| Wavelength | 0.71073 Å | |
| Crystal system | Hexagonal | |
| Space group | $P6_122$ | |
| Unit cell dimensions | a = 11.3851(8) Å | α = 90°. |
| | b = 11.3851(8) Å | β = 90°. |
| | c = 64.721(7) Å | $\gamma$ = 120°. |
| Volume | 7265.2(13) Å3 | |
| Z | 12 | |
| Density (calculated) | 1.181 Mg/m3 | |
| Absorption coefficient | 0.126 mm-1 | |
| F(000) | 2784 | |
| Crystal size | 0.380 x 0.331 x 0.134 mm3 | |
| Crystal color and habit | Colorless Block | |
| Diffractometer | Bruker Photon2 CMOS | |

| | |
|---|---|
| Theta range for data collection | 1.888 to 30.550°. |
| Index ranges | -16<=h<=16, -16<=k<=16, -92<=l<=90 |
| Reflections collected | 63449 |
| Independent reflections | 7401 [R(int) = 0.0386] |
| Observed reflections (I > 2sigma(I)) | 7034 |
| Completeness to theta = 25.242° | 100.0 % |
| Absorption correction | Semi-empirical from equivalents |
| Max. and min. transmission | 0.9185 and 0.8361 |
| Solution method | SHELXT (Sheldrick, 2014) |
| Refinement method | SHELXL-2018/3 (Sheldrick, 2018) Full-matrix least-squares on F2 |
| Data / restraints / parameters | 7401 / 0 / 411 |
| Goodness-of-fit on F2 | 1.152 |
| Final R indices [I>2sigma(I)] | R1 = 0.0378, wR2 = 0.0920 |
| R indices (all data) | R1 = 0.0404, wR2 = 0.0933 |
| Absolute structure parameter | 0.01(2) |
| Largest diff. peak and hole | 0.277 and -0.189 e.Å-3 |

**Table 1.9.** Crystal data and structure refinement for **L3b** (CCDC 2289935).

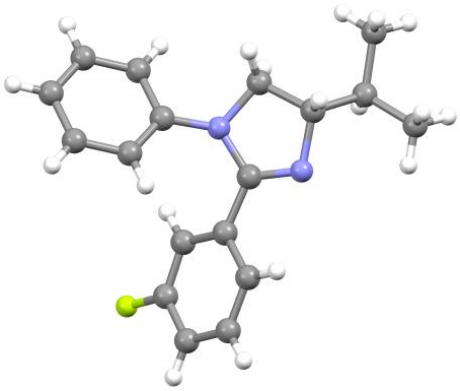


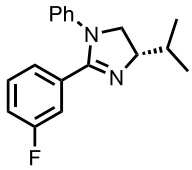


| | |
|---|---|
| Identification code | JF3154FMI (YPC-3-117) |
| Empirical formula | C25 H37 F N2 O2 Si |
| Formula weight | 444.65 |
| Temperature | 90(2) K |
| Wavelength | 0.71073 Å |
| Crystal system | Monoclinic |
| Space group | $P2_1$ |
| Unit cell dimensions | a = 10.4984(6) Å α = 90°. |
| | b = 23.5281(13) Å β = 109.2216(12)°. |
| | c = 11.1188(6) Å γ = 90°. |
| Volume | 2593.3(2) Å3 |
| Z | 4 |
| Density (calculated) | 1.139 Mg/m3 |
| Absorption coefficient | 0.120 mm-1 |
| F(000) | 960 |
| Crystal size | 0.269 x 0.249 x 0.196 mm3 |
| Crystal color and habit | Colorless Block |
| Diffractometer | Bruker Photon2 CMOS |
| Theta range for data collection | 2.229 to 27.463°. |
| Index ranges | -13<=h<=13, -30<=k<=30, -14<=l<=14 |
| Reflections collected | 23292 |
| Independent reflections | 11858 [R(int) = 0.0155] |
| Observed reflections (I > 2sigma(I)) | 10811 |
| Completeness to theta = 25.242° | 99.9 % |
| Absorption correction | Semi-empirical from equivalents |
| Max. and min. transmission | 0.9745 and 0.9363 |
| Solution method | SHELXT (Sheldrick, 2014) |

| | |
|---|---|
| Refinement method | SHELXL-2018/3 (Sheldrick, 2018) Full-matrix least-squares on F2 |
| Data / restraints / parameters | 11858 / 39 / 679 |
| Goodness-of-fit on F2 | 1.038 |
| Final R indices [I>2sigma(I)] | R1 = 0.0344, wR2 = 0.0829 |
| R indices (all data) | R1 = 0.0397, wR2 = 0.0860 |
| Absolute structure parameter | 0.009(16) |
| Largest diff. peak and hole | 0.149 and -0.209 e.Å-3 |

**Table 1.10.** Crystal data and structure refinement for **3a** (CCDC 2289936).

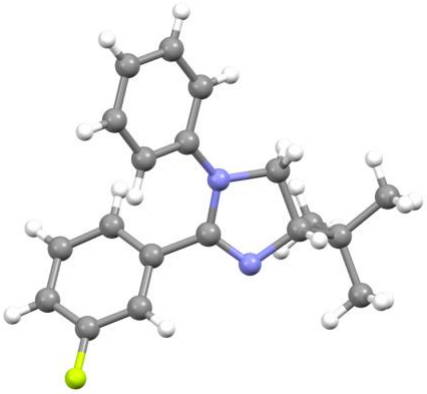


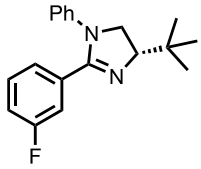



| | | |
|---|---|---|
| Identification code | JF3173FMI (YPC-4-4) | |
| Empirical formula | C18 H19 F N2 | |
| Formula weight | 282.35 | |
| Temperature | 190(2) K | |
| Wavelength | 0.71073 Å | |
| Crystal system | Orthorhombic | |
| Space group | $P2_12_12_1$ | |
| Unit cell dimensions | a = 11.6012(2) Å | α = 90°. |
| | b = 14.6138(3) Å | β = 90°. |
| | c = 17.9894(3) Å | $\gamma$ = 90°. |

| | |
|---|---|
| Volume | 3049.88(10) Å3 |
| Z | 8 |
| Density (calculated) | 1.230 Mg/m3 |
| Absorption coefficient | 0.081 mm-1 |
| F(000) | 1200 |
| Crystal size | 0.872 x 0.557 x 0.462 mm3 |
| Crystal color and habit | Colourless Block |
| Diffractometer | Bruker APEX-II CCD |
| Theta range for data collection | 1.795 to 27.556°. |
| Index ranges | -15<=h<=15, -19<=k<=18, -23<=l<=23 |
| Reflections collected | 25518 |
| Independent reflections | 7028 [R(int) = 0.0215] |
| Observed reflections (I > 2sigma(I)) | 6516 |
| Completeness to theta = 25.242° | 99.9 % |
| Absorption correction | Semi-empirical from equivalents |
| Max. and min. transmission | 0.9632 and 0.8900 |
| Solution method | SHELXT (Sheldrick, 2015) Acta Cryst., A71, 3-8 |
| Refinement method | SHELXL-2018/3 (Sheldrick, 2018) Full-matrix least-squares on F2 |
| Data / restraints / parameters | 7028 / 9 / 433 |
| Goodness-of-fit on F2 | 1.016 |
| Final R indices [I>2sigma(I)] | R1 = 0.0319, wR2 = 0.0772 |
| R indices (all data) | R1 = 0.0358, wR2 = 0.0798 |
| Absolute structure parameters | Flack = 0.04(19). Parsons = 0.03(18), Hooft = 0.07(17) |
| Largest diff. peak and hole | 0.186 and -0.168 e.Å-3 |

**Table 1.11.** Crystal data and structure refinement for **3b** (CCDC 2289937).

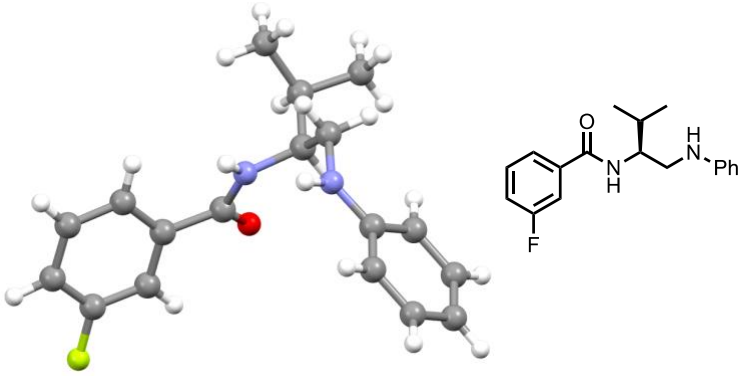





| | | |
|---|---|---|
| Identification code | JF3216KF (YPC-3-147) | |
| Empirical formula | C19 H21 F N2 | |
| Formula weight | 296.38 | |
| Temperature | 190(2) K | |
| Wavelength | 1.54178 Å | |
| Crystal system | Triclinic | |
| Space group | P1 | |
| Unit cell dimensions | a = 9.9901(3) Å | α= 60.8907(8)°. |
| | b = 10.2226(3) Å | β= 67.0468(9)°. |
| | c = 10.5066(3) Å | $\gamma$ = 63.2718(8)°. |
| Volume | 816.90(4) Å3 | |
| Z | 2 | |
| Density (calculated) | 1.205 Mg/m3 | |
| Absorption coefficient | 0.628 mm-1 | |
| F(000) | 316 | |
| Crystal size | 0.479 x 0.249 x 0.203 mm3 | |
| Crystal color and habit | Colorless Shard | |
| Diffractometer | Bruker Photon2 CMOS | |
| Theta range for data collection | 5.080 to 71.100°. | |
| Index ranges | -12<=h<=12, -12<=k<=12, -12<=l<=12 | |
| Reflections collected | 18398 | |

| | |
|---|---|
| Independent reflections | 5849 [R(int) = 0.0149] |
| Observed reflections (I > 2sigma(I)) | 5834 |
| Completeness to theta = 67.679° | 99.6 % |
| Absorption correction | Semi-empirical from equivalents |
| Max. and min. transmission | 0.8945 and 0.8531 |
| Solution method | SHELXT (Sheldrick, 2015) Acta Cryst., A71, 3-8 |
| Refinement method | SHELXL-2018/3 (Sheldrick, 2018) Full-matrix least-squares on F2 |
| Data / restraints / parameters | 5849 / 7 / 451 |
| Goodness-of-fit on F2 | 1.014 |
| Final R indices [I>2sigma(I)] | R1 = 0.0321, wR2 = 0.0893 |
| R indices (all data) | R1 = 0.0322, wR2 = 0.0894 |
| Absolute structure parameter | 0.07(14) |
| Largest diff. peak and hole | 0.197 and -0.226 e.Å-3 |

**Table 1.12.** Crystal data and structure refinement for **S2** (CCDC 2289938).

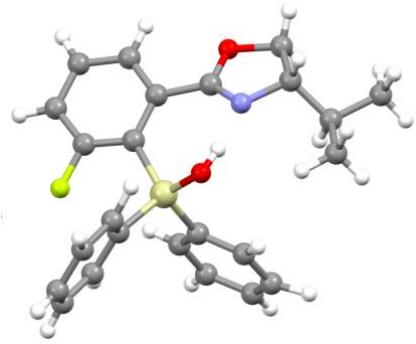


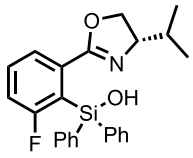

| | |
|---|---|
| Identification code | JF3275KFMI (YPC-4-138-SM) |
| Empirical formula | C18 H21 F N2 O |
| Formula weight | 300.37 |
| Temperature | 190(2) K |
| Wavelength | 1.54178 Å |

| | | |
|---|---|---|
| Crystal system | Orthorhombic | |
| Space group | $P2_12_12_1$ | |
| Unit cell dimensions | a = 5.2703(3) Å | α= 90°. |
| | b = 13.9801(9) Å | β= 90°. |
| | c = 21.4626(14) Å | $\gamma$ = 90°. |
| Volume | 1581.35(17) Å3 | |
| Z | 4 | |
| Density (calculated) | 1.262 Mg/m3 | |
| Absorption coefficient | 0.703 mm-1 | |
| F(000) | 640 | |
| Crystal size | 0.519 x 0.177 x 0.050 mm3 | |
| Crystal color and habit | Colorless Rod | |
| Diffractometer | Bruker Photon2 CMOS | |
| Theta range for data collection | 3.773 to 74.626°. | |
| Index ranges | -6<=h<=5, -17<=k<=16, -26<=l<=24 | |
| Reflections collected | 7941 | |
| Independent reflections | 3222 [R(int) = 0.0582] | |
| Observed reflections (I > 2sigma(I)) | 3093 | |
| Completeness to theta = 67.679° | 99.9 % | |
| Absorption correction | Semi-empirical from equivalents | |
| Max. and min. transmission | 0.8176 and 0.5381 | |
| Solution method | SHELXT (Sheldrick, 2015) Acta Cryst., A71, 3-8 | |
| Refinement method | SHELXL-2018/3 (Sheldrick, 2018) Full-matrix least-squares | |
| on F2 | | |
| Data / restraints / parameters | 3222 / 0 / 283 | |
| Goodness-of-fit on F2 | 1.050 | |
| Final R indices [I>2sigma(I)] | R1 = 0.0443, wR2 = 0.1179 | |
| R indices (all data) | R1 = 0.0455, wR2 = 0.1200 | |

| | |
|---|---|
| Absolute structure parameter | -0.03(13) |
| Largest diff. peak and hole | 0.227 and -0.168 e.Å-3 |

**Table 1.13.** Crystal data and structure refinement for **L1a** (CCDC 2289939).






| | | |
|---|---|---|
| Identification code | JF3112P1FMI (YPC-2-55) | |
| Empirical formula | C24 H24 F N O2 Si | |
| Formula weight | 405.53 | |
| Temperature | 100(2) K | |
| Wavelength | 0.71073 Å | |
| Crystal system | Triclinic | |
| Space group | P1 | |
| Unit cell dimensions | a = 10.6067(19) Å | α = 61.010(4)°. |
| | b = 10.8407(19) Å | β = 70.064(4)°. |
| | c = 10.999(2) Å | $\gamma$ = 89.897(5)°. |
| Volume | 1019.2(3) Å3 | |
| Z | 2 | |
| Density (calculated) | 1.321 Mg/m3 | |
| Absorption coefficient | 0.145 mm-1 | |
| F(000) | 428 | |
| Crystal size | 0.454 x 0.340 x 0.298 mm3 | |
| Crystal color and habit | Colorless Block | |

| | |
|---|---|
| Diffractometer | Bruker Photon2 CMOS |
| Theta range for data collection | 2.084 to 30.525°. |
| Index ranges | -15<=h<=15, -15<=k<=15, -15<=l<=15 |
| Reflections collected | 55770 |
| Independent reflections | 12230 [R(int) = 0.0151] |
| Observed reflections (I > 2sigma(I)) | 12023 |
| Completeness to theta = 25.242° | 99.9 % |
| Absorption correction | Semi-empirical from equivalents |
| Max. and min. transmission | 0.9624 and 0.9436 |
| Solution method | SHELXT (Sheldrick, 2014) |
| Refinement method | SHELXL-2018/3 (Sheldrick, 2018) Full-matrix least-squares on F2 |
| Data / restraints / parameters | 12230 / 5 / 715 |
| Goodness-of-fit on F2 | 1.020 |
| Final R indices [I>2sigma(I)] | R1 = 0.0280, wR2 = 0.0806 |
| R indices (all data) | R1 = 0.0284, wR2 = 0.0810 |
| Absolute structure parameter | -0.030(15) |
| Largest diff. peak and hole | 0.417 and -0.255 e.Å-3 |

## VII. References


(1) Marciniec, B.; Maciejewski, H. Transition Metal-Siloxide Complexes; Synthesis, Structure and Application to Catalysis. *Coord. Chem. Rev.* **2001**, *223* (1), 301–335. https://doi.org/10.1016/S0010-8545(01)00400-3.

(2) Krempner, C. Role of Siloxides in Transition Metal Chemistry and Homogeneous Catalysis. *Eur. J. Inorg. Chem.* **2011**, *2011* (11), 1689–1698. https://doi.org/10.1002/ejic.201100044.

(3) Franz, A. K.; Wilson, S. O. Organosilicon Molecules with Medicinal Applications. *J. Med. Chem.* **2013**, *56* (2), 388–405. https://doi.org/10.1021/jm3010114.

(4) Wolczanski, P. T. Chemistry of Electrophilic Metal Centres Coordinated by Silox (tBu3SiO), Tritox (tBu3CO) and Related Binfunctional Ligands. *Polyhedron* **1995**, *14* (22), 3335–3362. https://doi.org/10.1016/0277-5387(95)85014-7.

(5) Ali, A.; Langer, M.; Lorenz, V.; Hrib, C. G.; Hilfert, L.; Edelmann, F. T. Synthesis and Structure of Hexaphenyltrisiloxanediolates of Sodium, Titanium, and Iron. *J. Organomet. Chem.* **2015**, *776*, 163–169. https://doi.org/10.1016/j.jorganchem.2014.11.016.

(6) P. Richers, C.; A. Bertke, J.; B. Rauchfuss, T. Syntheses of Transition Metal Methoxysiloxides. *Dalton Trans.* **2017**, *46* (27), 8756–8762. https://doi.org/10.1039/C6DT04205H.

(7) Chandrasekhar, V.; Boomishankar, R.; Nagendran, S. Recent Developments in the Synthesis and Structure of Organosilanols. *Chem. Rev.* **2004**, *104* (12), 5847–5910. https://doi.org/10.1021/cr0306135.

(8) Prabusankar, G.; Murugavel, R.; Butcher, R. J. Synthesis, Spectral Studies, and Structural Characterization of a New Organosilanetriol, Its Amine Complexes, and a Surface Lewis Basic Cubic Aluminosilicate. *Organometallics* **2005**, *24* (9), 2124–2128. https://doi.org/10.1021/om049254.

(9) Notte, G. T.; Leighton, J. L. A New Silicon Lewis Acid for Highly Enantioselective Mannich Reactions of Aliphatic Ketone-Derived Hydrazones. *J. Am. Chem. Soc.* **2008**, *130* (21), 6676–6677. https://doi.org/10.1021/ja800830h.

(10) Sakaguchi, Y.; Iwade, Y.; Sekikawa, T.; Minami, T.; Hatanaka, Y. Chiral Silicon Lewis Acids Having a Pentacoordinate Stereogenic Silicon Center: 29Si NMR Studies and Application to Asymmetric Diels–Alder Reactions. *Chem. Commun.* **2013**, *49* (95), 11173. https://doi.org/10.1039/c3cc46501b.

(11) Maruoka, K.; Banno, H.; Yamamoto, H. Asymmetric Claisen Rearrangement Catalyzed by Chiral Organoaluminum Reagent. *J. Am. Chem. Soc.* **1990**, *112* (21), 7791–7793. https://doi.org/10.1021/ja00177a047.

(12) Zhang, H.; Zhao, D. Synthesis of Silicon-Stereogenic Silanols Involving Iridium-Catalyzed Enantioselective C–H Silylation Leading to a New Ligand Scaffold. *ACS Catal.* **2021**, *11* (17), 10748–10753. https://doi.org/10.1021/acscatal.1c03112.

(13) Chang, X.; Ma, P.; Chen, H.; Li, C.; Wang, P. Asymmetric Synthesis and Application of Chiral Spirosilabiindanes. *Angew. Chem. Int. Ed.* **2020**, *59* (23), 8937–8940. https://doi.org/10.1002/anie.202002289.

(14) Sore, H. F.; Galloway, W. R. J. D.; Spring, D. R. Palladium-Catalysed Cross-Coupling of Organosilicon Reagents. *Chem Soc Rev* **2012**, *41* (5), 1845–1866. https://doi.org/10.1039/C1CS15181A.

(15) Langenohl, F.; Rösler, J.; Zühlke, S.; Kirchhoff, J.; Strohmann, C. A Silicon-Stereogenic Silanol - $^{18}$O-Isotope Labeling and Stereogenic Probe Reveals Hidden Stereospecific Water Exchange Reaction. *Chem. – Eur. J.* **2023**, *29* (1), e202202935. https://doi.org/10.1002/chem.202202935.

(16) Golz, C.; Steffen, P.; Strohmann, C. Exploring Planar-Chiral Amino Siloxides. *Angew. Chem. Int. Ed.* **2017**, *56* (28), 8295–8298. https://doi.org/10.1002/anie.201703701.

(17) Özçubukçu, S.; Schmidt, F.; Bolm, C. Organosilanols as Catalysts in Asymmetric Aryl Transfer Reactions. *Org. Lett.* **2005**, *7* (7), 1407–1409. https://doi.org/10.1021/ol050242.

(18) Poulton, J. T.; Sigalas, M. P.; Folting, K.; Streib, W. E.; Eisenstein, O.; Caulton, K. G. RuHX(CO)(PR3)2: Can .Nu.CO Be a Probe for the Nature of the Ru-X Bond? *Inorg. Chem.* **1994**, *33* (7), 1476–1485. https://doi.org/10.1021/ic00085a043.

(19) Chisholm, M. H.; Cotton, F. A.; Extine, M. W.; Kelly, R. L. Reactions of Metal-to-Metal Multiple Bonds. 3. Addition of Nitric Oxide to Hexakis(Alkoxy)Dimolybdenum Compounds. Preparation

and Properties of Bis(Nitrosyl)Hexakis(Alkoxy)Dimolybdenum Compounds and Structural Characterization of the Isopropoxy Derivative. *J. Am. Chem. Soc.* **1978**, *100* (11), 3354–3358. https://doi.org/10.1021/ja00479a018.

(20) Fürstner, A. Alkyne Metathesis on the Rise. *Angew. Chem. Int. Ed.* **2013**, *52* (10), 2794–2819. https://doi.org/10.1002/anie.201204513.

(21) Heppekausen, J.; Stade, R.; Kondoh, A.; Seidel, G.; Goddard, R.; Fürstner, A. Optimized Synthesis, Structural Investigations, Ligand Tuning and Synthetic Evaluation of Silyloxy-Based Alkyne Metathesis Catalysts. *Chem Eur J* **2012**, *18*, 10281–10299.

(22) Fürstner, A. The Ascent of Alkyne Metathesis to Strategy-Level Status. *J. Am. Chem. Soc.* **2021**, jacs.1c08040. https://doi.org/10.1021/jacs.1c08040.

(23) Hillenbrand, J.; Leutzsch, M.; Yiannakas, E.; Gordon, C. P.; Wille, C.; Nöthling, N.; Copéret, C.; Fürstner, A. "Canopy Catalysts" for Alkyne Metathesis: Molybdenum Alkylidyne Complexes with a Tripodal Ligand Framework. *J. Am. Chem. Soc.* **2020**, *142* (25), 11279–11294. https://doi.org/10.1021/jacs.0c04742.

(24) Denmark, S. E.; Smith, R. C. Mechanistic Duality in Palladium-Catalyzed Cross-Coupling Reactions of Aryldimethylsilanolates. Intermediacy of an 8-Si-4 Arylpalladium(II) Silanolate. *J. Am. Chem. Soc.* **2010**, *132* (4), 1243–1245. https://doi.org/10.1021/ja907049y.

(25) Denmark, S. E. The Interplay of Invention, Discovery, Development, and Application in Organic Synthetic Methodology: A Case Study. *J. Org. Chem.* **2009**, *74* (8), 2915–2927. https://doi.org/10.1021/jo900032x.

(26) Denmark, S. E.; Ambrosi, A. Why You Really Should Consider Using Palladium-Catalyzed Cross-Coupling of Silanols and Silanolates. *Org. Process Res. Dev.* **2015**, *19* (8), 982–994. https://doi.org/10.1021/acs.oprd.5b00201.

(27) Tymonko, S. A.; Smith, R. C.; Ambrosi, A.; Ober, M. H.; Wang, H.; Denmark, S. E. Mechanistic Significance of the Si–O–Pd Bond in the Palladium-Catalyzed Cross-Coupling Reactions of Arylsilanolates. *J. Am. Chem. Soc.* **2015**, *137* (19), 6200–6218. https://doi.org/10.1021/jacs.5b02518.

(28) Huang, C.; Chattopadhyay, B.; Gevorgyan, V. Silanol: A Traceless Directing Group for Pd-Catalyzed *o* -Alkenylation of Phenols. *J. Am. Chem. Soc.* **2011**, *133* (32), 12406–12409. https://doi.org/10.1021/ja204924j.

(29) Huang, C.; Ghavtadze, N.; Chattopadhyay, B.; Gevorgyan, V. Synthesis of Catechols from Phenols via Pd-Catalyzed Silanol-Directed C–H Oxygenation. *J. Am. Chem. Soc.* **2011**, *133* (44), 17630–17633. https://doi.org/10.1021/ja208572v.

(30) Huang, C.; Ghavtadze, N.; Godoi, B.; Gevorgyan, V. Pd-Catalyzed Modifiable Silanol-Directed Aromatic C−H Oxygenation. *Chem. – Eur. J.* **2012**, *18* (32), 9789–9792. https://doi.org/10.1002/chem.201201616.

(31) Parasram, M.; Gevorgyan, V. Silicon-Tethered Strategies for C–H Functionalization Reactions. *Acc. Chem. Res.* **2017**, *50* (8), 2038–2053. https://doi.org/10.1021/acs.accounts.7b00306.

(32) Sieburth, S. M.; Fensterbank, L. Silanol Reactivity: Evaluation of Silanolate as a Metalation-Directing Group. *J. Org. Chem.* **1993**, *58* (23), 6314–6318. https://doi.org/10.1021/jo00075a026.

(33) Trost, B. M.; Chung, C. K. Vanadium-Catalyzed Addition of Propargyl Alcohols and Imines. *J. Am. Chem. Soc.* **2006**, *128* (32), 10358–10359. https://doi.org/10.1021/ja064011p.

(34) Trost, B. M.; Jonasson, C. Vanadium-Catalyzed *Anti* -Selective Additions of Allenols to Imines. *Angew. Chem. Int. Ed.* **2003**, *42* (18), 2063–2066. https://doi.org/10.1002/anie.200350890.

(35) Trost, B. M.; Oi, S. Atom Economy: Aldol-Type Products by Vanadium-Catalyzed Additions of Propargyl Alcohols and Aldehydes. *J. Am. Chem. Soc.* **2001**, *123* (6), 1230–1231. https://doi.org/10.1021/ja003629a.

(36) Noyori, R. Asymmetric Catalysis: Science and Opportunities (Nobel Lecture). *Angew. Chem. Int. Ed.* **2002**, *41* (12), 2008–2022. https://doi.org/10.1002/1521-3773(20020617)41:12<2008::AID-ANIE2008>3.0.CO;2-4.

(37) Fanourakis, A.; Docherty, P. J.; Chuentragool, P.; Phipps, R. J. Recent Developments in Enantioselective Transition Metal Catalysis Featuring Attractive Noncovalent Interactions between Ligand and Substrate. *ACS Catal.* **2020**, *10* (18), 10672–10714. https://doi.org/10.1021/acscatal.0c02957.

(38) MacMillan, D. W. C. The Advent and Development of Organocatalysis. *Nature* **2008**, *455* (7211), 304–308. https://doi.org/10.1038/nature07367.
(39) Connon, R.; Roche, B.; Rokade, B. V.; Guiry, P. J. Further Developments and Applications of Oxazoline-Containing Ligands in Asymmetric Catalysis. *Chem. Rev.* **2021**, *121* (11), 6373–6521. https://doi.org/10.1021/acs.chemrev.0c00844.
(40) Yoon, T. P.; Jacobsen, E. N. Privileged Chiral Catalysts. *Science* **2003**, *299* (5613), 1691–1693. https://doi.org/10.1126/science.1083622.
(41) Hartwig, J. F. Carbon–Heteroatom Bond Formation Catalysed by Organometallic Complexes. *Nature* **2008**, *455* (7211), 314–322. https://doi.org/10.1038/nature07369.
(42) Margalef, J.; Biosca, M.; de la Cruz Sánchez, P.; Faiges, J.; Pàmies, O.; Diéguez, M. Evolution in Heterodonor P-N, P-S and P-O Chiral Ligands for Preparing Efficient Catalysts for Asymmetric Catalysis. From Design to Applications. *Coord. Chem. Rev.* **2021**, *446*, 214120. https://doi.org/10.1016/j.ccr.2021.214120.
(43) Zeng, W.; Chen, G.-Y.; Zhou, Y.-G.; Li, Y.-X. Hydrogen-Bonding Directed Reversal of Enantioselectivity. *J. Am. Chem. Soc.* **2007**, *129* (4), 750–751. https://doi.org/10.1021/ja067346f.
(44) Pfaltz, A.; Drury, William J., I. Design of Chiral Ligands for Asymmetric Catalysis: From C2-Symmetric P,P- and N,N-Ligands to Sterically and Electronically Nonsymmetrical P,N-Ligands. *ChemInform* **2004**, *101*, 5723–5726. https://doi.org/10.1002/chin.200436268.
(45) Helmchen, G.; Pfaltz, A. PhosphinooxazolinesA New Class of Versatile, Modular P,N - Ligands for Asymmetric Catalysis. *Acc. Chem. Res.* **2000**, *33* (6), 336–345. https://doi.org/10.1021/ar9900865.
(46) Menges, F.; Neuburger, M.; Pfaltz, A. Synthesis and Application of Chiral Phosphino-Imidazoline Ligands: Ir-Catalyzed Enantioselective Hydrogenation. *Org. Lett.* **2002**, *4* (26), 4713–4716. https://doi.org/10.1021/ol027253c.
(47) Burk, M. J. C2-Symmetric Bis(Phospholanes) and Their Use in Highly Enantioselective Hydrogenation Reactions. *J. Am. Chem. Soc.* **1991**, *113* (22), 8518–8519. https://doi.org/10.1021/ja00022a047.
(48) Park, H.; Kumareswaran, R.; RajanBabu, T. V. Tunable Phosphinite, Phosphite and Phosphoramidite Ligands for the Asymmetric Hydrovinylation Reactions. *Tetrahedron* **2005**, *61* (26), 6352–6367. https://doi.org/10.1016/j.tet.2005.03.120.
(49) Feringa, B. L. Phosphoramidites: Marvellous Ligands in Catalytic Asymmetric Conjugate Addition. *Acc. Chem. Res.* **2000**, *33* (6), 346–353. https://doi.org/10.1021/ar990084k.
(50) Bartels, B.; Helmchen, G. Ir-Catalysed Allylic Substitution: Mechanistic Aspects and Asymmetric Synthesis with Phosphorus Amidites as Ligands. *Chem. Commun.* **1999**, No. 8, 741–742. https://doi.org/10.1039/a900864k.
(51) Schwarzer, M. C.; Fujioka, A.; Ishii, T.; Ohmiya, H.; Mori, S.; Sawamura, M. Enantiocontrol by Assembled Attractive Interactions in Copper-Catalyzed Asymmetric Direct Alkynylation of α-Ketoesters with Terminal Alkynes: OH···O/$Sp^3$-CH···O Two-Point Hydrogen Bonding Combined with Dispersive Attractions. *Chem. Sci.* **2018**, *9* (14), 3484–3493. https://doi.org/10.1039/C8SC00527C.
(52) Krueger, C. A.; Kuntz, K. W.; Dzierba, C. D.; Wirschun, W. G.; Gleason, J. D.; Snapper, M. L.; Hoveyda, A. H. Ti-Catalyzed Enantioselective Addition of Cyanide to Imines. A Practical Synthesis of Optically Pure α-Amino Acids. *J. Am. Chem. Soc.* **1999**, *121* (17), 4284–4285. https://doi.org/10.1021/ja9840605.
(53) Josephsohn, N. S.; Kuntz, K. W.; Snapper, M. L.; Hoveyda, A. H. Mechanism of Enantioselective Ti-Catalyzed Strecker Reaction: Peptide-Based Metal Complexes as Bifunctional Catalysts. *J. Am. Chem. Soc.* **2001**, *123* (47), 11594–11599. https://doi.org/10.1021/ja011875w.
(54) Matsuzawa, A.; Mashiko, T.; Kumagai, N.; Shibasaki, M. La/Ag Heterobimetallic Cooperative Catalysis: A Catalytic Asymmetric Conia-Ene Reaction. *Angew. Chem. Int. Ed.* **2011**, *50* (33), 7616–7619. https://doi.org/10.1002/anie.201102114.
(55) Narasaka, K.; Iwasawa, N.; Inoue, M.; Yamada, T.; Nakashima, M.; Sugimori, J. Asymmetric Diels-Alder Reaction Catalyzed by a Chiral Titanium Reagent. *J. Am. Chem. Soc.* **1989**, *111* (14), 5340–5345. https://doi.org/10.1021/ja00196a045.

(56) Corey, E. J.; Matsumura, Y. Evidence for the Importance of N-n-Attractive Interactions in Enantioselective Diels- Alder Reactions Chiral Catalysts of Type (R0)2TiC12. *Tetrahedron Lett.* **1991**, *32*, 6289–6292.
(57) Sangtrirutnugul, P.; Tilley, T. D. Silyl Derivatives of [Bis(8-Quinolyl)Methylsilyl]Iridium(III) Complexes: Catalytic Redistribution of Arylsilanes and Dehydrogenative Arene Silylation. *Organometallics* **2007**, *26* (23), 5557–5568. https://doi.org/10.1021/om700494q.
(58) Kitano, T.; Komuro, T.; Ono, R.; Tobita, H. Tandem Hydrosilylation/ *o* -C–H Silylation of Arylalkynes Catalyzed by Ruthenium Bis(Silyl) Aminophosphine Complexes. *Organometallics* **2017**, *36* (15), 2710–2713. https://doi.org/10.1021/acs.organomet.7b00528.
(59) Mo, Z.; Kostenko, A.; Zhou, Y.-P.; Yao, S.; Driess, M. Chelate Silylene–Silyl Ligand Can Boost Rhodium-Catalyzed C−H Bond Functionalization Reactions. *Chem. – Eur. J.* **2018**, *24* (55), 14608–14612. https://doi.org/10.1002/chem.201803089.
(60) Komuro, T.; Mochizuki, D.; Hashimoto, H.; Tobita, H. Iridium and Rhodium Complexes Bearing a Silyl-Bipyridine Pincer Ligand: Synthesis, Structures and Catalytic Activity for C–H Borylation of Arenes. *Dalton Trans.* **2022**, *51* (26), 9983–9987. https://doi.org/10.1039/D2DT01227H.
(61) Komuro, T.; Nakajima, Y.; Takaya, J.; Hashimoto, H. Recent Progress in Transition Metal Complexes Supported by Multidentate Ligands Featuring Group 13 and 14 Elements as Coordinating Atoms. *Coord. Chem. Rev.* **2022**, *473*, 214837. https://doi.org/10.1016/j.ccr.2022.214837.
(62) Yang, B.; Gao, J.; Tan, X.; Ge, Y.; He, C. Chiral PSiSi-Ligand Enabled Iridium-Catalyzed Atroposelective Intermolecular C−H Silylation. *Angew. Chem. Int. Ed.* **2023**, e202307812. https://doi.org/10.1002/ange.202307812.
(63) Gao, J.; He, C. Chiral Silanols: Strategies and Tactics for Their Synthesis. *Chem. – Eur. J.* **2023**, *29* (19), e202203475. https://doi.org/10.1002/chem.202203475.
(64) Bausch, C. C.; Pfaltz, A. *PHOX Ligands. In Privileged Chiral Ligands and Catalysts*; Wiley-VCH Verlag GmbH & Co. KGaA, 2011.
(65) Hargaden, G. C.; Guiry, P. J. Recent Applications of Oxazoline-Containing Ligands in Asymmetric Catalysis. *Chem. Rev.* **2009**, *109* (6), 2505–2550. https://doi.org/10.1021/cr800400z.
(66) Desimoni, G.; Faita, G.; Jørgensen, K. A. $C_2$ -Symmetric Chiral Bis(Oxazoline) Ligands in Asymmetric Catalysis. *Chem. Rev.* **2006**, *106* (9), 3561–3651. https://doi.org/10.1021/cr0505324.
(67) Min, T. *Doctoral Dissertation, University of California−Davis*; 2012.
(68) Diemoz, K. M. *Doctoral Dissertation, University of California−Davis*; 2018.
(69) Wilson, S. O.; Tran, N. T.; Franz, A. K. NMR and X-Ray Studies of Hydrogen Bonding for Amide-Containing Silanediols. *Organometallics* **2012**, *31* (19), 6715–6718. https://doi.org/10.1021/om300736n.
(70) Jagannathan, J. R.; Fettinger, J. C.; Shaw, J. T.; Franz, A. K. Enantioselective Si–H Insertion Reactions of Diarylcarbenes for the Synthesis of Silicon-Stereogenic Silanes. *J. Am. Chem. Soc.* **2020**, *142* (27), 11674–11679. https://doi.org/10.1021/jacs.0c04533.
(71) Kelly, A. T.; Franz, A. K. Metal-Free Synthesis of 1,3-Disiloxanediols and Aryl Siloxanols. *ACS Omega* **2019**, *4* (4), 6295–6300. https://doi.org/10.1021/acsomega.9b00121.
(72) Yang, W.; Liu, L.; Guo, J.; Wang, S.-G.; Zhang, J.-Y.; Fan, L.-W.; Tian, Y.; Wang, L.-L.; Luan, C.; Li, Z.-L.; He, C.; Wang, X.; Gu, Q.-S.; Liu, X.-Y. Enantioselective Hydroxylation of Dihydrosilanes to Si-Chiral Silanols Catalyzed by In Situ Generated Copper(II) Species. *Angew. Chem. Int. Ed.* **2022**, *61* (32), e202205743. https://doi.org/10.1002/anie.202205743.
(73) Jeon, M.; Han, J.; Park, J. Catalytic Synthesis of Silanols from Hydrosilanes and Applications. *ACS Catal.* **2012**, *2* (8), 1539–1549. https://doi.org/10.1021/cs300296x.
(74) Crawford, C. J.; Qiao, Y.; Liu, Y.; Huang, D.; Yan, W.; Seeberger, P. H.; Oscarson, S.; Chen, S. Defining the Qualities of High-Quality Palladium on Carbon Catalysts for Hydrogenolysis. *Org. Process Res. Dev.* **2021**, *25* (7), 1573–1578. https://doi.org/10.1021/acs.oprd.0c00536.
(75) Tran, N. T.; Wilson, S. O.; Franz, A. K. Cooperative Hydrogen-Bonding Effects in Silanediol Catalysis. *Org. Lett.* **2012**, *14* (1), 186–189. https://doi.org/10.1021/ol202971m.
(76) Liu, B.; Zhu, S.-F.; Zhang, W.; Chen, C.; Zhou, Q.-L. Highly Enantioselective Insertion of Carbenoids into N−H Bonds Catalyzed by Copper Complexes of Chiral Spiro Bisoxazolines. *J. Am. Chem. Soc.* **2007**, *129* (18), 5834–5835. https://doi.org/10.1021/ja0711765.

(77) Zhu, S.-F.; Zhou, Q.-L. Transition-Metal-Catalyzed Enantioselective Heteroatom–Hydrogen Bond Insertion Reactions. *Acc. Chem. Res.* **2012**, *45* (8), 1365–1377. https://doi.org/10.1021/ar300051u.
(78) Furniel, L. G.; Echemendía, R.; Burtoloso, A. C. B. Cooperative Copper-Squaramide Catalysis for the Enantioselective N–H Insertion Reaction with Sulfoxonium Ylides. *Chem. Sci.* **2021**, *12* (21), 7453–7459. https://doi.org/10.1039/D1SC00979F.
(79) Gillingham, D.; Fei, N. Catalytic X–H Insertion Reactions Based on Carbenoids. *Chem. Soc. Rev.* **2013**, *42* (12), 4918. https://doi.org/10.1039/c3cs35496b.
(80) Li, M.-L.; Yu, J.-H.; Li, Y.-H.; Zhu, S.-F.; Zhou, Q.-L. Highly Enantioselective Carbene Insertion into N–H Bonds of Aliphatic Amines. *Science* **2019**, *366* (6468), 990–994. https://doi.org/10.1126/science.aaw9939.
(81) Li, M.-L.; Pan, J.-B.; Zhou, Q.-L. Enantioselective Synthesis of Amino Acids from Ammonia. *Nat. Catal.* **2022**, *5* (6), 571–577. https://doi.org/10.1038/s41929-022-00779-2.
(82) Liu, Z.; Calvó-Tusell, C.; Zhou, A. Z.; Chen, K.; Garcia-Borràs, M.; Arnold, F. H. Dual-Function Enzyme Catalysis for Enantioselective Carbon–Nitrogen Bond Formation. *Nat. Chem.* **2021**, *13* (12), 1166–1172. https://doi.org/10.1038/s41557-021-00794-z.
(83) Yang, W.; Pu, M.; Lin, X.; Chen, M.; Song, Y.; Liu, X.; Wu, Y.-D.; Feng, X. Enantioselective Formal Vinylogous N–H Insertion of Secondary Aliphatic Amines Catalyzed by a High-Spin Cobalt(II) Complex. *J. Am. Chem. Soc.* **2021**, *143* (25), 9648–9656. https://doi.org/10.1021/jacs.1c04367.
(84) Lee, E. C.; Fu, G. C. Copper-Catalyzed Asymmetric N−H Insertion Reactions: Couplings of Diazo Compounds with Carbamates to Generate α-Amino Acids. *J. Am. Chem. Soc.* **2007**, *129* (40), 12066–12067. https://doi.org/10.1021/ja074483j.
(85) Zhu, S.-F.; Xu, B.; Wang, G.-P.; Zhou, Q.-L. Well-Defined Binuclear Chiral Spiro Copper Catalysts for Enantioselective N–H Insertion. *J. Am. Chem. Soc.* **2012**, *134* (1), 436–442. https://doi.org/10.1021/ja2084493.
(86) Zhu, Y.; Liu, X.; Dong, S.; Zhou, Y.; Li, W.; Lin, L.; Feng, X. Asymmetric N□H Insertion of Secondary and Primary Anilines under the Catalysis of Palladium and Chiral Guanidine Derivatives. *Angew. Chem. Int. Ed.* **2014**, *53* (6), 1636–1640. https://doi.org/10.1002/anie.201308501.
(87) Hansch, Corwin.; Leo, A.; Taft, R. W. A Survey of Hammett Substituent Constants and Resonance and Field Parameters. *Chem. Rev.* **1991**, *91* (2), 165–195. https://doi.org/10.1021/cr00002a004.
(88) Zhu, Y.; Liu, X.; Dong, S.; Zhou, Y.; Li, W.; Lin, L.; Feng, X. Asymmetric N□H Insertion of Secondary and Primary Anilines under the Catalysis of Palladium and Chiral Guanidine Derivatives. *Angew. Chem. Int. Ed.* **2014**, *53* (6), 1636–1640. https://doi.org/10.1002/anie.201308501.
(89) Shen, G.; Liu, H.; Chen, J.; He, Z.; Zhou, Y.; Wang, L.; Luo, Y.; Su, Z.; Fan, B. Zinc Salt-Catalyzed Reduction of α-Aryl Imino Esters, Diketones and Phenylacetylenes with Water as Hydrogen Source. *Org. Biomol. Chem.* **2021**, *19* (16), 3601–3610. https://doi.org/10.1039/D1OB00155H.
(90) Pan, J.; Zhang, X.; Shi, Y.; Han, A.; Chen, Y.; Ouyang, J.; Li, M.; Zhou, Q. A Spiro Phosphamide Catalyzed Enantioselective Proton Transfer of Ylides in a Free Carbene Insertion into N−H Bonds. *Angew. Chem. Int. Ed.* **2023**, *62* (15), e202300691. https://doi.org/10.1002/anie.202300691.
(91) Huang, W.-S.; Xu, Z.; Yang, K.-F.; Chen, L.; Zheng, Z.-J.; Xu, L.-W. Modular Construction of Multifunctional Ligands for the Enantioselective Ruthenium-Catalyzed Carbenoid N–H Insertion Reaction: An Enzyme-like and Substrate-Sensitive Catalyst System. *RSC Adv.* **2015**, *5* (58), 46455–46463. https://doi.org/10.1039/C5RA05804J.
(92) Zhao, P.; Huang, D.; Wang, F.; Han, T.; Yang, M.; Wang, K.; Hu, Y. Tin Powder-promoted Oxidation/Allylation of Glycine Esters: Synthesis of $\gamma$, $\delta$-unsaturated $\alpha$-amino Acid Esters. *Appl. Organomet. Chem.* **2022**, *36* (1). https://doi.org/10.1002/aoc.6479.
(93) Tian, H.; Xu, W.; Liu, Y.; Wang, Q. Unnatural α-Amino Acid Synthesized through α-Alkylation of Glycine Derivatives by Diacyl Peroxides. *Org. Lett.* **2020**, *22* (13), 5005–5008. https://doi.org/10.1021/acs.orglett.0c01574.

(94) Bachmann, S.; Fielenbach, D.; Jørgensen, K. A. Cu(I)-Carbenoid- and Ag(I)-Lewis Acid-Catalyzed Asymmetric Intermolecular Insertion of α-Diazo Compounds into N–H Bonds. *Org Biomol Chem* **2004**, *2* (20), 3044–3049. https://doi.org/10.1039/B412053A.

# Chapter Two: Mechanistic Insights into the Aminoamide Silanol Ligand in the Copper-catalyzed Enantioselective N−H Insertion Reaction*

## I. Introduction

This chapter delves deeper into the structural and mechanistic aspects of the aminoamide silanol ligand and its role as a ligand in the enantioselective N−H insertion, building upon the discovery discussed in Chapter One. The primary objectives are to gain a comprehensive understanding of how the individual elements − the amide, amino, and silanol functional groups − within the ligand structure contribute to its functionality and mode of interaction in the formation of the active metal complex during the enantioselective N−H insertion process. Additionally, we aim to identify the structural features of the ligand that contribute to the selectivity in the enantioselective N−H insertion. To achieve this goal, we conducted investigations, including silanol ligand analog studies, X-ray structural analysis, and a series of binding experiments using *in-situ* IR and NMR spectroscopy to probe metal-ligand interactions (Figure 2.1). Crystallization studies allow access to a sodium complex where X-ray structure analyses provided evidence of an H-bonding stabilized Na-siloxide complex. Additionally, we collaborated with Prof. Peng Liu at the University of Pittsburgh on density functional theory (DFT) calculations. The results support the silanol as a chelating group in the active complex. By integrating evidence from all the experiments, we propose the mechanism of the formation of the active catalyst complex and identify crucial structural features of the ligand that confer the enantioselective N−H insertion.

*Reproduced in part with permission from Chang, Y.-P.; Blanco-Herrero, K.; Alturaifi, T. M.; Fettinger, J. C.; Liu, P.; Franz, A. K. "Multifunctional Chiral Silanol Ligands for Enantioselective Catalysis." *Angew. Chem. Int. Ed. (manuscript under revision)*

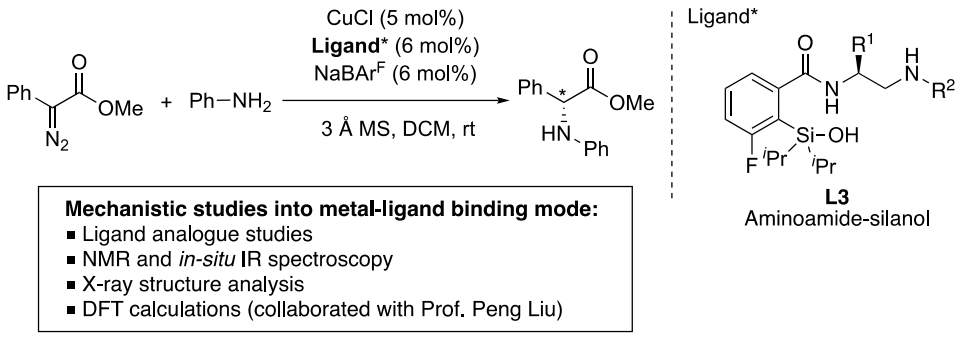



**Figure 2.1.** Project overview.

## II. Modularity of Aminoamide-silanol Ligands

The synthesis of versatile aminoamide-silanol ligands **L3** involves a streamlined and efficient four-step process. By utilizing commercially available starting materials, we can fine-tune the electronic and steric properties of the ligands (Figure 2.2A). Our exploration focused on varying $R^1$ (**L3b**–**d**), $R^3$ (**L3g**), and the aryl ring (**L3e**–**f**) in Chapter 1. In this section, we focus on examining the impact of altering the substituents $R^2$ on the amino group. The X-ray analysis of **L3a** revealed intramolecular H-bonding between the silanol and amino group, which could provide secondary structure elements and additional opportunities for tuning the electronic properties of the ligand (Figure 2.2B).

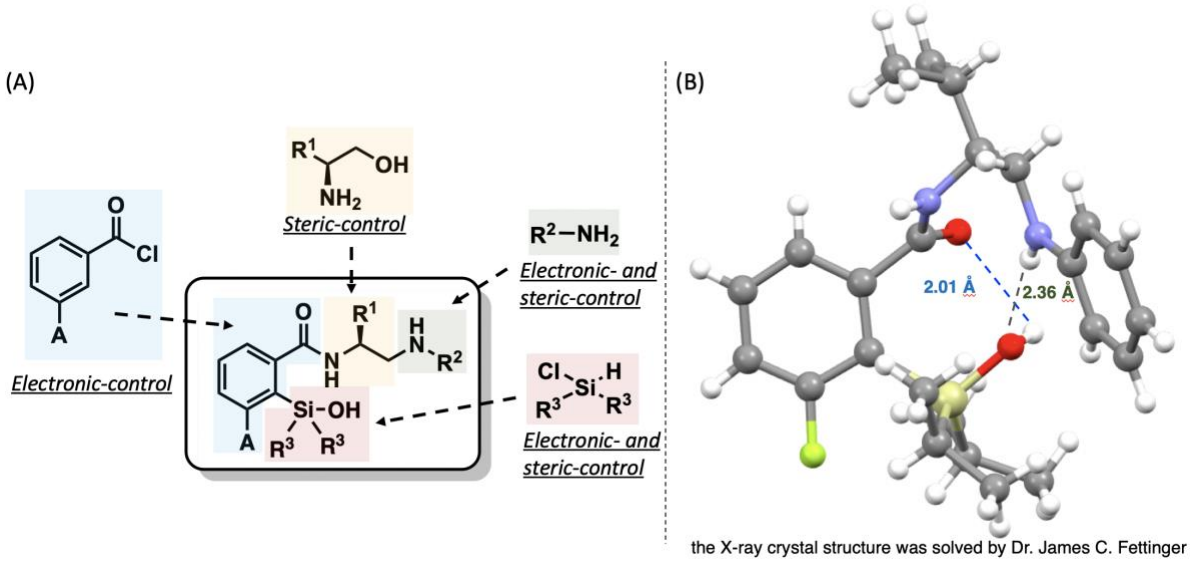
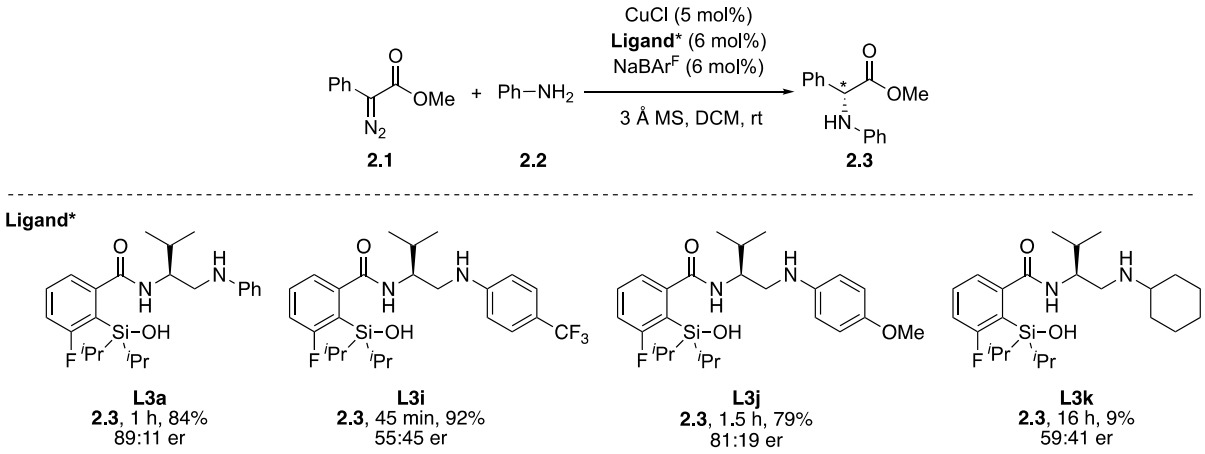



**Figure 2.2.** (A) Modular synthesis of aminoamide-silanol ligands. (B) X-ray analysis of **L3a**.

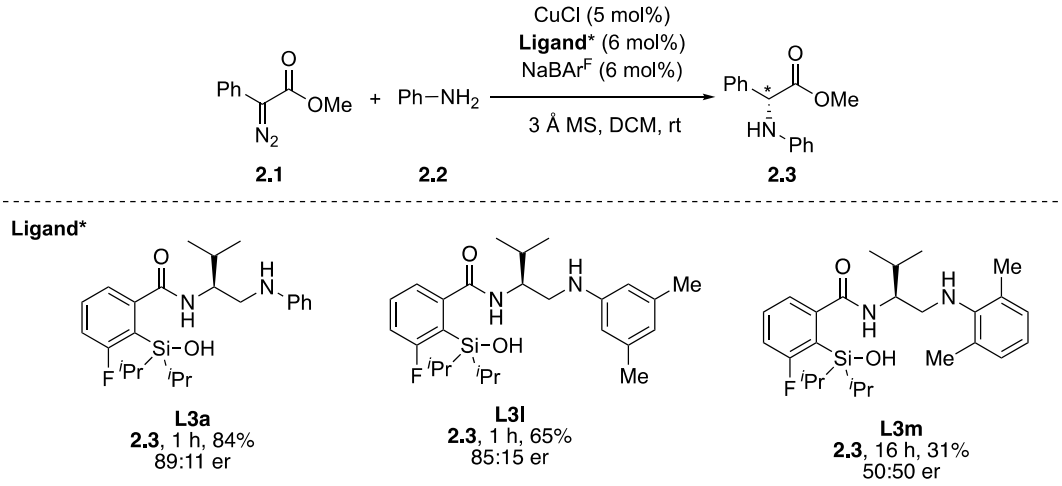
The results shown in Scheme 2.1 confirm that the substituents at the amino nitrogen have a distinct influence on both reactivity and enantioselectivity. First, it was noted that electronic modification via

para-substitution of the *N*-aryl ring with electron-withdrawing and electron-donating groups (**L3i**–**k**) significantly affected enantioselectivity. The introduction of an electron-withdrawing trifluoromethyl group at the para position significantly decreased the selectivity for the N–H insertion (55:45 er). In contrast, a slight decrease in selectivity was observed with the electron-donating methoxy group (81:19 er). Upon comparing *N*-phenyl (**L3a**) and *N*-cyclohexyl (**L3k**), the *N*-phenyl demonstrated superior reactivity (84% *vs.* 9% yield) and enantioselectivity (89:11 *vs.* 59:41 er). These results suggested that the binding interaction between the amino group and copper salt is crucial role in a metal-ligation site, impacting reactivity and selectivity.



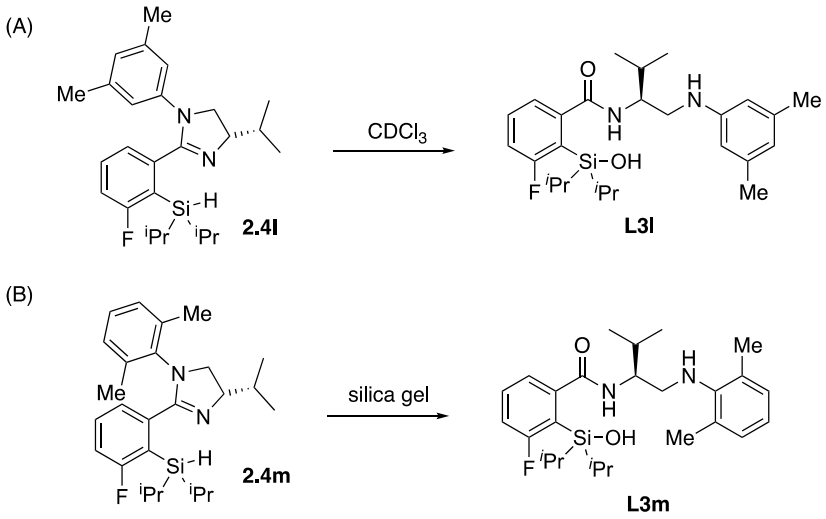

**Scheme 2.1.** Ligand analogs to enhance understanding of metal-ligand interactions in the enantioselective N–H insertion of α-phenyl-α-diazoesters with aniline.

Subsequently, an evaluation was conducted to assess the impact of ortho-substituents on the arylamine ring on the performance of the ligands (Scheme 2.2). Increasing the steric bulk on the *N*-aryl group (**L3l** *vs* **L3m**) resulted in low yield (65% *vs.* 31%) and selectivity (85:15 *vs.* 50:50 er) for the insertion product. This observed effect could be attributed to hindered addition to the sterically hindered metal-carbenoid complex.



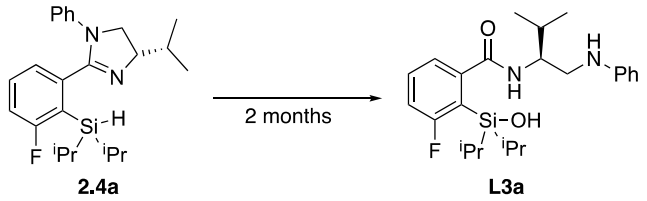

**Scheme 2.2.** Ligand screen for the steric bulk on the *N*-aryl group.

During the synthesis of **L3l** and **L3m**, it was observed that the respective imidazoline silanes (**2.4l** and **2.4m**) would readily convert to aminoamide silanol structures without the addition of a metal catalyst (Scheme 2.3). Specifically, the isolated silane **2.4l** undergoes hydrolysis and ring-opening into silanol **L3l** when exposed to air (Scheme 2.3A). The identification of the isolated silane product **2.4l** was confirmed through distinct peaks in the $^{1}$H NMR and $^{19}$F NMR spectra. Then, upon exposure to $CDCl_3$ while waiting to collect $^{13}$C NMR data overnight, it was observed that silane **2.4l** converted into aminoamide silanol **L3l**. Similarly, when imidazoline silane **2.4m** was exposed to silica gel for column chromatography, the silane reaction mixture interacted with silica gel to promote the formation of the intended silanol **L3m** (Scheme 2.3B).



**Scheme 2.3.** Observation of transformation of imidazoline silanes into aminoamide silanols upon exposure to $CDCl_3$ and/or silica gel.

Additionally, we observed the transformation of imidazoline silane **2.4a** into aminoamide silanol **L3a** while it was stored in a drawer on the benchtop for over two months in the absence of light (Scheme 2.4). This prompted us to conduct further investigation into the Pd-free hydrolysis process. Further discussion of the metal-free silane hydrolysis will be presented in the next section.




**2.4a** **L3a**

**Scheme 2.4.** Imidazoline silane transformed into aminoamide silanol while stored in the dark.

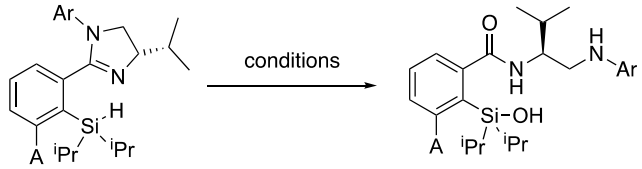
### III. Discussion of Pd-free Hydrolysis During Ligand Synthesis

For specific substrates (Table 2.1), it is notable that aminoamide silanol **L3** can form readily from imidazoline silane **2.4** without the use of any Pd catalyst. Although we acknowledge the potential presence of trace amounts of residual Pd or other metals in the chlorosilane reagent, the fact that we can successfully synthesize the ligand without the need to add any Pd reagent remains an appealing method. These observations suggest that the hydrolysis of both the silane and imidazoline are facilitated based on the structural features and is unlikely to be driven solely by Pd residues. The active silane might be the gateway to the aminoamide silanol. It is also noteworthy that several examples of metal-free silanol synthesis from silanes through organocatalysis, biocatalysis, photocatalysis, and electrochemical catalysis have been reported.[1–3]

Table 2.1 summarizes the observations made for the conversion of imidazoline silane under the Pd-free hydrolysis process. Certain observations were made as part of the intentional investigation of this process, while other observations were made during various storage conditions. Both imidazoline silanes **2.4a** and **2.4e** undergo complete conversion to **L3** under the Pd-free hydrolysis conditions (Table 2.1, entries 1 and 4). The presence of fluoride on the aryl group appears to influence the stabilization of imidazoline silane **2.4a** (Table 2.1, entry 3), consequently slowing down the conversion to the

corresponding aminoamide silanol **L3**. These results, combined with spectroscopic evidence, will be discussed in detail below.

**Table 2.1.** Examples of aminoamide silanol **L3** formation without Pd/C




**2.4a**, A = F, Ar = Ph
**2.4e**, A = H, Ar = Ph

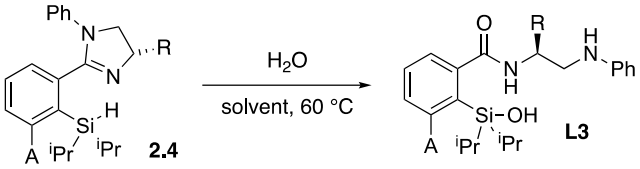
**L3a**, A = F, Ar = Ph
**L3e**, A = H, Ar = Ph

| Entry | A | Ar | **2.4** | Conditions | Time | Conversion of **2.4** (%)[b] |
|---|---|---|---|---|---|---|
| 1[a] | F | Ph | **2.4a** | $H_2O$, THF, 60 °C | 16 h | >95% |
| 2[a] | F | Ph | **2.4a** | $H_2O$, THF, rt | 16 h | <5% |
| 3 | F | Ph | **2.4a** | rt (benchtop) | 3 d | <5% |
| 4[a] | H | Ph | **2.4e** | $H_2O$, THF, 60 °C | 16 h | >95% |
| 5 | H | Ph | **2.4e** | rt (benchtop) | 3 d | 20% |
| 6 | F | 3,5-$(CH_3)_2$Ph | **2.4l** | $CDCl_3$, rt | 3 d | >95% |
| 7 | F | 2,6-$(CH_3)_2$Ph | **2.4m** | silica gel, rt | instant | >95% |

[a]Reactions performed under standard reaction conditions (General Procedure D-Method A in Chapter 1): silane **2.4** (0.1 mmol), $H_2O$ (1 mmol), solvent (0.15 M). [b]Conversion determined using $^{19}F$ NMR (if applied) or $^{1}H$ NMR spectroscopy.

Imidazoline silanes **2.4** with different steric groups were investigated for the potential of the hydrolysis reaction to proceed without a Pd catalyst (Table 2.2). When an *iso*-propyl group was used as the steric group, the aminoamide silanol product was generated after stirring overnight at 60 °C; for a 1-gram scale reaction, a longer reaction time was required for completion (Table 2.2, entries 1−2). When a *tert*-butyl group was used as the steric group, no aminoamide silanol formed after 7 d in the absence of Pd/C (Table 2.2, entries 4−5). Despite the intentional addition of HCl, the reactivity of silane **2.4b** remained low (Table 2.2, entry 6), suggesting that trace acid does not significantly promote silanol formation. When a phenyl group was used as the steric group, a slower silane conversion into aminoamide was observed, with only 45% conversion after 40 h. Without the presence of fluoride on the aryl group, the silanes showed higher reactivity, as shown in Table 2.1. Specifically, with *tert*-butyl group as the steric group, **2.4f** demonstrated only 23% conversion into **L3f** after 7 d (Table 2.2, entry 9).

**Table 2.2.** Scope of the Pd-free hydrolysis from imidazoline silane **2.4** to aminoamide silanol **L3**



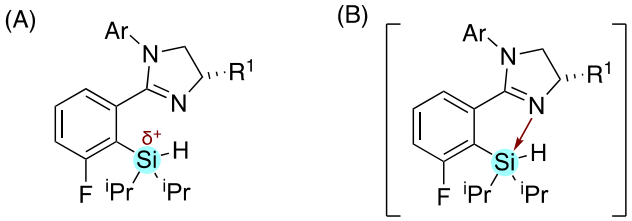

**2.4a**, A = F, R = $^{i}$Pr
**2.4b**, A = F, R = $^{t}$Bu
**2.4d**, A = F, R = Ph
**2.4e**, A = H, R = $^{i}$Pr
**2.4f**, A = H, R = $^{t}$Bu

**L3a**, A = F, R = $^{i}$Pr
**L3b**, A = F, R = $^{t}$Bu
**L3d**, A = F, R = Ph
**L3e**, A = H, R = $^{i}$Pr
**L3f**, A = H, R = $^{t}$Bu

| Entry[a] | A | R | **2.4** | Solvent[b] | Additive | Time | Conversion of silane (%)[c] |
|---|---|---|---|---|---|---|---|
| 1 | F | $^{i}$Pr | **2.4a** | THF | - | 16 h | >95% (63%) |
| 2[d] | F | $^{i}$Pr | **2.4a** | THF | - | 53 h | >95% (54%) |
| 3 | F | $^{i}$Pr | **2.4a** | 1,4-dioxane | - | 16 h | >95% |
| 4 | F | $^{t}$Bu | **2.4b** | 1,4-dioxane | - | 7 d | NR[e] |
| 5 | F | $^{t}$Bu | **2.4b** | THF | - | 3 d | NR |
| 6 | F | $^{t}$Bu | **2.4b** | 1,4-dioxane | HCl (1 mol%) | 3 d | 30% |
| 7 | F | Ph | **2.4d** | 1,4-dioxane | - | 40 h | 45% |
| 8 | H | $^{i}$Pr | **2.4e** | THF | - | 16 h | >95% (83%) |
| 9 | H | $^{t}$Bu | **2.4f** | 1,4-dioxane | - | 7 d | 23% |

[a]Reactions performed under standard reaction conditions (General Procedure D-Method A in Chapter 1): silane **2.4** (0.1 mmol), $H_2O$ (1 mmol), solvent (0.15 M). [b]Consistent results with both THF and 1,4-dioxane were obtained; however, for longer reaction times, 1,4-dioxane is preferred to prevent solvent evaporation. [c]Conversion determined using $^{19}F$ or $^{1}H$ NMR spectroscopy; isolated yield in parentheses. [d]Reaction performed with 954 mg (2.4 mmol) of silane. [e]No reaction.

One possible explanation for the high reactivity observed in specific imidazoline-silanes (Figure 2.3A, **2.4**) might result from intramolecular activation of the silane. This occurs via a dative bond between the imidazoline nitrogen and the electropositive silicon center (Figure 2.3B, [**2.4**]). The resulting pentacoordinate silane would exhibit increased reactivity at the silicon center, making it more susceptible to nucleophilic attack,[4] which in turn forms silanol. Table 2.2 suggests that the electron-withdrawing fluoride group may influence the formation of this dative bond in the aryl ring and the different steric effects of $R^1$.




**2.4**
tetracoordinate

[**2.4**]
pentacoordinate
*more electrophilic silicon*

**Figure 2.3.** Proposed dative bond formation between the nitrogen of imidazoline and silicon.

Spectroscopic data also supports that an intramolecular interaction may occur with the silane. The IR spectrum displayed a slight red-shift and significant broadening of Si−H stretching based on the steric effects (**2.4a**, $\nu$ = 2127 $cm^{-1}$ *vs* **2.4b**, $\nu$ = 2131 $cm^{-1}$), along with a downfield shift also observed in the $^{29}Si$ NMR spectrum (**2.4a**, δ = 2.05 ppm *vs* **2.4b**, δ = 1.81 ppm). The imidazoline-containing silane **2.4e** lacking an electron-withdrawing fluoride group in the aryl ring (Table 2.2, entry 8, **2.4e**) displays a more downfield shift in the $^{29}Si$ NMR spectrum (δ = 2.60 ppm). This supports that the silicon center is more electropositive. This observation is also supported by its heightened reactivity in the Pd-free hydrolysis. The fluoride on the aryl group decreases the chelating between the nitrogen of imidazoline and silicon, thereby stabilizing the imidazoline silane **2.4a** and slowing down the conversion to aminoamide silanol **L3a**. Specifically, when silane **2.4e** was stored on the benchtop for 3 d, 20% conversion of **2.4e** was observed, while no conversion was observed under the same conditions for **2.4a** (Table 2.1, entries 3 and 5). We acknowledge that the observations corresponding to entries 3 and 5 were not made on the same day, hindering a direct comparison. Nonetheless, we present these observations as they provide valuable insights into the reactivity of the silicon center, supporting the spectroscopic results that the absence of fluoride on the aryl ring leads to a more electropositive silicon center.

## IV. Mechanistic Studies of the Metal-ligand Binding Mode

### IVa. Silanol Ligand Analog Study

To identify the pivotal structural elements involved in metal-ligand binding, we synthesized and evaluated a series of specific silanol ligand analogs (Scheme 2.5, **L4**−**L7**). Our investigations confirmed the vital role played by the silanol in the enantioselectivity of the N−H insertion as discussed in Chapter 1. Subsequently, we hypothesized that the amide carbonyl, amine NH, and aryl amine groups also serve as essential components (Figure 2.4).

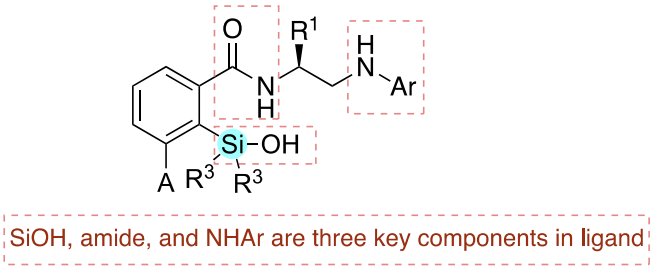
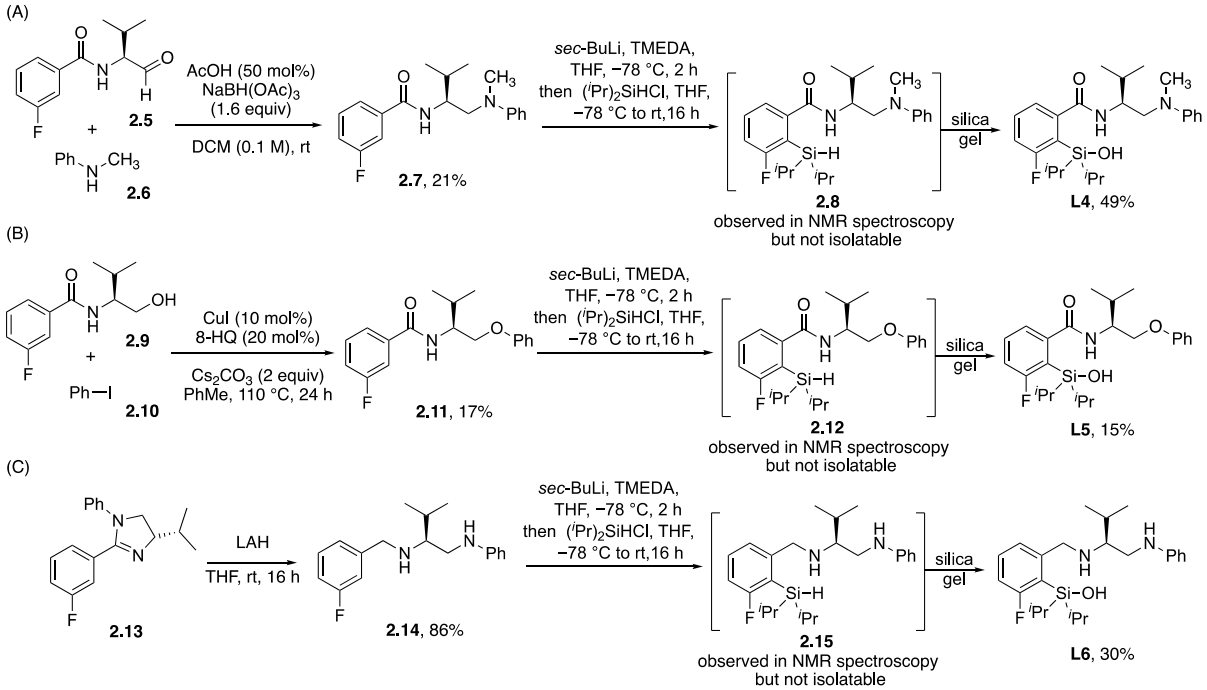


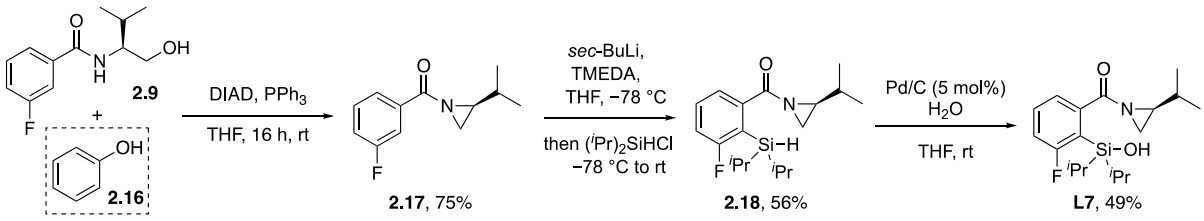

**Figure 2.4.** Essential chelating components on **L3**.

The precursors for each analog were synthesized and submitted to the standard silylation conditions to access silanol ligand analogs **L4**–**L7**. The *N*-methylated precursor **2.7** was generated via a reductive-amination of aldehyde **2.5** and *N*-methylaniline (Scheme 2.5A). The *O*-phenyl precursor **2.11** was synthesized using a copper-catalyzed C–O coupling (Scheme 2.5B). The low yield of **2.11** is attributed to the low conversion (20%) of starting material **2.9**. Diamine **2.14** was obtained upon reduction of imidazoline **2.13** using LAH (Scheme 2.5C). The respective chiral scaffolds (**2.7**, **2.11**, and **2.14**) underwent silylation through direct lithiation using *sec*-BuLi to form the corresponding silane. All the respective silane precursors (**2.8**, **2.12**, and **2.15**) exhibited high reactivity toward the silanol formation: Upon exposure of the silanes to silica gel, the target silanol products **L4**–**L6** were formed and isolated.



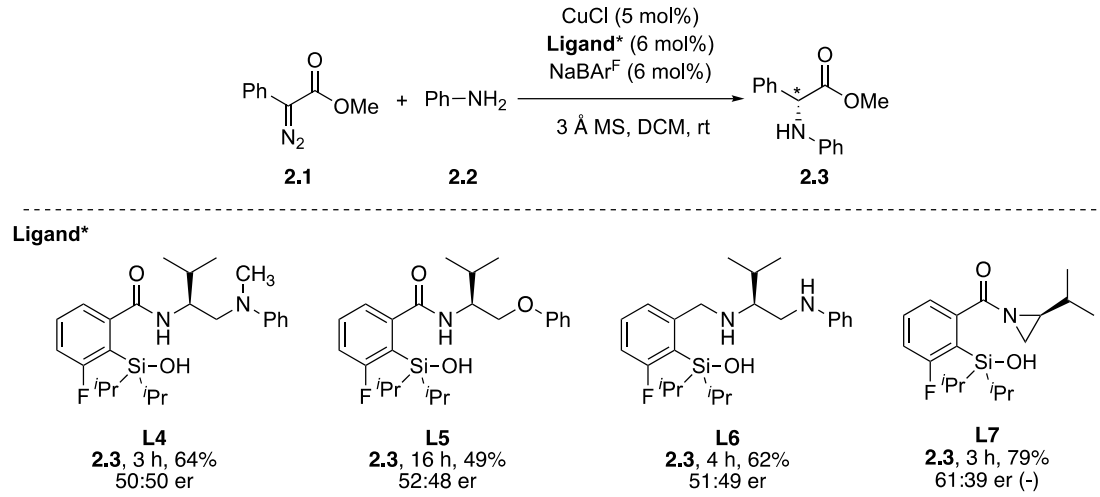

**Scheme 2.5.** Synthesis of **L4**–**L6**.

Aziridine **2.17** was obtained as the major product when **2.9** was exposed to Mitsunobu conditions initially intended to synthesize the phenyl ether **2.11 (**Scheme 2.6). The unexpected aziridine structure was confirmed using HRMS, and NMR spectroscopy, including $^{1}H$-$^{13}C$ HSQC and $^{1}H$-$^{13}C$ HMBC. Aziridine silanol **L7** was subsequently accessed through the standard route involving silylation. The spontaneous transformation of silane into silanol, as mentioned in Scheme 2.5, was not observed. The aziridine silane **2.18** is stable in silica column and was isolated. **L7** was obtained following hydrolysis using Pd/C conditions.




**Scheme 2.6.** Synthesis of unexpected aziridine scaffold.

The studies of the silanol ligand analogs revealed that the amide carbonyl, amine NH, and aryl amine groups play crucial roles in the catalytic process of enantioselective the N−H insertion (Scheme 2.7.). The *N*-methylated analog (**L4**) affords good yield (64%) of insertion product **2.3** but affords no selectivity. Similarly, the ether analog (**L5**), resulted in low enantioselectivity. These observations suggest that the H-bonding interaction between the NH-phenyl amine and the carbonyl group is critical to impart enantioselectivity. Evaluating a ligand analog (**L6**) with the carbonyl group of the amide removed resulted in a complete loss of enantioselectivity, suggesting the participation of the carbonyl oxygen in the binding process. The low selectivity observed for aziridine silanol ligand **L7**, lacking the amide N-H and the amino group, further emphasized the significance of the aminoamide scaffold in promoting high selectivity.



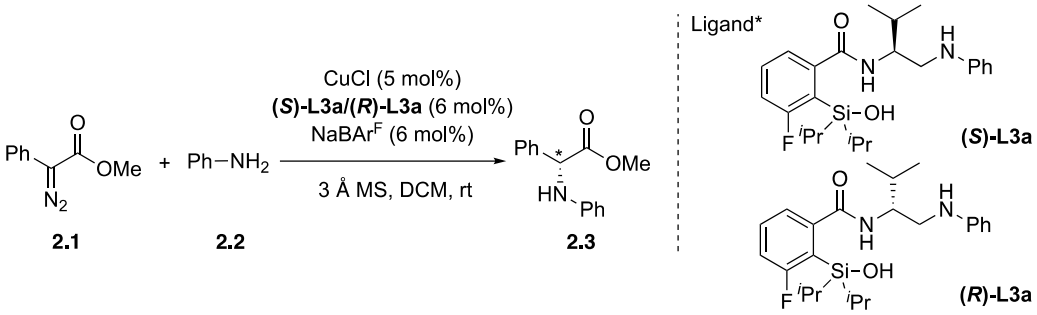

**Scheme 2.7.** Comparing ligand analogs in the N−H insertion reaction.

## IVb. Evaluation of Non-linear Behavior and M/L Ratio Experiments

To further understand the catalyst complex and mechanism involved, we investigated whether the silanol ligand exhibits a non-linear effect in the enantioselective N−H insertion reaction. A non-linear effect in enantioselective catalysis can have either a positive or negative correlation between the enantiopurity of the chiral ligand and the resulting enantiopurity of the product. This non-ideal behavior can arise from various factors, such as the presence of higher-order aggregates or dimeric forms of the catalyst, complicated reaction kinetics, or unexpected interactions between catalysts and substrates.[5–8]

We evaluated of potential non-linear behavior with **L3a** for the enantioselective N−H insertion (Table 2.3). In this case, we observed linear (ideal) behavior ($R^2 = 0.993$), suggesting the formation of a 1:1 metal/ligand complex (Figure 2.5).[7] This linear behavior suggests that the relationship between the enantiopurity of our chiral catalyst and the resulting product enantiopurity followed an expected pattern, indicating a simpler, more direct interaction between the catalyst and ligand in our N−H insertion.

**Table 2.3.** Evaluation of potential non-linear behavior with **L3a** for the enantioselective N−H insertion of α-phenyl-α-diazoesters with aniline[a]




| (*S*)-L3a (mol%) | (*R*)-L3a (mol%) | ee of ligand (%) | ee of product (%)[c] |
|---|---|---|---|
| 6.0 | 0.0 | 100[b] | 78 |
| 5.5 | 0.5 | 83.3 | 64 |
| 5.0 | 1.0 | 66.7 | 56 |
| 4.5 | 1.5 | 50.0 | 44 |
| 4.0 | 2.0 | 33.3 | 27 |
| 3.5 | 2.5 | 16.7 | 12 |
| 3.0 | 3.0 | 0 | 0 |

[a]Standard reaction conditions: **2.1** and **2.2** (0.2 mmol), CuCl (5 mol%), NaBAr$^F$ (6 mol%), (*S*)-**L3a**/(*R*)-**L3a** (6 mol% in total) and spherical 3Å mol sieves (50 mg) in DCM (0.05 M) at room temperature. [b]Determined using CSP-HPLC analysis with a Chiralpak AD-H column. [c]Determined using CSP-HPLC analysis with a Chiralpak OD-H column.

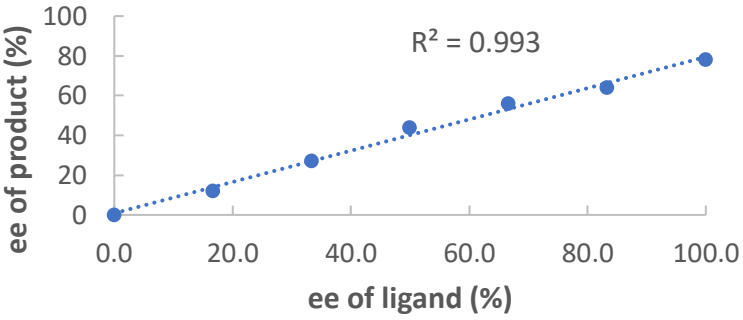
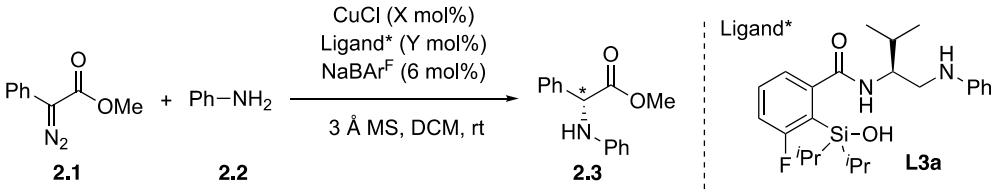



**Figure 2.5.** Linear behavior observed in the enantioselective N−H insertion of α-phenyl-α-diazoester with aniline.

Experiments comparing several M/L ratios were conducted to understand the impact of the stoichiometry between copper and **L3a** on the performance of enantioselective N−H insertion (Table 2.4). In the optimal condition, a slight excess of **L3a** was used to ensure that all copper is bound to the ligand to avoid an unselective background reaction (Table 2.4, entry 1).[9] Reducing the ligand loading to a 2:1 ligand-to-metal ratio maintained the enantioselectivity (89:11 *vs* 88:12 er, entry 2). This suggests a consistent metal-ligand coordination is operating despite varying M/L ratios, possibly due to

the high equilibrium constant favoring the complexation of **L3a** to copper. This prevents the dissociation of the active complex upon the addition of the aniline starting material (**2.2**). At M/L = 1/2, the enantioselectivity was slightly reduced (89:11 *vs* 84:16 er, entry 3) while the reactivity was slightly enhanced (83% *vs* 90% yield, entry 3). Overall, the comparable results across different M/L ratios suggest a high equilibrium constant for the complexation of **L3a** to Cu, ensuring the stability of active metal-ligand complexes under the optimal reaction conditions.

**Table 2.4.** Results of M/L ratio experiments.



**2.1** **2.2** **2.3**

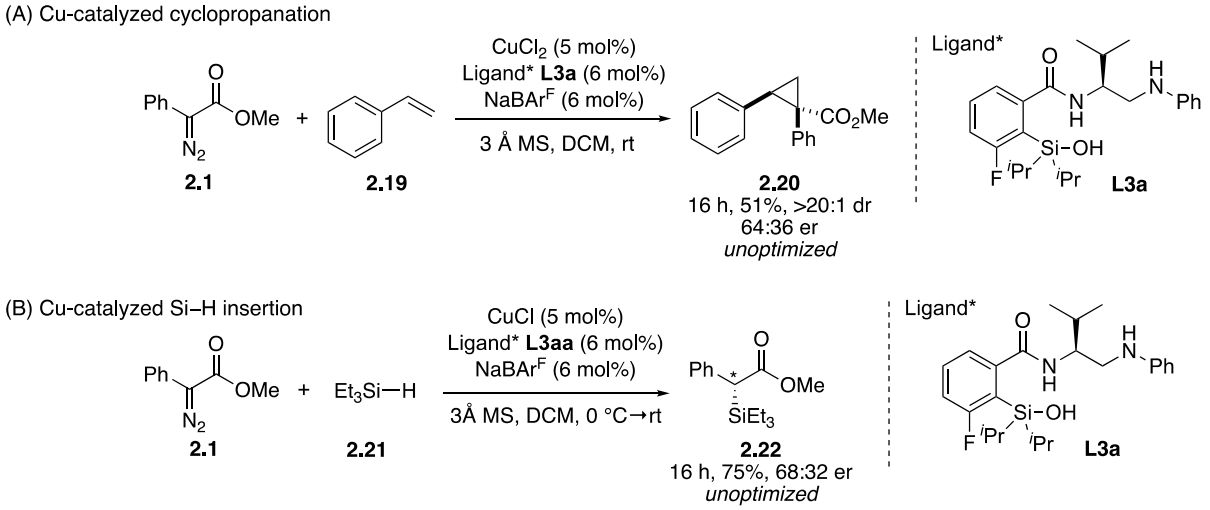
| Entry[a] | **M/L** | CuCl X (mol%) | Ligand Y (mol%) | Time (h) | Yield (%)[b] | er[c] |
|---|---|---|---|---|---|---|
| 1 | **1/1.2** | 5 | 6 | 1 | 83 | 89:11 |
| 2 | **2/1** | 5 | 2.5 | 1 | 70 | 88:12 |
| 3 | **1/2** | 5 | 10 | 1 | 90 | 84:16 |

[a]Reactions performed under standard reaction conditions (General procedure-**Procedure G**): Diazo compound **2.1** (0.2 mmol), aniline **2.2** (0.2 mmol), CuCl (X mol%), $NaBAr^F$ (6 mol%), ligand **L3a** (Y mol%), and activated spherical 3 Å mol sieves (50 mg) at room temperature. [b]NMR yield using Ph-TMS as internal standard [c]Determined using CSP-HPLC with a Chiralpak OD-H column.

## IVc. Investigation of the Silanol Ligand in Reactions with a Concerted Mechanism

Cyclopropanation and Si−H insertion reactions have been performed to provide mechanistic insights into the Cu/silanol system. Compared to N−H insertion reactions,[8–14] cyclopropanation[15–17] and Si−H insertion[18–20] reactions are generally accepted to proceed through concerted mechanisms.[21,21] These reactions do not rely on a proton-shuttle mechanism, so comparing to the N−H insertion can provide mechanistic insight into the specific role of aminoamide silanol as a proton shuttle or as a ligand in a Cu-siloxide complex. We performed cyclopropanation and Si−H insertion reactions and verified that the metal-siloxide complex forms and contributes to selectivity (Scheme 2.8). Using the aminoamide-silanol ligand **L3a**, we observed moderate activity and high diastereoselectivity (albeit low enantioselectivity) of the [Cu]/silanol system in a cyclopropanation reaction (Scheme 2.8A). Kevin

Blanco-Herrero is optimizing the reaction conditions for Si−H insertion (Scheme 2.8B), with enantioselectivities at 80:20 er when using toluene as the solvent at room temperature.

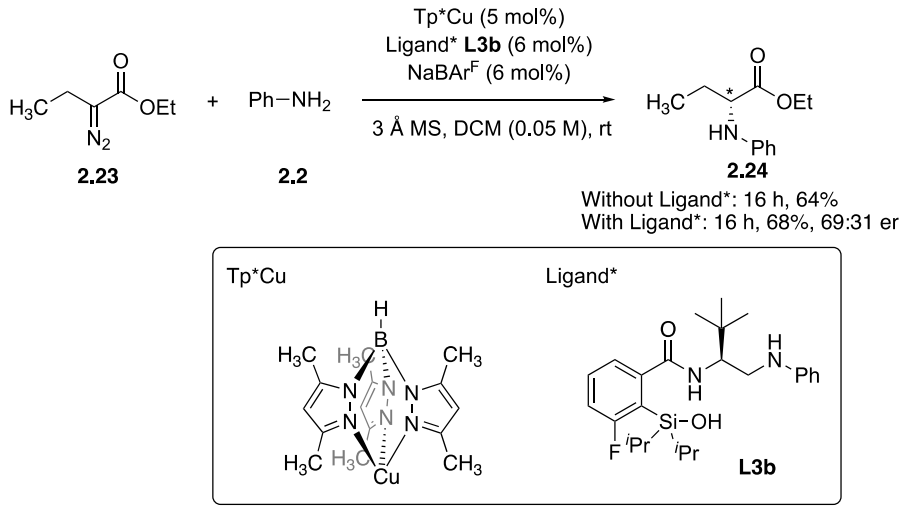



**Scheme 2.8.** Evaluation of **L3a** in (A) cyclopropanation and (B) Si−H insertion reactions.

## IVd. Silanols with Bulky [Cu] Catalyst

The second approach for evaluating the proton-shuttle capability of the silanol ligand involves using a bulky Cu catalyst that does not bind to any ligand. In a previous study, the Zhou group demonstrated the enantioselective N–H insertion reaction of α-diazobutanoates with benzylamine.[22,23] They employed an achiral transition-metal catalyst to generate the ylide intermediate, followed by a separate chiral catalyst for promoting enantioselective proton transfer. Through screening various transition metal catalysts and chiral H-bonding catalysts, the successful combination was found to be the homoscorpionate-coordinated copper complex tris(pyrazolyl)borate (Tp*Cu) with a chiral amino-thiourea catalyst. This cooperative interaction between an achiral transition-metal complex and a chiral hydrogen-bond donor, a thiourea catalyst, facilitates carbenoid insertions into the N–H bonds of aliphatic amines.

To assess the functionality of our silanol ligand, we tested it with Tp*Cu. If no selectivity is observed when using the bulky Tp*Cu, it would indicate that the silanol does not act as a proton transfer catalyst. However, the results demonstrated a slight selectivity (69:31 er) in the N–H insertion reaction when combining Tp*Cu with **L3b**, suggesting that silanol ligands have the potential to function as proton transfer catalysts (Scheme 2.9).

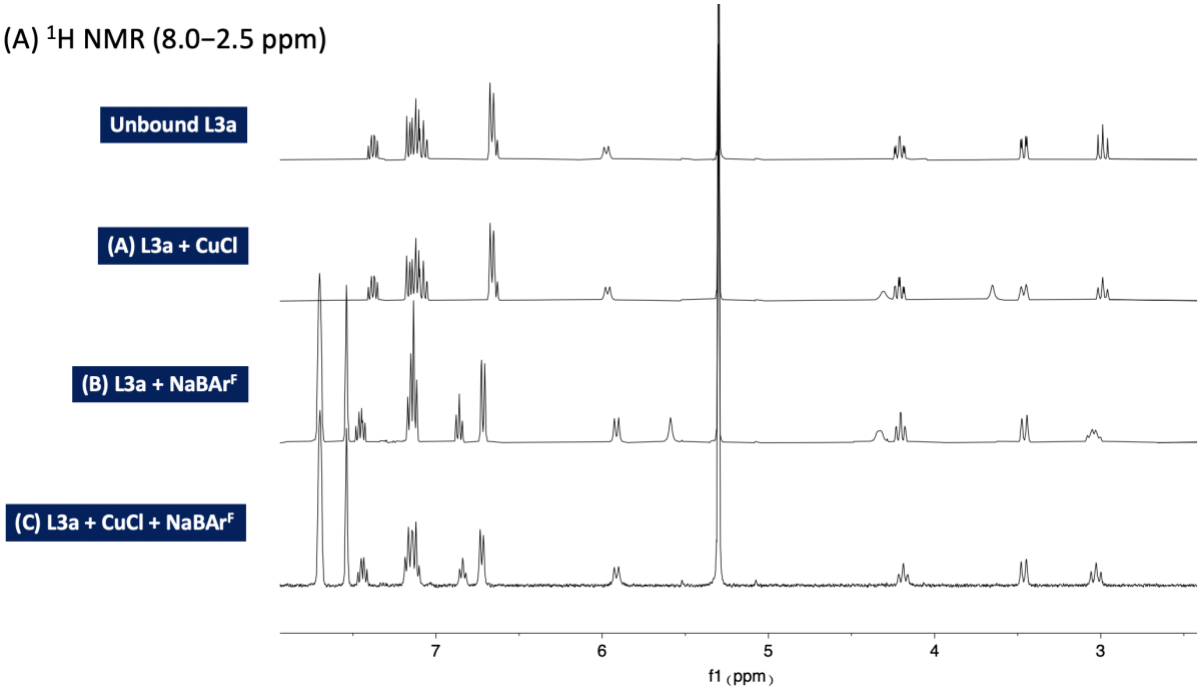



**Scheme 2.9.** Silanol **L3b** is capable of acting as a proton-shuttle catalyst with the bulky Tp*Cu catalyst.

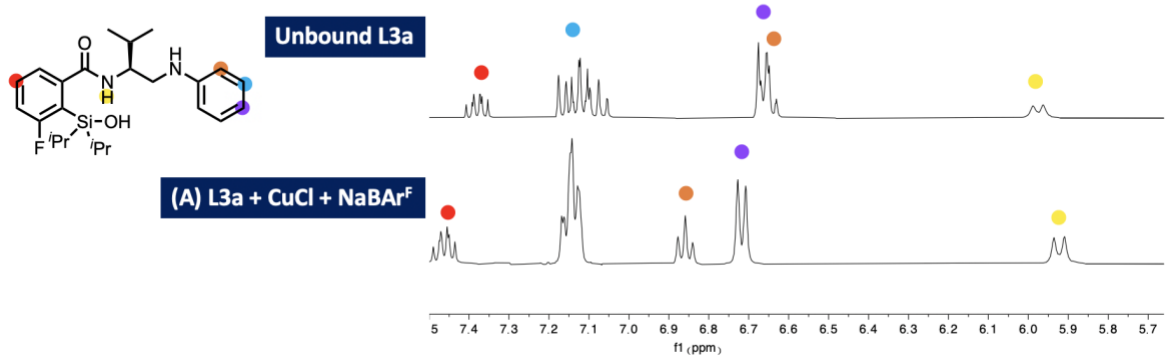
## IVe. Metal-ligand Binding Experiments using NMR and IR Spectroscopy

The investigation into the pre-complexation of the silanol ligand with the copper catalyst during the reaction involved detailed analysis using $^{1}$H and $^{29}$Si NMR spectroscopy (Figure 2.6). These analyses included the examination of NMR shift changes and peak disappearances. The $^{1}$H NMR spectra showed significant shifts in the protons on the phenyl ring linked to the amino group (Figure 2.6B), indicating potential arylamine protonation at the amino group. The essential role of the protonated amino group in metal binding is supported by the results from using **L3a** and **L3i**−**k** with varied electronic properties in the standard N−H insertion (Scheme 2.1). Additionally, the observation of a slight shift in the amide NH instead of its disappearance suggests secondary interactions involving the binding of the amide C=O to Cu (Figure 2.6B).[24–27] The NMR experiments for analysis of **L3a** when mixed solely with NaBAr$^{F}$ demonstrate a significant downfield shift in both $^{1}$H and $^{29}$Si NMR spectra (Figure 2.6C), indicating the essential role of NaBAr$^{F}$ in facilitating the formation of the Si-O-Na complex. In the absence of NaBAr$^{F}$, no apparent shifts in $^{1}$H and $^{29}$Si NMR spectra were observed. This observation, combined with the result of the N−H insertion without the addition of NaBAr$^{F}$ (50:50 er, Table 1.2), further supports the involvement of metal-siloxides in determining selectivity as opposed to the ligand acting solely as a proton shuttle or H-bonding catalyst.

(A) $^{1}$H NMR (8.0–2.5 ppm)




(B) $^{1}$H NMR (7.5–5.7 ppm)
400 MHz in $CD_2Cl_2$



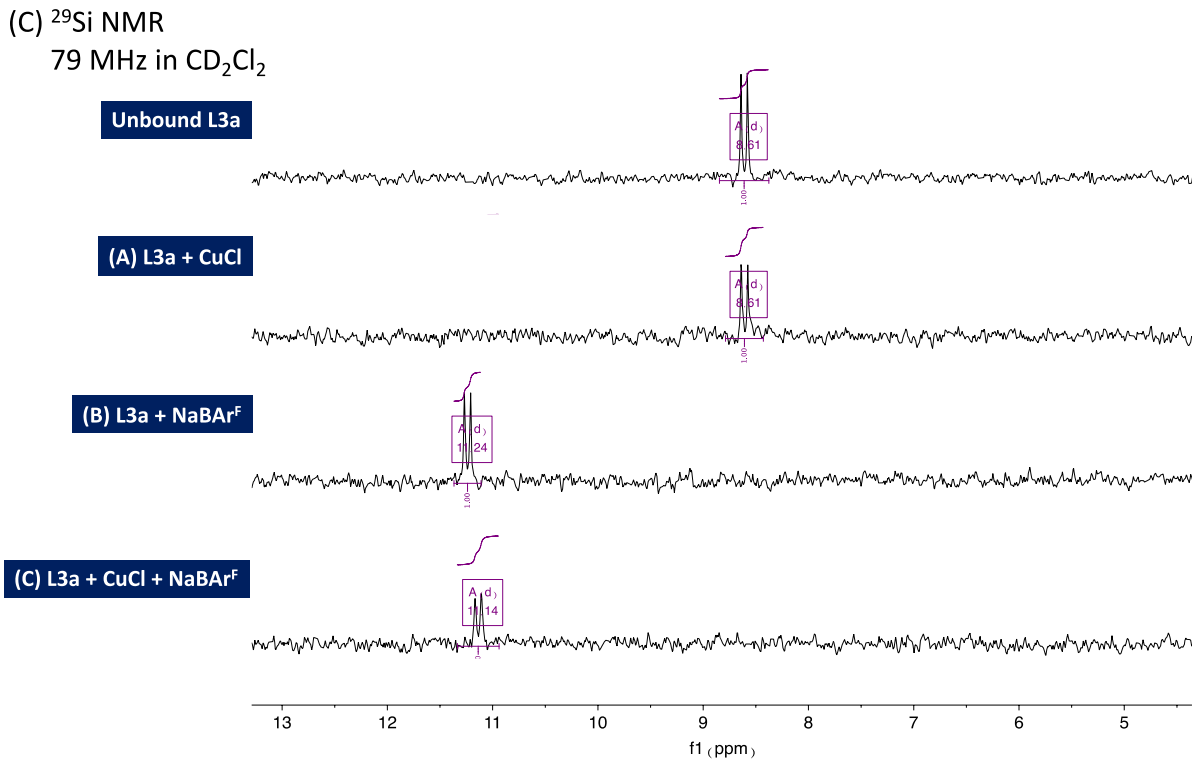



**Figure 2.6**. (A) $^{1}$H NMR (B) Zoomed in $^{1}$H NMR (C) $^{29}$Si NMR spectra of the mixture of CuCl, NaBAr$^{F}$, and ligand **L3a** in $CD_2Cl_2$.

## IVf. Results of NMR Binding Experiments with Different Metal Salts

We performed binding experiments for ligand **L3a** with different metal salts, including CuCl, CuMes, and $Sc(OTf)_3$. When aminoamide ligand **L3a** (at 0.02 M) was treated with each metal salt (1:1 ligand-to-metal ratio in $CD_2Cl_2$), $^{1}$H NMR spectra in Figure 2.7 provide evidence that supports the formation of a new metal-ligand complex with different metal-dependent binding modes. The disappearance of the amide NH, as observed in Figure 2.7C when **L3a** was mixed with $Sc(OTf)_3$, was noted. This observation was compared to the peak shifting observed when **L3a** was mixed with Cu (Figure 2.7A). The conclusion drawn for this comparison is that the amide C=O on **L3a** is bound to Cu in the metal-ligand complex.

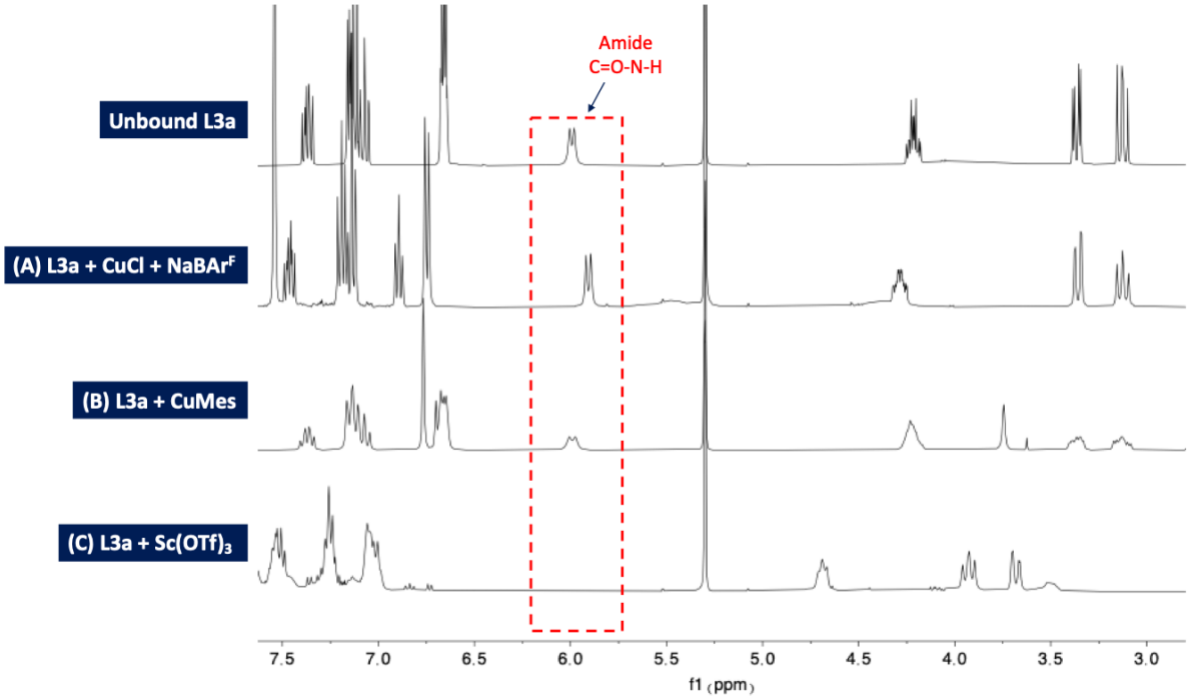



**Figure 2.7.** Comparison of $^1$H NMR spectra of **L3a** with various metal salts in $CD_2Cl_2$ at 0.02 M. Attention is drawn to the amide NH peak highlighted by the red dotted box. The disappearance of the amide NH peak when **L3a** is mixed with $Sc(OTf)_3$, compared to the peak shifting observed when **L3a** is mixed with [Cu], indicates that the amide C=O on **L3a** is bound to [Cu] in the metal-ligand complex.

In-situ IR spectroscopy was then used to analyze binding for the mixture of CuCl, NaBAr$^F$, and silanol ligand **L3a** (Figure 2.8). The mixture was stirred at room temperature for two hours to monitor the pre-complexation of the catalyst and ligand. The primary peak corresponding to (and used to track consumption of) a possible Si−OH stretch is at 1085 cm$^{-1}$.[28] The intensity of this peak was determined by integrating the area of the peak with a two-point baseline correction between 1124 cm$^{-1}$ and 1008 cm$^{-1}$. The primary peak corresponding to (and used to track the formation of) a possible Si−OM stretch is at 1131 cm$^{-1}$ (Figure 2.8A).[28] The intensity of this peak was measured with a two-point baseline correction between 1240 cm$^{-1}$ and 1100 cm$^{-1}$ (Figure 2.8B).

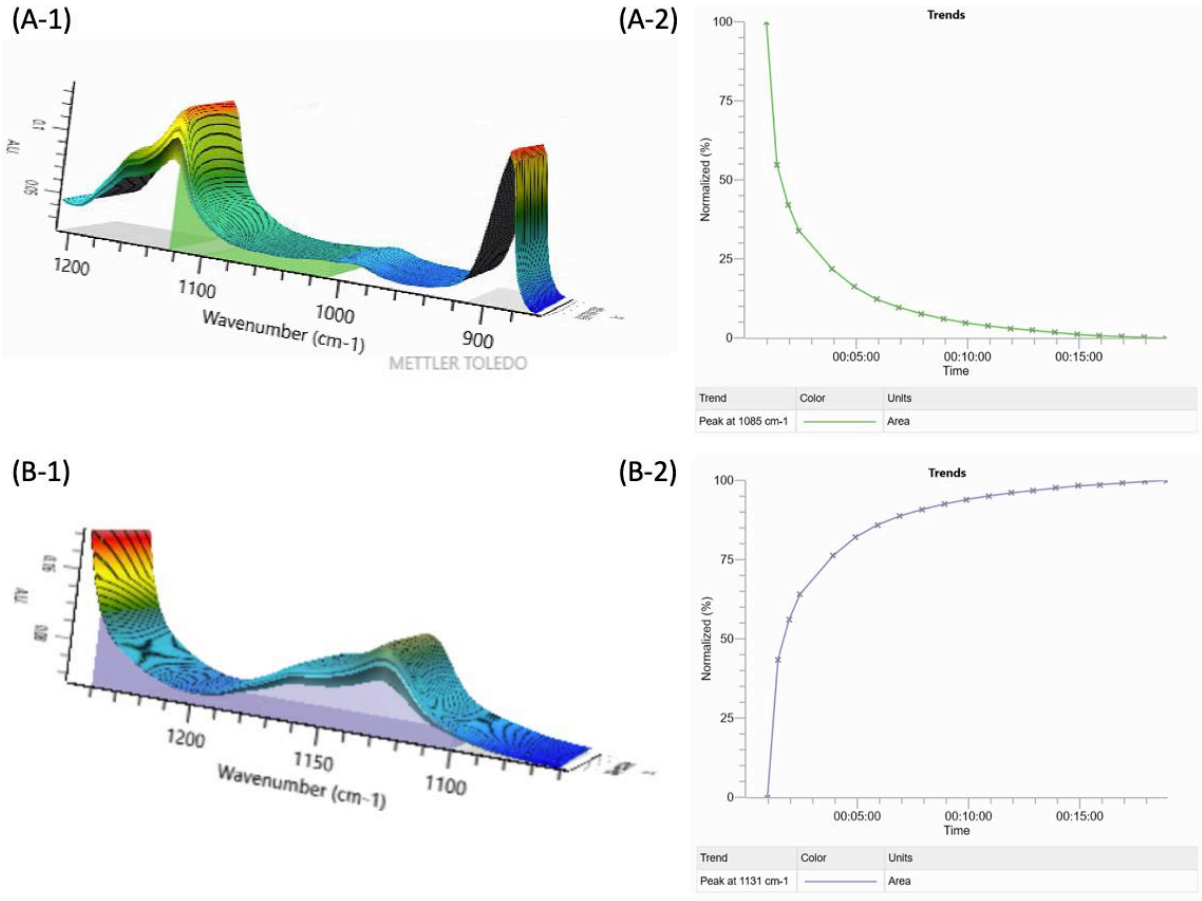



**Figure 2.8.** A-1) Representative in-situ IR spectrum showing temporal changes in the Si−OH stretching bands. The highlighted peak at 1085 $cm^{-1}$ was used for monitoring the Si−OH stretch. The peak intensity was measured by integrating the area of the peak with a two-point baseline correction applied between 1124 $cm^{-1}$ and 1008 $cm^{-1}$; A-2) Time-resolved in-situ IR monitoring of the Si−OH stretch at 1085 $cm^{-1}$; B-1) Representative in-situ IR spectrum showing temporal changes in the Si−OM stretching bands. The highlighted peak at 1131 $cm^{-1}$ was used for monitoring the Si−OM stretch. The peak intensity was measured by integrating the area of the peak with a two-point baseline correction applied between 1240 $cm^{-1}$ and 1100 $cm^{-1}$; B-2) Time-resolved in-situ IR monitoring of the Si−OM stretch at 1131$cm^{-1}$.

The disappearance of possible Si−OH stretches (1085 $cm^{-1}$) and the increase in Si−OM stretches (1131 $cm^{-1}$) are indicative of the interaction between the silanol ligand and CuCl (Figure 2.9). No change was observed in the signal at 1131 $cm^{-1}$ over the course of the reaction after the pre-complexation. Binding experiments performed using in-situ IR and NMR spectroscopy both indicated that the pre-complexation required only 30 minutes. However, it is crucial to acknowledge that the reaction times for N−H insertions varied, with some taking up to 8 hours, despite consistent yield and selectivity. To ensure consistent results, a 2-hour pre-complexation was adopted for all insertion reactions.

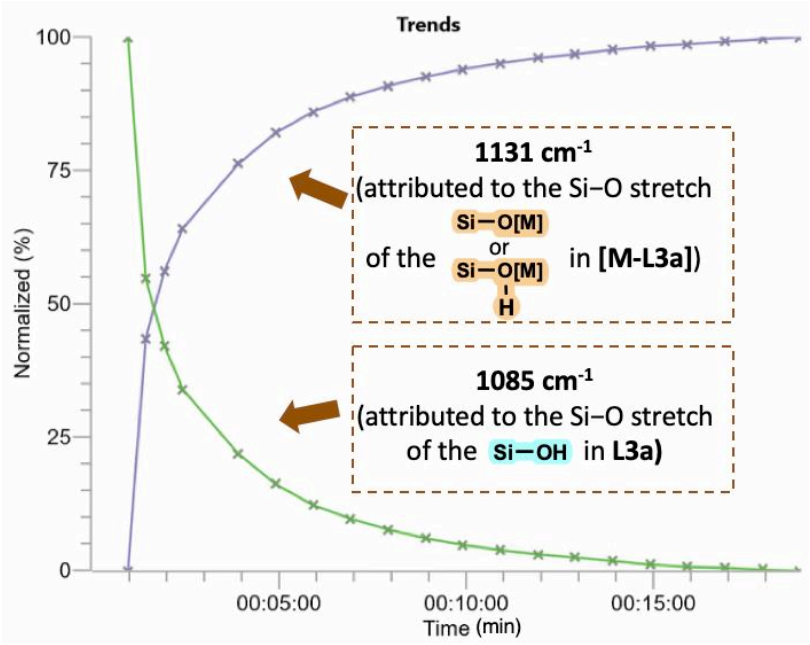



**Figure 2.9.** Stack of in-situ IR monitoring changes over time for both disappearance and appearance trends.

**IVg. Crystallization Experiments for the Understanding of Metal-ligand Binding Interactions**

Crystallization experiments provide key insight into the coordination mode for the metal-siloxide. Several metal-ligand recrystallization experiments including **L3a** with various metal mixtures were evaluated, including **L3a** (1.0 equiv) with these metals: CuCl, $NaBAr^F$, CuCl/$NaBAr^F$ (1:1 ratio), $Cu(OTf)_2$/$NaBAr^F$ (1:1 ratio), CuMes, $Pd(dba)_2$, and $Sc(OTf)_3$. Single crystals of $\mathbf{[(L3a)_2/Na\cdot(H_2O)_2]^+[BAr^F]^-}$ were grown from the mixture of **L3a**, CuCl, and $NaBAr^F$ (1.0 equiv each). While there is an absence of copper, the single crystal X-ray analysis of $\mathbf{[(L3a)_2/Na\cdot(H_2O)_2]^+[BAr^F]^-}$ confirms the formation of a sodium siloxide complex, and specifically indicates that an H-bonding interaction is contributing to the stabilization of the sodium-siloxide complex (Figure 2.10). Intramolecular H-bonding interactions are observed between the amino and silanol group, with additional intermolecular H-bonding between amino and amide groups. Additional H-bonds exist between water molecules and the silanol and amino groups.

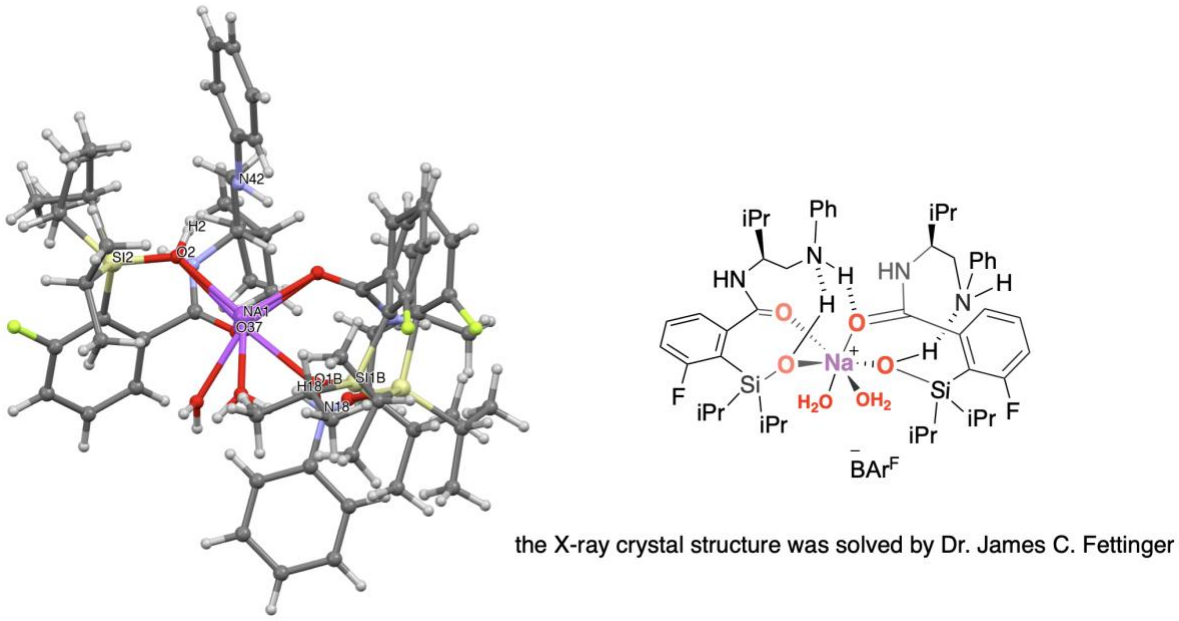



**Figure 2.10.** Single-crystal structure of complex $[(\mathbf{L3a})_2/\mathbf{Na}\cdot(\mathbf{H_2O})_2]^+[\mathbf{BAr^F}]^-$; the $BAr^{F-}$ anion has been omitted for clarity. Selected bond distances (Å), H-bonding interactions, and angles (deg): Si(2)−O(2): 1.634(4), Na(1)−O(2): 2.284(10), Na(1)−O(37): 2.441(8), O(2)−H(2)...N(42), N(18)−H(18)...O(37), ∠Si(2)−O(2)−Na(1): 133.7(2).

## IVh. DFT Calculations on the Metal-ligand Binding Modes

Given unresolved questions about the binding modes from the experimental results, we initiated a collaboration with Prof. Peng Liu at the University of Pittsburgh. In particular, our goal for the computational studies is to investigate whether the siloxide forms and protonates the amino group or if the silanol acts as a neutral ligand. Turki Alturaifi, a member of the Liu group, conducted the DFT calculations on the binding modes and conformations of the Cu-carbene complex with the silanol ligand (Figure 2.11). The calculations reveal the binding modes and conformations of the silanol ligand **L3a** with the proposed Cu–carbene complex,[8,12,22,29] supporting silanol as a chelating group in the active complex. The analysis demonstrates that the most stable conformation involves both the silanol and amide carbonyl oxygen atoms coordinating relatively strongly with the copper atom, with bond distances of 2.03 Å and 2.14 Å, respectively.

Additionally, intramolecular H-bonding between the silanol and amino group was observed, increasing the Lewis basicity of the silanol oxygen and further stabilizing the silanol-Cu coordination. The ten-membered ring (highlighted in yellow) adopts a chair–chair–half-chair conformation[30,31] with no noticeable transannular strain, and the *i*-Pr group at the stereogenic center is at the pseudoequatorial

position. These results were validated through the analog study previously discussed in Sections II and IVa in this chapter. Using silanol ligands with different *N*-substitution (**L3i**−**m**, Section II) and the silanol analogs with varying H-bonding capabilities (**L4**−**L7**, Section IVa) showed a distinct influence on reactivity and selectivity.

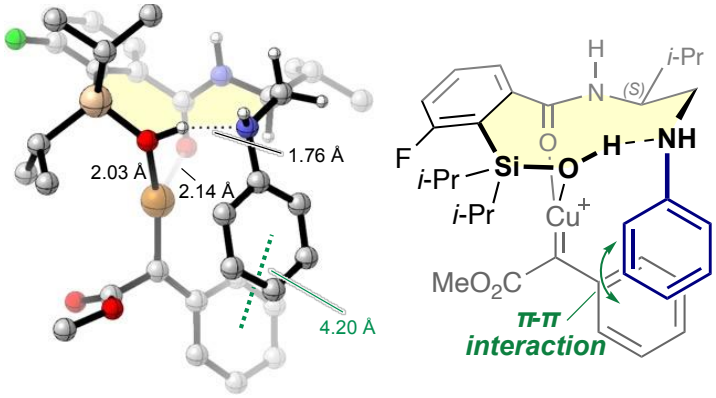
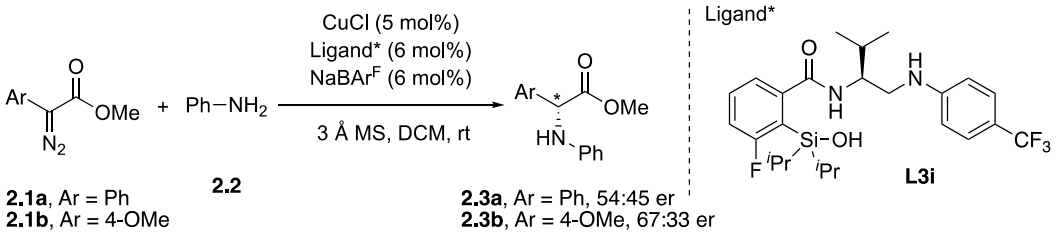



**Figure 2.11.** The lowest energy conformer of the proposed Cu-carbene intermediate, featuring the silanol ligand **L3a** and aryl diazoesters **2.1**, as determined by DFT calculations at the M06/6-311+G(d,p)–SDD(Cu)/SMD(DCM)//B3LYP-D3/6-31G(d)–SDD(Cu) level of theory.

The DFT calculations indicate a π-π interaction between the amino phenyl group on the ligand and the phenyl group on the carbene, with a distance of 4.20 Å between the centroids of the two benzene rings (Figure 2.11). We have evidence supporting π-π stacking, specifically with 3,5-$(CH_3)_2$ (**L3l**) and 2,6-$(CH_3)_2$ (**L3m**) on the amino aryl group as discussed in Section II. Notably, the use of the sterically bulky 2,6-$(CH_3)_2$ substituents on the ligand (**L3m**) resulted in a complete loss of enantioselectivity in the N−H insertion (**L3i**, 85:15 er *vs.* **L3m**, 50:50 er). In addition, a significant loss of enantioselectivity is also observed with *N*-cyclohexyl ligand (**L3k**, 59:41 er). Furthermore, a decrease in selectivity is observed when conducting the N−H insertion in aromatic solvents (89:11 *vs* 78:22 er).

We hypothesized that higher selectivity in the N-H insertions could be achieved by increasing π-π interactions through appropriately substituted benzene rings in the ligand and aryl diazoesters. When para-electron-withdrawing groups (**L3i**) were employed on the aryl amino group, the insertion product was obtained with an enantioselectivity of 54:45 er (**Scheme 2.10**). We anticipated that using **L3i** and p-OMe-Ph on the diazo **2.1b** would result in higher selectivity compared to the unsubstituted diazoester **2.1a**. However, while some improvement was observed, it was not significant (**2.3b**, 67:33 *vs.* **2.3a**, 55:45 er). This is attributed to the amino phenyl group on the ligand aligning directly over the

benzene ring on the carbene, as indicated by computational structure analysis (Figure 2.11). Any substitutions at the para-position of the amino aryl group could induce unfavorable steric effects, potentially destabilizing the π-π interaction and leading to low enantioselectivity of the insertion product **2.3**. This may explain why the enantioselectivity improvement observed with **L3i** is minimal. The π-π interaction inspires the future ligand design, a pursuit that James Vesto will continue to develop in collaboration with the Liu group.




**Scheme 2.10.** N−H insertions with increased π-π interaction between benzene rings in the Cu-complex.

## IVi. Proposed chiral induction model for the N−H insertions

Based on the DFT calculations and the absolute configuration of the N−H insertion products **2.3a**, we proposed a chiral induction model (**Figure 2.12**). From the DFT calculations, the *i*-Pr group at the stereogenic carbon is placed in a pseudo-equatorial position, stabilizing the intramolecular H-bond. In contrast, the phenyl group on the amino group engaging in π-π interaction with the phenyl group on the carbenoid is positioned in a pseudo-axial position. The electron-deficient Cu-carbene is then attacked by aniline **2.2** from the less-hindered *Re* face, followed by a configuration-retained proton transfer, ultimately leading to the formation of the insertion product with an *R* configuration.

Traditionally, N−H insertion reactions using aryl diazoacetates have resulted in low enantioselectivity compared to those using alkyl diazoacetates. This is because the general mechanism of N−H insertions involves a ylide intermediate. When the catalyst-associated ylide is favored, high enantioselectivity is usually observed.[8,29] On the other hand, when the substituents (*e.g.*, aryl groups) on the diazoester stabilize the free ylide, the free ylide tends to form preferentially. Without the chiral environment provided by the catalyst, the N−H insertion product **2.3** is obtained with no enantioselectivity. We propose that the critical factor enabling our silanol ligand **L3** to overcome this

limitation is the π-π interaction, which provides extra stability to the metal-ligand complex and the catalyst-associated ylide.

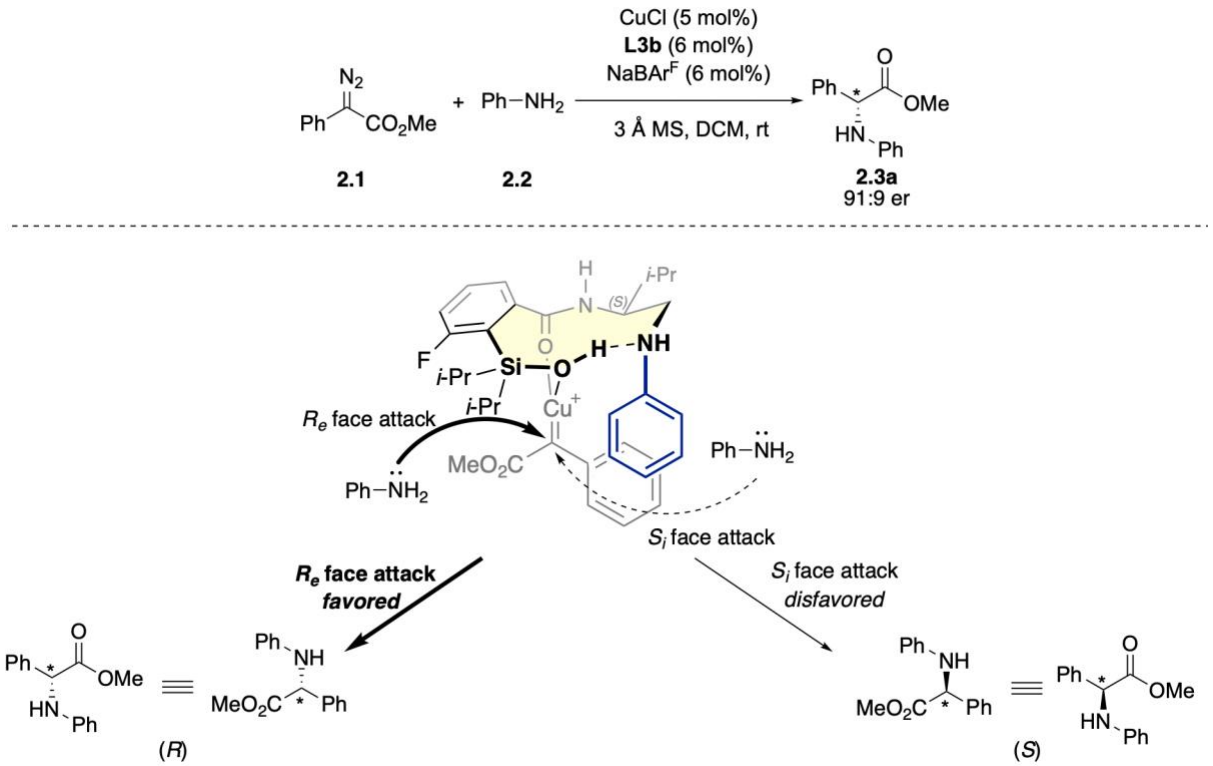



**Figure 2.12.** Proposed chiral induction model for the N−H insertions using phenyl diazoacetate.

Building on the DFT calculations and the absolute configuration of **2.3c**, a chiral induction model for the N−H insertions using alkyl diazoacetate was proposed (Figure 2.13), similar to phenyl diazoacetate. This model suggests a CH-π interaction between the alkyl R group and the phenyl group on the amino moiety of the ligand. We attribute the higher enantioselectivity (up to 98:2 er, **2.3d**) observed when using alkyl diazoacetate to two factors: 1) the less stable[32,33] and hence less preferentially formed free ylide intermediate,[8,29] and 2) the CH-π interaction within the metal-ligand complex.

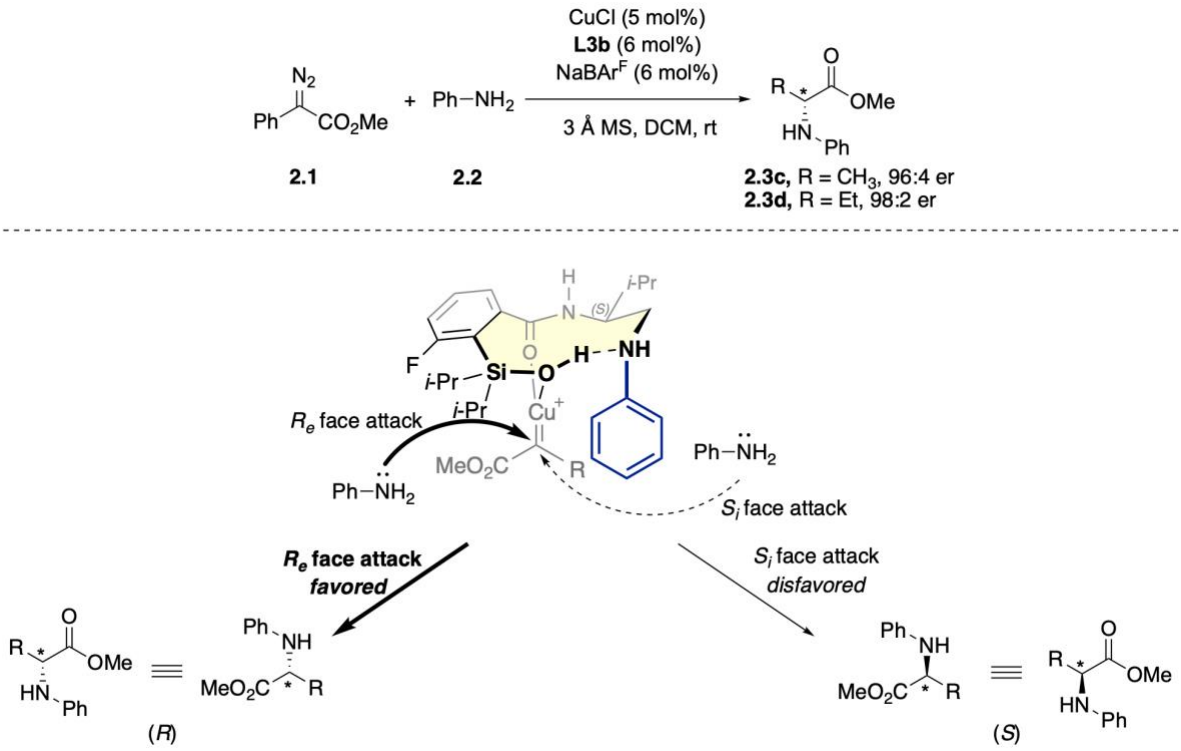
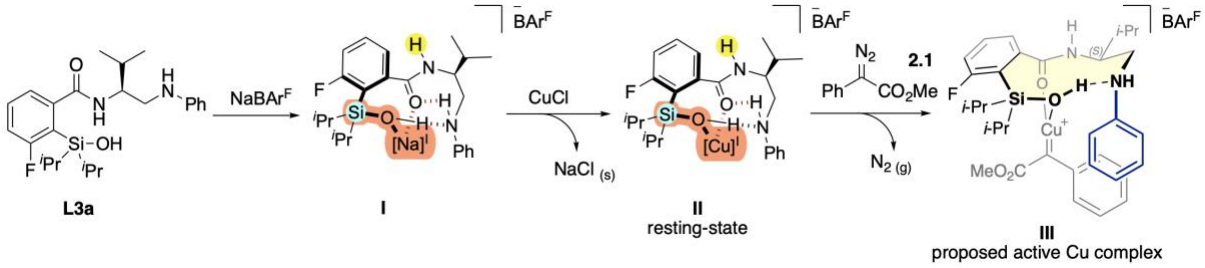



**Figure 2.13.** Proposed chiral induction model for the N−H insertions using alkyl diazoacetate.

## IVj. Proposed Mechanism of the Formation of Active Metal Complex

Based on the experimental results, we propose that the formation of the active diazo bound Cu complex **III** relies on the presence of $NaBAr^F$ to initially form the H-bond stabilized silanol-sodium complex **I** (Scheme 2.11). In addition, the binding experiments for **L3a** with just $NaBAr^F$ also exhibit a significant downfield shift in both $^1H$ and $^{29}Si$ NMR spectra, suggesting the presence of the sodium complex **I**. The observed changes in peaks corresponding to the *N*-phenyl moiety in the $^1H$ NMR spectrum suggests possible arylamine protonation due to $NaBAr^F$. However, complex **I** does not exhibit reactivity in N−H insertion with only $NaBAr^F$ and **L3a**, suggesting that the Na complex is not the catalytically active complex. We propose that complex **I** undergoes metathesis, replacing Na with Cu, leading to the formation of complex **II**, the H-bond stabilized silanol-copper resting state. This metathesis is facilitated by the precipitation of $NaCl_{(s)}$. Subsequently, upon the addition of diazoacetate **2.1**, complex **II** transforms into the active complex **III**. The collaboration with the Liu group on the DFT calculations for the proposed mechanism is currently ongoing.




**Scheme 2.11.** Proposed mechanism for the formation of the active copper complex based on the results of N−H insertions and spectroscopic binding experiments.

## V. Conclusions

This chapter has focused on illustrating the features of the chiral aminoamide silanol ligand, unveiling its pivotal role in forming a copper-siloxide complex and in enantioselective catalysis. The modular synthesis of the ligand allowed us to synthesize diverse ligand variants. These ligand variants provided the platform to assess the impact of both steric and electronic substituents on the reactivity and enantioselectivity of the N−H insertion reaction. Additionally, the strategic design and synthesis of silanol ligand analogs provided valuable insights into the functionality of the amide, amino, and silanol moieties in the catalytic process. Collaboration with Prof. Peng Liu for DFT calculations on the binding modes and conformations of the Cu-carbene complex with the silanol ligand further enhanced our understanding. Integration of DFT calculations with experimental results, ligand analog studies, spectroscopic analysis, and X-ray structural analysis suggest the significance of the silanol group as a key coordinating moiety involved in the formation of an H-bond stabilized silanol-copper carbenoid complex. Further studies on ligand modification and full DFT calculations on the mechanism are underway to deepen our understanding and refine our insights into the catalytic process.

## VI. Experimental Procedure and Characterization

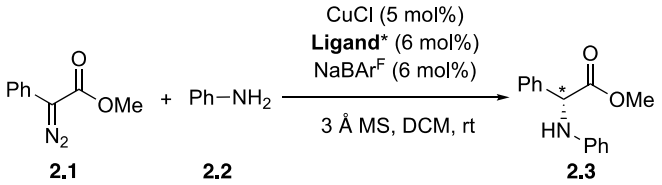
### VIa. General Information

Refer to Chapter 1 for the information of NMR instrumentation. In-situ infrared spectroscopic analysis and kinetics were performed using a Mettler Toledo ReactIR 700 (serial number B929971514) with a liquid $N_2$ MCT detector fitted with a DiComp probe (serial number B939349478). The system was

filled with liquid $N_2$ and allowed to cool for 1 h before experiments begun. Initial trends were found using iC IR 7.1 and further analyzed using Microsoft Excel.

## VIb. General Procedure

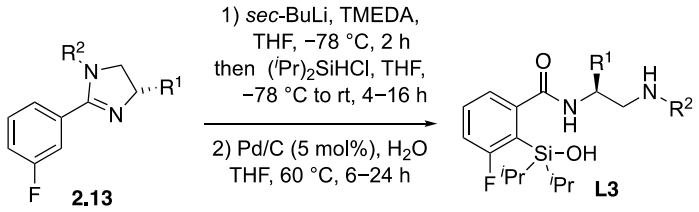
**Procedure J: Procedure for the enantioselective N−H insertions**




Refer the Procedure G in Chapter 1 for the N−H insertions. For the measurement of NMR yield, the reaction mixture was diluted with ~1 mL of $CDCl_3$, and phenyltrimethylsilane was added as an NMR internal standard. NMR yields were evaluated by acquiring $^1$H NMR spectra from a ~0.6 mL aliquot of the solution.

**Procedure K: Synthesis of silanol when there is an inseparable mixture for the silane**

*In this case of specific silanes ($R^1$ = iPr, $R^2$ = 4-$CF_3$Ph, 4-OMePh, and cyclohexyl), the silane compound and unreacted imidazoline are closely overlapping so that they cannot be separated using silica gel flash column chromatography, and the silanes are carried forward to the hydrolysis step where the silanol products are separated.*



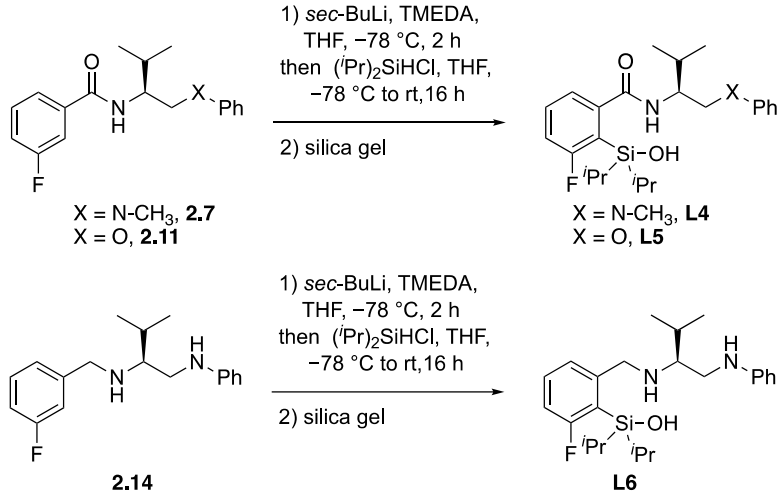

Step 1: Imidazoline **2.13** (1.0 equiv) was dissolved in THF (0.15 M) and purged under argon for 5 min. The reaction was cooled to –78 °C and tetramethylethylenediamine (TMEDA) (1.2 equiv, unless otherwise indicated) was added followed by the dropwise addition of *sec*-butyl lithium (1.4 M in cyclohexane, 1.2 equiv, unless otherwise indicated). The reaction was stirred at –78 °C for 2 h (unless otherwise indicated) and then chlorosilane (1.3 equiv, unless otherwise indicated) was added. The reaction was allowed to slowly warm to room temperature and then stirred for an additional 16−24 h at

which time it was quenched with saturated aq. $NaHCO_3$ (10 mL). The aqueous phase was extracted with diethyl ether (3 × 5 mL). The combined organic phase was dried over $MgSO_4$, filtered, and concentrated *in vacuo*. The reaction mixture was filtered through a silica plug (DCM/MeOH, 10:1 *v*/*v*) to yield a mixture of unreacted imidazoline and the corresponding silane, which is carried on directly to the next step without further purification. Confirmation of the silane product was achieved through distinctive peaks in $^{1}H$ NMR and $^{19}F$ NMR spectroscopy.

Step 2: Refer to Procedure D (Method B) in Chapter 1

**Procedure L: Synthesis of aminoamide silanol through an unstable silane (for the silanes that react with silica gel)**

*In this case of specific silanes (X = N-CH₃, O), the silane compounds reacted with silica gel and converted into the corresponding silanols.*

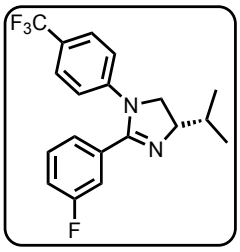



Aminoamide (1.0 equiv) was dissolved in THF (0.15 M) and the mixture was purged under argon for 5 min. The reaction was cooled to –78 °C and tetramethylethylenediamine (TMEDA) (3.0 equiv, unless otherwise indicated) was added followed by the dropwise addition of *sec*-butyl lithium (1.4 M in cyclohexane, 3.0 equiv, unless otherwise indicated). The reaction was stirred at –78 °C for 2 h and then diisopropylchlorosilane (3.1 equiv, unless otherwise indicated) was added. The reaction was allowed to slowly warm to room temperature and then stirred for an additional 16−24 h at which time it was quenched with 10 mL of saturated aq. $NaHCO_3$ (unless otherwise indicated). The aqueous phase was

extracted with diethyl ether (2 × 5 mL). The combined organic phase was dried over $MgSO_4$, filtered, and concentrated *in vacuo*. The silane product is unstable and found to react with silica gel to form the corresponding silanol. The crude mixture was wet loaded in $CHCl_3$ onto a silica gel flash column for purification. Note - $H_2$ gas evolution was observed on the silica gel surface. The silanol product was purified via the flash chromatography ($SiO_2$, hexanes/EtOAc/$Et_3N$, 140:20:1.5 *v*/*v*/*v*).

**VIc. Characterization Data**

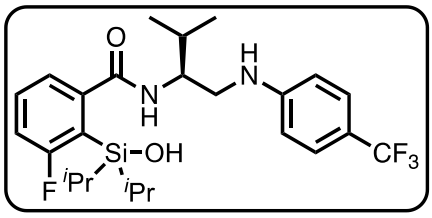
**(*S*)-2-(3-fluorophenyl)-4-isopropyl-1-(4-(trifluoromethyl)phenyl)-4,5-dihydro-1*H*-imidazole (2.13i)**




Synthesized according to the General Procedure B in Chapter 1 for imidazoline formation using β-hydroxy amide (**2.9**) (1.00 g, 4.44 mmol), thionyl chloride (1.30 mL, 17.8 mmol), $Et_3N$ (1.86 mL, 13.3 mmol) and 4-(trifluoromethyl)aniline (0.67 mL, 5.3 mmol). The reaction mixture was purified using flash column chromatography ($SiO_2$, gradient from 100% DCM to 20:1 DCM/MeOH) to give the imidazoline (**2.13i**) as a yellow oil (0.82 g, 53%).

$^1$H NMR (300 MHz, $CDCl_3$) δ 7.44 – 7.35 (m, 2H), 7.37 – 7.20 (m, 3H), 7.17 – 7.04 (m, 1H), 6.81 – 6.70 (m, 2H), 4.20 – 4.02 (m, 2H), 3.73 (ddd, *J* = 5.7, 5.6, 1.8 Hz, 1H), 2.03 – 1.82 (m, 1H), 1.05 (d, *J* = 6.8 Hz, 3H), 0.96 (d, *J* = 6.7 Hz, 3H); $^{13}$C{$^1$H} NMR (76 MHz, $CDCl_3$) δ 162.7 (d, *J* = 247.1 Hz), 159.3 (d, *J* = 2.7 Hz), 145.5 (d, *J* = 1.1 Hz), 133.4 (d, *J* = 7.9 Hz), 130.3 (d, *J* = 8.2 Hz), 126.1 (q, *J* = 3.8 Hz), 124.5 (d, *J* = 3.3 Hz), 124.4 (q, *J* = 33.0 Hz), 124.3 (q, *J* = 271.1 Hz), 120.9, 117.5 (d, *J* = 21.3 Hz), 115.9 (d, *J* = 22.9 Hz), 70.5, 55.9, 33.1, 18.9, 18.1; $^{19}$F{$^1$H} NMR (283 MHz, $CDCl_3$) δ –61.96, –111.96; HRMS (ESI/Orbitrap) m/z: $[M + H]^+$ Calcd for $C_{19}H_{19}F_4N_2$ 351.1484; Found 351.1472.

**(*S*)-3-fluoro-2-(hydroxydiisopropylsilyl)-*N*-(3-methyl-1-((4-(trifluoromethyl)phenyl)amino)butan-2-yl)benzamide (L3i)**



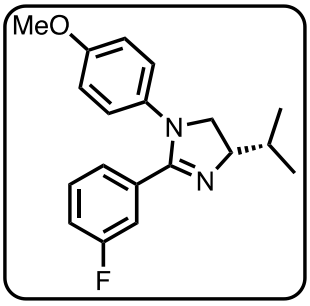

Synthesized according to the General Procedure K for silane formation using imidazoline (**2.13i**) (1.09 g, 3.12 mmol), *sec*-BuLi (1.4 M in cyclohexane, 2.67 mL, 3.74 mmol), TMEDA (0.56 mL, 3.74 mmol) and diisopropylchlorosilane (0.69 mL, 4.0 mmol). The reaction mixture was filter through a silica plug (DCM/MeOH, 10:1 *v*/*v*) to yield the mixture of unreacted imidazoline and silane (**2.13i**:**2.4i**, 1:3). The resulting mixture was carried on to the next step, and the imidazoline is removed after the purification in the next step. Confirmation of the silane product was achieved through distinctive peaks in $^{1}$H NMR and $^{19}$F NMR with δ −95.42 ppm.

For silanol formation using a mixture of imidazoline (**2.13i**) and silane (**2.4i**) from the previous step (1:3, 1.19 g, 2.56 mmol, calculated based off silane), Pd/C (10 wt%, 136 mg, 0.128 mmol) and $H_2O$ (0.46 mL, 25.6 mmol) was stirred in THF (0.15 M) at 60 °C for 6 h. The reaction mixture was purified using flash column chromatography ($SiO_2$, hexanes/EtOAc/$Et_3N$, 140:20:1.5 *v*/*v*/*v*) to give the silanol as a crystalline white solid (561 mg, 44%) over two steps. $R_f$ = 0.23 (hexanes/EtOAc/$Et_3N$, 7:1:0.15 *v*/*v*/*v*).

$^{1}$H NMR (400 MHz, $CDCl_3$) δ 7.42 – 7.32 (m, 3H), 7.14 – 7.03 (m, 2H), 6.68 (d, *J* = 8.6 Hz, 2H), 5.87 (d, *J* = 9.9 Hz, 1H), 4.86 (br, 1H), 4.29 (dddd, *J* = 9.9, 9.9, 5.9, 3.5 Hz, 1H), 3.53 (br, 1H), 3.40 (dd, *J* = 12.2, 3.5 Hz, 1H), 3.13 (dd, *J* = 12.2, 9.9 Hz, 1H), 2.05 – 1.92 (m, 1H), 1.37 – 1.23 (m, 2H), 1.17 – 0.98 (m, 15H), 0.92 (d, *J* = 7.5 Hz, 3H); $^{13}$C{$^{1}$H} NMR (101 MHz, $CDCl_3$) δ 173.1 (d, *J* = 2.3 Hz), 166.7 (d, *J* = 240.8 Hz), 150.9, 145.2 (d, *J* = 11.6 Hz), 131.6 (d, *J* = 9.1 Hz), 126.7 (q, *J* = 3.7 Hz), 125.2 (q, *J* = 270.4 Hz), 122.6 (d, *J* = 34.8 Hz), 122.6 (d, *J* = 2.6 Hz), 118.9 (q, *J* = 32.4 Hz), 116.9 (d, *J* = 27.6 Hz), 112.0, 55.1, 46.1, 31.3, 19.9, 18.4, 17.8 (d, *J* = 2.1 Hz), 17.4 (d, *J* = 1.5 Hz), 17.2 (d, *J* = 2.2 Hz), 14.2 (d, *J* = 1.8 Hz), 13.6 (d, *J* = 2.6 Hz), 13.2 (d, *J* = 1.1 Hz); $^{19}$F{$^{1}$H} NMR (376 MHz, $CDCl_3$)

δ –60.95 (3F), –94.71 (1F); $^{29}Si\{^{1}H\}$ NMR (79 MHz, $CDCl_3$) δ 9.86 (d, *J* = 4.9 Hz); IR (neat) 3344, 2945, 2866, 1616, 1596, 1533, 1325, 1105, 1065, 827 $cm^{-1}$; HRMS (ESI/Orbitrap) m/z: $[M - H_2O + H]^+$ Calcd for $C_{25}H_{33}F_4N_2OSi$ 481.2298; Found 481.2291; mp: 86−90 °C.

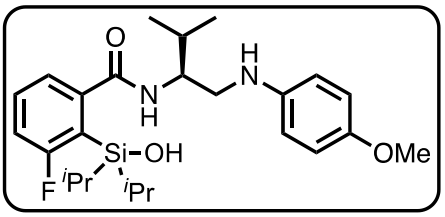
**(*S*)-2-(3-fluorophenyl)-4-isopropyl-1-(4-methoxyphenyl)-4,5-dihydro-1*H*-imidazole (2.13j)**




Synthesized according to the General Procedure B in Chapter 1 for imidazoline formation using β-hydroxy amide (**2.9**) (0.50 g, 2.22 mmol), thionyl chloride (0.65 mL, 8.9 mmol), $Et_3N$ (0.93 mL, 6.7 mmol) and *p*-anisidine (0.33 mL, 2.7 mmol). The reaction mixture was purified using flash column chromatography ($SiO_2$, gradient from 100% DCM to 10:1 DCM/MeOH) to give the imidazoline as a yellow oil (0.39 g, 53%).

$^{1}H$ NMR (400 MHz, $CDCl_3$) δ 7.28 – 7.15 (m, 3H), 7.05 – 6.96 (m, 1H), 6.81 – 6.68 (m, 4H), 4.11 – 3.98 (m, 2H), 3.74 (s, 3H), 3.55 (ddd, *J* = 5.3, 5.2, 2.0 Hz, 1H), 1.98 – 1.84 (m, 1H), 1.05 (d, *J* = 6.7 Hz, 3H), 0.96 (d, *J* = 6.7 Hz, 3H); $^{13}C\{^{1}H\}$ NMR (101 MHz, $CDCl_3$) δ 162.4 (d, *J* = 243.9 Hz), 156.5, 136.7, 133.7 (d, *J* = 7.7 Hz), 129.8 (d, *J* = 8.4 Hz), 125.2, 124.7 (d, *J* = 2.9 Hz), 116.8 (d, *J* = 20.9 Hz), 116.0 (d, *J* = 23.1 Hz), 114.3, 70.4, 57.5, 55.5, 33.3, 19.0, 18.1; $^{19}F\{^{1}H\}$ NMR (376 MHz, $CDCl_3$) δ –112.91; HRMS (ESI/Orbitrap) m/z: $[M + H]^+$ Calcd for $C_{19}H_{22}FN_2O$ 313.1716; Found 313.1708.

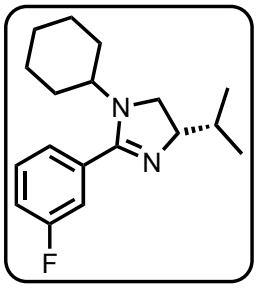
**(*S*)-3-fluoro-2-(hydroxydiisopropylsilyl)-*N*-(1-((4-methoxyphenyl)amino)-3-methylbutan-2-yl)benzamide (L3j)**




Synthesized according to the General Procedure K for silane formation using imidazoline (**2.13j**) (0.320 g, 1.00 mmol), *sec*-BuLi (1.4 M in cyclohexane, 0.88 mL, 1.2 mmol), TMEDA (0.18 mL, 1.2 mmol) and diisopropylchlorosilane (0.23 mL, 1.3 mmol). The reaction mixture was filter through a silica plug (DCM/MeOH, 10:1 *v*/*v*) to yield the mixture of unreacted imidazoline (**2.13j**) and the corresponding silane (**2.4j**), (**2.13j**:**2.4j**, 1:1). The resulting mixture was carried on to the next step. Confirmation of the silane product was achieved through distinctive peaks in $^{1}$H NMR and $^{19}$F NMR with δ -96.18 ppm. For silanol formation, a mixture of imidazoline (**2.13j**),silane (**2.4j**) (1:1, 236 mg, 0.553 mmol, calculated based off silane), Pd/C (10 wt%, 29 mg, 0.028 mmol) and $H_2O$ (0.10 mL, 5.5 mmol) in THF (0.15 M) was stirred at 60 °C for 16 h. The reaction mixture was purified using flash column chromatography ($SiO_2$, hexanes/EtOAc/$Et_3N$, 140:20:2.5 *v*/*v*/*v*) to give the silanol as a crystalline white solid (210 mg, 38%) over two steps. $R_f$ = 0.26 (hexanes/EtOAc/$Et_3N$, 7:1:0.15 *v*/*v*/*v*).

$^{1}$H NMR (400 MHz, $CDCl_3$) δ 7.35 (ddd, *J* = 8.2, 8.2, 5.8 Hz, 1H), 7.13 (d, *J* = 7.7 Hz, 1H), 7.06 (ddd, *J* = 8.5, 8.4, 1.0 Hz, 1H), 6.82 – 6.73 (m, 2H), 6.70 – 6.61 (m, 2H), 5.95 (d, *J* = 9.5 Hz, 1H), 4.24 (dddd, *J* = 9.5, 9.5, 6.1, 3.8 Hz, 1H), 3.88 (br, 2H), 3.74 (s, 3H), 3.33 (dd, *J* = 12.2, 3.8 Hz, 1H), 3.12 (dd, *J* = 12.2, 9.5 Hz, 1H), 2.06 – 1.92 (m, 1H), 1.36 – 1.21 (m, 2H), 1.12 – 1.02 (m, 12H), 0.99 (dd, *J* = 7.5, 1.3 Hz, 3H), 0.93 (dd, *J* = 7.5, 1.2 Hz, 3H); $^{13}$C{$^{1}$H} NMR (101 MHz, $CDCl_3$) δ 172.7 (d, *J* = 2.2 Hz), 166.8 (d, *J* = 240.6 Hz), 152.5, 145.4 (d, *J* = 11.4 Hz), 142.6, 131.4 (d, *J* = 9.2 Hz), 122.9 (d, *J* = 34.5 Hz), 122.8 (d, *J* = 2.6 Hz), 116.8 (d, *J* = 27.9 Hz), 114.8 (d, *J* = 53.9 Hz), 55.9, 55.4, 47.5, 31.1, 19.8, 18.5, 17.9 (d, *J* = 2.2 Hz), 17.8 (d, *J* = 2.2 Hz), 17.4, 14.2 (d, *J* = 2.2 Hz), 13.9 (d, *J* = 2.6 Hz); $^{19}$F{$^{1}$H} NMR (376 MHz, $CDCl_3$) δ –94.85; $^{29}$Si{$^{1}$H} NMR (79 MHz, $CDCl_3$) δ 8.79 (d, *J* = 4.8 Hz); IR (near) 3323, 2943, 2866, 1633, 1595, 1510, 1464, 1221, 1030, 883 cm$^{-1}$; HRMS (ESI/Orbitrap) m/z: [M – $H_2O$ + H]$^{+}$ Calcd for $C_{25}H_{36}FN_2O_2Si$ 443.2530; Found 443.2523.

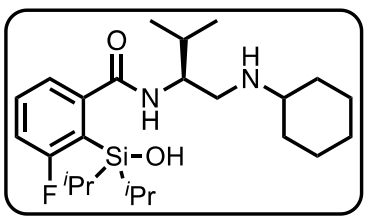
**(*S*)-1-cyclohexyl-2-(3-fluorophenyl)-4-isopropyl-4,5-dihydro-1*H*-imidazole (2.13k)**



Synthesized according to the General Procedure B in Chapter 1 for imidazoline formation using β-hydroxy amide (**2.9**) (0.676 g, 3.00 mmol), thionyl chloride (0.88 mL, 12 mmol), $Et_3N$ (1.25 mL, 9.00 mmol) and cyclohexyl amine (0.41 mL, 3.6 mmol). The reaction mixture was purified using flash column chromatography ($SiO_2$, gradient from 100% DCM to 10:1 DCM/MeOH) to give the imidazoline as a pale yellow oil (0.630 g, 69%).

$^1$H NMR (400 MHz, $CDCl_3$) δ 7.38 (ddd, *J* = 8.0, 8.0, 5.7 Hz, 1H), 7.30 – 7.23 (m, 1H), 7.19 (ddd, *J* = 9.3, 2.7, 1.5 Hz, 1H), 7.12 (dddd, *J* = 8.5, 8.5, 2.7, 1.2 Hz, 1H), 3.92 (ddd, *J* = 11.2, 8.8, 5.8 Hz, 1H), 3.50 (dd, *J* = 11.2, 9.5 Hz, 1H), 3.31 – 3.16 (m, 2H), 1.95 – 1.82 (m, 1H), 1.80 – 1.66 (m, 3H), 1.65 – 1.36 (m, 4H), 1.22 – 1.02 (m, 3H), 1.01 (d, *J* = 6.8 Hz, 3H), 0.94 (d, *J* = 6.7 Hz, 3H); $^{13}$C{$^1$H} NMR (101 MHz, $CDCl_3$) δ 164.5 (d, *J* = 2.6 Hz), 162.7 (d, *J* = 246.9 Hz), 130.3 (d, *J* = 8.1 Hz), 124.1 (d, *J* = 2.9 Hz), 116.9 (d, *J* = 20.9 Hz), 115.5 (d, *J* = 22.7 Hz), 69.3, 55.3, 46.9, 33.5, 31.5, 30.4, 25.8, 25.6, 25.5, 18.9, 18.0; $^{19}$F{$^1$H} NMR (376 MHz, $CDCl_3$) δ –112.44; HRMS (ESI/Orbitrap) m/z: $[M + H]^+$ Calcd for $C_{18}H_{26}FN_2$ 289.2080; Found 289.2073.

**(*S*)-*N*-(1-(cyclohexylamino)-3-methylbutan-2-yl)-3-fluoro-2-(hydroxydiisopropylsilyl)benzamide (L3k)**

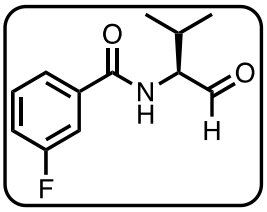


Synthesized according to the General Procedure K for silane formation using imidazoline (**2.13k**) (0.570 g, 1.98 mmol), *sec*-BuLi (1.4 M in cyclohexane, 1.69 mL, 2.37 mmol), TMEDA (0.36 mL, 2.37 mmol) and diisopropylchlorosilane (0.44 mL, 2.57 mmol). The reaction mixture was filter through a silica plug (DCM/MeOH, 10:1 *v*/*v*) to yield the mixture of unreacted imidazoline (**2.13k**) and the corresponding silane (**2.4k**). The resulting mixture was carried on to the next step. Confirmation of the product was obtained through diagnostic peaks in $^{1}$H NMR and $^{19}$F NMR with δ –96.45 ppm.

For silanol formation, a mixture of imidazoline (**2.13d**),silane (**2.4d**) (3:1, 200 mg, 0.500 mmol, calculated based off silane), Pd/C (10 wt%, 27 mg, 0.025 mmol) and $H_2O$ (90 µL, 5.0 mmol) in THF (0.1 M) was stirred at 60 °C for 40 h. The reaction mixture was purified using flash column chromatography ($SiO_2$, hexanes/EtOAc/$Et_3N$, 140:20:1.5 *v*/*v*/*v*) to give the silanol as a crystalline white solid (83 mg, 10%) over two steps. $R_f$ = 0.25 (hexanes/EtOAc/$Et_3N$, 7:1:0.15 *v*/*v*/*v*).

$^{1}$H NMR (400 MHz, $CDCl_3$) δ 7.37 (ddd, *J* = 8.2, 8.0, 6.1 Hz, 1H), 7.10 (dd, *J* = 7.5, 1.1 Hz, 1H), 7.03 (ddd, *J* = 9.1, 8.3, 1.1 Hz, 1H), 3.82 – 3.70 (m, 1H), 3.52 (dd, *J* = 10.8, 9.2 Hz, 1H), 3.16 (dd, *J* = 10.6, 9.3 Hz, 1H), 3.07 (dddd, *J* = 11.7, 11.7, 3.5, 3.5 Hz, 1H), 1.83 – 1.54 (m, 6H), 1.52 – 1.35 (m, 2H), 1.34 – 1.17 (m, 2H), 1.15 – 1.02 (m, 12H), 0.98 (ddd, *J* = 7.7, 7.7, 1.3 Hz, 6H), 0.92 (d, *J* = 6.7 Hz, 3H); $^{13}$C{$^{1}$H} NMR (151 MHz, $CDCl_3$) δ 166.90 (d, *J* = 238.7 Hz), 139.90 (d, *J* = 13.5 Hz), 131.25 (d, *J* = 8.6 Hz), 130.98 (d, *J* = 9.8 Hz), 125.43 (d, *J* = 2.3 Hz), 124.66 (d, *J* = 2.3 Hz), 123.53 (d, *J* = 34.7 Hz), 115.75 (d, *J* = 27.7 Hz), 70.74, 55.41, 47.60, 34.13, 32.32, 31.69, 30.40, 25.72, 25.52, 25.44, 19.94, 18.84, 17.79 (d, *J* = 2.2 Hz), 17.75 (d, *J* = 2.9 Hz), 17.36, 14.53, 14.17; $^{29}$Si{$^{1}$H} NMR (79 MHz, $CDCl_3$) δ 1.58 (d, *J* = 4.3 Hz); $^{19}$F{$^{1}$H} NMR (376 MHz, $CDCl_3$) δ –95.08; IR (neat) 3271, 2957, 2861, 1633, 1579, 1448, 1218, 1003, 883, 796, 605 cm$^{-1}$; HRMS (ESI/Orbitrap) m/z: $[M - H_2O + H]^+$ Calcd for $C_{24}H_{40}FN_2OSi$ 419.2894; Found 419.2895.

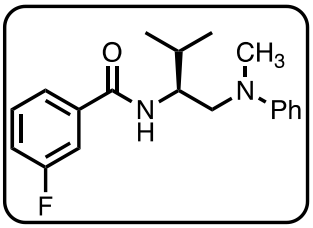
**(*S*)-3-fluoro-*N*-(3-methyl-1-oxobutan-2-yl)benzamide (2.5)**



Synthesized based on a reported procedure.[34] To a solution of β-hydroxy amide (**2.9**) (540 mg, 2.40 mmol, 1.0 equiv) in DCM at 0 °C, Dess-Martin periodinane (0.70 mL, 9.6 mmol, 4.0 equiv) was added portion-wise. After stirring 10 min, the reaction was allowed to warm to room temperature and stirred for 16 h. The reaction mixture was poured into aqueous solution of saturated $Na_2S_2O_3$/$NaHCO_3$ (10 mL, 1:1 *v*/*v*). The aqueous phase was extracted with DCM (2 × 20 mL), and the combined organic phase was dried over $MgSO_4$, filtered, and concentrated *in vacuo*. The resulting reaction mixture was purified using flash column chromatography ($SiO_2$, DCM/MeOH, 20:1 *v*/*v*) to give the aldehyde as a clear oil (617 mg, 89%). $R_f$ = 0.47 (DCM/MeOH, 20:1 *v*/*v*). The product was immediately used in the next step to prevent racemization.

$^1$H NMR (400 MHz, $CDCl_3$) δ 8.75 (s, 1H), 6.60 (ddd, *J* = 7.7, 1.3, 1.3 Hz, 1H), 6.54 (ddd, *J* = 9.4, 2.1, 2.1 Hz, 1H), 6.41 (ddd, *J* = 8.0, 7.9, 5.6 Hz, 1H), 6.22 (dddd, *J* = 8.3, 8.3, 2.6, 1.0 Hz, 1H), 6.05 (d, *J* = 7.7 Hz, 1H), 3.78 (dd, *J* = 7.7, 4.7 Hz, 1H), 1.53 – 1.37 (m, 1H), 0.08 (dd, *J* = 11.0, 6.9 Hz, 6H); $^{13}$C{$^1$H} NMR (101 MHz, $CDCl_3$) δ 199.9, 166.5 (d, *J* = 2.6 Hz), 162.7 (d, *J* = 247.6 Hz), 136.2 (d, *J* = 7.0 Hz), 130.3 (d, *J* = 7.7 Hz), 122.6 (d, *J* = 2.9 Hz), 118.8 (d, *J* = 21.3 Hz), 114.6 (d, *J* = 22.7 Hz), 63.8, 29.3, 19.1, 18.0; $^{19}$F{$^1$H} NMR (376 MHz, $CDCl_3$) δ –111.56; IR (neat): 3296, 3074, 2966, 1726, 1645, 1585, 1553, 1481, 1221, 752, 679 cm$^{-1}$; HRMS (ESI/Orbitrap) m/z: $[M + H]^+$ Calcd for $C_{12}H_{15}FNO_2$ 224.1087; Found 224.1082.

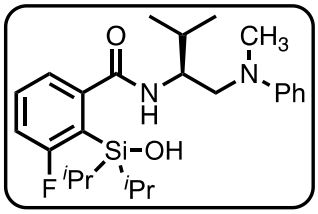
**(*S*)-3-fluoro-*N*-(3-methyl-1-(methyl(phenyl)amino)butan-2-yl)benzamide (2.7)**



To a solution of aldehyde (**2.5**) (220 mg, 0.987 mmol, 1.00 equiv) and acetic acid (28 μL, 0.49 mmol, 0.50 equiv) in DCM at 0 °C, N-methyl aniline (0.13 mL, 1.2 mmol, 1.2 equiv) was added. The solution was added to sodium triacetoxyborohydride (335 mg, 1.58 mmol, 1.60 equiv) and stirred overnight at room temperature. To quench the reaction, aq. 1M NaOH (5 mL) was added while stirring. The aqueous phase was extracted with DCM (2 × 10 mL), and the combined organic phase was dried over $MgSO_4$, filtered, and concentrated *in vacuo*. The resulting reaction mixture was purified using flash column chromatography ($SiO_2$, DCM/MeOH, 30:1 *v*/*v*) to give the product **2.7** as a white solid (65.7 mg, 21%). $R_f$ = 0.32 (DCM/MeOH, 30:1 *v*/*v*).

$^1$H NMR (400 MHz, $CDCl_3$) δ 7.33 – 7.19 (m, 3H), 7.17 – 7.05 (m, 2H), 6.80 (d, *J* = 8.3 Hz, 2H), 6.72 (dd, *J* = 7.3, 7.3 Hz, 1H), 5.82 (d, *J* = 9.4 Hz, 1H), 4.41 (dddd, *J* = 9.4, 9.3, 5.7, 5.5 Hz, 1H), 3.76 (dd, *J* = 14.9, 9.3 Hz, 1H), 3.37 (dd, *J* = 14.9, 5.7 Hz, 1H), 2.97 (s, 3H), 2.07 – 1.91 (m, 1H), 1.09 – 1.00 (m, 6H); $^{13}$C{$^1$H} NMR (101 MHz, $CDCl_3$) δ 166.5 (d, *J* = 2.6 Hz), 162.7 (d, *J* = 247.6 Hz), 150.2, 137.2 (d, *J* = 7.0 Hz), 130.1 (d, *J* = 7.7 Hz), 129.7, 122.3 (d, *J* = 3.3 Hz), 118.2 (d, *J* = 21.3 Hz), 116.8, 114.2 (d, *J* = 23.1 Hz), 112.6, 53.5 (d, *J* = 22.7 Hz), 38.4, 30.3, 19.8, 17.9; $^{19}$F{$^1$H} NMR (376 MHz, $CDCl_3$) δ –111.99; IR (neat): 3280, 3064, 2960, 2872, 1633, 1597, 1585, 1504, 1215, 744, 690 $cm^{-1}$; HRMS (ESI/Orbitrap) m/z: $[M + H]^+$ Calcd for $C_{19}H_{24}FN_2O$ 315.1872; Found 315.1873.

**(*S*)-3-fluoro-2-(hydroxydiisopropylsilyl)-*N*-(3-methyl-1-(methyl(phenyl)amino)butan-2-yl)benzamide (L4)**

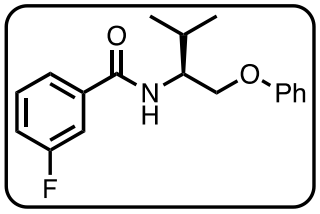



Synthesized according to the General Procedure L for silane formation using methylated-aminoamide (**2.7**) (120 mg, 0.382 mmol), *sec*-BuLi (1.4 M in cyclohexane, 0.65 mL, 0.92 mmol, 2.4 equiv), TMEDA (0.14 mL, 0.92 mmol, 2.4 equiv) and diisopropylchlorosilane (0.16 mL, 0.96 mmol, 2.5 equiv). The crude silane product reacted with silica gel and turned into the title silanol product on the surface

of the silica. The reaction mixture was purified using flash column chromatography ($SiO_2$, hexanes/EtOAc/$Et_3N$, 140:20:1.5 *v*/*v*/*v*) to give the silanol as a crystalline white solid (84 mg, 49%) over two steps. $R_f$ = 0.31 (hexanes/EtOAc/$Et_3N$, 7:1:0.15 *v*/*v*/*v*).

$^1$H NMR (400 MHz, $CDCl_3$) δ 7.30 – 7.20 (m, 2H), 7.14 (ddd, *J* = 8.0, 7.7, 6.0 Hz, 1H), 6.98 (ddd, *J* = 8.7, 8.4, 1.0 Hz, 1H), 6.84 – 6.76 (m, 2H), 6.75 (dddd, *J* = 7.2, 7.2, 1.0, 1.0 Hz, 1H), 6.39 (dd, *J* = 7.5, 1.0 Hz, 1H), 5.76 (d, *J* = 9.7 Hz, 1H), 4.41 (dddd, *J* = 9.7, 9.7, 5.5, 5.2 Hz, 1H), 3.89 (br, 1H), 3.72 (dd, *J* = 14.8, 9.7 Hz, 1H), 3.31 (dd, *J* = 14.9, 5.5 Hz, 1H), 2.97 (s, 3H), 2.05 – 1.88 (m, 1H), 1.33 – 1.16 (m, 2H), 1.15 – 0.97 (m, 12H), 1.00 – 0.83 (m, 6H); $^{13}$C{$^1$H} NMR (101 MHz, $CDCl_3$) δ 172.1 (d, *J* = 2.6 Hz), 166.8 (d, *J* = 239.9 Hz), 150.2, 144.9 (d, *J* = 11.7 Hz), 131.2 (d, *J* = 9.2 Hz), 129.8, 123.3 (d, *J* = 34.5 Hz), 123.0 (d, *J* = 2.6 Hz), 117.0, 116.8 (d, *J* = 27.9 Hz), 112.7, 53.7, 53.1, 38.3, 30.3, 19.7, 17.9 (d, *J* = 1.8 Hz), 17.9, 17.8 (d, *J* = 1.8 Hz), 17.5, 17.4, 14.5 (d, *J* = 2.9 Hz), 13.9 (d, *J* = 2.9 Hz); $^{19}$F{$^1$H} NMR (376 MHz, $CDCl_3$) δ –94.76; $^{29}$Si NMR (79 MHz, $CDCl_3$) δ 8.17 (d, *J* = 5.5 Hz); IR (neat): 3427, 2943, 2864, 1632, 1597, 1506, 1446, 1221, 858, 746 cm$^{-1}$; HRMS (ESI/Orbitrap) m/z: $[M + H]^+$ Calcd for $C_{25}H_{38}FN_2O_2Si$ 445.2686; Found 445.2678.

**(*S*)-3-fluoro-*N*-(3-methyl-1-phenoxybutan-2-yl)benzamide (2.11)**

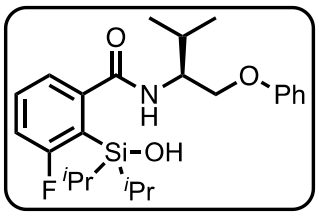



A 7 mL microwave vial containing $Cs_2CO_3$ (2.0 equiv, 1.96 mmol, 639 mg) and a stir bar was flame-dried under high vacuum (<1 torr). After the vial cooled to room temperature, it was purged with argon. β-Hydroxyamide (**2.9**) (1.5 equiv, 2.22 mmol, 500 mg), CuI (0.1 equiv, 0.15 mmol, 29 mg) and 8-hydroxyquinoline (0.2 equiv, 0.30 mmol, 44 mg) were added by difference (directly from reagent bottle or flask to reaction vial). The vial was re-purged with argon and sealed with a PTFE silicone septum, and anhydrous toluene (2 mL) was then added and the mixture was stirred for 24 h at 110 °C. To quench the reaction, $H_2O$ (3 mL) was added while stirring. The aqueous phase was extracted with DCM (2 ×

10 mL) and the combined organic phase was dried over $MgSO_4$, filtered, and concentrated *in vacuo*. The reaction mixture was purified using flash column chromatography ($SiO_2$, hexanes/EtOAc, 6:1 *v*/*v*) to give the product as a clear liquid (74.1 mg, 17%). $R_f$ = 0.27 (hexanes/EtOAc, 6:1 *v*/*v*).

$^1$H NMR (400 MHz, $CDCl_3$) δ 7.55 – 7.45 (m, 2H), 7.39 (ddd, *J* = 8.1, 7.9, 5.7 Hz, 1H), 7.33 – 7.26 (m, 2H), 7.19 (dddd, *J* = 8.3, 8.3, 2.6, 1.0 Hz, 1H), 6.97 (tt, *J* = 7.3, 1.1 Hz, 1H), 6.94 – 6.88 (m, 2H), 6.43 (d, *J* = 9.0 Hz, 1H), 4.24 (dddd, *J* = 9.3, 8.0, 3.4, 3.4 Hz, 1H), 4.18 (dd, *J* = 9.5, 3.4 Hz, 1H), 4.09 (dd, *J* = 9.5, 3.4 Hz, 1H), 2.18 (dqq, *J* = 8.0, 6.8, 6.8 Hz, 1H), 1.06 (dd, *J* = 6.8, 4.7 Hz, 6H); $^{13}$C{$^1$H} NMR (101 MHz, $CDCl_3$) δ 166.1 (d, *J* = 2.6 Hz), 162.9 (d, *J* = 248.0 Hz), 158.8, 137.1 (d, *J* = 7.0 Hz), 130.4 (d, *J* = 8.1 Hz), 129.7, 122.5 (d, *J* = 2.9 Hz), 121.4, 118.6 (d, *J* = 21.3 Hz), 114.6, 114.5 (d, *J* = 17.6 Hz), 67.8, 54.7, 29.7, 19.8, 19.5; $^{19}$F{$^1$H} NMR (283 MHz, $CDCl_3$) δ –111.74; HRMS (ESI/Orbitrap) m/z: $[M + H]^+$ Calcd for $C_{18}H_{21}FNO_2$ 302.1556; Found 302.1554.

**(*S*)-3-fluoro-2-(hydroxydiisopropylsilyl)-*N*-(3-methyl-1-phenoxybutan-2-yl)benzamide (L5)**

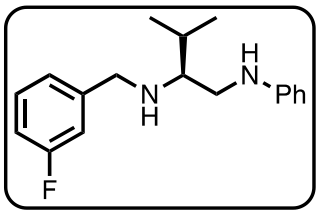



Synthesized according to the General Procedure L using **2.11** (70 mg, 0.23 mmol), *sec*-BuLi (1.4 M in cyclohexane, 0.35 mL, 0.49 mmol, 2.1 equiv), TMEDA (57 μL, 0.49 mmol, 2.1 equiv) and diisopropylchlorosilane (75 μL, 0.51 mmol, 2.2 equiv). The crude silane product reacted with silica gel and turned into the title silanol product on the surface of the silica. The reaction mixture was purified using flash column chromatography ($SiO_2$, hexanes/EtOAc, 6:1 *v*/*v*) to give the silanol as a clear liquid (15 mg, 15%) over two-steps. $R_f$ = 0.41 (hexanes/EtOAc, 6:1 *v*/*v*).

$^1$H NMR (400 MHz, $CDCl_3$) δ 7.37 (ddd, *J* = 8.3, 7.5, 5.8 Hz, 1H), 7.32 – 7.26 (m, 2H), 7.22 (dd, *J* = 7.5, 1.2 Hz, 1H), 7.08 (ddd, *J* = 9.1, 8.3, 1.1 Hz, 1H), 6.97 (tt, *J* = 7.4, 1.1 Hz, 1H), 6.95 – 6.90 (m, 2H), 6.36 (d, *J* = 9.4 Hz, 1H), 4.22 (dddd, *J* = 9.4, 8.0, 3.5, 3.5 Hz, 1H), 4.18 – 4.10 (m, 2H), 3.84 (s, 1H),

2.16 (dqq, $J$ = 8.2, 6.8, 6.8 Hz, 1H), 1.36 – 1.17 (m, 2H), 1.12 – 1.01 (m, 12H), 0.97 (dd, $J$ = 7.5, 1.3 Hz, 3H), 0.91 (dd, $J$ = 7.5, 1.3 Hz, 3H); $^{13}C\{^{1}H\}$ NMR (101 MHz, $CDCl_3$) δ 171.94 (d, $J$ = 2.2 Hz), 166.92 (d, $J$ = 240.3 Hz), 158.72, 145.08 (d, $J$ = 11.4 Hz), 131.38 (d, $J$ = 9.2 Hz), 129.72, 123.39 (d, $J$ = 34.1 Hz), 123.14 (d, $J$ = 2.9 Hz), 121.43, 117.05 (d, $J$ = 27.9 Hz), 114.71, 67.76, 55.15, 29.56, 19.75, 19.48, 17.83 (d, $J$ = 2.6 Hz), 17.75 (d, $J$ = 2.2 Hz), 17.42, 17.35, 14.19 (d, $J$ = 2.6 Hz), 14.13 (d, $J$ = 2.9 Hz); $^{29}Si\{^{1}H\}$ NMR (79 MHz, $CDCl_3$) δ 8.46 (d, $J$ = 5.1 Hz); $^{19}F\{^{1}H\}$ NMR (376 MHz, $CDCl_3$) δ – 94.60; IR (neat) 3296, 2943, 2866, 1635, 1597, 1497, 1240, 1221, 856, 752 $cm^{-1}$; HRMS (ESI/Orbitrap) m/z: $[M - H_2O + H]^+$ Calcd for $C_{24}H_{33}FNO_2Si$ 414.2264; Found 414.2253.

**(*S*)-*N*2-(3-fluorobenzyl)-3-methyl-*N*1-phenylbutane-1,2-diamine (2.14)**

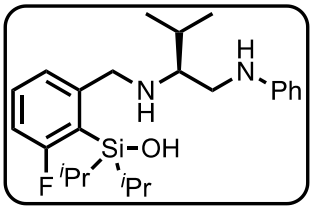



Imidazoline (**2.13**) (516 mg, 1.83 mmol, 1.0 equiv) was added directly into a flame-dried round bottom flask, dissolved in THF (2 mL) and purged with argon. Lithium aluminum hydride solution (4.0 M in $Et_2O$, 1.00 mL, 4.11 mmol, 2.25 equiv) was added dropwise at room temperature. After 16 h of stirring, the reaction was cooled to 0 °C, then was quenched with 20% KOH aqueous solution (0.70 mL) and further $H_2O$ (1 mL) was added. The aqueous phase was extracted with $Et_2O$ (3 × 3 mL) and the combined organic phase was dried over $MgSO_4$, filtered, and concentrated *in vacuo*. The resulting reaction mixture was purified using flash column chromatography ($SiO_2$, hexanes/EtOAc/$Et_3N$, 140:20:1.5 *v*/*v*/*v*) to yield the diamine as a pale yellow oil (471 mg, 86%). $R_f$ = 0.28 (hexanes/EtOAc/$Et_3N$, 7:1:0.15 *v*/*v*/*v*).

$^{1}H$ NMR (300 MHz, $CDCl_3$) δ 7.34 – 7.22 (m, 1H), 7.22 – 7.12 (m, 2H), 7.11 – 7.01 (m, 2H), 6.99 – 6.87 (m, 1H), 6.69 (dddd, $J$ = 7.2, 7.2, 1.1, 1.1 Hz, 1H), 6.64 – 6.53 (m, 2H), 4.13 (s, 1H), 3.81 (d, $J$ = 13.5 Hz, 1H), 3.74 (d, $J$ = 13.5 Hz, 1H), 3.20 (dd, $J$ = 12.0, 4.1 Hz, 1H), 2.94 (dd, $J$ = 12.0, 7.5 Hz, 1H), 2.61 (ddd, $J$ = 7.5, 5.7, 4.1 Hz, 1H), 2.07 – 1.85 (m, 1H), 1.00 (d, $J$ = 6.9 Hz, 3H), 0.95 (d, $J$ = 6.9 Hz,

3H); $^{13}C\{^1H\}$ NMR (101 MHz, $CDCl_3$) δ 163.1 (d, $J$ = 245.8 Hz), 148.9, 143.7 (d, $J$ = 7.0 Hz), 130.0 (d, $J$ = 8.4 Hz), 129.3, 123.7 (d, $J$ = 2.9 Hz), 117.4, 115.0 (d, $J$ = 21.3 Hz), 113.9 (d, $J$ = 21.3 Hz), 113.1, 61.8, 50.9 (d, $J$ = 1.8 Hz), 43.7, 29.4, 19.5, 18.4; $^{19}F\{^1H\}$ NMR (283 MHz, $CDCl_3$) δ –113.36; HRMS (ESI/Orbitrap) m/z: $[M + H]^+$ Calcd for $C_{18}H_{24}FN_2$ 287.1923; Found 287.1917.

**(*S*)-(2-fluoro-6-(((3-methyl-1-(phenylamino)butan-2-yl)amino)methyl)phenyl)diisopropylsilanol (L6)**



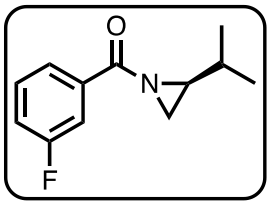

Synthesized according to the General Procedure L for silane formation using diamine (**2.14**) (204 mg, 0.713 mmol), *sec*-BuLi (1.4 M in cyclohexane, 1.02 mL, 1.43 mmol, 2.0 equiv), TMEDA (0.21 mL, 1.4 mmol, 2.0 equiv) and diisopropylchlorosilane (0.27 mL, 1.6 mmol, 2.2 equiv). The reaction mixture was quenched with brine (5 mL), and the aqueous phase was extracted with diethyl ether (4 × 5 mL, or until no organic compound was found in aqueous layer). The combined organic phase was dried over $MgSO_4$, filtered, and concentrated *in vacuo*.

The crude silane product reacted with silica gel and turned into the title silanol product on the surface of the silica. The reaction mixture was purified using flash column chromatography ($SiO_2$, hexanes/EtOAc/$Et_3N$, 140:20:1.5 *v*/*v*/*v*) to give the silanol as a clear oil (85 mg, 30%) over two steps. $R_f$ = 0.55 (hexanes/EtOAc/$Et_3N$, 7:1:0.15 *v*/*v*/*v*).

$^1H$ NMR (400 MHz, $CDCl_3$) δ 7.32 – 7.23 (m, 1H), 7.25 – 7.15 (m, 2H), 7.12 (d, $J$ = 8.3 Hz, 1H), 7.07 (dd, $J$ = 9.9, 2.5 Hz, 1H), 6.92 (ddd, $J$ = 8.0, 7.5, 2.6 Hz, 1H), 6.77 – 6.67 (m, 2H), 4.26 (dd, $J$ = 1.7, 1.7 Hz, 1H), 4.23 (d, $J$ = 15.9 Hz, 1H), 4.04 (d, $J$ = 15.9 Hz, 1H), 3.38 – 3.24 (m, 2H), 3.13 (dd, $J$ = 8.8, 5.8 Hz, 1H), 1.93 – 1.80 (m, 1H), 1.49 – 1.35 (m, 2H), 1.21 – 1.09 (m, 3H), 1.07 – 0.98 (m, 12H), 0.88 – 0.76 (m, 3H); $^{13}C\{^1H\}$ NMR (76 MHz, $CDCl_3$) δ 163.08 (d, $J$ = 245.5 Hz), 148.67, 144.31 (d, $J$ = 6.3 Hz), 129.73 (d, $J$ = 8.2 Hz), 129.24, 123.34 (d, $J$ = 2.7 Hz), 114.64 (d, $J$ = 21.5 Hz), 114.57, 113.61

(d, $J$ = 21.3 Hz), 62.03, 50.29 (d, $J$ = 1.9 Hz), 47.28, 28.97, 20.05, 18.35, 17.70, 17.47, 17.41 (d, $J$ = 1.6 Hz), 17.26, 15.50, 14.63, 14.34, 13.37; $^{19}F\{^{1}H\}$ NMR (283 MHz, $CDCl_3$) δ –113.57; $^{29}Si\{^{1}H\}$ NMR (79 MHz, $CDCl_3$) δ 10.61; IR (neat) 3280, 2994, 2949, 2837, 1448, 1409, 1113, 1013, 580 $cm^{-1}$; HRMS (ESI/Orbitrap) m/z: $[M + H]^+$ Calcd for $C_{24}H_{38}FN_2OSi$ 417.2737; Found 417.2722.

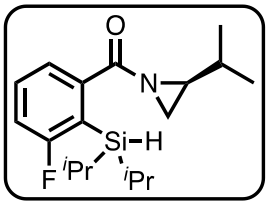
**(*S*)-(3-fluorophenyl)(2-isopropylaziridin-1-yl)methanone (2.17)**




Diisopropyl azodicarboxylate (DIAD) (1.4 equiv, 2.80 mmol, 0.49 mL) was added dropwise at room temperature to a solution of β-hydroxyamide (**2.9**) (451 mg, 2.00 mmol, 1.0 equiv), triphenylphosphine ($PPh_3$) (1.4 equiv, 2.80 mmol, 734 mg) and phenol (245 mg, 2.60 mmol, 1.3 equiv) in THF (4 mL, 0.5 M). The reaction was stirred for 16 h. To quench the reaction, sat. aq. $NaHCO_3$ (10 mL) was added while stirring. The aqueous phase was extracted with DCM (2 × 10 mL), and the combined organic phase was dried over $MgSO_4$, filtered, and concentrated *in vacuo*. The reaction mixture was purified using flash column chromatography ($SiO_2$, DCM/MeOH, 20:1 *v*/*v*) to give the silanol as a clear liquid (310 mg, 75%). $R_f$ = 0.55 (DCM/MeOH, 20:1 *v*/*v*).

$^{1}H$ NMR (400 MHz, $CDCl_3$) δ 7.74 (ddd, $J$ = 7.8, 1.3, 1.3 Hz, 1H), 7.65 (ddd, $J$ = 5.7, 2.7, 1.3 Hz, 1H), 7.37 (ddd, $J$ = 8.4, 7.8, 5.7 Hz, 1H), 7.16 (ddd, $J$ = 8.4, 2.7, 1.3 Hz, 1H), 4.42 (ddd, $J$ = 7.7, 7.5, 1.4 Hz, 1H), 4.19 – 4.04 (m, 2H), 1.86 (dqq, $J$ = 13.4, 6.8, 6.8 Hz, 1H), 1.03 (d, $J$ = 6.8 Hz, 3H), 0.93 (d, $J$ = 6.8 Hz, 3H); $^{13}C\{^{1}H\}$ NMR (101 MHz, $CDCl_3$) δ 162.6 (d, $J$ = 246.1 Hz), 162.5 (d, $J$ = 3.3 Hz), 130.2 (d, $J$ = 8.4 Hz), 130.0 (d, $J$ = 8.1 Hz), 124.1 (d, $J$ = 2.9 Hz), 118.3 (d, $J$ = 20.9 Hz), 115.4 (d, $J$ = 23.5 Hz), 72.8, 70.5, 33.0, 19.0, 18.2; $^{19}F\{^{1}H\}$ NMR (376 MHz, $CDCl_3$) δ –112.83; IR (neat) 2958, 2874, 1728, 1653, 1587, 1450, 1351, 1190, 968, 847 $cm^{-1}$; HRMS (ESI/Orbitrap) m/z: $[M + H]^+$ Calcd for $C_{12}H_{15}FNO$ 208.1137; Found 208.1128.

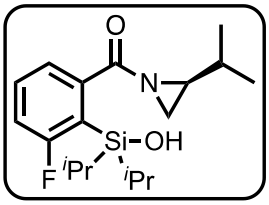
**(*S*)-(2-(diisopropylsilyl)-3-fluorophenyl)(2-isopropylaziridin-1-yl)methanone (2.18)**




Synthesized according to the General Procedure C in Chapter 1 for silane formation using aziridine (**2.17**) (279 mg, 2.93 mmol, 1.0 equiv), *sec*-BuLi (1.4 M in cyclohexane, 1.99 mL, 2.79 mmol, 3.0 equiv), TMEDA (0.42 mL, 2.79 mmol, 3.0 equiv) and diisopropylchlorosilane (0.49 mL, 2.88 mmol, 3.1 equiv). The reaction mixture was preliminary purified via flash column chromatography ($SiO_2$, 100% DCM) to yield the silane as a clear liquid (200 mg, 56%).

$^1$H NMR (400 MHz, $CDCl_3$) δ 7.53 (dd, *J* = 7.6, 1.2 Hz, 1H), 7.36 (ddd, *J* = 8.4, 7.6, 5.8 Hz, 1H), 7.08 (ddd, *J* = 8.4, 8.4, 1.2 Hz, 1H), 4.47 – 4.34 (m, 1H), 4.16 – 3.99 (m, 2H), 3.91 (ddd, *J* = 6.0, 4.1, 4.1 Hz, 1H), 1.95 – 1.78 (m, *J* = 6.7 Hz, 1H), 1.46 – 1.29 (m, 1H), 1.11 (dd, *J* = 7.3, 1.0 Hz, 6H), 1.06 (d, *J* = 6.7 Hz, 3H), 0.99 – 0.87 (m, 9H); $^{13}$C{$^1$H} NMR (101 MHz, $CDCl_3$) δ 167.2 (d, *J* = 240.6 Hz), 164.5 (d, *J* = 2.6 Hz), 137.4 (d, *J* = 11.4 Hz), 131.2 (d, *J* = 9.2 Hz), 125.3 (d, *J* = 2.9 Hz), 122.4 (d, *J* = 33.0 Hz), 117.0 (d, *J* = 27.5 Hz), 73.3, 70.5, 33.0, 19.5, 19.3, 18.7, 11.9 (d, *J* = 2.6 Hz), 11.8 (d, *J* = 2.6 Hz); $^{29}$Si{$^1$H} NMR (79 MHz, $CDCl_3$) δ 2.72 (d, *J* = 4.8 Hz); $^{19}$F{$^1$H} NMR (376 MHz, $CDCl_3$) δ – 95.69; IR (neat) 2956, 2862, 2121, 1655, 1595, 1429, 1223, 1095, 972, 800 cm$^{-1}$; HRMS (ESI/Orbitrap) m/z: $[M + H]^+$ Calcd for $C_{18}H_{29}FNOSi$ 322.2002; Found 322.1992.

**(*S*)-(3-fluoro-2-(hydroxydiisopropylsilyl)phenyl)(2-isopropylaziridin-1-yl)methanone (L7)**




Synthesized according to the General Procedure D in Chapter 1 for silanol formation using silane (**2.18**) (88 mg, 0.27 mmol), Pd/C (10 wt%, 12 mg, 0.014 mmol) and $H_2O$ (40 μL, 2.7 mmol) in THF (1.5 mL,

0.15 M) at room temperature for 4 h. The reaction mixture was purified using flash column chromatography ($SiO_2$, hexanes/EtOAc, 8:1 *v*/*v*) to give the silanol as a crystalline white solid (45 mg, 49%).

$^1$H NMR (400 MHz, $C_6D_6$) δ 8.50 (s, 1H), 7.85 (dd, *J* = 7.9, 1.2 Hz, 1H), 6.90 (ddd, *J* = 8.0, 7.9, 6.2 Hz, 1H), 6.79 (ddd, *J* = 9.4, 8.2, 1.2 Hz, 1H), 3.69 (dd, *J* = 9.5, 7.9 Hz, 1H), 3.58 (ddd, *J* = 9.5, 7.9, 7.9 Hz, 1H), 3.49 (dd, *J* = 7.9, 7.9 Hz, 1H), 1.64 – 1.49 (m, 2H), 1.47 – 1.32 (m, 7H), 1.24 (ddd, *J* = 7.5, 7.5, 1.3 Hz, 6H), 0.86 (d, *J* = 6.7 Hz, 3H), 0.64 (d, *J* = 6.7 Hz, 3H); $^{13}$C{$^1$H} NMR (101 MHz, $C_6D_6$) δ 167.41 (d, *J* = 236.6 Hz), 165.53 (d, *J* = 3.3 Hz), 135.29 (d, *J* = 12.5 Hz), 130.86 (d, *J* = 9.5 Hz), 127.71 (d, *J* = 2.2 Hz), 126.58 (d, *J* = 34.5 Hz), 118.34 (d, *J* = 29.0 Hz), 72.63, 69.83, 32.91, 18.67, 18.54, 18.37 (d, *J* = 2.9 Hz), 18.34 (d, *J* = 2.9 Hz), 18.01 (d, *J* = 1.1 Hz), 17.99 (d, *J* = 1.1 Hz), 15.63 (d, *J* = 4.4 Hz), 15.35 (d, *J* = 5.1 Hz); $^{29}$Si{$^1$H} NMR (79 MHz, $C_6D_6$) δ 6.20 (d, *J* = 7.0 Hz); $^{19}$F{$^1$H} NMR (376 MHz, $C_6D_6$) δ –93.04; IR (neat) 3058, 2956, 2864, 1641, 1595, 1419, 1248, 978, 893, 802 cm$^{-1}$; HRMS (ESI/Orbitrap) m/z: $[M + H]^+$ Calcd for $C_{18}H_{29}FNO_2Si$ 338.1951; Found 338.1940; $R_f$ = 0.57 ($SiO_2$, hexanes/EtOAc, 8:1 *v*/*v*).

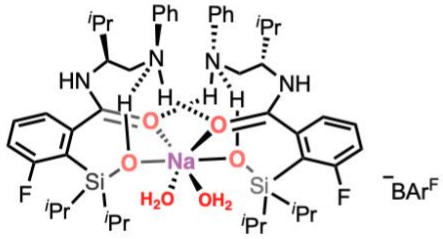
**VId. X-ray Crystallography Data**

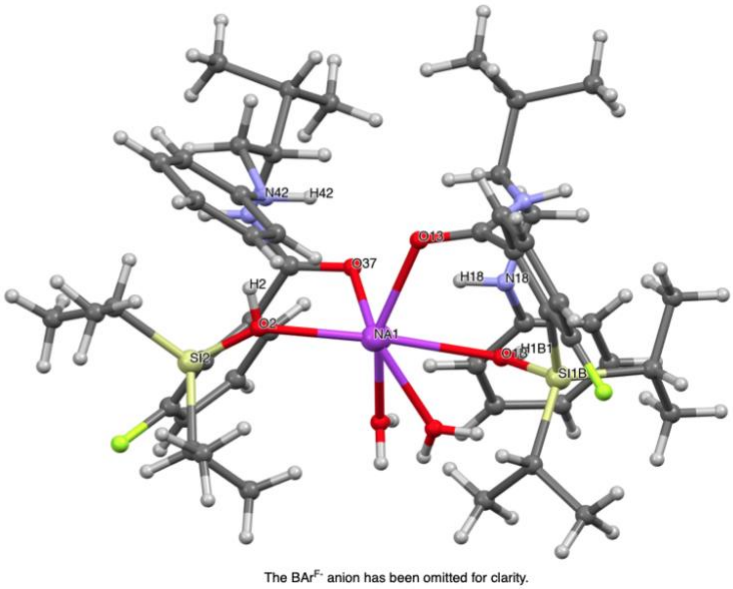
**Procedure: Crystallization of complex $[(L3a)_2/Na\cdot(H_2O)_2]^+[BAr^F]^-$**

A 7 mL vial containing 50 mg of 3Å molecular sieves and a stir bar was flame-dried under high vacuum (<1 torr). After the vial cooled to room temperature, it was purged with argon. CuCl (0.010 mmol, 0.050 equiv), $NaBAr^F$ (0.010 mmol, 0.050 equiv), and **L3a** (0.010 mmol, 0.050 equiv) were added by difference measurement (directly from reagent bottle or flask to reaction vial). The vial was re-purged with argon three times and capped with a septum and an Ar-balloon. Anhydrous DCM (0.60 mL) was then added, the resulting mixture was stirred (~270 rpm to avoid molecular sieves being ground) at room temperature. At 2 h, the solution (0.55 mL) of the mixture was filtered through Celite and transferred directly into an oven-dried, argon-purged NMR tube capped with a rubber septum. Single crystals were grown during slow solvent evaporation over two months.

***Note***: The crystallization process was conducted using the same preparation method as the N-H insertion (**Procedure G**), with the modification that the complex formed *in-situ* was filtered through Celite for crystallization purposes. Notably, the filtrate from this alternative setup was confirmed to catalyze the N-H insertion (Scheme 2.1), achieving 52% yield and 80:20 er over 16 h. The slower reaction rate and enantioselectivity compared to the standard reaction (1 h, 84%, 89:11 er) were attributed to the non-inert filtration under atmospheric conditions and moisture introduction from Celite.

**Table 2.5.** Crystal data and structure refinement for $[C_{48}H_{72}N_4O_5F_2Si_2Na][C_{32}H_{12}BF_{24}]$ (CCDC 2311643).




| | | |
|---|---|---|
| Identification code | JF3155FF (YPC-3-170) | |
| Empirical formula | C80 H84 B F26 N4 Na O5 Si2 | |
| Formula weight | 1765.49 | |
| Temperature | 90(2) K | |
| Wavelength | 0.71073 Å | |
| Crystal system | Triclinic | |
| Space group | P1 | |
| Unit cell dimensions | a = 12.8653(14) Å | α = 76.0784(15)°. |
| | b = 12.9386(14) Å | β = 80.3071(16)°. |

| | |
|---|---|
| | c = 14.2525(16) Å $\gamma$ = 65.8644(15)°. |
| Volume | 2094.9(4) Å3 |
| Z | 1 |
| Density (calculated) | 1.399 Mg/m3 |
| Absorption coefficient | 0.157 mm-1 |
| F(000) | 910 |
| Crystal size | 0.520 x 0.459 x 0.190 mm3 |
| Crystal color and habit | Colorless Plate |
| Diffractometer | Bruker Photon2 CMOS |
| Theta range for data collection | 1.740 to 27.509°. |
| Index ranges | -16<=h<=16, -16<=k<=16, -18<=l<=18 |
| Reflections collected | 33064 |
| Independent reflections | 19110 [R(int) = 0.0161] |
| Observed reflections (I > 2sigma(I)) | 16393 |
| Completeness to theta = 25.242° | 100.0 % |
| Absorption correction | Semi-empirical from equivalents |
| Max. and min. transmission | 0.9541 and 0.8636 |
| Solution method | SHELXT (Sheldrick, 2015) Acta Cryst., A71, 3-8 |
| Refinement method | SHELXL-2019/2 (Sheldrick, 2019) Full-matrix least-squares |
| on F2 | |
| Data / restraints / parameters | 19110 / 455 / 1442 |
| Goodness-of-fit on F2 | 1.033 |
| Final R indices [I>2sigma(I)] | R1 = 0.0596, wR2 = 0.1549 |
| R indices (all data) | R1 = 0.0702, wR2 = 0.1649 |
| Absolute structure parameter | 0.01(7) |
| Largest diff. peak and hole | 0.912 and -0.549 e.Å-3 |

## VII. References


(1) Huang, W.-S.; Xu, H.; Yang, H.; Xu, L.-W. Catalytic Synthesis of Silanols by Hydroxylation of Hydrosilanes: From Chemoselectivity to Enantioselectivity. *Chem. – Eur. J.* **2024**, *30* (2), e202302458. https://doi.org/10.1002/chem.202302458.

(2) Kelly, A. T.; Franz, A. K. Metal-Free Synthesis of 1,3-Disiloxanediols and Aryl Siloxanols. *ACS Omega* **2019**, *4* (4), 6295–6300. https://doi.org/10.1021/acsomega.9b00121.

(3) Limnios, D.; Kokotos, C. G. Organocatalytic Oxidation of Organosilanes to Silanols. *ACS Catal.* **2013**, *3* (10), 2239–2243. https://doi.org/10.1021/cs400515w.

(4) Brook, M. A. Silicon in Organic, Organometallic, and Polymer Chemistry; John Wiley & Sons, 2000; p 103−104.

(5) Blackmond, D. G. Kinetic Aspects of Nonlinear Effects in Asymmetric Catalysis. *Acc. Chem. Res.* **2000**, *33* (6), 402–411. https://doi.org/10.1021/ar990083s.

(6) Armstrong, B. M.; Sayler, R. I.; Shupe, B. H.; Stich, T. A.; Britt, R. D.; Franz, A. K. EPR Evidence for the Origin of Nonlinear Effects in an Enantioselective Cu(II)-Catalyzed Spiroannulation. *ACS Catal.* **2019**, *9* (2), 1224–1230. https://doi.org/10.1021/acscatal.8b03822.

(7) Kagan, H. B. Practical Consequences of Non-Linear Effects in Asymmetric Synthesis. *Adv. Synth. Catal.* **2001**, *343* (3), 227–233. https://doi.org/10.1002/1615-4169(20010330)343:3<227::AID-ADSC227>3.0.CO;2-X.

(8) Zhu, S.-F.; Xu, B.; Wang, G.-P.; Zhou, Q.-L. Well-Defined Binuclear Chiral Spiro Copper Catalysts for Enantioselective N–H Insertion. *J. Am. Chem. Soc.* **2012**, *134* (1), 436–442. https://doi.org/10.1021/ja2084493.

(9) Lee, E. C.; Fu, G. C. Copper-Catalyzed Asymmetric N−H Insertion Reactions: Couplings of Diazo Compounds with Carbamates to Generate α-Amino Acids. *J. Am. Chem. Soc.* **2007**, *129* (40), 12066–12067. https://doi.org/10.1021/ja074483j.

(10) Liu, B.; Zhu, S.-F.; Zhang, W.; Chen, C.; Zhou, Q.-L. Highly Enantioselective Insertion of Carbenoids into N−H Bonds Catalyzed by Copper Complexes of Chiral Spiro Bisoxazolines. *J. Am. Chem. Soc.* **2007**, *129* (18), 5834–5835. https://doi.org/10.1021/ja0711765.

(11) Saito, H.; Morita, D.; Uchiyama, T.; Miyake, M.; Miyairi, S. Cinchona Alkaloids Induce Asymmetry in the Insertion Reaction of Thermally Generated Carbenes into N−H Bonds. *Tetrahedron Lett.* **2012**, *53* (49), 6662–6664. https://doi.org/10.1016/j.tetlet.2012.09.087.

(12) Zhu, Y.; Liu, X.; Dong, S.; Zhou, Y.; Li, W.; Lin, L.; Feng, X. Asymmetric N□H Insertion of Secondary and Primary Anilines under the Catalysis of Palladium and Chiral Guanidine Derivatives. *Angew. Chem. Int. Ed.* **2014**, *53* (6), 1636–1640. https://doi.org/10.1002/anie.201308501.

(13) Hou, Z.; Wang, J.; He, P.; Wang, J.; Qin, B.; Liu, X.; Lin, L.; Feng, X. Highly Enantioselective Insertion of Carbenoids into N-H Bonds Catalyzed by Copper(I) Complexes of Binol Derivatives. *Angew. Chem. Int. Ed.* **2010**, *49* (28), 4763–4766. https://doi.org/10.1002/anie.201001686.

(14) Zhu, S.-F.; Zhou, Q.-L. Transition-Metal-Catalyzed Enantioselective Heteroatom–Hydrogen Bond Insertion Reactions. *Acc. Chem. Res.* **2012**, *45* (8), 1365–1377. https://doi.org/10.1021/ar300051u.

(15) Evans, D. A.; Woerpel, K. A.; Hinman, M. M.; Faul, M. M. Bis(Oxazolines) as Chiral Ligands in Metal-Catalyzed Asymmetric Reactions. Catalytic, Asymmetric Cyclopropanation of Olefins. *J. Am. Chem. Soc.* **1991**, *113* (2), 726–728. https://doi.org/10.1021/ja00002a080.

(16) Zhao, X.; Zhang, Y.; Wang, J. Recent Developments in Copper-Catalyzed Reactions of Diazo Compounds. *Chem. Commun.* **2012**, *48* (82), 10162. https://doi.org/10.1039/c2cc34406h.

(17) Doyle, M. P.; Duffy, R.; Ratnikov, M.; Zhou, L. Catalytic Carbene Insertion into C−H Bonds. *Chem. Rev.* **2010**, *110* (2), 704–724. https://doi.org/10.1021/cr900239n.

(18) Zhang, Y.-Z.; Zhu, S.-F.; Wang, L.-X.; Zhou, Q.-L. Copper-Catalyzed Highly Enantioselective Carbenoid Insertion into Si-H Bonds. *Angew Chem Int Ed* **2008**, *47* (44), 8496–8498. https://doi.org/10.1002/anie.200803192.

(19) Yang, L.-L.; Evans, D.; Xu, B.; Li, W.-T.; Li, M.-L.; Zhu, S.-F.; Houk, K. N.; Zhou, Q.-L. Enantioselective Diarylcarbene Insertion into Si–H Bonds Induced by Electronic Properties of the Carbenes. *J. Am. Chem. Soc.* **2020**, *142* (28), 12394–12399. https://doi.org/10.1021/jacs.0c04725.

(20) Xue, W.; Oestreich, M. Beyond Carbon: Enantioselective and Enantiospecific Reactions with Catalytically Generated Boryl- and Silylcopper Intermediates. *ACS Cent. Sci.* **2020**, *6* (7), 1070–1081. https://doi.org/10.1021/acscentsci.0c00738.
(21) Ren, Y.-Y.; Zhu, S.-F.; Zhou, Q.-L. Chiral Proton-Transfer Shuttle Catalysts for Carbene Insertion Reactions. *Org. Biomol. Chem.* **2018**, *16* (17), 3087–3094. https://doi.org/10.1039/C8OB00473K.
(22) Li, M.-L.; Yu, J.-H.; Li, Y.-H.; Zhu, S.-F.; Zhou, Q.-L. Highly Enantioselective Carbene Insertion into N–H Bonds of Aliphatic Amines. *Science* **2019**, *366* (6468), 990–994. https://doi.org/10.1126/science.aaw9939.
(23) Li, M.-L.; Pan, J.-B.; Zhou, Q.-L. Enantioselective Synthesis of Amino Acids from Ammonia. *Nat. Catal.* **2022**, *5* (6), 571–577. https://doi.org/10.1038/s41929-022-00779-2.
(24) Yao, L.; Ishihara, K. Enantioselective [1,3] O-to-C Rearrangement: Dearomatization of Alkyl 2-Allyloxy/Benzyloxy-1/3-Naphthoates Catalyzed by a Chiral π–Cu( II ) Complex. *Chem. Sci.* **2019**, *10* (8), 2259–2263. https://doi.org/10.1039/C8SC05601C.
(25) Smrečki, N.; Rončević, T.; Jović, O.; Kukovec, B.-M.; Maravić, A.; Gajski, G.; Čikeš-Čulić, V. Copper(II) Complexes with N ´ -Methylsarcosinamide Selective for Human Bladder Cancer Cells. *Inorganica Chim. Acta* **2019**, *488*, 312–320. https://doi.org/10.1016/j.ica.2019.01.013.
(26) Pantalon Juraj, N.; Tandarić, T.; Tadić, V.; Perić, B.; Moreth, D.; Schatzschneider, U.; Brozovic, A.; Vianello, R.; Kirin, S. I. Tuning the Coordination Properties of Chiral Pseudopeptide Bis(2-Picolyl)Amine and Iminodiacetamide Ligands in Zn( II ) and Cu( II ) Complexes. *Dalton Trans.* **2022**, *51* (44), 17008–17021. https://doi.org/10.1039/D2DT02895F.
(27) Yang, W.; Pu, M.; Lin, X.; Chen, M.; Song, Y.; Liu, X.; Wu, Y.-D.; Feng, X. Enantioselective Formal Vinylogous N–H Insertion of Secondary Aliphatic Amines Catalyzed by a High-Spin Cobalt(II) Complex. *J. Am. Chem. Soc.* **2021**, *143* (25), 9648–9656. https://doi.org/10.1021/jacs.1c04367.
(28) Launer, P. J.; Arkles, B. *Silicon Compounds: Silanes & Silicones In Infrared Analysis of Organosilicon Compounds*, 3rd ed.; Gelest Inc., 2013.
(29) Gillingham, D.; Fei, N. Catalytic X–H Insertion Reactions Based on Carbenoids. *Chem. Soc. Rev.* **2013**, *42* (12), 4918. https://doi.org/10.1039/c3cs35496b.
(30) Dragojlovic, V. Conformational Analysis of Cycloalkanes. *ChemTexts* **2015**, *1* (3), 14. https://doi.org/10.1007/s40828-015-0014-0.
(31) Wiberg, K. B. The C7−C10 Cycloalkanes Revisited. *J. Org. Chem.* **2003**, *68* (24), 9322–9329. https://doi.org/10.1021/jo030227n.
(32) Durán, R.; Herrera, B. Theoretical Study of the Mechanism of Catalytic Enanteoselective N–H and O–H Insertion Reactions. *J. Phys. Chem. A* **2020**, *124* (1), 2–11. https://doi.org/10.1021/acs.jpca.9b07274.
(33) Durán, R.; Herrera, B. Theoretical Study of the Substituent Effect on the O–H Insertion Reaction of Copper Carbenoids. *Theor. Chem. Acc.* **2022**, *141* (3), 15. https://doi.org/10.1007/s00214-022-02876-8.
(34) Kinens, A.; Sejejs, M.; Kamlet, A. S.; Piotrowski, D. W.; Vedejs, E.; Suna, E. Development of a Chiral DMAP Catalyst for the Dynamic Kinetic Resolution of Azole Hemiaminals. *J. Org. Chem.* **2017**, *82* (2), 869–886. https://doi.org/10.1021/acs.joc.6b02955.

# Chapter Three: NMR Quantification of Halogen-Bonding Donor Ability to Evaluate Catalyst Activity*

## I. Introduction

This chapter presents the development of an NMR quantification method of measuring halogen-bonding (X-bonding) donor abilities using a commercially available molecular probe, triethyl phosphine oxide (TEPO) with $^{31}$P NMR spectroscopy. The use of this $^{31}$P NMR quantification method provides a simple and rapid tool to quantify non-covalent interactions, enabling predictions for the design and applications of new organocatalysts.[1–5] X-bonding has emerged as new class of organocatalysts in recent years.[6–10] We aimed to extend the application of $^{31}$P NMR quantification to X-bonding, aiming to predict the catalytic abilities of novel XBDs, thereby advancing our understanding of X-bonding catalysis. In this project, a series of monodentate and bis(imidazolium) halogen-bond donors (XBDs) was quantified using $^{31}$P NMR spectroscopy (Figure 3.1). The measured $\Delta\delta(^{31}P)$ values correlate with calculated free energy $\Delta G^{\ddagger}$ of activation and catalytic activity for a Friedel−Crafts indole addition reaction. The data were able to be used to establish a scale for predicting the catalytic activity of XBDs. These results were compiled into a manuscript and published in *Organic Letters*.

*Reproduced in part with permission from Chang, Y.-P.; Tang, T.; Jagannathan, J. R.; Hirbawi, N.; Sun, S.; Brown, J.; Franz, A. K. *Org. Lett.* **2020**, *22* (16), 6647–6652. https://doi.org/10.1021/acs.orglett.0c02427. Copyright 2020 American Chemical Society.

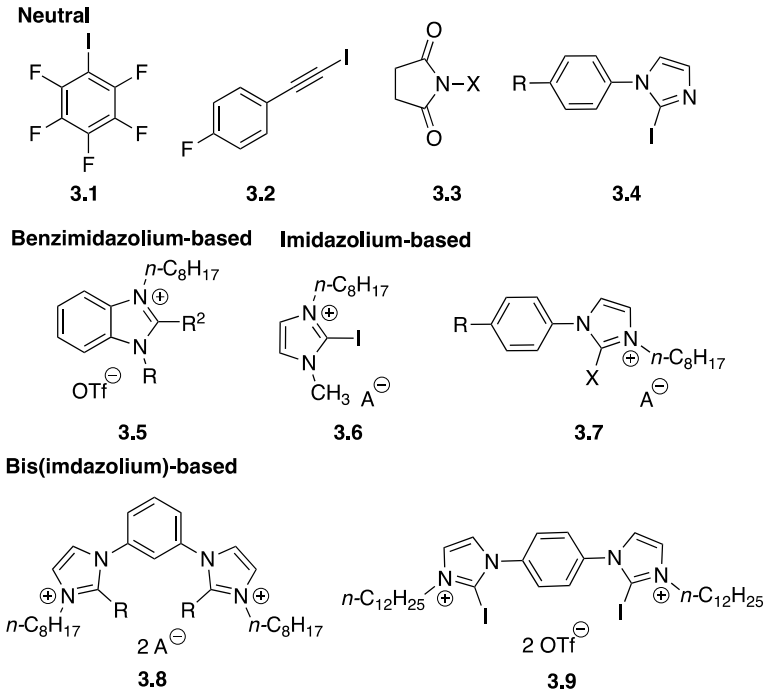



**Figure 3.1.** Halogen-bond donors studied in this chapter.

## Ia. Halogen-bonding

Halogen-bonding (X-bonding) is a noncovalent interaction between an electrophilic halogen atom and a Lewis base (LB) (Figure 3.2).[11,12] When a high-polarizability halogen atom is substituted, electron density undergoes redistribution, rendering the electrostatic potential anisotropic. This redistribution process gives rise to the formation of a sigma hole, which is localized 180° to the σ bond. The size of this σ hole, or the extent of electron density depletion, determines the X-bonding capability.[13] Consequently, we can modulate the X-bonding ability by varying the X-atom from iodine to chlorine. As polarizability increases in the order of F << Cl < Br < I , the sigma hole expands, leading to an enhanced X-bonding capability.[7] Halogen bond strength typically falls within the range of 1−30 kcal/mol, with the majority falling in the 1−5 kcal/mol range.[13] X-bonding ability can be altered by modifying the electronic properties of the attached residue (R group) on the X-atom. Owing to the high directionality and tunability, X-bonding has been utilized in crystal engineering and material science to control molecular assembly.[14–16] More recently, X-bonding has been applied to molecular recognition[17,18] and catalysis[6–10,19–25] in the solution-phase.[26]

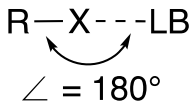
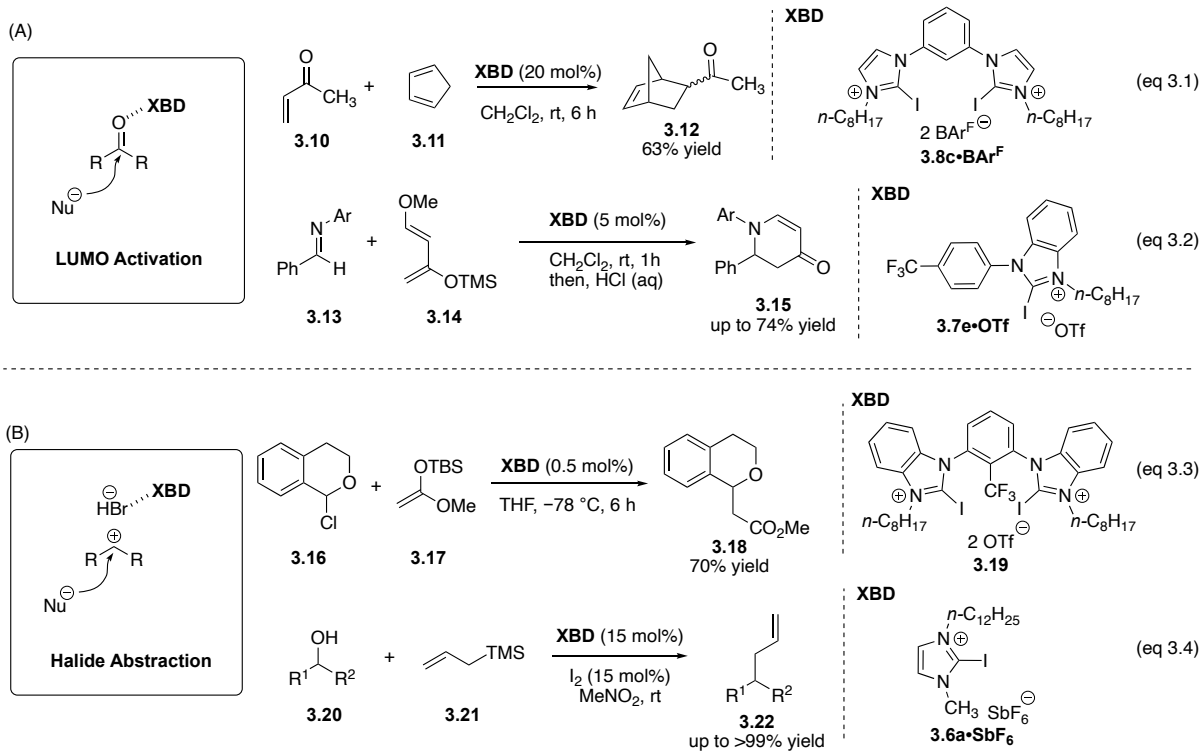



**Figure 3.2.** X-bonding: a noncovalent interaction between an electrophilic halogen atom (X) and a Lewis base (LB).

**Ib. X-bonding in Organocatalysis**

X-bonding has been extensively applied in materials and biorecognition but has not been widely utilized in organocatalysis until recent years.[6–10] In the field of organocatalysis, hydrogen-bonding (H-bonding) has traditionally held the utmost significance as an intermolecular interaction to increase the rate of reactions. However, researchers are now using X-bonding as a noncovalent interaction in organocatalysis due to its mild Lewis acid character and high directionality. The fundamental concept of activation through X-bonding is similar to H-bonding. When a Lewis acidic XB donor binds to a Lewis basic substrate, it has the potential to enhance the polarization of the substrate, thereby increasing its reactivity. X-bonding catalysis includes two distinct activation modes: LUMO activation (Scheme 3.1A) and halide abstraction (Scheme 3.1B).[7,8] The particular activation mode varies based on the nature of the substrates. In 2014, the Huber group reported the pioneering example of the activation of a carbonyl compound using XBDs (eq 3.1).[10] They used a Diels–Alder reaction as a benchmark reaction and provided evidence demonstrating that dicationic XBDs with non-coordinating counterions (**3.8c•BAr$^F$**) are capable of activating a carbonyl compound. Another example was reported by Minakata et al., who reported using 2-halogenoimidazolium salts (**3.7e•OTf**) to catalyze the aza-Diels-Alder reaction of aldimines **3.13** with Danishefsky's diene (**3.14**, eq 3.2).[21] The Huber group developed a class of rigid bis(halobenzimidazolium) compounds, such as **3.19**, as XBDs for halide abstraction catalysis. These XBDs efficiently catalyzed the reaction between 1-chloroisochroman (**3.16**) and a ketene silyl acetal **3.17** through halide abstraction, requiring a minimal catalyst loading as low as 2.5 mol% (eq 3.3).[20] In parallel, the Takemoto group devised a cocatalytic system involving XB donors and TMSX **3.21** to activate alcohols **3.20**, facilitating a direct dehydroxylative coupling reaction with diverse nucleophiles containing TMS groups (eq 3.4).[23]




**Scheme 3.1.** Activation modes of X-bonding catalysis: (A) LUMO activation and (B) halide abstraction.

## Ic. Quantification Methods of X-bonding

The investigation of X-bonding relies on high sensitivity techniques such as IR,[27] Raman,[28] UV−Vis,[29] and NMR[30–35] spectroscopies since X-bonding of organic scaffolds is a relatively weak interaction with a low association affinity to Lewis bases.[36–38] Due to the high versatility and capability of providing detailed structural information, solution-phase NMR spectroscopy, especially $^{1}$H and $^{19}$F NMR spectroscopies, are the most common techniques for analyzing the thermodynamic properties of X-bonding.[30–33] However, the quantification of X-bonding through $^{1}$H and $^{19}$F NMR chemical shifts are limited to at least two bonds away from the interaction site to the reporter nucleus.[35] The greater distance might decrease the magnitude of the changes in shift, and hence impede the accuracy of the X-bonding quantification (Figure 3.3A). $^{13}$C NMR spectroscopy can detect the electrostatic change of a carbon that is one bond away from the interaction site, and this method is less susceptible to medium (solvent, pH) effects, but the low sensitivity decreases the applicability of using $^{13}$C NMR spectroscopy to quantify X-bonding (Figure 3.3B).[33,34] A few examples of quantification of X-bonding using $^{15}$N NMR spectroscopy have also been reported.[35] However, even though the reporter nitrogen is directly

interacting with the halogen atom, the authors reported that the evaluation of weak X-bonding interactions was not sufficiently accurate (Figure 3.3C).

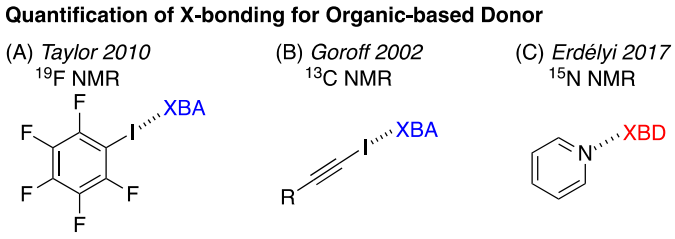



**Figure 3.3.** Previous works on quantification of X-bonding using NMR spectroscopy

## Id. Quantification of Lewis Acidity Using $^{31}$P NMR Spectroscopy

$^{31}$P NMR spectroscopy has been successfully applied to quantify noncovalent interactions upon binding to TEPO as a Lewis basic probe (Figure 3.4A).[1–5,39,40] First reported by Gutmann and Beckett to measure Lewis acidic solvents,[39,40] the Franz group and others have since adapted this method to quantify the H-bonding ability of various H-bond donors.[1–5] Previous work in the Franz group has successfully demonstrated the proportional relationship of H-bonding ability and catalytic activity for a variety of H-bonding donors (Figure 3.4B) and metal-ligand complexes using $^{31}$P NMR spectroscopy.[5]

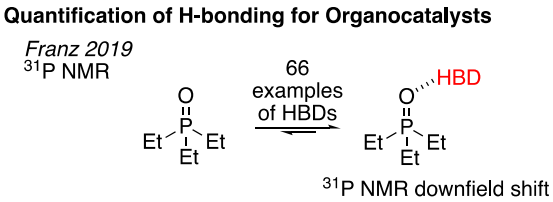



**Figure 3.4.** Quantification of H-bonding ability using $^{31}$P NMR reported by the Franz group.[5]

In addition to the application to H-bonding, our group has expanded the $^{31}$P NMR spectroscopy method to quantify X-bonding ability and correlated the catalytic ability of XBD organocatalysts (Figure 3.5). Nine classes of representative XBD compounds, including neutral (**3.1**–**3.4**), cationic benzimidazolium- (**3.5**),[20,21] imidazolium- (**3.6**–**3.7**),[20,21,23] and bis(imidazolium)-based[9,20] (**3.8**–**3.9**) structures were examined to quantify a total of 36 XBD examples. This work involved collaboration with Teresa Tang and Dr. Jake R. Jagannathan, who contributed to the $K_a$ calculations.

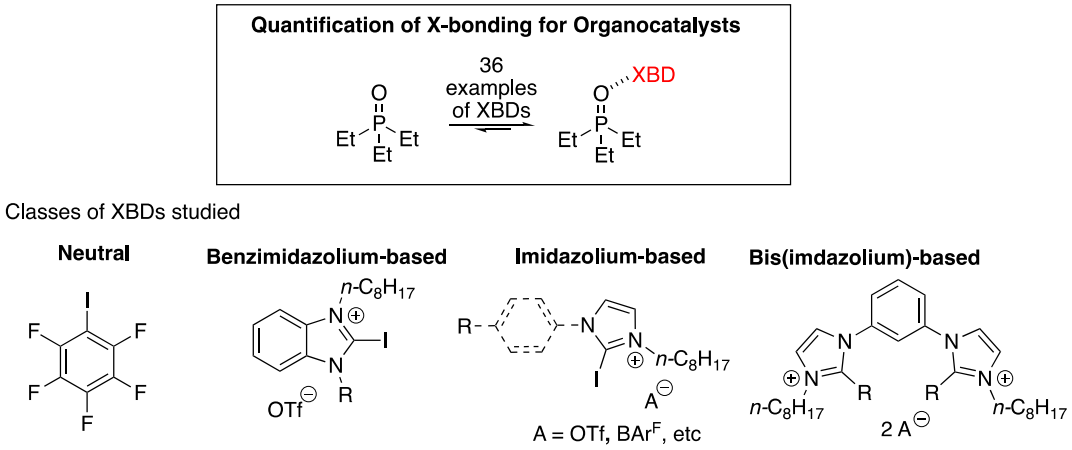



**Figure 3.5.** Project overview.

## II. Method Validation

To validate $^{31}$P NMR spectroscopy as a method to quantify X-bonding ability, factors such as the XBD−TEPO equilibrium, solvent interference and competition from other noncovalent interactions from impurities were carefully examined. Similar to TEPO binding to HBDs, downfield $^{31}$P NMR shifts (Δδ) are observed upon TEPO binding to XBDs (Figure 3.6). Stronger X-bonding ability is expected to correlate to larger Δδ($^{31}$P) values. When different probes such as d$^5$-pyridine and tetraethyl methylenebis(phosphonate) were evaluated, no obvious changes in chemical shift were observed. TEPO was determined to be the most safe, stable, and effective phosphorous probe compared to other options.

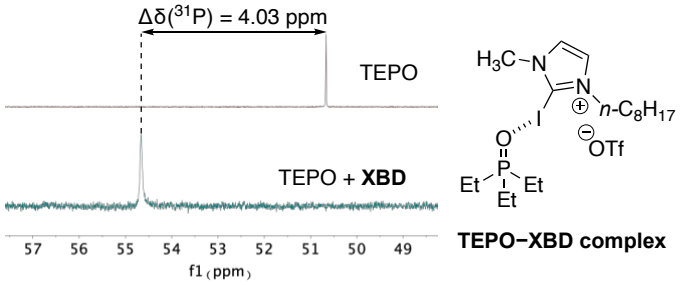



**Figure 3.6.** Example $^{31}$P NMR spectra for the downfield $^{31}$P NMR shifts Δδ($^{31}$P) upon TEPO binding to XBD (in $CD_2Cl_2$).

### IIa. Titration Experiments

To assess the XBD−TEPO binding equilibrium and optimal equivalents, I performed a series of titration experiments using 0.5−16 equivalents of XBD catalyst to identify the saturation point. The purpose of

this series of experiments is to observe and determine the equilibrium point of $^{31}$P NMR probe binding to XBDs. To determine the stoichiometry of TEPO binding to XBDs, I investigated **3.6•OTf**, **3.8c•OTf**, **3.7e•BAr$^F$**, and **3.8c•BAr$^F$** binding to TEPO as idealized representative examples due to their varied denticity and counteranions. The TEPO concentration was held constant at 15 mM for titration experiments and varying amounts of XBDs were added to give the desired equivalents. The results are summarized in Figure 3.7. For imidazolium- (**3.6•OTf**) and bis(imidazolium)-based triflate (**3.8c•OTf**) XBDs, saturation occurs at approximately 10 and 15 equivalents, respectively. With the weakly coordinating counteranion BArF (tetrakis[3,5-bis(trifluoromethyl)phenyl]borate), **3.7e•BAr$^F$** and **3.8c•BAr$^F$** XBDs possess enhanced binding ability and saturation was observed for each catalyst at ~5 equivalents. Preliminary association constants were calculated by Dr. Jake R. Jagannathan and detailed in his dissertation.[41]

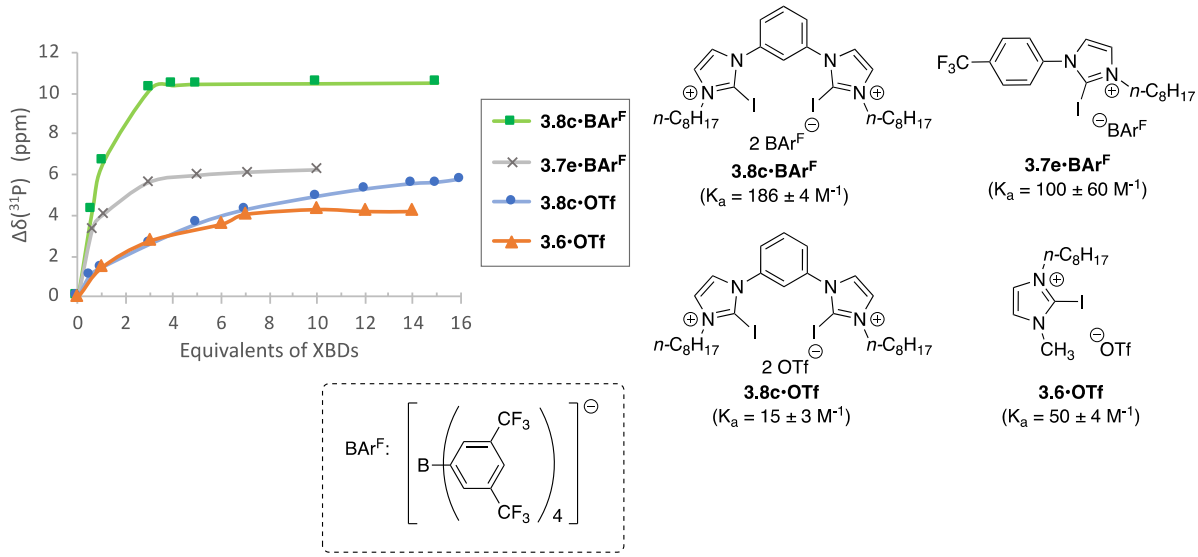



**Figure 3.7**. Titration experiments comparing XBDs and calculated binding constant $K_a$.

## IIb. Job Plots

Job plots were constructed for understanding the binding mode of TEPO probe and XBDs (Figure 3.8.). The Job plot can provide information about the binding stoichiometry between the TEPO probe and the XBD. For both **3.6•OTf** and **3.8c•OTf**, a maximum is observed in the curve at $X_A = 0.5$, which suggests a 1:1 binding stoichiometry between TEPO and each imidazolium- and bis-imidazolium salt. A slight asymmetry is observed in the plot of **3.8c•OTf**, which may be due to the formation of higher-order

species through possible π–π stacking interactions. Nevertheless, the stoichiometry confirms a 1:1 binding ratio of **3.8c•OTf** with TEPO.

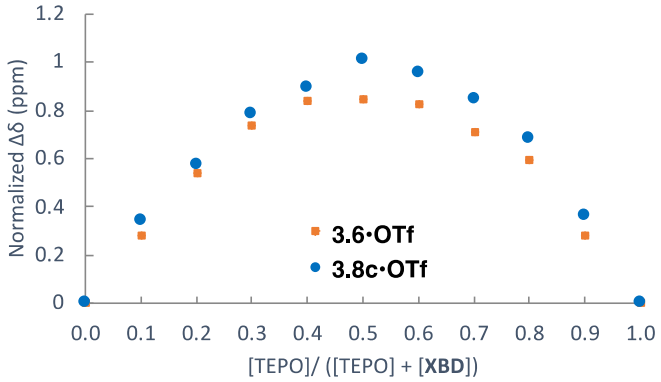
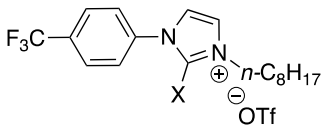



**Figure 3.8.** Job Plot of **3.6•OTf** and **3.8c•OTf** binding with TEPO, respectively (at 55 mM in $CD_2Cl_2$).

## IIc. Changing the Halogen-donating Atom on Substrates

To assure that TEPO is actually probing the X-bonding interactions and binding to the halogen atoms, a series of trifluoromethyl-phenyl imidazolium triflate salts with different X-atoms (**3.7e−7g•OTf**) were tested. Due to the increased polarizability of the halogen atom, resulting in enhanced sigma-hole interactions, the more electrophilic halogen atom (I > Br > Cl) should correlate with larger $\Delta\delta(^{31}P)$ values. Indeed, switching from iodo- to bromo- and chloro-substrates (in **3.7e−7g•OTf**) significantly decreased the $\Delta\delta(^{31}P)$ values (Table 1), matching a decrease in polarizability of the halogen substituents and hence the X-bonding ability. These results confirm that TEPO shift is reflecting the interaction between TEPO and the halogen atom.

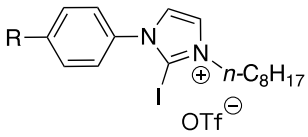



| | X | Δδ (ppm) | polarizability |
|---|---|---|---|
| **3.7e•OTf** | I | 5.28 | |
| **3.7f•OTf** | Br | 1.13 | |
| **3.7g•OTf** | Cl | 1.09 | |

**Figure 3.9.** $\Delta\delta(^{31}P)$ values (n = 3, STD < 0.1 ppm) confirm the X-atom is involved in XBD−TEPO binding.

## IId. Hammett Plot

To validate the use of $^{31}$P NMR spectroscopy to quantify electronic effects for X-bonding, a Hammett plot was created for a series of 2-iodoimidazolium triflate salts (**3.7a−7e•OTf**) with electronically varied substituents on the conjugated benzene ring (Figure 3.10). A linear relationship ($R^2 = 0.988$) was observed, indicating that $\Delta\delta(^{31}P)$ values can accurately quantify the electronic changes affecting X-bonding ability. This strong correlation validates the method using $^{31}$P NMR spectroscopy to quantify X-bonding abilities.




| | Δδ($^{31}$P) (ppm) | σ parameter |
|---|---|---|
| **3.7a•OTf**, R = OMe | 4.64 | −0.27 |
| **3.7b•OTf**, R = H | 4.79 | 0 |
| **3.7c•OTf**, R = Cl | 5.00 | 0.23 |
| **3.7d•OTf**, R = $OCF_3$ | 5.11 | 0.35 |
| **3.7e•OTf**, R = $CF_3$ | 5.29 | 0.54 |

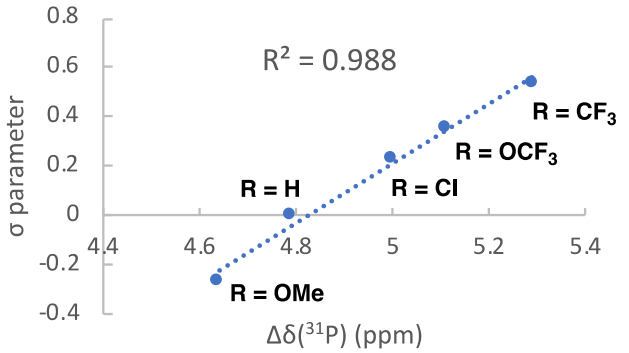



**Figure 3.10.** Correlation of $\Delta\delta(^{31}P)$ values (n = 3, STD < 0.1 ppm) and Hammett σ parameters for para-substituted phenyl-imidazolium triflates.

## IIe. Effect on Impurities on $\Delta\delta(^{31}P)$ Values

An integral part of this quantification method is to ensure the absence of any impurities, especially trace acids formed from the counter-anions. To obtain accurate and consistent results, it is essential to ensure that no residual triflic acid (TfOH) is present, which can lead to large $\Delta\delta(^{31}P)$ values due to TfOH−TEPO binding. During the initial development of the NMR quantification method, data inconsistencies were encountered, preventing the successful construction of a well-correlated Hammett plot. Consequently, this quantification method could not be validated. Upon detailed analysis and troubleshooting, it was determined that the inconsistency resulted from triflic acid impurities, which exhibited lower sensitivity to detection using $^{1}$H or $^{19}$F NMR spectroscopy compared to our quantification method. A series of experiments was performed that demonstrated that the purification methods from literature[9,10,20,21,42,43] could not consistently remove triflic acid completely (Figure 3.11).

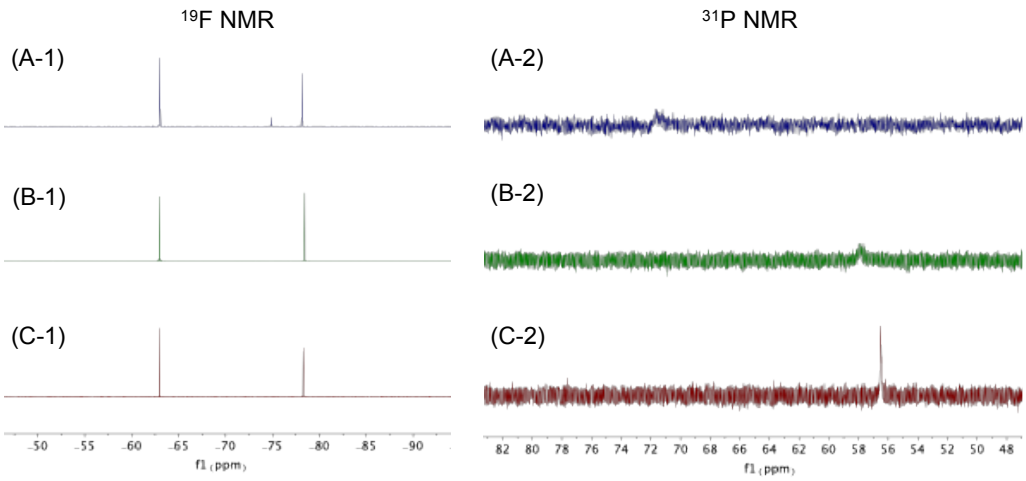



**Figure 3.11.** Comparing $^{19}$F NMR and $^{31}$P NMR spectra of **3.5d•OTf** before silica column (A), after the first silica column (B), after the second silica column (C).

To address this, we recognized that the use of TEPO binding could be established as an analytical method to assess the purity of XBD triflate salts. Through various experiments, we determined that $^{31}$P NMR spectroscopy and TEPO-binding experiments proved more effective in evaluating the purity of XBDs compared to $^{19}$F NMR spectroscopy (Figure 3.12). With this approach, we consistently obtained $\Delta\delta(^{31}P)$ values with standard deviation <0.10 ppm across different XBD batches. Subsequently, a Hammett plot ($R^2 = 0.988$) to validate this quantification method for X-bonding ability was constructed (Figure 3.10). Due to these developments, our method has been adopted by fellow researchers to verify the purity of their newly designed XBD catalysts.[44–53]

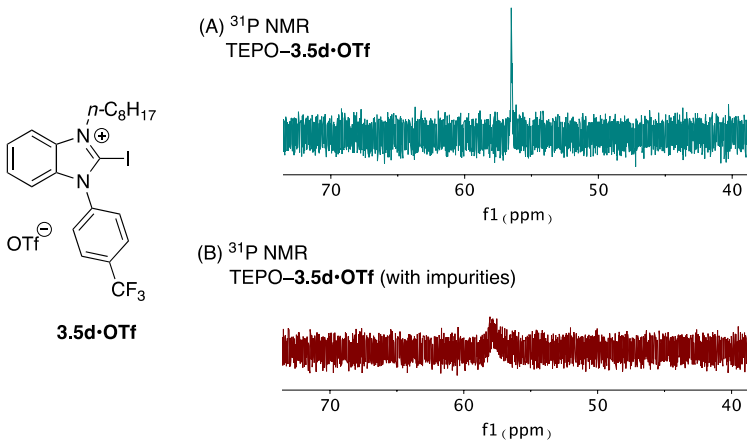



**Figure 3.12.** (A) Reliable and consistent $\Delta\delta(^{31}P)$ values are determined from sharp $^{31}$P NMR signals after rigorous purification (e.g. binding to **3.5d•OTf**). (B) Even when no TfOH is observed using $^{1}$H and $^{19}$F NMR spectroscopy, a broader peak is observed using $^{31}$P NMR spectroscopy (after extraction and the first silica column).

Water is also an impurity that would affect $\Delta\delta(^{31}P)$ values. TEPO is a highly hygroscopic compound. To work with TEPO, we developed the standard procedure for $^{31}P$ NMR measurement to obtain reliable and consistent $\Delta\delta(^{31}P)$ values. Typically, TEPO was used directly from the bottle as we received it. Over time, TEPO would appear wet or turn into a liquid. As a result, we developed a procedure for purifying TEPO to address this issue.

Control experiments were performed to investigate the impact of water on TEPO binding and the resulting $^{31}P$ NMR values attributed to the hygroscopicity of TEPO (Figure 3.13). Binding experiments with XBD (**3.1**) and HBD were performed using the standard procedure of $^{31}P$ NMR measurement (Figure 3.13A). The same procedure was performed except one drop of water was added into a 0.5 mL TEPO stock solution to make a wet TEPO solution (Figure 3.13B). Compared to the use of dried TEPO (Figure 3.13A), the trace amount of water broadened the $^{31}P$ NMR signal, attributed to the TEPO−$H_2O$ complex (Figure 3.13-B2−3). However, a sharp $^{31}P$ NMR signal could verify that the XBD binding was not affected by trace amounts of water (Figure 3.14).

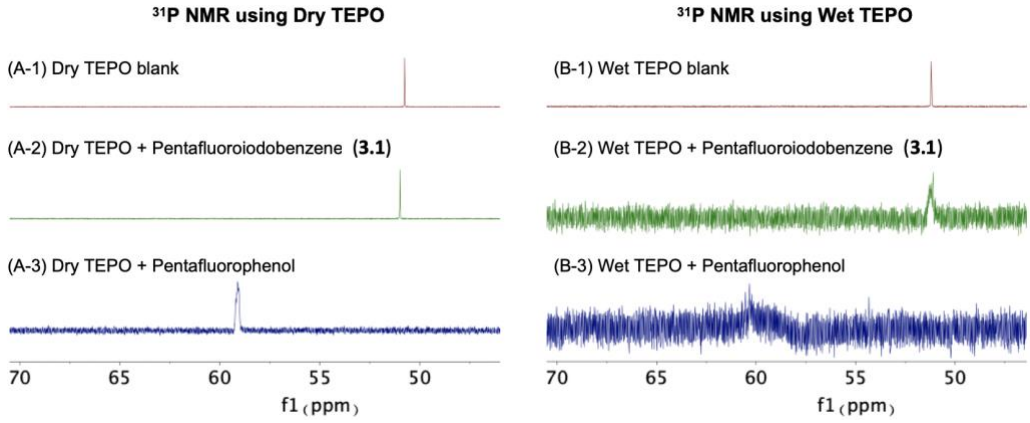



**Figure 3.13.** Comparing $^{31}P$ NMR spectra for binding experiments using (A) dried TEPO and (B) wet TEPO.

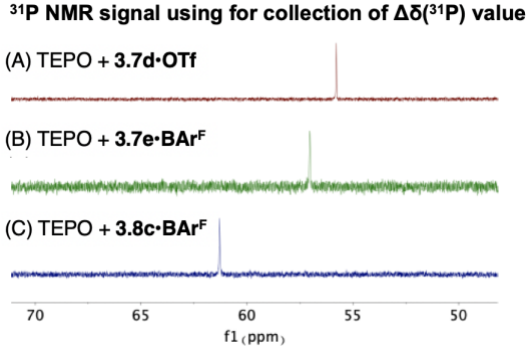



**Figure 3.14.** Examples for $^{31}P$ NMR spectra of binding experiments.

## III. Results and discussion

To build a scale to quantify the X-bonding ability of organocatalysts, Δδ($^{31}$P) values were measured for a variety of XBD compounds (Figure 3.15). All Δ$\delta$($^{31}$P) and $k_{obs}$ data are presented in Table 3.1. In this section, the results of Δ$\delta$($^{31}$P) NMR data of XBDs, categorized as neutral, mono-, and bi-dentate species, will be discussed.

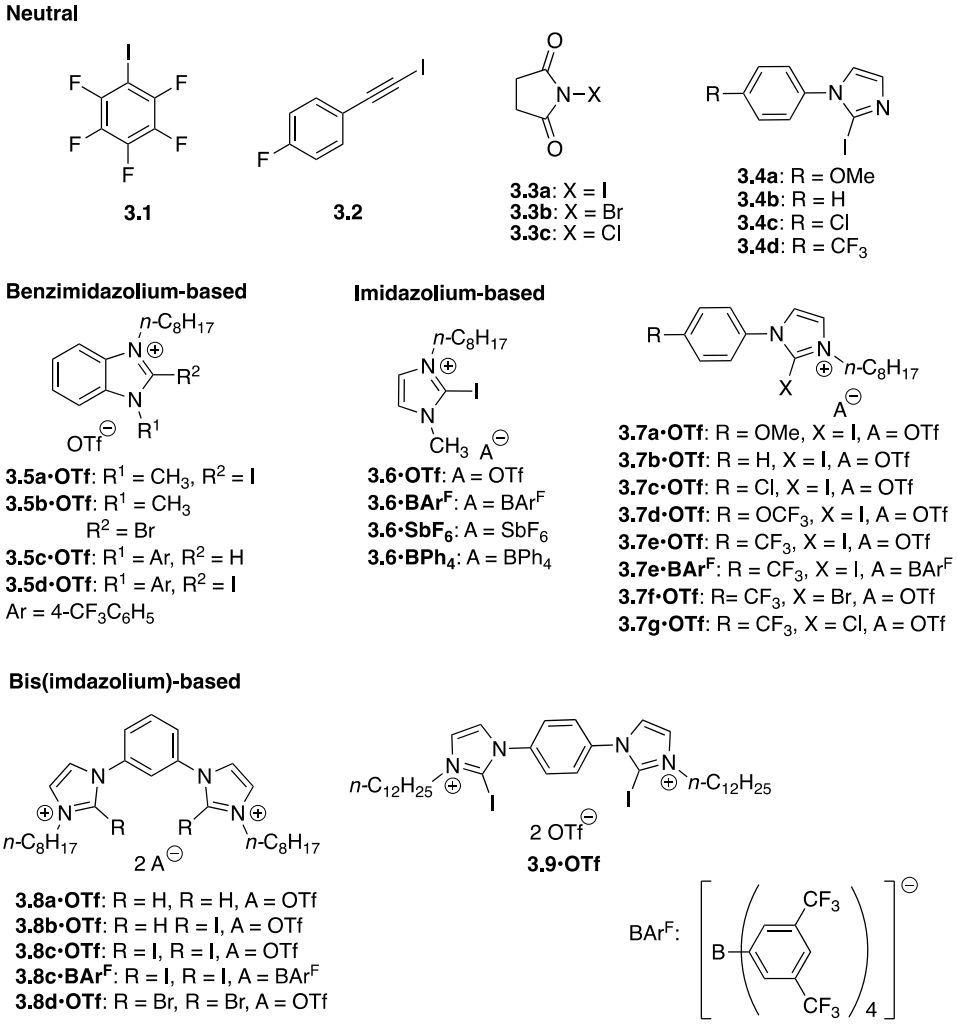



**Figure 3.15.** List of precursors or XBD catalysts studied.

**Table 3.1.** $\Delta\delta(^{31}P)$ measurements for TEPO binding of precursors or catalysts studied[a]

| XBD[a] | $\Delta\delta(^{31}P)$ (ppm) Trial 1[b] | $\Delta\delta(^{31}P)$ (ppm) Trial 2[b] | $\Delta\delta(^{31}P)$ (ppm) Trial 3[b] | Avg $\Delta\delta(^{31}P)$ (ppm)[c] | std dev. |
|---|---|---|---|---|---|
| **3.1** | 0.20 | 0.22 | 0.22 | **0.21** | 0.01 |
| **3.2** | 0.12 | 0.14 | 0.13 | **0.13** | 0.01 |
| **3.3a** | 10.01 | 9.99 | 9.97 | **9.99** | 0.02 |
| **3.3b** | 1.42 | 1.36 | 1.44 | **1.41** | 0.04 |
| **3.3c** | 1.34 | 1.41 | 1.38 | **1.38** | 0.04 |
| **3.4a** | 0.05 | 0.01 | 0.05 | **0.04** | 0.02 |
| **3.4b** | 1.11 | 1.05 | 1.05 | **1.07** | 0.03 |
| **3.4c** | 0.89 | 0.89 | 0.97 | **0.92** | 0.05 |
| **3.4d** | 0.88 | 0.89 | 0.89 | **0.89** | 0.01 |
| **3.5a•OTf** | 4.94 | 4.94 | 4.93 | **4.94** | 0.01 |
| **3.5b•OTf** | 1.77 | 1.64 | 1.61 | **1.67** | 0.09 |
| **3.5c•OTf** | 1.24 | 1.26 | 1.25 | **1.25** | 0.01 |
| **3.5b•OTf** | 5.77 | 5.74 | 5.76 | **5.76** | 0.02 |
| **3.6•OTf** | 4.06 | 4.02 | 4.01 | **4.03** | 0.03 |
| **3.6•BAr$^F$** | 5.75 | 5.65 | 5.66 | **5.68** | 0.06 |
| **3.6•$SbF_6$**[d] | 5.34 | 5.29 | 5.29 | **5.31** | 0.03 |
| **3.6•$BPh_4$**[d] | 4.62 | 4.49 | 4.46 | **4.52** | 0.09 |
| **3.7a•OTf** | 4.70 | 4.68 | 4.68 | **4.69** | 0.01 |
| **3.7b•OTf** | 4.79 | 4.78 | 4.78 | **4.78** | 0.01 |
| **3.7c•OTf** | 5.00 | 5.01 | 5.01 | **5.01** | 0.01 |
| **3.7d•OTf** | 5.12 | 5.10 | 5.11 | **5.11** | 0.01 |
| **3.7e•OTf** | 5.29 | 5.28 | 5.29 | **5.28** | 0.01 |
| **3.7e•BAr$^F$**[e] | 6.24 | 6.29 | 6.23 | **6.25** | 0.03 |
| **3.7f•OTf** | 1.43 | 1.44 | 1.39 | **1.42** | 0.03 |
| **3.7g•OTf** | 1.22 | 1.13 | 1.27 | **1.21** | 0.07 |
| **3.8a•OTf**[f] | 0.94 | 0.99 | 0.98 | **0.97** | 0.03 |
| **3.8b•OTf**[f] | 4.87 | 4.88 | 4.88 | **4.88** | 0.01 |
| **3.8c•OTf**[f] | 4.91 | 4.92 | 5.03 | **4.95** | 0.07 |
| **3.8c•BAr$^F$**[e] | 10.47 | 10.44 | 10.46 | **10.46** | 0.02 |
| **3.8d•OTf**[f] | 2.54 | 2.46 | 2.52 | **2.51** | 0.04 |
| **3.9•OTf**[g] | 4.01 | 3.90 | 3.89 | **3.91** | 0.07 |

[a]Experiments performed at 15 mM TEPO in $CD_2Cl_2$ with 10 equiv XBD unless otherwise indicated. [b]$\Delta\delta(^{31}P)$ = δ(XBD•TEPO complex) – δ(free TEPO). [c]Avg $\Delta\delta(^{31}P)$ values used for correlation. [d]One drop of 2,6-di-*tert*-butylpyridine (DTBP) was added into binding experiment. [e]Saturation occurs at approximately 5 equivalents; 5 equiv of XBD was used. [f]Using 15 equiv of XBD. [g]Using 3 equiv of XBD due to its low solubility.

## IIIa. Low $\Delta\delta(^{31}P)$ Values of Neutral XBDs

TEPO binding with most neutral XBDs (Figure 3.16, e.g. **3.1**−**2**, **3.4**) results in very low $\Delta\delta(^{31}P)$ values (0.04−1.07 ppm), indicating low X-bonding ability; however, X-bonding ability notably increased with a highly electronegative atom attached to the halogen atom (e.g. **3.3a**, $\Delta\delta(^{31}P)$ = 9.99 ppm). Without a

cationic charge on the XBD core, the $\Delta\delta(^{31}P)$ values are < 1.0 ppm and interactions are too weak to observe trends, highlighting the importance of the cationic charge for increasing the X-bonding ability (e.g. **3.4a−4d**). Despite the wide use of neutral XBDs in material science and molecular recognition, this $^{31}P$ NMR quantification method was unable to quantify them.

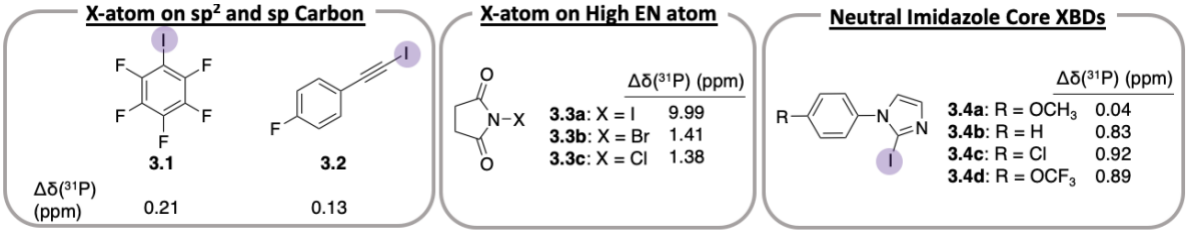



**Figure 3.16.** $\Delta\delta(^{31}P)$ values for neutral XBDs studied.

## IIIb. Structure Effect: Benzimidazolium- *vs* Imidazolium-based XBD

Next, this $^{31}P$ NMR quantification method was investigated to assess the effects of structure and counteranions on X-bonding ability (Figure 3.17). The larger $\Delta\delta(^{31}P)$ value of cationic benzimidazolium-based XBD (**3.5a•OTf**, $\Delta\delta(^{31}P)$ = 4.94 ppm) compared to cationic imidazolium-based XBD (**3.6•OTf**, $\Delta\delta(^{31}P)$ = 4.03 ppm) suggests higher X-bonding ability. This increased X-bonding ability is attributed to the extended aromaticity of the benzimidazolium core. The larger $\Delta\delta(^{31}P)$ value of **5a•OTf** also removes the potential for TEPO binding to be attributed to H-bonding interactions with C4 and C5 protons on the cationic imidazolium core. By increasing the electron deficiency of the benzimidazolium core (**3.5d•OTf**),[21] the largest $\Delta\delta(^{31}P)$ value among the cationic XBD triflates was observed (5.76 ppm). The non-iodinated imidazolium triflate (**3.5c•OTf**) was synthesized, and the $\Delta\delta(^{31}P)$ value was compared to ensure that TEPO is probing X-bonding ability rather than H-bonding ability.[21]

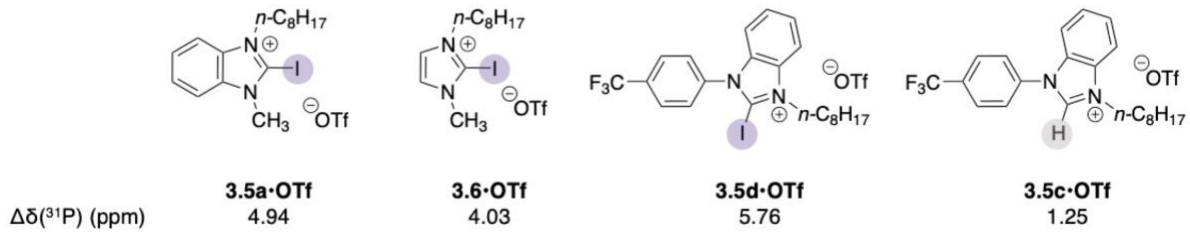



**Figure 3.17.** $\Delta\delta(^{31}P)$ demonstrates structure effect.

## IIIc. Counteranion Effect

The counteranion effect on X-bonding ability was studied by undergraduate student Teresa Tang (Figure 3.18A). Teresa investigated the effect of four different counteranions (OTf, $BAr^F$, $SbF_6$, and $BPh_4$) for imidazolium **3.6** on X-bonding interactions.[20,22] Initially, either no signal or a broad signal was detected in the $^{31}P$ NMR binding experiments when testing **3.6•BAr$^F$, 3.6•SbF$_6$** and **3.6•BPh$_4$**. We attributed this observation to the potential coordination of $[SbF_6]^-$ anions via a fluorine bridge, resulting in signal suppression.[54] In addition, $[BPh_4]^-$ is prone to hydrolysis,[55] to form an acid that binds to TEPO, thereby causing no signal to be observed. Therefore, we decided to add a hindered base, 2,6-di-tert-butylpyridine (DTBP), to abstract any acid that might be formed. A control experiment demonstrated that the addition of DTBP can recover the $^{31}P$ signal. Overall, an increase of signal to noise ratio is observed when DTBP was added in the $^{31}P$ quantification experiment (Figure 3.18B). The $\Delta\delta(^{31}P)$ values for **3.6•OTf, 3.6•BAr$^F$, 3.6•SbF$_6$** and **3.6•BPh$_4$** with DTBP follow the general trend of anion-coordinating ability. The largest $\Delta\delta(^{31}P)$ value (5.68 ppm) was measured for **3.6•BAr$^F$** matching the decreased coordinating ability for the $BAr^{F-}$ counterion and hence increased X-bonding ability. The $\Delta\delta(^{31}P)$ values for **3.6•SbF$_6$** and **3.6•BPh$_4$** were observed to generally follow the trend for anion-coordinating ability.[55]

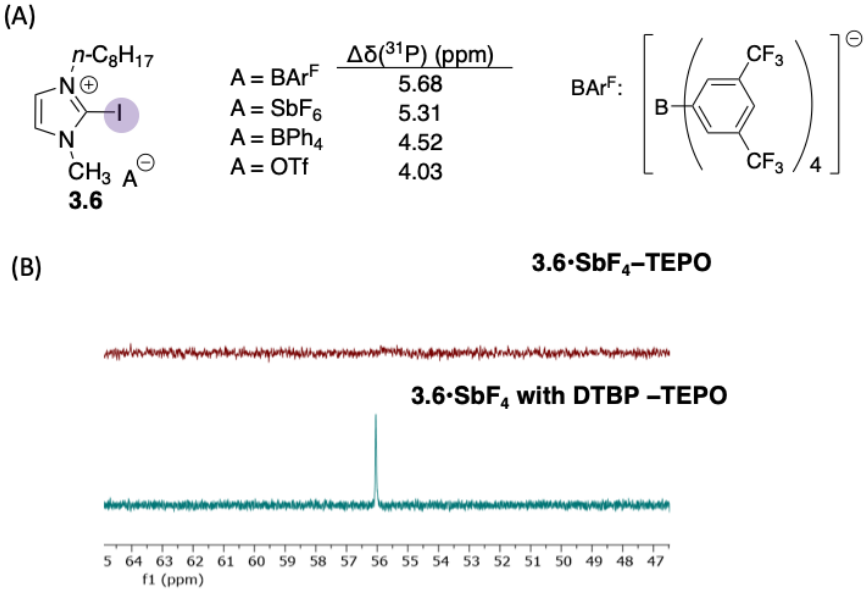



**Figure 3.18.** $\Delta\delta(^{31}P)$ demonstrates counteranion effect.

**IIId. Denticity Effect: Bis(imidazolium)-based XBDs**

To investigate the denticity effect based on substituent pattern for X-bonding ability, bis(imidazolium) salts **3.8**–**3.9** were synthesized and their X-bonding abilities were quantified using $^{31}$P NMR spectroscopy. The results were categorized into three classes for discussion. The first class includes the bis(imidazolium) triflate **3.8•OTf** (Figure 3.19). The Job plot indicated a 1:1 binding pattern between XBD and TEPO. However, similar $\Delta\delta(^{31}P)$ values were observed for meta-bis-(imidazolium) triflate **3.8c•OTf**, phenyl-imidazolium **3.6•OTf** and the mono-iodinated **3.8b•OTf**. These results suggest that the steric interactions of the meta-substituted bis(imidazolium) triflate do not favor bidentate X-bonding interactions with TEPO. In the second category, using a weakly coordinating counteranion, $BAr^{F-}$, led to distinct observations. Meta-substituted bis(imidazolium) $BAr^F$ **3.8c•BAr$^F$** exhibit nearly double the $\Delta\delta(^{31}P)$ value compared to unsubstituted **3.6•BAr$^F$**, suggesting that the bidentate X-bonding interactions with TEPO occurred with the weakly coordination $BAr^F$ counterion. This observation is consistent with previous crystallographic studies on imidazolium triflates, which highlighted interactions between the counteranion and halogen atoms, suggesting that charge separation enhances denticity.[20,42]

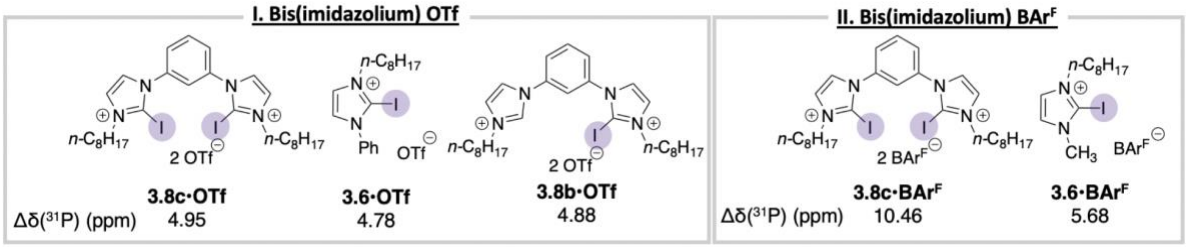



**Figure 3.19.** $\Delta\delta(^{31}P)$ values of bis(imidazolium) salts **3.8** and comparisons.

In the third category, we examined the denticity effect based on the substituent pattern by synthesizing and quantifying *meta*- (**3.8c•OTf**) and *para*-bis(imidazolium) triflate (**3.9•OTf**) (Figure 3.20). Due to the low solubility of the para-substituted bis(imidazolium) **3.9•OTf**, $\Delta\delta(^{31}P)$ values were collected using 3.0 equivalents of XBD (relative to TEPO) for the direct comparison between meta-substituted **3.8c•OTf** (2.58 ppm) and para-substituted bis(imidazolium) **3.9•OTf** (3.91 ppm). The *para*-substituted bis(imidazolium) **3.9•OTf** showed a larger $\Delta\delta(^{31}P)$ value, suggesting enhanced bidentate capability.

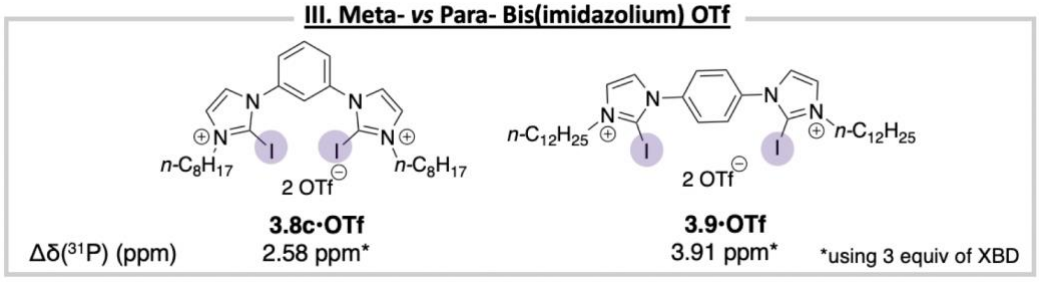
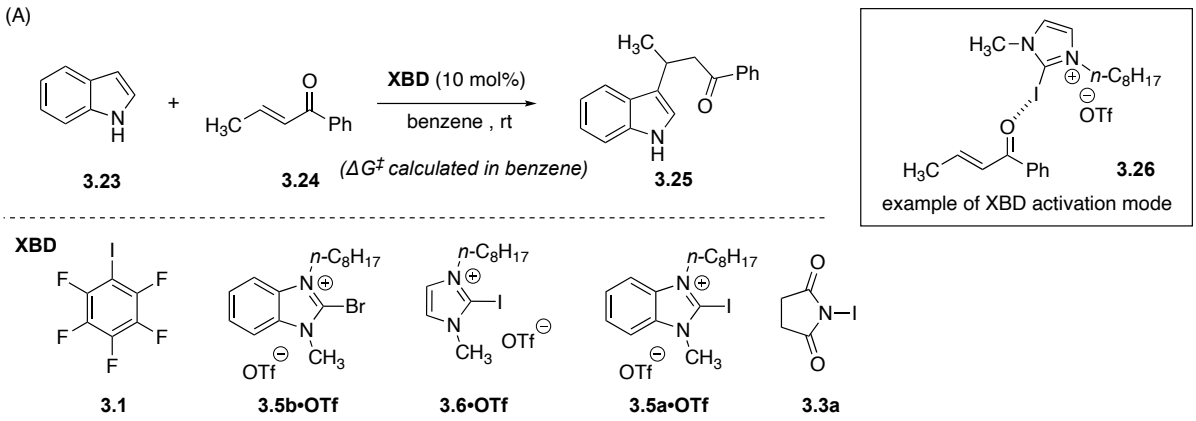



**Figure 3.20.** Δδ($^{31}$P) values of meta- and para-bis(imidazolium) triflates.

## IIIe. Correlation of Δδ($^{31}$P) and ΔG‡ values

The ability to correlate $^{31}$P NMR data with thermodynamic properties was explored by comparing measured Δδ($^{31}$P) values to previously calculated activation free energy (ΔG‡**)** values for reactions catalyzed by XBDs. This comparison was conducted using data for the Friedel−Crafts addition of indole **3.23** to *trans*-crotonophenone (**3.24**) catalyzed by XBD organocatalysts in benzene (Figure 3.21), reported by Breugst and coworkers.[43] A direct comparison between Δδ($^{31}$P) and calculated ΔG‡ values demonstrated a strong correlation ($R^2$ = 0.775, Figure 3.22). Considering the logarithm form of the Arrhenius equation, log Δδ($^{31}$P) values show a stronger correlation with ΔG‡ ($R^2$ = 0.899) compared to the direct Δδ($^{31}$P) values. This strong correlation between log Δδ($^{31}$P) values and calculated ΔG‡ values demonstrates the capability of correlating $^{31}$P NMR shifts with thermodynamic properties. The data also suggest that TEPO serves as a suitable isostere for carbonyl activation-type reactions.




(B) Δδ($^{31}$P) and calculated ΔG‡ values

| XBD | Δδ($^{31}$P) (ppm) | *ln* Δδ($^{31}$P) | *log* Δδ($^{31}$P) | ΔG‡ (kcal/mol)[a] |
|---|---|---|---|---|
| **3.1** | 0.21 | -1.56 | -0.68 | +41.0 |
| **3.5b•OTf** | 1.67 | 0.51 | 0.22 | +38.3 |
| **3.6•OTf** | 4.03 | 1.39 | 0.61 | +32.5 |
| **3.5a•OTf** | 4.94 | 1.60 | 0.69 | +31.5 |
| **3.3a** | 9.99 | 2.30 | 1.00 | +30.3 |

[a]Calculated activation free energies were reported by Breugst and coworkers

**Figure 3.21.** (A) a Friedel−Crafts addition catalyzed by XBD organocatalysts; (B) Δδ($^{31}$P) values and ΔG‡ values calculated in benzene for XBDs.[43]

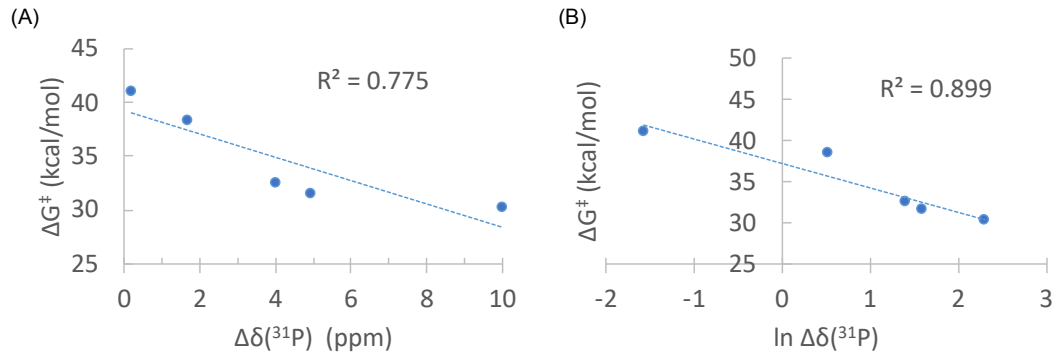



**Figure 3.22.** (A) Correlation between ΔG‡ values (calculated in benzene[43]) and Δδ($^{31}$P) values. (B) Correlation between ΔG‡ values (calculated in benzene[43]) and ln Δδ($^{31}$P) values. (C) Correlation between ΔG‡ values (calculated in benzene[7]) and log Δδ($^{31}$P) values.

## IIIf. Kinetic Analysis of Catalytic Activity in Friedel−Crafts Indole Additions

In order to evaluate the capability of TEPO binding and $^{31}$P NMR quantification to predict catalytic activity, the XBDs were investigated as catalysts in a Friedel−Crafts indole addition. The addition of indole to *trans*-crotonophenone was chosen as the model reaction (Figure 3.23A).[43] Trimethyl(phenyl)silane (Ph−TMS) was used as an NMR internal standard. The observed rate constants

($k_{obs}$) of the Friedel–Crafts addition reaction in $CD_2Cl_2$ were monitored using $^1H$ NMR spectroscopy (Figure 3.23B).

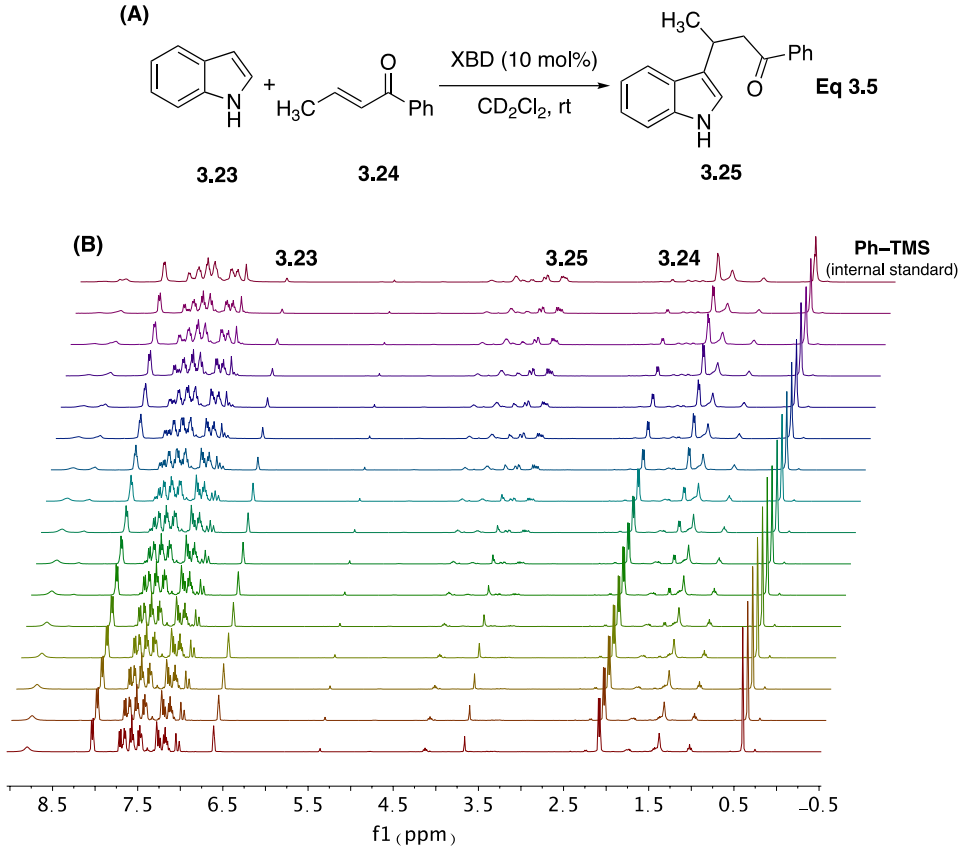



**Figure 3.23.** (A) The Friedel-Crafts reaction of indole **3.23** to *trans*-crotonophenone **3.24** as a model reaction. (B) Using $^1H$ NMR spectroscopy to monitor the consumption of indole **3.23** and formation of product **3.25**.

An induction period was observed in the initial phase of the kinetic reaction for some of the XBDs (Figure 3.24). The induction period was attributed to the dissociation of XBDs, which generates the active catalyst $\mathbf{3.7}^+$ (Scheme 3.2A).[43] Additionally, a correlation was noted between the induction period and the electron deficiency of the XBDs, with shorter induction periods observed for highly electrophilic R–I groups.

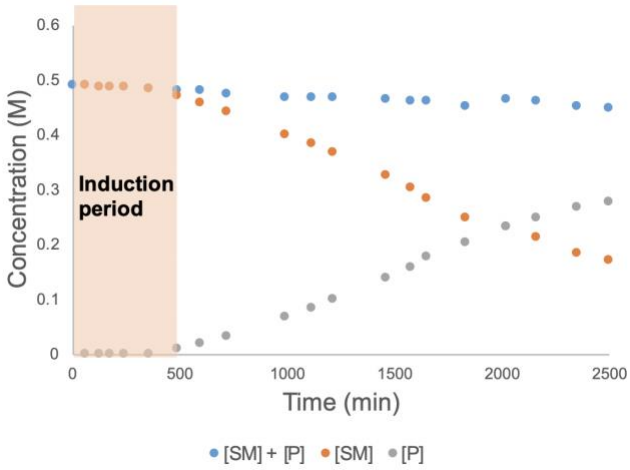
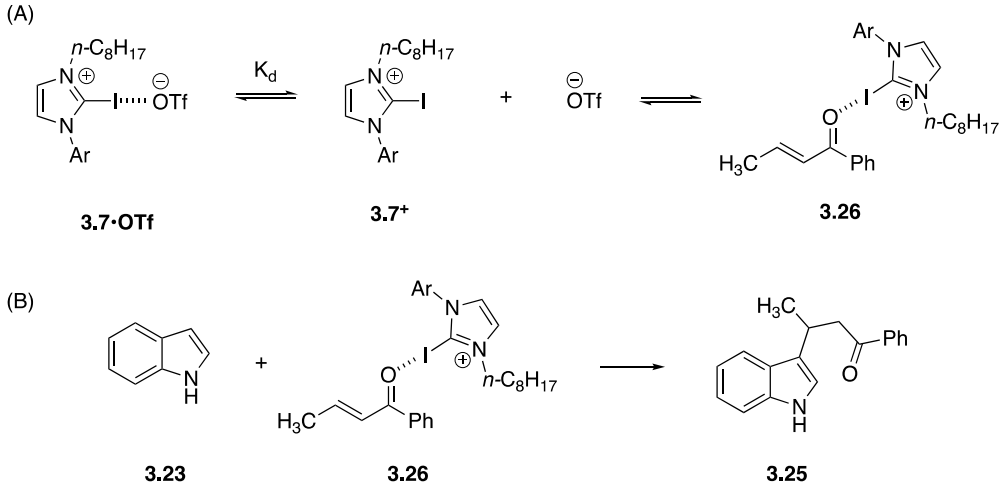



**Figure 3.24.** Reaction profile of indole addition to *trans*-crotonophenone catalyzed by **3.7b•OTf**.




**Scheme 3.2.** (A) Dissociation of XBD triflate salts and then association with *trans*-crotonophenone. (B) Indole addition to activated *trans*-crotonophenone.

In the post-induction period, the indole disappearance curve fit the first-order kinetics model. Moreover, we observed that if the conversion of the starting indole is more than 10%, the linear relationship between ln[Indole] vs time (min) is higher ($R^2$ = 0.988, 0.991 *vs* 0.996) (Figure 3.25A−C).

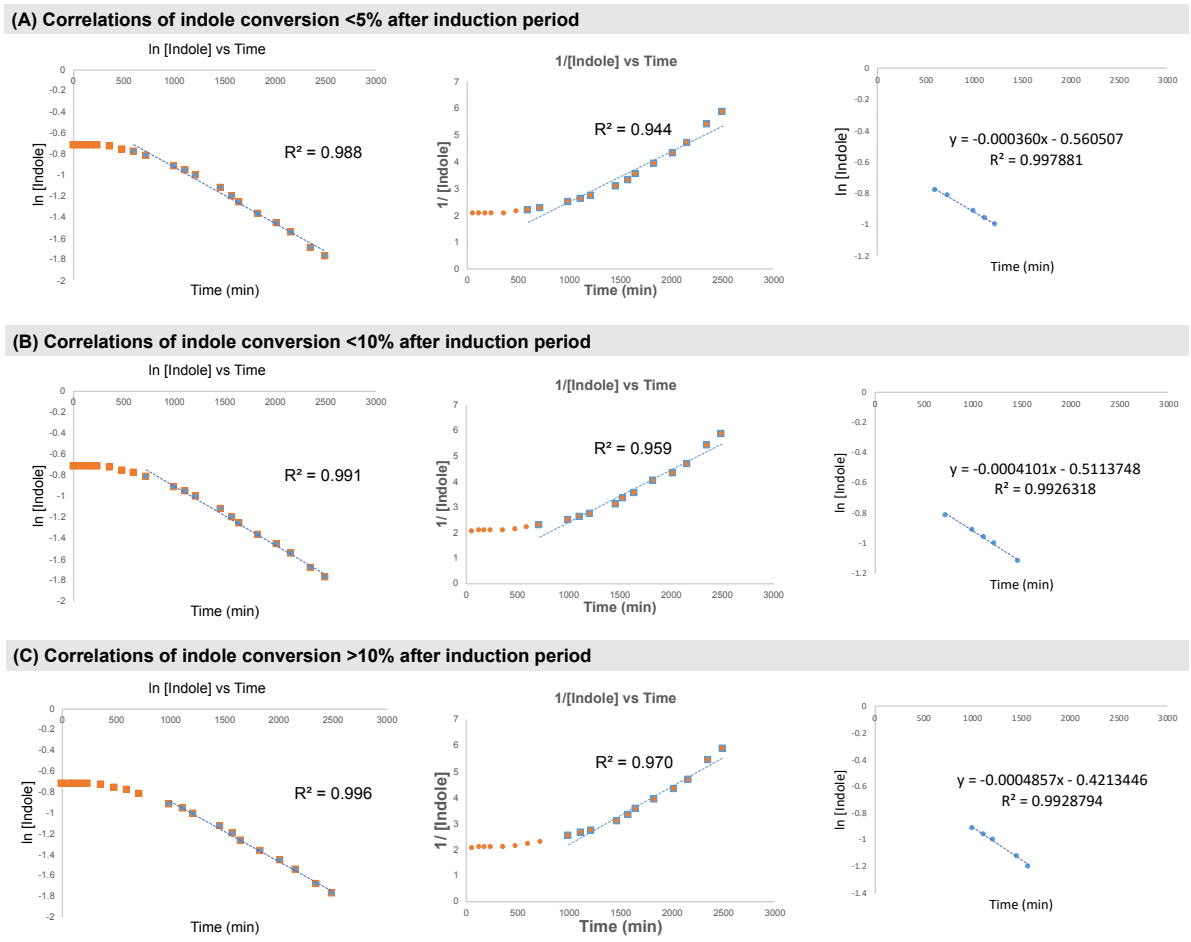



**Figure 3.25.** Examples of initial rate constant calculations for the model Friedel–Crafts addition catalyzed by **3.7b•OTf**.

After conducting a detailed analysis of the induction period kinetics, the $k_{obs}$ values were calculated according to a linear fit from the first-order plot for ln[Indole] vs time (min), using the initial five data points after more than 10% of indole was consumed (Figure 3.25C). These kinetic results are summarized in Table 3.2.

**Table 3.2.** $k_{obs}$ of indole Addition to t*rans*-crotonophenone reaction catalyzed by XBDs in $CD_2Cl_2$.

| entry[a] | XBD | Avg $\Delta\delta(^{31}P)$ (ppm)[c] | $k_{obs} \times 10^{-4}$ ($min^{-1}$) |
|---|---|---|---|
| 1 | **3.1** | 0.21 | NR[b] |
| 2 | **3.2** | 0.13 | -- |
| 3 | **3.3a** | 9.99 | --[c] |
| 4 | **3.3b** | 1.41 | --[c] |
| 5 | **3.3c** | 1.38 | -- |
| 6 | **3.4a** | 0.04 | -- |
| 7 | **3.4b** | 1.07 | -- |
| 8 | **3.4c** | 0.92 | -- |
| 9 | **3.4d** | 0.89 | -- |
| 10 | **3.5a•OTf** | 4.94 | 4.57 |
| 11 | **3.5b•OTf** | 1.67 | -- |
| 12 | **3.5c•OTf** | 1.25 | -- |
| 13 | **3.5b•OTf** | 5.76 | 13.00 |
| 14 | **3.6•OTf** | 4.03 | NR[b] |
| 15 | **3.6•BAr$^F$** | 5.68 | 5.77 |
| 16 | **3.6•$SbF_6$** | 5.31 | --[d] |
| 17 | **3.6•$BPh_4$** | 4.52 | --[d] |
| 18 | **3.7a•OTf** | 4.69 | 2.72 |
| 19 | **3.7b•OTf** | 4.78 | 4.86 |
| 20 | **3.7c•OTf** | 5.01 | 6.96 |
| 21 | **3.7d•OTf** | 5.11 | 7.16 |
| 22 | **3.7e•OTf** | 5.28 | 8.51 |
| 23 | **3.7e•BAr$^F$** | 6.25 | 11.47 |
| 24 | **3.7f•OTf** | 1.42 | NR[b] |
| 25 | **3.7g•OTf** | 1.21 | NR[b] |
| 26 | **3.8a•OTf**[h] | 0.97 | NR[b] |
| 27 | **3.8b•OTf**[h] | 4.88 | 8.23 |
| 28 | **3.8c•OTf**[h] | 4.95 | 9.21 |
| 29 | **3.8c•BAr$^F$** | 10.46 | 32.64 |
| 30 | **3.8d•OTf** | 2.51 | NR[b] |
| 31 | **3.9•OTf** | 3.91 | 8.28 |

[a]Observed rate constant ($k_{obs}$) of the XBD catalyzed Friedel−Crafts addition reaction in $CD_2Cl_2$ monitored using $^1H$ NMR spectroscopy [b]No reaction observed; $k_{obs}$ assumed to be zero. [c]Not reported; observed rate is attributed to *in-situ* formation of elemental halogens (e.g. $I_2$) rather than the respective XBD. [d]No reaction observed with DTP added.

## IIIg. Correlation of $\Delta\delta(^{31}P)$ and Catalytic Activity

The measured $\Delta\delta(^{31}P)$ values for XBDs were correlated to catalytic activity for a Friedel−Crafts indole addition (Eq 1 and Figure 3.26A).[28–30] When $\Delta\delta(^{31}P)$ is less than 4.03 ppm, such as for neutral XBDs and imidazolium **6•OTf**, the X-bonding interaction is too weak to facilitate the indole addition (Table 3.2, entries 1, 14, 24−26, and 30). XBDs with certain counteranions (Table 3.2, entries 16−17) could

not catalyze the Friedel−Crafts indole addition reaction, possibly due to the low dissociation tendancy of $[SbF_6]^-$ and $[BPh_4]^-$ counteranions. This resulted in reduced X-bonding ability because of the partial binding of iodine and the counteranions. When using *N*-bromo- and iodo-succinimide (Table 3.2, entries 3−4) as XBDs in the reaction, elemental halogens (e.g. $I_2$) were generated *in-situ*. These elemental halogens have superior X-bonding donating ability and would catalyze the reaction. Consequently, $k_{obs}$ values were not reported.

For the XBDs that have the capability to catalyze the Friedel−Crafts indole addition, a high correlation is observed between $\Delta\delta(^{31}P)$ values and $k_{obs}$ within the sub-class of monodentate triflate XBDs ($R^2$ = 0.922, Figure 3.26A). Moreover, a linear relationship was observed for Hammett σ parameters to the rate constants $k_{obs}$ for para-substituted phenyl-imidazolium triflate XBDs (Table 3.2, entries 18−22 and Figure 3.26B). The XBD with highest catalytic activity, bisimidazolium $BAr^F$ salt **3.8c•BAr$^F$** (Table 3.2, entry 29), was successfully predicted by the largest $\Delta\delta(^{31}P)$ value (10.46 ppm). Moreover, a linear correlation for XBDs ($R^2$ = 0.991) was observed within the sub-class of $BAr^F$ XBDs (Table 3.2, entries 15, 23, and 29). These correlations support that TEPO binding and $\Delta\delta(^{31}P)$ values can be a predictor of catalytic activity for carbonyl activation-type reactions within structural classes of XBDs.

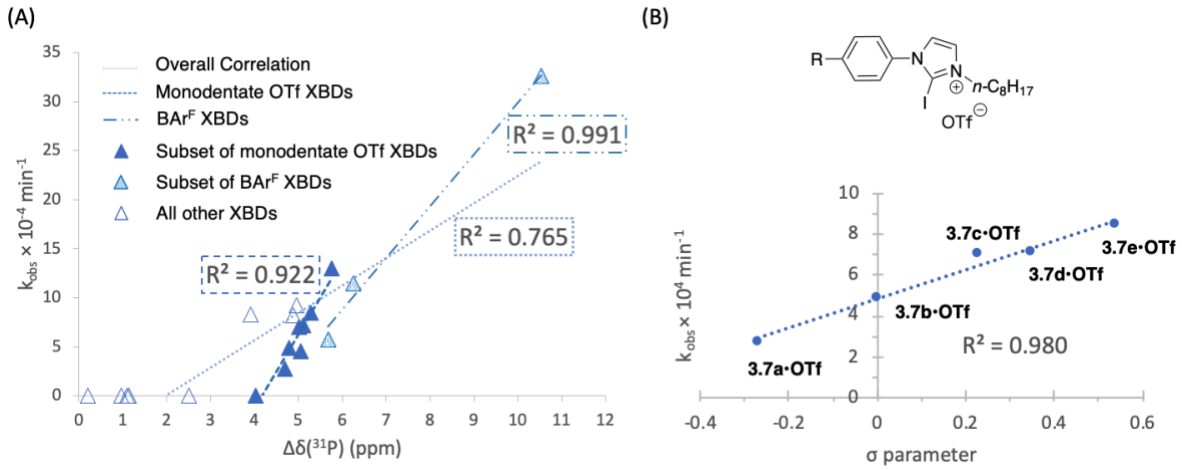



**Figure 3.26.** (A) Relationship between $\Delta\delta(^{31}P)$ and $k_{obs}$ (Table 3.1) for the Friedel−Crafts addition reaction of indole **3.23** to *trans*-crotonophenone **3.24** in $CD_2Cl_2$. (B) Correlation of Hammett σ parameters and $k_{obs}$.

## IV. Conclusions

In conclusion, a commercially available TEPO probe proved effective in quantifying X-bonding ability using $^{31}P$ NMR spectroscopy. Additionally, we demonstrated that TEPO binding serves as a sensitive indicator for the analysis of residual acidic impurities. We successfully correlated $\Delta\delta(^{31}P)$ values for TEPO binding with activation free energy values previously reported for a Friedel−Crafts indole addition reaction with *trans*-crotonophenone. Combining the previous work in our group on the quantification of H-bonding ability, we were able to build a common scale to make a comparison of several non-covalent interactions (Figure 3.27). X-bonding is a relatively weak non-covalent interaction with $\Delta\delta(^{31}P)$ values for TEPO binding up to 10.46 ppm compared to that of H-bonding (0.2−24.6 ppm)[5] and Lewis acid-ligand/counterion complexes (0.1−48.2 ppm).[3] As a result of these developments, our method has been adopted by fellow researchers to confirm the purity and X-bonding ability of their newly designed XBD catalysts.[44–53]

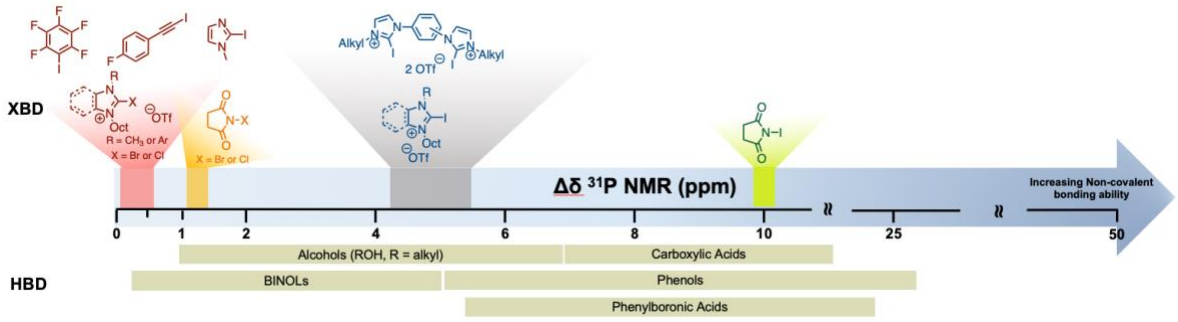



**Figure 3.27.** A unified scale of $\Delta\delta(^{31}P)$ values for TEPO binding in comparison to other non-covalent interactions.

## V. Experimental procedure and characterization

### Va. General Information

Materials **3.4−3.9** were synthesized according to procedures previously reported in literature.[20,21,23,43] Anhydrous dichloromethane ($CH_2Cl_2$) solvent was dispensed from a solvent purification system that passes solvent through two columns of dry neutral alumina. Deuterated dichloromethane ($CD_2Cl_2$) was obtained from Acros Organics. Triethylphosphine oxide (TEPO) was obtained from Sigma Aldrich.

**Procedure for TEPO Purification.** Wet TEPO (1 mL) was dissolved in dry $CH_2Cl_2$ (250 mL) and dried by rotary-evaporation. This process was repeated until the TEPO crystalized as the solution evaporated. The flask containing the resulting crystals was then placed under vacuum and filled with argon gas for storage.

**Synthesis and Physical Methods.** All reactions were performed in oven-dried and Ar-purged glassware (with aluminum foil wrapped around for dark conditions if necessary). All nuclear magnetic resonance (NMR) spectra were obtained on Bruker Nanobay AVIIIHD 400 (400 MHz for $^{1}H$; 100 MHz for $^{13}C$ 162 MHz for $^{31}P$) equipped with an autosampler and/or Varian VNMRS 600 (600 MHz for $^{1}H$; 151 MHz for $^{13}C$; 262 MHz for $^{31}P$), at room temperature. A 500 MHz Bruker Advance DRX (500 MHz for $^{1}H$; 202 MHz for $^{31}P$) was used for variable temperature experiments. Chemicals shifts were reported in parts per million (δ scale) and referenced according to TEPO as an external standard in $CD_2Cl_2$ for $^{31}P$ NMR signals.

## Vb. Experimental Procedures

**Experimental Procedure for TEPO Measurements:** The general procedure for measuring $^{31}P$ NMR shifts upon TEPO binding was adapted from several prior literature reports, including Gutmann and Beckett[39,40] for original TEPO studies, Hilt and coworkers[1,2] for measuring H-bond abilities of thioureas, and our group for NMR quantification of H-bond-activating effects.[5] An oven-dried 20-mL volumetric flask was purged with argon and charged with TEPO and $CH_2Cl_2$ was added to make the TEPO stock solution with concentration of 0.083 M. The respective XBDs **3.1−9•OTf** (10 equiv, 0.083 mmol, unless otherwise indicated) dissolved in 0.25 mL of $CH_2Cl_2$ and 0.2 mL of $CD_2Cl_2$, were added directly into an oven-dried and argon-purged NMR tube. Aliquots of the TEPO stock solution (0.1 mL) were transferred into the NMR tube and capped with a rubber septum. The $^{31}P$ NMR spectrum of each sample was immediately measured at room temperature with 32 scans and the $^{31}P$ NMR chemical shift was compared to a standard of TEPO solution (15 mM) to determine $\Delta\delta(^{31}P)$ values.

**General Procedure A- Halogenation:** Under an argon atmosphere, the respective imidazole-derivative was dissolved in dry THF (0.25 M). After cooling the solution to −78 °C, *n*-butyllithium (1.3 equiv,

unless otherwise indicated) was slowly added dropwise via a syringe and the solution was stirred at −78 °C for 2 h. A solution of the respective halogen source (1.2 equiv, unless otherwise indicated) in dry THF (1.0 M) was added dropwise via a syringe. The reaction flask was wrapped in aluminum foil and the reaction solution was stirred at room temperature overnight and then quenched with a saturated solution of $Na_2S_2O_3$. The crude product was extracted with $CH_2Cl_2$ and washed with a saturated brine solution. The collected organic layer was dried with $Na_2SO_4$ and vacuum filtered through a fritted filter. The crude product was concentrated by rotary evaporation and was purified using silica gel column chromatography.

**General Procedure B-Octylation:** The following procedure was modified from the octylation preparation developed by Huber and coworkers,[10] Minakata and coworkers[21] and Breugst and coworkers.[43] Under an argon atmosphere, the respective haloimidazole-derivative was dissolved in dry $CH_2Cl_2$ (0.125 M). Octyl triflate (1.5−4.8 equiv, specific amount of each substrate stated in its respective procedure) was added via a syringe. The reaction flask was wrapped in aluminum foil and the reaction solution was stirred at room temperature overnight. The resulting crude product was then purified using the purification procedure described below.

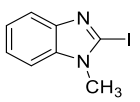
**Purification Procedure for XBD triflate salts.** XBD triflate salts were purified by a procedure adapted for the purification of imidazolium triflate salts as reported by Minakata and coworkers.[21] After the octylation of a neutral halogenated-imidazole derivative, the $CH_2Cl_2$ was removed under reduced pressure and the residue was washed with a $CH_2Cl_2$/hexanes mixture (1:5 *v*/*v*, 5 × 10 mL) to remove excess octyl triflate. The crude product with triflic acid was extracted with $CH_2Cl_2$ (3 × 10 mL) and saturated $Na_2CO_3$ aqueous solution (20 mL). The collected organic layer was dried over $Na_2SO_4$ and the solvent was evaporated. The crude product was purified by column chromatography on silica gel (MeOH/$CH_2Cl_2$, 1:9 *v*/*v*) twice to obtain the pure XBD triflate salts. The purity of the XBD salts was examined by a TEPO binding experiment as detailed in the Experimental Procedure for TEPO Measurements. A comparison of spectra before and after purification is shown in Figure 3.12.

**General Procedure C-Anion Exchange:** The following procedure was modified from the anion exchange procedure develop by Huber and coworkers,[10] Minakata and coworkers[21], and Breugst and coworkers.[43] Under an argon atmosphere, the respective imidazolium-based triflate salt was dissolved in a solvent mixture (the specific solvent composition ratios are indicated in its respective procedure). A metal salt containing the desired anion (1.3 equiv) was added to the reaction flask. The reaction flask was wrapped in aluminum foil and the reaction solution was stirred at room temperature overnight. The resulting crude product was then concentrated by rotary evaporation and purified by column chromatography (the specific silica gel column conditions are indicated in its respective procedure).

**Synthesis of Octyl Triflate:** The following procedure was modified from the preparation of alkyl triflates developed by Zeldin and coworkers.[56] Under an argon atmosphere, 1-octanol and 2,6-dimethylpyridine (1.6 equiv) were dissolved in dry $CH_2Cl_2$ (2.0 M). After cooling the solution to –78 °C, triflic anhydride (1.2 equiv) was slowly added dropwise via a syringe to the reaction flask. The reaction mixture was allowed to warm up to room temperature while being stirred for 20 min. The crude product was concentrated by rotary evaporation and re-dissolved in hexanes. The hexanes solution was filtered through a silica plug and concentrated down to yield octyl triflate as a clear liquid.

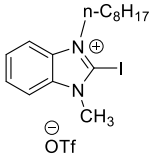
**Preparation of 2-iodo-3-octyl-1methyl-1H-benzimidazol-3-ium trifluoromethanesulfonate (3.5a•OTf):**

*Step 1: Synthesis of 1-methyl-2-iodo-1H-benzimidazole (**3.26**)*



This compound was synthesized following general procedure A with benzimidazole as the imidazole-derivative and $I_2$ as the halogen source. Yield: 33% (1.54 mmol, 0.397 g) as a white solid. $^1$H NMR spectral data matches that of a previous report.[57]

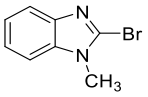
*Step 2: Synthesis of 2-iodo-3-octyl-1methyl-1H-benzimidazol-3-ium trifluoromethanesulfonate (**3.5a•OTf**)*



This compound was synthesized following general procedure B from **3.26** and octyl triflate (1.5 equiv). The reaction mixutre was purified according to the Purification Procedure for XBD triflate salts. Yield: 87% (1.33 mmol, 0.697 g) as a white solid. $^1$H NMR spectral data matches that of a previous report.[20]

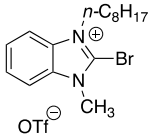
**Preparation of 2-bromo-3-octyl-1methyl-1H-benzimidazol-3-ium trifluoromethanesulfonate (3.5b•OTf):**

*Step 1: Synthesis of 1-methyl-2-bromo-1H-benzlimidazole (**3.27**)*



This compound was synthesized following general procedure A from benzimidazole and $CBr_4$ as the halogen source. Yield: 33% (1.65 mmol, 0.347 g) as a light brown solid. $^1$H NMR spectral data matches that of a previous report.[43]

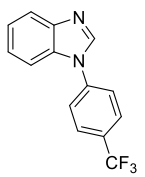
*Step 2: Synthesis of 2-bromo-3-octyl-1methyl-1H-benzimidazol-3-ium trifluoromethanesulfonate (**3.5b•OTf**)*



This compound was synthesized following general procedure B from **3.27** and octyl triflate (1.5 equiv). The reaction mixutre was purified according to the Purification Procedure for XBD triflate salts. Yield: 53% (0.53 mmol, 0.25 g) as a brownish yellow solid. $^1$H NMR spectral data matches that of a previous report.[20]

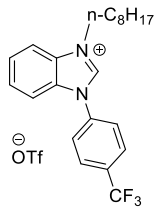
**Preparation of 2H-3-octyl-1phenyl-1H-benzimidazol-3-ium trifluoromethanesulfonate (3.5c•OTf):**

*Step 1: Synthesis of 1-(4-trifluoromethylphenyl)-2H-1H-benzimidazole (**3.28**)*



This compound was synthesized following the procedure reported by Minakata and coworkers. Yield: 47% (7.05 mmol, 1.50 g) as white solid. $^1$H NMR spectral data matches that of a previous report.[21]

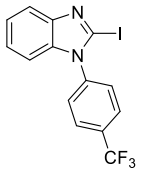
*Step 2: Synthesis of 2H-3-octyl-1-(4-trifluoromethylphenyl)-1H-benzimidazol-3-ium trifluoromethanesulfonate (**3.5c•OTf**)*




This compound was synthesized following general procedure B from **3.28** and octyl triflate (2.8 equiv). The reaction mixutre was purified according to the Purification Procedure for XBD triflate salts. Yield: 63% (0.71 mmol, 0.34 g) as a white solid. $^1$H NMR spectral data matches that of a previous report.[21]

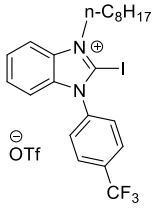
**Preparation of 2H-3-octyl-1-(4-trifluoromethylphenyl)-1H-benzimidazol-3-ium trifluoromethanesulfonate (3.5d•OTf):**

*Step 1: Synthesis of 1-(4-trifluoromethylphenyl)-2-iodo-1H-benzimidazole (**3.29**)*




This compound was synthesized following general procedure A from 1-(4-trifluoromethylphenyl)-2H-1H-benzimidazole as the imidazole-derivative and $I_2$ as the halogen source. Yield: 73% (4.13 mmol, 1.40 g) as a yellow solid. $^1$H NMR spectral data matches that of a previous report.[21]

*Step 2: Synthesis of 2-iodo-3-octyl-1-(4-trifluoromethylphenyl)-1H-benzimidazol-3-ium trifluoromethanesulfonate (**3.5d•OTf**)*




This compound was synthesized following general procedure B from **3.29** and octyl triflate (2.8 equiv). The reaction mixutre was purified according to the Purification Procedure for XBD triflate salts. Yield: 78% (2.34 mmol, 1.40 g) as a white solid. $^1$H NMR spectral data matches that of a previous report.[21]

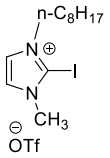
**Preparation of 2-iodo-3-octyl-1methyl-1H-imidazol-3-ium trifluoromethanesulfonate (3.6•OTf):**

*Step 1: Synthesis of 1-methyl-2-iodo-1H-imidazole (**3.30**)*



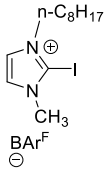

This compound was synthesized following general procedure A from imidazole as the imidazole-derivative and $I_2$ as the halogen source. Yield: 69% (5.52 mmol, 1.15 g) as a white solid. $^1$H NMR spectral data matches that of a previous report.[57]

*Step 2: Synthesis of 2-iodo-3-octyl-1methyl-1H-imidazol-3-ium trifluoromethanesulfonate (**3.6•OTf**)*



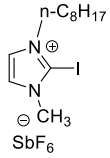
This compound was synthesized following general procedure B from **3.30** and octyl triflate (1.5 equiv). The reaction mixutre was purified according to the Purification Procedure for XBD triflate salts. Yield: 82% (4.53 mmol, 2.13 g) as a white solid. $^1$H NMR spectral data matches that of a previous report.[10]

**Preparation of 2-iodo-3-octyl-1methyl-1H-imidazol-3-ium tetrakis[3,5-bis(trifluoromethyl)phenyl]borate (3.6•BAr$^f$):**



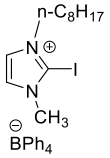
This compound was synthesized following general procedure C from **3.6•OTf** and NaBAr$^F$ as the metal salt. A mixture of ($CH_2Cl_2$/MeOH, 3:1 *v/v*) (12 mM) was used as reaction solvent. The crude product was purified by column chromatography on silica gel (MeOH/$CHCl_3$, 1:9 *v*/*v*). Yield: 89% (0.98 mmol, 1.16 g) as a pink solid. $^1$H NMR spectral data matches that of a previous report.[10]

**Preparation of 2-iodo-3-octyl-1methyl-1H-imidazol-3-ium hexaflurorantimonate (6•$SbF_6$):[10]**



This compound was synthesized following general procedure C from **3.6•OTf** and $AgSbF_6$ as the metal salt. Yield: 63% (1.58 mmol, 0.88 g) as a clear solid. A mixture of ($CHCl_3$/$Et_2O$, 1:1 *v/v*) (12 mM) was used as the reaction solvent. The crude solution was filtered through a celite pad with diethyl ether as the eluent before being concentrated down. The crude product was purified by column chromatography on silica gel (MeOH/$CHCl_3$, 1:9 *v*/*v*). $^1$H NMR (400 MHz, $CDCl_3$): δ 7.67 (s, 1H), 7.57 (s,1H), 4.14 (t, *J* = 7.50 Hz, 2H), 3.92 (s, 3H), 1.84 (s, 2H), 1.31 (d, *J* = 47.1 Hz, 10H), 0.88 (s, 3H); $^{13}$C NMR (100 MHz, $CDCl_3$) δ 127.2, 125.6, 94.1, 53.3, 39.8, 31.7, 29.6 , 29.0, 29.0, 22.6, 14.1; HRMS (ESI) m/z: $[M - SbF_6]^+$ Calcd for $C_{12}H_{22}IN_2$ 321.0822; Found 321.0814.

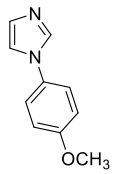
**Preparation of 2-iodo-3-octyl-1methyl-1H-imidazol-3-ium tetraphenylborate (3.6•$BPh_4$):[10]**



This compound was synthesized following general procedure C from **3.6•OTf** and $NaBPh_4$ as the metal salt. The crude product was purified by column chromatography on silica gel (MeOH/$CHCl_3$, 1:9 *v*/*v*). Yield: 86% (1.76 mmol, 1.13 g) as a white solid. $^1$H NMR (400 MHz, $CDCl_3$): δ 7.46 (s, 8H), 7.00 (t, *J* = 7.47 Hz, 8H), 6.86 (t, *J* = 7.47 Hz, 4H), 6.14 (s, 1H), 6.00 (s, 1H). 2.98 (s, 3H), 1.40 (m, 14H), 0.89 (t, *J* = 6.76 Hz, 3H); $^{13}$C NMR (100 MHz, $CDCl_3$) δ 164.8, 164.2, 163.8, 163.3, 136.2, 126.5, 125.9, 125.9, 125.8, 125.8, 124.7, 122.0, 52.4, 38.8, 31.7, 29.5, 29.0, 28.9, 26.1, 22.6, 14.1; HRMS (ESI) m/z: $[M - BPh_4]^+$ Calcd for $C_{12}H_{22}IN_2$ 321.0822; Found 321.0821.

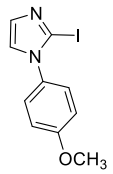
**Preparation of 2-iodo-3-octyl-1-(4-methoxyphenyl)-1H-imidazol-3-ium trifluoromethanesulfonate (3.7a•OTf):**

*Step 1: Synthesis of 1-(4-methoxyphenyl)-2H-1H-imidazole (**3.31**)*



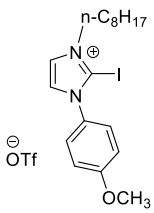
This compound was synthesized following the procedure reported by Minakata and coworkers. Yield: 83% (15.9 mmol, 2.78 g) as white solid. $^1$H NMR spectral data matches that of a previous report.[21]

*Step 2: Synthesis of 1-(4-methoxyphenyl)-2-iodo-1H-imidazole (**3.32**)*



This compound was synthesized following general procedure A with **3.31** and $I_2$ as the halogen source. Yield: 90% (6.89 mmol, 1.69 g) as a yellow solid. $^1$H NMR spectral data matches that of a previous report.[21]

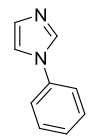
*Step 3: Synthesis of 2-iodo-3-octyl-1-(4-methoxyphenyl)-1H-imidazol-3-ium trifluoromethanesulfonate (**3.7a•OTf**)*



This compound was synthesized following general procedure B from **3.32** and octyl triflate (2.8 equiv). The reaction mixutre was purified according to the Purification Procedure for XBD triflate salts. Yield: 72% (2.16 mmol, 1.21 g) as a white solid. $^1$H NMR spectral data matches that of a previous report.[21]

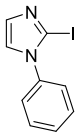
**Preparation of 2-iodo-3-octyl-1-(4-phenyl)-1H-imidazol-3-ium trifluoromethanesulfonate (3.7b•OTf):**

*Step 1: Synthesis of 1-phenyl-2H-1H-imidazole (**3.33**)*



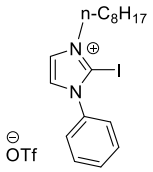
This compound was synthesized following the procedure reported by Minakata and coworkers.[6] Yield: 49% (11.8 mmol, 1.70 g) as white solid. $^1$H NMR spectral matches that of a previous report.[21]

*Step 2: Synthesis of 1-phenyl-2-iodo-1H-imidazole (**3.34**)*



This compound was synthesized following general procedure A with **3.33** and $I_2$ as the halogen source. Yield: 83% (4.61 mmol, 1.24 g) as a white solid. $^1$H NMR spectral data matches that of a previous report.[6]

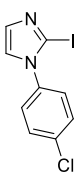
*Step 3: Synthesis of 2-iodo-3-octyl-1-phenyl-1H-imidazol-3-ium trifluoromethanesulfonate (**3.7b•OTf**)*



This compound was synthesized following general procedure B from **3.34** and octyl triflate (2.8 equiv). The reaction mixutre was purified according to the Purification Procedure for XBD triflate salts. Yield: 67% (2.01 mmol, 1.07 g) as a white solid. $^1$H NMR spectral data matches that of a previous report.[21]

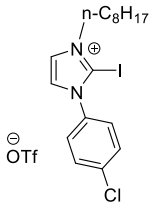
**Preparation of 2-iodo-3-octyl-1-(4-chlorophenyl)-1H-imidazol-3-ium trifluoromethanesulfonate (3.7c•OTf):**

*Step 1: Synthesis of 1-(4-chlorophenyl)-2-iodo-1H-imidazole (**3.35**)*



This compound was synthesized following general procedure A with 1-(4-chlorophenyl)-1H-imidazole as the imidazole-derivative and $I_2$ as the halogen source. This reaction yielded 78% (2.62 mmol, 798 mg) of **3.35** as a yellow solid. $R_f$ = 0.54 (EtOAc); $^1$H NMR (600 MHz, $CDCl_3$): δ 7.48 (d, *J* = 8.0 Hz, 2H), 7.30 (d, *J* = 8.0 Hz, 2H), 7.21 (s, 1H), 7.18 (s, 1H); $^{13}$C NMR (151 MHz, $CDCl_3$): δ 136.8, 135.2, 133.1, 129.6, 128.1, 124.7, 90.2; HRMS (ESI) m/z: $[M + H]^+$ Calcd for $C_9H_6ClIN_2$ 304.9342; Found 304.9346.

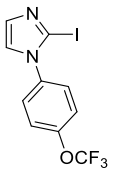
*Step 2: Synthesis of 2-iodo-3-octyl-1-(4-chlorophenyl)-1H-imidazol-3-ium trifluoromethanesulfonate (**3.7c•OTf**)*




This compound was synthesized following general procedure B with the compound from step 1 and octyl triflate (2.8 equiv). The reaction mixutre was purified according to the Purification Procedure for XBD triflate salts. The reaction was allowed to stir for 18 h to yield **3.7c•OTf** (66%, 1.34 mmol, 0.763 g) as a white solid. $R_f$ = 0.18 ($CH_3OH/CH_2Cl_2$, 1:9 *v*/*v*); $^1$H NMR (400 MHz, $CDCl_3$) δ 7.81 (d, *J* = 1.6 Hz, 1H), 7.66 (d, *J* = 1.6 Hz, 1H), 7.57 (d, *J* = 8.6 Hz, 1H), 7.49 (d, *J* = 1.6 Hz, 1H), 4.27 (t, *J* = 7.7 Hz, 2H), 1.96−1.87 (m, 2H), 1.46−1.23 (m, 10H), 0.89 (t, *J* = 7.1 Hz, 3H); $^{13}$C NMR (100 MHz, $CDCl_3$) δ 137.9, 134.8, 130.6, 128.1, 126.8, 126.4, 98.5, 53.9, 31.7, 29.6, 29.0, 28.9, 26.3, 22.6, 14.0; $^{19}$F NMR (376 MHz, $CDCl_3$) δ −78.2; HRMS (ESI) m/z: $[M - OTf]^+$ Calcd for $C_{18}H_{23}ClF_3IN_2O_3S$ 417.0594; Found 417.0589.

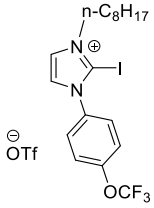
**Preparation of 2-iodo-3-octyl-1-(4-(trifluoromethoxy)phenyl)-1H-imidazol-3-ium trifluoromethanesulfonate (3.7d•OTf):**

*Step 1: Synthesis of 2-iodo-1-(4-(trifluoromethoxy)phenyl)-1H-imidazole (**3.36**)*




This compound was synthesized following general procedure A with 1-(4-(trifluoromethoxy)phenyl)-1H-imidazole as the imidazole-derivative and $I_2$ as the halogen source. This reaction yielded 34% (1.47 mmol, 0.522 g) of **3.36** as a light-yellow liquid. $R_f$ = 0.40 (EtOAc/Hexanes, 1:1 *v*/*v*); $^1$H NMR (400 MHz, $CDCl_3$) δ 7.40 (d, *J* = 8.7 Hz, 1H), 7.35 (d, *J* = 8.7 Hz, 1H), 7.22 (s, 1H), 7.20 (s, 1H); $^{13}$C NMR (151 MHz, $CDCl_3$) δ 136.7, 133.2, 128.4, 124.8, 121.7, 90.2; $^{19}$F NMR (376 MHz, $CDCl_3$) δ −57.9; HRMS (ESI) m/z: $[M + H]^+$ Calcd for $C_{10}H_6F_3IN_2O$ 354.9555; Found 354.9545.

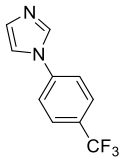
*Step 2: Synthesis of 2-iodo-3-octyl-1-(4-(trifluoromethoxy)phenyl)-1H-imidazol-3-ium trifluoromethanesulfonate (**3.7d•OTf**)*



This compound was synthesized following general procedure B from **3.36** and octyl triflate (2.8 equiv). The reaction mixutre was purified according to the Purification Procedure for XBD triflate salts. The reaction was allowed to stir for 18 h to yield **3.7d•OTf** (68%, 0.58 mmol, 0.36 g) as a white solid. $R_f$ = 0.52 (MeOH/$CH_2Cl_2$, 1:9 *v*/*v*) $^1$H NMR (400 MHz, $CDCl_3$) δ 7.83 (s, 1H), 7.68 (s, 1H), 7.61 (d, *J* = 8.3 Hz, 2H), 7.42 (d, *J* = 8.3 Hz, 2H), 4.26 (t, *J* = 7.8 Hz, 2H), 1.98−1.86 (m, 2H), 1.48−1.20 (m, 10H), 0.89 (t, *J* = 6.9 Hz, 3H); $^{13}$C NMR (151 MHz, $CDCl_3$) δ 150.9, 134.4, 128.7, 126.8, 126.3, 122.2, 98.9, 53.8, 31.6, 29.6, 29.0, 28.9, 26.3, 22.6, 14.0; $^{19}$F NMR (376 MHz, $CDCl_3$) δ −78.1, −57.9; HRMS (ESI) m/z: $[M - OTf]^+$ Calcd for $C_{19}H_{23}F_6IN_2O_4S$ 467.0807; Found 467.0805.

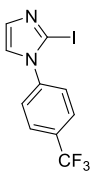
**Preparation of 2-iodo-3-octyl-1-(4-trifluorolmethylphenyl)-1H-imidazol-3-ium trifluoromethanesulfonate (7e•OTf) and 2-iodo-3-octyl-1-(4-trifluorolmethylphenyl)-1H-imidazol-3-ium tetrakis(3,5-bis(trifluoromethyl)phenyl)-borane (3.7e•BAr$^F$):**

*Step 1: Synthesis of 1-(4-trifluoromethylphenyl)-2H-1H-imidazole (**3.37**)*



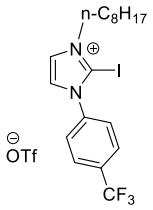
This compound was synthesized following the procedure reported by Minakata and coworkers. Yield: 49% (7.35 mmol, 1.56 g) as white solid. $^1$H NMR spectral data matches that of a previous report.[21]

*Step 2: Synthesis of 1-(4-trifluoromethylphenyl)-2-iodo-1H-imidazole (**3.38**)*



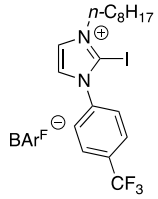
This compound was synthesized following general procedure A with the compound from step 1 (**3.37**) as the imidazole-derivative and $I_2$ as the halogen source. Yield: 90% (6.30 mmol, 1.72 g) as a yellow solid. $^1$H NMR spectral data matches that of a previous report.[21]

*Step 3: Synthesis of 2-iodo-3-octyl-1-(4-trifluoromethylphenyl)-1H-imidazol-3-ium trifluoromethanesulfonate (**7e•OTf**)*



This compound was synthesized following general procedure B from **3.38** and octyl triflate (2.8 equiv). The reaction mixutre was purified according to the Purification Procedure for XBD triflate salts. Yield: 71% (2.13 mmol, 1.28 g) as a yellow solid. $^{1}$H NMR spectral data matches that of a previous report.[21]

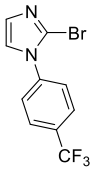
*Synthesis of **2-iodo-3-octyl-1-(4-trifluorolmethylphenyl)-1H-imidazol-3-ium tetrakis(3,5-bis(trifluoromethyl)phenyl)-borane (3.7e•BAr$^{F}$)***



This compound was synthesized following general procedure C with **3.7e•OTf** and $NaBAr^{F}$ as the metal salt. A mixture of ($CH_2Cl_2$/MeOH, 3:1 *v/v*) (12 mM) was used as reaction solvent The reaction mixutre was purified according to the Purification Procedure for XBD triflate salts. Yield: 80% (0.33 mmol, 0.43 g) as a pale yellow solid. $^{1}$H NMR (600 MHz, $CD_2Cl_2$) δ 7.97 (d, *J* = 8.2 Hz, 2H), 7.72−7.68 (m, 10H), 7.57−7.56 (m, 6H), 4.25 (t, *J* = 7.7 Hz, 2H), 1.97−1.92 (m, 2H), 1.47−1.26 (m, 10H), 0.89 (t, *J* = 6.6 Hz, 3H); $^{13}$C NMR (151 MHz, $CD_2Cl_2$) δ 161.8 (dd, *J* = 49.9 Hz), 138.3, 134.9, 128.9 (dddd, *J* = 31.5 Hz), 128.2 (q, *J* = 3.9 Hz), 127.3, 127.1, 126.3, 124.6 (q, *J* = 272.7 Hz), 117.6−117.5 (m), 54.5, 31.7, 29.7, 29.0, 28.9, 26.3, 22.6, 13.8; $^{19}$F NMR (376 MHz, $CD_2Cl_2$) δ −63.6, −62.8; HRMS (ESI) m/z calcd. For $C_{18}H_{23}F_3IN_2$ $[M - BAr^{F}]^{+}$ 451.0853, found 451.0855.

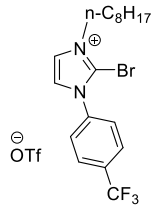
**Preparation of 2-bromo-3-octyl-1-(4-trifluorolmethylphenyl)-1H-imidazol-3-ium trifluoromethanesulfonate (3.7f•OTf):**

*Step 1: Synthesis of 1-(4-trifluoromethylphenyl)-2-bromo-1H-imidazole (**3.39**)*



This compound was synthesized following general procedure A with 1-(4-trifluoromethylphenyl)-2H-1H-imidazole as the imidazole-derivative and $CBr_4$ as the halogen source. Yield: 64% (1.51 mmol, 440 mg) as a brown solid. $^{1}$H NMR spectral data matches that of a previous report.[21]

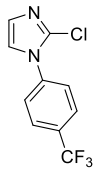
*Step 2: Synthesis of 2-bromo-3-octyl-1-(4-trifluoromethylphenyl)-1H-imidazol-3-ium trifluoromethanesulfonate (**7f•OTf**)*



This compound was synthesized following general procedure B with the compound from step 1 (**3.39**) and octyl triflate (2.8 equiv). The reaction mixutre was purified according to the Purification Procedure for XBD triflate salts. Yield: 61% (0.92 mmol, 0.51 g) as a brown solid. $^1$H NMR spectral data matches that of a previous report.[21]

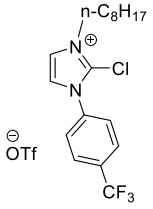
**Preparation of 2-chloro-3-octyl-1-(4-trifluorolmethylphenyl)-1H-imidazol-3-ium trifluoromethanesulfonate (3.6g•OTf):**

*Step 1: Synthesis of 1-(4-trifluoromethylphenyl)-2-chloro-1H-imidazole (**3.40**)*



This compound was synthesized following general procedure A with 1-(4-trifluoromethylphenyl)-2H-1H-imidazole as the imidazole-derivative and $C_2Cl_6$ as the halogen source. Yield: 86% (2.02 mmol, 498 mg) as a brown solid. $^1$H NMR spectral data matches that of a previous report.[21]

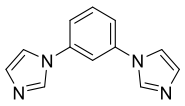
*Step 2: Synthesis of 2-chloro-3-octyl-1-(4-trifluoromethylphenyl)-1H-imidazol-3-ium trifluoromethanesulfonate (**3.7g•OTf**)*



This compound was synthesized following general procedure B with the compound from step 1 (**3.40**) and octyl triflate (2.8 equiv). The reaction mixutre was purified according to the Purification Procedure for XBD triflate salts. Yield: 40% (0.82 mmol, 0.42 g) as a yellow solid. $^1$H NMR spectral data matches that of a previous report.[21]

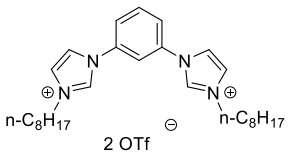
**Preparation of 1,1'-(1,3-phenylene)bis(3-octyl-1H-imidazol-3-ium) bistrifluoromethanesulfonate (3.7a•OTf):**

*Step 1: Synthesis of 1,1'-(1,3-phenylene)bisimidazole (**3.41**)*



This compound was synthesized from the coupling preparation procedure developed by Huber et. al. Yield: 59% (5.14 mmol, 1.08 g) as a white solid. $^1$H NMR spectral data matches that of a previous report.[9]

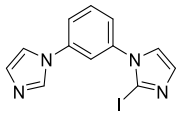
*Step 2: Synthesis of 1,1'-(1,3-phenylene)bis(3-octyl-1H-imidazol-3-ium) bistrifluoromethanesulfonate (**3.8a•OTf**)*




This compound was synthesized following general procedure B with **3.41** and octyl triflate (4.8 equiv). The reaction mixutre was purified according to the Purification Procedure for XBD triflate salts. Yield: 74% (1.27 mmol, 600 mg) as a white solid. $^1$H NMR spectral data matches that of a previous report.[42]

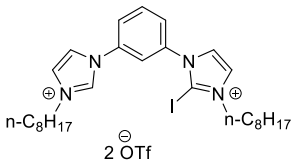
**Preparation of 2-iodo-3-octyl-1-(3-(3-octyl-1H-imidazol-3-ium-1-yl)phenyl)-1H-imidazol-3-ium bis-(trifluoromethane sulfonate) (3.7b•OTf):**

*Step 1: Synthesis of 1-(3-(1H-imidazol-1-yl)phenyl)-2-iodo-1H-imidazole (**3.42**)*



This compound was synthesized following general procedure A with **3.41** as the imidazole-derivative and $I_2$ as the halogen source. Yield: 48% (1.37 mmol, 0.459 g) as a yellow solid. $^1$H NMR spectral data matches that of a previous report.[42]

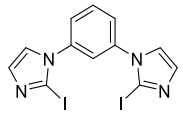
*Step 2: Synthesis of 2-iodo-3-octyl-1-(3-(3-octyl-1H-imidazol-3-ium-1-yl)phenyl)-1H-imidazol-3-ium bistrifluoromethanesulfonate (**3.8b•OTf**)*




This compound was synthesized following general procedure B from **3.42** and octyl triflate (4.8 equiv). The reaction mixutre was purified according to the Purification Procedure for XBD triflate salts. Yield: 75% (0.75 mmol, 0.67 g) as a white solid.[42]

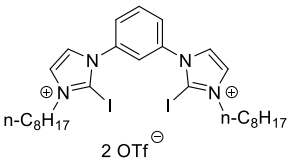
**Preparation of 1,1'-(1,3-phenylene)bis(2-iodo-3-octyl-1H-imidazol-3-ium) bis-(trifluoromethane sulfonate) (3.8c•OTf):**

*Step 1: Synthesis of 1,1'-(1,3-phenylene)bis(2-iodo-3-octyl-1H-imidazole) (**3.43**)*



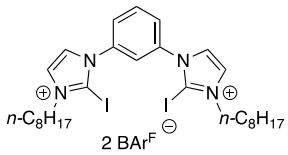
This compound was synthesized following general procedure A with **3.41** as the imidazole-derivative, *n*BuLi (2.3 equiv) and $I_2$ (2.2 equiv) as the halogen source. Yield: 64% (2.40 mmol, 1.12 g) as a yellow solid. $^1$H NMR spectral data matches that of a previous report.[20]

*Step 2: Synthesis of 1,1'-(1,3-phenylene)bis(2-iodo-3-octyl-1H-imidazol-3-ium) bis-(trifluoromethane sulfonate) (**3.8c•OTf**)*




This compound was synthesized following general procedure B from **3.43** and octyl triflate (4.8 equiv). The reaction mixutre was purified according to the Purification Procedure for XBD triflate salts. Yield: 70% (1.49 mmol, 1.47 g) as a white solid. $^1$H NMR spectral data matches that of a previous report.[20]

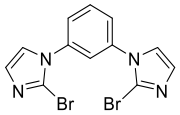
**Preparation of 1,1'-(1,3-phenylene)bis(2-iodo-3-octyl-1H-imidazol-3-ium) bis-(trifluoromethane sulfonate) (3.8c•BAr$^F$):**




This compound was synthesized following general procedure C with **3.8c•OTf** and NaBAr$^F$ (2.2 equiv) as the metal salt. A mixture of ($CH_2Cl_2$/MeOH, 3:1 *v/v*) (12 mM) was used as reaction solvent. The crude product was purified by column chromatography on silica gel (MeOH/$CH_2Cl_2$, 1:9 *v/v*). Yield: 77% (0.34 mmol, 0.81 g) as a yellow foam. $^1$H NMR spectral data matches that of a previous report.[10]

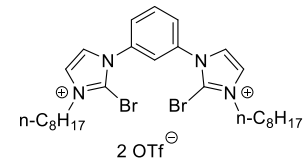
**Preparation of 1,1'-(1,3-phenylene)bis(2-bromo-3-octyl-1H-imidazol-3-ium) bis-(trifluoromethane sulfonate) (3.8d•OTf):**

*Step 1: Synthesis of 1,1'-(1,3-phenylene)bis(2-bromo-3-octyl-1H-imidazole) (**3.44**)*




This compound was synthesized following general procedure A with **3.41** as the imidazole-derivative, *n*BuLi (2.3 equiv) and $CBr_4$ (2.2 equiv) as the halogen source. Yield: 59% (1.12 mmol, 413 mg) as a brown solid. $^1$H NMR spectral data matches that of a previous report.[42]

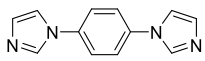
*Step 2: Synthesis of 1,1'-(1,3-phenylene)bis(2-bromo-3-octyl-1H-imidazol-3-ium) bis-(trifluoromethane sulfonate) (**3.8d•OTf**)*




This compound was synthesized following general procedure B with the compound from step 1 (**3.44**) and octyl triflate (4.8 equiv). The reaction mixutre was purified according to the Purification Procedure for XBD triflate salts. Yield: 62% (0.69 mmol, 0.62 g) as a light brown solid. $^1$H NMR spectral data matches that of a previous report.[20]

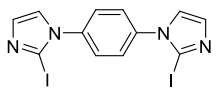
**Preparation of 1,1'-(1,4-phenylene)bis(2-iodo-3-dodecyl-1H-imidazol-3-ium) bis-(trifluoromethane sulfonate) (3.9•OTf):**

*Step 1: Synthesis of 1,4-di(1H-imidazol-1-yl)benzene (**3.45**)*



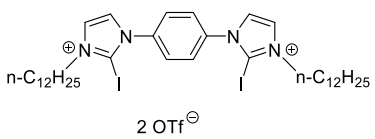

The following procedure was modified from the coupling preparation procedure developed by Huber[9] and Takemoto et. al.[10] Yield: 48% (4.80 mmol, 1.00 g) as a white solid.$^1$H NMR spectral data matches that of a previous report.[9]

*Step 2: Synthesis of 1,4-bis(2-iodo-1H-imidazol-1-yl)benzene (**3.46**)*



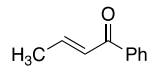

This compound was synthesized following general procedure A with the compound from step 1 (**3.45**) as the imidazole-derivative, *n*BuLi (2.3 equiv), and $I_2$ (2.2 equiv) as the halogen source. Yield: 64% (1.81 mmol, 0.84 g) as a yellow solid. $^1$H NMR spectral data matches that of a previous report.[9]

*Step 3: Synthesis of 1,1'-(1,4-phenylene)bis(2-iodo-3-dodecyl-1H-imidazol-3-ium) bis-(trifluoromethane sulfonate) (**3.9•OTf**)*




This compound was synthesized following general procedure B with **3.46**. Dodecyl triflate (4.8 equiv) was used in place of octyl triflate. The reaction mixutre was purified according to the Purification Procedure for XBD triflate salts. Yield: 69% (0.90 mmol, 0.99 g) as a white solid. $^1$H NMR data matches that of a previous report.[23]

**Synthesis of *trans*-1-Phenylbut-2-en-1-one (3.24)**




This compound was synthesized from the preparation developed by Breugst and coworkers. Yield: 48% (15.4 mmol, 2.26 g) as clear liquid. $^{1}$H NMR spectral data matches that of a previous report.[43]

## Vc. $^{31}$P NMR Spectroscopy Titration Data and Determination of Association Constants

**General Procedure of TEPO Titration Experiment (Figure 3.8)**[3]

The purpose of this experiment is to observe and determine the equilibrium point of $^{31}$P NMR probe binding to XBDs. To determine the stoichiometry of TEPO binding to XBDs, we investigated **3.6•OTf**, **3.8c•OTf**, **3.7e•BAr$^{F}$**, and **3.8c•BAr$^{F}$** binding to TEPO as an idealized representative example due to its denticity. TEPO concentration was held constant at 15 mM for titration experiments and varying amounts of XBDs were added to give the desired equivalents.

**Determination of Association Constants**[58,59]

Association constants were calculated using Microsoft Excel Solver to fit with the model equations below (Equation 3.1 and 3.2). $K_a$ was optimized and no constraints were used. Error was calculated as 95% confidence intervals based on the fit of the NMR data to the model.

(Equation 3.1)

(Equation 3.2)

$\Delta\delta = \delta_{complex} - \delta_{free}$; $\delta_{complex}$ = $^{31}$P chemical shift (ppm) of TEPO bound to XBD, estimated from extrapolation of where the binding curve levels off, $\delta_{free}$ = $^{31}$P chemical shift (ppm) of TEPO with no XBD present; $\delta_{obs,\ i}$ = $^{31}$P chemical shift (ppm) of TEPO at *i* equivalents of XBD. $R_0$ = initial concentration of TEPO and $S_i$ = concentration of XBD at *i* equivalents in molarity (M), $K_a$ = binding constant in $M^{-1}$. Data was verified with repeated experiments.[58,59]

**Table 3.3.** $\Delta\delta$($^{31}$P) data for TEPO titration experiment with 2-iodo-1-methyl-3-octyl-imidazoliumtrifluoromethanesulfonate (**3.6•OTf)**

| Equiv of XBD | $\Delta\delta(^{31}P)$ (ppm) |
|---|---|
| 1 | 1.47 |
| 3 | 2.77 |
| 6 | 3.89 |
| 7 | 4.09 |
| 10 | 4.33 |
| 12 | 4.23 |
| 14 | 4.23 |

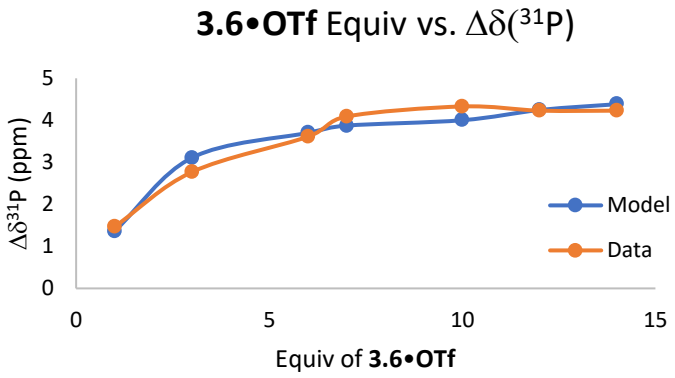



**Figure 3.28.** NMR binding study of TEPO (15 mM in $CD_2Cl_2$) in the presence of **3.6•OTf**. Shifts of 4.23 ppm are observed in the presence of 14 equivalents of **3.6•OTf**, binding constant of 50 ± 4 $M^{-1}$. (Orange curve indicates results from titration experiments; blue curve indicates model fit based on Eq 3.5 and 3.6).

**Table 3.4.** $\Delta\delta(^{31}P)$ data for TEPO titration experiment with 1,3-bis(3-octyl-1H-imidazolium)phenyl-bis(trifluoromethane sulfonate) (**3.8c•OTf**).

| Equiv of XBD | $\Delta\delta(^{31}P)$ (ppm) |
|---|---|
| 0.5 | 1.08 |
| 1.0 | 1.45 |
| 3.0 | 2.58 |
| 5.0 | 3.58 |
| 7.0 | 4.26 |
| 10.0 | 4.91 |
| 12.0 | 5.27 |
| 14.0 | 5.53 |
| 15.0 | 5.60 |
| 16.0 | 5.75 |

3.

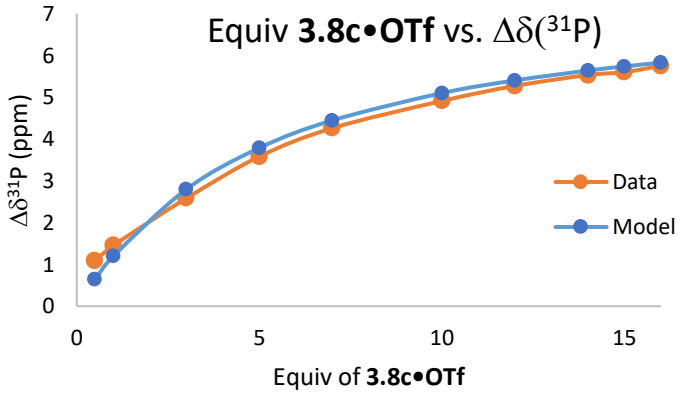



**Figure 3.29.** NMR binding study of TEPO (15 mM in $CD_2Cl_2$) in the presence of **3.8c•OTf**. Shifts of 5.75 ppm are observed in the presence of 16 equivalents of **3.8c•OTf**, binding constant of 15 ± 3 $M^{-1}$. (Orange curve indicates experimental results; blue curve indicates model fit based on Eq 3.5 and 3.6).

**Table 3.5.** $\Delta\delta(^{31}P)$ data for TEPO titration experiment with 2-iodo-3-octyl-1-(4-trifluorolmethylphenyl)-1H-imidazol-3-ium tetrakis(3,5-bis(trifluoromethyl)phenyl)-borane (**3.7e•BAr$^F$**).

| Equiv of XBD | $\Delta\delta(^{31}P)$ (ppm) |
|---|---|
| 0.6 | 3.38 |
| 1.0 | 4.05 |
| 3.0 | 5.64 |
| 5.0 | 5.97 |
| 7.1 | 6.13 |
| 10.0 | 6.25 |

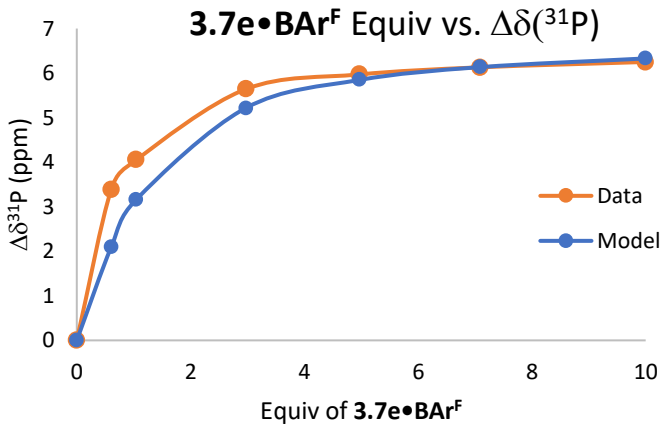



**Figure 3.30.** NMR binding study of TEPO (15 mM in $CD_2Cl_2$) in the presence of **3.7e•BAr$^F$**. Shifts of 6.25 ppm are observed in the presence of 10 equivalents of **3.7e•BAr$^F$**, binding constant of 100 ± 60 $M^{-1}$. (Orange curve indicates experimental results; Blue curve indicates model fit based on Eq 3.5 and 3.6).

**Table 3.6.** $\Delta\delta(^{31}P)$ data for TEPO titration experiment with 1,3-bis(3-octyl-1H-imidazolium)phenyl-tetrakis(3,5-bis(trifluoromethyl)phenyl)-borane (**3.8c•BAr$^F$**).

| Equiv of XBD | $\Delta\delta(^{31}P)$ (ppm) |
|---|---|
| 0.6 | 4.28 |
| 1.0 | 6.70 |
| 3.0 | 10.28 |
| 4.0 | 10.41 |
| 5.0 | 10.47 |
| 10.0 | 10.50 |
| 15.0 | 10.53 |

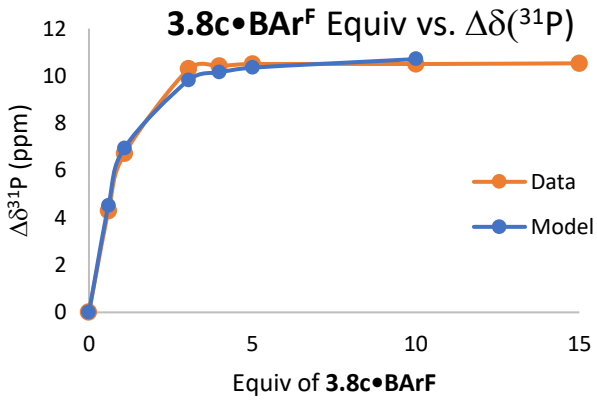



**Figure 3.31.** NMR binding study of TEPO (15 mM in $CD_2Cl_2$) in the presence of **3.8c•BAr$^F$**. Shifts of 10.53 ppm are observed in the presence of 15 equivalents of **3.8c•BAr$^F$**, binding constant of 186 ± 4 $M^{-1}$. (Orange curve indicates experimental results; Blue curve indicates model fit based on Eq 3.5 and 3.6). The association constant was calculated using 0.6 to 10 equivalents to limit over confidence of error.

## Vd. Job Plot Analysis of XBD Binding with TEPO

**Procedure for Job plot analysis of XBD binding with TEPO.** Stock solutions of XBD (55 mM) and TEPO (55 mM) in $CD_2Cl_2$ were prepared. To an oven-dried, argon-purged NMR tube, the XBD stock solution (540 µL) was added followed by TEPO stock solution (60 µL). In a subsequent measurement, the mole fraction of TEPO was varied from 0.1 to 0.9 with a final solution volume of 600 µL. The $^{31}P$

NMR spectrum of each sample was immediately collected at room temperature with 32 scans and compared to a standard of TEPO in $CD_2Cl_2$ (55 mM final concentration).

For **3.6•OTf** and **3.8c•OTf**, a maximum in the curve at $X_A = 0.5$ suggests a 1:1 binding stoichiometry between TEPO and each imidazolium- and bis-imidazolium salts.

**Table 3.7.** Values from Job Plot of **3.6•OTf** binding with TEPO (at 55 mM in $CD_2Cl_2$).

| Equiv of XBD | $\Delta\delta(^{31}P)$ (ppm) | $\Delta\delta(^{31}P) \times$ [TEPO]/ ([TEPO] + [**3.6•OTf**]) |
|---|---|---|
| 1.0 | 0.00 | 0.00 |
| 0.9 | 0.31 | 0.28 |
| 0.8 | 0.74 | 0.59 |
| 0.7 | 1.01 | 0.71 |
| 0.6 | 1.38 | 0.83 |
| **0.5** | **1.69** | **0.85** |
| 0.4 | 2.10 | 0.84 |
| 0.3 | 2.45 | 0.74 |
| 0.2 | 2.71 | 0.54 |
| 0.1 | 0.23 | 0.28 |

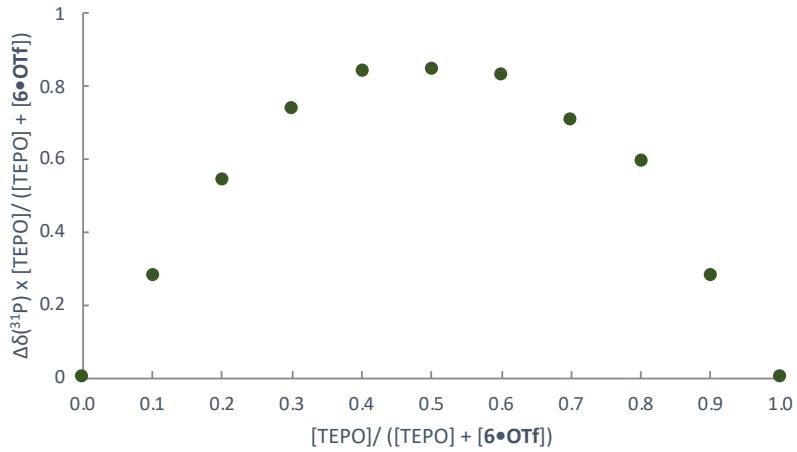



**Figure 3.32.** Job Plot of **3.6•OTf** binding with TEPO (at 55 mM in $CD_2Cl_2$).

**Table 3.8.** Values from Job Plot of **3.8c•OTf** binding with TEPO (at 55 mM in $CD_2Cl_2$).

| Equiv of XBD | $\Delta\delta(^{31}P)$ (ppm) | $\Delta\delta(^{31}P) \times$ [TEPO]/([TEPO] + [**3.8c•OTf**]) |
|---|---|---|
| 1.0 | 0.00 | 0.00 |
| 0.9 | 0.40 | 0.36 |
| 0.8 | 0.85 | 0.68 |
| 0.7 | 1.21 | 0.85 |
| 0.6 | 1.59 | 0.95 |
| **0.5** | **2.02** | **1.01** |
| 0.4 | 2.23 | 0.89 |
| 0.3 | 2.61 | 0.78 |
| 0.2 | 2.87 | 0.57 |
| 0.1 | 3.43 | 0.34 |

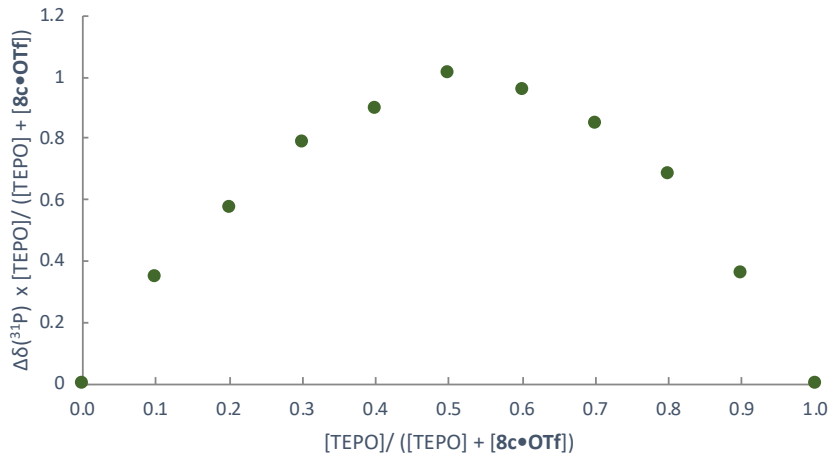



**Figure 3.33.** Job Plot of **3.8c•OTf** binding with TEPO (at 55 mM in $CD_2Cl_2$).

## Ve. Kinetic Analysis of Indole Addition to *trans*-Crotonophenone

**General Procedure for Measuring the Initial Rates of Indole Addition to *trans*-Crotonophenone.** Stock solutions of indole **3.23** (1.0 M) and *trans*-crotonophenone **3.24** (1.0 M) in $CD_2Cl_2$ were prepared. Selected catalysts from **3.1**−**3.9•OTf** (0.03 mmol) and trimethyl(phenyl)silane (amount was recorded after added) were weighed directly into an oven-dried and argon-purged NMR tube. Aliquots of **3.23** (0.3 mL, 0.3 mmol) and **3.24** (0.3 mL, 0.3 mmol) were transferred into the NMR tube, which was capped with rubber septum. The disappearance of the peak at δ = 6.55 ppm (1H for **3.23**) and the growth

of peaks at δ = 3.30, 3.51 and 3.85 ppm (1H for product **3.25**) were monitored by taking a $^1$H spectrum (four scans with a 25 second relaxation delay) every 1−8 h for up to three days. Trimethyl(phenyl)silane (δ = 0.34 ppm) was used as an internal standard, and the integrations were compared relative to integrations for indole **3.23** and product **3.25**.

Concentration of starting material **3.23** was calculated based on the raw integration of **3.25** and the known concentration of trimethyl(phenyl)silane.

(equation 3.3)

(equation 3.4)

**Vf. Kinetic Data for Indole Addition to *trans*-Crotonophenone Reaction Catalyzed by XBDs**

**Table 3.9.** $^1$H NMR data for the uncatalyzed indole addition.

| Time (min) | [SM] | [P] | [SM] + [P] |
|---|---|---|---|
| 0 | 0.514 | 0.001 | 0.516 |
| 291 | 0.511 | 0.002 | 0.513 |
| 725 | 0.507 | 0.001 | 0.508 |
| 1160 | 0.503 | 0.001 | 0.505 |
| 1449 | 0.504 | 0.001 | 0.505 |
| 1865 | 0.496 | 0.001 | 0.497 |
| 2218 | 0.498 | 0.001 | 0.499 |
| 2979 | 0.496 | 0.001 | 0.497 |
| 3352 | 0.494 | 0.001 | 0.496 |
| 3699 | 0.490 | 0.001 | 0.491 |
| 4059 | 0.489 | 0.001 | 0.490 |

No reaction observed

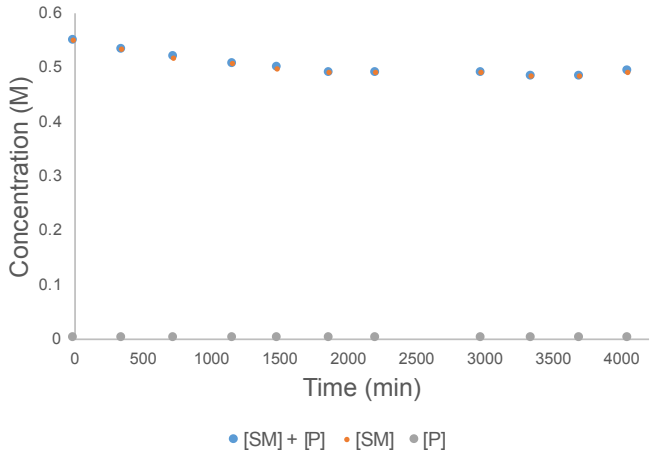
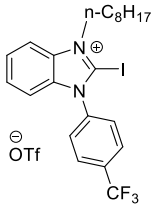



**Figure 3.34.** Reaction profile for the uncatalyzed reaction.

**Table 3.10.** $^{1}$H NMR data for the indole addition catalyzed by **3.5d•OTf**.

Average $k_{obs}$ = 13.00 × $10^{-4}$ $min^{-1}$

**Trial 1**

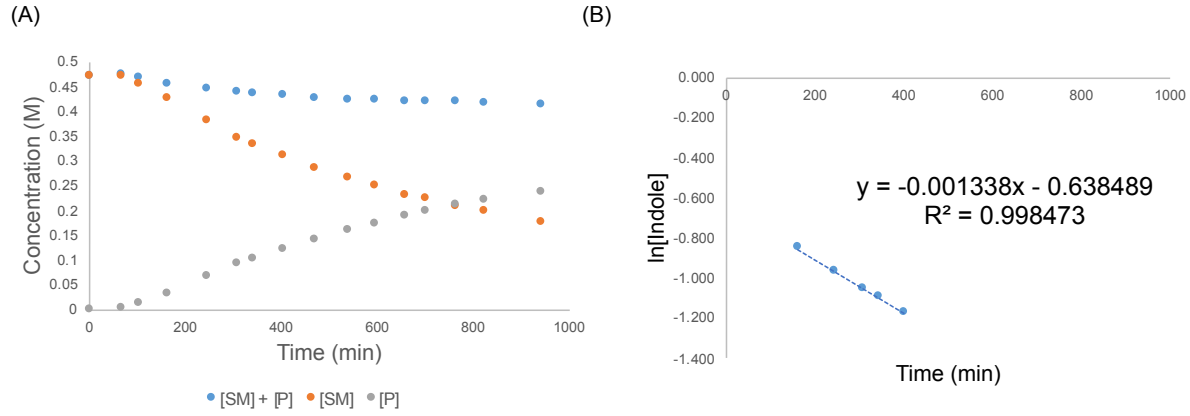



| Time (min) | [SM] | [P] | ln[SM] |
|---|---|---|---|
| 0 | 0.472 | 0.000 | -0.634 |
| 68 | 0.472 | 0.003 | -0.751 |
| 103 | 0.456 | 0.011 | -0.784 |
| 162 | 0.427 | 0.031 | -0.852 |
| 244 | 0.381 | 0.065 | -0.965 |
| 307 | 0.348 | 0.091 | -1.056 |
| 342 | 0.333 | 0.103 | -1.098 |
| 402 | 0.310 | 0.122 | -1.171 |
| 468 | 0.287 | 0.141 | -1.249 |
| 539 | 0.265 | 0.160 | -1.329 |
| 596 | 0.249 | 0.174 | -1.389 |
| 658 | 0.232 | 0.189 | -1.463 |
| 701 | 0.223 | 0.198 | -1.502 |
| 762 | 0.209 | 0.210 | -1.564 |
| 822 | 0.197 | 0.220 | -1.624 |
| 942 | 0.176 | 0.238 | -1.736 |

**Trial 2**

| Time (min) | [SM] | [P] | ln[SM] |
|---|---|---|---|
| 0 | 0.487 | 0.000 | -0.720 |
| 24 | 0.487 | 0.002 | -0.720 |
| 86 | 0.467 | 0.018 | -0.761 |
| 195 | 0.411 | 0.058 | -0.890 |
| 255 | 0.380 | 0.082 | -0.969 |
| 322 | 0.346 | 0.107 | -1.060 |
| 375 | 0.323 | 0.123 | -1.130 |
| 443 | 0.302 | 0.142 | -1.198 |
| 564 | 0.278 | 0.171 | -1.279 |
| 685 | 0.253 | 0.197 | -1.374 |
| 803 | 0.228 | 0.216 | -1.480 |
| 923 | 0.202 | 0.237 | -1.597 |
| 1280 | 0.158 | 0.278 | -1.847 |

**Trial 1**




**Trial 2**

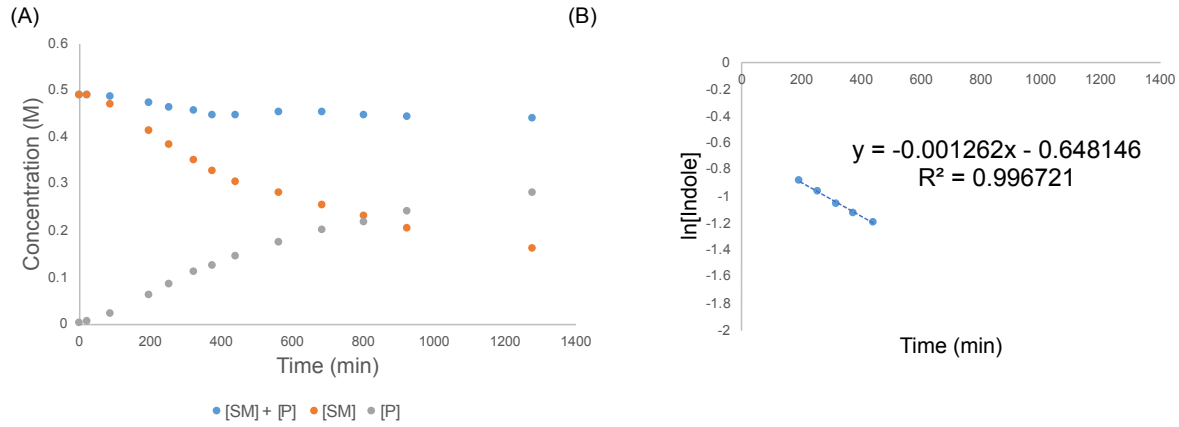
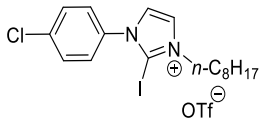



**Figure 3.35.** Data graphed for the indole addition catalyzed by **3.5d•OTf**: (A) Reaction profile. (B) Graph of ln[Indole] vs. time using the initial five data points after > 10% of the indole was consumed.

**Table 3.11.** $^1$H NMR data for the indole addition catalyzed by **3.7c•OTf**.

Average $k_{obs} = 7.03 \times 10^{-4}$ min$^{-1}$



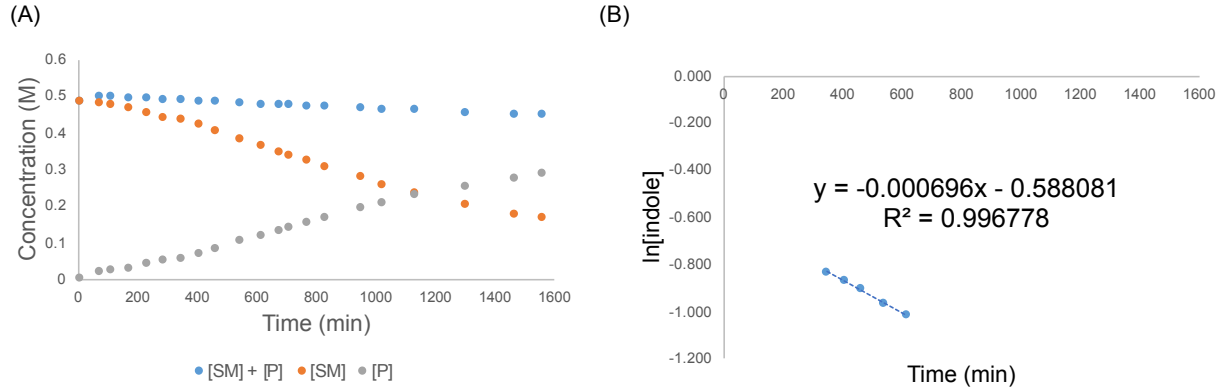

**Trial 1**

| Time (min) | [SM] | [P] | ln[SM] |
|---|---|---|---|
| 0 | 0.483 | 0.000 | -0.729 |
| 75 | 0.478 | 0.019 | -0.738 |
| 110 | 0.475 | 0.021 | -0.744 |
| 170 | 0.466 | 0.027 | -0.763 |
| 231 | 0.454 | 0.038 | -0.789 |
| 290 | 0.441 | 0.047 | -0.819 |
| 350 | 0.433 | 0.054 | -0.836 |
| 409 | 0.419 | 0.066 | -0.870 |
| 465 | 0.404 | 0.080 | -0.907 |
| 543 | 0.379 | 0.101 | -0.970 |
| 617 | 0.361 | 0.115 | -1.018 |
| 676 | 0.344 | 0.129 | -1.067 |
| 709 | 0.337 | 0.137 | -1.089 |
| 769 | 0.320 | 0.152 | -1.138 |
| 829 | 0.305 | 0.165 | -1.186 |
| 951 | 0.276 | 0.191 | -1.288 |
| 1024 | 0.257 | 0.207 | -1.359 |
| 1134 | 0.234 | 0.227 | -1.452 |
| 1302 | 0.201 | 0.252 | -1.604 |
| 1469 | 0.173 | 0.274 | -1.757 |
| 1562 | 0.163 | 0.284 | -1.813 |

**Trial 2**

| Time (min) | [SM] | [P] | ln[SM] |
|---|---|---|---|
| 0 | 0.487 | 0.000 | -0.720 |
| 21 | 0.487 | 0.000 | -0.720 |
| 210 | 0.450 | 0.012 | -0.799 |
| 222 | 0.447 | 0.014 | -0.805 |
| 277 | 0.437 | 0.023 | -0.828 |
| 398 | 0.409 | 0.047 | -0.895 |
| 523 | 0.382 | 0.074 | -0.963 |
| 639 | 0.353 | 0.102 | -1.042 |
| 765 | 0.321 | 0.132 | -1.136 |
| 879 | 0.291 | 0.159 | -1.235 |
| 999 | 0.260 | 0.185 | -1.346 |
| 1322 | 0.197 | 0.241 | -1.623 |
| 1904 | 0.116 | 0.308 | -2.158 |
| 2071 | 0.097 | 0.322 | -2.334 |

**Trial 1**




**Trial 2**

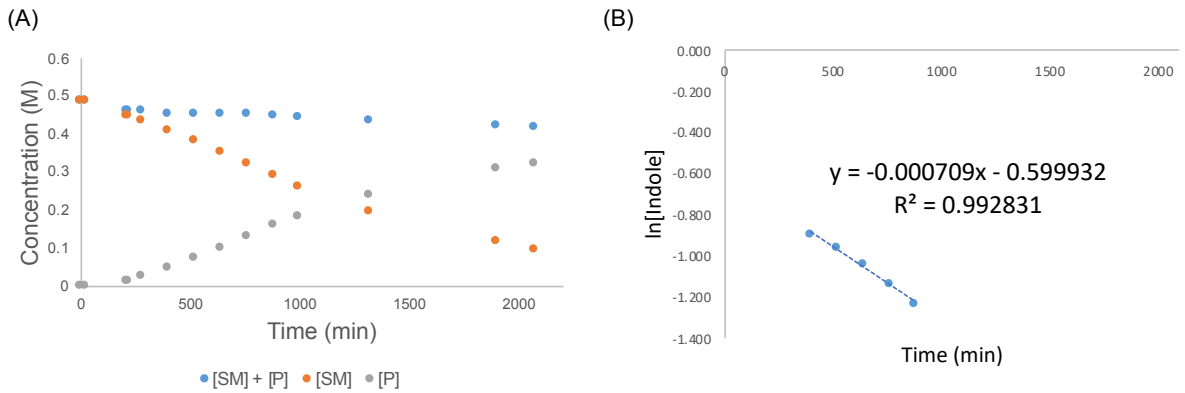
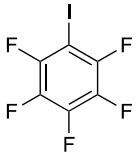



**Figure 3.36.** Data graphed for the indole addition catalyzed by **3.7c•OTf**: (A) Reaction profile. (B) Graph of ln[Indole] vs. time using the initial five data points after > 10% of the indole was consumed.

**Table 3.12**. $^{1}$H NMR data for the indole addition catalyzed by **3.1.**




| Time (min) | [SM] | [P] | [SM] + [P] |
|---|---|---|---|
| 0 | 0.547 | 0.000 | 0.547 |
| 351 | 0.530 | 0.001 | 0.532 |
| 739 | 0.515 | 0.001 | 0.517 |
| 1160 | 0.504 | 0.001 | 0.505 |
| 1498 | 0.496 | 0.001 | 0.497 |
| 1866 | 0.486 | 0.001 | 0.488 |
| 2218 | 0.488 | 0.001 | 0.489 |
| 2979 | 0.488 | 0.001 | 0.489 |
| 3353 | 0.480 | 0.001 | 0.481 |
| 3700 | 0.480 | 0.001 | 0.481 |
| 4060 | 0.489 | 0.001 | 0.490 |

No reaction observed

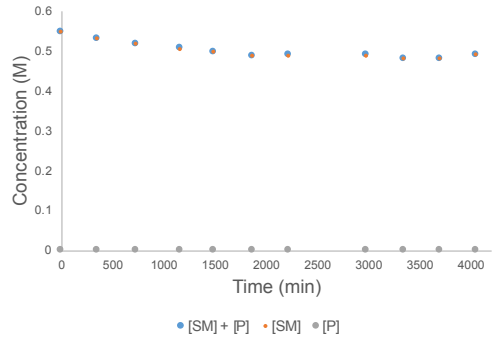
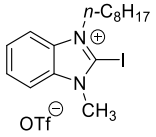



**Figure 3.37.** Reaction profile for the indole addition catalyzed by **1**.

**Table 3.13.** $^1$H NMR data for the indole addition catalyzed by **3.5a•OTf**.




| Time (min) | [SM] | [P] | ln[SM] |
|---|---|---|---|
| 0 | 0.498 | 0.000 | -0.698 |
| 33 | 0.498 | 0.000 | -0.698 |
| 110 | 0.498 | 0.001 | -0.698 |
| 206 | 0.491 | 0.004 | -0.710 |
| 310 | 0.485 | 0.009 | -0.725 |
| 356 | 0.482 | 0.010 | -0.730 |
| 478 | 0.471 | 0.017 | -0.754 |
| 537 | 0.467 | 0.022 | -0.761 |
| 598 | 0.459 | 0.026 | -0.778 |
| 657 | 0.453 | 0.030 | -0.791 |
| 809 | 0.436 | 0.046 | -0.830 |
| 897 | 0.424 | 0.056 | -0.859 |
| 1018 | 0.406 | 0.071 | -0.900 |
| 1137 | 0.387 | 0.087 | -0.949 |
| 1258 | 0.367 | 0.105 | -1.002 |
| 1377 | 0.346 | 0.123 | -1.062 |
| 1437 | 0.336 | 0.134 | -1.091 |
| 1577 | 0.311 | 0.153 | -1.168 |
| 1681 | 0.293 | 0.173 | -1.229 |
| 1934 | 0.253 | 0.213 | -1.376 |
| 2082 | 0.227 | 0.232 | -1.481 |
| 2218 | 0.205 | 0.250 | -1.585 |
| 2545 | 0.157 | 0.293 | -1.850 |
| 2715 | 0.148 | 0.305 | -1.907 |
| 2880 | 0.142 | 0.307 | -1.955 |
| 3122 | 0.132 | 0.315 | -2.025 |

$k_{obs} = 4.57 \times 10^{-4}$ min$^{-1}$

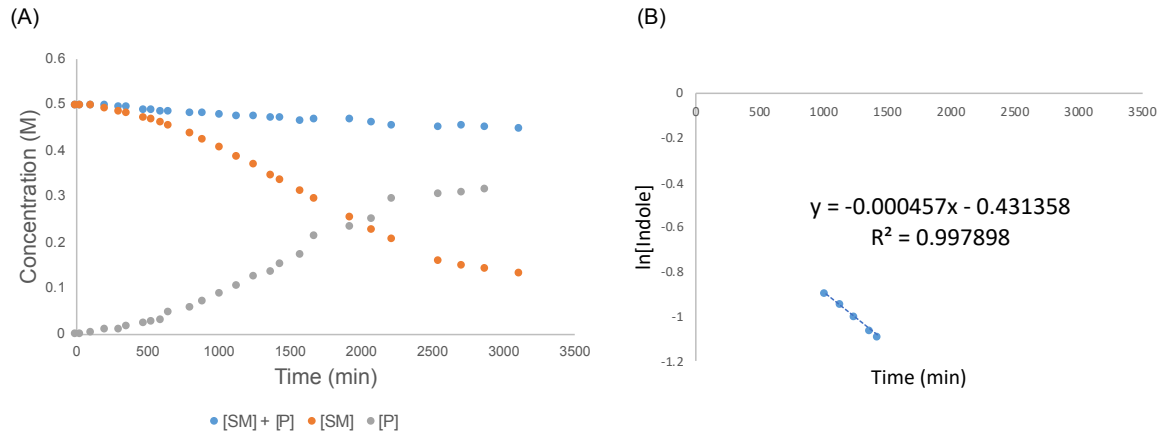
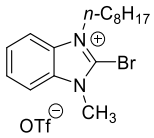



**Figure 3.38.** Data graphed for reaction catalyzed by **3.5a•OTf**: (A) Reaction profile. (B) Graph of ln[Indole] vs. time using the initial five data points after > 10% of the indole was consumed.

**Table 3.14.** $^{1}$H NMR data for the indole addition catalyzed by **3.5b•OTf**.




| Time (min) | [SM] | [P] | In[SM] |
|---|---|---|---|
| 0 | 0.438 | 0.002 | -0.826 |
| 179 | 0.401 | 0.015 | -0.914 |
| 360 | 0.380 | 0.033 | -0.967 |
| 495 | 0.367 | 0.047 | -1.004 |
| 721 | 0.347 | 0.067 | -1.058 |
| 901 | 0.332 | 0.082 | -1.102 |
| 1298 | 0.300 | 0.113 | -1.204 |
| 1461 | 0.287 | 0.125 | -1.248 |
| 1682 | 0.275 | 0.141 | -1.291 |
| 1841 | 0.264 | 0.150 | -1.332 |
| 2181 | 0.243 | 0.172 | -1.415 |
| 2520 | 0.225 | 0.188 | -1.491 |
| 2860 | 0.208 | 0.203 | -1.568 |
| 4415 | 0.156 | 0.247 | -1.855 |
| 4419 | 0.157 | 0.248 | -1.849 |
| 4422 | 0.157 | 0.252 | -1.851 |

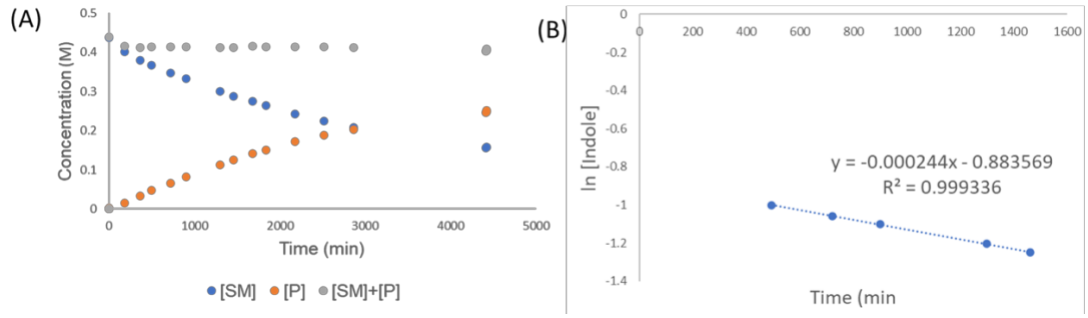
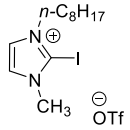



**Figure 3.39.** Data graphed for reaction catalyzed by **3.5b•OTf**: (A) Reaction profile. (B) Graph of ln[Indole] vs. time using the initial five data points after > 10% of the indole was consumed.

The $k_{obs}$ of **3.5b•OTf** was higher than expected. Although the catalyst used was purified multiple times using the general purification procedure, and $^{1}$H NMR spectra of **3.5b•OTf** show no observable impurities, we suspect that there was a trace amount of triflic acid present as the $^{31}$P NMR peak was not as intense compared to spectra of other XBDs. We speculate that the trace triflic acid caused the decomposition of the catalyst and thus the formation of bromine during the reaction. The reaction mixture was observed to be brown.

**Table 3.15.** $^{1}$H NMR data for the indole addition catalyzed by **3.6•OTf**.




| Time (min) | [SM] | [P] | [SM] + [P] |
|---|---|---|---|
| 0 | 0.451 | 0.003 | 0.454 |
| 240 | 0.451 | 0.003 | 0.454 |
| 401 | 0.451 | 0.003 | 0.453 |
| 603 | 0.450 | 0.003 | 0.453 |
| 780 | 0.449 | 0.003 | 0.452 |
| 961 | 0.447 | 0.004 | 0.451 |
| 1316 | 0.449 | 0.003 | 0.452 |
| 1501 | 0.447 | 0.003 | 0.450 |
| 1640 | 0.449 | 0.003 | 0.452 |
| 1823 | 0.445 | 0.003 | 0.448 |
| 2001 | 0.446 | 0.001 | 0.447 |
| 2181 | 0.445 | 0.003 | 0.448 |
| 2360 | 0.443 | 0.005 | 0.448 |
| 2540 | 0.444 | 0.003 | 0.447 |
| 2720 | 0.444 | 0.003 | 0.447 |
| 4100 | 0.443 | 0.005 | 0.449 |
| 3080 | 0.443 | 0.004 | 0.447 |
| 3260 | 0.440 | 0.006 | 0.446 |
| 3440 | 0.439 | 0.005 | 0.444 |
| 3680 | 0.437 | 0.008 | 0.445 |
| 3920 | 0.434 | 0.005 | 0.439 |
| 4220 | 0.432 | 0.012 | 0.445 |
| 4519 | 0.409 | 0.017 | 0.426 |
| 4759 | 0.404 | 0.021 | 0.424 |
| 5178 | 0.393 | 0.031 | 0.423 |

No reaction observed

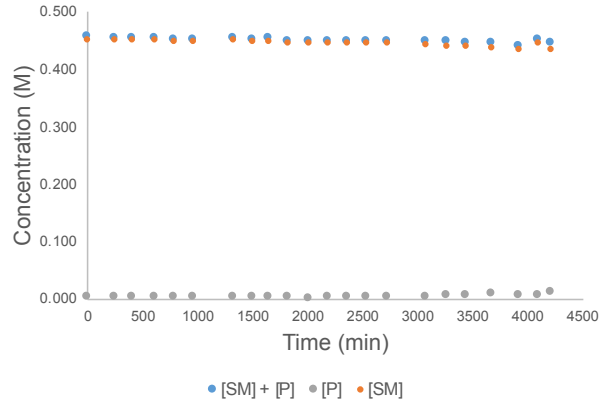
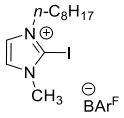



**Figure 3.40.** Reaction profile for the indole addition catalyzed by **3.6•OTf**.

**Table 3.16.** $^{1}$H NMR data for the indole addition catalyzed by **3.6•BAr$^{F}$**.




| Time (min) | [SM] | [P] | ln[SM] |
|---|---|---|---|
| 0 | 0.464 | 0.000 | -0.765 |
| 183 | 0.465 | 0.002 | -0.765 |
| 366 | 0.460 | 0.007 | -0.776 |
| 544 | 0.458 | 0.007 | -0.780 |
| 723 | 0.453 | 0.018 | -0.791 |
| 845 | 0.421 | 0.055 | -0.864 |
| 1144 | 0.349 | 0.116 | -1.053 |
| 1297 | 0.313 | 0.150 | -1.162 |
| 1430 | 0.291 | 0.165 | -1.235 |
| 1781 | 0.246 | 0.199 | -1.401 |
| 1961 | 0.234 | 0.214 | -1.451 |
| 2442 | 0.187 | 0.262 | -1.675 |
| 1602 | 0.267 | 0.184 | -1.321 |
| 2612 | 0.176 | 0.279 | -1.735 |
| 3030 | 0.147 | 0.311 | -1.917 |
| 3179 | 0.137 | 0.321 | -1.985 |
| 3358 | 0.127 | 0.331 | -2.061 |
| 3538 | 0.117 | 0.346 | -2.149 |
| 3719 | 0.107 | 0.354 | -2.235 |
| 4019 | 0.093 | 0.374 | -2.375 |
| 4523 | 0.078 | 0.390 | -2.549 |

$k_{obs} = 5.77 \times 10^{-4}$ min$^{-1}$

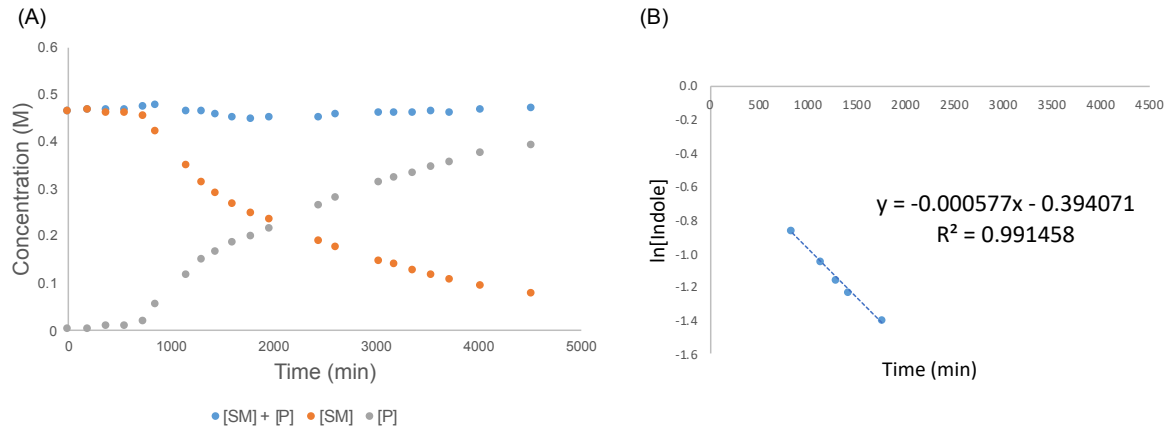
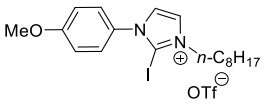



**Figure 3.41.** Data graphed for reaction catalyzed by **3.6•BAr$^F$**: (A) Reaction profile. (B) Graph of ln[Indole] vs. time using the initial five data points after > 10% of the indole was consumed.

**Table 3.17.** $^1$H NMR data for the indole addition catalyzed by **3.7a•OTf**.




| Time (min) | [SM] | [P] | ln[SM] |
|---|---|---|---|
| 0 | 0.453 | 0.000 | -0.792 |
| 54 | 0.453 | 0.000 | -0.792 |
| 117 | 0.453 | 0.000 | -0.792 |
| 172 | 0.453 | 0.000 | -0.792 |
| 232 | 0.451 | 0.000 | -0.797 |
| 352 | 0.451 | 0.000 | -0.797 |
| 472 | 0.449 | 0.002 | -0.801 |
| 592 | 0.441 | 0.006 | -0.819 |
| 712 | 0.437 | 0.010 | -0.828 |
| 988 | 0.415 | 0.026 | -0.879 |
| 1085 | 0.407 | 0.034 | -0.898 |
| 1181 | 0.397 | 0.042 | -0.923 |
| 1402 | 0.373 | 0.060 | -0.985 |
| 1522 | 0.360 | 0.073 | -1.023 |
| 1642 | 0.346 | 0.083 | -1.062 |
| 1762 | 0.326 | 0.103 | -1.122 |
| 1943 | 0.306 | 0.121 | -1.185 |
| 2092 | 0.284 | 0.139 | -1.259 |
| 2282 | 0.268 | 0.161 | -1.316 |
| 2430 | 0.250 | 0.175 | -1.385 |
| 2849 | 0.205 | 0.207 | -1.587 |
| 3023 | 0.185 | 0.220 | -1.689 |

$k_{obs} = 2.72 \times 10^{-4}$ min$^{-1}$

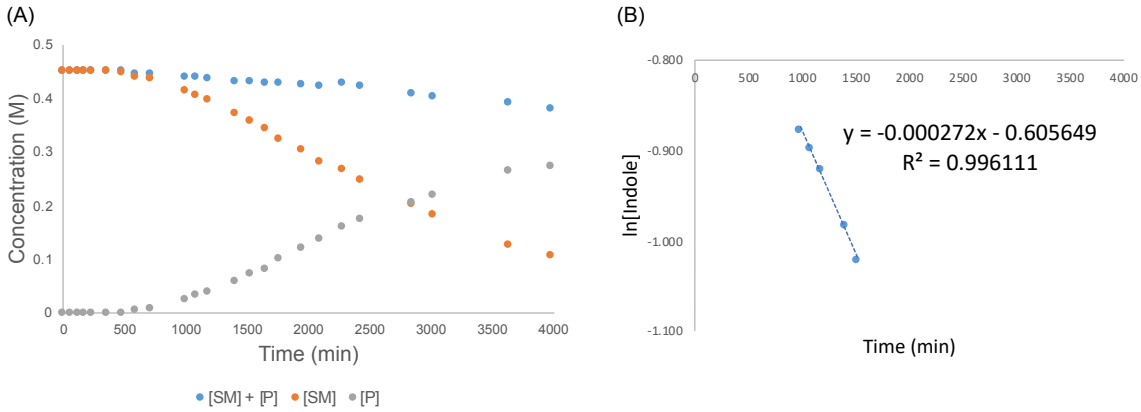
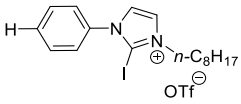



**Figure 3.42.** Data graphed for reaction catalyzed by **3.7a•OTf**: (A) Reaction profile. (B) Graph of ln[Indole] vs. time using the initial five data points after > 10% of the indole was consumed.

**Table 3.18.** $^1$H NMR data for the indole addition catalyzed by **3.7b•OTf**.




| Time (min) | [SM] | [P] | ln[SM] |
|---|---|---|---|
| 0 | 0.489 | 0.000 | -0.716 |
| 62 | 0.489 | 0.000 | -0.716 |
| 125 | 0.487 | 0.000 | -0.720 |
| 179 | 0.487 | 0.000 | -0.720 |
| 239 | 0.487 | 0.000 | -0.720 |
| 359 | 0.482 | 0.002 | -0.729 |
| 485 | 0.469 | 0.010 | -0.756 |
| 599 | 0.458 | 0.021 | -0.780 |
| 719 | 0.442 | 0.032 | -0.816 |
| 995 | 0.401 | 0.067 | -0.914 |
| 1114 | 0.383 | 0.083 | -0.959 |
| 1213 | 0.367 | 0.101 | -1.002 |
| 1461 | 0.326 | 0.139 | -1.122 |
| 1576 | 0.302 | 0.160 | -1.198 |
| 1649 | 0.283 | 0.177 | -1.264 |
| 1831 | 0.255 | 0.203 | -1.365 |
| 2017 | 0.233 | 0.232 | -1.456 |
| 2159 | 0.214 | 0.247 | -1.542 |
| 2350 | 0.185 | 0.267 | -1.686 |
| 2497 | 0.171 | 0.278 | -1.767 |

$k_{obs} = 4.86 \times 10^{-4}$ min$^{-1}$

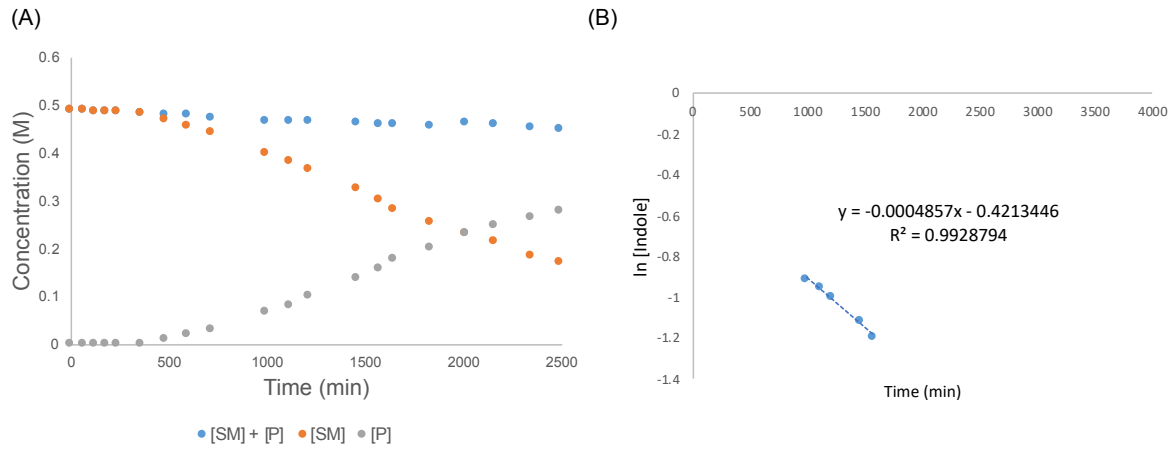
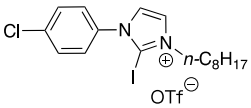



**Figure 3.43.** Data graphed for reaction catalyzed by **3.7b•Otf**: (A) Reaction profile. (B) Graph of ln[Indole] vs. time using the initial five data points after > 10% of the indole was consumed.

**Table 3.19.** $^{1}$H NMR data for the indole addition catalyzed by **3.7c•OTf**.




| Time (min) | [SM] | [P] | ln[SM] |
|---|---|---|---|
| 0 | 0.483 | 0.000 | -0.729 |
| 75 | 0.478 | 0.019 | -0.738 |
| 110 | 0.475 | 0.021 | -0.744 |
| 170 | 0.466 | 0.027 | -0.763 |
| 231 | 0.454 | 0.038 | -0.789 |
| 290 | 0.441 | 0.047 | -0.819 |
| 350 | 0.433 | 0.054 | -0.836 |
| 409 | 0.419 | 0.066 | -0.870 |
| 465 | 0.404 | 0.080 | -0.907 |
| 543 | 0.379 | 0.101 | -0.970 |
| 617 | 0.361 | 0.115 | -1.018 |
| 676 | 0.344 | 0.129 | -1.067 |
| 709 | 0.337 | 0.137 | -1.089 |
| 769 | 0.320 | 0.152 | -1.138 |
| 829 | 0.305 | 0.165 | -1.186 |
| 951 | 0.276 | 0.191 | -1.288 |
| 1024 | 0.257 | 0.207 | -1.359 |
| 1134 | 0.234 | 0.227 | -1.452 |
| 1302 | 0.201 | 0.252 | -1.604 |
| 1469 | 0.173 | 0.274 | -1.757 |

$k_{obs} = 6.96 \times 10^{-4}$ min$^{-1}$

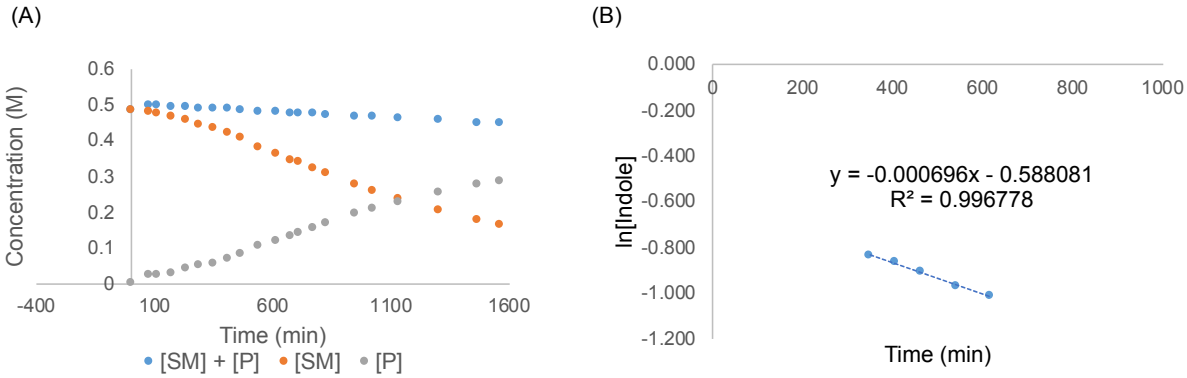
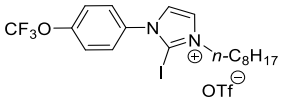



**Figure 3.44.** Data graphed for reaction catalyzed by **3.7c•OTf**: (A) Reaction profile. (B) Graph of ln[Indole] vs. time using the initial five data points after > 10% of the indole was consumed.

**Table 3.20.** $^{1}$H NMR data for the indole addition catalyzed by **3.7d•OTf**.




| Time (min) | [SM] | [P] | ln[SM] |
|---|---|---|---|
| 0 | 0.502 | 0.003 | -0.690 |
| 14 | 0.502 | 0.003 | -0.690 |
| 77 | 0.502 | 0.005 | -0.690 |
| 137 | 0.502 | 0.005 | -0.690 |
| 197 | 0.502 | 0.005 | -0.690 |
| 256 | 0.502 | 0.004 | -0.690 |
| 316 | 0.495 | 0.008 | -0.704 |
| 376 | 0.487 | 0.012 | -0.720 |
| 436 | 0.479 | 0.019 | -0.736 |
| 505 | 0.467 | 0.027 | -0.762 |
| 557 | 0.459 | 0.032 | -0.779 |
| 677 | 0.432 | 0.055 | -0.839 |
| 737 | 0.420 | 0.066 | -0.868 |
| 857 | 0.391 | 0.090 | -0.940 |
| 976 | 0.358 | 0.118 | -1.026 |
| 1097 | 0.322 | 0.140 | -1.132 |
| 1217 | 0.301 | 0.165 | -1.201 |
| 1276 | 0.289 | 0.177 | -1.242 |
| 1337 | 0.276 | 0.187 | -1.289 |
| 1696 | 0.214 | 0.239 | -1.542 |
| 1938 | 0.182 | 0.266 | -1.704 |

$k_{obs} = 7.16 \times 10^{-4}$ min$^{-1}$

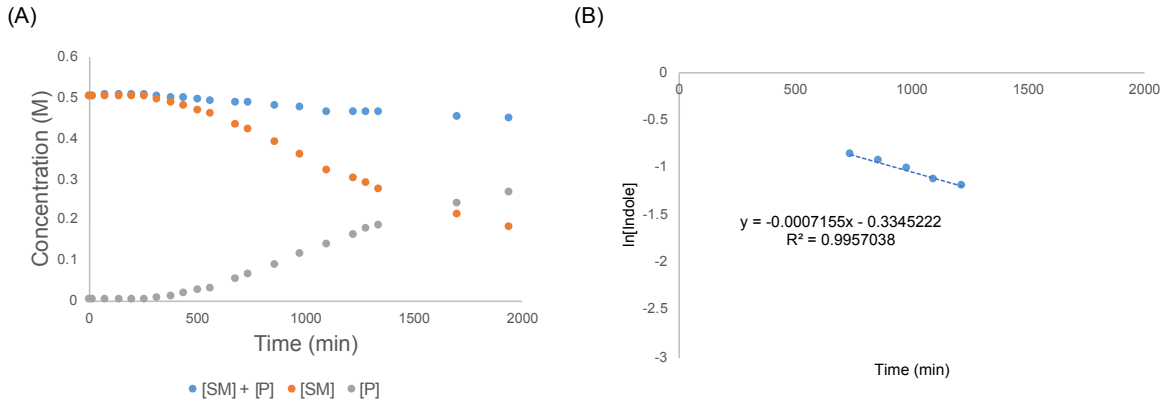
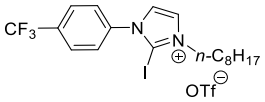



**Figure 3.45.** Data graphed for reaction catalyzed by **3.7d•OTf**: (A) Reaction profile. (B) Graph of ln[Indole] vs. time using the initial five data points after > 10% of the indole was consumed.

**Table 3.21.** $^{1}$H NMR data for the indole addition catalyzed by **3.7e•OTf**.




| Time (min) | [SM] | [P] | ln[SM] |
|---|---|---|---|
| 0 | 0.492 | 0.000 | -0.710 |
| 70 | 0.492 | 0.000 | -0.710 |
| 132 | 0.484 | 0.005 | -0.726 |
| 186 | 0.474 | 0.012 | -0.747 |
| 247 | 0.461 | 0.021 | -0.775 |
| 367 | 0.430 | 0.042 | -0.845 |
| 494 | 0.393 | 0.069 | -0.933 |
| 606 | 0.362 | 0.096 | -1.016 |
| 726 | 0.328 | 0.119 | -1.114 |
| 1003 | 0.254 | 0.175 | -1.369 |
| 1101 | 0.237 | 0.183 | -1.438 |
| 1197 | 0.222 | 0.200 | -1.505 |
| 1418 | 0.192 | 0.222 | -1.650 |
| 1546 | 0.178 | 0.235 | -1.727 |
| 1657 | 0.171 | 0.244 | -1.764 |
| 1838 | 0.156 | 0.254 | -1.860 |
| 2025 | 0.144 | 0.262 | -1.938 |
| 2167 | 0.138 | 0.267 | -1.984 |
| 2297 | 0.130 | 0.276 | -2.042 |
| 2445 | 0.123 | 0.280 | -2.093 |

$k_{obs} = 8.51 \times 10^{-4}$ min$^{-1}$

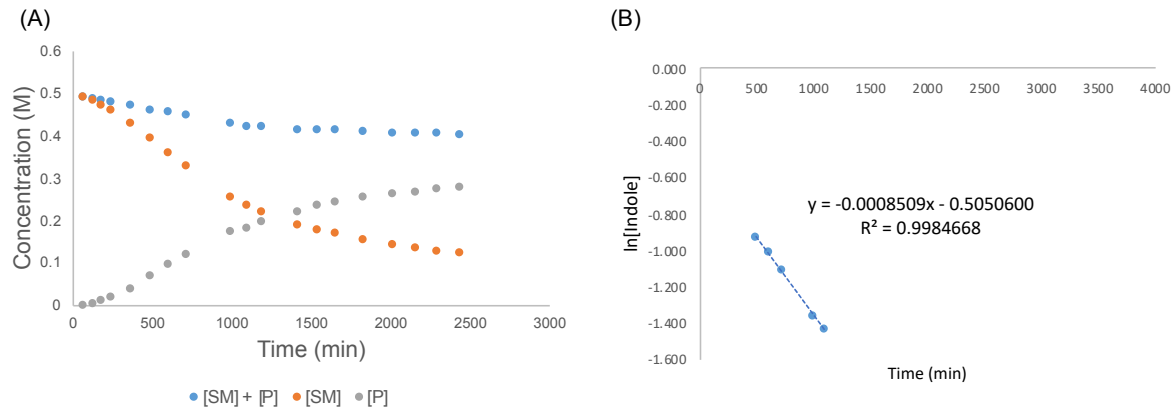
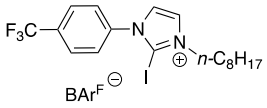



**Figure 3.46.** Data graphed for reaction catalyzed by **3.7e•OTf**: (A) Reaction profile. (B) Graph of ln[Indole] vs. time using the initial five data points after > 10% of the indole was consumed.

**Table 3.22.** $^{1}$H NMR data for the indole addition catalyzed by **3.7e•BAr$^{F}$**.




| Time (min) | [SM] | [P] | ln[SM] |
|---|---|---|---|
| 0 | 0.497 | 0.000 | -0.699 |
| 54 | 0.497 | 0.001 | -0.699 |
| 60 | 0.490 | 0.001 | -0.714 |
| 119 | 0.491 | 0.001 | -0.711 |
| 178 | 0.484 | 0.000 | -0.725 |
| 238 | 0.473 | 0.007 | -0.748 |
| 297 | 0.450 | 0.026 | -0.798 |
| 357 | 0.427 | 0.047 | -0.852 |
| 418 | 0.398 | 0.068 | -0.921 |
| 477 | 0.370 | 0.089 | -0.995 |
| 537 | 0.348 | 0.107 | -1.055 |
| 597 | 0.324 | 0.125 | -1.128 |
| 657 | 0.303 | 0.139 | -1.195 |
| 718 | 0.289 | 0.151 | -1.241 |
| 777 | 0.274 | 0.161 | -1.293 |
| 837 | 0.255 | 0.165 | -1.366 |
| 898 | 0.246 | 0.177 | -1.403 |

$k_{obs} = 11.47 \times 10^{-4}$ min$^{-1}$

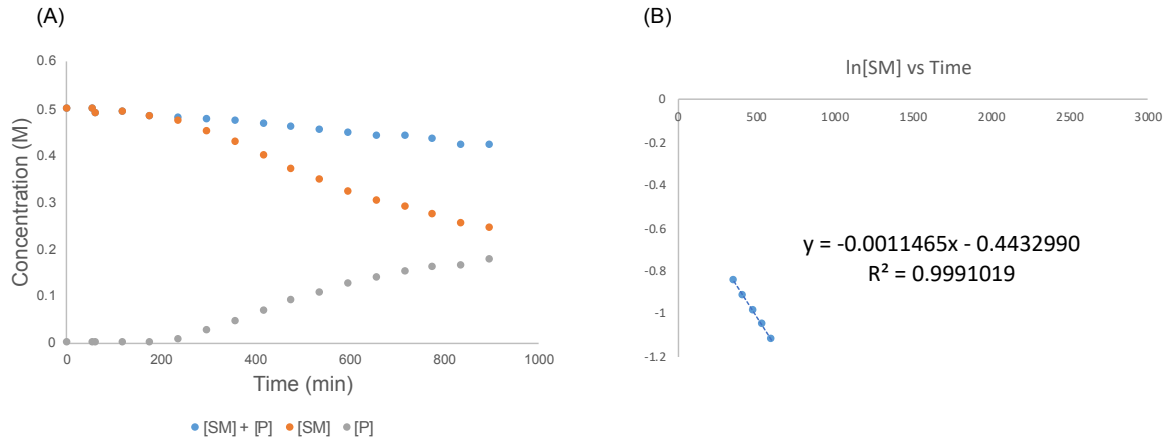
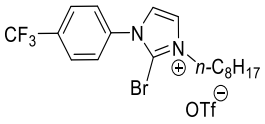



**Figure 3.47.** Data graphed for reaction catalyzed by **3.7e•BAr$^{F}$**: (A) Reaction profile. (B) Graph of ln[Indole] vs. time using the initial five data points after > 10% of the indole was consumed.

**Table 3.23.** $^{1}$H NMR data for the indole addition catalyzed by **3.7f•OTf**.




| Time (min) | [SM] | [P] | [SM] + [P] |
|---|---|---|---|
| 0 | 0.484 | 0.000 | 0.484 |
| 14 | 0.484 | 0.000 | 0.484 |
| 67 | 0.483 | 0.001 | 0.483 |
| 120 | 0.481 | 0.001 | 0.482 |
| 239 | 0.479 | 0.001 | 0.479 |
| 359 | 0.477 | 0.001 | 0.479 |
| 479 | 0.473 | 0.001 | 0.474 |
| 600 | 0.472 | 0.001 | 0.473 |
| 749 | 0.469 | 0.001 | 0.470 |
| 848 | 0.468 | 0.002 | 0.470 |
| 1021 | 0.459 | 0.001 | 0.460 |
| 1189 | 0.463 | 0.002 | 0.465 |

No reaction observed

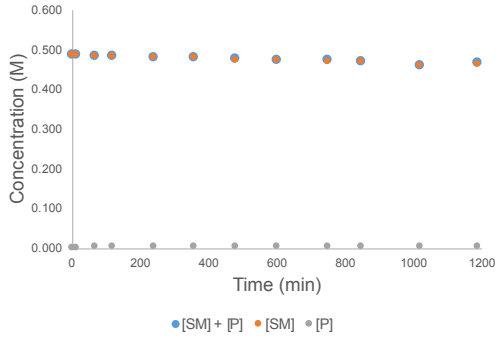
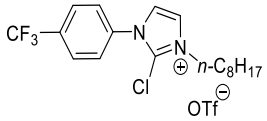



**Figure 3.48.** Reaction profile for reaction catalyzed by **3.7f•OTf**.

**Table 3.24.** $^{1}$H NMR data for the indole addition catalyzed by **3.7g•OTf**.




| Time (min) | [SM] | [P] | [SM] + [P] |
|---|---|---|---|
| 0 | 0.446 | 0.000 | 0.446 |
| 29 | 0.446 | 0.000 | 0.446 |
| 75 | 0.444 | 0.001 | 0.445 |
| 127 | 0.443 | 0.001 | 0.445 |
| 247 | 0.439 | 0.004 | 0.444 |
| 367 | 0.437 | 0.002 | 0.439 |
| 486 | 0.433 | 0.004 | 0.437 |
| 615 | 0.429 | 0.008 | 0.437 |
| 757 | 0.423 | 0.010 | 0.433 |
| 855 | 0.421 | 0.010 | 0.431 |
| 1029 | 0.413 | 0.017 | 0.430 |
| 1202 | 0.408 | 0.022 | 0.430 |

No reaction observed

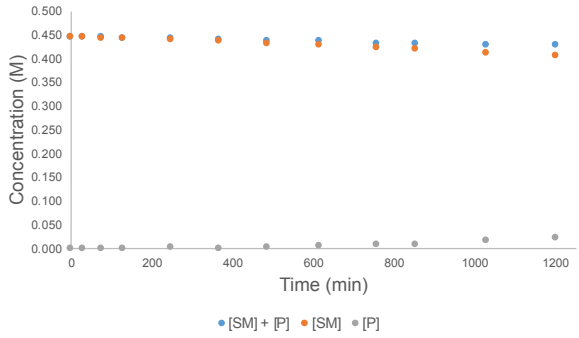
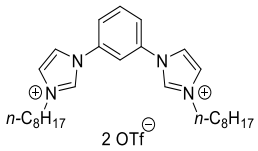



**Figure 3.49.** Reaction profile for reaction catalyzed by **3.7g•OTf**.

**Table 3.25.** [1]H NMR data for the indole addition catalyzed by **3.8a•OTf**.




| Time (min) | [SM] | [P] | [SM] + [P] |
|---|---|---|---|
| 0 | 0.494 | 0.000 | 0.494 |
| 83 | 0.494 | 0.000 | 0.494 |
| 160 | 0.485 | 0.001 | 0.486 |
| 277 | 0.482 | 0.001 | 0.483 |
| 404 | 0.483 | 0.001 | 0.484 |
| 668 | 0.483 | 0.001 | 0.484 |
| 758 | 0.483 | 0.001 | 0.484 |
| 879 | 0.483 | 0.000 | 0.483 |
| 1076 | 0.486 | 0.001 | 0.487 |
| 1325 | 0.490 | 0.001 | 0.491 |
| 1597 | 0.486 | 0.001 | 0.487 |
| 1767 | 0.487 | 0.001 | 0.489 |
| 1966 | 0.494 | 0.001 | 0.495 |
| 2842 | 0.494 | 0.000 | 0.494 |
| 3037 | 0.493 | 0.001 | 0.494 |
| 3332 | 0.493 | 0.000 | 0.493 |
| 3551 | 0.496 | 0.000 | 0.496 |

No reaction observed

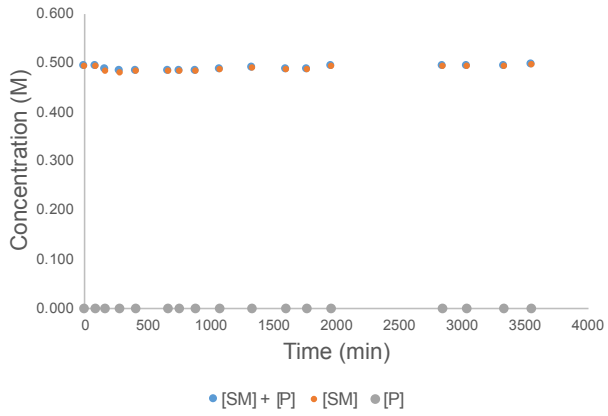
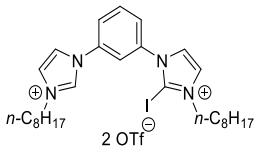



**Figure 3.50.** Reaction profile for reaction catalyzed by **3.8a•OTf**.

**Table 3.26.** $^{1}$H NMR data for the indole addition catalyzed by **3.8b•OTf**.




| Time (min) | [SM] | [P] | ln[SM] |
|---|---|---|---|
| 0 | 0.444 | 0.000 | -0.813 |
| 14 | 0.444 | 0.000 | -0.813 |
| 217 | 0.441 | 0.001 | -0.818 |
| 269 | 0.423 | 0.013 | -0.860 |
| 391 | 0.389 | 0.040 | -0.944 |
| 516 | 0.353 | 0.074 | -1.042 |
| 632 | 0.320 | 0.105 | -1.138 |
| 756 | 0.289 | 0.134 | -1.240 |
| 871 | 0.269 | 0.165 | -1.315 |
| 992 | 0.236 | 0.183 | -1.443 |
| 1892 | 0.121 | 0.283 | -2.115 |
| 2063 | 0.108 | 0.301 | -2.228 |

$k_{obs} = 8.23 \times 10^{-4}$ min$^{-1}$

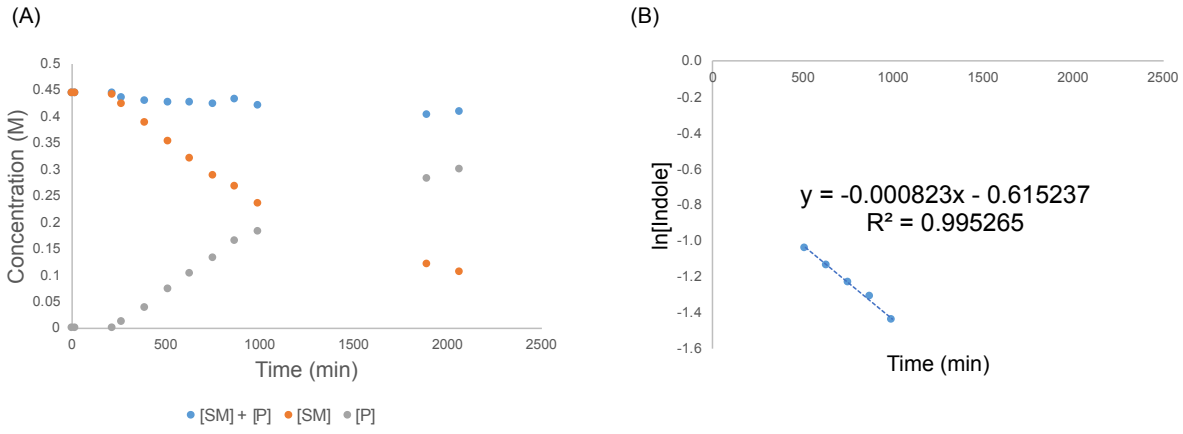
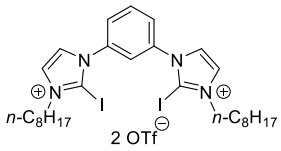



**Figure 3.51.** Data graphed for reaction catalyzed by **3.8b•OTf**: (A) Reaction profile. (B) Graph of ln[Indole] vs. time using the initial five data points after > 10% of the indole was consumed.

**Table 3.27.** $^{1}$H NMR data for the indole addition catalyzed by **3.8c•OTf**.




| Time (min) | [SM] | [P] | ln[SM] |
|---|---|---|---|
| 0 | 0.494 | 0.000 | -0.706 |
| 18 | 0.494 | 0.000 | -0.706 |
| 95 | 0.492 | 0.003 | -0.709 |
| 191 | 0.466 | 0.023 | -0.763 |
| 295 | 0.433 | 0.052 | -0.836 |
| 341 | 0.418 | 0.066 | -0.871 |
| 462 | 0.375 | 0.101 | -0.982 |
| 523 | 0.356 | 0.119 | -1.034 |
| 593 | 0.335 | 0.135 | -1.094 |
| 642 | 0.319 | 0.152 | -1.144 |
| 762 | 0.284 | 0.179 | -1.257 |
| 882 | 0.254 | 0.205 | -1.369 |
| 1003 | 0.228 | 0.227 | -1.477 |
| 1122 | 0.206 | 0.243 | -1.578 |
| 1243 | 0.190 | 0.260 | -1.660 |
| 1362 | 0.174 | 0.272 | -1.751 |
| 1422 | 0.167 | 0.276 | -1.791 |
| 1542 | 0.149 | 0.289 | -1.904 |
| 1663 | 0.141 | 0.297 | -1.960 |
| 1782 | 0.130 | 0.305 | -2.041 |
| 1902 | 0.120 | 0.312 | -2.118 |

$k_{obs} = 9.21 \times 10^{-4}$ min$^{-1}$

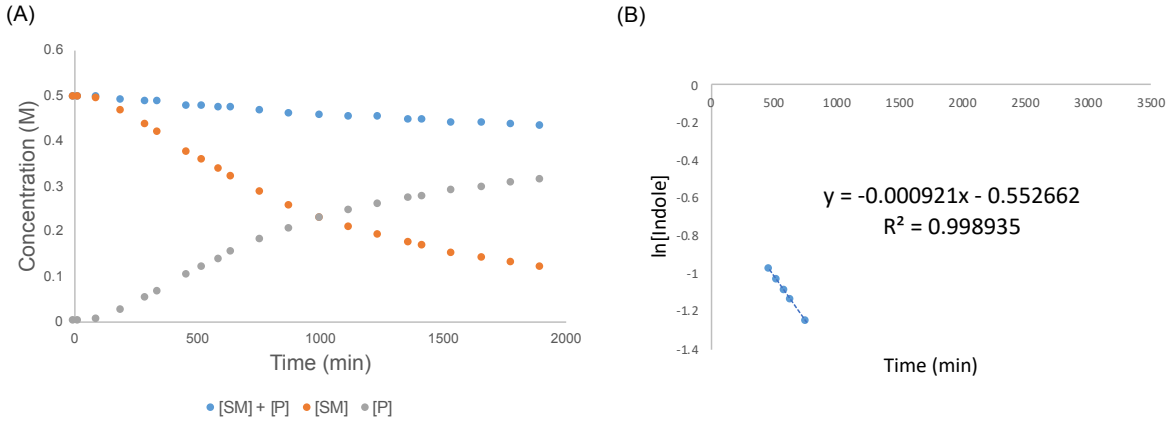
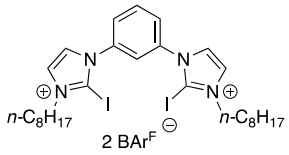



**Figure 3.52.** Data graphed for reaction catalyzed by **3.8c•OTf**: (A) Reaction profile. (B) Graph of ln[Indole] vs. time using the initial five data points after > 10% of the indole was consumed.

**Table 3.28.** $^1$H NMR data for the indole addition catalyzed by **3.8c•BAr$^F$**.




| Time (min) | [SM] | [P] | ln[SM] |
|---|---|---|---|
| 0 | 0.490 | 0.000 | -0.712 |
| 10 | 0.490 | 0.000 | -0.712 |
| 32 | 0.491 | 0.004 | -0.711 |
| 113 | 0.444 | 0.035 | -0.812 |
| 117 | 0.435 | 0.045 | -0.832 |
| 121 | 0.421 | 0.054 | -0.864 |
| 137 | 0.384 | 0.085 | -0.957 |
| 166 | 0.331 | 0.130 | -1.107 |
| 207 | 0.296 | 0.166 | -1.217 |
| 269 | 0.242 | 0.208 | -1.421 |
| 317 | 0.210 | 0.234 | -1.562 |
| 377 | 0.193 | 0.249 | -1.643 |
| 436 | 0.181 | 0.260 | -1.711 |
| 497 | 0.173 | 0.263 | -1.752 |
| 557 | 0.169 | 0.267 | -1.778 |
| 617 | 0.162 | 0.270 | -1.822 |
| 677 | 0.158 | 0.270 | -1.845 |
| 797 | 0.157 | 0.273 | -1.851 |
| 917 | 0.148 | 0.274 | -1.910 |

$k_{obs} = 3.26 \times 10^{-3}$ min$^{-1}$

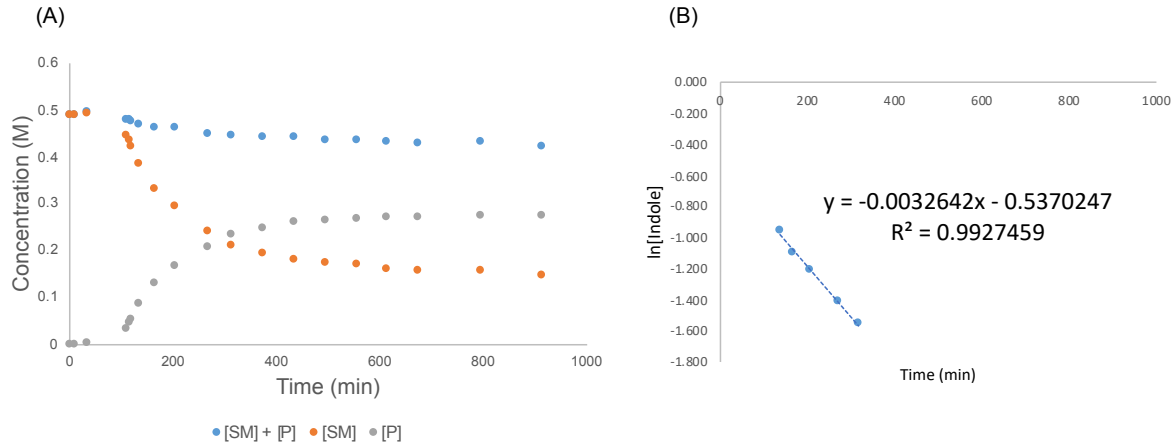
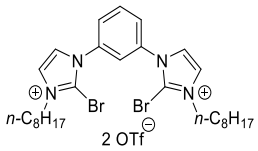



**Figure 3.53.** Data graphed for reaction catalyzed by **3.8c•BAr$^F$**: (A) Reaction profile. (B) Graph of ln[Indole] vs. time using the initial five data points after > 10% of the indole was consumed.

**Table 3.29.** $^{1}$H NMR data for the indole addition catalyzed by **3.8d•OTf**.




| Time (min) | [SM] | [P] | [SM] + [P] |
|---|---|---|---|
| 0 | 0.497 | 0.000 | 0.497 |
| 6 | 0.497 | 0.000 | 0.497 |
| 161 | 0.481 | 0.001 | 0.482 |
| 262 | 0.480 | 0.001 | 0.481 |
| 383 | 0.479 | 0.002 | 0.481 |
| 508 | 0.479 | 0.002 | 0.481 |
| 622 | 0.478 | 0.003 | 0.481 |
| 742 | 0.476 | 0.004 | 0.481 |
| 862 | 0.476 | 0.005 | 0.482 |
| 982 | 0.472 | 0.007 | 0.479 |
| 1883 | 0.467 | 0.014 | 0.481 |
| 2361 | 0.466 | 0.016 | 0.482 |

No reaction observed

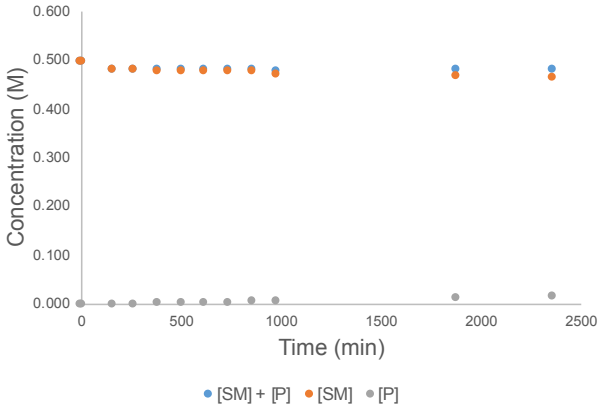
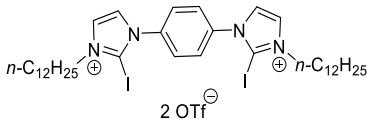



**Figure 3.54.** Reaction profile for reaction catalyzed by **3.8d•OTf**.

**Table 3.30.** $^1$H NMR data for the indole addition catalyzed by **3.9•OTf**.




| Time (min) | [SM] | [P] | ln[SM] |
|---|---|---|---|
| 0 | 0.496 | 0.000 | -0.702 |
| 25 | 0.493 | 0.000 | -0.708 |
| 102 | 0.496 | 0.000 | -0.702 |
| 199 | 0.497 | 0.000 | -0.699 |
| 302 | 0.499 | 0.000 | -0.695 |
| 348 | 0.499 | 0.000 | -0.695 |
| 470 | 0.496 | 0.000 | -0.702 |
| 530 | 0.496 | 0.000 | -0.702 |
| 590 | 0.495 | 0.000 | -0.704 |
| 649 | 0.492 | 0.000 | -0.710 |
| 770 | 0.488 | 0.000 | -0.717 |
| 889 | 0.474 | 0.006 | -0.746 |
| 1010 | 0.440 | 0.030 | -0.821 |
| 1129 | 0.393 | 0.063 | -0.933 |
| 1250 | 0.354 | 0.092 | -1.040 |
| 1369 | 0.322 | 0.115 | -1.132 |
| 1429 | 0.304 | 0.127 | -1.191 |
| 1549 | 0.278 | 0.144 | -1.280 |
| 1673 | 0.258 | 0.160 | -1.356 |
| 1791 | 0.241 | 0.168 | -1.421 |
| 1924 | 0.225 | 0.176 | -1.490 |
| 2031 | 0.213 | 0.183 | -1.544 |
| 2211 | 0.204 | 0.185 | -1.591 |
| 2393 | 0.189 | 0.189 | -1.668 |
| 2583 | 0.180 | 0.183 | -1.715 |
| 2933 | 0.175 | 0.194 | -1.745 |
| 3078 | 0.150 | 0.196 | -1.898 |

$k_{obs} = 8.28 \times 10^{-4}$ min$^{-1}$

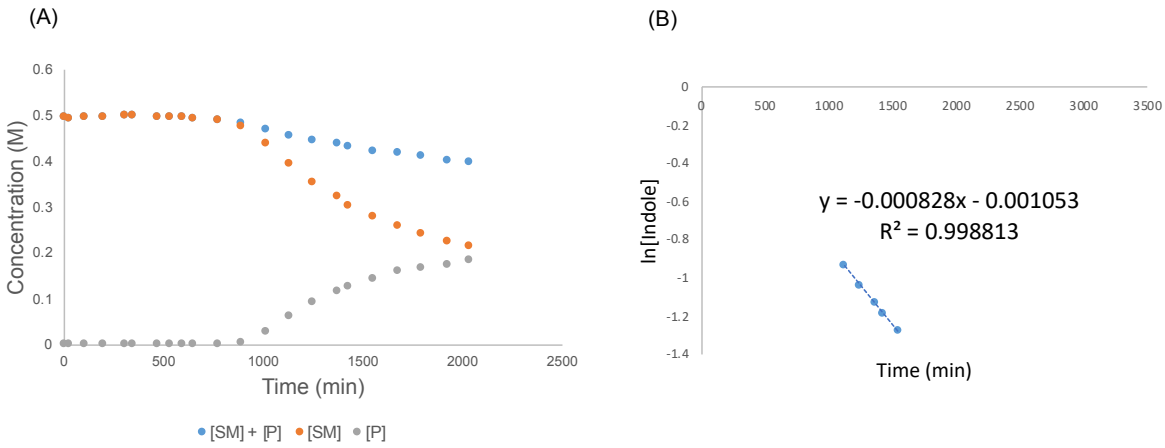



**Figure 3.55.** Data graphed for reaction catalyzed by **3.9•OTf**: (A) Reaction profile. (B) Graph of ln[Indole] vs. time using the initial five data points after > 10% of the indole was consumed.

## VI. References


(1) Noedling, A. R.; Jakab, G.; Schreiner, P. R.; Hilt, G. 31P NMR Spectroscopically Quantified Hydrogen-Bonding Strength of Thioureas and Their Catalytic Activity in Diels-Alder Reactions. *Eur. J. Org. Chem.* **2014**, *2014*, 6394–6398. https://doi.org/10.1002/ejoc.201402871.

(2) Noedling, A. R.; Muether, K.; Rohde, V. H. G.; Hilt, G.; Oestreich, M. Ferrocene-Stabilized Silicon Cations as Catalysts for Diels-Alder Reactions: Attempted Experimental Quantification of Lewis Acidity and ReactIR Kinetic Analysis. *Organometallics* **2014**, *33*, 302–308. https://doi.org/10.1021/om401040y.

(3) Jennings, J. J.; Wigman, B. W.; Armstrong, B. M.; Franz, A. K. NMR Quantification of the Effects of Ligands and Counterions on Lewis Acid Catalysis. *J. Org. Chem.* **2019**, *84*, 15845–15853. https://doi.org/10.1021/acs.joc.9b02107.

(4) Jagannathan, J. R.; Diemoz, K. M.; Targos, K.; Fettinger, J. C.; Franz, A. K. Kinetic and Binding Studies Reveal Cooperativity and Off-Cycle Competition for H-Bonding Catalysis with Silsesquioxane Silanols. *Chem. - Eur. J.* **2019**, *25*, 14953–14958. https://doi.org/10.1002/chem.201903693.

(5) Diemoz, K. M.; Franz, A. K. NMR Quantification of Hydrogen-Bond-Activating Effects for Organocatalysts Including Boronic Acids. *J. Org. Chem.* **2019**, *84*, 1126–1138. https://doi.org/10.1021/acs.joc.8b02389.

(6) Bamberger, J.; Ostler, F.; Mancheno, O. G. Frontiers in Halogen and Chalcogen-Bond Donor Organocatalysis. *ChemCatChem* **2019**, *11*, 5198–5211. https://doi.org/10.1002/cctc.201901215.

(7) Sutar, R. L.; Huber, S. M. Catalysis of Organic Reactions through Halogen Bonding. *ACS Catal.* **2019**, *9*, 9622–9639. https://doi.org/10.1021/acscatal.9b02894.

(8) Bulfield, D.; Huber, S. M. Halogen Bonding in Organic Synthesis and Organocatalysis. *Chem. - Eur. J.* **2016**, *22*, 14434–14450. https://doi.org/10.1002/chem.201601844.

(9) Walter, S. M.; Kniep, F.; Herdtweck, E.; Huber, S. M. Halogen-Bond-Induced Activation of a Carbon-Heteroatom Bond. *Angew. Chem. Int. Ed.* **2011**, *50*, 7187. https://doi.org/10.1002/anie.201101672.

(10) Jungbauer, S. H.; Walter, S. M.; Schindler, S.; Rout, L.; Kniep, F.; Huber, S. M. Activation of a Carbonyl Compound by Halogen Bonding. *Chem. Commun. Camb. U. K.* **2014**, *50*, 6281–6284. https://doi.org/10.1039/c4cc03124e.

(11) Cavallo, G.; Metrangolo, P.; Milani, R.; Pilati, T.; Priimagi, A.; Resnati, G.; Terraneo, G. The Halogen Bond. *Chem. Rev.* **2016**, *116*, 2478–2601. https://doi.org/10.1021/acs.chemrev.5b00484.

(12) Desiraju, G. R.; Ho, P. S.; Kloo, L.; Legon, A. C.; Marquardt, R.; Metrangolo, P.; Politzer, P.; Resnati, G.; Rissanen, K. Definition of the Halogen Bond (IUPAC Recommendations 2013). *Pure Appl. Chem.* **2013**, *85*, 1711–1713. https://doi.org/10.1351/pac-rec-12-05-10.

(13) Politzer, P.; Murray, J. S.; Clark, T. Halogen Bonding: An Electrostatically-Driven Highly Directional Noncovalent Interaction. *Phys. Chem. Chem. Phys.* **2010**, *12* (28), 7748. https://doi.org/10.1039/c004189k.

(14) Berger, G.; Soubhye, J.; Meyer, F. Halogen Bonding in Polymer Science: From Crystal Engineering to Functional Supramolecular Polymers and Materials. *Polym. Chem.* **2015**, *6*, 3559–3580. https://doi.org/10.1039/c5py00354g.

(15) Mukherjee, A.; Tothadi, S.; Desiraju, G. R. Halogen Bonds in Crystal Engineering: Like Hydrogen Bonds yet Different. *Acc. Chem. Res.* **2014**, *47*, 2514–2524. https://doi.org/10.1021/ar5001555.

(16) Metrangolo, P.; Neukirch, H.; Pilati, T.; Resnati, G. Halogen Bonding Based Recognition Processes: A World Parallel to Hydrogen Bonding. *Acc. Chem. Res.* **2005**, *38*, 386–395. https://doi.org/10.1021/ar0400995.

(17) Scholfield, M. R.; Vander Zanden, C. M.; Carter, M.; Ho, P. S. Halogen Bonding (X-Bonding): A Biological Perspective. *Protein Sci.* **2013**, *22*, 139–152. https://doi.org/10.1002/pro.2201.

(18) Metrangolo, P.; Resnati, G. Halogen versus Hydrogen. *Sci. Wash. DC U. S.* **2008**, *321*, 918–919. https://doi.org/10.1126/science.1162215.

(19) Kniep, F.; Rout, L.; Walter, S. M.; Bensch, H. K. V.; Jungbauer, S. H.; Herdtweck, E.; Huber, S. M. 5-Iodo-1,2,3-Triazolium-Based Multidentate Halogen-Bond Donors as Activating Reagents. *Chem. Commun. Camb. U. K.* **2012**, *48*, 9299–9301. https://doi.org/10.1039/c2cc34392d.

(20) Jungbauer, S. H.; Huber, S. M. Cationic Multidentate Halogen-Bond Donors in Halide Abstraction Organocatalysis: Catalyst Optimization by Preorganization. *J. Am. Chem. Soc.* **2015**, *137*, 12110–12120. https://doi.org/10.1021/jacs.5b07863.
(21) Takeda, Y.; Hisakuni, D.; Lin, C.-H.; Minakata, S. 2-Halogenoimidazolium Salt Catalyzed Aza-Diels-Alder Reaction through Halogen-Bond Formation. *Org. Lett.* **2015**, *17*, 318–321. https://doi.org/10.1021/ol503426f.
(22) Chan, Y.-C.; Yeung, Y.-Y. Halogen Bond Catalyzed Bromocarbocyclization. *Angew. Chem. Int. Ed.* **2018**, *57*, 3483–3487. https://doi.org/10.1002/anie.201800261.
(23) Saito, M.; Tsuji, N.; Kobayashi, Y.; Takemoto, Y. Direct Dehydroxylative Coupling Reaction of Alcohols with Organosilanes through Si-X Bond Activation by Halogen Bonding. *Org. Lett.* **2015**, *17*, 3000–3003. https://doi.org/10.1021/acs.orglett.5b01290.
(24) Squitieri, R. A.; Fitzpatrick, K. P.; Jaworski, A. A.; Scheidt, K. A. Synthesis and Evaluation of Azolium-Based Halogen-Bond Donors. *Chem. - Eur. J.* **2019**, *25*, 10069–10073. https://doi.org/10.1002/chem.201902298.
(25) Liu, X.; Ma, S.; Toy, P. H. Halogen Bond-Catalyzed Friedel-Crafts Reactions of Aldehydes and Ketones Using a Bidentate Halogen Bond Donor Catalyst: Synthesis of Symmetrical Bis(Indolyl)Methanes. *Org. Lett.* **2019**, *21*, 9212–9216. https://doi.org/10.1021/acs.orglett.9b03578.
(26) Erdelyi, M. Halogen Bonding in Solution. *Chem. Soc. Rev.* **2012**, *41*, 3547–3557. https://doi.org/10.1039/c2cs15292d.
(27) Laurence, C.; Queignec-Cabanetos, M.; Dziembowska, T.; Queignec, R.; Wojtkowiak, B. 1-Iodoacetylenes. 1. Spectroscopic Evidence of Their Complexes with Lewis Bases. A Spectroscopic Scale of Soft Basicity. *J. Am. Chem. Soc.* **1981**, *103*, 2567. https://doi.org/10.1021/ja00400a014.
(28) Fan, H.; Eliason, J. K.; Moliva A., C. D.; Olson, J. L.; Flancher, S. M.; Gealy, M. W.; Ulness, D. J. Halogen Bonding in Iodoperfluoroalkane/Pyridine Mixtures. *J. Phys. Chem. A* **2009**, *113*, 14052–14059. https://doi.org/10.1021/jp9057127.
(29) Wash, P. L.; Ma, S.; Obst, U.; Rebek, J. Jr. Nitrogen-Halogen Intermolecular Forces in Solution. *J. Am. Chem. Soc.* **1999**, *121*, 7973–7974. https://doi.org/10.1021/ja991653m.
(30) von der Heiden, D.; Vanderkooy, A.; Erdelyi, M. Halogen Bonding in Solution: NMR Spectroscopic Approaches. *Coord. Chem. Rev.* **2020**, *407*, 213147. https://doi.org/10.1016/j.ccr.2019.213147.
(31) Sarwar, M. G.; Dragisic, B.; Salsberg, L. J.; Gouliaras, C.; Taylor, M. S. Thermodynamics of Halogen Bonding in Solution: Substituent, Structural, and Solvent Effects. *J. Am. Chem. Soc.* **2010**, *132*, 1646–1653. https://doi.org/10.1021/ja9086352.
(32) Metrangolo, P.; Panzeri, W.; Recupero, F.; Resnati, G. Perfluorocarbon-Hydrocarbon Self-Assembly Part 16. 19F NMR Study of the Halogen Bonding between Halo-Perfluorocarbons and Heteroatom Containing Hydrocarbons. *J. Fluor. Chem.* **2002**, *114*, 27–33.
(33) Rege, P. D.; Malkina, O. L.; Goroff, N. S. The Effect of Lewis Bases on the 13C NMR of Iodoalkynes. *J. Am. Chem. Soc.* **2002**, *124*, 370–371. https://doi.org/10.1021/ja016290g.
(34) Glaser, R.; Chen, N.; Wu, H.; Knotts, N.; Kaupp, M. 13C NMR Study of Halogen Bonding of Haloarenes: Measurements of Solvent Effects and Theoretical Analysis. *J. Am. Chem. Soc.* **2004**, *126*, 4412–4419. https://doi.org/10.1021/ja0383672.
(35) Hakkert, S. B.; Graefenstein, J.; Erdelyi, M. The 15N NMR Chemical Shift in the Characterization of Weak Halogen Bonding in Solution. *Faraday Discuss.* **2017**, *203*, 333–346. https://doi.org/10.1039/c7fd00107j.
(36) Beale, T. M.; Chudzinski, M. G.; Sarwar, M. G.; Taylor, M. S. Halogen Bonding in Solution: Thermodynamics and Applications. *Chem. Soc. Rev.* **2013**, *42*, 1667–1680. https://doi.org/10.1039/c2cs35213c.
(37) Benesi, H. A.; Hildebrand, J. H. A Spectrophotometric Investigation of the Interaction of Iodine with Aromatic Hydrocarbons. *J. Am. Chem. Soc.* **1949**, *71*, 2703. https://doi.org/10.1021/ja01176a030.
(38) Klaeboe, P. The Raman Spectra of Some Iodine, Bromine, and Iodine Monochloride Charge-Transfer Coomplexes in Solution. *J. Am. Chem. Soc.* **1967**, *89*, 3667. https://doi.org/10.1021/ja00991a001.

(39) Mayer, U.; Gutmann, V.; Gerger, W. Acceptor Number. Quantitative Empirical Parameter for the Electrophilic Properties of Solvents. *Monatshefte Fuer Chem.* **1975**, *106*, 1235. https://doi.org/10.1007/bf00913599.
(40) Beckett, M. A.; Strickland, G. C.; Holland, J. R.; Varma, K. S. A Convenient NMR Method for the Measurement of Lewis Acidity at Boron Centers: Correlation of Reaction Rates of Lewis Acid Initiated Epoxide Polymerizations with Lewis Acidity. *Polymer* **1996**, *37*, 4629–4631. https://doi.org/10.1016/0032-3861(96)00323-0.
(41) Jagannathan, J. R. *Doctoral Dissertation, University of California−Davis*; 2021.
(42) Walter, S. M.; Kniep, F.; Rout, L.; Schmidtchen, F. P.; Herdtweck, E.; Huber, S. M. Isothermal Calorimetric Titrations on Charge-Assisted Halogen Bonds: Role of Entropy, Counterions, Solvent, and Temperature. *J. Am. Chem. Soc.* **2012**, *134*, 8507–8512. https://doi.org/10.1021/ja2119207.
(43) von der Heiden, D.; Detmar, E.; Kuchta, R.; Breugst, M. Activation of Michael Acceptors by Halogen-Bond Donors. *Synlett* **2018**, *29*, 1307–1313. https://doi.org/10.1055/s-0036-1591841.
(44) Weiss, R.; Aubert, E.; Groslambert, L.; Pale, P.; Mamane, V. Chalcogen Bonding with Diaryl Ditellurides: Evidence from Solid State and Solution Studies. *Chem. - Eur. J.* **2022**, *28*, e202200395. https://doi.org/10.1002/chem.202200395.
(45) Li, C.; Manick, A.-D.; Yang, J.; Givaudan, D.; Biletskyi, B.; Michaud-Chevalier, S.; Dutasta, J.-P.; Herault, D.; Bugaut, X.; Chatelet, B.; Martinez, A. The Chloroazaphosphatrane Motif for Halogen Bonding in Solution. *Inorg. Chem.* **2021**, *60*, 11964–11973. https://doi.org/10.1021/acs.inorgchem.1c01005.
(46) Sysoeva, A. A.; Novikov, A. S.; Il'in, M. V.; Suslonov, V. V.; Bolotin, D. S. Predicting the Catalytic Activity of Azolium-Based Halogen Bond Donors: An Experimentally-Verified Theoretical Study. *Org. Biomol. Chem.* **2021**, *19*, 7611–7620. https://doi.org/10.1039/d1ob01158h.
(47) Weiss, R.; Aubert, E.; Pale, P.; Mamane, V. Chalcogen-Bonding Catalysis with Telluronium Cations. *Angew. Chem. Int. Ed.* **2021**, *60*, 19281–19286. https://doi.org/10.1002/anie.202105482.
(48) Sun, J.; Decato, D. A.; Bryantsev, V. S.; John, E. A.; Berryman, O. B. The Interplay between Hydrogen and Halogen Bonding: Substituent Effects and Their Role in the Hydrogen Bond Enhanced Halogen Bond. *Chem. Sci.* **2023**, *14*, 8924–8935. https://doi.org/10.1039/d3sc02348f.
(49) Steinke, T.; Wonner, P.; Gauld, R. M.; Heinrich, S.; Huber, S. M. Catalytic Activation of Imines by Chalcogen Bond Donors in a Povarov [4+2] Cycloaddition Reaction. *Chem. - Eur. J.* **2022**, *28*, e202200917. https://doi.org/10.1002/chem.202200917.
(50) Zhang, Y.; Zhu, H.; Zhang, B.; Yang, H.; Tan, C.-H.; Wang, C.; Wen, J.; Zong, L. Hydrogen Bond-Enhanced Halogen Bonding Organocatalyst with C(Sp3)-Br and Sulfoxide Moieties. *ACS Catal.* **2023**, *13*, 7103–7109. https://doi.org/10.1021/acscatal.3c01131.
(51) Milic, M.; Targos, K.; Tellez Chavez, M.; Thompson, M. A. M.; Jennings, J. J.; Franz, A. K. NMR Quantification of Hydrogen-Bond-Accepting Ability for Organic Molecules. *J. Org. Chem.* **2021**, *86*, 6031–6043. https://doi.org/10.1021/acs.joc.0c02876.
(52) Kaasik, M.; Martonova, J.; Erkman, K.; Metsala, A.; Jarving, I.; Kanger, T. Enantioselective Michael Addition to Vinyl Phosphonates via Hydrogen Bond-Enhanced Halogen Bond Catalysis. *Chem. Sci.* **2021**, *12*, 7561–7568. https://doi.org/10.1039/d1sc01029h.
(53) Steinke, T.; Wonner, P.; Engelage, E.; Huber, S. M. Catalytic Activation of a Carbon-Chloride Bond by Dicationic Tellurium-Based Chalcogen Bond Donors. *Synthesis* **2021**, *53*, 2043–2050. https://doi.org/10.1055/a-1372-6309.
(54) Honeychuck, R. V.; Hersh, W. H. Coordination of "Noncoordinating" Anions: Synthesis, Characterization, and x-Ray Crystal Structures of Fluorine-Bridged Hexafluoroantimonate(1-), Tetrafluoroborate(1-), and Hexafluorophosphate(1-) Adducts of [R3P(CO)3(NO)W]+. An Unconventional Order of Anion Donor Strength. *Inorg. Chem.* **1989**, *28* (14), 2869–2886. https://doi.org/10.1021/ic00313a034.
(55) Krossing, I.; Raabe, I. Noncoordinating Anions—Fact or Fiction? A Survey of Likely Candidates. *Angew. Chem. Int. Ed.* **2004**, *43* (16), 2066–2090. https://doi.org/10.1002/anie.200300620.
(56) Fife, W. K.; Ranganathan, P.; Zeldin, M. A General Synthesis of 1-Alkyl-4-Vinylpyridinium Ions. Alkylation of 4-Vinylpyridine with Primary Alkyl Triflates. *J. Org. Chem.* **1990**, *55* (21), 5610–5613. https://doi.org/10.1021/jo00308a019.

(57) Baillie, S. E.; Bluemke, T. D.; Clegg, W.; Kennedy, A. R.; Klett, J.; Russo, L.; de Tullio, M.; Hevia, E. Potassium-Alkyl Magnesiates: Synthesis, Structures and Mg–H Exchange Applications of Aromatic and Heterocyclic Substrates. *Chem Commun* **2014**, *50* (85), 12859–12862. https://doi.org/10.1039/C4CC05305B.
(58) Thordarson, P. Determining Association Constants from Titration Experiments in Supramolecular Chemistry. *Chem Soc Rev* **2011**, *40* (3), 1305–1323. https://doi.org/10.1039/C0CS00062K.
(59) Diemoz, K. M.; Wilson, S. O.; Franz, A. K. Synthesis of Structurally Varied 1,3-Disiloxanediols and Their Activity as Anion-Binding Catalysts. *Chem. – Eur. J.* **2016**, *22* (51), 18349–18353. https://doi.org/10.1002/chem.201604103.

# Chapter Four: Evaluation of NMR Quantification for H-bonding Ability of Photoacids

## I. Introduction

This chapter presents a brief summary of work on the evaluation of an NMR quantification method for the H-bonding abilities of photoacids (PAs) using TEPO as the $^{31}$P NMR probe (Figure 4.1). The primary goal is this research is to establish an approach for evaluating and quantifying the H-bonding capabilities of photoacids, with the ultimate goal of expanding the applications of the $^{31}$P NMR quantification methods in our group, as outlined in Chapter 3. This chapter presents 1) assessment of in-situ LED-NMR spectroscopy, 2) identification of the optimal solvent for quantification, and 3) synthesis of merocyanine-type photoacids characterized by extended relaxation times.

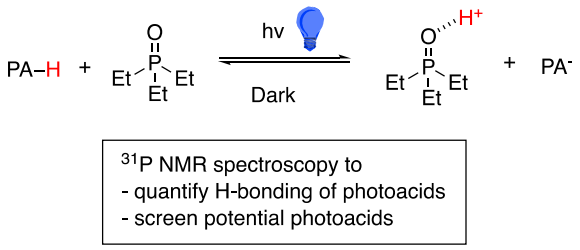



**Figure 4.1.** Objective of Appendix A.

### Ia. Photoacids

A photoacid refers to a molecule that undergoes a transformation into a more potent acid upon exposure to irradiation (Figure 4.2).[1–7] These molecules play a role in regulating proton transfer processes through light, functioning as a control switch between photons and protons. Proton transfer drives a multitude of chemical, material, and biological phenomena, including acid-catalyzed reactions,[8–16] the behavior of pH-sensitive materials,[17–21] and the intricate activities of enzymes.[22–27] The unique attribute of photoacids lies in their potential to exercise precise spatial and temporal control over proton transfer. This characteristic opens up possibilities for harnessing photoacids to convert light energy into alternative forms of energy, marking a promising avenue for innovative applications in diverse fields.

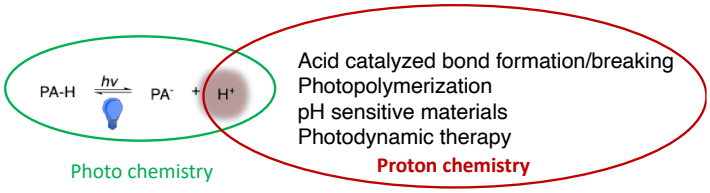



**Figure 4.2.** Application of photoacids.

There are two primary classes of photoacid compounds: irreversible and reversible (Figure 4.3).[1,2] The group of irreversible photoacids consists of photoacid generators (PAG), while the reversible group of photoacids consists of excited-state and metastable-state photoacids. Excited-state and metastable-state photoacids are molecules that possess highly acidic excited states. These photoacids are reversible since the relaxation process, which involves the transition from the excited state to the ground state, causes the molecule to revert to a low acidity state. Excited-state photoacids have a lifespan in the nanosecond range, while metastable-state photoacids have a longer lifespan of approximately 70 seconds. This research is focused on investigating reversible photoacids, which are widely used in acid catalysis .[8–16]

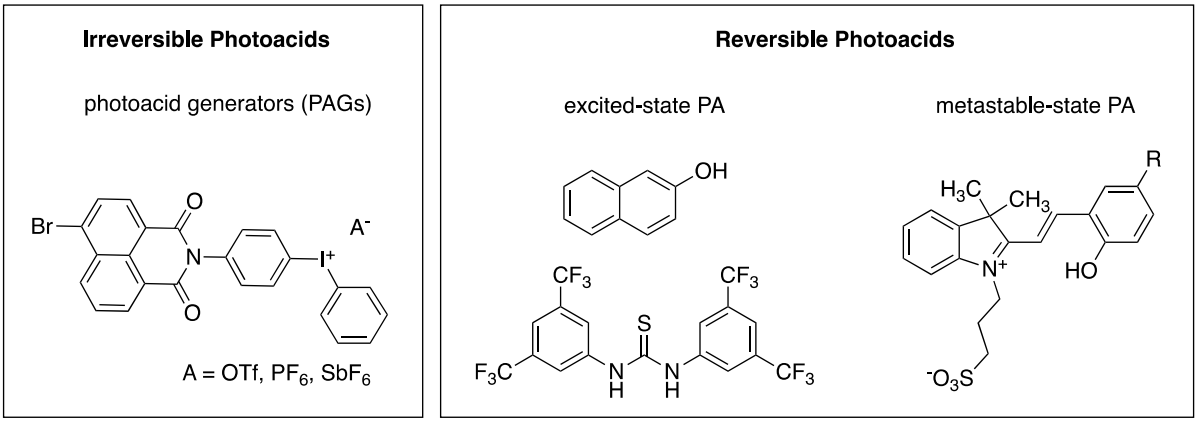


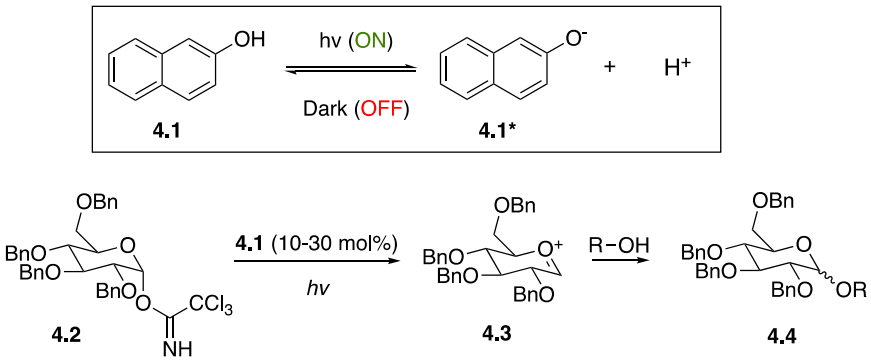

**Figure 4.3.** Examples of a PAG, excited-state photoacids, and a metastable-state photoacid.

## Ib. Photoacids in Catalysis

A reversible photoacid possesses the ability to release a proton upon exposure to light and retrieve the proton in the absence of light.[1,2] The liberated proton can be employed in acid catalysis for polymer or organic synthesis, offering a way to convert light energy into chemical energy. Photoacid catalysts,

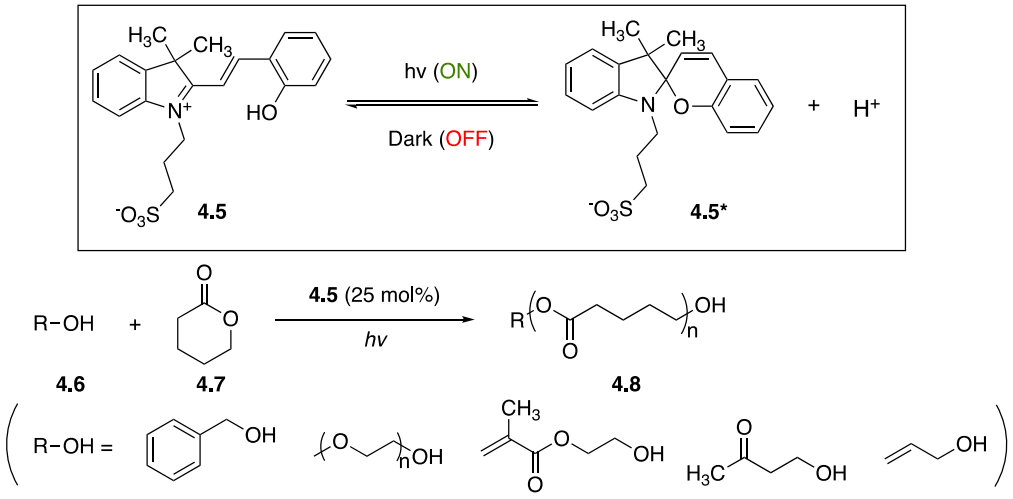
unlike Brønsted acids or Lewis acidic metals, are attractive alternatives due to their potential to overcome limitations such as restricted functional group compatibility or the need for air-free conditions.[3] These catalysts usually exist as stable weak acids in the absence of light and only exhibit strong acid properties upon light activation. Consequently, the reversible nature of such photoacids offers control over reactions involving proton concentration.[8,9,28]

Specific derivatives of phenol and naphthol have exhibited activity as photoacids, displaying increased acidity in their excited state, which has been effective in several acid-sensitive transformations. For example, a glycosylation reaction utilizing naphthol **4.1** was developed (Scheme 4.1).[12] The photocatalysts used in this process were successfully recovered and reused without any loss in catalytic activity.




**Scheme 4.1.** Glycosylation catalyzed by a naphthol photoacid.

In another example, the merocyanine-type photoacid stands out as the first photoacid with a prolonged relaxation time, garnering extensive study (Scheme 4.2).[9] Under blue light photoirradiation, the protonated merocyanine (**4.5**, MEH) undergoes trans-cis isomerization, leading to proton dissociation of cis-MEH and subsequent nucleophilic ring-closure to form a spiropyran (**4.5***, SP), releasing a proton. This process is reversible, with spiropyran **4.5*** converting back to **4.5** and reclaiming the proton in the absence of light. The *in-situ* generated proton serves as a catalyst for the ring-opening polymerization of cyclic esters, yielding well-defined polymers with controlled molecular weight. This provides temporal control of ring-opening polymerization in the presence or absence of light, enabling precise manipulation of molecular weight distributions.




**Scheme 4.2.** Ring-opening polymerization catalyzed by merocyanine-type photoacid **4.5**.

**Quantification of H-bonding abilities photoacids using constant illumination NMR spectroscopy**

Our goal was to employ $^{31}$P NMR spectroscopy to assess the H-bonding abilities of photoacids and screen potential candidates. Our initial strategy involved collaborating with the Olson lab to perform constant illumination NMR experiments.[29] To illuminate samples, we planned to employ a Mightex WheeLED light source equipped with a fiber optic cable directly inserted into the NMR tube.[30] This approach would allow us to potentially discover new and promising photoacids, even those with a short lifetime. A preliminary assessment to evaluate the feasibility and practicality of employing this technique was conducted.

## II. Results and Discussion

### IIa. Concentration Tests

To assess the feasibility of conducting constant illumination NMR experiments, the concentration limitations of our established $^{31}$P NMR quantification method within our research group were examined.[31–35] For constant illumination NMR experiments, as the fiber optic cable tip is positioned above the solvent, the NMR sample solution's concentration should ideally be less than 0.1 mM for effective light penetration through the NMR tube. In our previous $^{31}$P NMR quantification experiments, the sample concentrations ranged between 16 and 36 mM. Concentration tests using TEPO within a range of 0.5 to 32 mM, using three equivalents of 1-naphthol in a $CD_2Cl_2$/DCM (1/4, v/v) solution were

carried out (Figure 4.4). The results indicated that obtaining a $^{31}P$ NMR signal in a 0.5 mM TEPO solution required 1024 scans and an acquisition time exceeding one hour. Due to the impracticality caused by the extended acquisition time, testing the 0.1 mM sample was not continued. The possibility of using the 800 MHz Bruker Avance III equipped with Bruker CPTCI Cryoprobe was also considered. Unfortunately, the cryoprobe available in the UC Davis NMR facility is only compatible with $^{1}H$ and $^{13}C$ NMR spectroscopy. Due to the nanosecond lifetime of excited-state photoacids, screening them was not possible without employing constant illumination NMR spectroscopy. Consequently, attention was redirected towards meta-stable state photoacids, recognized for their longer lifetimes.

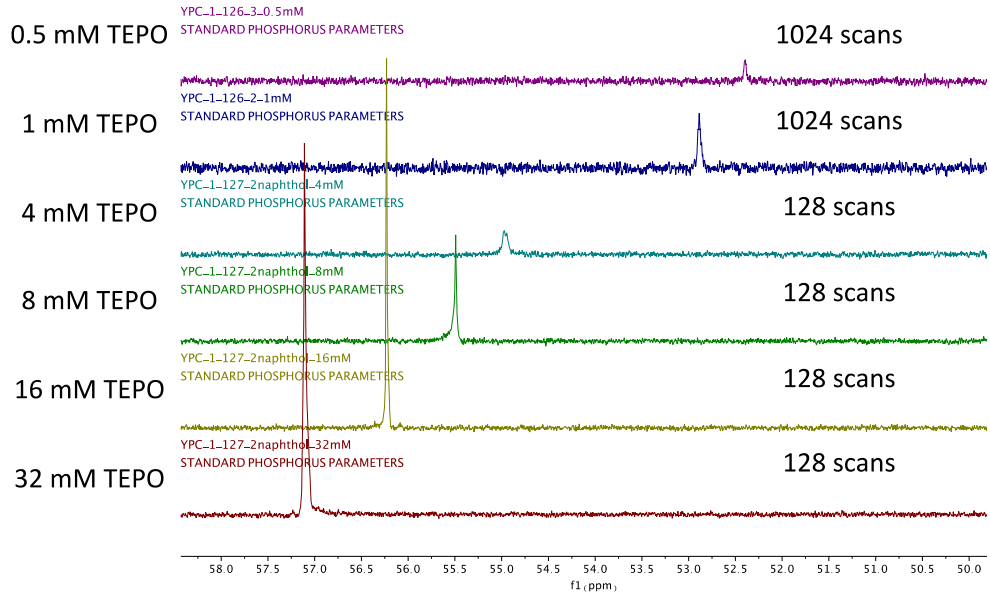
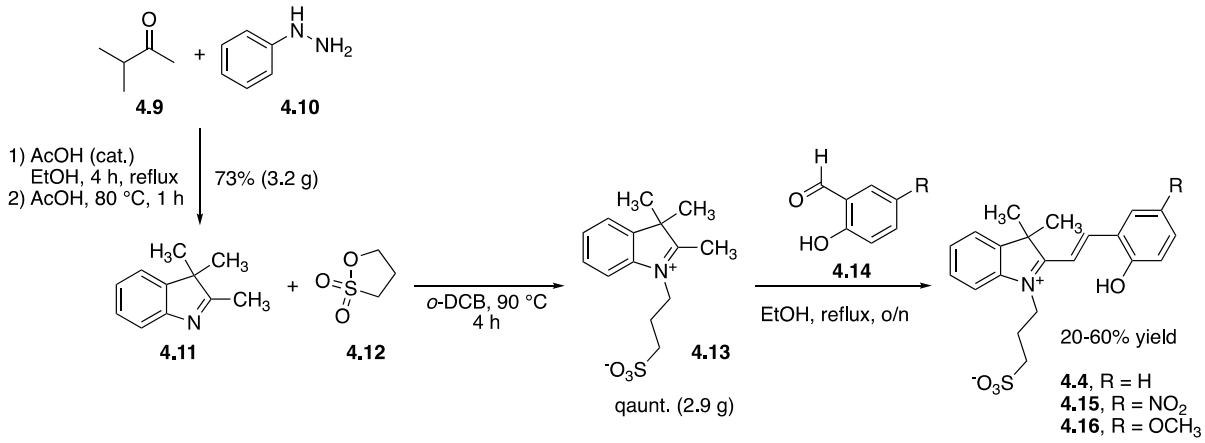



**Figure 4.4.** Concentration test ranging from 0.5 to 32 mM of TEPO to evaluate the signal/noise ratio of the $^{31}P$ signals.

## IIb. Synthesis of Merocyanine-type Photoacids (MEH)

The meta-stable state photoacids, specifically MEH **4.4**, **4.15**, and **4.16** were synthesized, following the procedure outlined in the literature (Scheme 4.3).[8,36] The synthesis involved several steps. Firstly, 2,3,3-trimethylindolenine (**4.11**) was synthesized via the Fischer indole synthesis method, using 3-methyl-2-butanone (**4.9**) and phenylhydrazine (**4.10**). Subsequently, the resulting 2,3,3-trimethylindolenine **4.11** was reacted with propane sultone (**4.12**) to yield the indolium species **4.13**. Finally, MEH was obtained through the condensation between indolium **4.13** and benzaldehydes (**4.14**). All the product yields are

consistent with the reported yields, except for the last step. There was a reduction in product yield due to product loss during recrystallization performed on a small scale (~200 mg).




**Scheme 4.3.** Synthesis of merocyanine-type photoacids (MEH).

## IIc. Solvent Screen

Evaluation of the MEH photoacids were conducted using deuterated solvent screening for the $^{31}P$ NMR quantification method. A mixture of $CD_2Cl_2$/DCM (1/4, v/v) was the original solvent used to study H-bonding ability because it would not interfere with the H-bonding interactions. However, this $CD_2Cl_2$/DCM solvent system could not be utilized due to the insolubility of MEH in this system. Consequently, a solvent screen was conducted using a good H-bonding donor, pentafluorobenzoic acid **4.17**, combined with 8 mM of TEPO in the corresponding solvent systems listed below (Figure 4.5). In a preliminary titration experiment, 3, 5, and 15 equivalents of **4.17** were tested using $D_2O$, MeOD, or a MeOD/$CDCl_3$ solvent mixture for the NMR quantification experiment. However, minimal shifts in $\Delta\delta(^{31}P)$ values were observed in these experiments, indicating that these solvents were not suitable for effective H-bonding quantification.

MeOD

| Equivalents | Δδ (ppm) |
|---|---|
| 3 | 0.05 |
| 5 | 0.11 |
| 15 | 0.23 |

D2O

| Equivalents | Δδ (ppm) |
|---|---|
| 3 | 0.03 |
| 5 | 0.06 |
| 15 | 0.07 |

MeOD/$CDCl_3$ (2/1, v/v)

| Equivalents | Δδ (ppm) |
|---|---|
| 3 | 0.04 |
| 5 | 0.08 |
| 15 | 0.23 |

MeOD/$CDCl_3$ (1/1, v/v)

| Equivalents | Δδ (ppm) |
|---|---|
| 3 | 0.09 |
| 5 | 0.12 |
| 15 | 0.26 |

MeOD/$CDCl_3$ (1/2, v/v)

| Equivalents | Δδ (ppm) |
|---|---|
| 3 | 0.14 |
| 5 | 0.26 |
| 15 | 0.64 |

**Figure 4.5.** Solvent test for the quantification of H-bonding using the $^{31}P$ NMR quantification method.

Next, H-bonding acceptor NMR solvents such as $d^6$-DMSO, $d^6$-acetone, and $d^3$-acetonitrile were evaluated. Notably, low $\Delta\delta(^{31}P)$ values were observed with $d^6$-DMSO. Using $d^6$-DMSO would have been ideal for quantifying H-bonding ability due to its common usage in MEH-related reactions. Distinct trends in the $\Delta\delta(^{31}P)$ values were noticeable in $d^6$-acetonitrile and $d^6$-acetone (Figure 4.6). Additionally, the $\Delta\delta(^{31}P)$ values in these two solvents closely resembled those observed in $CD_2Cl_2$/DCM (1/4, v/v). Consequently, the decision was made to use $d^6$-acetone as the deuterated solvent for the $^{31}P$ NMR quantification method of MEH, due to its lower cost.

$d^6$-DMSO

| Equivalents | Δδ (ppm) |
|---|---|
| 3 | 0.55 |
| 5 | 0.89 |
| 15 | 1.89 |

$d^6$-acetone

| Equivalents | Δδ (ppm) |
|---|---|
| 3 | 10.11 |
| 5 | 11.06 |
| 15 | 12.17 |

$d^3$-ACN

| Equivalents | Δδ (ppm) |
|---|---|
| 3 | 9.83 |
| 5 | 11.23 |
| 15 | 12.08 |

$CD_2Cl_2$/DCM (1/4, v/v)

| Equivalents | Δδ (ppm) |
|---|---|
| 3 | 10.09 |
| 5 | 11.94 |
| 15 | 13.72 |

**Figure 4.6.** Continued solvent test for the quantification of H-bonding using the $^{31}P$ NMR quantification method.

## IId. Assessment of the HBD−TEPO Binding Equilibrium in $d^6$-Acetone

After selecting $d^6$-acetone as the deuterated solvent for the $^{31}P$ NMR quantification method, the HBD−TEPO binding equilibrium was evaluated. To validate the bonding experiment in $d^6$-acetone, method validation including titration experiments, Job plot analysis, and Hammett plot analysis were conducted.

In both the titration and Job plot experiments, 4-trifluoromethylbenzoic acid (**4.18**) was chosen due to its comparable pKa to the merocyanine-type photoacids in their ground state (Figure 4.7). The titration experiment showed saturation at 10 equivalents, which is different from the saturation point observed in $CD_2Cl_2$/DCM (1/4, v/v) at 3 equivalents. The Job plot suggested a 1:1 binding stoichiometry between TEPO and HBD in $d^6$-acetone.

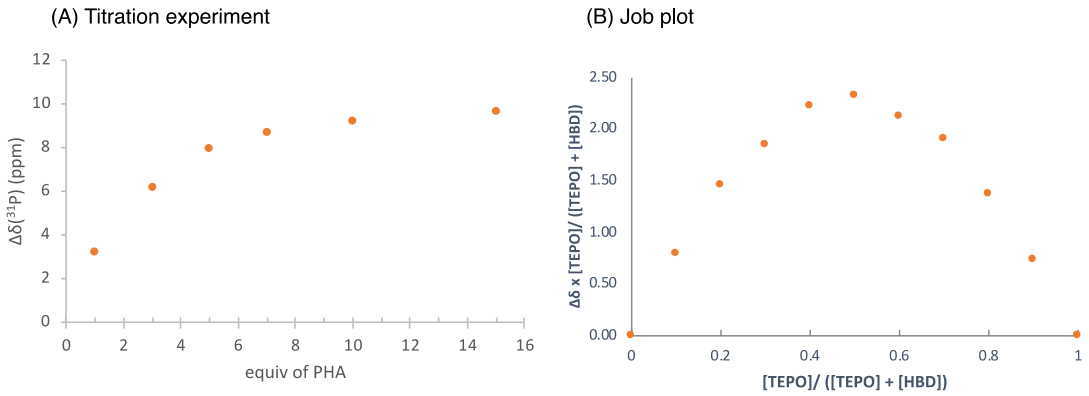
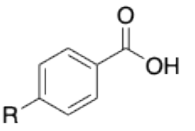



**Figure 4.7.** (A) Titration experiments of **4.18** with TEPO. (B) Job Plot of **4.18** binding with TEPO (at 8 mM in d$^6$-acetone).

To further validate the capability of $^{31}$P NMR spectroscopy and TEPO binding to quantify the electronic effects of H-bonding in d$^6$-acetone, a Hammett plot was made for a series of benzoic acids with electronically varied substituents on the para-position (Figure 4.8). A linear relationship ($R^2$ = 0.998) was observed for benzoic acids in 8 mM TEPO, indicating the accurate quantification of Δδ($^{31}$P) values for electronic changes influencing H-bonding ability in d$^6$-acetone. This strong correlation validates the $^{31}$P quantification method using d$^6$-acetone to quantify H-bonding abilities.




| R | σ parameter | Equiv of HBD | Δδ (ppm) |
|---|---|---|---|
| OMe | -0.27 | 10 | 7.29 |
| H | 0 | 10 | 8.05 |
| Cl | 0.23 | 10 | 8.53 |
| $CF_3$ | 0.54 | 10 | 9.27 |
| $NO_2$ | 0.78 | 10 | 9.85 |

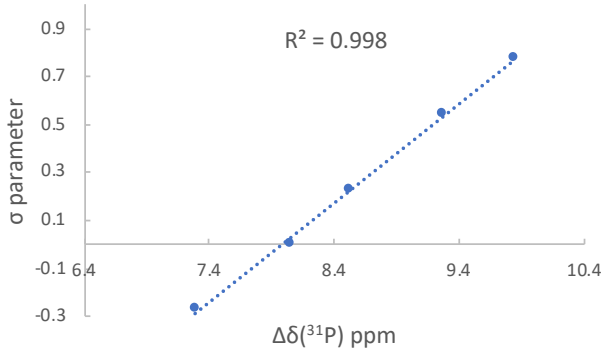



**Figure 4.8.** Correlation of Δδ($^{31}$P) values and Hammett σ parameters for para-substituted benzoic acids.

## IIe. Benchtop Irradiation of MEH

Following the validation of the $^{31}$P NMR method for quantifying H-bonding ability in d$^6$-acetone, the potential activation of the metastable-state photoacid, MEH **4.5**, was tested on the benchtop. The methodology involved exposing the NMR sample to blue LED light on the benchtop for five minutes,

followed by an immediate NMR scan after irradiation (Figure 4.9A). The feasibility of this approach was confirmed by initially utilizing $^1$H NMR spectroscopy to verify the method, referencing the reported $^1$H NMR spectra of **4.5** in d$^6$-DMSO before and after irradiation.[8] The results showed no observation of **4.5** during NMR acquisition period, demonstrating the successful tracking of **4.5*** using $^1$H NMR spectroscopy after the benchtop irradiation (Figure 4.9B). However, due to the low solubility of **4.5** in d$^6$-acetone (<2 mM), this benchtop irradiation method could not be applied in d$^6$-acetone for obtaining $^1$H NMR spectra.

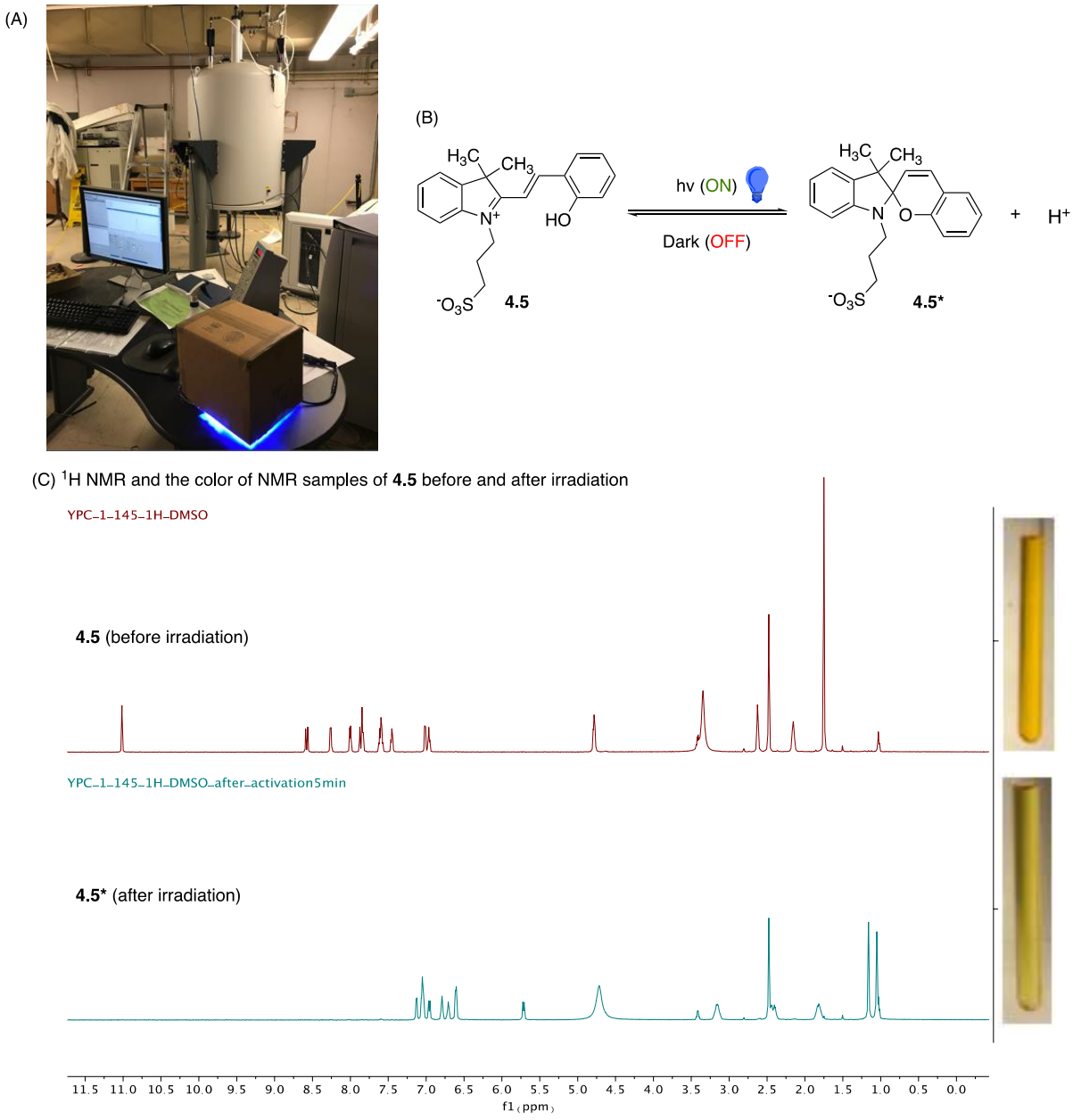



**Figure 4.9.** (A) Benchtop irradiation setup; (B) The transformation of **4.5** before and after irradiation; (C) $^1$H NMR spectra of **4.5** in d$^6$-DMSO before and after irradiation.

## IIf. Preliminary $^{31}$P NMR Quantification Experiments of MEH

Upon confirming the effectiveness of the benchtop irradiation of **4.5**, the $^{31}$P NMR quantification method in d$^6$-acetone was then tested based on the previous solvent screen. Due to the low solubility of **4.5** in most solvents except for DMSO, preparing an NMR sample with TEPO at 2 mM and photoacid **4.5** at 2 mM (1.0 equivalent each) was not possible in d$^6$-acetone. Consequently, the concentration and equivalence of the photoacid remained unknown. Nevertheless, $\Delta\delta(^{31}P)$ values were measured for (A) a TEPO-only sample as a blank and (B) TEPO with **4.5** before irradiation (Figure 4.10). The $\Delta\delta(^{31}P)$ value measured for the pre-irradiated **4.5** was 0.04 ppm, suggesting it to be a weak H-bonding donor. Following this, the same sample was exposed to blue light on the benchtop for three minutes a subsequent $^{31}$P NMR spectrum was obtained. The 2 mM TEPO solution required 256 scans, taking approximately 15 minutes acquisition time. However, this prolonged acquisition time raised concerns regarding the possibility of **4.5*** reverting back to **4.5**. Despite these challenges, a broad peak in the $^{31}$P NMR with a $\Delta\delta(^{31}P)$ value of 14.79 ppm was observed (Figure 4.10C), indicating that the irradiated **4.5*** species is a more potent H-bonding donor. The broad peak might be caused by the fast equilibrium between TEPO, **4.5***, and potentially **4.5** that reverted back. The $^{31}$P downfield shift before and after irradiation of photoacids, $\Delta\Delta\delta(^{31}P)^*$, is 14.75 ppm for **4.5**.

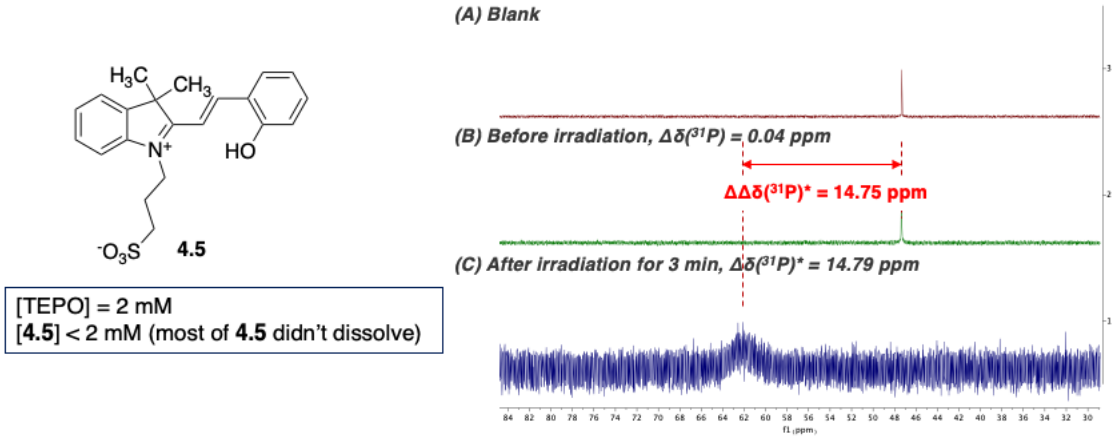



**Figure 4.10.** Preliminary results of $\Delta\Delta\delta(^{31}P)^*$ for **4.5**.

The preliminary $^{31}$P NMR experiments of **4.15** were also conducted. Similar to the findings with **4.5**, **4.15** was not very soluble in d$^6$-acetone. Consequently, the concentration and equivalence of **4.15** in the sample remained unknown. An observed $\Delta\Delta\delta(^{31}P)^*$ value of 5.41 ppm was obtained using

**4.15**. However, due to incomplete dissolution of both photoacids (**4.5** and **4.15**) in d$^6$-acetone, this comparison cannot be considered valid. Consequently, we proposed synthesizing the n-butyl MEH analog to enhance solubility and make the $^{31}$P NMR quantification feasible.[37,38]

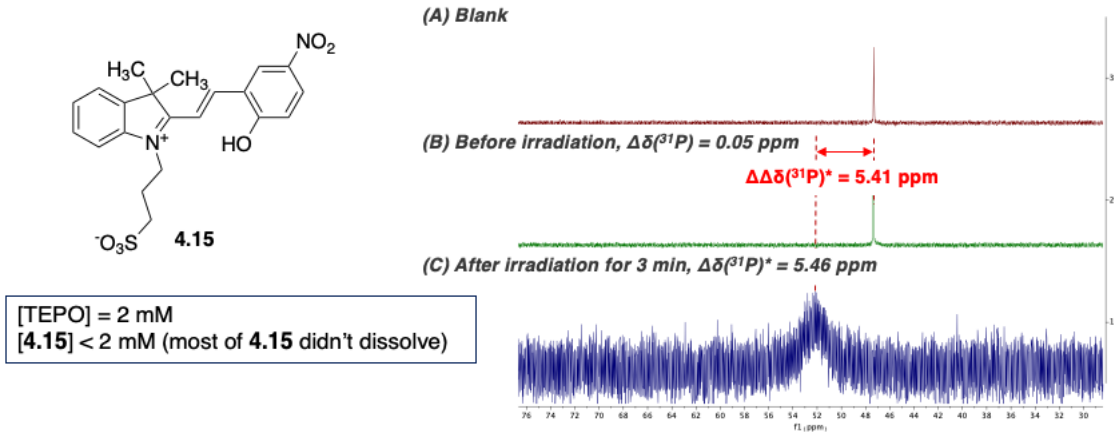
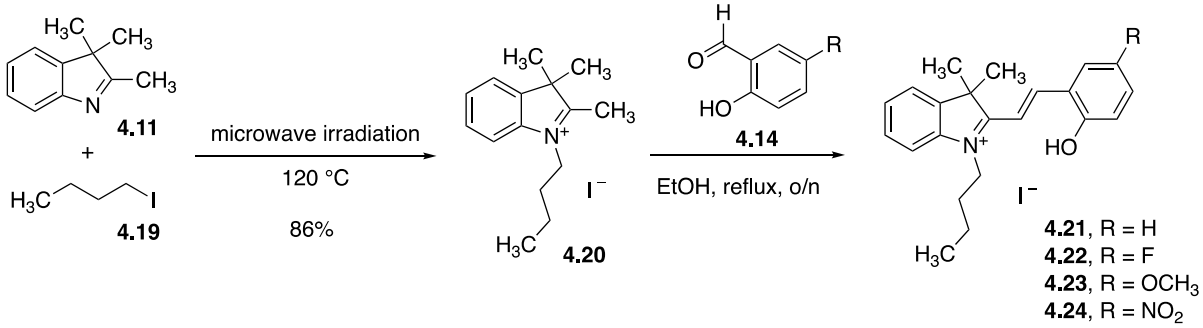



**Figure 4.11.** Preliminary results of ΔΔδ($^{31}$P)* for **4.15**.

## IIg. Evaluation of n-Butyl MEH for $^{31}$P NMR Quantification

We explored the potential of $^{31}$P NMR quantification for MEH by enhancing its solubility, achieved through the addition of an n-butyl chain onto the nitrogen of the indolium ring .[37,38] A series of several different n-butyl MEH compounds **4.21**−**4.24** with various substituents on the phenol ring were synthesized (Scheme 4.4).




**Scheme 4.4.** Synthesis of n-butyl MEH **4.21**−**4.24**.

Among these, **4.21** was selected for the titration experiment of the $^{31}$P NMR method with a TEPO concentration at 4 mM (Table 4.1). However, with five equivalents (20 mM) of MEH **4.21**, it was observed that only 87% of the compound converted into SP **4.21*** after the irradiation for 3 or 5

minutes due to limitations in light penetration at higher concentrations. Consequently, three equivalents were determined as the optimal amount of MEH for the quantification.

**Table 4.1.** $\Delta\Delta\delta(^{31}P)$* data for titration experiment with **4.21**.

| Entry[a] | X equiv of MEH to TEPO | [**4.21**] (mM) | $\Delta\delta(^{31}P)$[b] (ppm) | $\Delta\delta(^{31}P)$*[c] (ppm) | $\Delta\Delta\delta(^{31}P)$*[d] (ppm) |
|---|---|---|---|---|---|
| 1[e] | 1 | 4 | 2.25 | 9.28 | 7.03 |
| 2[e] | 3 | 12 | 4.19 | 17.23 | 13.04 |
| 3[f] | 5 | 20 | 4.62 | 17.41 | 12.79 |

[a]Experiments performed at 4 mM TEPO in $d^6$-acetone with X equiv of **4.21**. [b]$\Delta\delta(^{31}P)$ = δ(MEH•TEPO complex) – δ(free TEPO). [c]$\Delta\delta(^{31}P)$* = δ(SP•TEPO complex) – δ(free TEPO). [d]$\Delta\Delta\delta(^{31}P)$* = $\Delta\delta(^{31}P)$* – $\Delta\delta(^{31}P)$. [e] >95% conversion of MEH to SP after irradiation for 3 min determined using $^1H$ NMR spectroscopy. [f]87% conversion of MEH to SP after irradiation for 3 min determined using $^1H$ NMR spectroscopy.

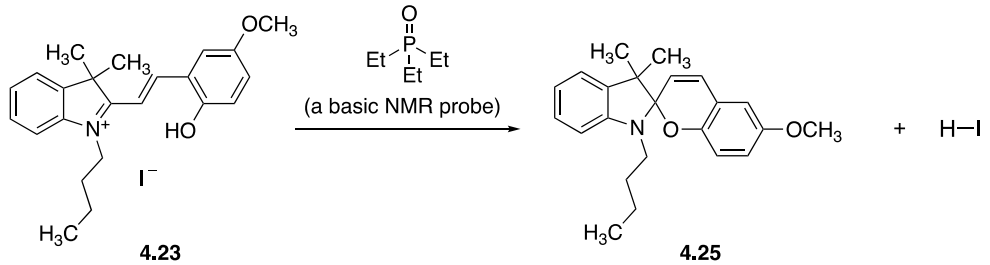
To verify the $^{31}P$ NMR quantification method, $\Delta\Delta\delta(^{31}P)$* values were measured for MEH **4.21**−**4.24** to ascertain if a linear relationship existed in the Hammett plot (Table 4.2). While entries 1 and 2 generally followed the anticipated trend, an unexpected negative $\Delta\Delta\delta(^{31}P)$* value was observed during the evaluation of **4.23** (entry 4). Upon adding TEPO solution to **4.23**, a color change was observed. This change might be attributed to TEPO's basic nature, potentially facilitating the formation of spiropyran (**4.25**, Scheme 4.5). Consequently, in the presence of TEPO, the irradiation of the MEH might not solely induce cyclization in the binding experiments, resulting in inaccurate quantification outcomes. Furthermore, the low solubility of **4.24** rendered the $\Delta\Delta\delta(^{31}P)$* measurement invalid due to the unknown amount of MEH in the solution (entries 4–5).

Due to the combined challenges posed by TEPO's basicity and solubility issues, the number of MEH samples that could be tested was limited. Considering these limitations, we opted to discontinue further testing of MEH compounds.

**Table 4.2.** $\Delta\Delta\delta(^{31}P)$* data for Hammett plot with **4.21**−**4.24**

| Entry[a] | MEH | $\sigma_p$ parameter | X equiv of MEH | [MEH] (mM) | $\Delta\delta(^{31}P)$[b] (ppm) | $\Delta\delta(^{31}P)$*[c] (ppm) | $\Delta\Delta\delta(^{31}P)$*[d] (ppm) |
|---|---|---|---|---|---|---|---|
| 1 | **4.21** | H = 0 | 3 | 12 | 4.19 | 17.23 | 13.04 |
| 2 | **4.22** | F = 0.06 | 3 | 12 | 5.43 | 13.92 | 8.49 |
| 3[e] | **4.23** | $OCH_3$ = –0.27 | 3 | 12 | 5.08 | 3.10 | –2.40 |
| 4[f] | **4.24** | $NO_2$ = 1.27 | 3 | 12 | 4.28 | 10.39 | 6.11 |
| 5[f] | **4.24** | $NO_2$ = 1.27 | 1 | 4 | 4.69 | 11.97 | 7.28 |

[a]Experiments performed at 4 mM TEPO in $d^6$-acetone with X equiv of MEH. [b]$\Delta\delta(^{31}P)$ = δ(MEH•TEPO complex) – δ(free TEPO). [c]$\Delta\delta(^{31}P)$* = δ(SP•TEPO complex) – δ(free TEPO). [d]$\Delta\Delta\delta(^{31}P)$* = $\Delta\delta(^{31}P)$* – $\Delta\delta(^{31}P)$. [e]SP formed upon the addition of TEPO. [f]MEH was not fully dissolved.




**Scheme 4.5.** The formation of spiropyran **4.25** upon the addition of TEPO solution.

### III. Conclusions and Future Work

In conclusion, a series of experiments was performed to evaluate a quantification method for H-bonding abilities of photoacids using $^{31}P$ NMR spectroscopy; however, the overall goals of the project were not acheived. These experiments included assessment of the concentration limit and solvent selection. It was confirmed that $d^6$-acetone is suitable for quantifying H-bonding based on the linear correlation observed in the Hammett plot. However, a significant hurdle emerged concerning the use of the TEPO NMR probe. It became evident that TEPO had the potential to alter the reaction profile of MEH in binding experiments, making it unsuitable for this specific type of photoacid.

Despite this setback, our interest persists in exploring potential excited-state photoacids. To further this exploration, we initiated a collaboration with Dr. Derrick Kaseman and Dr. Ping Yu in the UC Davis NMR facility. Our plan involved acquiring an NMRtorch tube to illuminate NMR samples, a new development in 2022 enabling in-situ illumination of NMR samples at higher concentrations, up to 6 mM.[39] Unfortunately, the project was suspended upon the departure of Dr. Derrick Kaseman from UC Davis. This remains a promising option that may be continued in the future.

## IV. Experimental Procedure

### General information

Deuterated acetone ($d^6$-acetone), deuterated water, deuterated DMSO, and deuterated MeOH were obtained from Acros Organics. Triethylphosphine oxide (TEPO) was obtained from Sigma Aldrich.

### Experimental Procedure for $^{31}$P NMR Measurement of PHAs

An oven-dried 20-mL volumetric flask was purged with argon and charged with TEPO and diluted with $d^6$-acetone to make the TEPO stock solution with a concentration of 4 mM. The respective PHA (6 equiv, 0.006 mmol, unless otherwise indicated) dissolved in 0.25 mL of $d^6$-acetone was added directly into an oven-dried and argon-purged NMR tube. Aliquots of the TEPO stock solution (0.25 mL) were transferred into the NMR tube, which was capped with a rubber septum. The $^{31}$P NMR spectrum of each sample was immediately measured at room temperature with 256 scans and the $^{31}$P NMR chemical shift was compared to a standard of TEPO solution (15 mM) to determine $\Delta\delta(^{31}P)$ values. For the measurement of $\Delta\delta(^{31}P)$* values, the same NMR sample was irradiated under blue LED light for 3 min, and the $^{31}$P NMR spectrum was measured.

## V. References


(1) Zivic, N.; Kuroishi, P. K.; Dumur, F.; Gigmes, D.; Dove, A. P.; Sardon, H. Recent Advances and Challenges in the Design of Organic Photoacid and Photobase Generators for Polymerizations. *Angew. Chem. Int. Ed.* **2019**, *58* (31), 10410–10422. https://doi.org/10.1002/anie.201810118.

(2) Liao, Y. Design and Applications of Metastable-State Photoacids. *Acc. Chem. Res.* **2017**, *50* (8), 1956–1964. https://doi.org/10.1021/acs.accounts.7b00190.

(3) Twilton, J.; Le, C.; Zhang, P.; Shaw, M. H.; Evans, R. W.; MacMillan, D. W. C. The Merger of Transition Metal and Photocatalysis. *Nat. Rev. Chem.* **2017**, *1* (7), 0052. https://doi.org/10.1038/s41570-017-0052.

(4) Solntsev, K. M.; Tolbert, L. M.; Cohen, B.; Huppert, D.; Hayashi, Y.; Feldman, Y. Excited-State Proton Transfer in Chiral Environments. 1. Chiral Solvents. *J. Am. Chem. Soc.* **2002**, *124* (31), 9046–9047. https://doi.org/10.1021/ja026896k.

(5) Ireland, J. F.; Wyatt, P. A. H. Acid-Base Properties of Electronically Excited States of Organic Molecules. In *Advances in Physical Organic Chemistry*; Elsevier, 1976; Vol. 12, pp 131–221. https://doi.org/10.1016/S0065-3160(08)60331-7.

(6) Wan, Peter.; Shukla, Deepak. Utility of Acid-Base Behavior of Excited States of Organic Molecules. *Chem. Rev.* **1993**, *93* (1), 571–584. https://doi.org/10.1021/cr00017a024.

(7) Shizuka, H. Excited-State Proton-Transfer Reactions and Proton-Induced Quenching of Aromatic Compounds. *Acc. Chem. Res.* **1985**, *18* (5), 141–147. https://doi.org/10.1021/ar00113a003.

(8) Shi, Z.; Peng, P.; Strohecker, D.; Liao, Y. Long-Lived Photoacid Based upon a Photochromic Reaction. *J. Am. Chem. Soc.* **2011**, *133* (37), 14699–14703. https://doi.org/10.1021/ja203851c.

(9) Fu, C.; Xu, J.; Boyer, C. Photoacid-Mediated Ring Opening Polymerization Driven by Visible Light. *Chem. Commun.* **2016**, *52* (44), 7126–7129. https://doi.org/10.1039/C6CC03084J.

(10) Das, A.; Banerjee, T.; Hanson, K. Protonation of Silylenol Ether via Excited State Proton Transfer Catalysis. *Chem. Commun.* **2016**, *52* (7), 1350–1353. https://doi.org/10.1039/C5CC08081A.

(11) Salem, Z. M.; Saway, J.; Badillo, J. J. Photoacid-Catalyzed Friedel–Crafts Arylation of Carbonyls. *Org. Lett.* **2019**, *21* (21), 8528–8532. https://doi.org/10.1021/acs.orglett.9b02841.

(12) Iwata, R.; Uda, K.; Takahashi, D.; Toshima, K. Photo-Induced Glycosylation Using Reusable Organophotoacids. *Chem Commun* **2014**, *50* (73), 10695–10698. https://doi.org/10.1039/C4CC04753B.

(13) Yi, H.; Niu, L.; Wang, S.; Liu, T.; Singh, A. K.; Lei, A. Visible-Light-Induced Acetalization of Aldehydes with Alcohols. *Org. Lett.* **2017**, *19* (1), 122–125. https://doi.org/10.1021/acs.orglett.6b03403.

(14) Das, A.; Ayad, S.; Hanson, K. Enantioselective Protonation of Silyl Enol Ether Using Excited State Proton Transfer Dyes. *Org. Lett.* **2016**, *18* (20), 5416–5419. https://doi.org/10.1021/acs.orglett.6b02820.

(15) Zhao, G.; Wang, T. Stereoselective Synthesis of 2-Deoxyglycosides from Glycals by Visible-Light-Induced Photoacid Catalysis. *Angew. Chem. Int. Ed.* **2018**, *57* (21), 6120–6124. https://doi.org/10.1002/anie.201800909.

(16) Strada, A.; Fredditori, M.; Zanoni, G.; Protti, S. Acid Catalyzed Formation of C-C and C-S Bonds via Excited State Proton Transfer. *Molecules* **2019**, *24* (7), 1318. https://doi.org/10.3390/molecules24071318.

(17) Steidl, L.; Jhaveri, S. J.; Ayothi, R.; Sha, J.; McMullen, J. D.; Ng, S. Y. C.; Zipfel, W. R.; Zentel, R.; Ober, C. K. Non-Ionic Photo-Acid Generators for Applications in Two-Photon Lithography. *J Mater Chem* **2009**, *19* (4), 505–513. https://doi.org/10.1039/B816434G.

(18) Maity, C.; Hendriksen, W. E.; van Esch, J. H.; Eelkema, R. Spatial Structuring of a Supramolecular Hydrogel by Using a Visible-Light Triggered Catalyst. *Angew. Chem. Int. Ed.* **2015**, *54* (3), 998–1001. https://doi.org/10.1002/anie.201409198.

(19) Li, X.; Fei, J.; Xu, Y.; Li, D.; Yuan, T.; Li, G.; Wang, C.; Li, J. A Photoinduced Reversible Phase Transition in a Dipeptide Supramolecular Assembly. *Angew. Chem. Int. Ed.* **2018**, *57* (7), 1903–1907. https://doi.org/10.1002/anie.201711547.

(20) Zhang, H.; Zeng, H.; Priimagi, A.; Ikkala, O. Programmable Responsive Hydrogels Inspired by Classical Conditioning Algorithm. *Nat. Commun.* **2019**, *10* (1), 3267. https://doi.org/10.1038/s41467-019-11260-3.

(21) Ivan, M. G.; Scaiano, J. C. (tito). Photoimaging and Lithographic Processes in Polymers. *John Wiley Sons Ltd* **2010**, 479–507. https://doi.org/10.1002/9780470594179.ch12.
(22) Mayer, G.; Heckel, A. Biologically Active Molecules with a "Light Switch." *Angew. Chem. Int. Ed.* **2006**, *45* (30), 4900–4921. https://doi.org/10.1002/anie.200600387.
(23) Emond, M.; Sun, J.; Grégoire, J.; Maurin, S.; Tribet, C.; Jullien, L. Photoinduced pH Drops in Water. *Phys. Chem. Chem. Phys.* **2011**, *13* (14), 6493. https://doi.org/10.1039/c0cp02464c.
(24) Yue, X.; Yanez, C. O.; Yao, S.; Belfield, K. D. Selective Cell Death by Photochemically Induced pH Imbalance in Cancer Cells. *J. Am. Chem. Soc.* **2013**, *135* (6), 2112–2115. https://doi.org/10.1021/ja3122312.
(25) Abeyrathna, N.; Liao, Y. A Reversible Photoacid Functioning in PBS Buffer under Visible Light. *J. Am. Chem. Soc.* **2015**, *137* (35), 11282–11284. https://doi.org/10.1021/jacs.5b06218.
(26) Johns, V. K.; Wang, Z.; Li, X.; Liao, Y. Physicochemical Study of a Metastable-State Photoacid. *J. Phys. Chem. A* **2013**, *117* (49), 13101–13104. https://doi.org/10.1021/jp409111m.
(27) Lawler, C.; Fayer, M. D. Proton Transfer in Ionic and Neutral Reverse Micelles. *J. Phys. Chem. B* **2015**, *119* (19), 6024–6034. https://doi.org/10.1021/acs.jpcb.5b02753.
(28) Liu, J.; Tang, W.; Sheng, L.; Du, Z.; Zhang, T.; Su, X.; Zhang, S. X.-A. Effects of Substituents on Metastable-State Photoacids: Design, Synthesis, and Evaluation of Their Photochemical Properties. *Chem. – Asian J.* **2019**, *14* (3), 438–445. https://doi.org/10.1002/asia.201801687.
(29) Zhu, J. S.; Larach, J. M.; Tombari, R. J.; Gingrich, P. W.; Bode, S. R.; Tuck, J. R.; Warren, H. T.; Son, J.-H.; Duim, W. C.; Fettinger, J. C.; Haddadin, M. J.; Tantillo, D. J.; Kurth, M. J.; Olson, D. E. A Redox Isomerization Strategy for Accessing Modular Azobenzene Photoswitches with Near Quantitative Bidirectional Photoconversion. *Org. Lett.* **2019**, *21* (21), 8765–8770. https://doi.org/10.1021/acs.orglett.9b03387.
(30) Feldmeier, C.; Bartling, H.; Riedle, E.; Gschwind, R. M. LED Based NMR Illumination Device for Mechanistic Studies on Photochemical Reactions – Versatile and Simple, yet Surprisingly Powerful. *J. Magn. Reson.* **2013**, *232*, 39–44. https://doi.org/10.1016/j.jmr.2013.04.011.
(31) Diemoz, K. M.; Franz, A. K. NMR Quantification of Hydrogen-Bond-Activating Effects for Organocatalysts Including Boronic Acids. *J. Org. Chem.* **2019**, *84* (3), 1126–1138. https://doi.org/10.1021/acs.joc.8b02389.
(32) Chang, Y.-P.; Tang, T.; Jagannathan, J. R.; Hirbawi, N.; Sun, S.; Brown, J.; Franz, A. K. NMR Quantification of Halogen-Bonding Ability To Evaluate Catalyst Activity. *Org. Lett.* **2020**, *22* (16), 6647–6652. https://doi.org/10.1021/acs.orglett.0c02427.
(33) Jennings, J. J.; Wigman, B. W.; Armstrong, B. M.; Franz, A. K. NMR Quantification of the Effects of Ligands and Counterions on Lewis Acid Catalysis. *J. Org. Chem.* **2019**, *84* (24), 15845–15853. https://doi.org/10.1021/acs.joc.9b02107.
(34) Jagannathan, J. R.; Diemoz, K. M.; Targos, K.; Fettinger, J. C.; Franz, A. K. Kinetic and Binding Studies Reveal Cooperativity and Off-Cycle Competition for H-Bonding Catalysis with Silsesquioxane Silanols. *Chem. – Eur. J.* **2019**, *25* (65), 14953–14958. https://doi.org/10.1002/chem.201903693.
(35) Jennings, J. J.; Milic, M.; Targos, K.; Franz, A. K. NMR Quantification of H-Bond Donating Ability for Bioactive Functional Groups and Isosteres. *Eur J Med Chem* **2020**, *207*, 112693. https://doi.org/10.1016/j.ejmech.2020.112693.
(36) Mason, S. J.; Hake, J. L.; Nairne, J.; Cummins, W. J.; Balasubramanian, S. Solid-Phase Methods for the Synthesis of Cyanine Dyes. *J. Org. Chem.* **2005**, *70* (8), 2939–2949. https://doi.org/10.1021/jo0479415.
(37) Shumburo, A.; Biewer, M. C. Stabilization of an Organic Photochromic Material by Incorporation in an Organogel. *Chem. Mater.* **2002**, *14* (9), 3745–3750. https://doi.org/10.1021/cm020421a.
(38) Moo, J. G. S.; Presolski, S.; Pumera, M. Photochromic Spatiotemporal Control of Bubble-Propelled Micromotors by a Spiropyran Molecular Switch. *ACS Nano* **2016**, *10* (3), 3543–3552. https://doi.org/10.1021/acsnano.5b07847.
(39) Bramham, J. E.; Golovanov, A. P. Sample Illumination Device Facilitates in Situ Light-Coupled NMR Spectroscopy without Fibre Optics. *Commun. Chem.* **2022**, *5* (1), 90. https://doi.org/10.1038/s42004-022-00704-5.

# Appendix A: Photoredox Catalysis for the Synthesis of Functionalized Polyhedral Oligomeric Silsesquioxanes

## I. Introduction

This appendix presents the development of the first photocatalysis methodology for the functionalization of higher-order siloxane structures, specifically polyhedral oligomeric silsesquioxanes (POSSs). The Franz lab is dedicated to pioneering synthetic strategies for creating silicon-containing nanomaterials with specific functionalities. POSS is an important building block for nanomaterials in a wide range of fields, making it a key frontier molecule in hybrid nanomaterial science and engineering (Figure 5.1).[1–3] When integrated into materials, the inorganic siloxane core within POSS structures has shown to be a versatile and effective additive. POSSs enhance the thermal and chemical stability of the hybrid nanomaterials compared to unmodified counterparts. Additionally, the organic groups ($R^1$) attached to the siloxane scaffold facilitate the solubilization of POSSs in organic solvents, thereby streamlining processing and functionalization procedures.[4] Various synthetic strategies allow for the incorporation of suitable mono-functionalized ($R^2$) POSS derivatives into polymers as side chains. This approach offers diverse functional polymeric materials with adjustable physical properties tailored for specific applications.

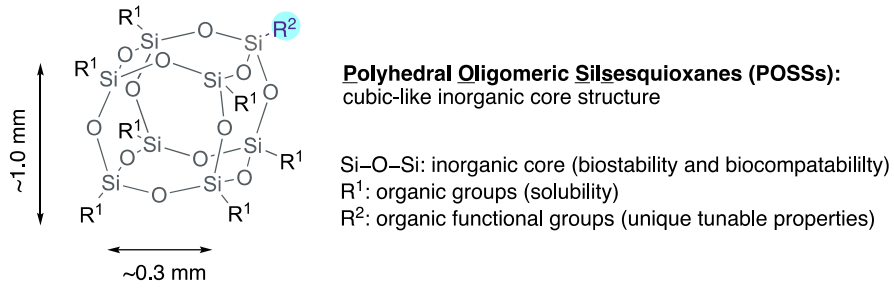



**Figure 5.1.** Polyhedral oligomeric silsesquioxanes (POSSs).

Our goal was to demonstrate a new method of POSS functionalization using carbenes. We proposed incorporating cyclopropanes onto POSS structures **5.3** from allyl-POSS **5.1**, a transformation not previously demonstrated on POSS nanomaterials. Initial attempts using transition-metal catalysis methods for this purpose were unsuccessful. Andrew Huss made a breakthrough by employing photoredox catalysis to introduce alkylbromide groups—precursors for synthesizing cyclopropanes—

onto the POSS **5.2**. My collaboration with Andrew primarily focused on optimizing the organophotoredox methodology, exploring substrate scope, and assessing the feasibility of cyclopropanation within the photoredox reaction (Figure 5.2). This work represents the first example of functionalizing POSS nanomaterials using photoredox catalysis, potentially leading to exciting new possibilities in nanomaterial research and engineering.

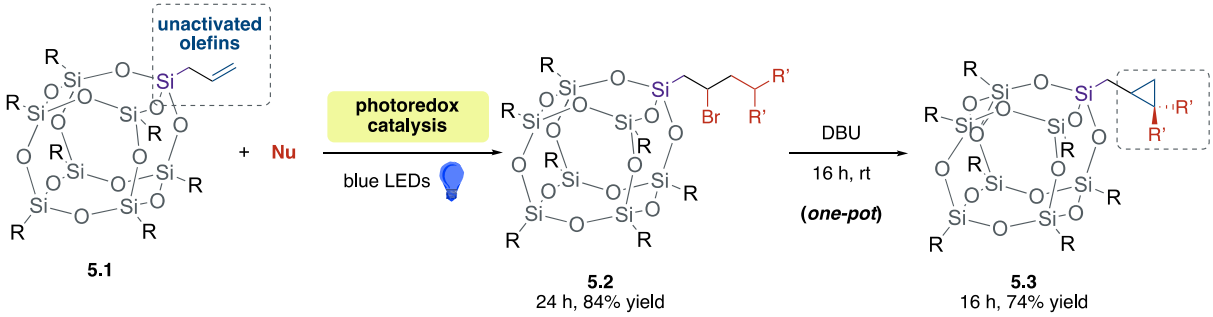
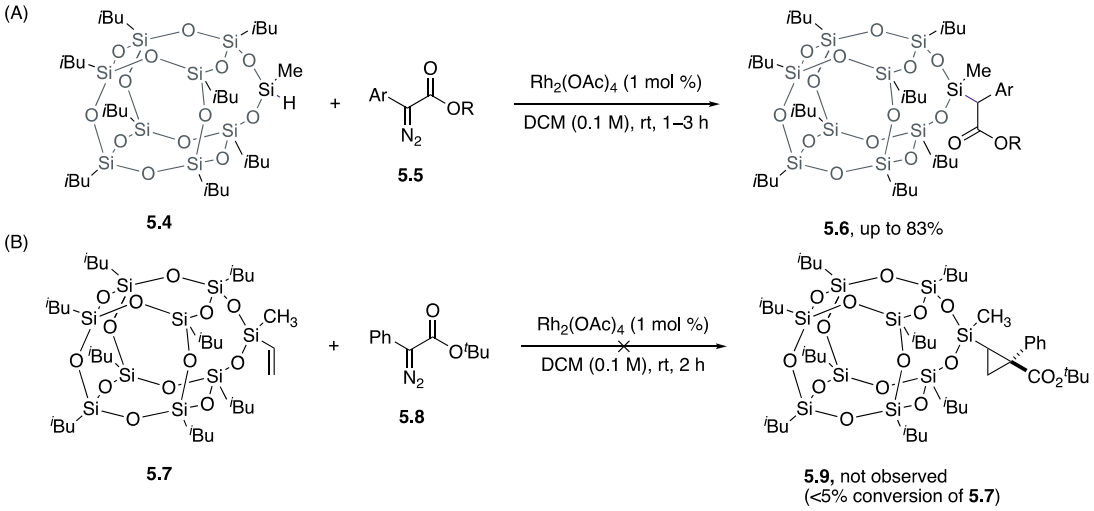



**Figure 5.2.** Project overview.

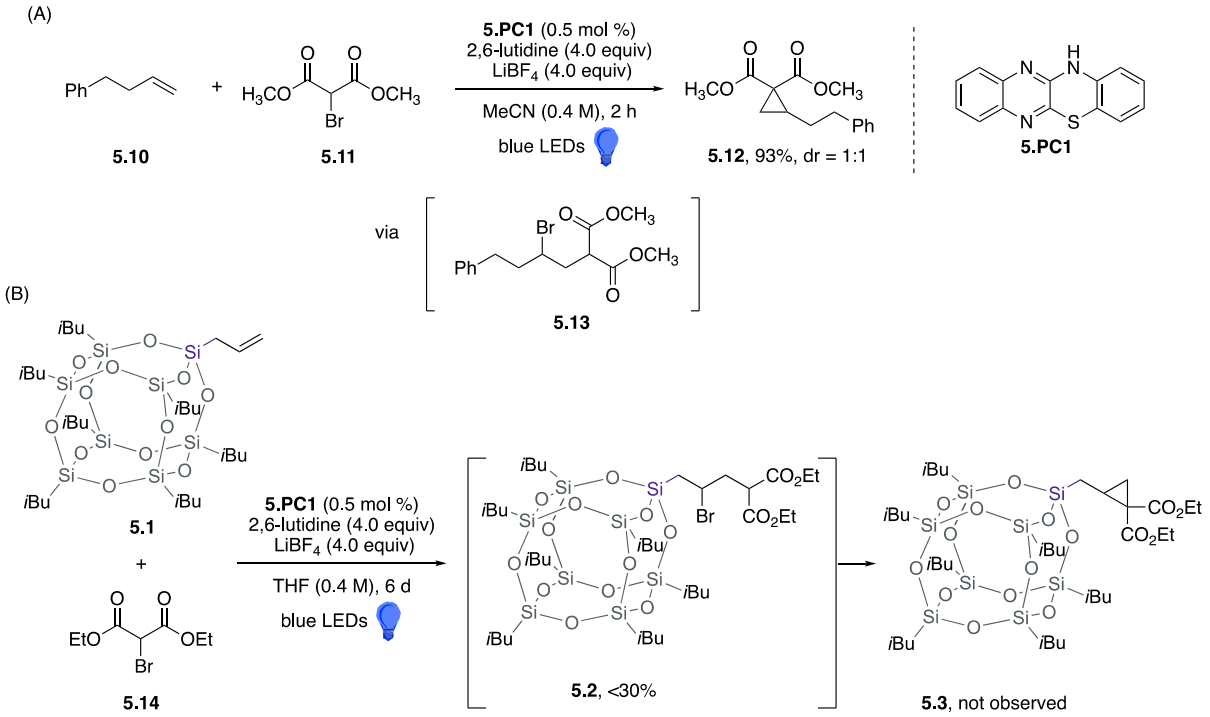
### Functionalization of POSS

Previous lab members Dr. Jake Jagannathan and Karina Targos developed the Rh-catalyzed carbene insertion into Si−H bonds for the synthesis of functionalized POSSs (Scheme 5.1A).[5] We envisioned the use of a carbene to install a cyclopropane onto POSS by adapting the previous method using Rh-catalyzed carbene insertion with a diazoester carbene precursor (Scheme 5.1B). However, the inherent unreactive nature of the olefin on POSS posed a significant challenge, thereby limiting the range of available synthetic approaches for functionalization. Unfortunately, attempts to employ Rh-catalyzed carbene insertion were unsuccessful. Andrew conducted extensive experiments utilizing various transition metals with both donor/acceptor carbenes and acceptor/acceptor carbenes, and with POSSs containing vinyl or allyl groups, yet yielding no success.




**Scheme 5.1. (**A) Rh-catalyzed carbene insertion into Si−H bonds. (B) Attemped cyclopropanation through Rh-catalyzed carbene insertion.

Using the organophotocatalyst benzothiazinoquinoxaline **5.PC1**,[6,7] Carreira and coworkers have successfully achieved cyclopropanation of inactivated olefins with α-bromo-β-ketoesters or α-bromomalonates **5.11** (Scheme 5.2A).[7] $LiBF_4$ was added to facilitate the enolization of the intermediate malonate. Without the addition of $LiBF_4$, the intermediate alkylbromide **5.13** was isolated in 75% yield. In this project, Andrew made a breakthrough by adapting Carreira's organophotocatalysis method. Initially, when employing this reported method in THF, the preliminary yield of alkylbromide **5.2** was below 30% after 6 days (Scheme 5.2B). Notably, although the optimal solvent in the prior report was MeCN, allyl-POSS **5.1** displayed insolubility in MeCN, resulting in no observed reaction. At this point, I collaborated closely with Andrew to fine-tune and optimize the photocatalysis reaction. The methodology presented here offers a diverse range of polymeric materials whose reactive organic moieties ($R^2$, Figure 5.1) are uniquely functionalized via organophotoredox catalysis.




**Scheme 5.2.** (A) Previous example of organophotocatalyzed cyclopropanation of unactivated olefins. (B) Preliminary experiment conducted by Andrew Huss.

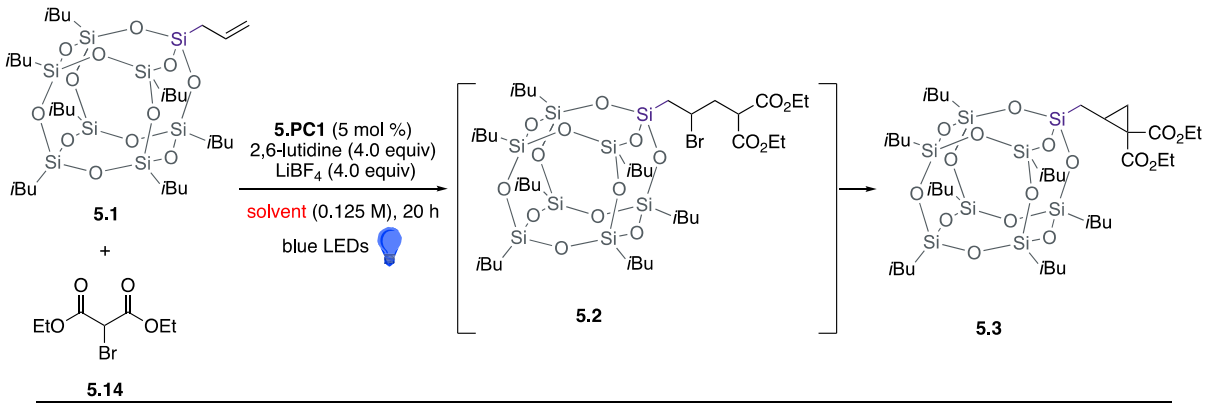
## II. Method Development

This section will detail the optimization of new functionalized POSS through photoredox catalysis. The data, including contributions from Andrew Huss, provide insights into the optimization process. The initial attempts to optimize the conditions for POSS functionalization through photoredox catalysis encountered significant challenges. First, the 6-day duration for the reaction rendered the optimization process impractical and ineffective. Moreover, we proposed that the partial solubility of allyl-POSS **5.1** in THF at 0.4 M in the preliminary experiment affected the reactivity. To improve the practicality of the optimization process, we increased **5.PC1** loading to 5 mol%, decreased the reaction concentration to 0.125 M, and reduced the reaction time to 20 h, regardless of whether or not the allyl-POSS starting material was consumed.

**IIa. Solvent Screen**

The results of the solvent screen for the photoredox reaction are presented in Table 5.1. No cyclopropane product **5.3** was observed. Nevertheless, we proceeded to optimize the yield of intermediate bromide **5.2**. Following the evaluation of single-component solvents (Table 5.1, entries 1−5), it was observed that DCM exhibited the highest reactivity, achieving >95% conversion of **5.1**. However, the reaction in DCM was not as clean as when using THF. In THF, the reaction proceeds without generating any side products. To enhance reactivity while preserving chemoselectivity, we opted to screen a solvent mixture of DCM/THF and hexanes/THF. The optimal solvent composition determined from these screenings was DCM/THF (1/1, v/v), consistently giving **5.2** in 83% yield (the average of three trials).

**Table 5.1.** Solvent screen for the photoredox catalysis for functionalizing POSS.




| Entry[a] | Solvent | Conversion of **5.1** (%)[b] | **5.2** yield (%)[b] | **5.3** yield (%) |
|---|---|---|---|---|
| 1[c] | THF | 64 | 66 | <5 |
| 2 | Sulfolane | 25 | <5 | <5 |
| 3[d] | n-butyl acetate | >95 | 84 | <5 |
| 4 | PhCl | 62 | 54 | <5 |
| 5[c] | DCM | >95 | 70 | <5 |
| 6[e] | DCM/THF (1/1) | 87 | 83 (84) | <5 |
| 7 | DCM/THF (9/1) | 87 | 62 | <5 |
| 8 | DCM/THF (1/2) | 86 | 79 | <5 |
| 9 | DCM/THF (1/4) | 79 | 71 | <5 |
| 10[d] | DCM/THF (2/1) | 92 | 87 | <5 |
| 11[d] | DCM/THF (4/1) | >95 | 85 | <5 |
| 12[c] | hexanes/THF (1/1) | 83 | 83 | <5 |
| 13 | hexanes/THF (2/1) | 89 | 82 | <5 |
| 14[d] | hexanes/THF (1/2) | 73 | 61 | 27 |
| 15 | THF/ACN (4/1) | 6 | 9 | <5 |
| 16[f] | DCM/THF (1/1) | 88 | 79 | <5 |

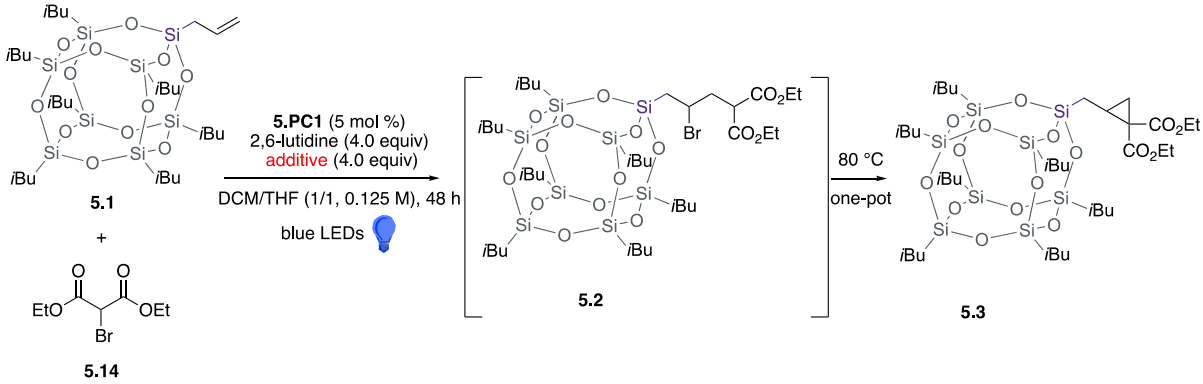
[a]Reactions were performed with allyl-POSS **5.1** (0.250 mmol), bromomalonate **5.14** (0.475 mmol), **5.PC1** (5 mol%), 2,6-lutidine (1.0 mmol), and $LiBF_4$ (1.0 mmol) in 2 mL of solvent at 440 nm blue LED (36-watt Kessil 440 nm PR160L lamp at 100% intensity). [b]NMR yield using benzylbenzoate as an internal standard. Isolated yield in parenthesis. [c]Average of two trials. [d]Reactions were conducted by Andrew Huss. [e]Average of three trials. [f]Reaction concentration at 0.19 M (**5.1** was not fully dissolved at 0.2 M).

## IIc. Additive Screen

Initially, the solvent screen did not afford any cyclopropane product **5.3**. Despite screening two base additives, $Cs_2CO_3$ and $K_2CO_3$, the desired cyclopropane remained undetected (Table 5.2). In an effort

to ensure the formation of the cyclopropane product, after the photocatalysis reaction for 48 h, the mixture was cooled and subsequently stirred at 80 °C for 1−2 d. Eventually, cyclopropane **5.3** was observed in both reactions with the base additives and subsequently isolated in 58% yield (Table 5.2, entry 1). When no additive was included, an 84% conversion to bromide intermediate **5.2** was observed (entry 3). It became clear that the cyclopropanation could be accessed after the photoredox process upon the inclusion of heat and either additive.

**Table 5.2.** Additive screen for the photoredox catalysis for functionalizing POSS.

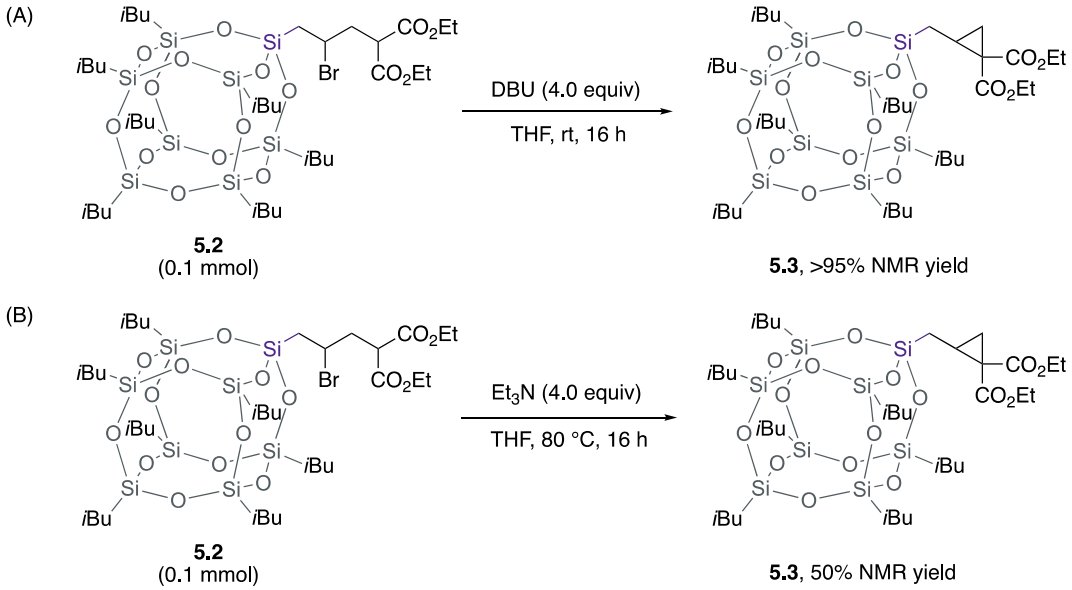



| Entry[a] | Additive | Conversion of **5.1** to **5.2** (%)[b] | Conversion of **5.2** to **5.3** (%)[b] | **5.3** yield (%)[b] |
|---|---|---|---|---|
| 1 | $Cs_2CO_3$ | 58 | >95 | (52)[c] |
| 2 | $K_2CO_3$ | 85 | >95 | 85[d] |
| 3 | -- | 84 | <5 | <5 |

[a]Reactions performed under standard reaction conditions: allyl-POSS **5.1** (0.250 mmol), bromomalonate **5.14** (0.475 mmol), **5.PC1** (5 mol%), 2,6-lutidine (1.0 mmol), additive (1.0 mmol) ) in 2 mL of DCM/THF (1/1) at 440 nm blue LED (36-watt Kessil 440 nm PR160L lamp at 100% intensity). [b]Conversion determined using $^1$H NMR spectroscopy. Isolated yield in parenthesis. [c]**5.2** completely consumed in 1 d. . [d]**5.2** completely consumed in 2 d.

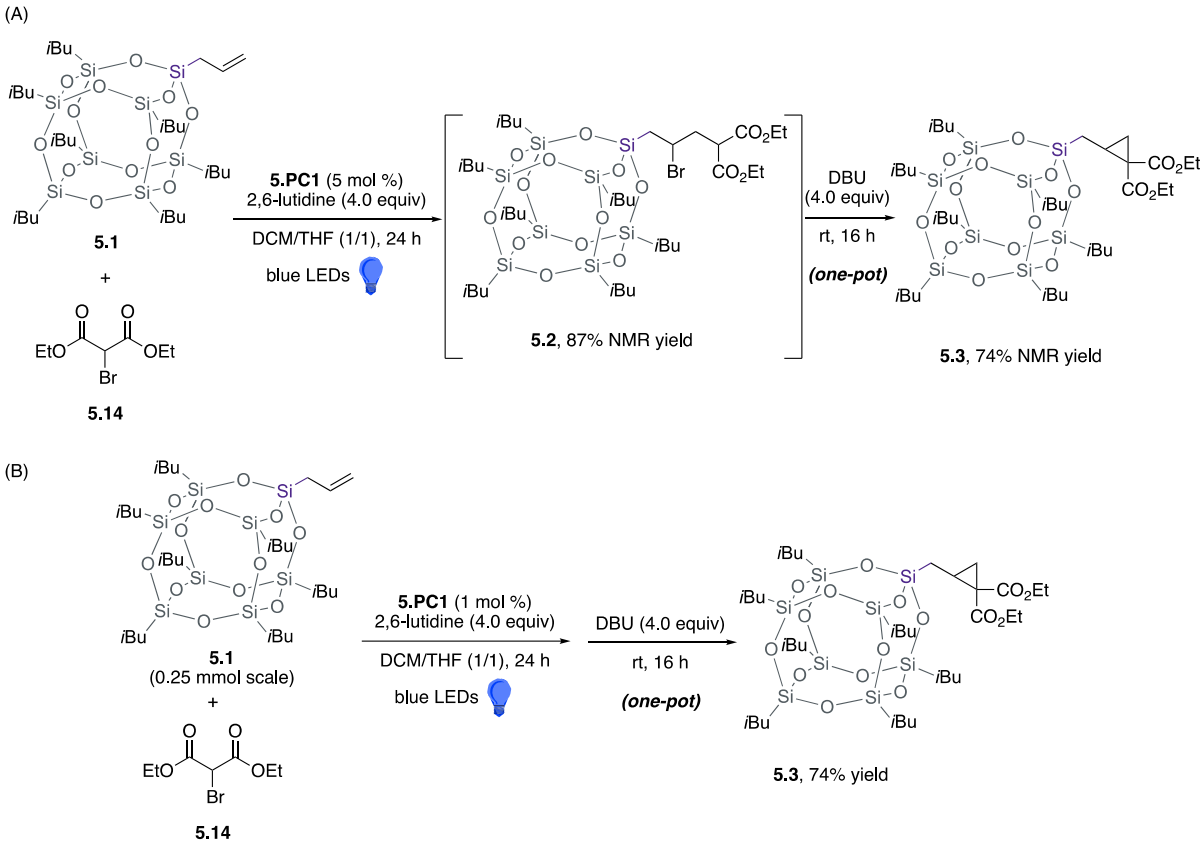
## IId. Base Screen

Inspired by the encouraging results of the base additive screen, we set out to identify the appropriate base for enolization and subsequent nucleophilic addition to generate cyclopropane **5.3**. To that end, the isolated bromide intermediate (**5.2**) was treated with DBU or $Et_3N$ (Scheme 5.3). At room temperature, using DBU resulted in a >95% NMR yield of **5.3**. Conversely, using $Et_3N$ at elevated temperature resulted in a 50% NMR yield.




**Scheme 5.3.** Organic base screen for generating **5.3** from purified **5.2**.

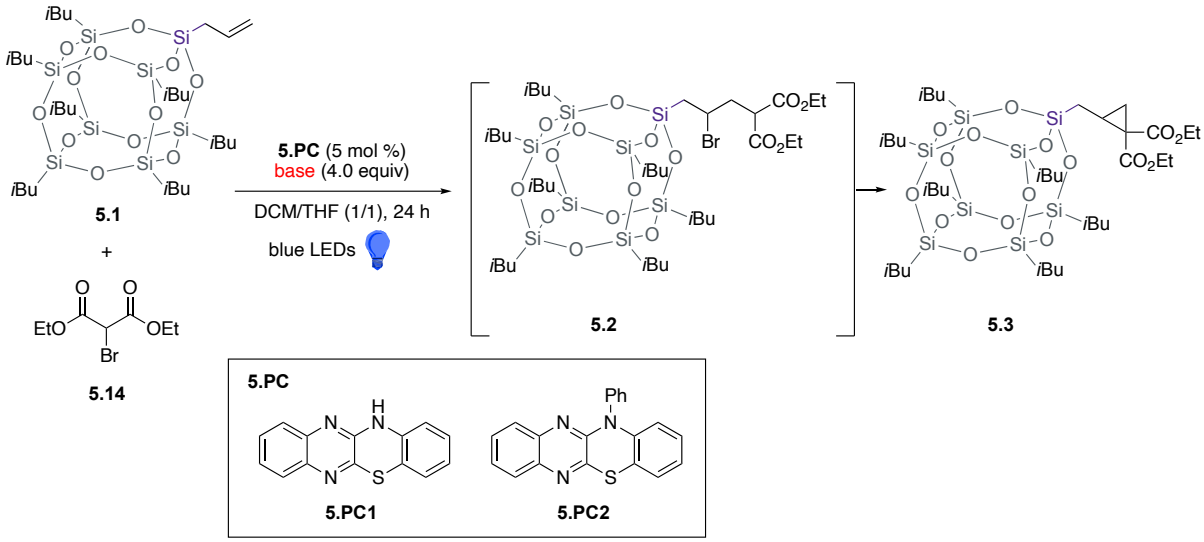
The subsequent evaluation involved testing the one-pot reaction approach (Scheme 5.4). A 74% NMR yield was achieved using a 5 mol% loading of **5.PC1** (Scheme 5.4A). Under the optimal conditions with 1 mol% of **5.PC1** loading and a 24 hour photocatalysis reaction time, the mixture underwent treatment with four equivalents of DBU for 16 h. Cyclopropane **5.3** was then isolated in 74% yield (Scheme 5.4B).




**Scheme 5.4.** Synthesis of cyclopropane **5.3** in a one-pot reaction.

An investigation aiming to generate cyclopropane **5.3** during the photocatalysis reaction was conducted and is presented in Table 5.3. Substituting the base from pyridine-like bases to others yielded no conversion of **5.1** (Table 5.3, entries 3−7). Using a mixture of 2,6-lutidine/DBU did produce cyclopropane **5.3** by photoredox reaction; however, the yield was low after 24 h (Table 5.3, entries 8−10). Notably, a distinctive color change occurred upon the addition of DBU to the reaction mixture. We presumed that DBU deprotonated the benzothiazine proton on **5.PC1**, rendering the catalyst inactive, resulting in no observable reaction (Table 5.3, entry 6). Subsequently, **5.PC2** was synthesized[7] and assessed for making cyclopropane **5.3** by a photoredox reaction. Yet, 5 mol% of **5.PC2** loading resulted in only 34% of bromide intermediate **5.2** and 10% of **5.3** (Table 5.3, entry 12). Under the optimal conditions with 1 mol% **5.PC2** loading, the yield increased to 46% of bromide intermediate **5.2** and 22% of **5.3** (Table 5.3, entry 13). Although we anticipated the yield could be higher with extended time, it was concluded that generating the cyclopropane was more efficient in a one-pot manner. Since this methodology represents the first example of functionalizing POSS using photoredox catalysis, we redirected our focus to synthesizing the bromide compound **5.2**.

**Table 5.3.** Base screen for the photoredox catalysis for functionalizing POSS.



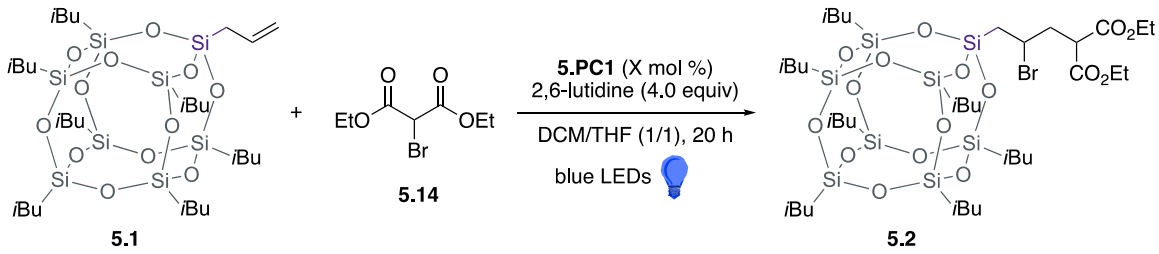

| Entry[a] | **5.PC** | Base | Time (h) | Conversion of **5.1** (%)[b] | **5.2** yield (%)[b] | **5.3** yield (%)[b] |
|---|---|---|---|---|---|---|
| 1 | **PC1** | 2,6-lutidine | 20 | 87 | 83 | <5 |
| 2[c] | **PC1** | pyridine | 20 | 80 | 77 | <5 |
| 3[c] | **PC1** | DMAP | 20 | <5 | <5 | <5 |
| 4 | **PC1** | $Et_3N$ | 20 | <5 | <5 | <5 |
| 5 | **PC1** | DIPEA | 20 | <5 | <5 | <5 |
| 6 | **PC1** | DBU | 20 | <5 | <5 | <5 |
| 7 | **PC1** | DABCO | 24 | <5 | <5 | <5 |
| 8 | **PC1** | 2,6-lutidine (4.0 equiv) /DBU (4.0 equiv) | 24 | 20 | <5 | 19 |
| 9 | **PC1** | 2,6-lutidine (4.0 equiv) /DBU (1.0 equiv) | 24 | 59 | 58 | trace |
| 10 | **PC1** | 2,6-lutidine (4.0 equiv) /DBU (0.5 equiv) | 24 | 90 | 87 | 3 |
| 11 | **PC2** | 2,6-lutidine (4.0 equiv) /DBU (4.0 equiv) | 24 | >95 | <5 | <5 |
| 12 | **PC2** | 2,6-lutidine (4.0 equiv) /DBU (1.0 equiv) | 24 | 48 | 34 | 10 |
| 13 | **PC2** 1mol% | 2,6-lutidine (4.0 equiv) /DBU (1.0 equiv) | 24 | 74 | 46 | 22 |

[a]Reactions were performed with allyl-POSS **5.1** (0.250 mmol), bromomalonate **5.14** (0.475 mmol), **5.PC** (5 mol%, unless indicated), and base (as indicated) in 2 mL of DCM/THF (1/1) at 440 nm blue LED (36-watt Kessil 440 nm PR160L lamp at 100% intensity). [b]NMR yield using benzylbenzoate as an internal standard. [c]Reactions were conducted by Andrew Huss.

## IIe. Catalyst Loading Screen

Lastly, a screening of catalyst loading was conducted (Table 5.4). Even though the tested catalytic loading amounts gave results that were within an acceptable error range, we chose to use a 1 mol% loading of **5.PC1** due to its higher yield and relatively low loading amount. The control experiment without exposure to blue LED light but heated to 40 °C did not yield an observable reaction (Table 5.4, entry 4). Andrew conducted the catalyst screening, equivalance studies, and remaining control experiments; however, the data from these experiments will not be provided here. Thus, the optimized conditions consist of 1 mol % **5.PC1**, 1.7 equiv of bromomalonate **5.14**, and 4.0 equiv of 2,6-lutidine (Table 5.4, entry 3).

**Table 5.4.** Catalyst loading screen for the photoredox catalysis for functionalizing POSS.



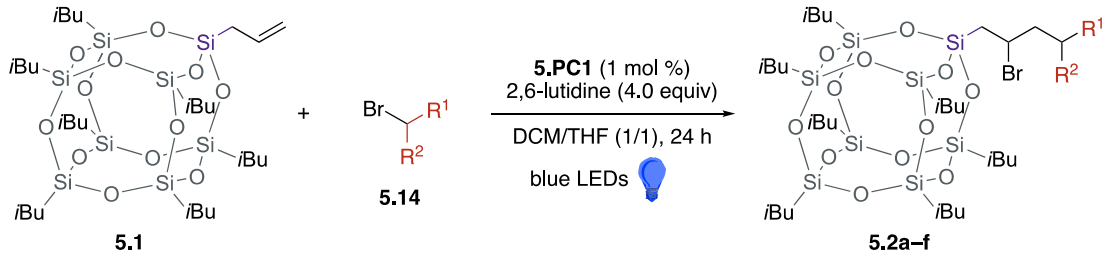

| Entry[a] | X mol% | Conversion of **5.1** (%)[b] | **5.2** yield (%)[b] |
|---|---|---|---|
| 1 | 5 | 90 | 84 |
| 2 | 2 | 90 | 86 |
| 3 | 1 | 92 | 89 |
| 4 | 0.5 | 91 | 87 |
| 5[c] | 1 | <5 | <5 |

[a]Reactions were performed with allyl-POSS **5.1** (0.250 mmol), bromomalonate **5.14** (0.475 mmol), **5.PC** (mol% as indicated), and 2,6-lutidine (1.0 mmol) in 2 mL of DCM/THF (1/1) at 440 nm blue LED (36-watt Kessil PR160L lamp at 100% intensity). [b]NMR yield using benzylbenzoate as an internal standard. [c]Without blue LED light, at 40 °C.

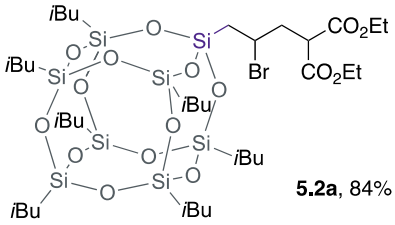
## III. Substrate Scope

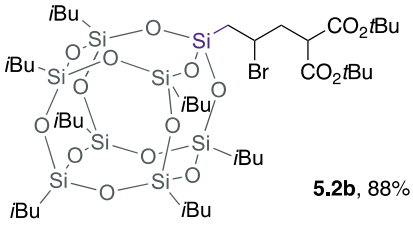
Having established the optimized conditions, we explored the substrate scope for functionalizing ally-POSS with various alkylbromides (Scheme 5.5 and Scheme 5.6). The scheme only presents the substrates that were synthesized and characterized independently as part of this thesis research. The transformation exhibited adaptability to a range of activated alkylbromides. Di-tert-butyl

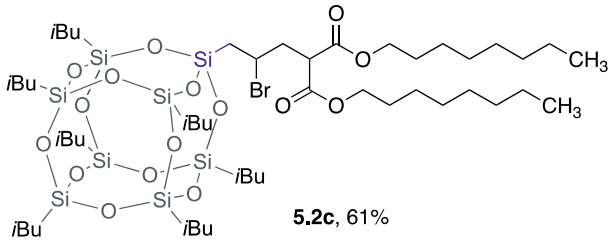
bromomalonate and the long-chain di-$^{n}$octyl bromomalonate provided the alkylbromides **5.2b** and **c** in 88% and 61% yields, respectively. Additionally, the mono-activated bromides, α-bromo ethyl acetate and α-bromo acetonitrile, were compatible with the reaction. While the reaction rate was initially low using 1 mol% of **5.PC1**, increasing the catalyst loading to 5 mol% resulted in a 67% yield of the desired ester **5.2d** and a 67% yield of the nitrile **5.2e**. Bromoacetophenone and bromoacetamide were incompatible with the reaction conditions despite their potentials as valuable coupling partners in future applications. For the reaction with bromoacetophenone, 68% of allyl-POSS **5.1** starting material was recovered, yet the desired product **5.2f** was not obtained. Bromoacetamide did not dissolve in DCM/THF, leading to no conversion of allyl-POSS **5.1** when reacted with bromoacetamide **5.14g**.



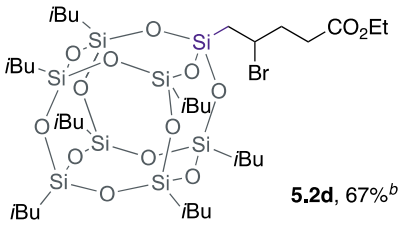

**di-activated bromides**

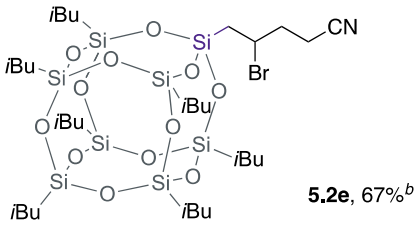


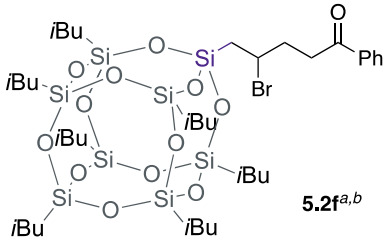



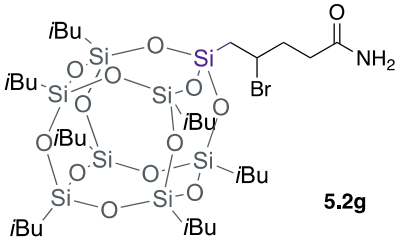

**mono-activated bromides**




***unsuccessful substrates***

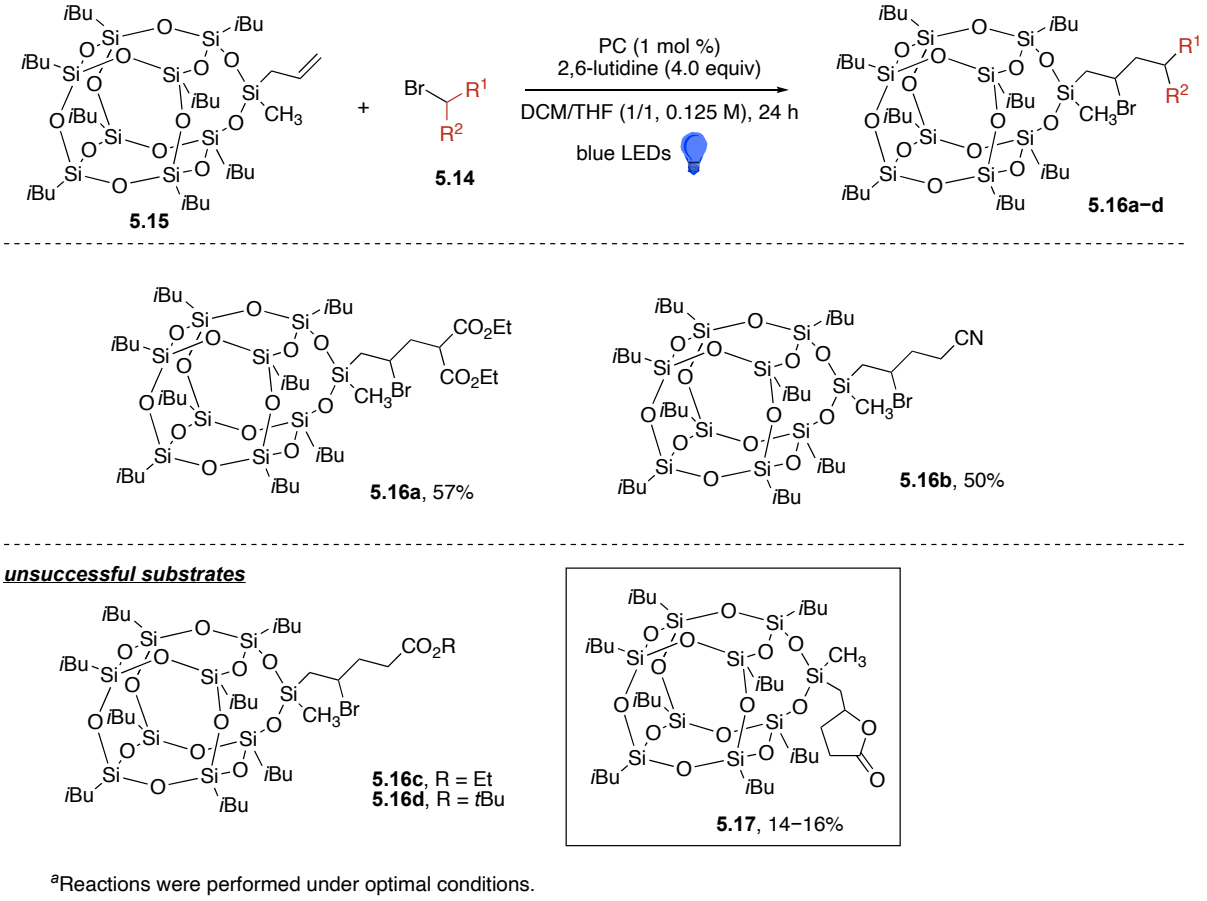



[a]Reactions were performed under optimal conditions. [b]5 mol% of **5.PC1** was used.

**Scheme 5.5.** Scope of the photocatalysis of corner allyl-POSS **5.1** with alkylbromides **5.14**.[a]

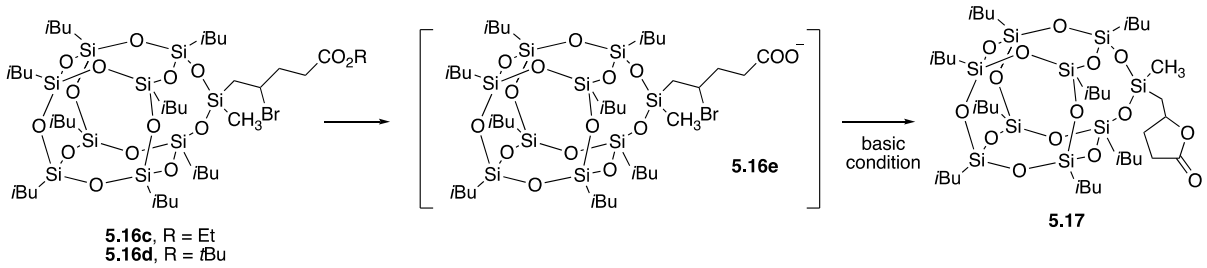
The examination of the substrate scope involving edge allyl-POSS **5.15** and alkylbromides was conducted (Scheme 5.6). The edge allyl-POSS **5.15** reacted with bromomalonate in the photocatalysis reaction, giving a 57% yield of **5.16a**. Additionally, the mono-activated bromide α-bromo acetonitrile showed compatibility with the reaction, yielding 50% of **5.16b**.




[a]Reactions were performed under optimal conditions.

**Scheme 5.6.** Scope of the photocatalysis of edge allyl-POSS **5.15** with alkylbromides.[a]

When α-bromo ethyl acetate and *tert*-butyl acetate were used, the desired products **5.16c** and **d** were not observed. Instead, lactone compound **5.17** was isolated as the major product in 16% and 14% isolated yields, respectively. Additionally, 62% and 60% of the allyl-POSS **5.15** starting material were recovered in these reactions, respectively. The formation of lactone compound **5.17** is attributed to an intramolecular $S_N2$ reaction in which carboxylate **5.18** attacked the bromide, resulting in the generation of lactone **5.17** (Scheme 5.7).

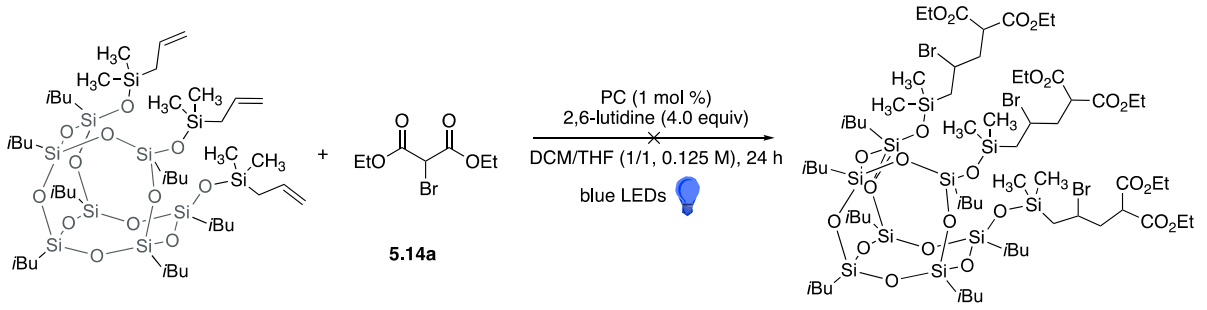



**5.16c**, R = Et
**5.16d**, R = *t*Bu

**Scheme 5.7.** Proposed reaction for the formation of **5.17**.

### Scope of functionalization POSS with three allyl groups

POSS **5.19** with three allyl groups was subjected to the optimized conditions with this photoredox method (Scheme 5.8). The desired product **5.20** was not observed despite the complete consumption of allyl-POSS **5.19** using 1.5 equivalents of bromomalonate per allyl group. Instead, five unidentified compounds (each <10%) were isolated, along with a 40% isolated yield of desilylated product **5.21**. However, the mechanism leading to the formation of this unexpected compound remains elusive. It is possible that radical generation was involved under the influence of blue LED irradiation. Notably, the starting material experienced desilylation, which is likely attributed to the basic conditions under the optimized conditions.




**5.19**

**5.14a**

**5.20**, ***not observed***

**5.21**, proposed structure of the major product based on NMR spectroscopy and HRMS

**Scheme 5.8.** Functionalization POSS with three allyl groups through the photoredox reaction.

## IV. Conclusions

We developed a novel metal-free photocatalytic methodology for functionalizing POSS, generating a new C−C bond. Our initial exploration into transition-metal catalysis to incorporate cyclopropanes onto POSS structures transformed into a new direction with photocatalysis. Andrew Huss's significant breakthrough employing photoredox catalysis to introduce alkyl bromide groups onto POSS nanomaterials redirected our approach. Collaborating closely with Andrew, our efforts focused on optimizing the organophotocatalytic methodology and exploring substrate scope. In addition, we demonstrated a one-pot process to form a cyclopropane POSS. This pioneering work marks the first successful functionalization of POSS nanomaterials via photoredox catalysis, offering promising prospects in nanomaterial research and engineering.

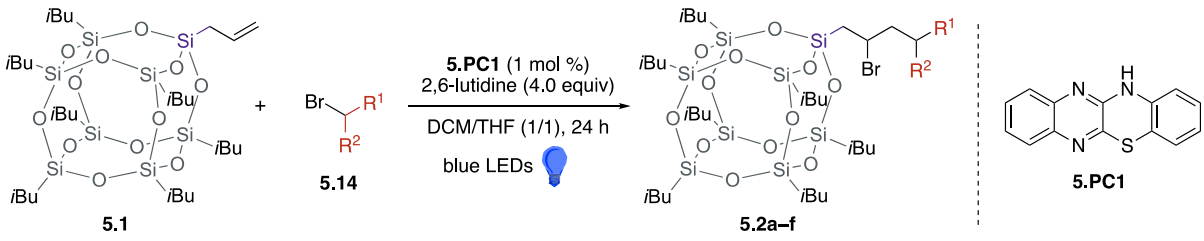
## V. Experimental Procedure and Characterization

### Va. General Information

**Synthesis, Purification, and Analysis.** All the solvent and reagents, unless otherwise noted, were purchased from commercial sources. Refer to Chapter 1 for the information of NMR spectroscopy.

### Vb. General Procedure

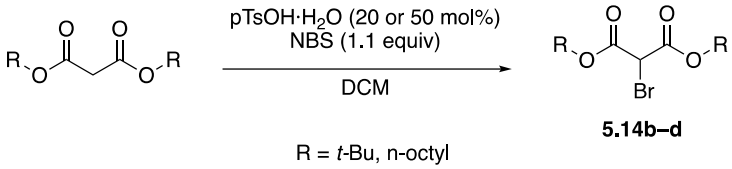
**Procedure A: Procedure for the photoredox catalysis for functionalizing POSS**




To a 7 mL microwave vial charged with a magnetic stir bar and **5.PC1** (0.6 mg, 0.003 mmol, 1 mol%) in 2 mL of DCM/THF (1/1, *v*/*v*) was sequentially added allyl POSS **5.1** or **5.15** (1.0 equiv, 0.25 mmol), 2,6-lutidine (4.0 equiv, 1.0 mmol), and alkylbromides **5.14** (1.7 equiv, 0.475 mmol). The vial was sealed with a PTFE silicone septum. The reaction was irradiated under 440 nm blue LED (36-watt Kessil 440 nm PR160L lamp at 100% intensity) for the indicated duration. The reaction mixture was diluted with

DCM and concentrated *in vacuo*. The products were purified using flash column chromatography ($SiO_2$, gradient from 100% hexanes to 15:1 hexanes/EtOAc) to yield the corresponding functionalized POSS.

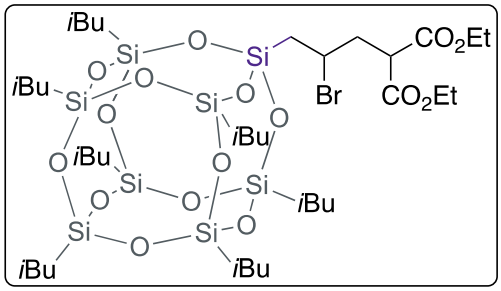
**Procedure B: Synthesis of di-alkyl bromomalonates**




A 50-mL round bottom flask containing a stir bar was flame-dried under high vacuum (<1 torr). After the flask cooled to room temperature, it was purged with argon. *p*-Toluenesulfonic acid monohydrate (0.2 or 0.5 equiv, as indicated) was added to a solution of dioctyl malonate (1.0 equiv) in DCM (0.1 M). The reaction mixture was cooled to 0 °C and N-bromosuccinimide (1.10 equiv) was added in 5 portions over ~5 min. The reaction was allowed to warm to room temperature and stirred for 2 h (unless otherwise indicated). After complete conversion of starting material, the reaction was quenched with saturated aq. $NaHCO_3$ (20 mL) and washed with saturated aq. $Na_2S_2O_3$ (20 mL) and brine (20 mL). The aqueous phase was extracted with DCM (3 × 20 mL). The combined organic phase was dried over $MgSO_4$, filtered, and concentrated *in vacuo*. The products were purified using flash column chromatography ($SiO_2$, hexanes/EtOAc, 95:5 *v*/*v*) to yield the corresponding di-alkyl bromomalonates.

## Vc. Characterization Data

(**5.2a**)

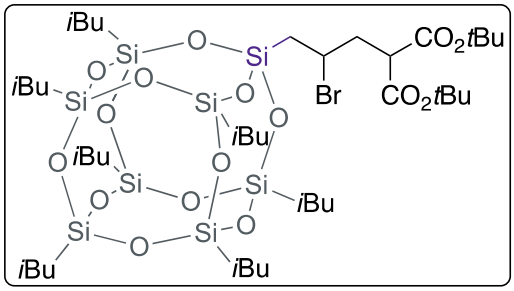



Synthesized according to the General Procedure A using allyl POSS **5.1** (214 mg, 0.25 mmol), bromo diethylmalonate **5.14a** (80.9 µL, 0.425 mmol), **5.PC1** (0.6 mg, 0.0025 mmol), and 2,6-lutidine (116 µL, 1.00 mmol). The reaction mixture was purified using flash column chromatography ($SiO_2$, gradient

from 100% hexanes to 15:1 hexanes/EtOAc) to give the functionalized POSS **5.2a** as a white solid (230 mg, 84%).

$^{1}$H NMR (400 MHz, $CDCl_3$) δ 4.27 – 4.14 (m, 5H), 3.75 (dd, *J* = 10.5, 3.9 Hz, 1H), 2.56 (ddd, *J* = 15.0, 10.5, 2.7 Hz, 1H), 2.24 (ddd, *J* = 15.0, 11.0, 4.0 Hz, 1H), 1.92 – 1.78 (m, *J* = 6.8 Hz, 7H), 1.61 (dd, *J* = 15.0, 6.6 Hz, 1H), 1.52 (dd, *J* = 15.1, 8.2 Hz, 1H), 1.27 (td, *J* = 7.1, 4.4 Hz, 6H), 0.95 (d, *J* = 6.6 Hz, 42H), 0.61 (dd, *J* = 9.3, 7.1 Hz, 14H); $^{13}$C NMR (101 MHz, $CDCl_3$) δ 169.03, 168.54, 61.68, 61.48, 51.38, 50.16, 40.39, 26.46, 25.83, 23.99, 22.62, 22.46, 14.28, 14.19; $^{29}$Si NMR (79 MHz, $CDCl_3$) δ $^{29}$Si NMR (79 MHz, $CDCl_3$) δ -21.96, -67.45, -67.86, -67.89; HRMS (ESI/Orbitrap) m/z: $[M + H]^+$ Calcd for $C_{38}H_{80}BrO_{16}Si_8$ 1095.2784; Found 1095.2793; $R_f$ = 0.67 (hexanes/EtOAc, 20:1 *v*/*v*).

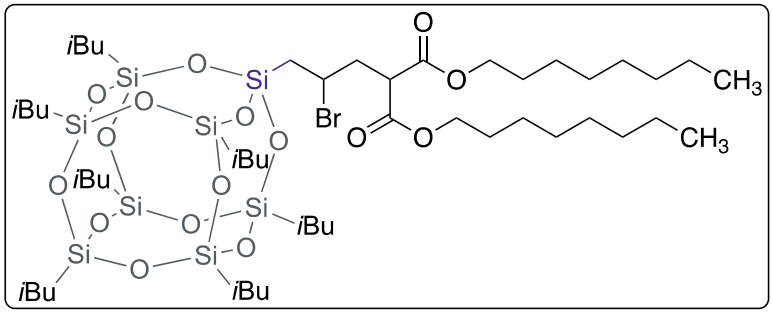
(**5.2b**)




Synthesized according to the General Procedure A using allyl POSS **5.1** (214 mg, 0.25 mmol), bromomalonate **5.14b** (97.7 µL, 0.425 mmol), **5.PC1** (0.6 mg, 0.0025 mmol), and 2,6-lutidine (116 µL, 1.00 mmol). The reaction mixture was purified using flash column chromatography ($SiO_2$, gradient from 100% hexanes to 15:1 hexanes/EtOAc) to give the functionalized POSS **5.2b** as a white solid (254 mg, 88%).

$^{1}$H NMR (400 MHz, $CDCl_3$) δ 4.28 (dddd, *J* = 11.0, 10.4, 7.0, 2.9 Hz, 1H), 3.56 (dd, *J* = 10.3, 4.0 Hz, 1H), 2.49 (ddd, *J* = 15.0, 10.4, 2.9 Hz, 1H), 2.17 (ddd, *J* = 15.0, 11.0, 4.0 Hz, 1H), 1.97 – 1.79 (m, 7H), 1.63 (dd, *J* = 14.7, 7.0 Hz, 1H), 1.60 – 1.51 (m, 1H), 1.49 (s, 9H), 1.48 (s, 9H), 0.97 (d, *J* = 6.8 Hz, 42H), 0.63 (dd, *J* = 11.5, 7.1 Hz, 14H); $^{13}$C NMR (101 MHz, $CDCl_3$) δ 168.35, 167.96, 81.62, 81.47, 53.22, 50.47, 40.41, 28.10, 28.06, 26.63, 25.86, 25.83, 25.80, 24.03, 24.01, 23.99, 22.64, 22.58, 22.53, 22.51, 22.47; $^{29}$Si NMR (79 MHz, $CDCl_3$) δ -21.94, -67.45, -67.80, -67.88, -67.91.

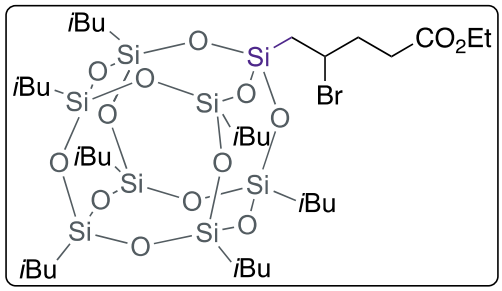
(**5.2c**)




Synthesized according to the General Procedure A using allyl POSS **5.1** (214 mg, 0.25 mmol), bromomalonate **5.14c** (173 mg, 0.425 mmol), **5.PC1** (0.6 mg, 0.0025 mmol), and 2,6-lutidine (116 µL, 1.00 mmol). The reaction mixture was purified using flash column chromatography ($SiO_2$, gradient from 100% hexanes to 15:1 hexanes/EtOAc) to give the functionalized POSS **5.2c** as a white solid (194 mg, 61%).

$^1$H NMR (400 MHz, $CDCl_3$) δ 4.25 (dddd, $J$ = 11.4, 7.7, 6.9, 2.8 Hz, 1H), 4.13 (q, $J$ = 7.0 Hz, 4H), 3.78 (dd, $J$ = 10.3, 4.0 Hz, 1H), 2.57 (ddd, $J$ = 14.9, 10.3, 2.8 Hz, 1H), 2.27 (ddd, $J$ = 14.9, 11.0, 4.0 Hz, 1H), 1.87 (heptdd, $J$ = 7.2, 7.2, 7.2 Hz, 7H), 1.65 (qd, $J$ = 7.0, 4.4 Hz, 4H), 1.61 – 1.56 (m, 1H), 1.57 – 1.51 (m, 1H), 1.39 – 1.24 (m, 20H), 0.98 (d, $J$ = 6.6 Hz, 42H), 0.95 – 0.86 (m, 6H), 0.64 (t, $J$ = 8.6 Hz, 14H); $^{13}$C NMR (101 MHz, $CDCl_3$) δ 169.11, 168.65, 65.88, 65.70, 51.29, 50.15, 40.49, 31.94, 29.36, 29.33, 28.69, 28.62, 25.97, 25.94, 25.84, 24.00, 23.98, 22.79, 22.62, 22.46, 14.23; $^{29}$Si NMR (79 MHz, $CDCl_3$) δ -21.96, -67.46, -67.87, -67.90, -73.01; HRMS (ESI/Orbitrap) m/z: $[M + H]^+$ Calcd for $C_{50}H_{104}BrO_{16}Si_8$ 1263.4662; Found 1263.4674; $R_f$ = 0.67 (hexanes/EtOAc, 20:1 *v*/*v*).

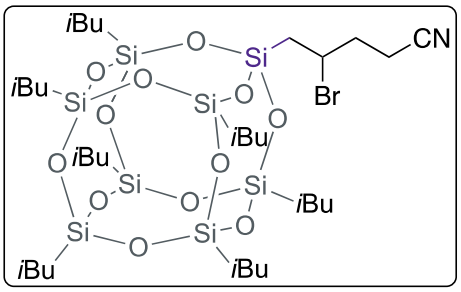
(**5.2d**)



Synthesized according to the General Procedure A using allyl POSS **5.1** (214 mg, 0.25 mmol), ethyl bromoacetate **5.14d** (47.1 µL, 0.425 mmol), **5.PC1** (3.1 mg, 0.0125 mmol), and 2,6-lutidine (116 µL, 1.00 mmol). The reaction mixture was purified using flash column chromatography ($SiO_2$, gradient from 100% hexanes to 15:1 hexanes/EtOAc) to give the functionalized POSS **5.2d** as a white solid (171 mg, 67%).

$^1$H NMR (400 MHz, $CDCl_3$) δ 4.36 (dddd, $J$ = 9.0, 9.0, 5.8, 3.2 Hz, 1H), 4.16 (q, $J$ = 7.1 Hz, 2H), 2.63 (ddd, $J$ = 16.3, 9.7, 5.3 Hz, 1H), 2.50 (ddd, $J$ = 16.3, 9.7, 5.8 Hz, 1H), 2.30 (dddd, $J$ = 14.7, 9.0, 6.0, 3.2 Hz, 1H), 2.08 (dddd, $J$ = 14.7, 9.7, 9.0, 5.3 Hz, 1H), 1.88 (hept, $J$ = 6.8 Hz, 7H), 1.64 (dd, $J$ = 15.1, 5.8 Hz, 1H), 1.55 (dd, $J$ = 15.1, 9.0 Hz, 1H), 1.28 (t, $J$ = 7.1 Hz, 3H), 0.98 (dd, $J$ = 6.8, 1.9 Hz, 42H), 0.63 (dd, $J$ = 7.1, 4.9 Hz, 14H); $^{13}$C NMR (101 MHz, $CDCl_3$) δ 172.72, 60.55, 52.54, 36.08, 32.82, 26.23, 25.83, 24.04, 24.01, 23.99, 22.66, 22.61, 22.59, 22.55, 22.50, 14.40; $^{29}$Si NMR (79 MHz, $CDCl_3$) δ -21.95, -67.47, -67.70, -67.78, -67.84, -67.90; HRMS (ESI/Orbitrap) m/z: $[M + H]^+$ Calcd for $C_{35}H_{76}BrO_{14}Si_8$ 1023.2572; Found 1023.2599; $R_f$ = 0.75 (hexanes/EtOAc, 20:1 *v*/*v*).

(**5.2e**)

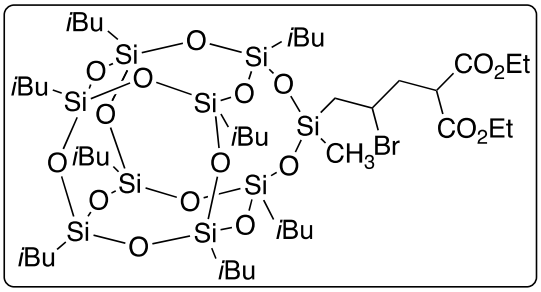



Synthesized according to the General Procedure A using allyl POSS **5.1** (214 mg, 0.25 mmol), bromoacetonitrile **5.14e** (29.6 µL, 0.425 mmol), **5.PC1** (3.1 mg, 0.0125 mmol), and 2,6-lutidine (116 µL, 1.00 mmol). The reaction mixture was purified using flash column chromatography ($SiO_2$, gradient from 100% hexanes to 15:1 hexanes/EtOAc) to give the functionalized POSS **5.2e** as a white solid (165 mg, 67%).

$^1$H NMR (400 MHz, $CDCl_3$) δ 4.34 (dddd, $J$ = 9.7, 9.7, 5.6, 2.9 Hz, 1H), 2.71 – 2.51 (m, 2H), 2.32 (dddd, $J$ = 14.7, 8.8, 7.2, 2.9 Hz, 1H), 2.09 (dddd, $J$ = 14.7, 9.9, 8.6, 5.1 Hz, 1H), 1.97 – 1.79 (m, $J$ = 6.8 Hz, 7H), 1.68 (dd, $J$ = 15.0, 5.6 Hz, 1H), 1.53 (dd, $J$ = 15.0, 9.9 Hz, 1H), 0.98 (dd, $J$ = 7.0, 4.8 Hz,

42H), 0.65 (dd, $J$ = 8.2, 7.0 Hz, 14H); $^{13}$C NMR (101 MHz, $CDCl_3$) δ 118.70, 50.48, 36.49, 26.06, 25.84, 25.82, 24.04, 23.99, 22.59, 22.55, 22.51, 16.39; $^{29}$Si NMR (79 MHz, $CDCl_3$) δ -21.94, -67.36, -67.77, -67.81, -73.40; HRMS (ESI/Orbitrap) m/z: $[M + H]^+$ Calcd for $C_{33}H_{71}BrNO_{12}Si_8$ ; Found 976.2316; $R_f$ = 0.75 (hexanes/EtOAc, 20:1 *v*/*v*).

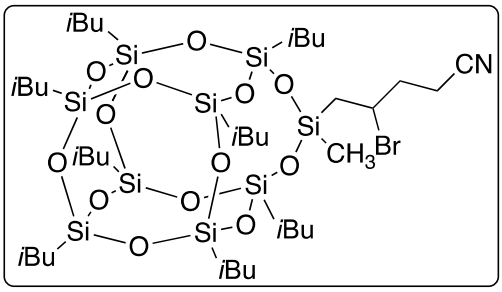
(**5.2f**)




Synthesized according to the General Procedure A using allyl POSS **5.15** (243 mg, 0.25 mmol), bromo diethylmalonate **5.14a** (80.9 μL, 0.425 mmol), **5.PC1** (0.6 mg, 0.0025 mmol), and 2,6-lutidine (116 μL, 1.00 mmol). The reaction mixture was purified using flash column chromatography ($SiO_2$, gradient from 100% hexanes to 15:1 hexanes/EtOAc) to give the functionalized POSS **5.2f** as a white solid (171 mg, 57%).

$^1$H NMR (400 MHz, $CDCl_3$) δ 4.34 – 4.16 (m, 5H), 3.80 (dd, $J$ = 10.5, 3.9 Hz, 1H), 2.53 (ddd, $J$ = 15.0, 10.4, 2.8 Hz, 1H), 2.26 (ddd, $J$ = 15.0, 11.0, 3.9 Hz, 1H), 1.95 – 1.78 (m, 8H), 1.65 – 1.53 (m, 2H), 1.30 (td, $J$ = 7.1, 4.5 Hz, 6H), 1.04 – 0.92 (m, 48H), 0.67 – 0.54 (m, 16H), 0.26 (s, 3H); $^{13}$C NMR (101 MHz, $CDCl_3$) δ 169.09, 168.75, 61.68, 61.56, 51.62, 51.38, 40.60, 31.23, 25.98, 25.96, 25.92, 25.90, 25.88, 25.81, 24.22, 24.15, 24.08, 24.02, 23.73, 23.69, 23.58, 23.24, 23.22, 23.18, 23.16, 22.62, 22.60, 14.25, 14.20, -0.16; $^{29}$Si NMR (79 MHz, $CDCl_3$) δ -26.94, -55.73, -67.04, -68.76, -68.81, -68.94, -68.96, -69.03, -69.13; HRMS (ESI/Orbitrap) m/z: $[M + H]^+$ Calcd for $C_{43}H_{92}BrO_{17}Si_9$ 1211.3441; Found 1211.3451; $R_f$ = 0.75 (hexanes/EtOAc, 20:1 *v*/*v*).

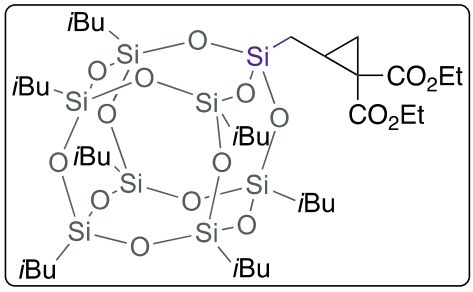
(**5.2g**)




Synthesized according to the General Procedure A using allyl POSS **5.15** (243 mg, 0.25 mmol), bromo diethylmalonate **5.14a** (80.9 µL, 0.425 mmol), **5.PC1** (0.6 mg, 0.0025 mmol), and 2,6-lutidine (116 µL, 1.00 mmol). The reaction mixture was purified using flash column chromatography ($SiO_2$, gradient from 100% hexanes to 10:1 hexanes/EtOAc) to give the functionalized POSS **5.2f** as a white solid (136 mg, 50%).

$^1$H NMR (400 MHz, $CDCl_3$) δ 4.38 (dddd, $J$ = 9.4, 9.4, 6.0, 2.9 Hz, 1H), 2.70 – 2.50 (m, 2H), 2.32 (dddd, $J$ = 14.6, 8.6, 7.3, 2.9 Hz, 1H), 2.17 – 2.03 (m, 1H), 1.96 – 1.78 (m, 8H), 1.61 (dd, $J$ = 14.9, 6.0 Hz, 1H), 1.51 (dd, $J$ = 14.9, 9.4 Hz, 1H), 1.03 – 0.92 (m, 48H), 0.67 – 0.56 (m, 16H), 0.24 (s, 3H); $^{13}$C NMR (101 MHz, $CDCl_3$) δ 118.72, 51.82, 36.69, 30.45, 25.95, 25.89, 25.86, 25.80, 24.25, 24.14, 24.12, 24.08, 24.01, 23.79, 23.75, 23.58, 23.18, 23.12, 22.59, 22.57, 16.31, 0.05, -4.13; $^{29}$Si NMR (79 MHz, $CDCl_3$) δ -27.41, -55.72, -66.98, -68.60, -68.74, -68.80, -68.85, -68.89, -68.93, -68.98; HRMS (ESI/Orbitrap) m/z: $[M + H]^+$ Calcd for $C_{38}H_{83}BrNO_{13}Si_9$ 1092.2971; Found 1092.2979; $R_f$ = 0.70 (hexanes/EtOAc, 20:1 *v*/*v*).

**(5.3)**

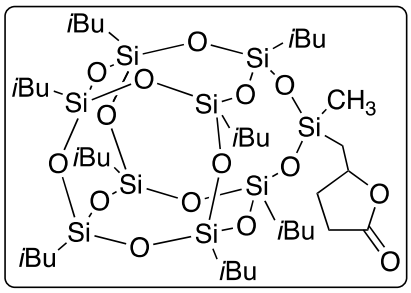



To a 7 mL microwave vial charged with a magnetic stir bar and **5.PC1** (0.6 mg, 0.0025 mmol, 1 mol%) in 2 mL of DCM/THF (1/1, *v*/*v*) was sequentially added allyl POSS **5.1** or **5.15** (1.0 equiv, 214 mg, 0.25 mmol), 2,6-lutidine (4.0 equiv, 116 µL, 1.0 mmol), and bromo diethylmalonate **5.14a** (1.7 equiv, 80.9

μL, 0.425 mmol). The vial was sealed with a PTFE silicone septum. The reaction was irradiated under 440 nm blue LED (36-watt Kessil lamp at 100% intensity). After 24 h irradiation DBU (4.0 equiv, 150 μL, 1.00 mmol) was added. The reaction was stirred at room temperature for an additional 16 h. The reaction mixture was then diluted with DCM and extracted with brine. The aqueous phase was extracted with DCM (3 × 2 mL). The combined organic phase was dried over $MgSO_4$, filtered, and concentrated *in vacuo*. The products were purified using flash column chromatography ($SiO_2$, gradient from 100% hexanes to 15:1 hexanes/EtOAc) to yield the corresponding functionalized cyclopropane POSS **5.3** as a white solid (188 mg, 74%).

$^1$H NMR (400 MHz, $CDCl_3$) δ 4.31 – 4.12 (m, 4H), 2.00 (dddd, $J$ = 12.1, 9.0, 7.6, 3.2 Hz, 1H), 1.87 (dpd, $J$ = 11.2, 6.7, 1.9 Hz, 7H), 1.45 (dd, $J$ = 9.0, 4.6 Hz, 1H), 1.36 (dd, $J$ = 7.5, 4.6 Hz, 1H), 1.29 (dt, $J$ = 11.2, 7.1 Hz, 6H), 1.09 (dd, $J$ = 14.9, 3.3 Hz, 1H), 0.97 (dd, $J$ = 6.7, 1.7 Hz, 42H), 0.63 (dd, $J$ = 7.0, 1.9 Hz, 14H), 0.27 (dd, $J$ = 14.9, 11.8 Hz, 1H); $^{13}$C NMR (101 MHz, $CDCl_3$) δ 170.56, 168.35, 61.39, 34.97, 25.85, 25.84, 25.83, 25.79, 24.02, 23.99, 23.68, 22.80, 22.63, 22.56, 22.34, 14.39, 14.23, 11.91; $^{29}$Si NMR (79 MHz, $CDCl_3$) δ -21.97, -67.50, -67.88, -69.99; HRMS (ESI/Orbitrap) m/z: $[M + H]^+$ Calcd for $C_{38}H_{79}O_{16}Si_8$ 1015.3522; Found 1015.3539; $R_f$ = 0.54 (hexanes/EtOAc, 20:1 *v*/*v*).

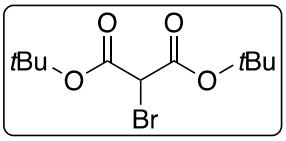
(**5.17**)




$^1$H NMR (400 MHz, $CDCl_3$) δ 4.68 (dddd, $J$ = 10.6, 8.5, 6.0, 4.7 Hz, 1H), 2.56 – 2.46 (m, 2H), 2.47 – 2.35 (m, 1H), 1.93 – 1.86 (m, 1H), 1.90 – 1.76 (m, 9H), 1.37 (dd, $J$ = 14.1, 4.8 Hz, 1H), 1.02 (dd, $J$ = 14.1, 10.6 Hz, 1H), 0.95 (dd, $J$ = 6.6, 4.1 Hz, 48H), 0.63 – 0.52 (m, 18H); $^{13}$C NMR (101 MHz, $CDCl_3$) δ 177.30, 79.52, 30.58, 29.76, 28.25, 25.97, 25.94, 25.89, 25.87, 25.84, 25.79, 24.96, 24.23, 24.13, 24.08, 24.01, 23.80, 23.23, 23.21, 23.16, 22.56; $^{29}$Si NMR (79 MHz, $CDCl_3$) δ -26.25, -66.96, -66.99,

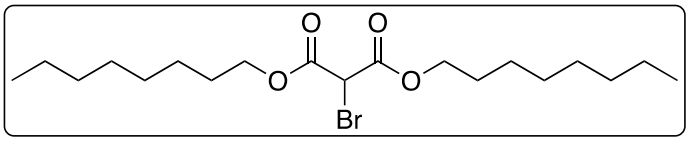
-68.78, -68.88, -68.91, -68.95, -69.05, -69.10; HRMS (ESI/Orbitrap) m/z: $[M + H]^+$ Calcd for $C_{38}H_{83}O_{15}Si_9$ 1031.3655; Found 1031.3665; $R_f$ = 0.23 (hexanes/EtOAc, 20:1 *v*/*v*).

(**5.14b**)




Synthesized according to the General Procedure B using dioctyl malonate (1.12 mL, 5.00 mmol), *p*-TsOH·$H_2O$ (190 mg, 1.00 mmol, 0.2 equiv), and N-bromosuccinimide (979 mg, 5.50 mmol). The products were purified using flash column chromatography ($SiO_2$, hexanes/EtOAc, 95:5 *v*/*v*) to give the di-tert-butyl bromomalonates **5.14b** as a colorless oil (1.21 mg, 83%). $^1$H NMR spectral data matches that of a previous report.[8]

(**5.14c**)




Synthesized according to the General Procedure B using dioctyl malonate (500 µL, 1.43 mmol), *p*-TsOH·$H_2O$ (95 mg, 0.72 mmol, 0.5 equiv), and N-bromosuccinimide (280 mg, 1.57 mmol). After the reaction was stirred at room temperature for 2 h, it was heated to 30 °C and stirred for an additional 16 h. The products were purified using flash column chromatography ($SiO_2$, hexanes/EtOAc, 95:5 *v*/*v*) to give the di-octyl bromomalonates **5.14b** as a colorless oil (490 mg, 84%).

$^1$H NMR (300 MHz, $CDCl_3$) δ 4.83 (s, 1H), 4.22 (t, *J* = 6.7 Hz, 4H), 1.75 – 1.59 (m, 4H), 1.43 – 1.21 (m, 20H), 0.88 (t, *J* = 7.0 Hz, 6H); $^{13}$C NMR (76 MHz, $CDCl_3$) δ 164.81, 67.47, 42.64, 31.90, 29.29, 29.25, 28.47, 25.80, 22.77, 14.22; $R_f$ = 0.37 (hexanes/EtOAc, 20:1 *v*/*v*).

## VI. References


(1) Li, Z.; Kong, J.; Wang, F.; He, C. Polyhedral Oligomeric Silsesquioxanes (POSSs): An Important Building Block for Organic Optoelectronic Materials. *J. Mater. Chem. C* **2017**, *5* (22), 5283–5298. https://doi.org/10.1039/C7TC01327B.

(2) *Polyhedral oligomeric silsesquioxane/epoxy coatings: a review*. https://doi.org/10.1680/jsuin.20.00037.

(3) Moo, J. G. S.; Presolski, S.; Pumera, M. Photochromic Spatiotemporal Control of Bubble-Propelled Micromotors by a Spiropyran Molecular Switch. *ACS Nano* **2016**, *10* (3), 3543–3552. https://doi.org/10.1021/acsnano.5b07847.

(4) Cordes, D. B.; Lickiss, P. D.; Rataboul, F. Recent Developments in the Chemistry of Cubic Polyhedral Oligosilsesquioxanes. *Chem. Rev.* **2010**, *110* (4), 2081–2173. https://doi.org/10.1021/cr900201r.

(5) Jagannathan, J. R.; Targos, K.; Franz, A. K. Synthesis of Functionalized Silsesquioxane Nanomaterials by Rhodium-Catalyzed Carbene Insertion into Si−H Bonds. *Angew. Chem. Int. Ed.* **2022**, *61* (1). https://doi.org/10.1002/anie.202110417.

(6) Fischer, D. M.; Freis, M.; Amberg, W. M.; Lindner, H.; Carreira, E. M. Organophotocatalytic Carbo-Heterofunctionalization of Unactivated Olefins with Pendant Nucleophiles. *Chem. Sci.* **2023**, *14* (26), 7256–7261. https://doi.org/10.1039/D3SC02250A.

(7) Fischer, D. M.; Lindner, H.; Amberg, W. M.; Carreira, E. M. Intermolecular Organophotocatalytic Cyclopropanation of Unactivated Olefins. *J. Am. Chem. Soc.* **2023**, *145* (2), 774–780. https://doi.org/10.1021/jacs.2c11680.

(8) Kelley, A. M.; Haywood, R. D.; White, J. C.; Petersen, K. S. Enantioselective Desymmetrizations of Diesters to Synthesize Fully Substituted Chiral Centers of 3,4-Dihydrocoumarins and Related Compounds. *ChemistrySelect* **2020**, *5* (10), 3018–3022. https://doi.org/10.1002/slct.202000312.